

ICONST EST 2023

International Conferences on Science and Technology

Engineering Science and Technology

August 30 - September 1, 2023 in Budva, MONTENEGRO

ABSTRACTS & PROCEEDINGS BOOK

ICONST EST 2023

International Conferences on Science and Technology

Engineering Science and Technology

August 30 - September 1, 2023 in Budva, MONTENEGRO

Editors

Dr. Mustafa Karaboyacı
Dr. Abdullah Beram
Dr. Hamza Kandemir
Dr. Serkan Özdemir

Technical Editors

MSc. Tunahan Çınar
MSc. Şerafettin Atmaca
Ma. Fıratcan Çınar

Cover design & Layout

Dr. Okan Koç

Copyright © 2023

All rights reserved. The papers can be cited with appropriate references to the publication. Authors are responsible for the contents of their papers.

Published by

Association of Kutbilge Academicians, Isparta, Türkiye
E-Mail: info@kutbilge.org

Publication Date: 20/10/2023
ISBN: 978-625-98911-1-8

ICONST EST 2023

International Conferences on Science and Technology

Engineering Science and Technology

August 30 - September 1, 2023 in Budva, MONTENEGRO

Scientific Honorary Committee

- Prof. Dr. Rade RATKOVIC, Fakultet za biznis i turizam Budva University, Montenegro
Prof. Dr. Mehmet SALTAN, Suleyman Demirel University, Türkiye
Prof. Dr. İlker Hüseyin ÇARIKÇI, Member of Council of Higher Education, Türkiye
Prof. Dr. Yılmaz ÇATAL, Isparta University of Applied Sciences, Türkiye
Prof. Dr. Vujadin VEŠOVIĆ, Faculty of Transport Communications and Logistics, Montenegro
Prof. Dr. Mentor ALİSHANI, University of Prizren, Kosovo
Prof. Dr. Edmond HAJRIZI, University for Business and Technology, Kosovo
Prof. Dr. Naime BRAJSHORI, Kolegji Heimerer, Kosovo
Prof. Dr. Nermina HADŽI GRAHIĆ, University of Tuzla, Bosnia and Herzegovina
Prof. Dr. Kseanela SOTIROFSK, University of Durres, Albania
Prof. Dr. Kürşad ÖZKAN, Isparta University of Applied Sciences, Türkiye

Organizing Committee

- Dr. Mustafa Karaboyacı, Suleyman Demirel University, Türkiye
Dr. Hamza Kandemir, Isparta University of Applied Science, Türkiye
Dr. Serkan Özdemir, Isparta University of Applied Science, Türkiye
Dr. Abdullah Beram, Pamukkale University, Türkiye
Dr. Ergin Kala, University of Prizren, Kosovo
Dr. Joanna Machnik-Slomka, Silesian University of Technology, Poland
Dr. Elzbieta Pawlowska, Silesian University of Technology, Poland
Dr. Fatmir Mehmeti, Prizren University, Kosovo
Prof Dr. Indrit Bimi, Durres University, Albania
Dr. Viliem Kurtulaj, Qiriazi University, Albania
Ma. Dragana Zecevic, Fakultet za biznis i turizam Budva University, Montenegro

Technical Committee

- MSc. Şerafettin Atmaca, Suleyman Demirel University, Türkiye
MSc. Tunahan Çınar, Düzce University, Türkiye
Ma. Fıratcan Çınar, Isparta University of Applied Sciences, Türkiye

ICONST EST 2023

International Conferences on Science and Technology

Engineering Science and Technology

August 30 - September 1, 2023 in Budva, MONTENEGRO

Scientific Committee

- Dr. Alev Akpınar Borazan, Bilecik Seyh Edebali University, Turkey
Dr. Amer Kanan, Al-Quds University, Palestine
Dr. Andrea G. Capodaglio, University of Pavia, Italy
Dr. Aybeyan Selim, International Vision University, North Macedonia
Dr. Apostolos Kiritsakis, Alexander Tech. Educational Ins. of Thessaloniki, Greece
Dr. Ayodeji Olalekan Salau, Obafemi Awolowo University, Nigeria
Dr. Bülent Derviş, International Vision University, North Macedonia
Dr. Cristian Fosalau, Technical University of Iasi, Romania
Dr. Driton Vela, University of Business and Technology, Kosovo
Dr. Eda Mehmeti, University of Business and Technology, Kosovo
Dr. Elvida Pallaska, University of Business and Technology, Kosovo
Dr. Ernek A. Aubakirov, Al – Farabi Kazakh National University, Kazakhstan
Dr. Fecir Duran, Gazi University, Turkey
Dr. Gauss M. Cordeiro, Federal University of Pernambuco, Brazil
Dr. Gholamhossein Hamedani, Marquette University, USA
Dr. Gülcan Özkan, Süleyman Demirel University, Turkey
Dr. Hamid Doost Mohammadian, FHM University of Applied Sciences, Germany
Dr. Ines Bula, University of Business and Technology, Kosovo
Dr. Izabela Zimoch, Silesian University of Technology, Poland
Dr. Joanna Boguniewicz-Zabłocka, Opole University of Technology, Poland
Dr. Kari Heliövaara, University of Helsinki, Finland
Dr. Kłosok-Bazan Iwona, Opole University of Technology, Poland
Dr. Kubilay Akçadoğan, Niğde Ömer Halisdemir University, Turkey
Dr. Leyla Tavacıoğlu, Istanbul Technical University, Turkey
Dr. Lulzim Beqiri, University for Business and Technology, Kosovo
Dr. Mathew Ademola Jayeola, Obafemi Awolowo University, Nigeria
Dr. Mehmet Kılıç, Suleyman Demirel University, Turkey
Dr. Mehmet Kitiş, Suleyman Demirel University, Turkey
Dr. Merita Barani, University for Business and Technology, Kosovo
Dr. Meruyert Kaygusuz, Pamukkale University, Turkey
Dr. Mirosław Kwiatkowski, AGH- University of Science And Technology, Poland
Dr. Mohd Aswadi Bin Alias, University Kuala Lumpur- Bm1, Malaysia
Dr. Muhamet Ahmeti, University of Business and Technology, Kosovo
Dr. Naushad Ali Mamode Khan, University of Mauritius, Mauritius
Dr. Nicholas Baldacchino, Malta College of Arts, Science & Technology, Malta
Dr. Nuray Benli Yıldız, Duzce University, Turkey
Dr. Rahmon Ariyo Badru, Obafemi Awolowo University, Nigeria
Dr. Ramazan Şenol, Suleyman Demirel University, Turkey
Dr. Salina Muhamad, Universiti Selangor, Malaysia
Dr. Sami Makolli, University of Business and Technology, Kosovo
Dr. Serhat Oğuzhan Kıvrak, Hitit University, Turkey
Dr. Shpend Dragusha, University of Business and Technology, Kosovo
Dr. Şule Sultan Uğur, Suleyman Demirel University, Turkey
Dr. Valmir Hoxha, University of Business and Technology, Kosovo
Dr. Vehebi Sofiu, University of Business and Technology, Kosovo
Dr. Vincenzo Naddeo, University of Salerno, Italy
Dr. Zhandos T. Mukayev, Shakarim State University of Semey, Kazakhstan

ICONST 2023

International Conferences on Science and Technology Engineering Science and Technology Life Science and Technology Natural Science and Technology

August 30 - September 1, 2023 in Budva, MONTENEGRO

Dear Readers;

The sixth of ICONST organizations was held in Budva/Montenegro between August 30 - September 1, 2023 with the theme of '*science for sustainable technology*' again. In recent years, weather changes due to climate change have reached a perceptible level for everyone and have become a major concern. For this reason, scientific studies that transform technological progress into a sustainable one is seen as the only solution for humanity's salvation. Here we ask ourselves "which branch of science is responsible for sustainability?". Sustainability science is an interdisciplinary field of study that covers all basic sciences with social, economic, ecological dimensions. If we consider technology as the practical application of scientific knowledge, the task of scientists under these conditions is to design products that consume less energy, require less raw materials, and last longer.

ICONST organizations organize congresses on sustainability issues of three main fields of study at the same time in order to present different perspectives to scientists. This year, 136 papers from 22 different countries presented by scientists in **ICONST Organizations**.

89 papers from 14 countries presented in our **International Conference on Engineering Science and Technology** organized under ICONST organizations. Türkiye leads the way with 48.8% of the participants, followed by Poland with 17.9%, Kosovo with 8.3%, Algeria, Azerbaijan and Montenegro with %4.8, Hungary with 2.4, Italy, Iraq, North Macedonia, Netherland, Iran, Bangladesh and South Africa with 1.2%.

25 papers from 11 countries presented in our **International Conference on Life Science and Technology** organized under ICONST organizations. Türkiye leads the way with 40% of the participants, followed by North Macedonia with 13%, Kosovo and Poland with 8.7%, Sweden, Finland, United Kingdom, Czech Republic, Portugal, Iran and Slovakia with 4.3%.

Finally, 22 papers from 9 countries presented in our **International Conference on Natural Science and Technology** organized under ICONST organizations. Türkiye leads the way with 45.5% of the participants, followed by Kosovo, Russia, Poland and Azerbaijan with 9.1% and India, Ethiopia, Serbia and Albania with 4.5%.

As ICONST organizations, we will continue to organize organizations with the value you deserve in order to exchange ideas against the greatest threat facing humanity, to inspire each other and to contribute to science. See you at your future events.

ICONST Organizing Committee

ICONST EST 2023

International Conferences on Science and Technology

Engineering Science and Technology

August 30 - September 1, 2023 in Budva, MONTENEGRO

Contents

Paper	Presentation Type	Country	Page
Location Detection of Water and Sewer Pipelines Using IMU Sensor Akif Demircali, Omer Boyaci	Oral Presentation	Türkiye	1
3D Printers: The Future Role and Application Areas of Technology Sertaç Salçini	Oral Presentation	Kosovo	2
Electricity Generation from Jerusalem Artichoke Waste by <i>Leuconostoc mesenteroides</i> in a Microbial Fuel Cell Ömer Boyacı, Büşra Onat, Zeynep Onat	Oral Presentation	Türkiye	3
Energy Storage Types in Transportation Vehicles-A Review- Özge Küçükkör, Ali Burak Gögebakan, Ömür Küçükkör, Serkan Özeçoğlu, Mine Sertsöz	Online Presentation	Türkiye	5
Influence of the Content of Recycled Artificial Leather Waste in Particleboards on Their Selected Properties Katarzyna Bartoszuk, Grzegorz Kowaluk	Oral Presentation	Poland	6
Performance Analysis of SRF and CSD Based Algorithms for Voltage Control of Self-Excited Induction Generator Ali Sait Özer, Hulusi Karaca	Oral Presentation	Türkiye	8
Development of Microsphere Releasing Hydrogel System for Local Delivery of Anti-cancer Agents After Tumor Removal Neslihan Barer, Bugse Tunc, Bengi Yilmaz, Yuk Yin Ng, Ali Deniz Dalgic	Oral Presentation	Netherlands	9
The Use of Chestnut Starch as a Binding Mass Filler in the Plywood Technology Julia Dasiewicz, Grzegorz Kowaluk	Oral Presentation	Poland	10
Preliminary Characterization of Functional Features of Biopolymer – Suberinic Acid Residue Blends Aleksandra Ježo, Grzegorz Kowaluk	Oral Presentation	Poland	11
Waste Banana Peel Flour as a Filler in Plywood Binder Matylda Wojciechowska, Grzegorz Kowaluk	Oral Presentation	Poland	12

Application Of Artificial Intelligence Technologies In The Detection Of Explosives	Poster Presentation	Azerbaijan	13
Saida Ahmadova			
Detection of financial flash crash anomalies in real time using observations of the signal and its statistical properties in a preset time window	Online Presentation	Poland	14
Adam Galuszka, Tomasz Dzida, Eryka Probierz, Karol Jedrasiak, Tomasz Wisniewski			
Influence of Sr doping on the microstructure, morphology and optical properties of ZnO thin films prepared by SILAR method	Online Presentation	Algeria	15
Mokrani Nourelhuoda, Ghettaf Temam Elhachemi, Ben Temam Hachemi, Barkat Hadjer			
Build Your Own Defense: Prevention of Ransomware	Online Presentation	Türkiye	16
Mahmut Tokmak			
Determination of Direct Tensile Strength by Non-Destructive Test	Oral Presentation	Türkiye	17
Mustafa Kanik, Zülfü Gürocak			
LCA Comparison Of Digestate Management	Online Presentation	Türkiye	18
Sıdıka Tuğçe Dağhoğlu, Melike Güler			
Investigating Electromagnetic Radiation for Improved Drying Efficiency	Oral Presentation	Poland	19
Magdalena Zielinska, Zhongli Pan, Ragab Gebreil			
Laboratory-Type Silage Production, Data Acquisition and Control System Sensor Performance Tests; Module-A Example	Oral Presentation	Türkiye	20
Fulya Tan, Figan Dalmış, Ersen Okur, İbrahim Savaş Dalmış			
Understanding the Outlines of Blockchain Integrations for Supply Chain Management in Healthcare Industry	Oral Presentation	Türkiye	22
Murat Tahir Çaldağ, Ebru Gökcalp			
Classification of TMJ Sounds by Using One Dimensional Convolutional Neural Networks	Oral Presentation	Türkiye	23
Uğur Taşkıran			
Classification of Motor Imagery Tasks Using Imaginary Coherence	Online Presentation	Türkiye	24
Fatih Ekrem Onat, Ahmet Ademoğlu			
Evaluation of Gamma Attenuation Coefficient for Monoatomic and Composit Absorbers: Experimental Measurements and XCom data	Online Presentation	Algeria	25
Boukhalfa-Salma, Khelifi-Rachid			
Adsorption Based Surfactant Removal - A Case Study in Industrial Wastewater Treatment	Oral Presentation	Italy	26
Iwona Klosok-Bazan, Joanna Boguniewicz-Zablocka, Andrea G. Capodaglio, Mustafa Karaboyacı			
Combination of GRAVEL unfolding package and Geant4 simulation for radioactivity monitoring: Application to gamma spectrometry technic	Online Presentation	Algeria	27
Boukhalfa-Salma and Khelifi-Rachid			

Integration of Renewable Energy Sources in the SMART Vehebi Sofiu, Sami Gashi, Besa Veseli, Faton Maloku, Muhaxherin Sofiu	Oral Presentation	Kosovo	28
Hygienic Surfaces and the Evolution of House Applications with Smart Materials: A Comprehensive Overview Halit Coza, Mahmed Sari Njjar	Online Presentation	Türkiye	29
The Impact of Electric Vehicles on Environment, Energy Systems, and the Economy Ahmad Al-Sarraj, Fatih Yigit, Ahmet Kabul	Oral Presentation	Iraq	30
Characteristics of Wood Particles Recovered from Post-Consumer Windows and Doors Joinery Anita Wronka, Grzegorz Kowaluk	Oral Presentation	Poland	31
Application of Post-Consumer Wood-Based Composites for Liquid Biofuels Purposes Aneta Skreęta, Jan Szadkowski	Oral Presentation	Poland	32
Empowering Sustainable Urban Transformation in developing societies: Lessons from the "Smart City Kosova" Initiative Shqiprim Ahmeti, Besa Veseli	Online Presentation	Kosovo	33
Analysis of The Efficient Recover of Li And Cobalt Metals From The Spent LIB Based on A Case Study Joanna Boguniewicz-Zablocka, Mustafa Karaboyacı and Domenico Guida	Oral Presentation	Poland	34
Estimating health exposure to nitrates (V) from drinking water- a case study Iwona Klosok-Bazan, Izabela Zimoch	Oral Presentation	Poland	35
Extended Reality as a Visual Tool for Architectural Fabrication and Inspection Faruk Can Ünal	Online Presentation	Türkiye	36
An assessment of over-tourism risk in Safranbolu, Turkey Büşra Nur Gündoędu, Sırma Turgut	Online Presentation	Türkiye	37
The Enneagram and Conflict Resolution in the New Design of Universal Systems in the Era of Digital Nomadism Özğü Hafizoęlu	Oral Presentation	Türkiye	38
Prioritizing Port`s Development Direction by Analytic Heirarchy Process Method Deda Delović	Oral Presentation	Montenegro	39
Incorporation of Different Anthocyanin Sources to SLA Resin at Different Solvent Compositions: An Optimization Study Munever Beyza Karabiyik, Kardelen Sena Kirdi, Sevil Cikrikci Erunsal	Online Presentation	Türkiye	40
Food Waste Management Elvin Shaliyev	Oral Presentation	Azerbaijan	41
Analysis of Parameters of Treated Effluents from On-Site Sewage Treatment Plants Monika Pawlita-Posmyk, Małgorzata Wzorek	Oral Presentation	Poland	42
Latest Developments and Applications in The Field of Biotechnology Kamila Sobkowiak	Oral Presentation	Poland	43

Influence of Sr doping on the microstructure, morphology and optical properties of ZnO thin films prepared by SILAR method Mokrani Nourelhuoda, Ghettaf Temam Elhachemi, Ben Temam Hachemi, Barkat Hadjer	Online Presentation	Algeria	44
Computer Science and Informatics: Journey from Past to Present and Future Berkan Başa	Oral Presentation	Kosovo	45
Effects of computer science and informatics on the education system Akif Gaş	Oral Presentation	Kosovo	46
Human-Machine Collaboration Systems in Mechanical Engineering Abbas Hasanov	Oral Presentation	Azerbaijan	47
Disaster Management Strategies Faruk Bojaxhi	Oral Presentation	Kosovo	48
Biomass Efficiency in Production of Green Energy Ylli Kortoçi	Oral Presentation	Kosovo	49
Food Safety and Microbiology Management Kamila Sobkowiak	Oral Presentation	Poland	50
The Importance of Technology in Access to Clean Water: Sustainable and Universal Access to Water Resources Elsever Şukurov	Oral Presentation	Azerbaijan	51
Truck and Van Trip Generation at Logistical Sites Gürkan Günay, Gökmen Ergün, Iğın Gökaşar	Oral Presentation	Türkiye	52
Chemical Waste Reduction and Recycling Strategies Iwona Klosok-Bazan, Joanna Boguniewicz-Zablocka, Mustafa Karaboyacı	Oral Presentation	Poland	53
Design and Optimization of Low Voltage Induction Motor for Standalone PV Systems by FEM Mustafa Tumbek, Enagnon Anpolinaire Dantondii	Oral Presentation	France	54
Sustainable innovation management in water and wastewater companies in Poland Joanna Machnik-Słomka, Elżbieta Pawłowska	Oral Presentation	Poland	55-60
Estimation of Direct Tensile Strength by a Non-Destructive Test Mustafa Kamk, Zülfü Gürocak	Oral Presentation	Türkiye	61-69
The Importance of Carbon Fibers: Research on Türkiye and The World Tugay Üstün, Sinan Can Altuntaş	Oral Presentation	Türkiye	70-78
Visualization of beetle brain with analog artificial intelligence Zoltán Attila Godó	Poster Presentation	Hungary	79-84
Biometric Personal Classification by EMG Signals Using The AlexNet Method Bekir Bilgin, Mehmet İsmail Gürsoy, Ahmet Alkan	Online Presentation	Türkiye	85-90
Design and analysis of geothermal energy-driven combined plant for the production of power, freshwater and heating Fatih Yılmaz	Online Presentation	Türkiye	91-97

The Preservation Proposal for Zion Orphanage of Zincidere Büşra Uzaslan, Gonca Büyükmihçi	Online Presentation	Türkiye	98-108
Assessment of Cargo Hold Wastage Due to Corrosion in General Cargo Ships: Nonlinear approach Špiro Ivošević, Nataša Kovač	Oral Presentation	Montenegro	109-117
Comparison of The Mechanical Properties of Cellulose Paper Reinforced Hybrid Composites Servet Tulum, Tuncer Demirel	Oral Presentation	Türkiye	118-126
Nonlinear Seismic Analysis Of A 24 Stories Reinforced Concrete Building İsra Yılmaz, Muhammet Karaton	Oral Presentation	Türkiye	127-136
Seismic Performance Evaluation of Different Structural Systems Fidan Guzel, Yunus Dere	Online	Türkiye	137-145
Studies of motion and the creation of movement-inspired architectural spatial forms Ferenc Sebestény	Online Presentation	Hungary	146-150
Evaluation of Critical Success Factors for Digital Education with Hesitant Fuzzy Linguistic MCDM Approach Esin Mukul, Gülçin Büyüközkan, Merve Güler	Oral Presentation	Türkiye	151-158
The Influence of Strontium on Eutectic Modification in Al-Si Alloys Biljana Zlaticanin, Sandra Kovačević	Poster Presentation	Montenegro	159-161
Structure and Simulation of Single Phase Seven Level Inverter Abdullatif Emlik, Ali Bekir Yıldız	Online Presentation	Türkiye	162-169
Assessment of The Seismic Hazard For Adıyaman With Deterministic Analysis Due To Probable Earthquake In The Akçadağ Segment (Malatya Fault) Seyhan Okuyan Akcan, Senem Tekin, Fatih Tekir, Mehmet Fatih Boybey, Oğuzhan Çetindemir	Online Presentation	Türkiye	170-177
Development and analysis of a solar PV/T and wind-based system for power and freshwater generation; a comprehensive thermodynamic assessment Fatih Yılmaz	Online Presentation	Türkiye	178-184
Classification of mechanical faults in electric motors based on power spectral density of vibration signal Yunus Emre Acar	Oral Presentation	Türkiye	185-191
Use of Green Synthesis Carbon Dots Derived from Pumpkin Waste in Food Packaging Cemhan Doğan, Nurcan Doğan	Oral Presentation	Türkiye	192-197
The Investigation of Performance Analyses of a Stirling Engine with Bell-Crank Drive Mechanism Derviş Erol	Oral Presentation	Türkiye	199-206
Prioritization of Cybersecurity Strategies: A Hesitant Fuzzy Linguistic MCDM Approach Merve Güler, Gülçin Büyüközkan, Esin Mukul	Oral Presentation	Türkiye	207-214

Analysis and Comparison of Commonly Used Three Level Inverter Topologies Berkay Sabuncu, Ali Bekir Yıldız	Online Presentation	Türkiye	215-225
The Effect of Titanium Contents on the Structure and Properties of the Al-Si Alloys Biljana Zlaticanin, Sandra Kovačević	Poster Presentation	Montenegro	226-228
Determination of the optimum operational conditions for leaching of Mg and Fe from chromium ore processing tailings by different acid solutions Hüseyin Yazıcı	Oral Presentation	Türkiye	229-241
Simulating Input Motion Recordings at Fatih Downhole Array Yusuf Guzel	Online Presentation	Türkiye	242-249
Performance comparison of feature extraction methods in Brain MRI images Züleyha Yılmaz Acar, Fatih Başçiftçi, Kamil Aykutaalp Gündüz	Oral Presentation	Türkiye	250-257
Maximum Power Point Transfer of Off-Grid Stored Energy and Battery Management System Design and Implementation Onur Emre Golen, Mehmet Ali Ustuner, Mohammed Ruhul Amin Bhuiyan, Hayati Mamur	Oral Presentation	Bangladesh	258-262
Stacked Autoencoder Feature Selection Based Zero Day Threat Detection Mahmut Tokmak, Mike Nkongolo	Online Presentation	South Africa	263-273
İlçelerde Bulunan Pazar Yeri Sayılarının Yeterliliklerinin Araştırılması Durdane Tay, Görkem Gülhan	Online Presentation	Türkiye	274-286
Development of Gas-Cooled Modular Reactor Based Helium Gas Turbine with Bottoming Transcritical CO ₂ Rankine Cycle and Hydrogen Production Gamze Soyuturk, Onder Kizilkan, Shoaib Khanmohammadi	Online Presentation	Iran	287-294
Dynamic modeling of a photovoltaic/thermal (PV/T) collector for Isparta Gamze Soyuturk, Onder Kizilkan	Online Presentation	Türkiye	295-305
The Effect of Grape Seed on Phenolic Properties in Different Fermentation Applications and Production Process in Wine Produced from Öküzgözü Grape Alev Akpınar Borazan, Berrin Bozan	Online Presentation	Türkiye	306-310
A Barrier-Free City Proposal for Disabled Individuals Gostivar/North Macedonia Example Ayşe Arıcı	Online Presentation	North Macedonia	311-321
Comparison of Two Sensorless Control Methods for PMSM based on High-Frequency Signal Injection Fehmi Sevilmiş	Oral Presentation	Türkiye	322-326
APF Based Control Algorithm for Voltage Regulation of Self Excited Induction Generator Using DSTATCOM Ali Sait Özer, Hulusi Karaca, Fehmi Sevilmiş	Oral Presentation	Türkiye	327-332
A Comparative Study on Effects of The Number of Hidden Layers in Classification of Induction Motor Rotor Faults with Deep Neural Network Hayri Arabacı	Oral Presentation	Türkiye	333-340

Location Detection of Water and Sewer Pipelines Using IMU Sensor

Akif Demircali¹, Omer Boyaci*²

Abstract: Drinking water is one of our most valuable natural resources. Drinking water pipelines carry water between sources and destinations. Similarly, sewer and drainpipes carry wastewater and various liquids from customer to the processing plants. Inspection and maintenance of water and sewer pipelines are crucial to maintaining a firm water supply, protecting the supply, and preventing contamination and clearing blockages from leaky sewer pipes. Because pipes are often located underground and come in different sizes and configurations, inspection of pipelines, including leak detection and fluid quality monitoring, is difficult. As it is known, there is no detailed location data of all old drinking water and sewerage pipeline networks in local governments. In excavations to be made for maintenance, repair and renovation works, it is important to correctly determine positions of the relevant lines. In this study, an IMU sensor-based location algorithm has been developed for the location detection of drinking water and sewer pipeline networks. The developed algorithm uses the acceleration, gyroscope and magnetometer data recorded by the IMU sensor that is left to pipeline while there is liquid flow. In this way, movements such as rotation around itself can be observed, as well as the instantaneous progress of the left sensor in liquid in the x, y and z axes. The IMU sensor used is the MPU9250 on the 9-axis Razor IMU M0 development board developed by SparkFun. The corresponding development board allows data to be saved on the SD card and transmitted via various communication protocols. With the developed system, precise location determination is made and the integration of the obtained data on the map is carried out. In addition, since the data obtained in the developed system includes rotational movements of the sensor in the liquid, it also allows interpretation of unusual flows of the liquid and potential leaks.

Keywords: Pipeline, Sewer, Position Detection, IMU Sensor.

¹Address: Pamukkale University, Faculty of Engineering, Denizli/Turkiye

²Address: Pamukkale University, Cardak Organized Industrial Zone Vocational School, Denizli/Turkiye

*Corresponding author: omerboyaci@pau.edu.tr

3 | r i t e r s | h e F u t u r e | l e a | A | l i c a t i | A r e a s | e c h | l | y

Serta Salini*¹

Abstract This paper aims to examine the future potential and broad application areas of 3D printer technology. 3D printers are an innovative technology that works on the principle of layer by layer construction of objects. This technology offers advantages such as optimizing production processes, providing design freedom, and enabling rapid prototype development. This paper will address the evolution of 3D printers and their future role. 3D printers are devices that construct objects layer by layer, utilizing various materials. This technology provides a range of advantages, including reducing production costs, facilitating customized production, and speeding up the prototyping process. This paper discusses the evolution of 3D printers and their potential future role. 3D printers create three-dimensional objects by layering different materials. Basic printing techniques such as Fused Deposition Modeling (FDM), Stereolithography (SLA), and Selective Laser Sintering (SLS) are elaborated upon in this section. The role of material selection and its impact on the design process are also examined. 3D printers offer advantages across a wide range of industries, from manufacturing to healthcare, education, and even space exploration. This section delves into the flexibility of design, customized production, and reduced waste production. It also highlights the improvements made in rapid prototyping processes. Despite its advantages, 3D printer technology faces challenges such as material quality, printing speed, cost factors, and difficulties in large-scale production. Various application-specific challenges are also addressed, considering different sectors. 3D printers have the potential to make significant impacts in various fields. Bioprinting could revolutionize the medical field by enabling the production of customized organs and tissues. In the construction sector, complex geometric structures can be efficiently built. Additionally, there is substantial potential in fields like space exploration, food production, and education. 3D printer technology holds the potential to transform industries in the future. By discussing the fundamental principles, current advantages, and future potential, this paper emphasizes the role of 3D printers in global innovation and production processes.

Keywords 3D printing, additive manufacturing, future technology, application areas, innovation

¹Address: University of Priština, Ukshin Hoti, Priština, Kosovo

* Corresponding author: sertacsalcini@gmail.com

Electricity Generation from Jerusalem Artichoke Waste by Electrochemical Microbial Fuel Cell

Ömer Boyacı^{*1}, Şra Öat¹, Eyüp Öat¹

Abstract As an alternative to fossil fuels the search for renewable energy sources has become increasingly important in recent years. We should develop renewable energy sources and make them sustainable and use them. The applicability of the generated electricity to real life processes is as important as generating electricity. From this point of view it is aimed to make biochemical electricity production using food waste and microorganisms and how to make this electricity applicable. We determined the food waste and microorganism in our project by taking advantage of the outputs of our TUBITA 220 B Symbiotic Water Kefir Production with Immune Boosting Jerusalem Artichoke Additive study we did last year. We are considering using Jerusalem artichoke peels as food waste. The reason for this is that the best food source used by the microorganism we will use in the other project is yams and peels. The microorganism is *Leuconostoc mesenteroides* and according to the result we obtained from water kefir production *Leuconostoc mesenteroides* is the probiotic bacterium that forms the basic flora that develops and adapts the most with the contribution of yams in the drink. At this point it will be ensured that *Leuconostoc mesenteroides* can realize electricity production by using yams peels as substrate. Previous studies have utilized algae and *Shewanella putrefaciens* as microbial fuel cells. Electricity generation from disaccharides usually D cellobiose, D maltose, glucose and acetate and wastewater such as whey, olive blackwater as substrates has been studied. The substrate in this study Jerusalem artichoke peels and the bacterial species *Leuconostoc mesenteroides* have not been studied before and are thought to contribute to the literature if investigated. R & D studies will be carried out to determine the capacity of this probiotic bacterium *Leuconostoc mesenteroides* to generate electricity and how the electricity produced can be evaluated with the analyses we aim to make.

Keywords Biochemical electricity production, microbial fuel cells, probiotic bacterium

¹Address: Pamukkale University, Engineering Faculty, Şardak Organized Industrial Zone Vocational School, Denizli, Türkiye

* Corresponding author: omerboyaci@pau.edu.tr

Energy Storage Systems in Transportation Vehicles A Review

Özge Karadağ¹, Ali İsmail Çelebi², Ömer Karadağ³, Serdar Özdemir², İsmail Sertöz^{*}

Abstract Today transportation is responsible for on average 30% of total energy consumption. While the increase and development of transportation vehicles continues with the advancing technology, the efficient use of energy in parallel with this progress is one of the important research topics. After these vehicles are supplied with energy in some way, renewable or non-renewable sources, how vehicles manage their energy consumption is a key point in energy efficiency, but it is not enough on its own. Because after the correct energy management, all components used in the vehicle must be efficient. In this study, energy storage options, which are perhaps the most difficult to choose from all these components, were investigated. Because when choosing an energy storage method and type, not only its efficiency, but also its economic aspect and environmental effects should be considered. There are many energy storage types. These are generally classified as chemical, thermal, electrical, and mechanical energy storages. They are also divided into many types within themselves. Thanks to this study, the advantages and disadvantages of storage options, which was carried out according to the mode of transportation (road, airway, rail system and sea), were investigated and samplings from the world were presented. Thus, it will be a resource for vehicle designers and researchers.

Keywords Energy Storage, Transportation Vehicles, Energy Efficiency, Environmental Impact

¹Address: Apadokya University Vocational School of Apadokya, Nevşehir, Türkiye

²Address: Eskisehir Technical University Railway Systems Department Postgraduate, Eskisehir, Türkiye

³Address: Apadokya University Political Science and Public Administration Postgraduate, Nevşehir, Türkiye

Address: Eskisehir Technical University Railway Systems Department, Eskisehir, Türkiye

* Corresponding author: msertoz@eskisehir.edu.tr

Value of the Text: Cycle Artificial Leather Waste in Particleboards Their Selected Properties

Katarzyna Bartosz¹, Ryszard Kowaluk^{*2}

Abstract Upholstery leather commonly known as artificial leather is a fabric plastic layered composite that looks like natural leather. Due to a broad range of advantages, artificial leather is commonly used as an upholstery material in the renovation and production of furniture or even car upholstery. The material is distinguished by its flexibility and perfect imitation of eco-leather. The aim of the research was to manage the artificial upholstery leather waste by adding previously disintegrated pieces of artificial leather with different content (0, 2, and 4) by weight to particleboards. The tests of selected mechanical properties (bending strength and modulus of elasticity) as well as screw withdrawal resistance and physical properties (density, profile thickness, swelling after water immersion) have been completed. The dimensional characterization of produced waste upholstery fabric particles has been also done. The mechanical properties of the boards deteriorated with the increase in the amount of artificial leather in tested particleboards. However, for most of the features of the tested board variants, the minimum requirements of European standards for furniture boards were met. It can be concluded that depending on the further use of the board, there is the possibility of using recovered pieces of leatherette as a reasonable addition to wood fibres in the production of particleboards. Thus, it is possible to positively contribute to tackling climate change and to circular economy due to the extension of carbon sequestration in recovered waste upholstery materials.

Keywords: recycling, particleboard, artificial leather, upholstery, furniture, circular economy

Article title: The presented study was completed within the activity of the Student Furniture Scientific Group of the Institute of Wood Science and Technology

¹**Address:** Faculty of Wood Technology, Warsaw University of Life Sciences - SGGW, Warsaw, Poland

²**Address:** Department of Technology and Entrepreneurship in Wood Industry, Institute of Wood Sciences and Furniture, Warsaw University of Life Sciences - SGGW, Warsaw, Poland

*** Corresponding author:** ryszard.kowaluk@sggw.edu.pl



er rma ce A alysis S F a S ase Al rithms r lta e tr I
Sel cite ucti e erat r

Ali Sait Özer¹, Hulusi Karaca*²

Abstract Self excited induction generator (SEIG) can be a good option for remote areas without grid connectivity. However, it is known that SEIG requires reactive power for voltage stability during load changes. Distributed static compensator (DSTATCOM) is a suitable option to provide the required reactive power. Various control algorithms have been developed to control DSTATCOM. Synchronous reference Frame (SRF) based and current synchronous detection (CSD) based algorithms are commonly used methods in the literature. This article tests the performance of these two theories under balanced, unbalanced, and nonlinear load conditions. It has been demonstrated that the SRF based method is simpler and more effective than the CSD based method.

Key words Distributed static compensator (DSTATCOM), Self excited induction generator (SEIG), wind energy conversion systems (ECS), Current synchronous detection (CSD) method

¹Address: Onyia Technical University, Department of Control and Automation Technology, Onyia, Turkey

²Address: Selçuk University, Department of Electrical and Electronics Engineering, Onyia, Turkey

* Corresponding author: hkaraca@selcuk.edu.tr

Development of a Hydrogel System for Local Delivery of Anti-cancer Agents: A Preliminary Study

Eslihan Arar¹, Umut C¹, Etilmaz², Umut³, Ali Ezelic^{1*}

Abstract One of the treatment approaches for solid tumors is the removal of tumor with surgical operation and application of systemic chemotherapy alongside local radiotherapy. However, the fact that tumor and healthy tissue do not have a clear border limits the surgeon's ability to remove all the tumor cells from the healthy tissue. For this reason, after the tumor is removed, some micro tumor tissues and cells are left in the wound area. The remaining cancerous cells are known to cause reappearance of tumor and cancer to metastasize to other tissues of the body. Systemic chemotherapy and local radiation therapy is applied to eliminate the remaining cancerous cells to prevent reoccurrence of the cancer. However, systemic chemotherapy can lead to serious side effects since anti-cancer agent can distribute systemically and targeted drug dose may not be achieved at the operation site. Novel local drug delivery approaches are needed to be developed to overcome systemic toxicity of drugs and create an efficient anti-cancer treatment. In this study, a hydrogel was fabricated to have micro chambers on the surface which will carry and deliver anti-cancer drug loaded microspheres. Anti-cancer drug doxorubicin was encapsulated into microspheres and drug release was studied. Scanning electron microscopy was used to show successful encapsulation of microspheres into micro chambers. Anti-cancer effect of the produced hydrogel microsphere system was tested in vitro on both monolayer and spheroid models formed by breast cancer cell line MCF 7 and the hydrogel was successfully reduced cancer cell viability. When the anti-cancer drug loaded microspheres were released from the hydrogel polymer scaffold was able to support viability of healthy cells which was shown by testing the proliferation of mouse fibroblast cell line L 2 on the hydrogel. This hydrogel microsphere system which has the capacity to kill cancer cells is expected to create an environment for normal tissue cells to proliferate over time for the healing of the scar tissue after the release of cancer drug.

Keywords Microsphere, Hydrogel, Local drug delivery, Post Operative Treatment, Doxorubicin

¹Address: Istanbul Bilgi University, Faculty of Engineering and Natural Sciences, Istanbul, Turkey

²Address: University of Health Sciences, Institute of Hamidiye Health Sciences, Istanbul, Turkey

³Address: University of Applied Sciences, Institute of Life Sciences, Utrecht, Utrecht, Netherlands

* Address: Etilmaz, Bilgi.edu.tr

The use of Chestnut Starch as a Natural Filler in the Production of Plywood

Julia Asienczyk¹, Ryszard Kowaluk^{*2}

Abstract Fillers play a crucial role in the production of plywood glues providing enhanced performance and stability to the end product. Plywood being a composite material requires fillers to improve its mechanical properties, adhesion, and overall quality. One common filler used in plywood glues is calcium carbonate. It acts as a bulking agent, increasing the volume and density of the adhesive mixture while reducing production costs. Calcium carbonate also enhances the glue's viscosity, ensuring proper bonding and uniform application during the plywood manufacturing process. Another widely used filler is rye or wheat flour, which consists of finely ground grains. The flour not only improves the adhesive's viscosity but also contributes to the overall strength and stability of the plywood. It helps to prevent warping and enhances dimensional stability, making the final product more durable. Additionally, other fillers like talc or clay minerals may be incorporated into the glues to improve their adhesive properties and increase moisture resistance. Chestnut starch is a type of vegetable flour made by grinding edible chestnuts into a powder. It has a different texture and properties than traditional wheat or rye flour. When used as a binder filler in plywood technology, it can be biodegradable and environment friendly. In the study, there were produced five types of plywood with 0, 5, 10, 15, and 20 parts by weight chestnut flour and one reference. All samples were produced in laboratory conditions and the selected mechanical and physical properties of the produced boards were studied. The mechanical properties of the boards increased with the addition of chestnut flour. In some tests, the results even met the highest requirements of European standards for plywood. According to this finding, a well-chosen addition of rice flour could be positively considered in plywood production. Research is still being conducted to improve the performance of plywood bonded with chestnut starch.

Keywords plywood, chestnut starch, binder

Article title The presented study was completed within the activity of the Student Furniture Scientific Group of the Faculty of Wood Technology, SGGW, Warsaw, Poland

¹**Address** Faculty of Wood Technology, Warsaw University of Life Sciences - SGGW, Warsaw, Poland

²**Address** Department of Technology and Entrepreneurship in Wood Industry, Institute of Wood Sciences and Furniture, Warsaw University of Life Sciences - SGGW, Warsaw, Poland

* **Corresponding author** r.kowaluk@sggw.edu.pl

Primary Characteristics of Functional Features of Polymer Suberin Acid Residues

Aleksandra¹, Kowaluk^{*2}

Abstract Polymer blends have gained significant attention in the field of materials science due to their unique properties and versatile applications. At the same time, more attention is paid to a circular economy including the usage of biodegradable resources. While biopolymers have numerous advantages, there are also challenges associated with their production. However, ongoing research and technological advancements have widespread adoption of biopolymers in various industries, including wood engineering. Therefore, in light of previous research findings, this study aims to prepare and evaluate blends of biopolymers, specifically poly(lactide) (PLA), polycaprolactone (PCL), and modified starch, with the incorporation of up to 10% suberin acid residues (SAR). The previous research showed that suberin acid residues (SAR) remaining from the extraction of birch bark are a promising bioresource that fits into the idea of upcycling. The blends have been produced through extrusion to form granules. The characteristics of the resulting biopolymer blends were assessed using scanning electron microscopy (SEM), spectroscopic techniques such as infrared absorption spectroscopy (IR), and thermal analysis methods including differential scanning calorimetry (DSC), thermogravimetry (TGA), and thermomechanical analysis (TMA). This research aims to address the following questions: What are the key characteristics of the biopolymer blends concerning their suitability for use in wood-based composite technology? What potential applications can be explored for the produced blends in wood technology? Can the prepared blends serve as raw materials for composite production or as binders? Is it feasible to create films/coatings on wood and wood composites? This study will show new promising paths to follow in the next research.

Keywords: polymer blends, suberin acid residues, biopolymers, polymer wood coatings, usage of polymer blends in wood engineering

Acronyms: The presented study was partially completed within the activity of the Student Furniture Scientific Group (Główna Naukowe Meblarstwa) under the BarkBuild project. The BarkBuild project is funded under the ERA-NET Cofund ForestValue program through Vinnova (Sweden), Valsts izglītības atbalsta aģentūra (Latvia), Ministry of Education, Science and Sport (IA) (Slovenia), Academy of Finland, The Research Council of Norway, and the National Science Centre (Poland), contract no. 202/03/N/0003.

The ForestValue program received funding from the Horizon 2020 Research and Innovation program of the European Union under grant agreement No. 773324.

¹**Address:** Faculty of Wood Technology, Warsaw University of Life Sciences - SGGW, Warsaw, Poland. ORCID: 0000-0002-2113-3411

²**Address:** Department of Technology and Entrepreneurship in Wood Industry, Institute of Wood Sciences and Furniture, Warsaw University of Life Sciences - SGGW, Warsaw, Poland. ORCID: 0000-0003-4310-4010

* **Corresponding author:** egor.kowaluk@sggw.edu.pl

Waste banana peel Flour as a Filler in Plywood Binder

Magdalena Ciechowska¹, Ryszard Kowaluk^{*2}

Abstract Waste banana peel flour has gained attention as a potential filler in plywood binders due to its abundance, low cost, and positive environmental impact. Banana peels, which are typically discarded as waste, can be processed into flour and incorporated into plywood binders, offering several advantages. Firstly, banana peel flour acts as a natural filler, increasing the volume and reducing the amount of more expensive fillers required in plywood production. This can lead to cost savings without compromising the overall quality of the plywood. Secondly, banana peels contain a significant amount of cellulose, which contributes to the strength and stability of the binder. The cellulose fibers present in the peel flour improve the adhesive's mechanical properties, enhancing the plywood's resistance to warping, bending, and cracking. Furthermore, banana peels are rich in phenolic compounds, such as tannins, which possess adhesive properties. These compounds can enhance the bonding strength between the veneer layers in plywood, resulting in improved overall structural integrity. Using waste banana peel flour as a filler in plywood binders also presents environmental benefits. By repurposing banana peels, which would otherwise end up in landfills, it reduces waste and promotes sustainability. The study aimed to investigate the influence of various contributions of banana peel flour in bonding mass on the properties of plywood produced with such an investigated binder. The following plywood features have been tested: modulus of rupture and modulus of elasticity, bonding quality, shear strength, and in-wood damage, and density profile. The achieved results have been referred to as the control plywood produced with regular, industrially composed bonding mass. The structure of banana peel has been also characterized as well. The results have shown that waste banana peel flour can be a valuable replacement of commercially applied filler in plywood technology.

Keywords: plywood, binder, glue, filler, banana peel, waste

Abstract: The presented study was completed within the activity of the Student Furniture Scientific Group of the Faculty of Wood Technology, SGGW, Warsaw, Poland.

¹**Address:** Faculty of Wood Technology, Warsaw University of Life Sciences - SGGW, Warsaw, Poland

²**Address:** Department of Technology and Entrepreneurship in Wood Industry, Institute of Wood Sciences and Furniture, Warsaw University of Life Sciences - SGGW, Warsaw, Poland

* **Corresponding author:** Ryszard Kowaluk, r.kowaluk@sggw.edu.pl



Applicati Artificiali e tecnologie in the detection of explosives

Saida Ahmedova*¹

Abstract Terrorist incidents in the world have once again proved that terrorism remains a global problem in the face of aviation security systems. Historically, as a result of the countermeasures taken in this direction, it was possible to weaken the wave of terrorism relatively, but this problem has not yet been fully resolved. The act of terrorism is carried out by means of terrorism. Terrorist tools consisting of dangerous items and substances are carried on board the plane or in the airport area on persons or in cargo, baggage and hand luggage carried in HG, bypassing inspection control. Therefore, the first of the countermeasures against a terrorist act is to detect the person who committed the terrorist act and the means of terrorism. Using artificial intelligence technologies in the detection of explosives is recognized as a current research area.

Keywords Explosive substance, plastic explosive device, portable, ray television complex, non-metallic objects.

¹Address National Aviation Academy, Transport technologies, Baku, Azerbaijan.

* **Corresponding author** saidaahmedovabaku@gmail.com

Effect of a financial flash crash anomalies in real time signal observations the signal and its statistical properties in a reset time

Adam Galuska¹, Masz Zia², Ryabierz¹, Karlewska², Maszysie²

Abstract As data collection tools continue to evolve there are now solutions that enable their analysis through digital platforms. These platforms offer automated financial planning services utilizing algorithms and requiring minimal human oversight. Such platforms gather financial information and future goals from clients utilizing this data to offer consulting services and automate the investment of client funds often leveraging data from various reports.

The integration of artificial intelligence (AI) in data analysis is becoming increasingly prevalent with around 70% of companies planning to implement AI-based solutions in the next year according to research. The rapid advancement of data-driven technologies and AI has created promising development prospects for organizations actively involved in these domains.

To summarize the market gaps identified include the absence of AI-based tools to support the investment process, the lack of a tool to identify historical events similar to the current situation by distinguishing current data from archival records using proprietary models based on deep networks, and the need for improved detection of flash crashes in financial threats. While there have been some works on mini flash crash detection and specific historical flash analysis, comprehensive solutions are still lacking.

Within the proposed detection of flash anomalies based on observation of the signal under study within a preset assumed time window is proposed. The size of the time window (signal length) is adjusted dynamically depending on the nature of the signal.

Assumptions of the method

For a signal in a time window the parameters of the normal distribution of this signal can be determined in confidence intervals for the mean value and standard deviation.

The onset of an anomaly is considered to be the moment when the observed current value of the signal exceeds a threshold value depending on the estimates of the mean value and standard deviation.

Parameterization of the algorithm (i.e. calibration of the threshold value) depends on the reference data of the type of anomaly under study.

Parameterization of the algorithm involves assuming different dependencies of the threshold value on normal distribution estimates and checking the best fit.

Anomaly detection occurs in real time (i.e. the time to analyze the tested signal for the occurrence of an anomaly is significantly shorter (i.e. at least 10 times) than the size of the tested time window).

Acknowledgement

The work has been developed within grant No. POIR.0.0.0.00.0.2. GP Data Platform as an innovative system using artificial intelligence techniques to support investment decisions on the capital market and implemented by Warsaw Stock Exchange SA in 2023. The work of Adam Galuska was partially supported by the SUT under B grant (the subsidy for maintaining and developing the research potential in 2023).

Keywords machine learning, anomaly detection, flash crash, signal analysis

¹**Address** Silesian University of Technology, Faculty of Automatic Control, Electronics and Computer Sciences, Akademicka, Gliwice, Poland

²**Address** Warsaw Stock Exchange, ul. Sienkiewicza 4, Warsaw, Poland

* **Corresponding author** adam.galuska@polsl.pl



Influence of Sr doping on the microstructure, morphology and optical properties of ZnO thin films prepared by SILAR method

Nourelhouda Mokrani^{1,*}, Hetta Emam Hachemi¹, Ezzamel Hachemi¹, Farhat Hachemi¹

Abstract The present study focused on the properties of Sr doped ZnO thin films using the successive ionic layer adsorption and reaction (SILAR) method. The X-ray diffraction results show that the ZnO and Sr doped ZnO samples exhibit hexagonal wurtzite structure having preferential growth along the (001) plane. The maximum crystallite size of 4 nm was observed for Sr doped ZnO 3 wt% sample. The SEM analysis revealed that the samples exhibit agglomerated grains and the EDX spectrum of the Sr doped ZnO 3 and 7wt% samples showed the presence of Zn, Sr and O elements. The UV-vis transmission spectrum of the Sr doped ZnO 7 wt% sample revealed that it has higher transmission in the UV region. Finally, Sr doping has a significant impact on the physical and chemical properties of SILAR deposited ZnO films.

Keywords ZnO thin films, SILAR, XRD, UV-vis

¹Address: Physics Laboratory of Thin Layers and Applications, Biskra University, BP 4, RP Biskra 07000, Algeria

* Corresponding author: nourelhouda.mokrani@univ-biskra.dz

Utilization of Open Source Technologies in RansomwareMahmut Mehmet Akif Ersoy^{*1}

Abstract Ransomware attacks have become a formidable menace in the digital environment causing severe disruptions and economic losses for businesses and individuals alike. This study presents a thorough examination of the growing threat landscape of ransomware, elucidating its various attack vectors, techniques, and implications. Moreover, it outlines a multifaceted and proactive approach to prevent ransomware incidents, offering practical strategies and best practices for achieving cybersecurity resilience. The study begins by highlighting the escalating frequency and sophistication of ransomware attacks, underlining the urgent need for robust prevention measures. It explores the primary methods employed by threat actors to propagate ransomware, such as phishing emails, exploit kits, and malicious downloads, to raise awareness about the evolving attack vectors. One of the core aspects of ransomware prevention lies in employee education and awareness. This study emphasizes the significance of ongoing cybersecurity training to empower employees in recognizing and reporting potential threats. By fostering a security-first culture, organizations can significantly reduce the risk of successful ransomware infiltrations. To fortify defenses, the study advocates for stringent software management practices. Regular updates and patching of operating systems, applications, and security tools are crucial to mitigating vulnerabilities that ransomware can exploit. Additionally, it stresses the importance of employing sophisticated endpoint protection solutions that utilize artificial intelligence and behavioral analysis to detect and neutralize ransomware in real time. Creating and maintaining secure data backups is another pivotal aspect of ransomware prevention. The study highlights the benefits of implementing a well-defined data backup strategy, encompassing both on-site and off-site solutions, to facilitate rapid recovery without capitulating to ransom demands. Furthermore, adopting a zero-trust security model and network segmentation can significantly limit the lateral movement of ransomware within an organization's infrastructure. By compartmentalizing critical assets, businesses can minimize the extent of potential damage in case of an intrusion. In conclusion, this study underscores the necessity of a holistic and proactive approach to prevent ransomware attacks. By combining employee education, vigilant software management, robust endpoint protection, comprehensive data backups, and stringent network segmentation, organizations can enhance their cybersecurity resilience against the persistent and ever-evolving ransomware threat. Implementing these strategies will enable businesses and individuals to defend their digital assets, safeguard sensitive data, and thwart ransomware actors effectively.

Keywords Malware, Ransomware, Build Own Defense, Prevention of Ransomware

¹Author: Burdur Mehmet Akif Ersoy University, Bucak, İliha Tolunay School of Applied Technology and Management, Burdur, Turkey

* Corresponding Author: mahmuttokmak@mehtemetafik.edu.tr

etermination of Direct Tensile Strength by Non-destructive Test

Mustafa Kaşıkçı^{*1}, İlhan Karaca¹

Abstract Depending on the type of stress affecting a material it exhibits various strength characteristics such as compression tensile shear bending and torsional strength Among these uniaxial compression and tensile strengths hold significant importance in rock mechanics applications and serve as indispensable parameters in geotechnical designs Engineering geological studies often focus on unconfined compressive strengths assuming that the rock is under compaction conditions However numerous researchers have emphasized that the tensile strength also plays a crucial role in determining the strength of rock material or rock mass against failure They have highlighted its significance during the design stage Unlike uniaxial compressive strength which has standardized testing methods rock tensile strength is determined using different test methods These methods can be categorized into two main classes direct and indirect tensile tests Direct tensile tests are conducted along the axis of the specimen using various test apparatus However these tests often present significant challenges in obtaining accurate and reliable results On the other hand indirect tensile tests offer an alternative approach and are preferred by designers due to their simplicity and ease of application Among the indirect methods the most commonly used one is the Brazilian test method Designers often use the values obtained through indirect methods directly as the tensile strength of the rock material Alternatively they may calculate the direct tensile strength (DTS) of the rock using empirical equations proposed in relevant studies As an alternative to direct and indirect methods used to determine the tensile strength of rock materials there are studies that propose empirical equations to estimate the tensile strength of rock materials based on various mechanical properties In these studies independent variables such as uniaxial compressive strength point load strength direct shear strength and sonic velocity (SV) have been used In this study two sample groups andesite and marl were subjected to testing to uncover the correlation between DTS and SV The study utilized a total of 20 samples to analyze this relationship The individual evaluations of the groups yielded correlation coefficient (r) values of 0.4 and 0.2 respectively However when all the samples were collectively analyzed the r value significantly increased to 0.8 and a very strong positive correlation has been identified between these two parameters

Keywords Tensile strength direct tensile test sonic wave test non-destructive test

¹Address: Firat University Faculty of Engineering Department of Geological Engineering
Elazığ, Türkiye

*Corresponding author: mkanik@firat.edu.tr

Amiris i estate a a eme t

Sı r a u e a lı lu^{*1}, eli e ler²

Abstract Digestate is a versatile material with abundant nutrients organic matter and moisture making it highly suitable for various applications in agriculture soil development and energy production. The digestate is divided into a liquid and solid phase once it exits the reactor while the liquid phase can be used in a variety of ways including fertilizer and the production of algae the solid phase can be used as compost or fertilizer. The LCA method suggests which scenario should be more environmentally beneficial in this aspect. This abstract investigates different techniques involving digestate utilization as an output substitution for conventional products and the application of allocation methods to equitably distribute environmental impacts and benefits. To determine the environmental advantages of digestate usage critical impact categories like greenhouse gas emissions energy consumption and land use are analyzed. The primary objective of this study is to assess and compare the environmental consequences of techniques used to assess both the solid and liquid phases of digestate. To achieve this goal a comparative analysis is conducted comparing the effectiveness and environmental impact of the proposed acclimation method to existing approaches. By undertaking this comparative analysis the study aims to contribute significantly to the advancement of knowledge on the environmental sustainability of digestate thereby offering valuable insights for optimizing its management and fostering the transition towards a circular economy. This research underlines the significance of incorporating comparative analysis within the life cycle assessment (LCA) framework to identify the most environmentally friendly options for acclimating digestate. Through such analysis the study advocates the adoption of more sustainable waste management strategies enhancing the potential for sustainable development and reduced environmental impact.

Keywords digestate LCA sustainability waste management

¹Address Ege University Centre for Environmental Studies I mir T rkiye

²Address Ege University Faculty of Engineering I mir T rkiye

* Address i author tugce daglioglu ege.edu.tr

Ac le me ts

he auth rs ish t tha

AK u er the ra t 121

r the i a cial su rt this stu y

vesti ati lectr ma etic a iati r m r ve ryi icie cy

a ale a ieli s a*¹, h li a ², a ab ebreil²

Abstract Hot air convective drying (HACD) is time consuming and it may result in low quality of final product. Therefore, the aim of this study is to present a modern method of drying intensification using electromagnetic intensification. The use of microwaves (M) or infrared radiation (IR) may contribute to reducing time or high product quality. Microwave volumetric heating (MVH) is a method of using microwaves to evenly heat the entire volume of material. During IR heating, the energy can be rapidly transmitted from the emitter to foodstuffs in the form of waves without heating the surrounding environment, leading to low heat losses and reduced damage to product quality. The intensification of heat and mass transfer processes due to microwave or infrared radiation induced heating effect was analyzed. Several innovative processing technologies based on M or IR heating have been developed for processing high moisture fruits and vegetables covered with thick surface layer which is a barrier to heat and mass transfer processes. They have also been used to produce functional dried snacks from e.g. fermented beetroots. Different types of intermittent drying have been introduced, for example, intermittent microwave convective drying. The regular IR equipment used electricity as the energy source, while the catalytic infrared (CIR) device used natural gas or propane to generate heat energy by the oxidative reactions in the presence of oxygen under the action of a catalyst. The drying kinetics, effective moisture diffusivity, drying time, changes in material temperature, specific energy consumption were evaluated under different conditions and optimal conditions were defined. The obtained results allow stating that M and IR make the drying process more effective and enhance the drying efficiency of final products without significant deterioration of product quality and elevation of material temperature. The applications of new M or IR based processing technologies should bring significant economic and environmental benefits to the food industry and society.

Key words: microwaves, electric infrared radiation, catalytic infrared radiation, drying kinetics, drying efficiency.

Acknowledgements: This study was supported by the Development Program of the University of Warmia and Mazury in Olsztyn (Project no. PO/R.03.0.00.00/3.0/7) and the Polish National Science Center grant No. 2020/37/B/N/00/7, title: The effect of ultrasound, microwaves, infrared radiation and reduced pressure on the dehydration and drying kinetics of beetroots and the University of Warmia and Mazury in Olsztyn grant No. 000/0.

¹**Address:** Department of Systems Engineering, University of Warmia and Mazury in Olsztyn, Olsztyn, Poland.

²**Address:** Department of Biological and Agricultural Engineering, University of California, Davis, Davis, CA, USA.

* **Corresponding author:** m.ielinska@uwm.edu.pl

Abstract: The primary objective of this study is to investigate the performance of sensors integrated into the laboratory type silage production data acquisition and control system. The system developed through the TUBITA 2002 project is a PLC controlled and multi sensor system designed to enable numerous studies aimed at improving silage quality.

Fulya A¹, Fırat Almış², Feri Özürlü, Savaş Almış^{*1}

Abstract The primary objective of this study is to investigate the performance of sensors integrated into the laboratory type silage production data acquisition and control system. The system developed through the TUBITA 2002 project is a PLC controlled and multi sensor system designed to enable numerous studies aimed at improving silage quality.

The system consists of grinding, weighing, silo data acquisition and control units. It provides the capability to apply change simulate various parameters during the silage production process. The silo unit is composed of two modules: module A (compression principle) and module B (vacuum principle). This research focuses on measurements conducted with plexiglass silos (24 cm³) in the module A unit. Plexiglass silos were equipped with oxygen sensor (0-100%), carbon dioxide sensor (0-1000 ppm), temperature sensor (0-30°C, 0-100°C), humidity sensor (0-100%), pH sensor (2-12) and pressure sensor (0-1000 mbar).

The sensors were placed on specially designed silo covers. The research utilized second crop silage corn material with a dry matter content (DM) of 32%. Four different compression forces were applied during the experiments. Time measurements during silage production (total cycle, application, waiting times) were defined on the setup page of the main screen. Sensor measurements were recorded as one data per second by connecting them to the data recording unit using 4-20 mA analog sensors. Due to the abundance of data, average values were taken. The data were displayed and monitored on the HMI operator panel programmed with ENDA V2.0 editor software and stored in Excel format. The measurements were carried out during the silage aerobic and post silage anaerobic periods.

According to the research results, it was observed that the six tested sensors performed accurate readings. However, issues related to the oxygen and carbon dioxide sensors were encountered. Due to the difficulty in reading at points with very low oxygen content, it was decided to be supported by controlling with sensors of different types and specifications. During measurements conducted at the compression stage in module A, the pressure values varied between 0.34-0.7 bar with increasing compression force. The temperature ranged from 33°C, humidity from 0-100%, pH from 2-12, O₂ level from 0-1000 mmol/L and CO₂ level from 0-40 mmol/L. The measured value ranges in silage varied depending on the duration of silage and accurate measurements were obtained in the desired direction. Sensor placements were updated considering measurement accuracy.

Keywords: Sensor, silage, silage production, simulation

¹A. Almış, Tekirdağ Namık Kemal University, Faculty of Agriculture, Tekirdağ, Türkiye

²A. Almış, Tekirdağ Namık Kemal University, Vocational College of Technical Sciences, Tekirdağ, Türkiye

³A. Almış, Tekirdağ Namık Kemal University, Ordu Faculty of Engineering, Tekirdağ, Türkiye

* Corresponding author: idalmis@nku.edu.tr

Analysis of the Effects of the Number of Hidden Layers in Fault Classification of Induction Motors

Hayri Arabaci*¹

Abstract Induction motors are widely used in industry. The motors are of solid construction. However, in case of any failure, it causes the system to which it is connected to stop or operate inefficiently. For this reason, it is important to detect the faults of induction motors. In few decades, studies on fault detection have been carried out using many methods in the literature. Motor current is the most used motor parameter for fault detection. In the studies, the frequency spectrum of the motor current is generally used as a feature. Machine learning and especially artificial neural networks are used in fault classification. In recent years, deep learning approaches have started to be used in this field as well. The deep neural network (DNN) comes to the fore in deep learning approaches because it requires less processing capacity. One of the parameters affecting the accuracy of the results obtained with DNN is the number of hidden layers. For this reason, in this study, the effects of the number of hidden layers on classification accuracy in the detection of broken rotor bar faults were investigated. Three different motors for experimental work were operated at rated loads in four different conditions: one broken bar fault, 2 broken bars fault, and 3 broken bars fault. The motor current for each condition was sampled and saved. The frequency spectrum of the currents was obtained using the fast Fourier transform. These frequency spectrums are used as input data for the deep neural network. The network was trained and tested on nine different hidden layers. The obtained test results were compared based on both the detection errors of the healthy motors and the test errors. The test results obtained show that test errors increase in cases where the number of hidden layers is low or high, and it gives the best results when the number of hidden layers is three. The error rate of 0.2% in the optimum network structure showed that the DNN approach could be used for rotor fault detection.

Keywords Deep neural network, fault classification, hidden layers, induction motor, rotor faults

¹Address: Selcuk University, Faculty of Technology, Onyia T. rkiye

*Corresponding author: hayriarabaci@selcuk.edu.tr

Outliers in Blockchain Integration in Supply Chain Management in the Healthcare Industry

Barış Akın^{*1}, Mustafa Özalp²

Abstract Emerging technologies present opportunities to improve systems existing features and add innovative additions. Blockchain as an emerging technology is featured with decentralized structure, transparent way of working, improved traceability and integration of cryptography based methods for extra security. Since the healthcare systems are required to be safe and fast as possible, blockchain integration is a viable choice. Supply chain management (SCM) of healthcare systems are concerned with the flow of information, product, service and finances throughout the stakeholders that are participating in the creation, distribution and utilization. The increased number of stakeholders on supply chains in healthcare industry arises security, privacy and transparency challenge that can be minimized with blockchain solutions. The aim of this study is to identify the outlying factors of blockchain integrated SCM systems in healthcare industry and provide a framework for further analysis.

In order to identify the outlying factors, a systematic literature review (SLR) is conducted. The results of the review presented fourteen factors that are determined as significant drivers for the subject. The factors identified are compatibility, complexity, perceived benefit, security, privacy, standardization, IT infrastructure, financial resources, human resources, competencies, organizational culture, stakeholder participation, collaboration, top management support, competitive pressure, government support and inter-organizational trust.

The research model is established with the identified factors according to Technology Organization Environment (TOE) framework. The reasoning behind the selection of TOE framework is to provide a holistic and structural model that is well accepted in the domain. This study provides insights and determines the outliers with a holistic framework on blockchain integrated supply chains in healthcare industry. Another contribution of this study is to raise awareness by presenting a comprehensive framework for business managers, customers and researchers on blockchain solutions in SCM systems.

Keywords: Blockchain Integration, Supply Chain Management, Healthcare Industry, TOE Framework

¹Address: Baskent University, Department of Technology and Knowledge Management, Ankara, Türkiye

²Address: Hacettepe University, Department of Computer Engineering, Ankara, Türkiye

*Corresponding author: baris@baskent.edu.tr

Classification of Temporomandibular Joint Sounds

Aras Selcuk^{*1}

Abstract The Temporomandibular joint (TMJ) is the joint which connects the jawbone to the skull which are located at each side of the skull. Temporomandibular joint Disorder (TMD) is generally defined as any problem arising from improper TMJ movement. TMD symptoms generally appear as pain in the jawbone and muscles which control the jaw movement. One of the diagnostic methods used by physicians is to listen to sounds produced by the joint during opening and closing of the jaw. In this research, previously collected TMJ sounds are used to diagnose TMD by using one-dimensional 1D convolutional neural networks (CNN), a subclass of deep learning algorithms. Results are then compared to the results of previously used two deep learning algorithms known as two-dimensional CNN, generally used for image processing, and LSTM network, generally used for time series analysis.

Keywords Temporomandibular joint Disorder, Sound Classification, Deep Learning, 1D CNN

¹Address: Selcuk University, Technology Faculty, Manisa, Turkey

*Corresponding author: aras@selcuk.edu.tr

Classification of Motor Imagery Signals Using Imaginary Coherence

Fatih Özat^{*1}, Ahmet A. Emel²

Abstract Electroencephalogram (EEG) motor imagery signals are widely used for the implementation of brain computer interfaces (BCI). Recently, functional connectivity measures have attracted attention as it can be used to capture statistical dependencies between EEG channels. However, functional connectivity during motor imagery tasks have not been fully explored. This study aims to use imaginary part of coherency or imaginary coherence as a functional connectivity metric for the classification of left hand/right hand motor imagery. To that end, multichannel EEG signals from 10 subjects were first decomposed into intrinsic mode functions (IMFs) using multivariate empirical mode decomposition and imaginary coherence values were calculated between same level IMFs across different EEG channels as a function of time and frequency. Statistical descriptors such as mean, standard deviation and variance were calculated for resulting connectivity functions for each channel combination as features for model training. Train-test split, leave-one-subject-out and inter-subject training schemes were used to train the models. With train-test split scheme, best accuracy was achieved with gradient boosting classifier (GBC) as 0.7. With inter-subject training, the average accuracy was obtained as 0.6 and maximum accuracy for a single subject as 0.7 with GBC. Finally, with leave-one-subject-out scheme, the average accuracy was 0.6 with maximum accuracy of 0.7 for a single subject using logistic regression model. Results show that while the performance of the models has variability across subjects, imaginary coherence can be used as a feature for distinguishing left hand/right hand motor imagery tasks.

Keywords Motor imagery, Electroencephalogram, Empirical mode decomposition, Functional connectivity, Imaginary coherence

¹**Address** Bogaçi University, Institute of Biomedical Engineering, Istanbul, Türkiye
İstanbul Kültür Teknik Üniversitesi, Elektrik Elektronik Fakültesi, İstanbul, Türkiye

²**Address** Bogaçi University, Institute of Biomedical Engineering, Istanbul, Türkiye

* **Corresponding Author** fatih.onat@boun.edu.tr

Experimental Measurement of the Mass Attenuation Coefficient of Monoatomic and Composite Materials

Uhal a Salma*¹, Kheli i achi ¹

Abstract Background Radiation shielding materials are carefully chosen for radiation exposure safety background decreasing in spectrometry measurement especially in the laboratory decreasing particle intensity and also to studying material attenuation proprieties etc Objective In this work we aim to evaluate the dependency or not of attenuation coefficient with several parameters including incident source beam energy and the chemical characteristics for mono atomic and composite target i.e density and effective atomic number and b comparing the experimental values of the massi ue attenuation coefficient with the theoretical Com data Methods The experimental values of the attenuation coefficient of five different types of samples were calculated for different gamma rays energies emitted from standard radioactive sources namely Europium 2 Cobalt 0 and Cesium 37 where the experimental setup was based on the transmission method The employed spectrometer is a 3 3 scintillator detector Besides the empirical results the Com data is directly used to extract the theoretical values of the massi ue attenuation coefficient of the studied samples Results The obtained results were in good agreement with the theoretical Com data The use of monoatomic and composite material allows for several results a high dependency on attenuationcoefficient with incident gamma energy b the linear attenuation decrease for high density values chemical composition and sample density Conclusion In this study a procedure for measurement of experimental combined with the theoretical Com data is followed The attenuation coefficient increase for low energy values a high fraction of gammas are attenuated for high density values The obtained results will be valuable for the estimation of massi ue attenuation coefficient density and effective atomic number if the data are correlated as a mathematical mapping problem i.e data extrapolation

Key r s Attenuation coefficient Com gamma radiation Transmission method

¹A rress Blida University Faculty of Sciences Department of Physics Laboratory of Theoretical Physics and Interaction of Radiations with Matter Blida Algeria

* rres i auth r boukhalfasalma gmail com

Abstract: The summary text should be written in 10 punto in Times New Roman between 200-300 words with a single line spacing. There will be no Turkish abstract in articles written only in English. It should not use Bold and italic spelling. The summary text should be written in 10 punto in Times New Roman between 200-300 words with a single line spacing. There will be no Turkish abstract in articles written only in English. It should not use Bold and italic spelling. The summary text should be written in 10 punto in Times New Roman between 200-300 words with a single line spacing. There will be no Turkish abstract in articles written only in English. It should not use Bold and italic spelling. The summary text should be written in 10 punto in Times New Roman between 200-300 words with a single line spacing. There will be no Turkish abstract in articles written only in English. It should not use Bold and italic spelling. The summary text should be written in 10 punto in Times New Roman between 200-300 words with a single line spacing. There will be no Turkish abstract in articles written only in English. It should not use Bold and italic spelling.

Abstract: The summary text should be written in 10 punto in Times New Roman between 200-300 words with a single line spacing. There will be no Turkish abstract in articles written only in English. It should not use Bold and italic spelling. The summary text should be written in 10 punto in Times New Roman between 200-300 words with a single line spacing. There will be no Turkish abstract in articles written only in English. It should not use Bold and italic spelling. The summary text should be written in 10 punto in Times New Roman between 200-300 words with a single line spacing. There will be no Turkish abstract in articles written only in English. It should not use Bold and italic spelling. The summary text should be written in 10 punto in Times New Roman between 200-300 words with a single line spacing. There will be no Turkish abstract in articles written only in English. It should not use Bold and italic spelling.

Abstract The summary text should be written in 10 punto in Times New Roman between 200-300 words with a single line spacing. There will be no Turkish abstract in articles written only in English. It should not use Bold and italic spelling. The summary text should be written in 10 punto in Times New Roman between 200-300 words with a single line spacing. There will be no Turkish abstract in articles written only in English. It should not use Bold and italic spelling. The summary text should be written in 10 punto in Times New Roman between 200-300 words with a single line spacing. There will be no Turkish abstract in articles written only in English. It should not use Bold and italic spelling. The summary text should be written in 10 punto in Times New Roman between 200-300 words with a single line spacing. There will be no Turkish abstract in articles written only in English. It should not use Bold and italic spelling. The summary text should be written in 10 punto in Times New Roman between 200-300 words with a single line spacing. There will be no Turkish abstract in articles written only in English. It should not use Bold and italic spelling. The summary text should be written in 10 punto in Times New Roman between 200-300 words with a single line spacing. There will be no Turkish abstract in articles written only in English. It should not use Bold and italic spelling.

Keywords 10 punto Times New Roman not italic between 4-6 words

¹**Address** Department of Thermal Engineering and Industrial Facilities, Opole University of Technology, 45-040 Opole, Poland

²**Address** Department of Civil Engineering - Architecture, University of Pavia, 27100 Pavia, Italy

³**Address** Seyman Demirel University, Engineering Faculty, Chemical Engineering Department, Isparta, Turkey

* **Corresponding author**: Boguniewicz, ablocka@p.edu.pl

Restoration of Gamma Spectrometry Data by Monte Carlo Simulation

Ummalqadiriyyah Salma^{*1}, Khelilouche Achiche¹

Abstract

Methods In this work we consist to combine GRAVEL unfolding package and Geant4 as Monte Carlo code for spectra unfolding and detector response function respectively without passing via more literature details the overlap problem is successfully applied for gamma spectrometry analysis It consists to restore the incident spectrums counted via calibrated gamma ray spectrometer The employed spectrometer was a ^{137}Cs iodine sodium scintillator detector with an energy resolution equal to 7% at ^{137}Cs peak To assume the convergence of the restored spectrum combined with the existing positive solution the original spectrum $T(E)$ a minimum value of σ^2 must be obtained by increasing the number of iteration For this reason and during the iteration procedure the algorithm runs the logarithms of σ values Therefore in each iteration previous solution is considered It should be noted that the number of iterations is not arbitrary In this work 10 000 iterations were made

Results For proposal application for non identical conditions i.e different gamma ray peaks the deconvoluted area is defined here by the real distribution of the coming signal to the instrument detector without the contributions of the other contributions e.g background radiation electronic noise escape peaks etc After restoring the incident spectrum the specific activities can easily be calculated where the restored area describes the real activity of the radionuclide without the contribution of other radionuclides

Conclusion The specific activities of natural radionuclides namely ^{238}U Uranium ^{232}Th Thorium and ^{40}K Potassium were determined via poor energy resolution gamma spectrometry technic The combination of the GRAVEL unfolding algorithm and Geant4 code is powerful solution for poor resolution detector

Keywords Gamma Spectrometry GRAVEL Monte Carlo Uranium Potassium Thorium

¹Address Blida University Faculty of Sciences Department of Physics Laboratory of Theoretical Physics and Interaction of Radiations with Matter Blida Algeria

* Corresponding author boukhalqadiri@gmail.com

te rati e e able er y S urces i the S A

ehebi S iu¹, Sami ashi¹, esa eseli¹, Fat al u¹, uha heri S iu¹

Abstract The demands of the global market for environmental protection have significantly increased the need for our country to follow the basic EU legislation for climate change renewable energy and simplified regulation on the implementation of policies according to the European directives for generation of electricity The challenge of this work is the adaptation of the current network with new generating capacities that come from alternative energy The integration of the advanced network increases the adaptability of the modern network and the functionali ation of effective generators with a reliable consumption system Part of this work is the research of future visions related to the optimi ation of user power and planned control with the mix of generating energy sources in the distribution of network The integration of the renewable energy network and the moderni ation of the SMART network is dedicated to being the bearer of the development and follow up of technological steps to the constant threats to sustainable development The ob ective of this work is the development of new economic frameworks that include services and the lowest costs for energy facilities related to the efficiency and effectiveness of technological users Simulative modulation improves the reliability of the energy transition with a range of the best services rather than focusing on the use of traditional fossil fuels

Key r s RES distribution network environment strategies innovation of technologies

¹A rres BT Higher Education Institution Faculty of Engineer of Energy alabria 0000
Pristina osovo

* rres i auth r sami gashi ubt uni net

Hygienic Surfaces and the Evolution of House Applications with Smart Materials: A Comprehensive Overview

Halit İsa^{*1}, Şahme Sari Kar²

Abstract This paper explores two revolutionary trends reshaping interior design and construction: hygienic surfaces and smart materials integration in house applications. With a growing focus on health, cleanliness, and sustainability, these innovative approaches have the potential to redefine living spaces, creating safer, more efficient, and adaptable environments for occupants. The first part examines hygienic surfaces, engineered materials, and coatings designed to resist dirt, grime, and microbial growth. They play a vital role in maintaining higher hygiene standards, especially in critical spaces like hospitals, clinics, and kitchens. Antimicrobial coatings containing silver ions or copper effectively inhibit bacteria and microorganisms, while non-porous tiles and laminates facilitate easy cleaning by preventing dirt adherence. Additionally, self-cleaning surfaces employing photocatalysis or hydrophobic properties ensure a more sterile environment by breaking down and repelling dirt and grime. The second part delves into smart materials integrated into house applications, capable of responding to external stimuli and adapting their properties accordingly. Smart windows, for example, adjust tint or transparency based on light conditions, regulating indoor temperature and reducing energy consumption. Self-healing materials extend the lifespan of household items by autonomously repairing minor damages or scratches. Shape-memory alloys offer efficient space utilization and customization in adaptive furniture and structures. Smart lighting systems adjust brightness and color temperature based on occupants' preferences, enhancing comfort and well-being. The integration of sensing materials embedded with advanced sensors enables real-time monitoring of temperature, humidity, and occupancy, facilitating better indoor environment control and energy management. The confluence of hygienic surfaces and smart materials presents a transformative opportunity for the evolution of house applications. Combining these technologies enables homes to foster healthier living environments, reducing infection risks and enhancing overall quality of life for residents. As technology continues to advance, further groundbreaking innovations are expected to redefine the way we design, build, and interact with our living spaces, offering unprecedented levels of safety, sustainability, and comfort.

Keywords: Hygienic Surfaces, Antimicrobial Coatings, Interior Design, Health, Indoor Environment

¹**Address:** Pamukkale University, Faculty of Architecture and Design, Department of Architecture, Denizli, Türkiye

²**Address:** Pamukkale University, Faculty of Technology, Department of Biomedical Engineering, Denizli, Türkiye

* **Corresponding Author:** hal@pau.edu.tr

The Impact of Electric Vehicles on the Environment, Energy Systems, and the Economy

Ahmed Al Sarra^{*1}, Fatih Altunali², Ahmet Kabul²

Abstract Energy efficiency is becoming more important for many equipment and devices that are used to provide people with comfort as conventional energy resources are depleting and environmental harm from their use is growing. Utilizing domestic and renewable energy sources has replaced energy efficiency as the fundamental policy of nations. Electric vehicles are now widely used, and many nations with environmental concerns have boosted their incentives, which may have significant environmental, energy, and economic repercussions. Countries have set a variety of goals in their energy policies for a more habitable environment and a reduction in their reliance on foreign energy sources, and steps are being taken in this regard. Countries promote the usage of electric cars while attempting to limit the environmental harm caused by transportation. This study discusses the effects of electric vehicles on the environment, energy systems, the economy, and the employment market. The widespread usage of electric vehicles has the potential to have a positive influence on the environment by lowering greenhouse gas emissions and enhancing air quality. Analysis of the effects of EVs on energy systems includes consideration of topics including the rise in electricity demand, grid integration, and charging infrastructure. The effects on energy distribution and consumption are also covered. Regarding the economy, the spread of electric vehicles has the potential to open up new job opportunities in the automotive industry. In this framework, topics including home production, employment expansion, and industry restructuring are considered. Finally, it should be underlined that policies and incentives are crucial to the spread of EVs. There are suggestions for effective policy changes, infrastructural upgrades, and international cooperation tactics. This report is a crucial resource for comprehending the difficulties and possibilities that businesses may encounter when they make the switch to electric vehicles. Electric vehicles can help nations move closer to having a sustainable transportation system. However, further analysis is needed, as well as changes to policy.

Keywords Electric vehicles, energy efficiency, environmental impact, sustainability

¹Ahmed Al Sarra, Ministry of higher education and scientific research, consultancy Department, Baghdad, IRA

²Ahmet Kabul, Isparta University of Applied Science, Faculty of Technology, Isparta, Turkey

* Corresponding author: ahmed.emad.4@gmail.com

Characteristics of Recycled Wood from Post-Consumer Window and Door Joinery

Anita Wróńska¹, Krzysztof Kalużny¹

Abstract Wooden doors and windows recycling plays a crucial role in promoting sustainability and reducing the environmental impact of the construction industry. Recycling these products allows for the efficient reuse of valuable wood resources, minimizing the need for fresh timber extraction and reducing waste, for example with the purpose of wood chips production for the particleboard industry. Using post-consumer wood from window and door joinery is often not fully utilized due to the variety of coatings and paints which are used on these materials. Due to the fact that the coatings on the wood need to be stripped away before this wood can be recycled, it can be expensive. There are several volatile compounds which are contained in varnishes and oils that are released when such wood is burned. Based on the characterization, we can determine how varnish, paint, or veneer influence the geometry of particles after industrial cutting. In order to characterize the recycled wood raw material, tests such as sieve analysis and fractional composition of the particles, water absorption, as well as Total Volatile Organic Compounds (TVOC) emission will be carried out. Based on the results of this study, a decision can be made about how to reuse raw wood most effectively. In addition to the environmental benefits, wooden doors and windows recycling also offers economic advantages. Recycling creates job opportunities in the collection, processing, and manufacturing sectors. It contributes to a circular economy model where materials are kept in use for as long as possible, reducing the need for resource extraction and supporting local industries.

Acceptance The presented study was completed within the activity of the Student Furniture Scientific Group of the Faculty of Wood Sciences and Furniture Technology, Lodz University of Technology.

Keywords recycling, upcycling, particleboard, post-consumer, window, circular economy

¹Address: Department of Technology and Entrepreneurship in Wood Industry, Institute of Wood Sciences and Furniture, Lodz University of Life Sciences, SGGW, Nowoursynowska Street 46, 91-424 Lodz, Poland

* Corresponding author: anita.wronka@sggw.edu.pl

**Application of post consumer waste materials
in liquid biofuels production**Agneta Sierota¹, Aleksandra Szafraniec²

Abstract The development of the economy involves an increasing demand for basic raw materials such as metal ores, wood fibre materials, etc. which have limited capacity or resources in the Earth's crust. Industrial development in the 20th and 21st centuries will be confronted with the need to switch to other raw materials, plastics, or to reuse a raw material after its useful life or waste material. The repeated use of biological raw material such as wood or its processing by products is associated with a decrease in the mechanical parameters of the raw material used in industry, an increase in the mineral impurities content and hindered processing of the raw material after a certain time, micronisation of the structural components of the biomass occurs. Therefore, such biomass should be removed from the production process, e.g. in furniture factories or paper mills, and used in another industry. The aim of this study was to use post consumer biomass in liquid biofuel, bioethanol, technology. For ethanol production, simple sugars are used, which are converted to ethanol and carbon dioxide in a biochemical process by yeasts or bacteria. In order to verify the efficiency of the process, the chemical composition of the post consumer biomass will be characterised to determine the content of sugars, lignin, hemicelluloses and associated substances. Enzymatic hydrolysis of the biomass will be carried out to verify the potential of the post consumer biomass as a feedstock for liquid biofuels.

Abstract This project was completed by the activity of the Chemical Food Technology Student Scientific Group of the Chemical Technology in Drewno. The part of the presented study was completed thanks to the activity of the Student Furniture Scientific Group of the Institute of Furniture Technology in Drewno.

Keywords bioethanol, woody biomass, post consumer material, hydrolysis, chemical composition

¹**Address** Faculty of Food Technology, Warsaw University of Life Sciences - SGGW, Warsaw, Poland

²**Address** Department of Food Science and Food Protection, Institute of Food Sciences and Furniture Technology, Warsaw University of Life Sciences - SGGW, Warsaw, Poland. ORCID: 0000-0002-34473-2

* **Corresponding author**: an.sadkowska@sggw.edu.pl

Smart City Development in Montenegro: A Collaborative Effort for Sustainable Urban Development

Shqipëri Ahmeti^{*1}, Veseljević¹

Abstract The Smart City Montenegro initiative a collaborative effort aiming to involve five international universities seeks to drive sustainable urban development in Montenegro's municipalities. By leveraging digital technology and interdisciplinary expertise the project aims to create a National Strategy for Smart and Sustainable Urban Development as well as Smart City Strategies for seven major municipalities in Montenegro. These strategies encompass various dimensions of urban life from sustainable living and efficient resource use to participatory governance and improved mobility. The initiative recognizes that Smart City development is complex and context specific necessitating customized solutions for each municipality. The project spans three distinct phases involving data collection stakeholder engagement and the formulation of comprehensive strategies. These strategies address both technological and non technological aspects with action plans devised to achieve tangible outcomes. The impact of the initiative is broad involving planning experts young professional employment international academic collaboration and expert guidance. Ultimately the goal is to transform these municipalities into interconnected smart cities fostering holistic development citizen well being and environmental sustainability. The project signifies a significant step toward addressing urbanization challenges and promoting a brighter more interconnected urban future in Montenegro. This conference paper tends to share a real life experience of a long term initiative for making cities of a society in transition smart sustainable and climate neutral. The paper adopts a deductive method to explore the conceptual framework of smart cities and sustainable development. It analyzes various dimensions and domains of smart urbanization considering the intricacies of contextual relevance. This analytical foundation is followed by an exploration of the cities and municipalities involved in the project shedding light on their unique profiles and challenges. Additionally the paper delves into specific suggestions and concrete projects proposed by the initiative's authors illustrating the tangible outcomes of the project's meticulous planning and execution.

Keywords Smart City Montenegro sustainable development digital technology interdisciplinary collaboration Smart City Strategies climate neutral cities

¹Address: Institution of Higher Education UBT College Montenegro

* Corresponding author: shqipri.ahmeti@ubt.edu.me

Analysis of the lithium recovery from spent Lithium Ion Batteries A Case Study

Małgorzata Boguniewicz^{1,*}, Mustafa Karabacı² and Mehmet Ural³

Abstract From the point of view of environmental protection the recovery of major components or valuable resources and the preservation of natural resources through the recycling of used LIBs is very desirable and its importance will grow in the future. To achieve future e-waste management policy goals efficient recycling systems based on metals recovery should be used more widely. In this work the review of the current status of recycling techniques and technologies concerning spent lithium ion batteries (LIBs) is presented. The most common treatment processes include pyrometallurgy, hydrometallurgy and biometallurgy. The single recycling processes were summarized and some examples of typical combined processes were described. The case study from Italy and Poland region shows that there is great potential for investors interested in recovering lithium and cobalt from spent lithium ion batteries (LIBs).

Keywords Lithium ion battery recycling, environmental protection, resource recovery, sustainable e-waste management, metal recycling technologies

¹**Address** Department of Thermal Engineering and Industrial Facilities, Faculty of Mechanical Engineering, Opole University of Technology, Pr. S. Kowalska 7, Street 4/7, Opole, Poland

²**Address** Seyman Demirel University, Engineering Faculty, Chemical Engineering Department, Isparta, Türkiye

³**Address** Department of Industrial Engineering, University of Salerno, 40-4 Fisciano, Italy

* **Corresponding author** boguniewicz@ablocka.poznan.pl

Estimation of health exposure to nitrates in drinking water a case study

Krzysztof Aza^{*1}, Zabela Imch²

Abstract Nitrates in water occur due to fertilization of fields in agriculture due to leaking septic tanks and in extreme cases due to dumping of waste with high concentrations of nitrates from factories or through municipal sewage. The presence of nitrates in water is harmful to human health. Studies conducted indicate the occurrence of a number of adverse symptoms in both animals and humans exposed to the consumption of water with elevated nitrate and nitrite content. Nitrates (V) are not toxic compounds. Their harmfulness is due to their oxidizing properties and ability to reduce to nitrate (III). They can cause oxidation of hemoglobin to methemoglobin, anemia, oxidation of vitamin A, the deficiency of which causes a number of dangerous disorders, impaired utilization of nutrients such as proteins and fats, and failure to absorb B vitamins. Nitrite poisoning is particularly dangerous for young children, mainly infants, as it can cause methemoglobinemia. Therefore, the WHO recommended nitrate (V) level is 50 mg/L. The article will present an estimation of health exposure to nitrate (V) delivered with water to consumers in a small distribution system exploiting aquifer groundwater resources. The average daily production of water in 2017-2022 varied from 10 m³ to 100 m³. The analysis of the dynamics of changes in the multiplicity of nitrate concentrations in water for years 2017-2023 shows a clear upward trend. According to the ongoing water quality monitoring, nitrate concentrations of 40 mg/L were recorded in April 2022 and 43 mg/L in December 2022. Another test performed in March 2022 showed nitrate concentrations close to the maximum allowable value in drinking water and was then 40 mg/L. In March 2022, more than 10% exceedance of the parametric value was recorded, the nitrate concentration was then 70 mg/L. The health risk of nitrates (V) included in tap water was assessed by comparing the acceptable daily intake (ADI) with the value of the estimated daily intake (EDI). Based on the results of conducted analyses, the following conclusions were drawn: the water in the analyzed system, despite the exceedance of parametric values, does not pose a potential health risk for adults; the calculated limiting safe concentration of nitrates in drinking water for adults is the level of 50 mg/L for the adopted ADI value of 3 mg/kg body weight per day and the weight of an adult of 70 kg. Taking into account the guidelines and recommendations of the WHO, which allows the temporary supply of water with a nitrate concentration of 100 mg/L, the water in the analyzed system can be used for the preparation of food for newborns and infants under 3 months of age. Nevertheless, information campaigns should be conducted among pregnant women and mothers of children under 3 years of age on the potential health risks of exposure to methemoglobinemia. This campaign should include a piece of information on the orders to use products with low nitrate and high antioxidant content in the diet. In the situation of nitrate concentrations in the water above 100 mg/L, a ban on the use of water for children's consumption should be implemented. And in the situation of the occurrence of contamination in the water at the level of the calculated limit, the safe concentration of nitrates (V) in drinking water for adults above 50 mg/L for a period of 10 days, absolutely ban on drinking water must be obligatory.

Keywords: drinking water, nitrates (V), health exposure, risk assessment

¹**Address:** Opole University of Technology, Faculty of Mechanical Engineering, Department of Thermal Engineering and Industrial Facilities, Mikolajczyka, Opole 42-27, Poland

²**Address:** Silesian University of Technology, Faculty of Energy and Environmental Engineering, Institute of Water and Wastewater Engineering, Konarskiego, Gliwice 44-100, Poland

* **Corresponding author:** klosok@pau.edu.pl

Extended Reality as a Visual Tool for Architectural Fabrication and Inspection

Farukcanunal

Abstract This study explores the transformative role of extended reality as an innovative visual tool within the processes of architectural fabrication and inspection. By seamlessly merging virtual and physical environments, extended reality offers architects, designers, and engineers an unprecedented level of visualization, interaction, and quality control throughout the architectural lifecycle. This study presents the potential of extended reality in architectural fabrication and inspection through case studies, technological explorations, and critical analysis. The integration of extended reality in fabrication processes aids in streamlining workflows, reducing errors, and optimizing material usage, ultimately leading to more efficient and sustainable construction practices. It enables real-time overlay of digital information onto physical structures, facilitating on-site comparisons between digital models and actual construction progress for architectural inspection. This real-time alignment enhances error detection, expedites issue resolution, and ensures adherence to design specifications, thereby elevating the overall construction quality. This study highlights the convergence of digital visualization and tangible craftsmanship and demonstrates how extended reality's immersive capabilities provide users with a comprehensive toolkit to push the boundaries of manufacturing, enhance collaboration, and increase the precision and excellence of the product. The digital transformation of architecture has blurred the boundaries between the physical and virtual realms, and the integration of extended reality in architectural fabrication and inspection processes signifies a paradigmatic shift in the field.

Keywords Extended reality, visual tool, architectural fabrication, architectural inspection

Address Yeditepe University, Faculty of Architecture, Department of Architecture, Istanbul, Turkey

Corresponding Author farukcanunal@yeditepe.edu.tr

An Assessment of Over Tourism Risk in Safranbolu, Turkey

Şirvanur Çelebi¹, Sırma Çelebi²

Abstract While tourism can be seen as a way to integrate historical sites with contemporary life, it has become increasingly clear that this seemingly innocent activity has negative effects, especially when it comes to historical sites that have turned into popular tourist attractions. Overtourism is a global serious threat to the conservation of the underlying values and Outstanding Universal Values of heritage sites. This worry has grown, particularly in light of the growing number of visitors and the uncontrolled tourism development. Safranbolu as a World Heritage Site since 2014 has been a popular tourist destination for decades thanks to its authentic architectural fabric and well-protected traditional Ottoman houses. As a matter of fact, the number of tourists visiting between 2000 and 2022 has increased almost 7 times, and Safranbolu is confronting an enduring continuous trend of tourism growth. This study aims to evaluate the over-tourism risk in Safranbolu, Turkey in the context of Butler's 2000 Tourism Area Life Cycle and Doxey's 1975 Irritation Index approaches. To do this, using qualitative and quantitative methods, the data obtained from secondary documents on tourism development, tourism statistics, and the results of the survey conducted with 200 participants in April 2022 are evaluated together. The findings demonstrate that tourism in Safranbolu is still in a development stage, and residents have mixed feelings about how they are affected. This research highlighted that there is a potential of overtourism, but that it has not yet turned into a significant issue.

Keywords Over Tourism, Heritage Historical Sites, Residents, Doxey, Butler

¹Address: Republic of Türkiye Ministry of Culture and Tourism, Istanbul, Türkiye

²Address: Yıldırım Technical University, Faculty of Architecture, Department of Urban Planning, Istanbul, Türkiye

*Corresponding author: nur.gundogdu@std.yildi.edu.tr

The Parameters of Conflict Resolution in the Digital Nomad Era in Universal Systems

Özhan Özlü*¹

Abstract Every year and at every age humans move. From one idea to another, from one house to another, from one school to another, from one job to another, from one city to another, from one country to another, from one culture to another. No time is the Digital Nomad era more true than today. Covid-19 caused the biggest mass movement and made every country, family, culture, and workplace rethink new parameters for how people live and work, causing an explosion in digital nomadism that creates digital, physical, and transitional conflicts all over the world, individually or socially, since World War II. Natural and artificial pressures like climate change and international crises are also huge emerging factors in the Digital Nomad era as people move to adapt to the changing ecological environment. In this paper, first, the main theme of conflict resolution emerges from the above-mentioned changing ecological environment. Secondly, divergent identities of four generations: Boomers, Gen X, Millennials, and Gen Z, and how these hard-wired systems of brains can affect, enhance, impair, and change their adaptation in this new era to ignite a world demanding sustainable solutions that shifts to implement lasting changes through unity is discussed. Finally, the individual and social behavioral types in the pre/post pandemic world are addressed through the Enneagram. As the era of the digital nomad is operating through cognitive, physical, and emotional transitions, the design and management logic of this emerging world is appearing with conflicts like precise and fully interconnected and in real time, asynchronous and synchronous. These conflicts are being addressed through the Enneagram to ignite and unite humans and organizations. On a generational basis, Baby Boomers, Gen X, Millennials, and now Gen Z are living different inputs to shape and reshape the world. They all have a different generational characteristic that can be explained with Enneagram strategies. Given the monumental post-pandemic paradigm shift of Covid-19, generational identity is a proven design and management parameter that can help individuals and organizations identify strengths and weaknesses and become more efficient and productive as mankind is forced to adapt under stress to new demands on health care, financial, industrial, construction, and government systems. Given this paradigm shift through the Enneagram strategies, identifying individual, organizational, and generational skills can show how to utilize divergence for a better future. The divergence within and between four generations will show three hard-wired syndromes: Flight, Freeze, and Fight, which compose the obstacles that can cause resistance to change, resistance to adapt, and resistance to evolve. As a result, the divergence can be woven together to reduce conflicts to figure out the most efficient solutions to global problems in the new emerging digital world.

Keywords Unity, Conflict Resolution, Design Management, Generations, Enneagram, Digital Nomadism

¹Address: Pamukkale Üniversitesi, Faculty of Architecture and Design, Denizli, Türkiye

*Corresponding author: dro.gutr@gmail.com

Port Development Trends Directly by Analytic Hierarchy Process

Deda Lović^{*1}

Abstract Ports are no longer the simple maritime services providers of the past. They are multimodal transport and logistics centres, focal points of leisure and tourism and hubs for sustainable industry and clean energy (ESPO 2022). They have a huge potential for job creation and investment. The European Commission has estimated that by 2030 between 10 000 and 20 000 new jobs can be created in ports (European Commission 2023). Pre-existing megatrends, generators of port development, are UNCTAD 2022 geopolitical, technological and environmental. In the recent technology in maritime report by the American Bureau of Shipping (ABS 2022), future maritime technologies are organised into three major categories or trends: digitalisation, AI, digital twins, autonomous operations, applied research, new materials, green ecosystems, blue economies, and clean energy transition. As well, Deloitte Global Port Advisory, in their Study published in 2020, recognised following key development trends in the port sector in the time horizon to 2030: Space productivity, Port infrastructure, Changes in supply and demand, More technological solutions, More cyber risk, Less focus on physical infrastructure investments, Shift from big, bigger, biggest to green, greener, greenest, Sustainability, etc. There are different important deadlines which ports have to take into account when creating development strategies/plans. For example, in line with the upcoming new Alternative Fuels Infrastructure Regulation, 2030 will be the deadline for having shore-side electricity infrastructure in place (ESPO 2023). The transition to sustainable ports, digital nodes, and energy hubs requires radical system-led changes based on new knowledge and innovation. All previously mentioned require extensive innovation and transformational capabilities in ports (Lind 2023). Realising a modal shift to more sustainable transport modes is one of the domains in which digitalisation can be an enabler, improving the integration of the freight transport system (European Environment Agency 2022). Acting in accordance with new trends/demands have to be followed by huge investments. On the <https://maritime-executive.com> is available information that, for example, The Biden Administration in USA announced an additional 4 billion in funding for new programs that are designed to support the electrification of US ports as well as to reduce emissions to air in the ports. If all mentioned is taken into consideration, it becomes clear how challenging is proper definition/selection of development priorities of a port. After a theoretical analysis of port development trends, in this paper, an approach to selecting port development priorities based on Analytic Hierarchy Process (AHP) method is proposed. Object of the research is Port of Bar, Montenegro. Selection of development priorities is done having as the base following four criteria: level of revenues/profit, level of productivity, contribution to safety/security in the port, contribution to environmental protection in the port. AHP Hierarchy framework used was a three-level model: level 0 - goal, level 1 - criterion, level 2 - choice.

Keywords: Port Development Trends, Analytic Hierarchy Process

¹Address: Deda Lović, Port of Bar, Obala 3, ul. 2, 85000 Bar, Montenegro

*Corresponding author: deda.lovic@gmail.com

Colorimetric Indicators for 3D Printing: A Study on Anthocyanin Sources in SLA Resin

Uğur Evvereyza Karabiyi¹, Karale Seva Kirici¹, Sevil Cikrikci Gidatarim^{*1}

Abstract In recent years 3D printing (3DP) has gained so much attention in different fields from biomedical to food applications. Since it enables us to fabricate complex geometries, manipulate surface area, or formulate personalized dosages, different printing techniques might be used for personalized, efficient, and economical productions. One of the examples from the food side could be the fabrication of colorimetric indicators. Printing pH-sensitive indicators at varying dimensions and shapes is possible depending on your demand. Stereolithography (SLA) is one of the printing techniques based on photopolymerization reaction using laser light and liquid photosensitive resin. Although commercial SLA resins are already available in the markets, they do not show any sensing or other kind of properties. Under the light of these findings, this study aims to add a colorimetric response functionality to regular SLA resin during environmental changes. For this purpose, different kinds of anthocyanin (ACN) sources (black carrot powder, red beet powder, red cabbage juice) were added to SLA resin (clear color) at varying ACN:SLA resin ratios (20:0, 0:0, 0:20) to examine their color intensity after printing. At this stage, they were printed only in single rectangular form (x0 x0 cm). Additionally, the ethanol:water ratio (20:0, 0:0, 0:20) was changed during sample preparation to check the solvent effect on the color. The results showed that the highest color intensity and stability were observed in the samples prepared by 2 w/w black carrot solution, 0:0 ethanol:water mixture combined with 0:0 ACN:SLA resin. This outcome is the starting point for designing anthocyanin-added SLA resin-based indicators. In this way, they could be used as a sensor in various food products to monitor food freshness. As a further step, they need to be investigated for pH sensitivity, changing their colors at different conditions, because environmental pH differs during food spoilage, and printed samples might be indicative of such changes by giving a color response.

Keywords: SLA resin, 3D printing, anthocyanins, indicator, color

¹Address: Onyia Food and Agriculture University, Faculty of Engineering and Architecture, Onyia, Türkiye

*Corresponding author: sevil.cikrikci@gidatarim.edu.tr

This study is licensed under a Creative Commons Attribution 4.0 International License. <https://creativecommons.org/licenses/by/4.0/>

Food Waste Management

Ivi Shaliyev*¹

Abstract Food engineering plays an important role in food production and processing. However, the food waste generated during these processes poses a major problem both environmentally and economically. This article addresses the importance of effectively managing food waste in the field of food engineering.

Sources of food waste vary from the consumer level to the production stage. This article examines the causes and formation processes of food waste in detail. It also addresses strategies to reduce food waste by designing and improving food production processes. Management of food waste is of great importance in terms of sustainability and environmental protection. This article discusses reducing the environmental impact of food waste through methods such as recycling, composting, and energy production. It also addresses the impacts of reducing food waste on food safety and economic efficiency.

This study emphasizes the importance of food waste management in the field of food engineering and indicates the necessity of focusing on this issue in terms of environmental sustainability, economic efficiency, and food safety. Food engineers play an important role in effectively managing food waste, and increasing work in this area could be a critical step for the future of the food industry.

Keywords Food waste, sustainability, utilization, recycling

¹Address: A.T.A. Food Safety Agency of the Republic of Azerbaijan

* Corresponding author: elvin.shaliyev@gmail.com

Analysis of parameters created by the On-Site Sewage Treatment Plants

Magdalena Smy¹, Aneta Zreba^{*2}

Abstract Domestic sewage treatment solutions such as septic tanks or on-site wastewater treatment plants are widely favoured by homeowners especially in areas where conventional sewage system connections are not feasible. This is especially relevant to rural areas characterised by dispersed settlements situated on hilly and mountainous terrains. The operation of on-site sewage treatment plants must ensure the preservation of the natural environment and the parameters must adhere to the legal standards. To assess the environmental impact, a specific on-site sewage treatment plant was selected for evaluation. Over the course of one year, parameters in treated effluents including total suspended solids, COD_{Cr} and BOD were closely monitored. The year-long monitoring process provided valuable insights into the plant's effectiveness in meeting environmental protection goals and complying with regulatory standards. The studies revealed that the tested on-site sewage treatment plants operated according to the manufacturer's specifications and met the requirements defined by the law. It can be concluded that despite testing several on-site sewage treatment devices, each of them operates differently. However, the most crucial aspect is that their operation is correct. The variations in the operation of domestic treatment plants stem from factors such as the quantity and quality of sewage directed to the treatment plant, as well as the adherence to proper usage rules by the system's users.

Keywords on-site sewage treatment plant, treated effluents, environment, parameters

¹Address: Opole University of Technology, Faculty of Mechanical Engineering, Opole, Poland

²Address: Opole University of Technology, Faculty of Mechanical Engineering, Opole, Poland

* Address: imw@orek.pole.edu.pl

Applications in the Field of Biotechnology

Kamila Sobiechowska^{1*}

Abstract In our rapidly developing technological world the concept of biotechnology has an important place. Biotechnology can be defined as a branch of science that aims to manipulate the genes, cells and biological processes of organisms by bringing together life sciences and technology. This discipline enables revolutionary innovations in many fields such as agriculture, medicine, food industry, energy production and environmental protection.

The basis of biotechnology is to understand the structure and functioning of genetic materials: DNA and RNA. Genetic science aims to discover the genes that determine the characteristics of organisms and to give new features to living things by manipulating the genes through this information.

For example, in the agricultural field, biotechnology aims to obtain more durable, productive and nutritious products by changing the genes of plants and animals. Thanks to biotechnology in the field of medicine, the diagnosis and treatment of many diseases have become more effective. mRNA vaccines during the COVID period can be given as an example of biotechnological development. Bioenergy is one of the most important contributions of biotechnology in the energy sector. Renewable energy resources such as biomass energy, biogas and biohydrogen are developed with biotechnology.

Despite all these positive aspects, advances in the field of biotechnology also raise ethical and social problems. Issues such as possible risks of genetic changes and confidentiality of genetic information are the subject of debate.

In this study, biotechnology studies on agriculture, medicine, food and environment were compiled and important benefits that will increase our ability to control the forces of nature were determined. However, the points where these powers should be used consciously and ethical rules should be taken into consideration are also stated.

Keywords Biotechnology, food, agriculture, medicine, environment, ethics

¹Address: Lodz University of Technology, Chemistry Faculty, Lodz, Poland

* Corresponding author: camilla.rivero@gmail.com



Influence of Sr doping on the microstructure, morphology and optical properties of ZnO thin films prepared by SILAR method

Nourelhouda Mokrani^{1,*}, Hetta Hachemi¹, Ezzamel Hachemi¹, Farhat Hachemi¹

Abstract The present study focused on the properties of Sr doped ZnO thin films using the successive ionic layer adsorption and reaction (SILAR) method. The X-ray diffraction results show that the ZnO and Sr doped ZnO samples exhibit hexagonal wurtzite structure having preferential growth along the (001) plane. The maximum crystallite size of 4 nm was observed for Sr doped ZnO 3 wt% sample. The SEM analysis revealed that the samples exhibit agglomerated grains and the EDX spectrum of the Sr doped ZnO 3 and 7wt% samples showed the presence of Zn, Sr and O elements. The UV-vis transmission spectrum of the Sr doped ZnO 7 wt% sample revealed that it has higher transmission in the UV region. Finally, Sr doping has a significant impact on the physical and chemical properties of SILAR deposited ZnO films.

Keywords Sr doped ZnO thin films, SILAR, XRD, UV-vis

¹Address: Physics Laboratory of Thin Layers and Applications, Biskra University, BP 4, RP Biskra 07000, Algeria

* Corresponding author: nourelhouda.mokrani@univ-biskra.dz

Computer Science and Informatics Survey and Future

Branislava Čučević¹

Abstract This paper presents a comprehensive review of the past, present and future of computer science and informatics. Computer science represents one of the most important technological advances in human history, and advances in this field have transformed and shaped the way we live on Earth. The foundations of computer science were built on mathematical logic and theories of computation. In the 19th and 20th centuries, computers started with mechanical devices and over time electronic computers were developed. During the Second World War, the first computers such as the ENIAC appeared. Then, with revolutionary advances in programming, personal computers and the software industry emerged. Today, computer science is in every aspect of our lives with technologies such as smartphones, laptops, cloud computing and data centers. The internet has revolutionized communication and information flow between people. Areas such as Big Data analytics, artificial intelligence and machine learning have had a huge impact on business, medicine, transportation and many other sectors. The future of computer science and computing looks very exciting. Technologies such as artificial intelligence, autonomous vehicles, the Internet of Things (IoT), quantum computing, etc. will cause major changes in the coming years. Artificial intelligence will enable the development of systems with human-like thinking abilities, while IoT will make our lives smarter and more efficient with increased communication between objects. Quantum computers, on the other hand, have great potential to solve problems of complexity that traditional computers cannot. In conclusion, the field of computer science and informatics is rapidly evolving and has a profound impact on our world. This journey from the past to the present will lead to even more exciting technologies and innovations in the future. Keeping abreast of changes in this field and understanding how to use these technologies is an important requirement for individuals and societies.

Keywords Computer Science, History of Informatics, Technology Development, Artificial Intelligence, Data Analytics, Internet of Things, Future Technologies

¹Address: Priren University, Faculty of Computer Science, Priren, Kosovo

*Corresponding author: besaberkant@gmail.com

Effects of computer science and informatics on the education system

A i aš*¹

Abstract In the era of digital transformation computer science and informatics has become an important element in the field of education. Technological devices and the internet, which have become an integral part of students' daily lives, should be integrated into the educational process. Computer science and informatics help students understand and use these technologies effectively. Interactive educational tools make students more interested in the lessons. This contributes to making learning processes more effective. Computer science and informatics education provides students with important digital skills. These skills are of great importance not only in education but also in the business world of the future. Training educators in computer science and informatics contributes to the effective use of this field in classrooms. School administrators should also be informed about updating the technological infrastructure and using resources effectively. Distance education has become increasingly important, especially due to global events. Computer science and informatics help in the successful implementation of such educational methods. Students who master technology can compete in the workforce of the future. Computer science and informatics education prepares students for this and increases their ability to adapt to new technologies. As a result, computer science and informatics in education improves student achievement, makes teachers' jobs easier, and helps build the skills needed for the future workforce. In the era of digital transformation, these fields should become a fundamental part of the education system.

Key words Educational Technologies, Computer Science Education, Informatics Education, Digital Skills, Student Achievement, Interactive Education, Future Workforce

¹**Address** Pri ren University, Faculty of Computer Science, Pri ren, osovo

* **Corresponding author** akifgas@hotmail.com

Human Machine Collaboration Systems in Mechanical Engineering

Abbas Hasav^{*1}

Abstract Mechanical engineering plays an important role in a wide range of areas from industrial processes to product design. However, the automation of traditional machines and the interaction of people with machines are undergoing significant change with developing technology. This article discusses a new paradigm in mechanical engineering, highlighting the importance and application areas of human-machine collaboration systems.

The article begins by introducing the basic concepts and components of human-machine collaboration systems. These systems enable people to collaborate with machines to create more efficient and flexible production processes. Technologies such as collaborative robots, smart manufacturing cells, and unmanned aerial vehicles have great potential in industrial applications. The design and control of human-machine collaboration systems are of great importance in terms of safety, ergonomics, and human factors. The article examines key components such as interfaces, control systems, and learning algorithms used to optimize the interaction of humans with machines. Mechanical engineers play an important role in this new paradigm. Integration of human-machine collaboration systems in design, production, and process improvement helps create more competitive and flexible businesses.

In conclusion, this article encourages mechanical engineers to be interested in human-machine collaboration systems. These systems will play an important role in the future of the industry and offer great potential to increase productivity, reduce error rates, and improve occupational safety.

Keywords Mechanical engineering, collaboration, learning algorithms

¹Address: Amelioration and Water Farm Open Joint Stock Company, A. Erbai an

* Corresponding author: mirtelekom2@gmail.com

Disaster Management Strategies

Faruk Boaxhi¹*

Abstract Disaster management represents a very important interdisciplinary field that studies the effects of natural disasters on people's quality of life and environmental sustainability and develops strategies to reduce or manage these effects

The study examines disaster management strategies used to increase the resilience of infrastructure water resources waste management and energy systems in regions where natural disasters are common Disaster management and environmental engineering play a critical role in pre disaster preparedness response during disaster and post disaster recovery The study also considers the impact of disasters on environmental factors such as environmental pollution waste management and water supply Evaluates the short and long term effects of disasters on the environment and the reflections of these effects on environmental engineering practice

Forests play an important role in mitigating the effects of natural disasters Forest management aims to use and protect forests in a sustainable manner Forests can increase ecosystem resilience by preserving biodiversity This can speed up the natural recovery process after a disaster Environmental and forest management plays a critical role in minimizing the effects of natural disasters and protecting natural resources Bringing these two fields together is an important step towards the goal of building a safer and more sustainable world for future generations This article reveals the relationship between the common working points of these two fields and sustainability

Keywords Natural disasters forests water air engineering strategies

¹**Address** University of Priren Forestry and Environment Faculty Rruga e Shkronave nr 20000 Priren osovo

* **Corresponding author** faruk.boaxhi@uni-priren.com

Biomass energy production efficiency

Uroš Krtić¹

Abstract Today's energy needs must be compatible with environmental protection and sustainability goals. Biomass energy stands out as an energy source that meets these needs and minimizes environmental impacts. Because biomass fuels are considered a part of the carbon cycle, plants produce oxygen by taking carbon dioxide from the atmosphere during photosynthesis. Plant materials used in biomass energy production release this carbon back into the atmosphere when converted into energy. This makes the circulation of carbon sustainable.

Efficiency is critical for the effective use of biomass energy. Technological advances in recent years have made biomass conversion processes more effective. For example, anaerobic digestion techniques for biogas production and high efficiency reactors developed for thermal conversion have increased biomass productivity. Biomass conversion processes can be carried out by thermal, biochemical, and biological methods. The efficiency of these processes is increased and energy output is maximized. In particular, methods such as biomass gasification and pyrolysis have significantly increased biomass productivity.

Biomass energy production also plays an important role in waste management. Biomass resources such as agricultural waste and wood residues are evaluated correctly and create a solution in waste management. Additionally, afforestation projects for biomass energy production are critical to maintain the balance of ecosystems.

Biomass efficiency is an important step on the path to a sustainable future. Biomass efficiency and green energy play a critical role in reducing the environmental impact of fossil fuels and building a sustainable future. Thanks to technological advances and scientific research, biomass energy is becoming more effective and efficient day by day. In this study, energy production methods using efficient methods from forest industry waste in parallel with the developing technology are discussed.

Keywords Biomass, green energy, sustainability, Efficiency

¹**Address** University of Montenegro, Faculty of Life and Environmental Sciences, Ruga e Škronave nr. 20000, Prirenje, Montenegro

* **Corresponding author** yllikortici@uni-priren.com

Food Safety and Microbiology Management

Kamila Sibińska

Abstract Food safety covers the measures taken to ensure that individuals living all over the world have access to healthy and safe foods. An integral part of this process is microbiology management. Microbiology is a critical discipline for improving food safety by studying the potential hazards that microorganisms (bacteria, viruses, fungi) can cause in foods.

Food safety is a comprehensive field that investigates how microorganisms, toxins, and other contaminants that can harm the health of consumers can be controlled in food production and processing processes. The article discusses the challenges faced by food engineers in food safety and microbiology and the strategies they can use to overcome these challenges. Microbiological contamination poses a major threat to food safety. This article examines how the design and management of food processing processes, hygiene practices, microbiological testing methods, and food safety management systems can be improved. With the rapidly growing world population, the demand for food production is also increasing. Therefore, microbiology management and food safety are increasingly important. With advancing technology and research, more effective food safety strategies will be developed, and stronger foundations will be laid for future food production.

In conclusion, this study addresses the food industry's duty to protect consumer health and ensure the safety of food products by emphasizing the critical importance of food safety and microbiology management. In this study, the relationship between the correct management of microorganisms and safe production in the food industry is questioned. In this way, healthier food consumption and safe nutrition can be ensured for future generations.

Keywords: Microbiology, food, sustainable production, food safety

¹Address: Lodz University of Technology, Chemistry Faculty, Lodz, Poland

* Corresponding author: camilla.rivero@gmail.com



Technology for Sustainable and Universal Access to Water Resources

Alma Mater University^{*1}

Abstract Clean water is a basic requirement for human survival and healthy living and technology is an important tool in meeting this requirement. Water treatment systems are a fundamental element to transform contaminated water into clean water. Advanced treatment technologies ensure that water is free of contaminants and made potable. Smart water distribution systems and monitoring technologies ensure efficient management of water resources and reduce water leakages. Technology for sustainable use of water resources helps us better understand the water cycle and effectively reuse water. Technology plays an important role in preparing for emergencies such as water crises or natural disasters. Ensuring the security of water supply and treatment equipment is critical. For people living in areas far from water sources, portable water purifiers increase access to clean water and reduce health problems. Ultimately, access to clean water is a fundamental right for people to survive and live healthy lives. Technology is an important tool for protecting, purifying and distributing water resources and plays a critical role in tackling the water crisis. Investing in technological innovation for sustainable and universal access to water resources is vital to preserve clean water resources for future generations.

Keywords Clean Water, Water Treatment Technologies, Sustainable Water Resources, Water Crisis, Universal Access

¹ Alma Mater University, Faculty of Agriculture, Open Joint Stock Company "Agricultural University of Montenegro"

* Corresponding author: elik000@hotmail.com



Freight Trip Generation at Logistical Sites

Gurkan Gunay^{*1}, Mehmet İlhan², İbrahim Aşar³

Abstract It is known that freight transportation planning differs a lot from passenger transportation planning. Trip generation is the first step of transportation planning, and there are significant differences in passenger and freight trip generation mechanisms. In freight transportation, trip generation patterns of freight vehicles differ across various logistical site types. This study aims to develop freight trip generation models for trucks and vans in different logistical site types. In order to serve this goal, two specific objectives are pursued: First, to identify similarities and create homogeneous logistical site type groups based on freight trip generation patterns of vans and trucks using Analysis of Covariance (ANCOVA). Second, to develop specific regression models for freight trip generation patterns of these groups. It aims to understand whether a single regression model can examine a group. For this, the market segmentation method is used. However, this paper investigates freight trip generation of only one specific homogeneous logistical site type group, the one with the highest number of truck and van trips. The data used in this study is from the Aegean Logistics Master Plan in Turkey. The results indicate that homogeneous logistical site type groups can be created using ANCOVA. Further, according to the result of market segmentation analysis, these groups' trip generation behavior can be explained using a single regression equation.

Keywords Freight trip generation, truck, van, ANCOVA, market segmentation

¹A. Gunay, Istanbul Bilgi University, Faculty of Engineering and Natural Sciences, Department of Civil Engineering, Kağıtçıbaşı Cd. No: 23340, Eyupsultan, Istanbul, Turkey

^{2,3}A. İlhan, Bogaçi University, Faculty of Engineering, Department of Civil Engineering, 34342 Bebek, Istanbul, Turkey

* Corresponding author: gurkan.gunay@bilgi.edu.tr

Chemical Waste Reduction and Recycling Strategies

Małgorzata Kłosa^{*1}, Aleksandra Uściągalska¹, Mustafa Karabıyıcı²

Abstract The chemical industry produces large amounts of waste around the world and managing this waste can have negative impacts on the environment. This article highlights the importance of chemical waste reduction and recycling strategies. Chemical waste management plays a critical role in achieving sustainability goals.

The study addresses strategies to reduce chemical waste through source reduction, recycling, and reuse. Waste reduction involves changes to chemical processes and the design of products. This minimizes environmental impacts by reducing waste generation at the source. Recycling means reprocessing and gaining value from chemical waste. This strategy encourages recycling of waste into resources and reduces depletion of natural resources. The study provides information on the effectiveness and economic benefits of recycling processes. Chemical waste management is closely related to legal regulations, industry standards, and environmental policies. Therefore, the study highlights the importance of compliance with appropriate regulations for chemical industry enterprises.

In conclusion, this study addresses the environmental and economic benefits of chemical waste reduction and recycling strategies. Chemical engineers can contribute to the development of environmentally friendly and sustainable production processes by adopting waste management strategies. Zero waste processes, which are the most effective method for reducing waste, are discussed in the study. In addition, theoretical and field information has been provided to help understand that these strategies are of critical importance in achieving long-term sustainability goals for businesses and societies.

Keywords Chemical industry, waste management, zero emission, waste reduction

¹**Address** Department of Thermal Engineering and Industrial Facilities, Opole University of Technology, 45-040 Opole, Poland

²**Address** Seyman Demirel University, Engineering Faculty, Chemical Engineering Department, Isparta, Türkiye

* **Corresponding author** | klosok@pau.edu.pl

Design and Optimization of Low Voltage Induction Motor for Standalone PV Systems by FEM

Mustafa Tumbek*¹, Enagnon Appolinaire Dantondji²

Abstract: Photovoltaic (PV) cells were in widespread production by the end of the 1950s, and by the end of the decade were primarily used to power satellites in orbit around the earth. In the following years, the development in the manufacturing and the increase in the efficiency of the PV modules helped to reduce the costs and give opportunities for many remote applications that require low power. The aim of the study is to improve the performance of the induction motor for off-grid PV systems, which are often used in remote locations where grid connection is not feasible. By optimizing the shape of the motor's slots, the researchers aim to increase the motor's torque and efficiency, thereby improving the overall performance of the PV system. The use of finite element method (FEM) allows a detailed analysis of the motor's electromagnetic properties, enabling the design to be fine-tuned for maximum performance. This approach is particularly important for off-grid PV systems, where efficiency and reliability are critical to providing consistent power to remote applications. Overall, this study highlights the ongoing efforts to improve the performance of off-grid PV systems, which play an important role in providing clean energy to off-grid locations. The study aims to contribute to the further development of renewable energy technologies by focusing on induction motor design.

Keywords: Shape Optimization, Induction Motor Design, Low Voltage Motor Design, PV systems.

¹**Address:** Pamukkale University, Faculty of Engineering, Denizli/Turkiye

²**Address:** Paris-Saclay University, Faculty of Engineering and Systems Sciences, Paris / France

***Corresponding author:** mustafatumbek@pau.edu.tr

Sustainable innovation management in water and wastewater utilities

Anna Machnik-Szymańska¹, Iwona Szymańska²

Abstract Due to contemporary trends in the area of environmental protection social and economic development the issue of sustainable innovation management is becoming more and more popular among researchers and business managers. Activities in this area are particularly relevant to water and wastewater companies because of water which as a valuable and indispensable resource plays a particular role in social economic and environmental development. It is therefore necessary not only to manage its resources responsibly but also to protect it from pollution. To ensure this it is important to sustainably manage innovations implement eco innovations and measure their impact on the environment society and the economy. The innovative activities of enterprises are important not only for improving the competitiveness of the economy but also for reducing the negative impact on the environment and improving the quality of human life. The purpose of the article is to identify the role of innovation management in sustainable development in water and wastewater enterprises in Poland. In order to achieve the formulated objective literature research documentary research and the case study method of a purposefully selected company operating in the water and sewage sector in Poland were used. The example of the company under study shows its activity for sustainable management translating into environmental social and economic effects.

Keywords sustainable management innovation management eco innovation water and wastewater companies

¹Anna Szymańska Silesian University of Technology Faculty of Organization and Management Lublin Poland

²Iwona Szymańska Silesian University of Technology Faculty of Organization and Management Lublin Poland

* Corresponding author: iwona.machnik-slojka@polsl.pl

1. INTRODUCTION

Sustainable innovation management is an important issue increasingly being addressed by both researchers and practitioners. Schiederig et al. (2022) Indeed due to contemporary challenges sustainability has become a fundamental element of enterprise innovation strategies. Berkhout (2014) Enterprises are even forced to target sustainable innovation management using dynamic innovation capabilities. Dynamic innovation capabilities are necessary to effectively and efficiently implement innovations including eco innovations or sustainable development innovations that affect social economic and environmental development.

Innovation activities in the area of sustainable management are particularly important for water and wastewater companies. This is important because of the role these enterprises play in environmental social and economic development. These enterprises should responsibly manage water resources and protect them from pollution which is the basis for proper water management and the development of various ecosystems. GUS (2022) Rational efficient and sustainable water management ensuring access to water for the entire population is one of the fundamental tasks of any state. In this a large role at the regional and local level is played precisely by water and wastewater companies which are an important part of the ecosystem.

It may be helpful for these enterprises to sustainably managing innovation and targeting the creation and implementation of so called eco innovations which can help improve people's quality of life the competitiveness of the economy as well as reduce the negative impact on the environment.

Identifying the role of innovation management in the sustainable development of water and wastewater utilities in Poland is the purpose of the article.

2 A A A HO

In order to realize the formulated objective the research methodology was adapted which included

- theoretical cognitive research
- documentary research
- qualitative research using a case study

Theory cognitive research focused on a literature review of the role and importance of sustainable innovation management in companies and related eco innovation

Qualitative research was carried out using the case study method of a water and sewerage company purposely selected for the study operating Silesian province in Poland. The research included an interview with the management of the studied enterprise on the topic of sustainable innovation management

The research was complemented by desk research focusing on strategic documents, reports on innovation management, implementation of innovations in water and sewage enterprises and documents of the studied water and sewage enterprise

3 H SS A O A OF S S A A O A O A A O A S

Due to the growing importance of the concept of sustainability in the aspect of innovation management, some authors focus on the relationship between these constructs, e.g. Cillo et al. (2020). Many articles are devoted to this issue, but few authors focus on explaining the construct of sustainable innovation management. In attempting to define and understand sustainable innovation management, it is necessary to start from the definition of innovation management, where many authors refer to the basic functions of management. This approach is also taken in the Oslo Manual (2005). According to this Manual, innovation management is defined as *all systematically carried out activities of planning, management and control of internal and external resources for innovation* (Oslo Manual, 2005). Sustainable innovation management can therefore refer to these functions with a direction towards sustainability. In sustainable innovation management, it is worth emphasizing the importance of proper management by companies of both internal and external relationships (Berkhout, F., 2004). This is because it has a significant impact on the effective management of innovation processes, which increases the chances of success and competitiveness of these companies. With regard to managing sustainable innovation, Aagaard (2005) points to three key elements: a way of managing and measuring that ensures a higher level of ethical, social and environmentally friendly approaches; targeting the results of innovation management processes towards sustainable innovation; and ensuring effective and efficient external cooperation within the innovation management process (Aagaard, 2005). Forming good relationships with different stakeholder groups is related to the concept of CSR, which plays an important role in the context of sustainable management (Lein, 2005). This concept emphasizes ethical behavior towards one's stakeholders (Usman, Amran, 2005). Such conduct increases the chances of success and raising competitive advantage (Dluhoš, 2002; Ue, Lu, 2002; R. Griffin, 2003). Griffin (2003) points out that CSR is an organization's responsibilities to strengthen and protect the community. The ISO 26000 definition of CSR emphasizes an organization's responsibility to take action toward the environment and society based on ethical behavior toward stakeholders to achieve sustainable development (ISO 26000, 2006).

Contemporary innovation management, conditioned by a turbulent environment, requires the effective use of dynamic innovation capabilities (Bessant, Philips, 2003). They are essential to the management of innovation processes in enterprises (Cheng, Chen, 2003). Dynamic capabilities relate to the capacity to integrate and reconfigure different capabilities in response to the rapid pace of change (Teece et al., 1997). Thus, in sustainable innovation management, it is important to use different capabilities to manage innovation processes. A high level of dynamic innovation capabilities related to eco innovation research and internationalization, among others, is essential for sustainable innovation management in companies (Chakrabarty, Gang, 2002). In order to effectively implement innovation, companies should target the effective use of dynamic innovation capabilities.

This is because sustainable innovation management involves the creation and implementation of innovations, particularly sustainable innovations or eco innovations. Sustainable innovation can be understood as innovation that affects social, environmental and economic outcomes in the area of sustainable development (Boons et al., 2003).

In the field of sustainable innovation management, eco innovation plays an important role, which is of great importance for achieving the goals of the European Green Deal through better use of resources, reduction of negative environmental impact and positive social and economic impact (<https://green-business.ec.europa.eu/eco-innovation/en>). Eco

innovation also aims to support a closed loop industrial transformation <https://green.business.ec.europa.eu/eco-innovation/en>

The approach adopted in the article considers the relationship between the sustainable management of innovation, eco innovation and the effects achieved, see Figure 1

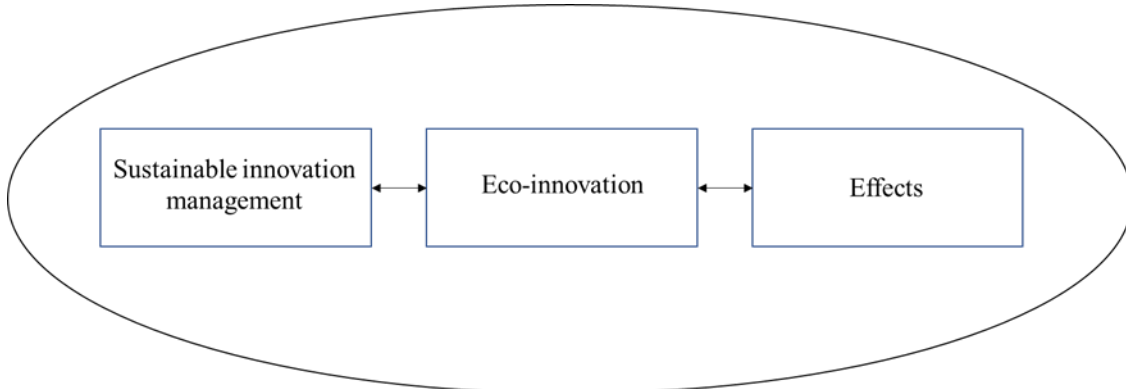


Figure 1 Relationship between sustainable innovation management, eco innovation and impact

At the level of EU member states, the eco innovation index is measured, which takes into account 2 indicators. Depending on the results obtained, individual countries are included in one of three groups: eco innovation leaders group, average Eco innovation performers group, eco innovation catching up group. The performance of individual countries according to the Eco Innovation Index 2022 for 2021 is shown in Figure 2.

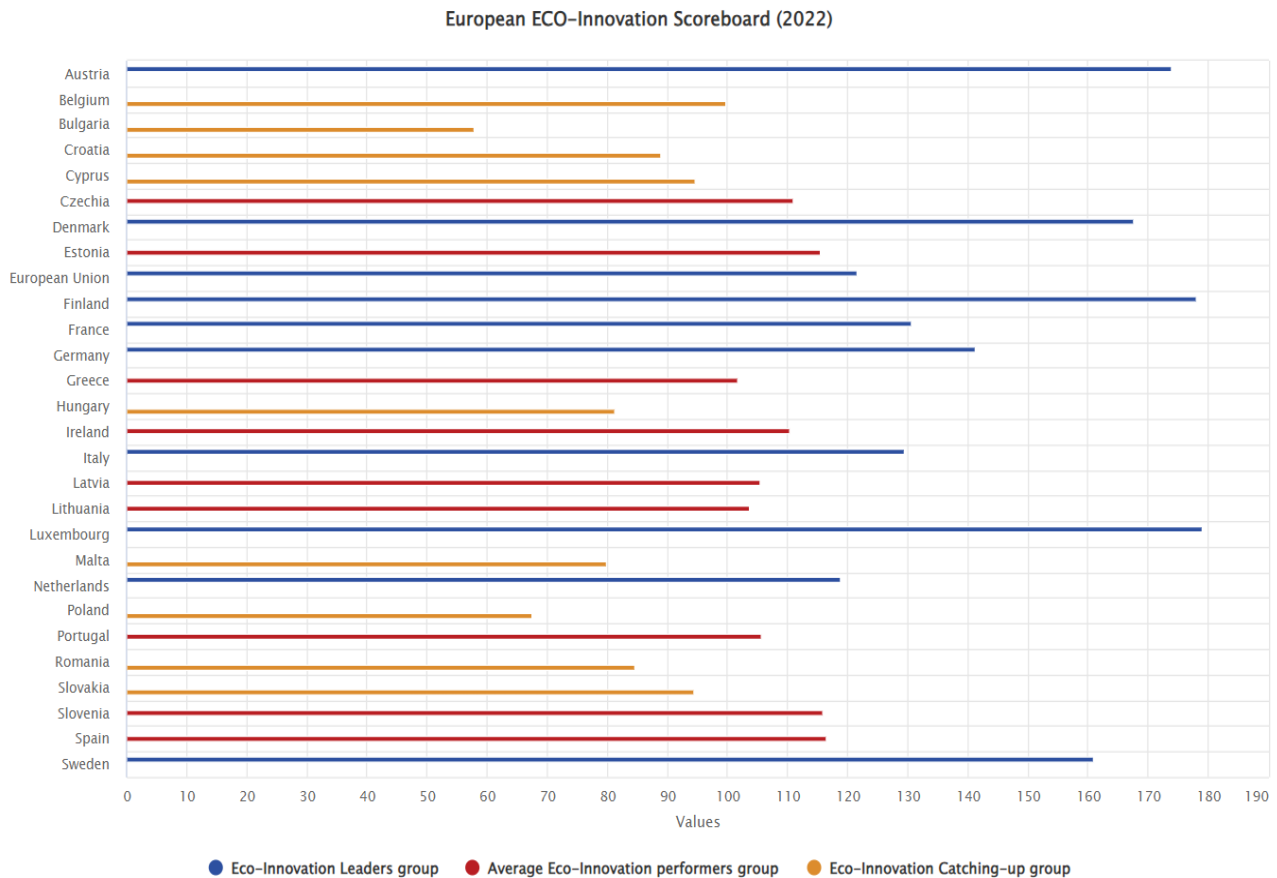


Figure 2 The Eco Innovation Index 2022

Read Eco Innovation at the heart of European policies, European Commission <https://green.business.ec.europa.eu/eco-innovation/en>, accessed 2 May 2023

According to The Eco Innovation Index 2022 collecting data from EU member states and beyond countries with the highest Eco innovation indexes include Luxembourg 7.02 Finland 7.0 Austria 7.3 Denmark 7.4 Sweden 7.0 <https://greenbusiness.ec.europa.eu/eco-innovation/en>. The indicator for the European Union is 7.247 Poland on the other hand ranks below the EU average with an indicator of 7.37 <https://greenbusiness.ec.europa.eu/eco-innovation/en>. As relatively strong points of Poland can be considered social behavior water productivity scientific publications while as weak points especially those related to eco innovation activities the number of ISO 400 certificates and patents related to eco innovation asi.ska.gov.pl 2022

O S A FF S OF S S A A O A O A A A A
S A S S O A AS S

Sustainable innovation management for water and wastewater enterprises given their role and mission to society is particularly important. Surveys conducted in Poland on the innovative activities of enterprises show that in 2020-2022 among enterprises classified as manufacturing in the Sewage Collection and Treatment Sewerage division there were 27% of innovative enterprises i.e. those that introduced at least one innovation in the period under consideration (GUS 2022). On the other hand, in the section water collection, treatment and supply innovative enterprises accounted for 22.4%. Innovation activities of enterprises in the years 2020-2022. Statistical analyses (GUS, arsaw.scein.gov.pl 2022).

Sustainable innovation management the implementation of eco innovation in enterprises based on accepted standards should contribute according to the formulated objectives to the achievement of sustainable development goals and translate into expected effects. According to the Oslo Manual 2005 effects that have an impact on society, the environment or the economy should result from the formulated goals in the area of innovation and be related, for example, to reducing the negative impact of activities on the environment, achieving benefits for the environment or society through improved safety and health (Oslo Manual 2005, 20).

In order to identify the effects resulting from sustainable innovation management activities of the water and sewerage company purposely selected for the study in Poland a qualitative research was conducted. As part of this research management was interviewed and desk research was conducted. The analyzed enterprise is engaged in water and wastewater management at the local level in the Silesian Voivodeship. One of the company's priorities is an environmental policy focused on the protection of natural resources, monitoring of environmental impact, sustainable development. In this regard, the company is ISO 4001 certified, which is the standard in the area of environmental management. The company is also focused on improving the efficiency of energy use, developing an energy management system with ISO 50001 Energy Management System certification. The company is also certified as an integrated management system in accordance with ISO 9001.

Based on the qualitative research carried out, effects affecting sustainability resulting from the activities of the studied water and sewerage company operating in the Silesian province in Poland were identified. The identified effects in the social, environmental and economic areas are shown in Table 1.

Table 1 Identified effects in the social, environmental and economic areas

Area	Effects
Social	increase the environmental awareness of the company's employees improved relations with stakeholders improvement of working conditions increase in pro-environmental behavior improving environmental conditions of the local community improvement of the company's image
Environmental	lower energy consumption at various stages of the process, water supply and wastewater treatment better waste management reduction in consumption of raw materials/resources reduction of pollution
Economic	cost reduction through greater energy savings lower costs due to better management of resources, raw materials savings resulting from more efficient waste management savings in operating costs

Source: own study

The analysed company through the implementation of a modern pro environmental policy improvement of management standards tries to reduce the negative impact on the environment in a systematic and continuous manner building lasting and positive relations with various groups of external stakeholders

The company is also focused on implementing pro environmental innovations in particular to improve energy efficiency water treatment processes

S S O A O S O S

In view of the growing global pressure to protect the environment and offset negative environmental impacts an increasingly conscious orientation of companies towards sustainable management has become evident over the past few years This is increasingly associated with the creation of enterprise innovation strategies focused on the creation and implementation of eco innovations for stakeholder value creation

Sustainable innovation management for water and wastewater utilities due to their role and mission to society is particularly important Today's challenges and global conditions are forcing companies to apply new methods and mechanisms for managing innovation focused on sustainability This increasingly requires a holistic approach to innovation management that makes effective use of dynamic innovation capabilities

The example of the analysed water and sewage company located in Poland indicates that aspects of sustainable innovation management are important to the company The company takes a number of measures focused on sustainable and responsible management As the results of the research conducted at this company show sustainable management translates into not only economic but also environmental and social effects

Given the limitations of research focusing on a single case study further research directions could take into account the more cross sectional nature of quantitative research

ethics committee Approval
 N A

peer review
 Externally peer reviewed

Author contributions
 Conceptualization M S E P Investigation M S E P Material and Methodology M S E P Supervision M S E P Visualization M S E P Writing Original Draft M S E P Writing review Editing M S E P Other All authors have read and agreed to the published version of manuscript

Conflict of interest
 The authors have no conflicts of interest to declare

Financial support
 The authors declared that this study has received no financial support

F S

Aagaard A 20 Managing Sustainable Innovation in Altenburger R Eds Innovation Management and Corporate Social Responsibility CSR Sustainability Ethics Governance Springer Cham
<https://doi.org/10.1007/978-3-319-32322-2>

Berkhout F 2014 Sustainable innovation management in Dodgson M Gann D M Phillips N Eds The Oxford Handbook of Innovation Management Oxford University Press

Bessant Phillips 2013 Innovation management and dynamic capability in Harland C Nassimbeni G Schneller E Eds The SAGE handbook of strategic supply management London Sage Publications Ltd pp 33-37

Boons F Montalvo C Guistagner M 2013 Sustainable innovation business models and economic performance An overview Journal of Cleaner Production 4 pp

- Chakrabarty S, Sang L. (2022) The Long Term Sustenance of Sustainability Practices in MNCs: A Dynamic Capabilities Perspective of the Role of R & D and Internationalization. *Journal of Business Ethics*. 20 pp. 2027. <https://doi.org/10.1007/s10551-022-4223-2>
- Cheng C C, Chen S. (2023) Breakthrough innovation: the roles of dynamic innovation capabilities and open innovation activities. *Journal of Business Industrial Marketing*. 20 pp. 444-444
- Cillo V, Petrucci AM, Ardito L, Del Giudice M. (2022) Understanding sustainable innovation: A systematic literature review. *Corporate Social Responsibility and Environmental Management*. John Wiley & Sons. 2022. 02.02
- Eco Innovation at the heart of European policies. European Commission. <https://green-business.ec.europa.eu/eco-innovation/en> accessed 2 May 2023
- Foss N, Levin P G. (2020) Stakeholders and Corporate Social Responsibility: An Ownership Perspective. Sustainability: Stakeholder Governance and Corporate Social Responsibility. *Advances in Strategic Management*. Vol. 3. Emerald Publishing Limited. pp. 7-3
- Griffin R. (2023) *Fundamentals of management*. Cengage Learning Inc. Florence
- Innovation activities of enterprises in the years 2020 - 2022. Statistical analyses. GUS. Warszawa. Scecin
- International Organization for Standardization. ISO 2000. Specjalna Odpowiedzialność. 2020. Szwajcaria
- Instytut Statystyki. (2022) *Eco Innovation Country Profile 2022. Poland*. Ecorys
- Oslo Manual 2020. Guidelines for Collecting, Reporting and Using Data on Innovation. 4th Edition. The Measurement of Scientific, Technological and Innovation Activities. 2020. OECD Eurostat
- Oslo Manual 2020. Guidelines for Collecting, Reporting and Using Data on Innovation. 4th Edition. The Measurement of Scientific, Technological and Innovation Activities. 2020. OECD Eurostat
- Schiederig T, Tietje F, Herstatt C. (2022) Green innovation in technology and innovation management: an exploratory literature review. *R & D Management*. 42.2
- Teece D J, Pisano G, Shuen A. (1997) Dynamic capabilities and strategic management. *Strategic Management Journal*. 18.7
- Usman A B and Amran N A B. (2020) Corporate social responsibility practice and corporate financial performance: evidence from Nigeria companies. *Social Responsibility Journal*. Vol. 16, No. 4. pp. 74-73
- Uduo D, Lu L, Dymek M. (2022) Corporate Social Responsibility and Profitability: The Moderating Role of Firm Type in Chinese Appliance Listed Companies. *Energies*. 14.227. <https://doi.org/10.3390/en14020227>
- Statystyczny Urząd w Warszawie. (2022) *Statystyka w gospodarce w Polsce 2022*. GUS. Urząd Statystyczny w Białymostku. Warszawa. Biały Białystok
- Uduo D, Lu L. (2020) Strategic stakeholder management, environmental corporate social responsibility engagement, and financial performance of stigmatized firms derived from Chinese special environmental policy. *Business Strategy and the Environment*. 2020. 027-044. <https://doi.org/10.1002/bse.2222>

Estimation of Direct Tensile Strength by a Non-Destructive Test

Mustafa Kaşıkçı¹, İlhan Karaca¹

Abstract Depending on the type of stress affecting a material it exhibits various strength characteristics such as compression tensile shear bending and torsional strength Among these uniaxial compression and tensile strengths hold significant importance in rock mechanics applications and serve as indispensable parameters in geotechnical designs Engineering geological studies often focus on unconfined compressive strengths assuming that the rock is under compaction conditions However numerous researchers have emphasized that the tensile strength also plays a crucial role in determining the strength of rock material or rock mass against failure They have highlighted its significance during the design stage

Unlike uniaxial compressive strength which has standardized testing methods rock tensile strength is determined using different test methods These methods can be categorized into two main classes direct and indirect tensile tests Direct tensile tests are conducted along the axis of the specimen using various test apparatus However these tests often present significant challenges in obtaining accurate and reliable results On the other hand indirect tensile tests offer an alternative approach and are preferred by designers due to their simplicity and ease of application Among the indirect methods the most commonly used one is the Brazilian test method Designers often use the values obtained through indirect methods directly as the tensile strength of the rock material Alternatively they may calculate the direct tensile strength DTS of the rock using empirical equations proposed in relevant studies

As an alternative to direct and indirect methods used to determine the tensile strength of rock materials there are studies that propose empirical equations to estimate the tensile strength of rock materials based on various mechanical properties In these studies independent variables such as uniaxial compressive strength point load strength direct shear strength and sonic velocity SV have been used

In this study two sample groups andesite and marl were subjected to testing to uncover the correlation between DTS and SV The study utilized a total of 20 samples to analyze this relationship The individual evaluations of the groups yielded correlation coefficient r values of 0.4 and 0.2 respectively However when all the samples were collectively analyzed the r value significantly increased to 0.8 and a very strong positive correlation has been identified between these two parameters

Keywords Tensile strength direct tensile test sonic wave test non-destructive test

¹Address: Firat University Faculty of Engineering Department of Geological Engineering Elazığ, Türkiye

*Corresponding author: mkanik@firat.edu.tr

1. INTRODUCTION

Stresses that act on any selected cross-sectional area can be classified into four types: normal stresses (compression and tension), shear stress, torsional stress, and bending stress. The resistance that a material exhibits against these different types of stresses is defined as strength. Among these strength types, compressive and tensile strengths hold significant importance in rock mechanics applications and are considered indispensable parameters in geotechnical designs. Goodman (1969) states that engineering studies often focus on the unconfined compressive strength, assuming the rock is subjected to compression. However, he emphasizes that tensile strength is also a crucial parameter in determining the resistance of rock materials or rock masses against failure.

In engineering applications, the tensile strength has been emphasized to hold an equally important position as the compressive strength. Various researchers have highlighted this fact in their studies. For instance, Diederichs and Kaiser (1999) state that tensile strength is a critical controlling property in determining the critical span of underground openings. Similarly, Cai et al. (2000) and Pine et al. (2007) have shown through their research that tensile stresses can significantly influence slope stability. Hang (2003) expressed the necessity of considering tensile strength in design for blasting due to its value being lower than the uniaxial compressive strength. Huang et al. (2020) conducted a study where they found that during tunnel excavation within a slope supported by diaphragm walls, deformation could induce tensile stresses in pre-stressed rock bolts. These tensile stresses can counteract the tensile stresses in the geological formation where rock bolts

are installed highlighting the importance of tensile strength in stability. In conclusion, accurately determining the strength of rock materials under tensile conditions plays a vital role in ensuring safe and economically sound engineering designs.

Unlike uniaxial compressive strength, different test methods have been proposed to determine the tensile strength of rock. These methods can be divided into two main categories: direct and indirect tensile test methods. Direct methods involve applying tensile stress along a single axis using different testing apparatus. On the other hand, indirect tensile tests can be performed using various methods. There are five types of indirect tests used to determine the tensile strength of rock materials: three point bending, four point bending, disk bending, ring tension test, and Brazilian test. Among these, the Brazilian test method is the most commonly used. While the direct tensile method is the fundamental testing approach, it comes with significant challenges related to precise alignment and sample preparation, which can affect obtaining accurate and successful test results. Moreover, as the sample size increases, the presence of micro-cracks within the rock material can pose difficulties in directly pulling the rock sample during testing (Goodman, 1966). On the contrary, the test methods used for indirectly determining tensile strength are simpler and more easily applicable. Therefore, the relationships between direct and indirect tensile strengths have been investigated by different researchers, and attempts have been made to establish these relationships. Figure 1 compares data obtained from various indirect tensile tests with data from direct tensile methods. When examining Figure 1, it can be observed that the results closest to those of direct tensile methods are obtained from the hydraulic fracturing method. However, the hydraulic fracturing method is one of the in situ testing methods, and determining the tensile strength using this method indirectly is much more challenging compared to the Brazilian method. While the Brazilian method is simple, its results do not represent the direct tensile strength (DTS) of the rock material. Results obtained from indirect methods tend to be higher than those obtained from direct methods (Lanphumesri, 2010; Fuenkaorn and Lanphumesri, 2010).

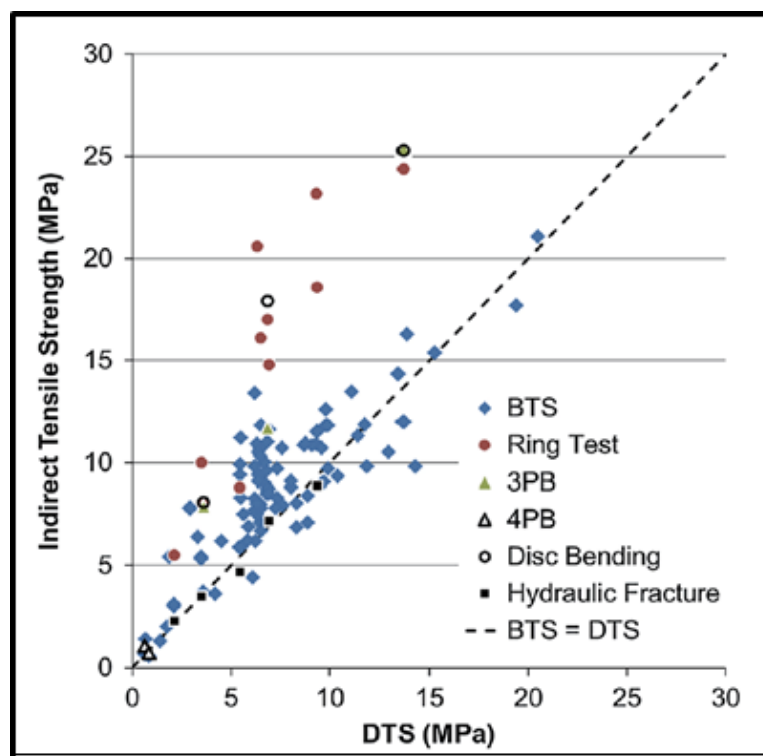


Figure 1 Comparison between DTS and various alternative indirect tensile testing methods (Perras, M. A. & Diederichs, 2014)

Furthermore, there are studies conducted by various researchers (Schrier, 1966; Suluk u and Ulusay, 2000; Mishra and Basu, 2012; Amshidi and Fereidooni, 2022) aimed at predicting the tensile strength of rock materials. In these studies, empirical equations were proposed where Brazilian tensile strength, uniaxial compressive strength, and direct shear strength of the rock material were used as independent variables. These equations allow for the estimation of the tensile strength of rock materials. Apuani et al. (1977) and Handelwal (2013) have also examined the relationships between Brazilian tensile strength and sonic velocity of rock materials. However, there is no existing study that investigates the relationships between the DTS of rock materials and their physical properties. In this study, experimental investigations were conducted to examine the relationships between DTS and SV in two different rock groups: andesite and marl. The

The prepared specimens following the guidelines of ISRM 2007 for the direct tensile test were kept in an oven at 100 C for 24 hours before attaching the tensile grips. After removing the specimens from the oven, steel grips were attached to the specimens using Loctite EA340 epoxy adhesive. To prevent movement of the grips, the specimens and steel grips were wrapped with paper tape and placed in a vacuum sealed environment for 3 days to allow the epoxy to fully cure and achieve sufficient tensile strength. Fig. 4



Figure 3 The specimens used for the direct tensile strength test

Afterward, the tensile tests were conducted using a uniaxial press with the help of an apparatus. The apparatus used and a view of the failed samples can be seen in Figure 5. All the experimental results from the tests are provided in Table 1.



Figure 4 Curing phase of the specimens

Table 1 The statistical evaluation of the experimental results

Group	Sample	Direct Tensile Strength				Statistical			
		Area	Area	Average	Standard Deviation	Area	Area	Average	Standard Deviation
Control	0	4.7		3.34	0.3	33	2	2	223.33
Adhesive	0	7.2	4.07	0.0	0.0	3702	327	34.7	30.7
All	20	7.2		4	32	3702	2	323.4	32.42

According to Table the highest DTS value of 7.2 MPa was obtained from the andesite group while the lowest average DTS value of MPa was obtained from the marl group. The highest SV value of 3702 m sec was observed in the andesite group and the lowest SV value of 2 m sec was recorded in the marl group.



Figure The apparatus used for the direct tensile test, the grips utilized, and the failed samples.

3 STATISTICAL ANALYSIS

The most common statistical method used to determine relationships between two parameters is simple or multiple regression analysis. These analyses aim to identify cause and effect relationships between two or more variables and use this relationship to make predictions or estimations related to the subject.

In this analysis method, a mathematical model is used to explain the relationship between two or more variables, and this model is called the Regression Model. The simple regression model can be represented as $y = a + bx$, where

y is the dependent (outcome) variable and is assumed to have some error

x is the independent (cause) variable and is assumed to be measured without error

a is the regression constant value and represents the value of y when x is 0

b is the regression coefficient, indicating the amount of change in y in its own unit corresponding to a unit change in x .

In this study, simple regression analyses were performed to establish the relationships between DTS and SV. These analyses were conducted for each sample group separately and for all groups together to examine the relationships comprehensively.

3.1 Simple regression analysis for the marl group samples

In this group, the samples are sedimentary origin marls, and upon evaluating the data from the experiments conducted on the cores of this group using a simple regression analysis, Fig. the correlation coefficient r was determined to be 0.2. This value indicates a strong positive correlation between DTS and SV in the marl group samples.

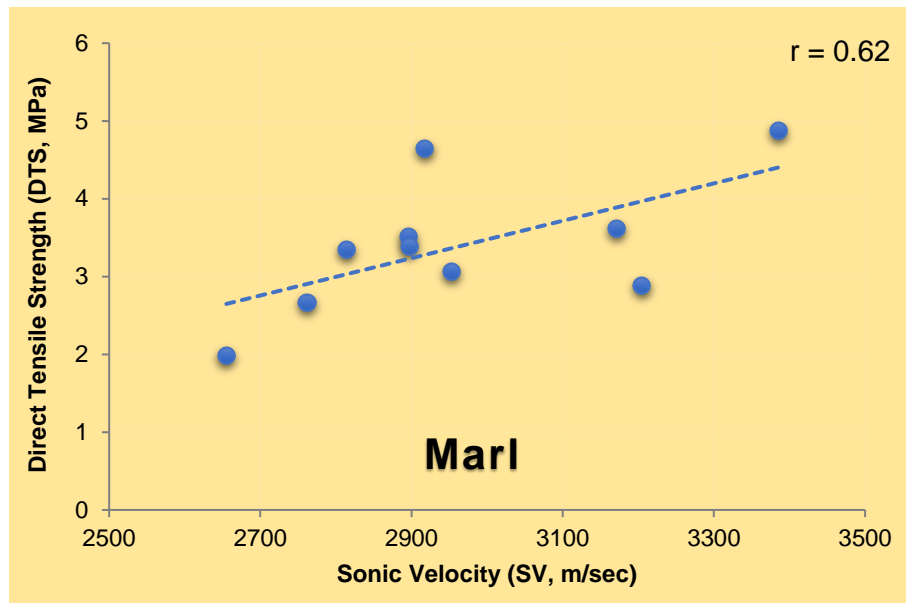


Figure Data distribution graph for marl samples

3.2 Simple regression analysis for the andesite samples

The samples in this group consist of volcanic origin andesites. Upon evaluating the results of the experiments conducted on andesite cores using a simple regression analysis, a strong positive relationship with an r value of 0.4 between DTS and SV of andesites has been determined. Fig. 7

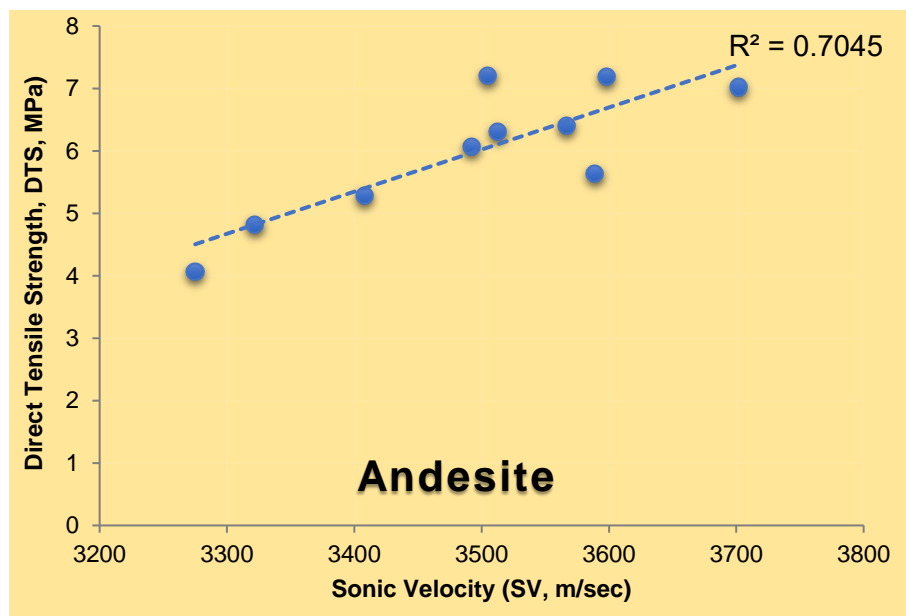


Figure Data distribution graph for andesite samples

3.3 Overall evaluation

In this study data for marl and andesite samples were evaluated together to explore the relationship between DTS and SV of the specimens. The data distribution graph for the regression analysis where DTS is the dependent variable and SV is the independent variable is provided in Figure 1. According to the results of the regression analysis there is a very strong positive correlation between DTS and SV. The r value is 0.89 and the equation describing the correlation is as follows:

$$DTS = 0.0045 SV - 9.805$$

2

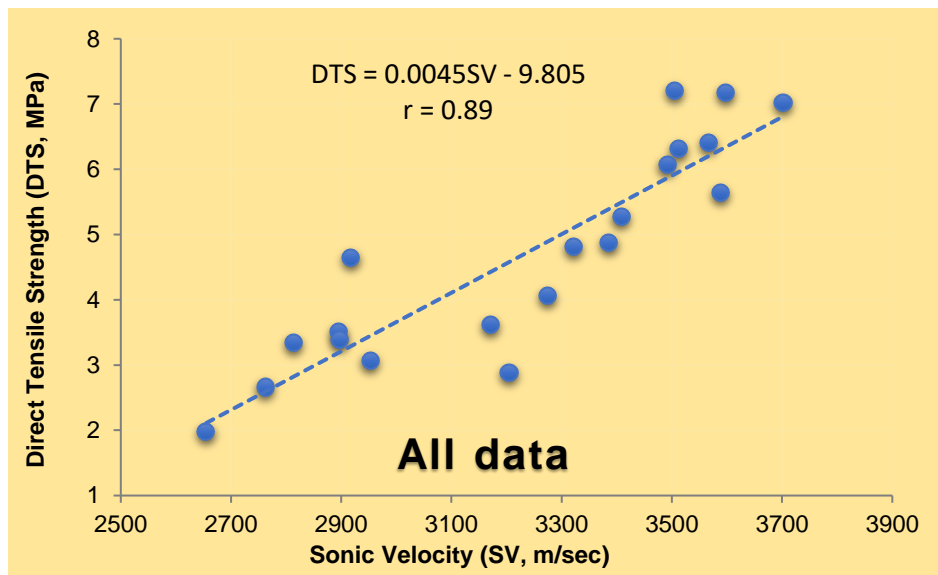


Figure 1. Data distribution graph for both groups

5. CONCLUSIONS

In the literature there are numerous studies on determining the DTS of rock materials using indirect methods. The results of these studies indicate that the values obtained through indirect methods for the tensile strength are generally higher than the actual DTS values of the rock materials. Andreev, a; Andreev, b; Gorski and Conlon, 2007; lanphumeesri, 2010; Fuenkaorn and lanphumeesri, 2010; Perras and Diederichs, 2014; Jensen, 2010; Liao et al., 2010. Although there are contrasting views, Coviello et al., 2000; Li and Wong, 2012, the prevailing opinion is in line with the findings from the widely used indirect method, Brazilian test. To overcome this issue, it may be possible to explore the relationships between the rock's direct tensile strength and other physical and mechanical properties. Therefore, this study was conducted with the aim of addressing this significant gap in the literature, even if only to a limited extent.

In this study, the relationships between the DTS and SV values of rock materials were examined using the simple regression method. For this purpose, experimental studies were conducted on core samples of marl and andesite rocks, and the obtained results were statistically evaluated to determine the relationships between the DTS and SV of the rock materials. As a result of the regression analyses, an empirical equation was proposed, which can be used to predict the DTS of rock materials.

Similar studies in the literature, Apuani et al., 2017; handelwal, 2013, have investigated the relationships between tensile strength obtained from Brazilian tests and SV for rock materials. However, this study is the first to examine the relationship between DTS and SV for rock materials. The evaluation of the results obtained from the experimental studies through regression analyses indicates strong positive relationships, with an r value of 0.2 for the marl group rocks and an r value of 0.4 for the andesite rocks.

The combined evaluation of data from both rock groups yields an r value of 0.89, indicating a very strong positive correlation between the DTS and SV through regression analysis. The empirical equation derived from this study for the determined correlation is highly effective and can be used by engineers to predict the DTS of rock materials. In future experimental studies conducted on different lithologies with new data, it will be possible to establish more reliable empirical equations that represent this relationship even better.

ACKNOWLEDGMENTS

All studied data presented in this study were obtained under a research project 22 0 7 supported by T BITA The Scientific and Technological Research Council of Turkey

ethics committee Approval
N/A

Peer review
Externally peer reviewed

Author contributions

Conceptualization M Investigation M G Material and Methodology M G Supervision M G
Visualization M Writing Original Draft M G Writing review Editing M G Other All authors have read and agreed to the published version of manuscript

Conflict of interest

The authors have no conflicts of interest to declare

Funding

The authors declared that this study has received financial support under a research project 22 0 7 supported by T BITA The Scientific and Technological Research Council of Turkey

References

- Andreev G A a Review of the Brazilian test for rock tensile strength determination Part I calculation formula
Min Sci Technol 33 44 4
- Apuani T Ting M S Butenuth C De Freitas M H 7 Measurements of the relationship between sonic wave velocities and tensile strength in anisotropic rock Geological Society London Special Publications 22 07
- Andreev G A b Review of the Brazilian test for rock tensile strength determination Part II contact conditions Min Sci Technol 33 47 4
- Cai M Kaiser P Martin C 200 Quantification of rock mass damage in underground excavations from microseismic event monitoring Int Rock Mech Min Sci 3 3 4
- Coviello A Lagioia R Nova R On the measurement of the tensile strength of soft rocks Rock Mech Rock Eng 200 3 4 2 273
- Diederichs M S Kaiser P Tensile strength and abutment relaxation as failure control mechanics in underground excavations Int Rock Mech Min Sci 3
- Fuenkaorn lanphumeesri S 20 Laboratory determination of direct tensile strength and deformability of intact rocks Geotech Test 34
- Goodman RE Introduction to Rock Mechanics 2nd ed New York Wiley
- Gorski B Conlon B L Unggren B 2007 Forsmark Site investigation Determination of the direct and indirect tensile strength on cores from borehole FM0 D S B P 07 7 Svensk mbr alehantering AB
- Huang F hang M ang F Ling T H ang L 2020 The failure mechanism of surrounding rock around an existing shield tunnel induced by an adjacent excavation Computers Geotechnics 7
- amshidi A Fereidooni D 2022 Evaluation of the block punch index test for predicting the strength of sandstones Scientific quarterly journal of Iranian Association of Engineering Geology 0
- ensen S S 20 Experimental Study of Direct Tensile Strength in Sedimentary Rocks Norwegian University of Science and Technology master thesis p

- Handelwal M 2013 Correlating P wave Velocity with the Physico Mechanical Properties of Different Rocks Pure Appl Geophys 70 07 4
- Ianphumeesri S 2010 Direct tension testing of rock specimens Suranaree University of Technology master thesis 04p
- Li D, Long L 2012 The Brazilian disc test for rock mechanics applications: review and new insights Rock Mech Rock Eng 4 2 2 2 7
- Liao, Hu B, Tang C A 2012 Numerical investigation of rock tensile strength determined by direct tension Brazilian and three point bending tests Int Rock Mech Min Sci 2 32
- Mishra D A, Basu A 2012 Use of the block punch test to predict the compressive and tensile strengths of rocks International Journal of Rock Mechanics Mining Sciences 27
- Perras M A, Diederichs M S 2014 A Review of the Tensile Strength of Rock: Concepts and Testing Geotech Geol Eng 32 2 4
- Pine R, Owen D, Coggan 2007 A new discrete fracture modelling approach for rock masses Geotech 2007 7 7 7 7
- Schrier van der S The block punch index test Bulletin of Engineering Geology and the Environment 3 2 2
- Sulukcu S, Ulusay R 2000 Evaluation of the block punch index test with particular reference to the size effect failure mechanism and its effectiveness in predicting rock strength International Journal of Rock Mechanics and Mining Sciences 3 0
- Ulusay R, ve Hudson A 2007 The blue book: the complete ISRM suggested methods for rock characterisation testing and monitoring 74 200 ISRM and Turkish National Group of ISRM Ankara
- Yang 2012 Free Surface and Swelling in Blasting Rock Fracture and Blasting Theory and Applications 23 2 4 <https://doi.org/10.1007/978-1-4020-0007-7>

Carbon Fibers Research for the World

Mustafa Siğirici¹, Siğirici Altu taş¹

Abstract Carbon fibers one of the engineering materials are one of the materials preferred by designers. Since these fibers have many forms they also play an important role in the development of high tech products. Since carbon fibers are the main element especially in fiber reinforced composites they allow the emergence of different shapes. This is the only reason why carbon fibers are in the form of fiber and weaving. Despite the fact that these materials have different forms their great advantages compared to traditional materials pave the way for their use in products produced in daily life. However the high production cost of carbon fibers hinders the development in this field even if it is a little bit. Carbon fibers used in fields such as defense aviation and space are turning into a strategic material from the point of view of countries. Countries want to make their own production of this product to meet their own needs but they also import it. For this reason research on carbon fibers is still ongoing. In this study the interest of G 20 countries towards this material was investigated by using secondary data. In this direction export and import figures were examined and country based percentages of these figures were revealed. However due to the fact that this product is a strategic product historical data could not be obtained only 2022 and later data were obtained and it was revealed that some countries did not share this information. In addition data for 2022 and 2023 for Turkey have been reached and detailed analysis has been made on a country basis.

Keywords Carbon fiber imports export data

¹Address: Baskent University, Ahramanka Vocational School, Ankara, Turkey

*Corresponding author: tugayustun@baskent.edu.tr

1

Srekli gelişmeye devam etmekte olan teknolojiyle beraber mühendislik malzemeleri önem kazanmaktadır. Bu mühendislik malzemelerinden bir de kompozitlerdir ve kendi içerisinde de çeşitli sınıflara ayrılmaktadır. Özellikle son yıllardan dolayı endüstriyel ve ticari olarak birçok uygulama alanına sahip olan elyaf takviyeli kompozitler bu sınıfın en önemli malzemeleri olarak karşımıza çıkmaktadır. Agarwal vd. (2017) Metal malzemeler ile karşılaştırıldığında birçok uygulama alanının temel sebebinde düşük yoğunluklar bundan dolayı ayrılmaktadır. Yüksek dayanım sergilemeleri olarak gösterilebilir. Mallick (2007) çalışmada 2000 yılında Bu malzemelerle elektronik kartlar, robotik kollar gibi elektronik gerektiren ürünleri gibi enerji depolama, rulmanlar gibi makine, havacılık ve savunma gibi birçok sektörde kullanılmaktadır. Gay (2014)

Elyaf takviyeli kompozit malzemelerin temel bileşenlerinden biri olan elyaflar kompozite güçlü ve sağlam katkı sağlarlar. 2023 Elyaf lar kendi içinde doğal ve sentetik olarak iki sınıfa ayrılırken sentetik elyaflardan biri olan karbon elyaflar birçok ara tirmacının ilgisini çekmektedir. Aslında karbon elyafların keşfedilmesi çok eski dönemlere dayanmaktadır. Thomas Edison elektrik lambalarının geliştirilmesinde pamuk ipliğini karbonla ederek karbon elyaf elde etmiş ve bunu kullanmıştır. Edison (1877) Bu süreçte yapılan çalışmalarla men tungsten tellerin icadıyla karbon elyaf kullanımı son bulmuştur. Dupont firması tarafından geliştirilen poliakrilonitril (PAN) den elde edilen elyaflar ile birlikte karbon elyafın temeli oluşturulmuştur. Hout (2010) lerleyen süreçlerde Amerika ve İngiltere başta olmak üzere birçok ülke havacılık ve ulaşım alanındaki çalışmaların artmasıyla karbon elyaf üretimi ve kullanılan karbon elyafların geliştirilmesi konularındaki ara tirmaların hızlanmasıyla birlikte 2023 yılında geliştirilen karbon elyaflar ile birlikte yüksek dayanım, korozyon direnci, yanma sıcaklığı, elektriksel iletkenlik, biyolojik uyumluluk, düşük genleşme gibi avantajlardan bahsedilebilir. Gevrekler (2015) ve başlıca özellikleri ve üretim maliyeti gibi olumsuzlukları da vardır. Başpa (2022) Bu malzemelerin avantajları ve dezavantajlarından bahsetmemiştir. Karbon dioksit malzemeleri ile karşılaştırıldığında nemli ortamlarda kullanılmaması, bakıldığında diğer malzemelerden 7 kat daha hafiftir. Başpa (2022) Genel olarak karbon elyaflar diğer malzemelerle karşılaştırıldığında dayanım ve iletkenlik özelliklerine sahiptir.

retim a s ndan incelendi inde di er geleneksel mal emelere g re birtak m orluklar bulunan karbon elyaf lar n retim maliyetleri di er mal emelere g re daha y ksektir arbon elyaf retiminde bir nc l mal eme kullan lmakla beraber bu mal emeden retilen liflerin karboni asyonu ile ger ekle tirilir arbon elyaf n genel olarak retim a amalar lif yapma stabili asyon karboni asyon y ey iyile tirme ve kaplama olarak s ralanabilir Ma umdar 200 arbon elyaf n retim a malar ayn olup kullan lan nc l mal emeler de i mektedir PAN nc l nde karbon elyaf retimi g n m de en ok tercih edilen bir y ntem olup Poliakrilonitril PAN hammaddesinden yap lmaktadır Ticari karbon elyaf retiminin 0 PAN nc l mal emesi ile ger ekle tirilmektedir nl 2023 Di er bir nc l mal eme olan ift ile karbon elyaf retimini 0 larda ticarile tirilmi tir ift petrol veya k m r katran ndan retilir ve PAN ba l elyaf larla k yasland nda elektriksel ve termal ellikleri daha geli mi tir Ba pai 202 ift nc l kullan larak retilen karbon elyaf lar n PAN a ile retilen karbon elyaf larla k yasla daha ucu ve daha y ksek oryantasyona sahip olmas da bir di er avanta lar aras nda g sterilebilir Morgan 200

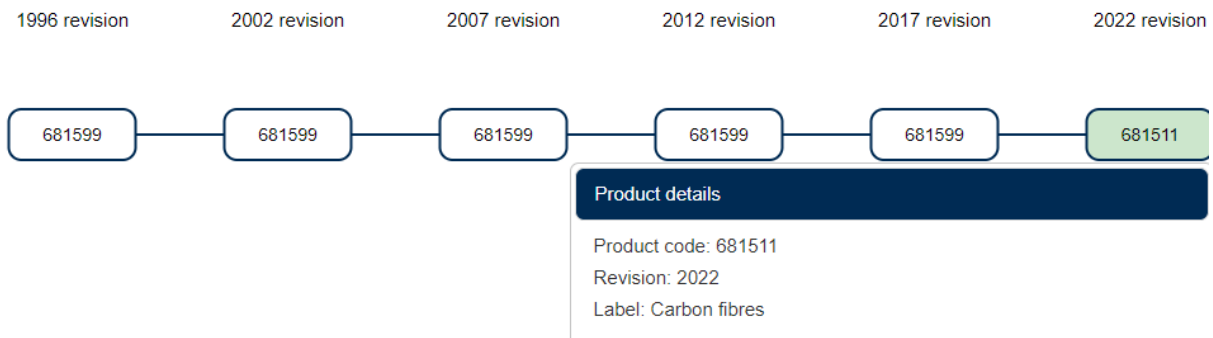
Bu al man n amac strate ik m hendislik mal emelerinden bir olan karbon elyaf lar n ikincil verilerden elde edilerek sekt rel de erlendirmesi yap lmaktadır Hem D nya da hem de T rkiye de e itli sekt rlerde kullan lan karbon elyaf ve karbon elyaftan mensucat r nlerinin ithalat ve ihracat rakamlar da lkeler ba nda k yaslamas yap lm t r

2 A A O

arbon elyaf lar lkelerin retimini yapmak ve geli tirmek istedi i strate ik bir mal eme olmas ndan dolay s rekli ara t r lmas yap lmakta olan g ncel bir konudur thalat ve ihracatta yer alan bu r n e itli ekillerde ticarete konu olmaktadır D nyada ve T rkiye de ticarete konu olan r nlerden olan karbon elyaf ve karbon elyaftan retilen mensucat TD dokuma r n olan eyler dokuma emtialar n n G mr k Tarife statistik Po isyon GT P numaralar s ras ile 000000 ve 2000000 2 eklindedir Bahsi ge en GT P kodu terimi ise T C Ticaret Bakanl taraf ndan T rk G mr k Tarife Cetvelinde kullan lan 2 rakaml kod olarak belirtilmektedir Bu kodun ilk rakam D nya G mr k rg t ne ye t m lkelerce kullan lan Armoni e Sistem HS Harmoni ed System Nomanklat r kodunu 7 inci rakaml Avrupa Birli i lkeleri taraf ndan kullan lan ombine Nomanklat r Combined Nomenclature CN kodunu 0 uncu rakaml farkl vergi uygulamalar m nedeniyle a lan po isyonlar g steren kodlar n 2 inci rakamlar ise istatistik kodlar n g sterme i in kullan lmaktadır T C Ticaret Bakanl 2023 ve 2 olarak belirlenen ve se ilen GT P kodlar 2022 HS revii yonunda olu turulmu ve sisteme d hil edilmi tir 2022 y l na kadar GT P kodlu r n olan arbon Elyaf ve 2 GT P kodlu r n olan arbon Elyaftan Mensucat GT P kodlu r n alt nda ve kapsam nda D nyada ve T rkiye de uluslararası ticarete ithalata ve ihracata konu olmu tur 2022 y l nda HS revii yonu olan GT P kodlar Resim de g sterilmektedir

a

Harmonized System revisions correspondences



b

Harmonized System revisions correspondences

E



e il 1 2022 l a ve b 2 HS odlar Reviyonu Trademap 2023

Uluslararası Ticaret Odası tarafından kurulan ve yürütmekte olan Trademap.org internet sitesi 220 lkenin ve b lgenin harmoni e sisteminde kayıtlı bulunan 300 r n n i erekle tasarlanmış Trademap.org internet sitesi sisteme dahil olan lkelerin ilgili resmi istatistik kurumlarının veri tabanlarından ilgili r nlerin ihracat ve ithalat rakamlar n e itli l tler aylık 3 aylık aylık yıllık kg ton lt para birimi vb do rultunda kendi b nyesine aktarmaktadır internet sitesini kullanan ara t rmac lar lkelerin ilgili r nlerdeki d nya pay na yeni pa arlara rekabet i pa arlara ihracat ithalat detayları tablolar grafikler ve haritalar ekinde ula bilmektedir s aca Trademap.org sitesi uluslararası ticaretin ve i olanaklarının geli tirilebilmesi i in kullanılan istatistik bilgileri sa layan veri tabanı niteli inde bir sistemdir

GT P kodlu r n olan Ta tan ve Minerallerden Di er E ya ba l kl r n tan m i erisinde bir ok mineral madde ve r n olmas dolay s ile bu r nlerin D nyadaki ve T rkiye deki ticari verilerine do ru ekinde ula lsa bile ilgili r nler olan arbon Elyaf ve arbon Elyaftan Mensucat ilgili verilerden 2022 y l na kadar elde edilememi tir Bu duruma istinaden arbon Elyaf ve arbon Elyaftan Mensucat r nleri ile ilgili 2022 HS reviyonu ile birlikte 2022 ve 2023 ay verileri bu al mada ele al narak tablolarda kullan lm t r

3 A

arbon Elyaf ve arbon Elyaftan Mensucat ile ilgili bilgiler kar la t r lmas yapıl rken ncelikle T rkiye ye ait veriler yer alm t r Tablo 1 ve Tablo 2 de T rkiye nin ihracat verileri bulunmaktadır GT P kodlu karbon elyaf r n n n 2022 y l nda T rkiye den D nyaya ihracat rakam 4 milyon 3 bin Amerikan dolar ekinde ger ekle mi tir Ayn GT P kodlu r n n T rkiye den D nyaya 2023 y l Ocak ay ihracat verisi ise 0 bin Amerikan dolar ekinde bilgi yer almaktadır Trademap 2023

Tablo 1 GT P odlu arbon Elyaf r n n n T rkiye den D nyaya hracat Verileri 2022 2023M0 Trademap 2023

r K u	r a mı	r iye i yaya hracatı 2 22 e i e er mily
000000	arbon Fiber	4 3

Tablo 2 den anla labilece i ere 2 GT P kodlu karbon elyaftan mensucat r n n n 2022 y l nda T rkiye den D nyaya ihracat rakam 7 milyon 0 bin Amerikan dolar ekinde ger ekle mi tir Ayn GT P kodlu r n n T rkiye den D nyaya 2023 y l Ocak ay ihracat verisi ise milyon 7 bin Amerikan dolar ekinde trademap.org sitesinden elde edilmi tir Her iki karbon elyaf r n birlikte ele al nd taktirde T rkiye 2022 y l nda yakla k milyon 00 bin Amerikan dolar ihracat ger ekle tirmi tir

Tablo 2 GT P Numaralı Karbon Elyaf Tanımlı Mensucat Ürünleri'nin Türkiye'den Dışarıya İhracat Verileri 2022-2023M0 Trademap 2023

Kod	Adı	2022 İhracat Değeri (Milyon \$)
2000000	Karbon Elyaf Tanımlı Mensucat	70

Bu şekilde Türkiye'nin bu ürünlerin ithalat rakamları trademap sitesinden alınmış olup, ikiye katlanarak ihracat ve ithalat verileri incelenmiştir. GT P kodlu karbon elyaf ürününde 2022 yılında Türkiye'nin dışarıya ihracat yaptığı toplam rakam 70 milyon 22 bin Amerikan doları şeklinde görülmüştür. Aynı GT P kodlu ürünün Türkiye'nin dışarıya 2023 yıl Ocak ayı ithalat verisi ise 4 milyon bin Amerikan doları şeklinde Trademap.org sitesinden elde edilmiştir.

Tablo 3 GT P Numaralı Karbon Elyaf Ürünleri'nin Türkiye'nin Dışarıya İthalat Verileri 2022-2023M0 Trademap 2023

Kod	Adı	2022 İthalat Değeri (Milyon \$)
000000	Karbon Fiber	47,22

Tablo 4 GT P Numaralı Karbon Elyaf Tanımlı Mensucat Ürünleri'nin Türkiye'nin Dışarıya İthalat Verileri 2022-2023M0 Trademap 2023

Kod	Adı	2022 İthalat Değeri (Milyon \$)
2000000	Karbon Elyaf Tanımlı Mensucat	70

Tablo 4'ten anlaşılacağı üzere GT P kodlu karbon elyaf tanımlı mensucat ürününde 2022 yılında Türkiye'nin dışarıya ihracat yaptığı toplam rakam 70 milyon bin Amerikan doları şeklinde görülmüştür. Aynı GT P kodlu ürünün Türkiye'nin dışarıya 2023 yıl Ocak ayı ithalat verisi ise 4 milyon bin Amerikan doları şeklinde trademap.org sitesinden elde edilmiştir.

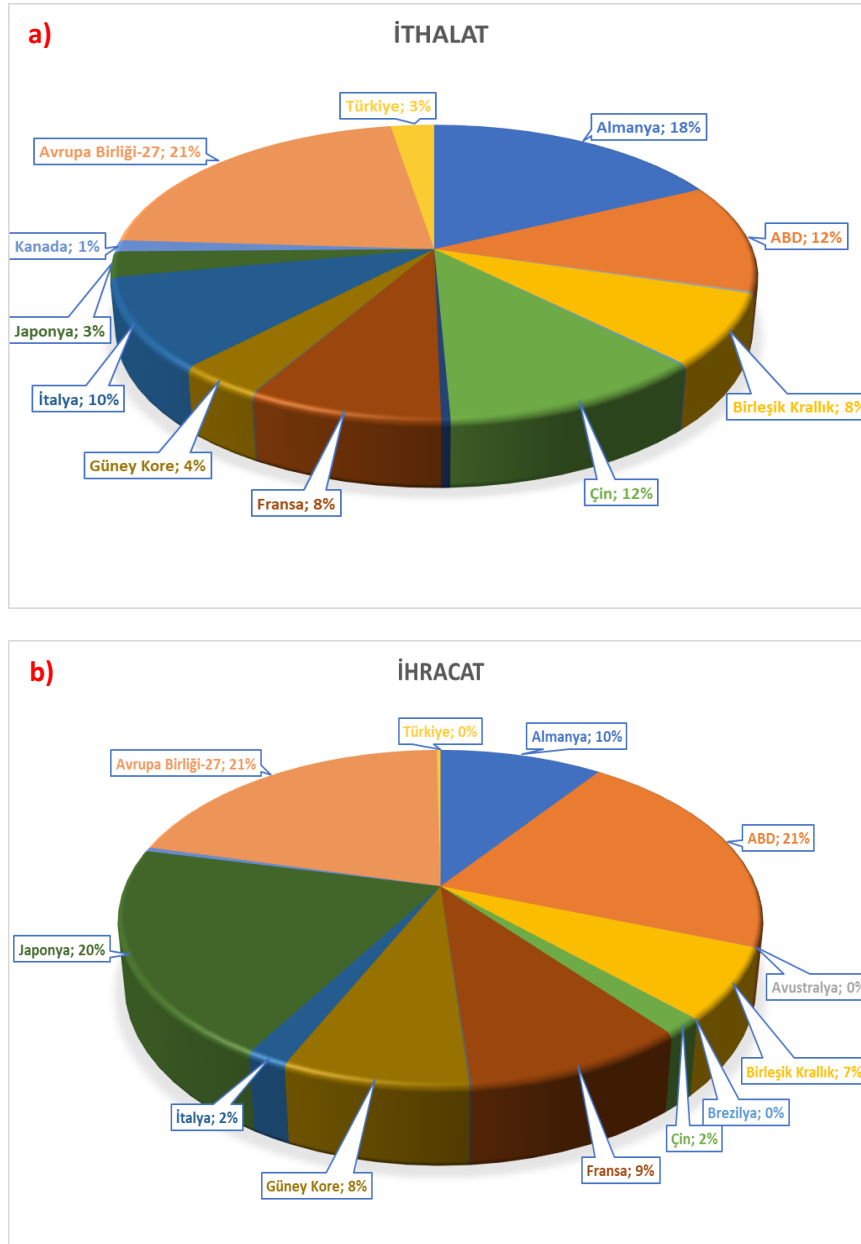
İkiye katlanarak ele alınan bu ürünlerin G 20ye Dışarıya İhracat ve İthalat Verileri'nin bir araya getirilen platformunda yer alan ülkelerin dışarıya ihracat verileri G 20ye dahil olan ülkelerde 2022 yılına ait GT P kodlu ürünlerin ikiye katlanarak ithalat ve ihracat verileri Tablo 4'te paylaşılmıştır.

abl odlu GT P r nlerinin G 20 deki Ticari Verileri 2022 000 Amerikan dolar Trademap 2023

1 11 Karb lya		
2 l eleri	thalat	hracat
Almanya	334 00	2 2 42
ABD	224	4 0
Ar antin	Bilgi ok	Bilgi ok
Avustralya	4 33	2
Birle ik rall k	4 2	47 4 0
Bre ilya	2 2	4
in	2 027	3 3 4
Endone ya	7 7	0
Fransa	7	204 2
G ney Afrika	2	2 02
G ney ore	70 47	70 40
Hindistan	Bilgi ok	Bilgi ok
talya	7 2	3 3 2
aponya	2 74	43 227
anada	23 47	7
Meksika	Bilgi ok	Bilgi ok
Rusya	Bilgi ok	Bilgi ok
Suudi Arabistan	Bilgi ok	Bilgi ok
Avrupa Birli i 27 Almanya Fransa talya Hari	40 727	44 2
T rkiye	47 22	4 3
lam	0	2 0 3

Trademap.org sitesinde ba lkelerin ilgili r nlerde ithalat ve ihracat verileri payla lmad ndan dolay veri bilgisine ula lamam olup ticari verilere eklenmemi tir

G 20 lkelerinin ihracat ve ithalat y deleri ise ekil 2 de verilmi tir 2022 y l nda GT P kodlu r nde G 20 lkeleri aras nda lkesel ba da en fa la ihracat ABD aponya Almanya ekleinde s ralanm t r En fa la ithalat ise Almanya ABD in ekleinde meydana gelmi tir lgili sekt rde toplam milyar milyon Amerikan dolar ekleinde ithalat 2 milyar milyon Amerikan dolar ihracat meydana gelmi tir



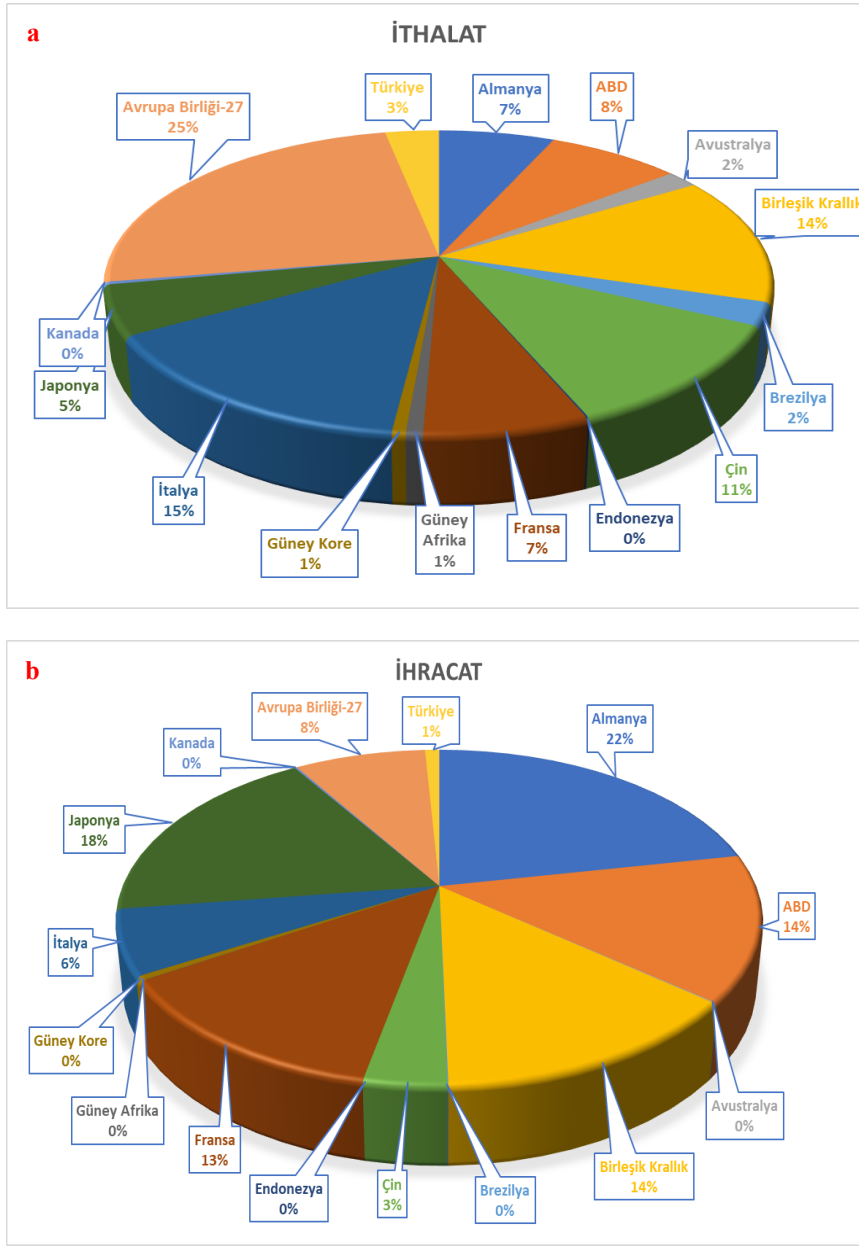
e il 2 GT P kodlu r nde G 20 lkelerin a thalat y deleri b hrcat y deleri

G 20 ye d hil olan lkelerde 2022 y l na ait 2 GT P kodlu r nlerin lke ba l ithalat ve ihracat verileri Tablo da payla lm t r Ayr ca G 20 lkelerinin ihracat ve ithalat y deleri ise ekil 3 te verilmi tir 2022 y l nda 2 GT P kodlu r nde G 20 lkeleri aras nda lkesel ba da en fa la ihracat Almanya aponya ABD ekinde s ralanm t r En fa la ithalat ise talya Birle ik rallık in ekinde meydana gelmi tir lgili sekt rde toplam 4 milyon Amerikan dolar ekinde ithalat 2 milyon Amerikan dolar ihracat meydana gelmi tir

abl 2 odlu GT P r nlerinin G 20 deki Ticari Verileri 2022 000 Amerikan dolar Trademap 2023

2 l eleri	1 12 Karb lya ta e sucat	thalat	hracat
Almanya	3 7		0 2
ABD	42		40
Ar antin	Bilgi ok		Bilgi ok
Avustralya	0 0		
Birle ik rall k	7 70		2 243
Bre ilya	3 4 4		37
in	3 3		2 02
Endone ya	4 4		Bilgi ok
Fransa	3 042		07 2
G ney Afrika	3 3		22
G ney ore	3 70		3 3
Hindistan	Bilgi ok		Bilgi ok
talya	2 74		37
aponya	2 3		
anada	0		
Meksika	Bilgi ok		Bilgi ok
Rusya	Bilgi ok		Bilgi ok
Suudi Arabistan	Bilgi ok		Bilgi ok
Avrupa Birli i 27 Almanya Fransa talya Hari	3 330		3 7
T rkiye	7 0 0		7 0
lam	4 30		2 7

Trademap.org sitesinde ba lkelerin ilgili r nlerde ithalat ve ihracat verileri payla lmad ndan dolay veri bilgisine ula lamam olup ticari verilere eklenmemi tir



Şekil 3 2 GT P kodlu rinde G 20 lkelerin a thalat y deleri b hracat y deleri

A A SO A

Mhendislik mal emelerinden biri olan karbon elyaflar n ticarete konu olan ihracat ve ithalat anlam nda G 20 lkeleri a s ndan incelemesi yap lm t r Ticarete konu olan r nlerden olan karbon elyaf ve karbon elyaftan retelen mensucat emtialar n n GT P numaralar vas tas yla 2022 y l na ait ikincil verilerden faydalanarak T rkiye ve G 20 lkeleri ba l bak lm t r Her iki GT P numaras na bak ld nda en fa la ihracat ABD aponya Almanya En fa la ithalat ise Almanya ABD in ekinde s ralanmaktadır T rkiye ba nda bireysel olarak bak ld nda ise her iki GT P numaras 2022 y l na ait verilerinde yakla k milyon 00 bin Amerikan dolar ihracat ger ekle tirirken milyon Amerikan dolar da ithalat yapm t r

KA AK A

- Agarwal B D Broutman L 0 Analysis and performance of fiber composites Second edition John Wiley Sons
- Ba pai P 202 Applications of carbon fiber carbon fiber reinforced plastic recycled carbon fiber reinforced polymers Carbon Fiber Second Edition 3
- Edison T A 7 Electric lamp Patent US 223
- Gay D 2022 Composite materials design and applications CRC press
- Hout R C 0 Orlon Acrylic Fiber Chemistry and Properties Textile Research Journal 20 7 0
- HS odlar 2022 <https://www.trademap.org/Index.aspx> Eri im Ha iran 2023
- o o lu H 2023 At k arbon Elyaf eniden ullan m in Polimer Matrisli Hibrit ompo it Mal eme Geli tirilmesi Geb e Teknik niversitesi Fen Bilimleri Enstit s
- Mallick P 2007 Fiber reinforced composites materials manufacturing and design CRC press
- Ma umdar S 200 Composites manufacturing materials product and process engineering CrC press
- Morgan P 200 Carbon fibers and their composites CRC press
- T rkiye Cumhuriyeti Ticaret Bakanl 2022 <https://ticaret.gov.tr/gumruk-islemleri-sikca-sorulan-sorular-ticari-tarife> Eri im Ha iran 2023
- nl S 2023 Polimer matrisli elyaf takviyeli kompo it mal eme imalat ve balistik elliklerin incelenmesi Sakarya niversitesi Fen Bilimleri Enstit s
- ang R M heng S R heng P G 20 Polymer matrix composites and technology Elsevier

Visualization of beetle brain with artificial intelligence

Attila ^{1*}

Abstract The closest possible analogy of artificial neural networks to the living nervous system can bring us closer to understanding the independent reactions induced by connectomics. We can assume that a similar data flow takes place in the living nervous system but the visibility of which has not yet been resolved. The 4 dimensional visualization of AI analog signals with colors developed by us provides insight into the learning process of the neural network. The learning of the AI is caused by pleasant or unpleasant signals from the sensors of a beetle robot. So stroking or hitting the robot triggers the reorganization of the weights of the AI node. The output of the neural network controls the movement of the robot beetle. We managed not only to implement the visualization but also to create an effective didactic tool for teaching AI to programming master university students.

Keywords connectomics visualiser neural network beetle brain artificial intelligence

University of Debrecen Faculty of Informatics Department of Information Technology
Debrecen Hungary

Corresponding author: oltan.godo@inf.unideb.hu

1 Introduction

The more we know about the functioning of the living nervous system the more new questions arise. We know exactly the connection between the nerve cells of some simpler organisms. This is connectomics. The nematode *Caenorhabditis Elegans* C. Elegans for example is such a reference organism whose anatomy is well mapped (White et al).

During a very exciting research Timothy Busbice (Timothy B. 2014) created a program that can be started three hundred and two times where each program inherits the attributes one of each of the worms 302 neurons and uses interprocess communications to connect the programs together in a manner similar to that of synaptic communication. Mapping the entire connectome into a framework whereby sensory input can be derived from robotic sensors and directed to connectome sensory neurons which in turn activates interneurons which activate motor neurons and muscle output can be accumulated to activate robotic motors. The simulated connectome and connectome framework allows for a biological simulation and study of the entire connectome from sensory input to muscular output.

The experiments discussed in his paper show that the connectome alone is enough to give rise to experimental behaviors shown in the biological organism. This in part answers the age old question of whether the connectome alone can have value in determining animal phenotypes. The connectomics of more complicated organisms has only recently been processed at the level of the fruit fly *Drosophila melanogaster*. This is already the result of enormous research work. The brain of the fruit fly contains 27,700 neurons (Dorkenwald S. 2023). How so many neurons can perform such a complex function as flying (Takemura S. et al. 2023) is still an area of intense research today.

The closer analogy of artificial neural networks with the living nervous system can bring us closer to understanding the independent reactions induced by connectomics. However

modeling the analog characteristics of the living nervous system results in an unprocessable amount of information. Therefore, visualizing the process of learning and rebuilding AI helps the human brain see the previously invisible processes inside the neural network. Boyle [20, 2]. The closest possible analogy assumes that a similar data flow takes place in the living nervous system, but the visibility of which has not yet been resolved.

2 Objectives

- Novel 4-dimensional visualization of neural network AI
- Visualization of analog signals with colors
- Visualization of the reorganization and learning mechanism of AI
- Output control of a beetle robot
- Realization of AI through the signals of the beetle robot's sensory organs, sensors, and visualization
- Creating an AI learning process with reflexes

2 Material and Methods

The neural network visualization software was created under the Linux operating system in the C++ programming language. The beetle is directly controlled by an Arduino Uno microcontroller. The movement is done by Adafruit 220 servo motors. The distance is detected by the Arduino ST-06 Ultrasonic sensor. The mechanical receptors are replaced by the Honeywell SEN-VIB0 vibration sensor. The communication between the PC and Arduino with the USB chip.

3 Artificial Intelligence: Imitating the Beetle Brain

The beetle's brain is a neural network program developed by us. The software is capable of generating a three-dimensional neural network of any size. The number of nodes of the neural network is given in the program argument. Thus, it starts with the allocation of memory of the required size. Each node is stored in an array data structure. Weights, i.e., connections between nodes, are stored in a separate dynamic data structure. Thus, the number of connections between nodes is arbitrary. During the operation of the neural network, the number of connections can change without limitation. So, during the learning process, new connections can be created, which shows analogous characteristics to the plasticity of the living nervous system. In addition, redundant, i.e., unused, connections can be built up, which is similar to the apoptosis of living systems. With the characteristics of the dynamic structure of the neural network, we tried to achieve the best similarity of the characteristics of the living nervous system.

Nodes represent individual neurons. The weights between the nodes are the axons and dendrites. Since the communication of nerve cells in synapses is one-way, the weights of the neural network are also limited to one-way traffic. In the living nervous system, the synapses of axons release neurotransmitters across the presynaptic membrane. It diffuses across the synaptic cleft and binds to receptors on the postsynaptic membrane. Here, it causes a local potentiation, which triggers the further stimulation of the targeted nerve cell. That is, information passes from one nerve cell to another in one direction. Even so, the one-way weights between the nodes of the neural network function as synapses.

3 Visualizations

One of the great innovations of the project is the visualization of neural processes. Since neural processes are extremely fast and moreover represent analog values, our idea is visualization with colors. It is true that neurons work digitally. That is, there is a resting potential. This is an average voltage difference of 0 mV measured on both sides of the nerve cell membrane. When an information signal passes through the membrane of the nerve cell, a series of local potential changes passes through it. At these points, the resting potential changes to a so-called action potential, the average value of which is 30 mV . The cell has no choice, no way back. That is, if an action potential is triggered, the all-or-nothing law comes into effect. So when the process starts, it changes completely into an action potential and then back into a resting potential. This is welcome for us bioinformaticians, since the cell works roughly with discrete values. In other words, we can distinguish between a binary resting potential of 0 and an action potential of value

However, the information is carried by the frequency, which is basically an analog signal. And the frequency is not only affected by the information content. But it is influenced by many analogous processes. In other words, if there is a signal with a certain frequency, it is not certain that the same frequency will reach the central nervous system. A number of things influence this. The channels of the nerve cell membrane, the ions, the capacity of the sodium-potassium ion pump, responsible for recovery, the condition of the synapses, the amount of neurotransmitters, their release, their rate of elimination, etc. We also think differently when we are hungry, dehydrated, didn't get enough sleep, or drank alcohol, etc. In other words, we influenced the quality of neural information processes.

In the neural network, this can be modeled in many different ways. There are many theories about this. They are all different, try to model the processes of the living nervous system as best as possible. The more or the more typical physiological features are described with the models, the greater the analogy with the functioning of the living nervous system.

Our AI model system also searches for optimal solutions. Therefore, the weights between the nodes transmit an analog signal. These can be summed up, and the nodes only transmit signals above the threshold value.

We solved the visualization of many and fast analog signals with colors. Thus, during the operation of AI, we practically see the communication between neurons and its weight, that is, the strength of the analog signal, which is analogous to the signal frequency of the communication between neurons. It's like looking into the brain and seeing the thoughts. It's a stunning sight.

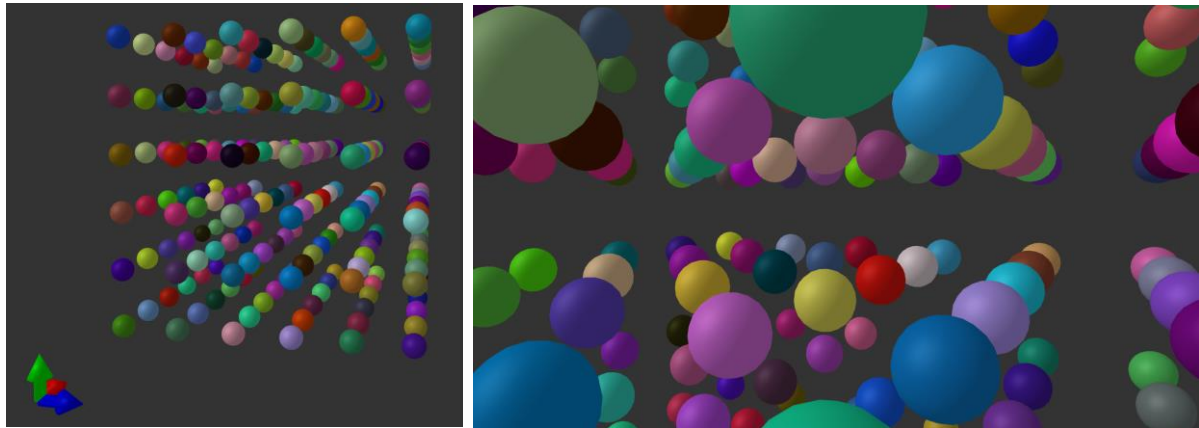


Figure 1 The colors of the analog signals running in the neural network

The visualization is performed by an independent software called visualiser. It is separate software because we have ensured the universality and free development of the system. The program is extremely close to hardware, made in the C programming language based on Linux and uses the OpenGL library. A file created in virtual memory is used for communication. The file contains exactly three times as many bytes as the number of nodes in the neural network. One node is described by three RGB bytes. The nodes can record True Color color values, that is, in principle, they can display 16.7 million analog values. The program reads the file at a very high speed and if there is a change in it, it is displayed immediately. Thus, we can create the AI neural network in any programming language.

We can operate it, store it, save it. But the visualization is solved by an independent program running in parallel. This makes the system very efficient and fast.

3.2.3. Results and Conclusions

It has proven to be a particularly effective tool in university education. University students can start their project work in the field of AI immediately and do not have to worry about complicated visualization. As soon as a network has been declared and the data has appeared in the array, the contents of the memory section can be paged out one by one into the file by writing a block. And the visualiser displays it immediately. The memory state of the three or more precisely four-dimensional arrays along with changes over time can be monitored in real time, and the processes can be visualised. Thus, they quickly gain a sense of success in AI programming and immediately see the results and continuous operation of their program. The visualiser provides extremely advanced visualization. The three-dimensional neural network object can be rotated as desired using the mouse. Furthermore, we can zoom in and get into its interior, as if we ourselves were tiny signs in a living brain. Meanwhile, signals are constantly rushing around us, from node to node. Informative for researchers and a fascinating sight for students. In this way, we also utilize its didactic significance.

4.1.2. Results and Conclusions

We did not upload the known connectomics of a living species into our neural network, but a fictitious initial connection system. Then we started teaching AI. We also tried to implement

learning in a model as close to life as possible. That's why we created the body of the beetle. This is still under development, but we are currently building a robot beetle controlled by Arduino microcontrollers and powered by servo motors. The outputs of the AI, which controls the muscles in the living nervous system, here the equivalent of the muscles are the motors. So the outputs move the beetle robot. The AI's inputs are the beetle's senses. In this case, a phototransistor, which is an analogue of the eye, an ultrasonic distance sensor and some vibration sensors, which represent the beetle's mechano-receptors.



Figure 1 Robot beetle

During the teaching process, reflexes can be built up with pleasant and unpleasant stimuli. Pleasant reinforcement is, for example, stroking, weak vibration. Unpleasant reinforcement is, for example, hitting the beetle, strong vibration on the vibration sensors, or for example, bright light on the phototransistors. So teaching AI is teaching a robot beetle. By stroking or beating with a stick. The independent movement resulting from the connector is confirmed or extinguished. This affects the AI system and relationships are built or broken because of it. Thus, AI is taught with a completely novel input. On the one hand, the system is much closer to living systems than previous learning mechanisms. On the other hand, the visualiser immediately shows the changes in the brain AI when the beetle is poked. That is, the rushing cavalcade of colors shows the analog signals running on nodes and weights. As we vexation the beetle, the operation and restructuring of the AI neuron network changes, which is immediately visible. This is a highly effective teaching and learning reinforcement for University students as well.

Further developments

We will supplement our system with a neural network built from real hardware. We are currently developing a real neural network built from $x \times x$ nodes. Here, the nodes are represented by STM32 microcontrollers and the weights are represented by the analog and digital data lines between them. Learning is provided by the use or inactivation of data lines by logically creating arbitrarily long data paths between nodes that are far from each other. We connect the hardware neural network with the software neural network. Thus, a neural network and the real neuron network will jointly form the AI.

discussions

We managed to create a visualization that can show the internal data flow of an analog neural network created in any programming language. We can track data traffic in real time, which is indicated by TrueColor colors. During the learning process, connections are built, rebuilt, or destroyed in the neural network. The change of AI can therefore be visualized in real time. During our current development, we modeled the brain of a fictitious beetle, which is similar to the connectomics of already known living nervous systems. So far, the nervous system of *Caenorhabditis Elegans* (*C. Elegans*), consisting of 302 neurons, has been fully modeled. The fruit fly's nervous system contains too many neurons in comparison. Our AI system controls a robot imitating a beetle with its output. The beetle's sensors correspond to living senses. Vibration, distance, and light sensors are input signals given to AI. We achieve the training of our system by vexating the beetle robot. That is, we caress or hit, which sends pleasant or unpleasant, i.e., strong or weak, vibration signals to the neural network. As a result, the neural network is rebuilt, which our visualization system makes immediately visible. The novel learning model is extremely spectacular and shows a closer analogy with living systems. The spectacular visualization and the visibility of the inner workings of AI have a great didactic value in the University Education of programming students. The closest possible analogy to living systems, such as connecting AI with a hardware neural network and teaching AI with reflexes, helps to build more natural artificial systems. We need to understand what phenomena in living systems are caused by connectomics alone and what carries the higher organization above the entity of living beings.

References

Boyle H, Berri Sand, Cohen N. 2022. Gait modulation in *C. elegans*: an integrated neuromechanical model. *Front. Comput. Neurosci.* 16:1033. doi: 10.3389/fncom.2022.1000030

Dorkenwald S, Matsliah A, Sterling AR, Schlegel P, Ulu SC, McEllar CE, et al. 2023. Neuronal wiring diagram of an adult brain. *bioRxiv* 2023.07.27.456144

Raphael Norman Tena, Erik Johnson, William R. Gray, Roncal. 2023. Training a neural model using the *C. elegans* connectome to perform exploration tasks. *Society for Neuroscience* 2023. URL: <https://www.huapl.edu/isc/publication/3>

Takemura S, et al. 2023. The Connectome of the Male *Drosophila* Ventral Nerve Cord. *bioRxiv* doi: <https://doi.org/10.1101/2023.07.04.543777> Timothy Busbice. 2024. Extending the *C. Elegans* Connectome to Robotics. *SOLID 2024 conference*. URL: <https://goo.gl/pxavv>

White G, Southgate E, Thomson N, and Brenner S. 1986. The structure of the nervous system of the nematode *Caenorhabditiselegans*. *Philos. Trans. R. Soc. Lond. B* 314:31-340. doi: 10.1098/rstb.1986.0086

Biometric Personal Classification by Signals in the AlexNet Method

Emre Kirilci¹, Mehmet Smailov², Ahmet Alpa³

Abstract Person classification systems are technologies developed to recognize individuals based on their physical or behavioral characteristics. These systems use features such as a person's fingerprint, face, iris structure, vein pattern, and speech. These features may be insufficient to protect personal data in terms of risks arising from information leakage, theft, fraud, or personal faults. For higher security, electrical signal-based bioelectric systems that include both biometric and behavioral features are needed. Bioelectrical signal measurements such as EEG and EMG allow for the obtaining of unique bioelectrical signatures that reflect the unique physiological characteristics of each individual. EMG signals include both conscious hand and wrist movements and the physiological characteristics of the person. These EMG signals are unique to each individual and can be identified using these features. In this study, it is aimed at identifying the person with the deep learning algorithm by determining the features in the EMG signals. In this study, the Gesture Recognition and Biometrics ElectroMyogram (GrabMyo) dataset from the open access PhysioNet database was used. A person recognition model was developed using the signals obtained from the fist movements of the hands of 10 different people with a 2-channel EMG device. The data were recorded with the EMG device for 10 seconds at a sampling frequency of 2048 Hz. Each person repeated the fist movement of the hand seven times. In this study, the Continuous Wavelet Transform (CWT) method was used to obtain the feature vector. The data obtained from each channel was divided into 100 ms (2048 samples) windows, and 10 scalogram images (227 x 227) were obtained. A total of 20 scalogram images were obtained from 2 channels, and a total of 10 scalogram images were obtained from one person since each person repeated the first movement seven times. The created scalogram images were classified using the AlexNET algorithm, one of the deep learning methods. In the model developed in the classification process, 80% of the dataset was used for training and 20% for testing. As a result of classification, 93% accuracy was found. The obtained results show that the proposed method can recognize people with high accuracy. It is thought that it can be widely used in financial instruments, military fields, telephones, and communication application areas that require a very high level of security.

Keywords EMG, Personal Classification, Continuous Wavelet Transform, AlexNet

¹**Address** ahramanmara S te mam University, Electrical Electronics Engineering Department, ahramanmara, T rkiye

²**Address** Adiyaman University, Electrical and Energy Department, Adiyaman, T rkiye

³**Address** ahramanmara S te mam University, Electrical Electronics Engineering Department, ahramanmara, T rkiye

* **Corresponding Author** mgursoy@adiyaman.edu.tr

1

Elektromiyografi (EMG) kasların elektriksel aktivitesini ölçmek için kullanılan bir testtir. Kaslarda kas lifleri elektriksel sinyaller üretir. EMG bu sinyalleri ölçerek kasların ne kadar iyi çalıştığını ve sinirlerin kaslara sinyal gönderip göndermediği hakkında bilgi verebilir. Phinyomark, Limsakul and Phukpattaranont (2017), Shin, Ung and Lim (2017). Elektro kaslar ve miyografi ise kasların aktivitesini ölçme anlamına gelir. EMG vücudtaki kasların kasılmalarını sırasında ettikleri elektriksel sinyalleri kaydederek ölçer. Kasların sinirler tarafından kontrol edilir ve sinirler kaslara beyinden gelen elektriksel sinyalleri ileterek onları hareket ettirir. EMG elektrot adı verilen küçük metal elektrotlar kullanılarak bu kaslardan elde edilen elektriksel sinyalleri kaydeder. Elektrotlar cilt yüzeyine yerleştirilir ve kaslardan gelen elektriksel aktiviteyi algılar. Başta Periferik nöropati, kas distrofisi, Miyoklonus, Titreme, Amyotrofik lateral skleroz, ALS, Polimiyozit, Romatoid artrit, kas yaralanmaları olmak üzere birçok hastalığın kullanılmaktadır. EMG bir nörolojik veya fizik tedavi uzmanı tarafından yapılmaktadır. Shioi et al. (2017), Taar (2022), Venugopalan et al. (2017).

İnternet sistemleri bir kişinin kimliğini doğrulamak için veya sınırlamak için kullanılan teknolojilerdir. Bu sistemler bir kişinin benzersiz fiziksel veya davranışsal özelliklerini kullanarak tanımlanmasını gerçekleştirir. İnternetin kullanılması farklı kimlik tanıma sistemleri türleri bulunmaktadır. Biyometrik Tanıma Sistemleri kişilerin

ben ersi fi iksel veya davran sal elli klerini kullanarak kimlik do rulama veya tan ma i lemidir Fan et al 2022 Lu et al 2020 Parmak i i tan ma y tan ma iris tan ma retina taramas parmak damar el geometrisi ses tan ma ve y r me biyometrisi gibi farkl biyometrik elli kler kullan larak ki iler tan n r

Tan ma Sistemleri tan ma sistemleri ki ilerini kullanarak kimlik do rulama veya tan ma i lemini ger ekle tiren bir biyometrik tan ma t r d r tan ma y n ben ersi elli klerini ve yap lar n kullanarak ki ileri s n fland r r veya e le tirir Parmak i Tan ma Sistemleri Parmak i i tan ma ki ilerini kullanarak kimlik do rulama veya tan ma yapar Parmak i leri parmaklar n d y eyindeki ben ersi desenler sayesinde her ki i i in farkl d r Sesi Tan ma Sistemleri Ses tan ma sistemleri ki ilerini sesini kullanarak kimlik do rulama veya tan ma i lemleri ger ekle tirir i ilerini konu ma tar lar ses tonlar ve di er ses elli kleri kullan larak ki iler tan n r Retina Tarama Sistemleri Retina tarama g n retina tabakas ndaki ben ersi damar desenlerini kullanarak ki i tan mada kullan lan bir biyometrik tan ma t r d r Parmak Damar Tan ma Sistemleri Parmak damar tan ma parmaklar n i y eyindeki damar desenlerini kullanarak kimlik do rulama veya tan ma yapar El Geometrisi Tan ma Sistemleri El geometrisi elin genel ekli ve parmaklar n u nluklar gibi elli klerini kullanarak ki ileri s n fland r r Gui et al 20 im and Pan 20 7 Lu et al 2020

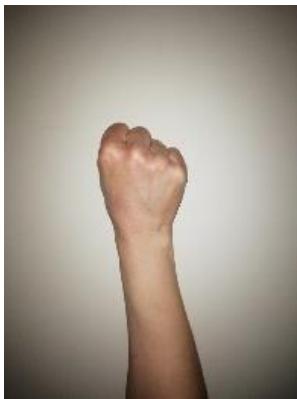
i i tan ma sistemleri g venlik eri im kontrol doland r c l k nleme ki i tan ma ve di er uygulamalarda kullan l r Ancak bu sistemlerin etik ve gi lilik konular g n nde bulundurularak uygulanmas nemlidir i sel verilerin g venli inin sa lanmas ve k t ama l kullan m n nlenmesi i in uygun nlemler al nmal d r

2 A A O

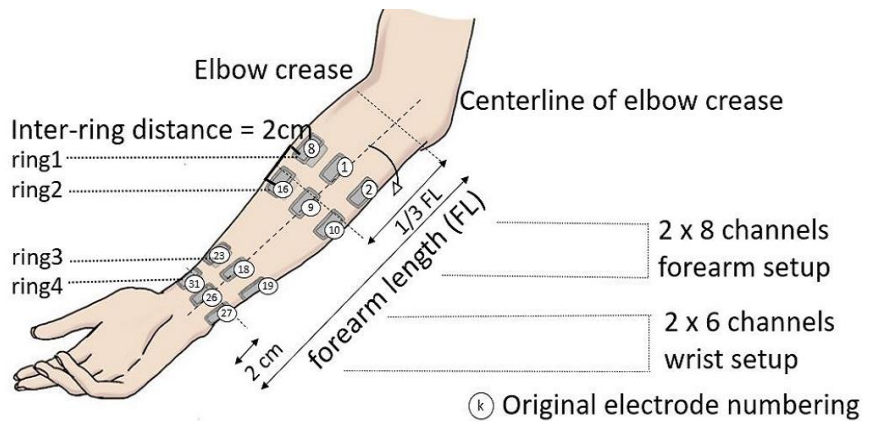
Bu al mada C Ty ntemi ile EMG sinyallerindeki elli k vekt r elde edlmi tir Bu elli k vekt rlerinin 227 x 227 boyutunda her bir ki iye ait 0 tane scalogram g r nt leri bulunmu tur Olu turulan scalogram g r nt leri derin renme y ntemlerinden AlexNET algoritmas kullan larak s n fland rma i lemi yap lm t r

2 1 eriseti

Bu al mada a k eriimli PhysioNet veritaban ndan Gesture Recognition and Biometrics electroMyogram GrabMyo veriseti kullan lm t r Pradhan He and iang 2022 0 farkl ki iden elin yumruk hareketlerinden 2 kanall kanal kol 2 kanal bilek EMG ciha ile elde edilen sinyalleri kullanarak ki i tan ma modeli geli tirilmi tir ekil EMG ciha ile veriler 204 H rnekleme frekans ile saniye s resince kaydedilmi tir ekil 3 Her ki i elin yumruk hareketini 7 defa tekrar etmi tir



a



b

ekil a Elin yumruk hareketi b EMG l m b lgeleri

Her kanaldan elde edilen veriler 00 ms 024 rnek pencerelelere ayr larak 0 tane 227 x 227 boyutunda scalogram g r nt s elde edildi 2 kanaldan toplam 2 0 scalogram g r nt s ve her ki i yumruk hareketini 7 defa tekrar etti inden bir ki iden toplam 0 scalogram g r nt s elde edildi Olu turulan scalogram g r nt leri Derin renme y ntemlerinden AlexNET algoritmas ile s n fland rma i lemi yap ld S n fland rma i leminde Geli tirilen modelde verisetinin 0 e itimi in 20 testi in kullan ld S n fland rma sonucunda 3 do ruluk bulunmu tur Elde edilen sonu lar nerilen y ntemin y ksek do rulukta ki i tan yabildi ini g stermektedir ok y ksek seviyede g venlik

gerektiren finansal ara larda askeri alanlarda telefon ve ileti im uygulama alanlar nda yayg n olarak kullan labilece i d n lmektedir

2.2 ti u us avelet ra s rm

Continuous avelet Transform C T bir sinyal veya aman serisi verisini farkl l eklerde anali etmek i in kullan lan bir aman frekans anali y ntemidir C T aman ve frekans bilgisini ayn anda elde edebilme yetene i sayesinde ba di er aman frekans d n mlerine g re avanta l d r C T nin temel amac sinyaldeki amanla de i en frekans bile enlerini belirlemektir Sinyaldeki farkl frekans bile enlerinin aman i indeki varl n ve iddetini a a karmak bir ok farkl uygulama i in nemlidir C T ellikle dura an olmayan ve aman i inde de i en sinyallerin anali inde faydal d r Lu et al 20 a 2020

Matematiksel olarak C T sinyali bir anali i levi olan dalgac kla wavelet s erek elde eder Dalgac k belirli bir ellik ve l ekte bir t r abl on i levi olarak d n lebilir Bu i lem sinyalin farkl aman noktalar nda dalgac kla apra korelasyonunu hesaplayarak ger ekle tirilir Bu apra korelasyon i lemi aman frekans u ay nda da l m elde etmek i in sinyalin farkl aman noktalar nda dalgac kla rt me d eyini l er Lu et al 20 b

$$CWT(a, b) = \int_{-\infty}^{\infty} x(t) \frac{1}{\sqrt{a}} \psi \left(\frac{t-b}{a} \right) dt$$

Burada x t giri sinyali ψ t wavelet fonksiyonu a kayd rma parametresi aman ve b l ek parametresi frekans temsil etmektedir

C T sinyallerin ve veri setlerinin amanla de i en elliklerini belirlemek g r lt leri gidermek s k t rma ve veri s k t rma ses ve g r nt i leme biyomedikal sinyallerin anali i ve di er e itli uygulamalarda kullan l r C T e itli dalgac k t rleri ve parametrelerle uygulanabilir ve anali edilen sinyalin elliklerine uygun olarak uyarlanabilir C T nin uygulamalar bilgi i lem m hendislik t p finans ve daha bir ok disiplinde geni bir yelpa ede bulunmaktad r G ne and Akkaya 2023

C T bir sinyali veya aman serisini farkl l eklerde anali etmek i in kullan lan bir aman frekans d n m y ntemidir Bu d n m sinyali bir anali i levi olan dalgac k wavelet ile s erek ger ekle tirilir Lu et al 2020

2.3 Ale

AlexNet 20 2 y l nda Alex ri hevsky Ilya Sutskever ve Geoffrey Hinton taraf ndan geli tirilen bir evri imli sinir a CNN mimarisidir ri hevsky Sutskever and Hinton 20 7 Bu mimari ImageNet Large Scale Visual Recognition Challenge ILSVRC yar mas nda b y k bir ba ar elde ederek derin renmenin pop ler hale gelmesine nemli katk da bulunmu tur Do an and T rko lu 20

AlexNet g r nt s n fland rma g revlerini ger ekle tiren bir derin renme modelidir Temel olarak bir evri imli sinir a d r ve verileri konvol syon aktivasyon fonksiyonlar havu lama pooling ve tam ba lant katmanlar kullanarak s n fland r r AlexNet nceki d nemlerdeki geleneksel s n fland rma y ntemlerine k yasla daha derin ve daha geni bir mimari kullanarak o d nem i in olduk a b y k ve ba ar l bir model olmu tur To a ar Ergen and yurt 2020

AlexNet in temel ellikleri unlard r

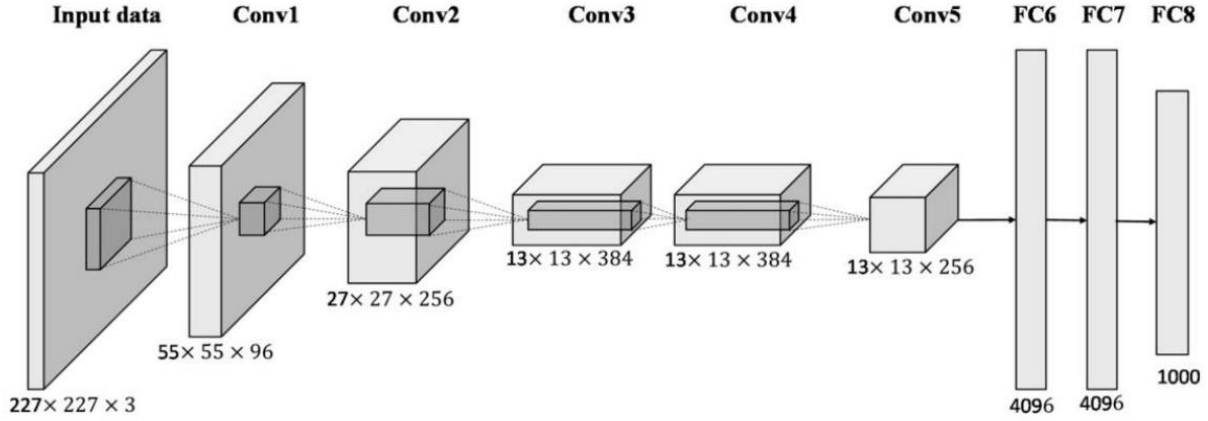
Evri im atmanlar Evri im katmanlar veriler erinde renilebilir filtrelerin uygulanarak ellik haritalar n n elde edilmesini sa lar Bu katmanlar g r nt deki nemli ellikleri alg lamak i in kullan l r

Aktivasyon Fonksiyonlar AlexNet evri im katmanlar n n ard ndan ReLU Rectified Linear Unit aktivasyon fonksiyonunu kullan r ReLU do rusal olmayan bir aktivasyon fonksiyonudur ve a n non lineer elliklerini renmesine yard mc olur

Havu lama atmanlar Havu lama katmanlar boyut a altma ve invaryans de i me lik sa lamak i in kullan l r AlexNet maksimum havu lama max pooling kullanarak boyut a altma i lemi yapar

Tam Ba lant atmanlar Son evri im katmanlar n n ard ndan tam ba lant fully connected katmanlar kullan l r Bu katmanlar s n fland rma i in ellikleri birle tirir ve son kt lar elde eder ri hevsky et al 20 7

AlexNet ImageNet veri k mesinde 000 farkl nesne s n f n tan mak i in e itilmi tir ve o d nemdeki di er y ntemlere g re b y k bir performans art sa lam t r ri hevsky et al 20 7 Ayr ca AlexNet derin renmenin pop lerli ini art rm ve g n m de kullan lan bir ok derin renme modelinin temelini olu turmu tur ekil 2

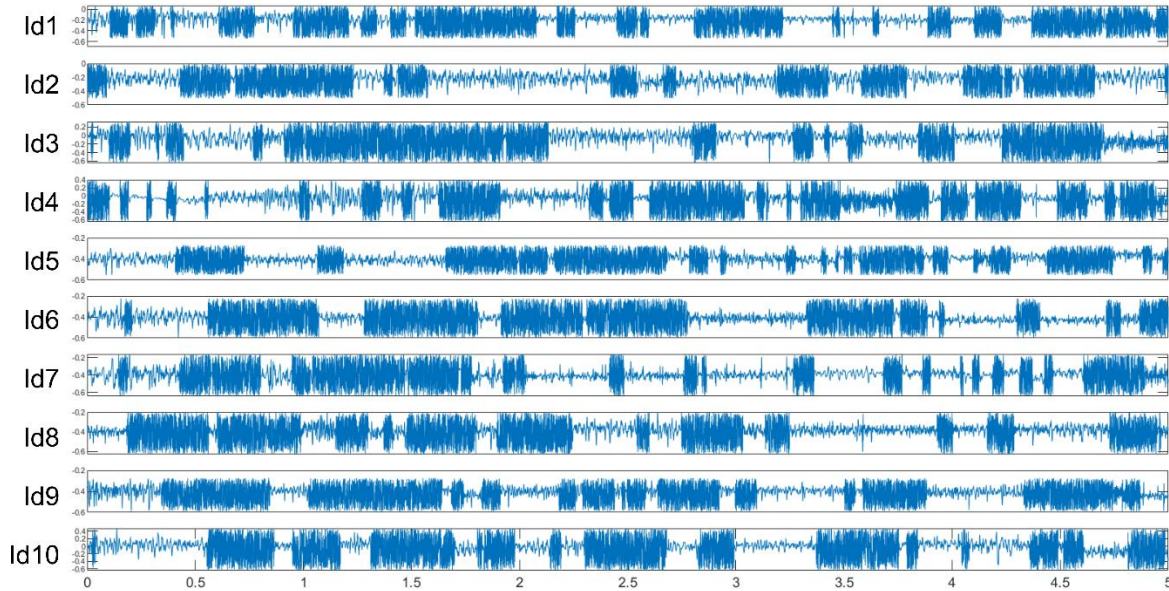


ekil 2 AlexNet derin renme mimarisi Do an and T rko lu 20

3 A

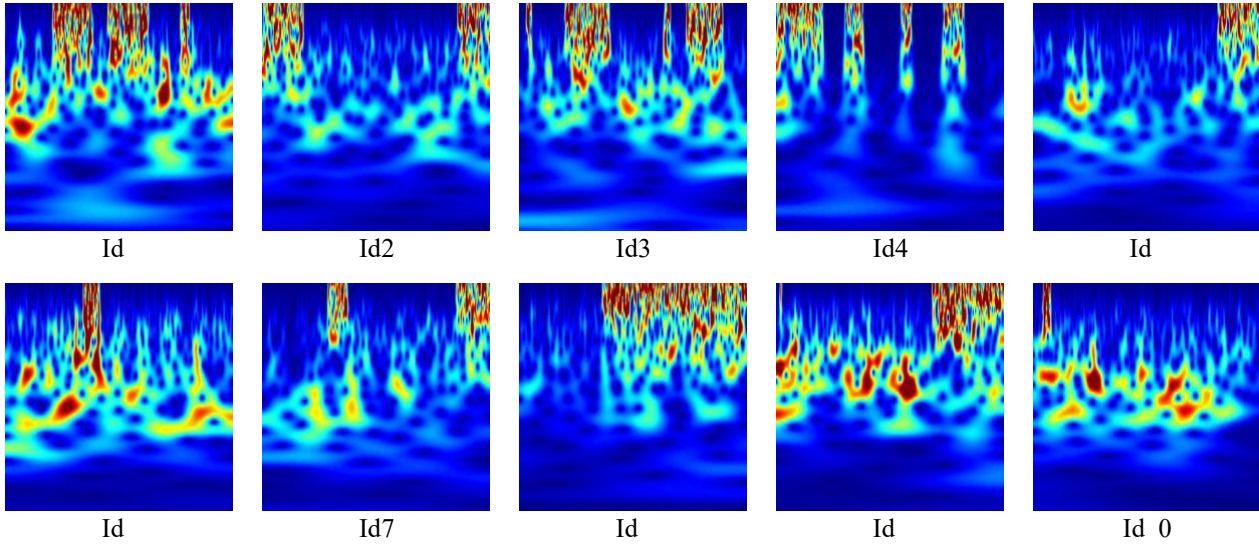
Bu al mada geli tirilen model MATLAB program ile geli tirilmi tir indows i letim sistemi ile IntelCore i7 2 2 GH i lemci ve 32 GB RAM elliklerine sahip bilgisayar kullan lm t r

A k eri imli PhysioNet veri taban ndan Gesture Recognition and Biometrics ElectroMyogram GrabMyo veri seti kullan ld umruk hareket r nt s i in 0 s n fl ki i tan ma problemi olu turuldu ullan lan 2 kanall EMG ciha ile 0 farkl ki inin ellerinin yumruk hareketlerinden elde edilen sinyaller ekil 3 de g sterilmektedir



Zaman (saniye)
 ekil 3 0 ki iye ait EMG sinyalleri

Her bir g n ll den elde edilen saniye u nlu undaki sinyaller 2 0 ms lik 2 rnek pencerelelere ayr ld Her bir penceredeki veriler C T y ntemi ile anali edilerek 227 x 227 boyutunda skalogram g r nt leri olu turuldu ekil 4



ekil 4 Bilek hareketlerinin skalogram g r nt leri

C T y ntemi ile olu turulan skalogram g r nt leri Derin renme y ntemlerinden AlexNET algoritmas ile sn fland rma i lemi yap lm tr Veri setinin 0 e itim ve kalan 20 k sm testi lemi i in ayr lm tr AlexNET algoritmas nda e itim fonksiyonu i in adam fonksiyonu kullan ld Toplam 0 epoc ile e itim i lemi tamamland Sn fland rma i lemi sonucunda 3 do ruluk oran ile sonu lar elde edildi Sn fland rma i lemi sonucunda elde edilen kar kl k matrisi confusion matrix ekil de g sterilmektedir

		Confusion Matrix											
		0	1	3	0	2	1	2	0	1			
Output Class	ID1	339 8.6%	0 0.0%	1 0.0%	3 0.1%	0 0.0%	2 0.1%	1 0.0%	2 0.1%	0 0.0%	1 0.0%	0 0.0%	97.1% 2.9%
	ID10	0 0.0%	374 9.5%	7 0.2%	5 0.1%	0 0.0%	4 0.1%	5 0.1%	5 0.1%	2 0.1%	3 0.1%	0 0.0%	92.3% 7.7%
	ID2	7 0.2%	2 0.1%	372 9.5%	1 0.0%	3 0.1%	6 0.2%	3 0.1%	3 0.1%	2 0.1%	5 0.1%	0 0.0%	92.1% 7.9%
	ID3	1 0.0%	1 0.0%	0 0.0%	360 9.2%	0 0.0%	4 0.1%	2 0.1%	0 0.0%	0 0.0%	3 0.1%	0 0.0%	97.0% 3.0%
	ID4	0 0.0%	0 0.0%	0 0.0%	2 0.1%	375 9.6%	1 0.0%	1 0.0%	1 0.0%	5 0.1%	2 0.1%	0 0.0%	96.9% 3.1%
	ID5	8 0.2%	1 0.0%	2 0.1%	4 0.1%	3 0.1%	360 9.2%	1 0.0%	5 0.1%	5 0.1%	1 0.0%	0 0.0%	92.3% 7.7%
	ID6	5 0.1%	1 0.0%	4 0.1%	2 0.1%	3 0.1%	2 0.1%	375 9.6%	2 0.1%	7 0.2%	3 0.1%	0 0.0%	92.8% 7.2%
	ID7	4 0.1%	5 0.1%	3 0.1%	9 0.2%	0 0.0%	1 0.0%	0 0.0%	363 9.3%	4 0.1%	3 0.1%	0 0.0%	92.6% 7.4%
	ID8	9 0.2%	0 0.0%	1 0.0%	3 0.1%	5 0.1%	5 0.1%	0 0.0%	3 0.1%	363 9.3%	2 0.1%	0 0.0%	92.8% 7.2%
	ID9	19 0.5%	8 0.2%	2 0.1%	3 0.1%	3 0.1%	7 0.2%	4 0.1%	8 0.2%	4 0.1%	369 9.4%	0 0.0%	86.4% 13.6%
		86.5% 13.5%	95.4% 4.6%	94.9% 5.1%	91.8% 8.2%	95.7% 4.3%	91.8% 8.2%	95.7% 4.3%	92.6% 7.4%	92.6% 7.4%	94.1% 5.9%	93.1% 6.9%	
		ID1	ID10	ID2	ID3	ID4	ID5	ID6	ID7	ID8	ID9		
		Target Class											

A A

Bu al mada elin yumruk hareketi s ras nda kaydedilen EMG sinyallerini kullanarak ki i tan ma i in renme tabanlı bir yakla m geli tirilmi tir nerilen modelde yumruk hareketi s ras nda kolda olu an EMG sinyallerinin ki i tan ma problemlerinde y ksek do rulukta sonu lar elde etti i g sterilmi tir C T y ntemi ile elde edilen ellik vekt r derin renme algoritmalar ndan AlexNET y ntemi ile 3 sn fland rma ba ar s sa lam tr Bu sonu lar do rusal olmayan EMG sinyallerinin fi yolo ik ve davran sal biyometrik ki i tan ma probleminin ba ar s n g sterilmektedir i inin davran sal yumruk hareketi ile kol ve bilek kaslar nda meydana gelen fi yolo ik EMG elektriksel sinyallerin ba kalar taraf ndan kopyalanama olmas y ksek g venlik gerektiren durumlarda ok y ksek g venlik sa layaca d n lmektedir

ti Kurul O ayı

N A

İlkar Atışması

araştırmacıların beyan edecekleri karıştırmaları yoktur

Finansal deste

araştırmacıların bu alanın herhangi bir maddi destek almadığını beyan etmişlerdir

KAĞIT AKIŞI

- Doğan Ferdi and Ibrahim Tırkoğlu 2022 Derin öğrenme Algoritmalarının Karşılaştırılması: Sınıflandırma Başarımlarının Karşılaştırılması The Comparison Of Leaf Classification Performance Of Deep Learning Algorithms *Molecular Plant-Microbe Interactions* 22 2 23
- Fan Jiahao, Inyuan Jiang, Yangu Liu, Jianhao Lin, Ming Chen, Yun Dai, Metin Akay and Fei Chen 2022 Cancelable HD SEMG Biometric Identification via Deep Feature Learning *IEEE Journal of Biomedical and Health Informatics* 24 7 2331 doi: 10.1109/BHI.2023.10474
- Gui Jiong, Maria V. Rui, Blondet Sarah, Laslo and Hanpeng Lin 2022 A Survey on Brain Biometrics *ACM Computing Surveys* doi: 10.1145/323032
- Güneş Harun and Abdullah Erhan Akkaya 2023 Using Wavelet Analysis and Deep Learning for EMG Based Hand Movement Signal Classification *Sakarya University Journal of Science* 27 2 42 doi: 10.15014/SAUFENBILDER.2023.74
- Limin Su and Sung Bum Pan 2023 A Study on EMG Based Biometrics *Journal of Internet Services and Information Security (JISIS)* 7 2 3 doi: http://dx.doi.org/10.2277/ISIS.2023.7.2.3
- Rihevsky Alex, Ilya Sutskever and Geoffrey E. Hinton 2023 ImageNet Classification with Deep Convolutional Neural Networks *Communications of the ACM* 64 0 4303 doi: 10.1145/36033
- Lu Li, Ingnan Mao, Uiyang Guangxin, Ding and Hiwei Hang 2023 An EMG Based Personal Identification Method Using Continuous Wavelet Transform and Convolutional Neural Networks Pp. in *BioCAS 2019 - Biomedical Circuits and Systems Conference, Proceedings* IEEE
- Lu Li, Ingnan Mao, Uiyang Guangxin, Ding and Hiwei Hang 2023 An EMG Based Personal Identification Method Using Continuous Wavelet Transform and Convolutional Neural Networks *BioCAS 2019 - Biomedical Circuits and Systems Conference, Proceedings* 3 34 doi: 10.1109/BIOCAS.2019.230
- Lu Li, Ingnan Mao, Uiyang Guangxin, Ding and Hiwei Hang 2023 A Study of Personal Recognition Method Based on EMG Signal *IEEE Transactions on Biomedical Circuits and Systems* 4 4 doi: 10.1109/TBCAS.2020.3004
- Phinyomark A., C. Limsakul and P. Phukpattaranont 2023 Application of Wavelet Analysis in EMG Feature Extraction for Pattern Classification *Measurement Science Review* 24 2 42 doi: 10.2478/v10040-020-0009-y
- Pradhan Ashirbad, Jiyuan He and Ning Jiang 2022 Multi Day Dataset of Forearm and Wrist Electromyogram for Hand Gesture Recognition and Biometrics *Scientific Data* 10 doi: 10.1038/s41598-022-03170-3
- Shin Siho, Aehyo Jung and Joun Tae Lim 2023 A Study of an EMG Based Authentication Algorithm Using an Artificial Neural Network *Proceedings of IEEE Sensors* 2023 Decem 3 doi: 10.1109/ICSENS.2023.10234
- Shiohira Ryohei, Shinichi Ito, Momoyo Ito and Minoru Fukumi 2023 Personal Authentication Based on Wrist EMG Analysis by a Convolutional Neural Network Pp. 2 in *5th IIAE International Conference on Intelligent Systems and Image Processing*
- Taibeyda 2022 Deep Biometric Identification Method Using Forearm Electromyography Signal *Arabian Journal for Science and Engineering* doi: 10.1007/s33022-020-0
- Toğar Mesut, Burhan Ergen and Fatih Yurt 2020 EvrimSEL Sinir Ağ Modellerinde Etkinlik Seviyelerini Ullanarak İki Grubun Terinin Sınıflandırılması *Firat Üniversitesi Mühendislik Bilimleri Dergisi* 32 47 doi: 10.3234/fumbd.2023.7330
- Venugopalan Shreyas, Felix Uefei, Benjamin Cowley and Marios Savvides 2023 Electromyograph and Eye-tracking Dynamics for Spoof Resistant Biometric Authentication *IEEE Computer Society Conference on Computer Vision and Pattern Recognition Workshops* 2023 Octob 0 doi: 10.1109/CVPRW.2023.73032

Thermodynamic analysis of a geothermal energy driven combined cycle power plant for clean water production

Fatih Ilmaz^{*1}

Abstract Geothermal energy is gaining importance day by day because it is an energy source that is least affected by environmental impacts among renewable energy sources. In this work, a comprehensive thermodynamic examination of a geothermal energy assisted combined system for clean water, power, and heating generation purposes is presented. This study mainly consists of a flash Binary power plant. As a subsystem, the secondary system consists of an organic Rankine cycle and a reverse osmosis unit (RO) for clean water production. In addition, a comparison of the efficiency with different refrigerants is carried out. The irreversibility occurring in the systems are determined and the parameters affecting the system performance change are analysed by parametric analyses. According to the analysis results, it has a net power generation capacity of 07 kW. In addition, the total hot water production capacity is determined as 4 kW. Moreover, the energy performance of the whole system is calculated as 0.70 and the exergy performance as 2.00.

Keywords Geothermal energy, Organic Rankine cycle, Reverse osmosis, Exergy analysis

¹Address: Department of Mechatronics Engineering, Faculty of Technology, Isparta University of Applied Sciences, Isparta, Turkey

*Corresponding author: fatiyilma7@gmail.com

1. Introduction

Energy usage is one of the key indicators showing countries' development level and societies' living standards. Population growth, urbanization, industrialization, and technological development straight enlargement energy consumption. This increase has led to environmental problems in parallel. Currently, about 60% of electricity is still generated from fossil fuels (Aushik et al., 2020). Therefore, the use and production of energy is one of the most important environmental issues and one of the most important ways to overcome environmental problems is renewable energy sources. Renewable energy sources are depicted that solar, biomass, hydraulic, wind, and geothermal sources. Among these energy sources, geothermal energy is contained as thermal energy in the earth's interior. The source of this heat is linked to the internal structure of our planet and the physical processes that occur there (Barbier, 2002). Moreover, among these resources, electricity generation from geothermal energy has a significant potential for Turkey. It can be applied for purposes such as electricity, heating, and cooling, as well as being the oldest renewable energy source. Today, the most mutual technique is the low-temperature Flash Binary power generation system (Ilmaz, 2020).

The use of the geothermal energy in the diverse combined systems for beneficial products also affects the method to be switching a clean and sustainable future. Herein, the geothermal energy powered combined plant comes to the fore. In the open literature, there are several papers about geothermally driven integrated plants. Anoglu et al. (2010) investigated a geothermally driven plant with a PEM unit for the generation of hydrogen. They investigated the performance of the model including energy and exergy performance methods. The exergy efficiency of their plant, Case 1, is determined as 2.00. The author (Ilmaz, 2022) proposed a geothermal driven multigeneration plant for the production of beneficial products. The paper is investigating a thermodynamic and environmental assessment. Total energy and exergy efficiency are determined as 2.00 and 2.40, respectively. Furthermore, in 2023, Vaccari et al. (2023) examined a geothermal plant in terms of environmental performance for different configurations. Also, Huang et al. (2023) developed a single flash geothermal power plant that includes transcritical CO₂. They computed that the total plant's exergetic efficiency is figured as 32.4%. Continue Guler et al. (2023) designed and developed a geothermal energy driven power plant that advanced exergoeconomic analysis method. They found the cost per CO₂ emission of the system as 0.04 \$/kWh.

As shown in the short literature investigation of the above mentioned the different design of geothermal energy based power plant has gained more and more importance day by day for acquiring more power and more efficiency. The proposed paper investigates the thermodynamic performance analysis of the flash Binary geothermal plant for producing power, heating, and fresh water. To generate these valuable outputs, a system is designed and then the overall system is examined with energetic and exergetic efficiencies methods.

2 A A A HO

In this developed study, a geothermal energy supported system was designed and then a comprehensive thermodynamic analysis was carried out. The system definition and analysis method will be mentioned in the subsections.

2.1 System description

The developed geothermal energy based cycle, which is exemplified in Figure 1, is proposed and analyzed. The system is made up of the main four sub-cycles which are a geothermal cycle, ORC, RO, and domestic water preparation.

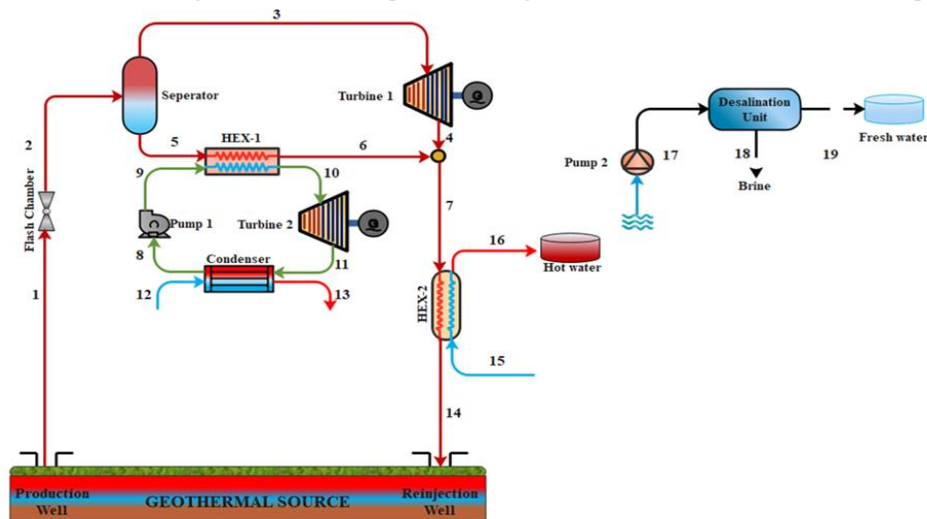


Figure 1 Representation plan of the developed system

Briefly, geothermal energy from underground enters the flash chamber and comes to the separator as a steam-water mixture. Then, in the separator, the saturated steam (point 3) and the saturated liquid separate at point 4 and go to the subsystems. Steam expands in Turbine 1 and electricity generation occurs. The geothermal source at point 1 provides the necessary thermal energy for the R-34a fluid ORC system, and the ORC system operates. In the hot water preparation unit, it is possible to produce hot water between 40–60 °C for domestic applications. Finally, clean water is obtained with the RO unit. The whole system continues to work simultaneously.

2.2 Thermodynamic performance analysis

In this developed study, a detailed thermodynamic performance investigation is conducted and analyzed using the energy and exergy efficiency methods. Generally, a thermodynamic analysis employed general four balance equations which are mass, energy, entropy, and finally exergy. These thermodynamic balance formulations can be depicted below (Cengel and Boles, 2002; Bejan et al., 2009; Dincer, 2020).

$$\sum \dot{m}_i = \sum \dot{m}_e \tag{1}$$

$$\sum \dot{m}_i h_i + \sum \dot{Q}_i + \sum \dot{W}_i = \sum \dot{m}_e h_e + \sum \dot{Q}_e + \sum \dot{W}_e \tag{2}$$

$$\sum \dot{m}_i s_i + \sum \left(\frac{\dot{Q}_i}{T} \right) + \dot{S}_{gen} = \sum \dot{m}_e s_e \tag{3}$$

$$\sum \dot{m}_i ex_i + \dot{E}x_i^Q + \dot{E}x_i^W = \sum \dot{m}_e ex_e + \dot{E}x_e^Q + \dot{E}x_e^W + \dot{E}x_D \tag{4}$$

In these formulations the subscripts i and e define the inputs and outputs of the system components. Then the terms h , s , \dot{Q} and \dot{W} represent specific enthalpy, specific entropy, heat transfer and work respectively. The terms $\dot{E}x^Q$, $\dot{E}x^W$ and ex in Equation 4 are work heat and specific exergies and can be formulated as follows:

$$\dot{E}x^Q = \left(1 - \frac{T_0}{T_k}\right) \dot{Q}$$

$$\dot{E}x^W = \dot{W}$$

The specific exergy can be written as below after disregarding the potential and kinetic energy terms:

$$ex = (h - h_0) - T_0(s - s_0) + ex_{ch}$$

herein the ex_{ch} terms define the chemical exergy. To sum up, the thermodynamic efficiencies can be modeled as:

$$\eta_{sys} = \frac{\dot{W}_{net} + \dot{Q}_{hot\ water} + \dot{m}_{fw} h_{fw}}{\dot{m}_1 h_1 - \dot{m}_{14} h_{14}}$$

$$\psi_{sys} = \frac{\dot{W}_{net} + \dot{E}x_{hot\ water} + \dot{m}_{fw} ex_{fw}}{\dot{m}_1 ex_1 - \dot{m}_{14} ex_{14}}$$

3 S S A S S O

To perform the thermal performance examination of this paper, the Engineering Equation Solver (EES) program is employed and also some acceptance is presented in Table . Moreover, this study is modeled as steady state flow condition. Kinetic and potential energy changes are ignored. Pumps and turbines have isentropic efficiency and the heat loss between plant's apparatuses and the environment is neglected. In light of Table assumption and inputs values, the analysis base case results are tabulated in Table 2. Based on herein values, the system net power production load is M and the freshwater generation rate is 4 kg/s respectively. Also, total system energy and exergy efficiencies are determined as 0 and 20 .

Table The design parameters and input variables for the developed system

arameters	alue	it
P_1	00	°C
T_1	0	kPa
\dot{m}_{geo}	00	kg/s
r_{pFC}	3	
$\eta_{is,T1}$		%
$\eta_{is,P1}$	2	%
orking fluid	R 34a	
ε_{HEX}	0	%
T_{17}	30	°C
P_{17}	0 32	kPa
Sea water salinity rate	42000	ppm
Freshwater salinity rate	0	ppm
Brine salinity rate	70000	ppm
Pinch point temperature	0	°C
T_0	0	°C
P_0	0 32	kPa

Table 2 Thermodynamic analysis results of the developed geothermal power plant

arameters	alue
\dot{W}_{T1}	04 k
\dot{W}_{T2}	2 7 k
\dot{W}_{net}	07 k
\dot{m}_{fw}	4 kg/s
$\dot{Q}_{heating\ load}$	4 k
η_{SG}	7 %
η_{sys}	0 %
ψ_{SG}	23 %
ψ_{sys}	2 0 %

After the given case study results there are some parametric studies are also conducted and presented here Figure 2 illustrates the impact of geothermal temperature on the net power rate It is noted that the net power rate rises with the geothermal temperature Looking at another perspective Figure 3 presents the variation in the heating and freshwater rate versus geothermal source temperature Finally the effect of the geothermal source temperature on the plant efficiency is also given in Figure 4 To sum up the geothermal temperature on the plant products and performance has a positive effect which increases both system performance and generated products

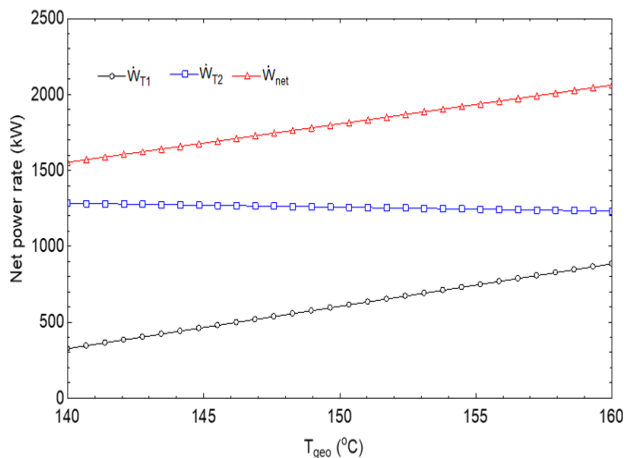


Figure 2 Variation of net power rate with a different geothermal source temperature

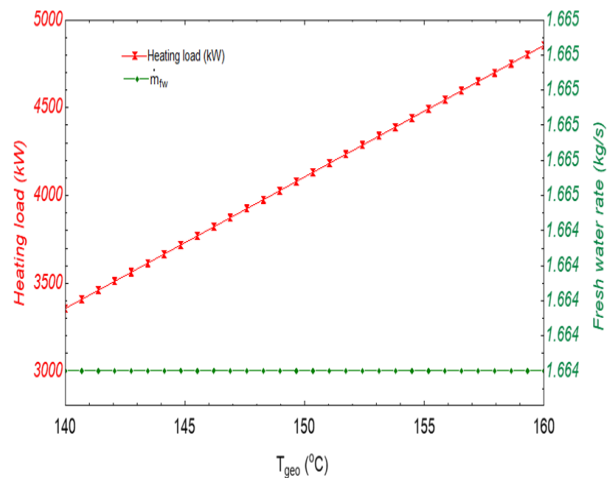


Figure 3 Variation of heating load and freshwater rate with a different geothermal source temperature

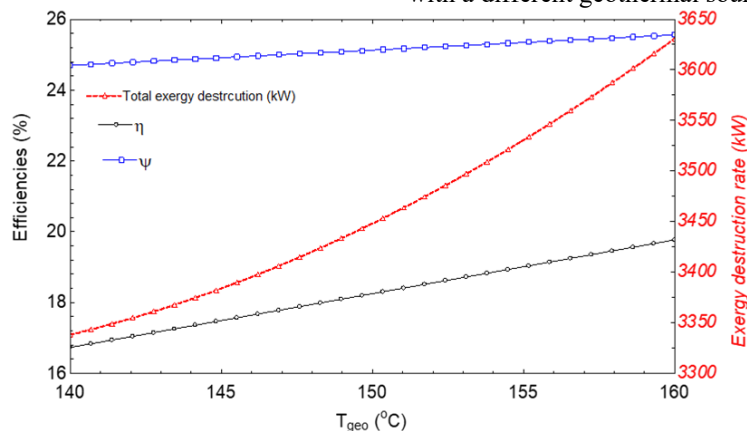


Figure 4 Variation of efficiencies and irreversibility rate with a different geothermal source temperature

Another important factor is the geothermal source capacity which is the mass flow rate Increasing the geothermal capacity from 0 kg s to 20 kg s leads to an increase in the generated heat and freshwater capacities as shown in Figure and also increases the system performance Figure As indicated in Figure the heating load is increased

linearly however the fresh water is not increased linearly the plant s energetic and exergetic efficiencies are directly goes up with the capacity increase as indicated in Figure

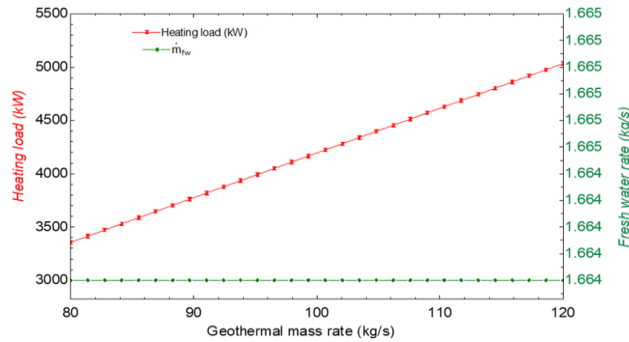


Figure The effect of geothermal capacity on heating and fresh water rate

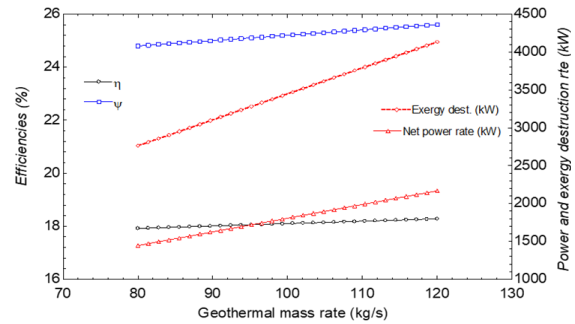


Figure The influence of geothermal capacity on efficiencies and products of the overall system

Figure 7 and Figure examine the effects of the increase in steam quality going to the separator on the system According to Figure 7 since the increase in steam quality is directly related to the mass flow to the subsystems the amount of power produced increases in Turbine and decreases in Turbine 2 But as a result net production increases Figure presents the total system efficiency and exergy destruction variation according to steam quality As a result of the increase in system efficiency the total exergy destruction decreases

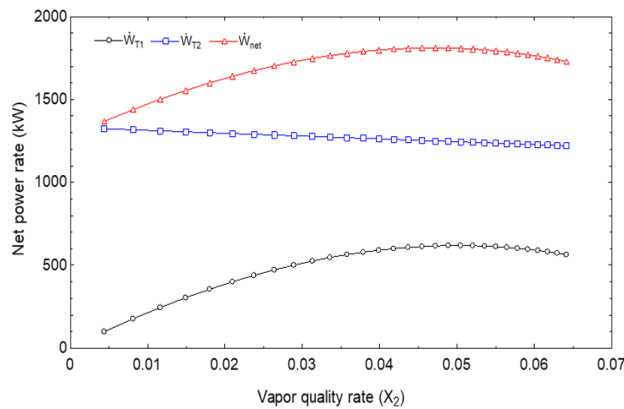


Figure 7 Net power rates varying against vapor quality ratio

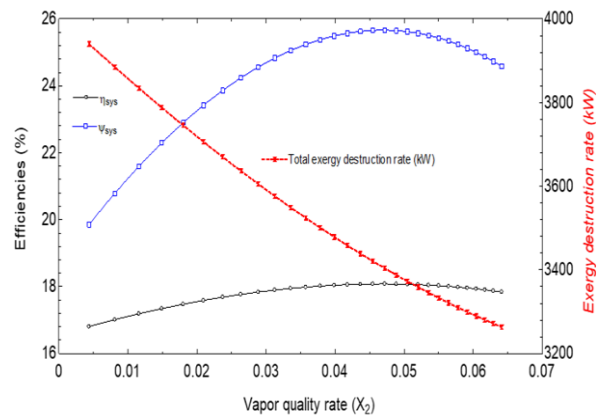


Figure Overall system efficiencies and irreversibility rate varying against vapor quality ratio

Finally the system performances of the power only single generation SG and trigeneration system electricity clean water and heating are compared and revealed in Figure As seen in the figure the whole system is more efficient than single systems Therefore it is possible to achieve higher efficiency by designing geothermal energy systems with low efficiencies for multiple generation purposes

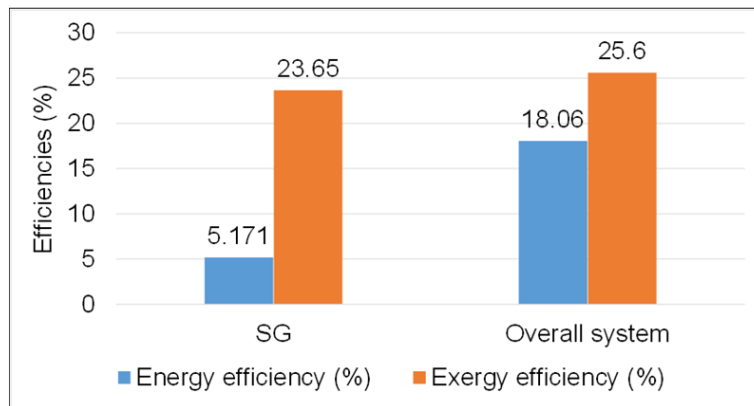


Figure Performance comparison of SG and total plant

O S O

In this designed study a thermodynamic performance investigation of the geothermal energy supported integrated system for power heating and clean water production is carried out To determine the system performance parametric studies are carried out by applying both energy and exergy efficiency methods Some important results that emerged as a result of the examination findings can be written as

The net power production is calculated as 07 k In addition the net domestic hot water production capacity was determined as 4 k

The clean water production capacity of this system is 4 kg s

The energetic and exergetic efficiencies for the total model are figured as 0 and 2 0

It has been determined that both the increase in geothermal temperature and the rise in geothermal capacity have a positive impact on the plant s performance

The increase in steam quality also increases the system s performance

F S

Barbier E 2002 Geothermal energy technology and current status an overview *Renewable and sustainable energy reviews* 6 2 3

Be an A George T Moran M Thermal design and optimi ation iley

Cengel A Boles MA Thermodynamics an engineering approach th ed Mc New ork McGraw Hil 20 20

Dincer I Thermodynamics A Smart Approach USA ohn iley Sons Ltd 2020

G ler O V G rb E Georgiev A G e eba A 2023 Advanced Exergoeconomic Assessment of CO2 Emissions Geo Fluid and Electricity in Dual Loop Geothermal Power Plant *Energies* 16 34

Huang Abed A M Eldin S M Aryanfar Garc a Alcara L 2023 Exergy analyses and optimi ation of a single flash geothermal power plant combined with a trans critical CO2 cycle using genetic algorithm and Nelder Mead simplex method *Geothermal Energy* 11 20

anoglu M Bolatturk A ilma C 20 0 Thermodynamic analysis of models used in hydrogen production by geothermal energy *International journal of hydrogen energy* 35 7 3 7

aushik S C Reddy V S Tyagi S 20 Energy and exergy analyses of thermal power plants A review *Renewable and Sustainable energy reviews* 15 4 7 72

Vaccari Marco et al Rigorous simulation of geothermal power plants to evaluate environmental performance of alternative configurations *Renewable Energy* 207 2023 47 4 3



ilma C 20 Thermo-economic cost analysis and comparison of methodologies for Dora II binary geothermal power plant *Geothermics* 75 4 7

ilma F 2022 Development and modeling of the geothermal energy based multigeneration plant for beneficial outputs Thermo-economic and environmental analysis approach *Renewable Energy* 189 074 0

İncidere Yetimhanesi'nin Korunması ve Restorasyonu

Şirvan Zengin^{*1}, Çağrı Mihri²

Abstract Historical buildings are documents that help us understand the architectural features, social and economic status, culture, and values of the society in which they were built and help us establish a connection between the past and the present. To ensure physical and cultural continuity, it is important to understand and evaluate the values of cultural heritage.

The documentation of cultural heritages constitutes the beginning of the conservation activities. The documentation studies include the recording of the current station of the heritage and demonstrate the original values and the periods and stages that the building has undergone. Documentation of cultural heritages constitutes a source for archive studies and is important for the accessibility of heritages and for the management and supervision of activities that will affect cultural heritage in the future with information.

This study includes documentation studies, surveys, restitution, and restoration decisions of Dar-ı Leytam of İncidere. The building located in İncidere town of Kayseri, including its architectural structure, physical condition, materials, and construction techniques. The building is one of the dar-ı leytams established in many cities of Anatolia, especially in Istanbul, to shelter orphaned children and to provide them with a profession to bring them into society with the rapid increase in the number of orphans in a very short time after the Balkan Wars and World War I. The building was one of the 3 dar-ı leytams in Kayseri. The study aims to transfer the building to the future, to participate in modern life, and to set an example for similar studies.

Keywords Conservation, Dar-ı Leytam, Orphanage, İncidere

¹Araştırma Gözetmeni, Erciyes University, Faculty of Architecture, Kayseri, Türkiye

²Araştırma Gözetmeni, Erciyes University, Faculty of Architecture, Kayseri, Türkiye

* İletişim Bilgisi: buscagli@ulakbim.gov.tr

1. GİRİŞ

Kayseri'deki Talas İlçesi İncidere Mahallesi Hürriyet Sokak'ta yer almaktadır. Yapının kitabesi bulunmamaktadır. İncidere Belediyesi tarafından 7 Aralık 1922 tarihli 2 sayılı karar ile okulda kullanılan mekânın unvanı ve diploma tescilinin iptaliyle yapıya yeni bir ismi verilmesi için Miss Griber tarafından yetimhane olarak yaptırıldığı bilgisi aktarılmıştır. İncidere Belediyesi tarafından 2017 yılında Miss Griber ismiyle bahsedilen kentin Maria Gerber oldu. Bu yapı, Miss Maria Gerber tarafından Türkiye'de bulunduğu dönemde kaleme alınan kitapta Kayseri yakınlarında yer alan İncidere'deki İncidere Yetimhanesi'nin inşaatına 1904 yılında başlanıp ve 2 yıl içinde tamamlandığı belirtilmektedir. Gerber tarafından yetimhane olarak inşa edilen yapı, Eski Eserler ve Mimarlar Genel Müdürlüğü tarafından 23.03.2003 tarih ve 33/7 envanter numaralı karar ile tescillenmiştir.



Figure 1. İncidere yetimhanesi yapısının 2024 yılına kadar Ali Peker tarafından

etimhane geni bir arazi iinde in a edilmi olup in a edildi i arazi nin etraf ihata duvar ile evrenmi tir Arazinin ku eyinde g n m e gelememi ama rhane yap s ve bir d nem ce aevi olarak kullan lan yatakhane binas bu binan n ku eyinde g n m e gelebilmi olan tescilli bir hamam yurdu n ku eybat s nda muhdes su deposu ve g neydo usunda tek katl m temilat yer almaktadr ap n n iinde yer ald ara ide g ney cephenin a ld avlunun ku eybat duvar nda yuvarlak kemerli bir e me avlunun g neyinden basamak ile k sa lanan ta d emeli bir merasim alan ve merasim alan n n ku eyinde b st g n m e gelememi olan b st kaidesi merasim alan n n g neyinde seki gen planl havu ve havu un da g neyinde a a land r lm geni bir alan bulunmaktadr Figure 2

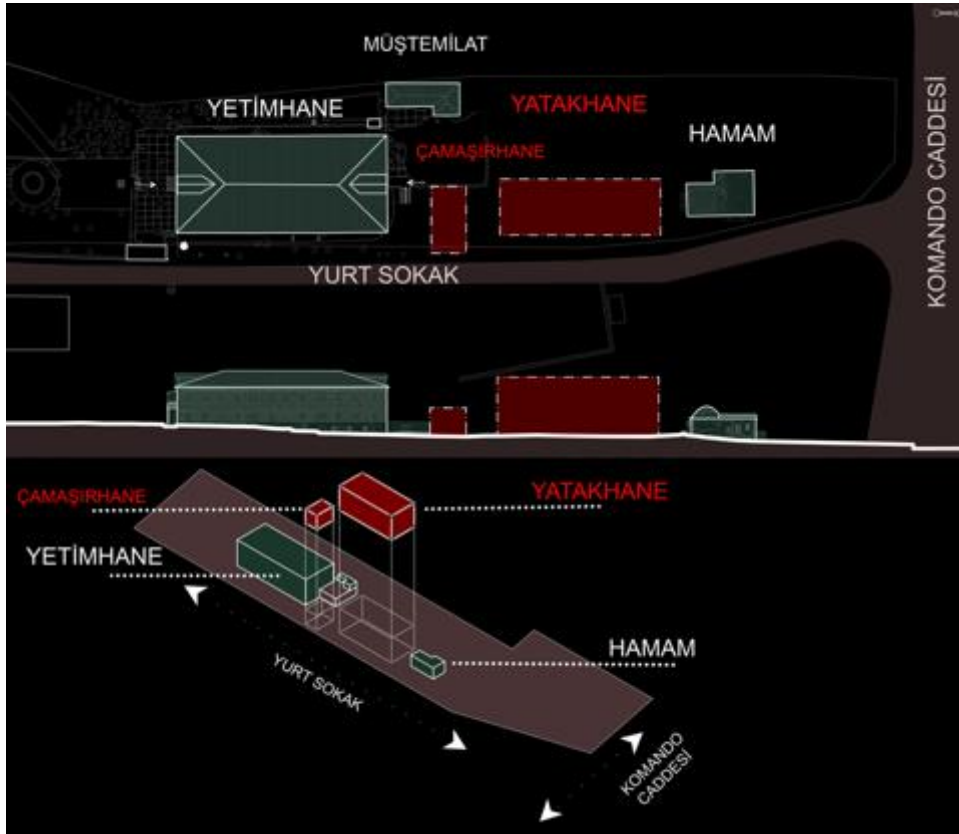


Figure 2: Vaizet Plan arazi iindeki mevcut ve amana y k lan yap lar U aslan 2022

2

A A A

ap n n belgeleme al malar yap ya arar vermeden hassas ve do ru ekilde tespiti i in la er tarama y ntemi ile ger ekle tirilmi tir ap n n l m nde kullan lan la er taray c 3 0 yatay 270 d ey olmak ere geni a ile tarama ve foto rafla belgelemenin yan s ra tan mlanan k smi alan ve y eylemlere odaklanarak bu b lgelerin detayl ve hassas taranmas ve foto raflanmas elliklerine de sahiptir Mekanlar aras ndaki ba lant n n kurulmas i in cihaza b t nle mi pusula altimetre e im l er ellikleri ile birlikte A4 boyutlu siyah beya referans ka tlar ve 2 adet referans k releri Sphere kullan lm t r



Figure 3: Pointcab program ndan al nan data g r n m a Restorasyon 202

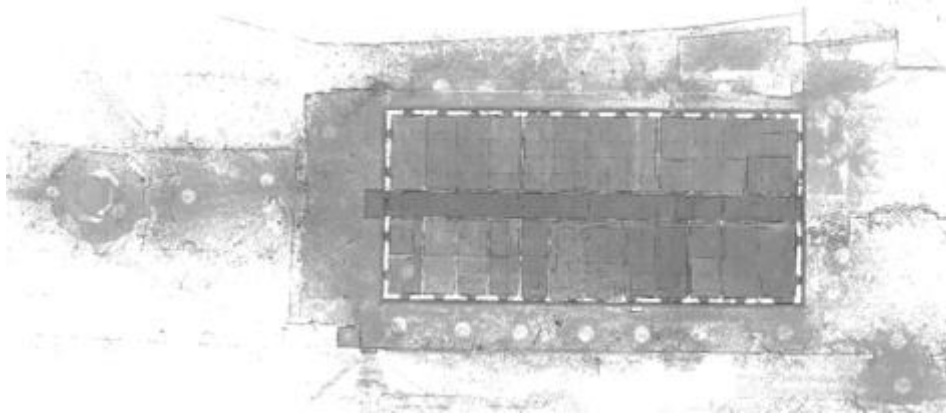


Figure 3 PointCab den alınan istasyonların data görünümü a Restorasyon 202

apın elemanları duvar ve döşeme kaplamaları vb yerlerde 1 metre ile ayrıntılı olarak alınarak detay çizimleri sahada elle yapılmıştır. Alınan detay çizimleri ile her tarayıcı verileri ile birlikte değerlendirilmiştir. Apın tıbbi bölümlerinin ayrıntılı ve eksiksiz belgelenmesi için yapıya farklı noktalardan foto raf çekimleri yapılmıştır. Yapı bileşenleri hem genel hem de detaylı olarak belgelenmiştir. Bu çekimlerden elde edilen foto raflar hem yapının cephe ve plan düzeyindeki tüm elemanları derinliği ile ölçüme vb yapı bileşenlerinin belgelenmesinde her tarayıcı verileri ile birlikte kullanılarak değerlendirilmiştir. Laser tarama sonucunda nokta bulutları ve elde edilen diğer veriler plan ve cephe çizimlerinde kullanılmıştır. Figure 3 ve 4

2.1.1.1. Zemin Katı

Zemin kat mekanlarının iki girişi bulunmaktadır. Bunlardan birisi cephenin ortasında dikey giriş cephenin ortasında yer almaktadır. İkinci girişi birbirini ile aynı düzende kurgulanmıştır. Zemin kat mekanları küçümsümlü ve konumlanan koridorun iki yanında sıralanmaktadır. Zemin kat 4 mekandan oluşmaktadır. Stüdyo katı girişinde bu koridordan sağlanmaktadır. Figure 4



Figure 4 Zemin kat koridoru birinci katta kapatılmış merdiven Ulaşan 202

Bodrum kat yerleşim alanı yetimhanenin inşaat edildiği arazinin doğu batı ve küçümsümlü doğu batıdaki kot farkından dolayı küçümsümlü kesiminde kesim olarak oluşturulmuştur. Figure 5 Bodrum kat mekandan oluşmaktadır. Mekanların duvarlar kesme ve molotai çeri siva d emeler beton yapı stüdyo katları ise betonarmedir. Bodrum katı bahçeye doğu yönünde yer alan iki farklı kapı ile ulaşmaktadır.

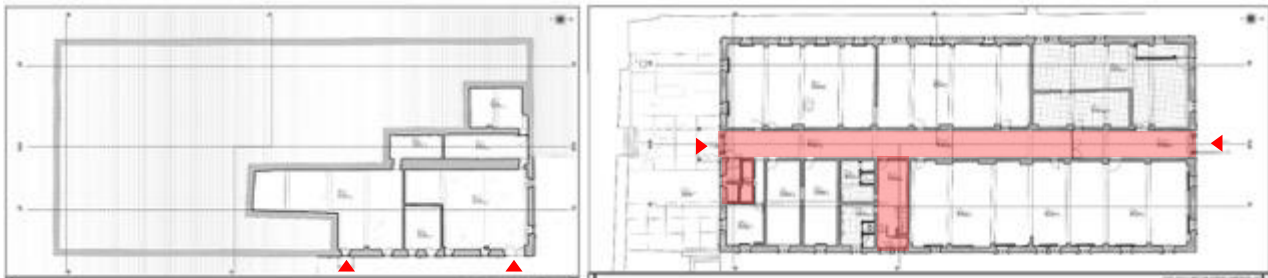


Figure 5 Bodrum kat ve zemin kat planları ve ölçümleri Ulaşan 202

Birinci kat kotuna ulaşım iki merdiven ile sağlanabilmektedir. Merdivenlerden emin kat r 1 ve planında yer alan numaralı odanın doğusunda yer alan sonradan üst kattan kapatılan merdiven kullanılmamaktadır. Figure 7 Birinci kat koridorun iki yanında konumlanan 2 mekandan oluşmaktadır. Birinci katta gney yönünde konumlanan balkon ferforje korkuluk ile sınırlanmıştır. Figure 7 Balkonun detaylı muhtesim mozaik sırt sırtı ise ahap sundurma atdır.

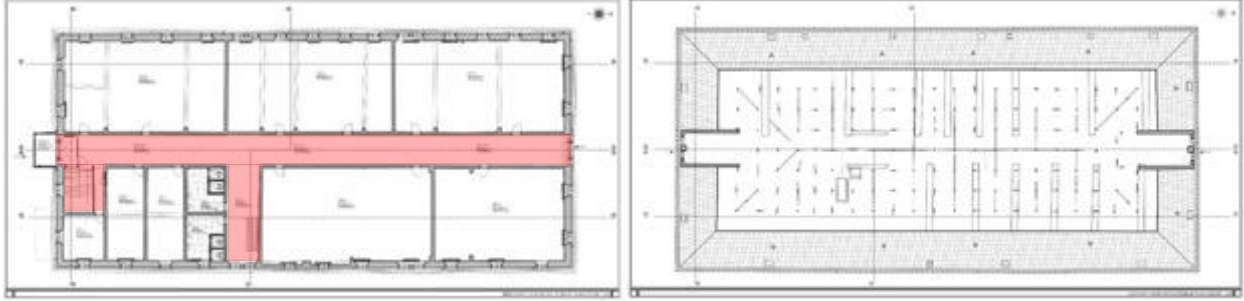


Figure 7 Birinci kat ve üst kat planı r 1 ve iimi U aslan 202

etimhanenin üst katına ilk birinci katta yer alan 0 numaralı mekanın gneybatısındaki demir merdiven ile sağlanmaktadır. Figure 7 Üst katın detaylı muhtesim betonarme olup birinci katın betonarme kirişleri 30 cm kadar üst katın detaylı muhtesiminden taşınmıştır. Üst katın üst sırt sırtı ahap strüktür ile taşınmaktadır. Üst katın üst kısmında gney yönünde genel niçli cihannmalar yer almaktadır. Figure 7 ve



Figure 8 Üst katın üst kısmındaki cihannmalar ve üst katın taşınması U aslan 202

2.2. Cepheleri

apının cepheleri ortas kabartılmış renkli ande it mal emeden yama tekni inde inşa edilmiştir. Doğru cephe bodrum kat mekanlarının girişi barındıran cephe dir. Bu girişler muhtesim demir doğrama kapılar ile kapatılmıştır. Cephenin bodrum kat girişlerinin bulunduğu kısmın seviyesi muhtesim imento esaslı harç ile sıvanmıştır. Cephenin üst kat mekanlarının yer aldığı seviyede aynı yatay aksta 4 adet pencere bulunur. Figure 7 Pencere bölükleri dikdörtgen formda basık kemerli taş ve çelikten yapılmıştır. Üst katın üst kısmında gney yönünde genel niçli cihannmalar yer almaktadır. Figure 7 ve

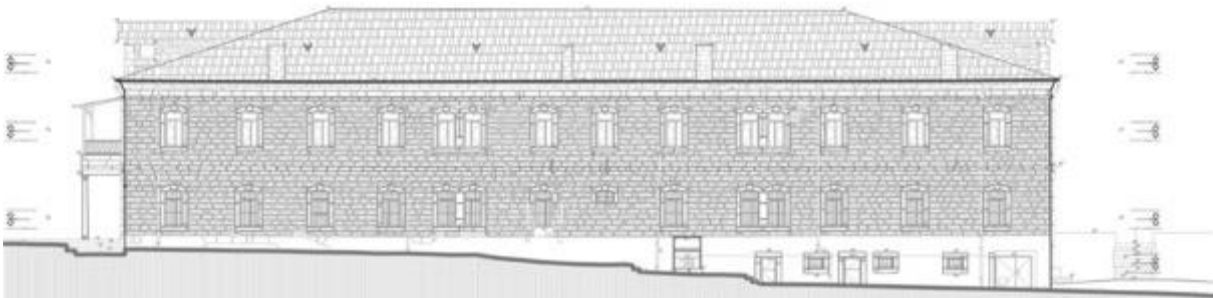


Figure 9 Doğru cephe r 1 ve iimi U aslan 202

ap n n bat cephesi emin kat mekanlar n n yer ald seviyede ayn yatay aksta 2 adet pencere bo lu u a l m t r Figure 0 Pencere bo luklar dikd rtgen formlu bas k kemerli ta s veli olup ah ap do ramal bir kanad a l r olmak ere ift kanatlı pencere ile i ten kapat lm t r Pencere bo luklar d tan demir parmaklıklar ile rt lm t r Cephenin st kat emin kattan cephe boyunca yatay ta silme ku a ile vurgulanarak ayr lm t r Cephenin birinci kat na da alt kattaki gibi ayn yatay aksta ve formda adet pencere a l m olup bu pencereler emin kattaki gibi demir parmaklıklar ile kapat lmam t r st kat n tavan seviyesi cepheden d a ta r lm bir adet ta silme ku a ile vurgulanm t r Cephenin sa ak seviyesinde de iki kademeli silme ku a yer almaktadır

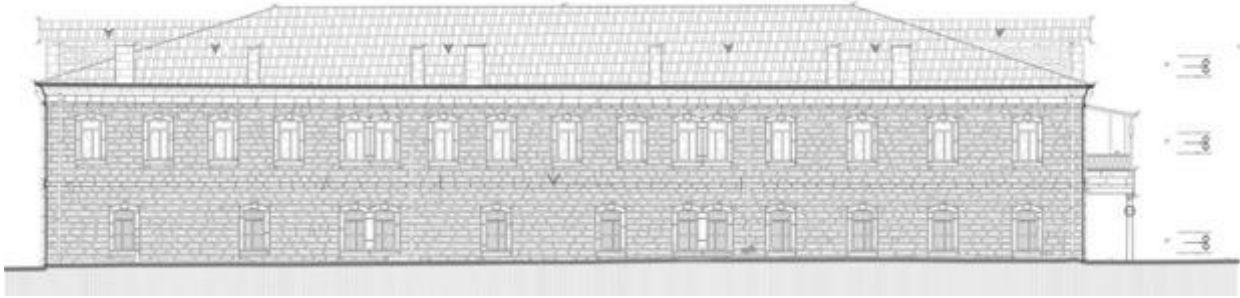


Figure 1 Bat cephe R l ve i imi U aslan 202

ap n n ku ey cephesi yap n n iki giri inden birini bar nd rmakta olup yap n n konumlandır ld geni ara iye a l maktadır ap n n do u ve bat s ndaki kot fark ndan dolay cephenin do usunda bodrum kat n n da cephesi alg lanırken bat s nda kot y kseldi i i in sadece emin kat mekan n n cephesi alg lanmaktadır Figure ap a kl n n bulundu u b l m cephegedeki k rm renkli ande it ta lar ndan farklı olarak gri renkli ta lar ile olu turularak vurgulanm t r ap a kl yuvarlak kemerli olup a kl k iki yandan birer adet dar formlu yuvarlak kemerli pencere a kl ile s n rland r lm t r ap a kl ift kanatlı demir do rama kap ile rt lm t r ap a kl n n st b l m n n iki yan ndaki bo luklar a kl ile ayn hi aya denk gelen st kat balkon giri i ve g ney cephegedeki balkon ve revaklı b l m g n ne al nd nda bu b l mde bulunmas gereken balkon ve giri in n ndeki revak k sm n n n g n m e gelememi i anla lmaktadır emin kat giri kap s n n iki yan nda iki er adet ayn yatay aksta d rt adet pencere yer almaktadır Pencere bo luklar dikd rtgen formlu bas k kemerli ta s veli olup ah ap do ramal bir kanad a l r olmak ere ift kanatlı pencere ile kapat lm t r Pencere bo luklar d tan demir parmaklıklar ile rt lm t r Cephenin st kat emin kattan cephe boyunca yatay ta silme ku a ile vurgulanarak ayr lm t r st kat n ortas ndaki alt kattaki giri kap s ile ayn dikey aksta dikd rtgen formlu kap a kl yer almaktadır ap a kl ift kanatlı demir do rama kap ile kapat lm t r ap iki yandan dar formlu yuvarlak kemerli birer adet pencere a kl ile s n rland r lm t r ap n n a ld balkon alt katta bulunmas gereken revaklı b l m gibi g n m e gelememi tir

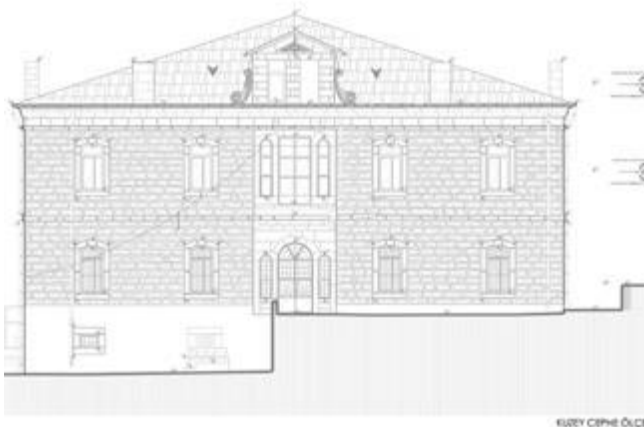


Figure 11 u ey Cephe R l ve i imi ve Foto raf U aslan 202

u ey ve g ney cephelerde giri ler ile ayn dikey aksta at dan ta r lm cihann ma yer almaktadır Cihann man n ku ey cephesine iki adet dikd rtgen formlu pencere bo lu u a l m pencerelerin do ramalar g n m e gelememi tir Cihann ma iki yandan birer adet yekpare vol t ile s n rland r lm t r Cihann man n gen al nl n n y eyinde gen formlu ta s sleme panosu yer almaktadır Figure



Figure 12 Güney Cephe Rölövesi ve Fotoğrafı Uslan 202

apın güney cephesi salta d emeli bahçeye almaktadır. Cephenin emin kat seviyesinin ortasında yapının iki girişi kapısından biri konumlandırılmıştır. Figure 2'ye göre yapıya ulaşım için iki adet sütun ile oluşturulmuş revak balmından sağlanmaktadır. Revak balmı ahap ve cam balmı ile kapatılmıştır. Ahap akları yuvarlak kemerli olup aklın iki yandan birer adet dar formlu yuvarlak kemerli pencere akları ile sınırlanmıştır. Ahap akları yuvarlak kemerli demir do ramakap ile örtülmüştür. Cephenin üst kat emin kattan cephe boyunca yatay taş silme kuşağı ile vurgulanarak ayrılmıştır. Üst katın ortasındaki alt kattaki giriş kapısı ile aynı dikey eksende dikdörtgen formlu kapı akları yer almaktadır. Ahap akları çift kanatlı demir do ramakap ile kapatılmıştır. Ahap iki yandan dar formlu yuvarlak kemerli birer adet pencere akları ile sınırlanmıştır. Ahapın nala balkonundan S formu ferforaj ile çevrelenmiş olup üstten ahap sundurmalı çatı örtülmüştür. Figure 2



Figure 13. 03 ve 04 numaralı mekanlar Uslan 202

2.3.3 Analizi ve Alışmaları

Malzeme Analizi

apının beden duvarlarında kırma tonlu bosalı ande it taşı mal emeli balmı duvarlarında kesme taşı mal emeli avluda demesinde salta bodrum kat mekanlarında molo taşı mal emeli kullanılmıştır. Mekanda taşı olarak betonarme kolon kiriş ve döşeme sistemleri yer almaktadır. Figure 3 Döşeme mal emesi emin kat koridorunda g n taşı döşemenin bir kısmı gr lmele birlikte diğer mekanların döşeme kaplamalarında muhdes moaik mal emeli ve beton ahap kullanılmıştır. Duvarlarda yer alan taş yastıklar g n de ahap tavan ve he neleri üretmektedir. Figure



Figure 1 Malzeme Analizi Kesit ve Cephe Rölövesi Leant Uslan 202

Ah ap mal eme yap n n mekan giri kap lar nda pencere s velerinde ve at kat nda g r lmektedir ap n n ana giri ve bodrum kat giri kap lar nda pencere korkuluklar nda muhdes demir mal eme kullan lm tr Islak hacim mekanlar nda d eme ve duvarlarda fayans kaplama ve pvc mal emeden retilmi kap lar yer almaktadır



Fi ure 1 g n ve muhdes yap elemanlar U aslan 202

a ısıl zulmalar

ap daki bo ulmalar mal eme sorunlar yap sal sorunlar ve muhdes olarak ba l k alt nda incelenmi tir Mal eme sorunlar ba l alt nda rutubetlenme yosunlanma bitkilenme g r len beden duvarlar d etkenler sebebiyle r yen ah ap elemanlar koro yona u rayan metal elemanlar ve e itli mal eme kay plar belirlenmi ve belgelenmi tir Figure mekan duvarlar nda s va d k lmeleri neme ba l karama ve kirlenmeler g lemlenmektedir



Fi ure 1 Hasar Anali i Le ant ve Plan i im rne i U aslan 202

ap sal sorunlar ba l nda ilk olarak yap n n cephelerinde g r len s va d k lmesi atlaklar incelenmi tir Cephede muhdes tesisat elemanlar n n monta s ras nda kesme ta y eyler arar g r m t r ap sal problemlere sebep olan suyun yap dan u akla t r lamamas ta y eylerde nemlenme bitkilenme ve yosunlanmalar s val k s mlarda s va d k lmelerine sebep olmu tur Muhdes eklentiler kap pencere do ramalar i mekanlarda d emeler muhdes beton ap ve duvarlarda imento esasl s valar tesisat eklentileri olarak incelenmi tir



Fi ure 1 Hasar Analizi Le ant Plan Cephe i im rnekleri U aslan 202

2 S S O A A A

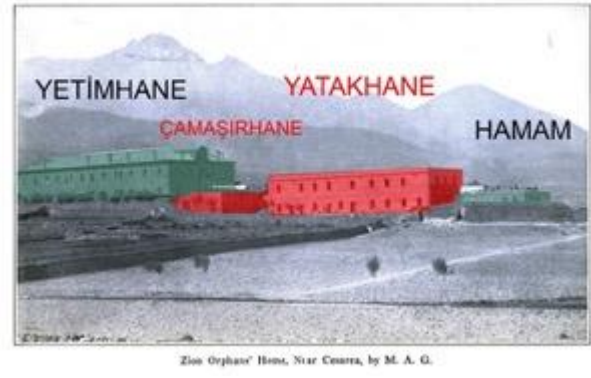
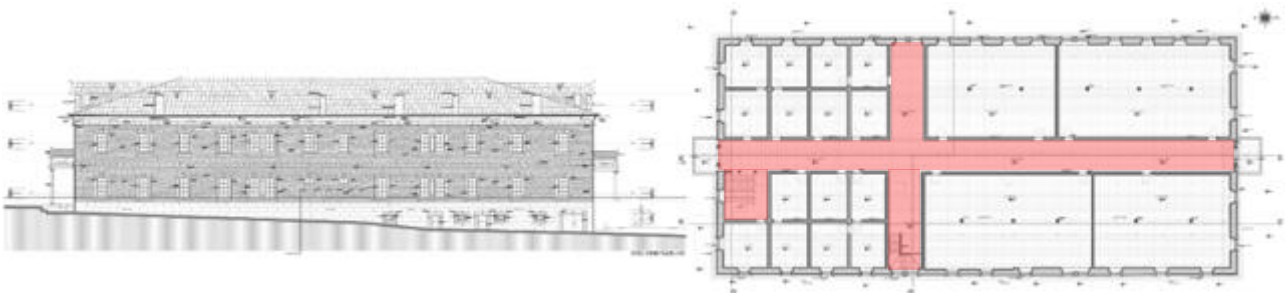


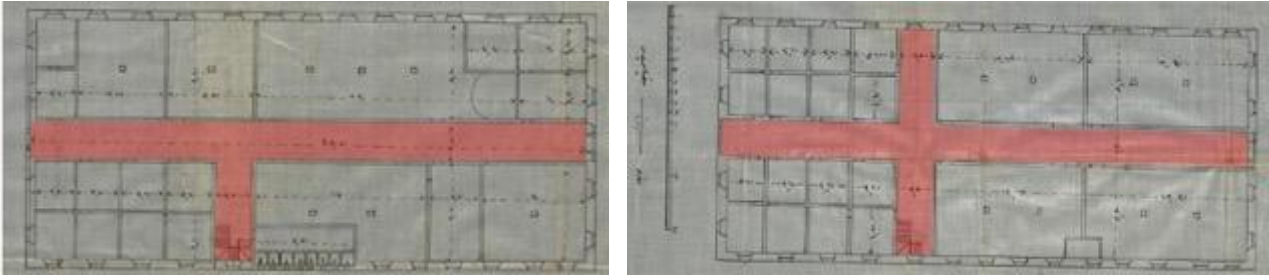
Figure 18. Zincidere yetimhanesi tarihi bilinmeyen fotoğraf ve Gerber'in kitabında yer alan foto altlık olarak kullanılarak kaldırılan yapılar ve 2021 yılındaki mevcut yapıların işlendiği görsel (Url 1 ve Gerber, 1917).

Restit syon al mas i in ncelikle yap n n kendisi incelenerek yap daki i ler ve mal emelerin detayl de erlendirilmesi yap lm t r ap ile ilgili eski foto raf ve belgelerin elde edilmesi i in Ba bakanl k Osmanl Ar ivi ayseri l t r Varl klar n oruma B lge urulu ar ivi ki isel foto raf ar ivleri ve kaynak yay nlar ara t r lm t r



Fi ure 1 Restit syon Do u cephesi ve Birinci at Plan a Restorasyon 202

Ba bakanl k Osmanl ar ivinde yer alan va iyet plan g ney ve do u cephesi i imleri ile kat planlar n n yer ald belge BOA 0 ile yap n n g ncel durumu k yasland nda farkl l klar oldu u g r lmektedir Ar iv i imlerinde cephelerde yer alan a kl k say lar n n farkl oldu u ve yap daki i lerden bu a kl klardan do u cephesinde yer alan havalandırma pencerelerinin sonradan kapat ld anla lmaktadır Figure 2



Fi ure 2 Ba bakanlık Osmanlı Ar ıvi 37 2 7 003 numaral belge de yer alan yap ın n emin kat ve birinci kat i imleri BOA Bab ali Evrak Odas Evrak BEO 37 2 7 003 H 22 0 32 M 30 0 0

Planlar incelendi inde emin katta fonksiyon de i ikli i sebebiyle mekanlarda de i iklikler yapıld ı ve ar ıvi i imlerinde yer almayan yap ın n g neydo usunda yer alan merdivenin ise l leri kullan lan mal emeler de erlendirildi inde g n oldu u d n lmektedir ap ın n d emelerinin betonarme d eme ile de i tirildi i g n d emelerin ah ap oldu u duvarlarda g r len he en kiri ler i in ta yast ki leri ile desteklenmektedir Birinci katta ar ıvi i imleri ile yap ın n g ncel durumunda balkonlar ve g neydo usunda yer alan merdiven d nda farklı k bulunmamaktadır Figure 20



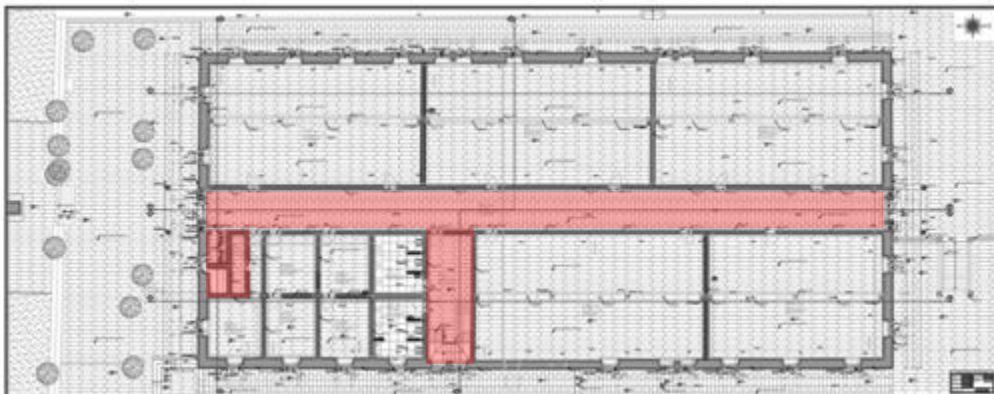
Şark cihetinin (doğu cephe) görünüşü

Fi ure 21 Ba bakanlık Osmanlı Ar ıvi 37 2 7 003 numaral belge de yer alan yap ın n cephe i imleri BOA Bab ali Evrak Odas Evrak BEO 37 2 7 003 H 22 0 32 M 30 0 0

ap ın n at s ar ıvdeki i imler ile farklı k g sterse de eski foto raflardan g n m deki gibi oldu u g r lmektedir Figure at ar ıvde yer alan i imlerde be ik at ve kalkan duvar n n erinde kap ve yanlar nda pencereler yer alacak ekilde g r l rken g n m de k rma at ve kalkan duvarlar yerine de cihann malar yer almaktadır Elde edilen i imler eski foto raflar ve ayn d nemdeki ben er yapı lar ile yap ın n g ncel durumu kar la tr larak restit syon paftalar ha rlanm tr

S O A S O Ö S

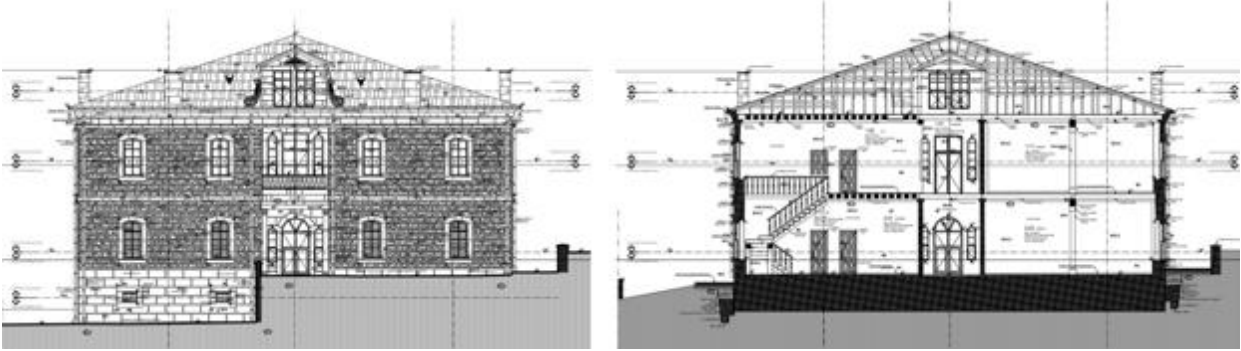
ap ın n restorasyonunda yap ın n g n niteliklerinin ortaya kar lmas ı g n bi imlerin korunmas hedeflenmi tir ap ya en a m dahale yapı lmas temel ilkesi nda g n elemanlara yapı lan olumsuz m dahalelerin yapı ya arar vermeden u akla tr lmas ve g n niteliklerin iyile tirilerek korunmas ad na m dahale kararlar geli tirilmi tir ap ın n g n i Levin s rd r lmesi a da koruma anlay gere i ve kent belle i aidiyet hissi yapı sal ve mekansal m dahalelerin en a a indirilmesi s rd r lebilirlik avanta lar sebebiyle nerilmektedir



Fi ure 22 Restorasyon emin at Plan a Restorasyon 202

Mal Ararlar G n m de kullan lmayan yap ge ir di d nemler boyunca farkl kurumlar taraf ndan e itim yap s olarak kullan lm ayn parseli payla t ce aevine ek at lye olarak kullan ld d nemde de g ni levini dolayl olarak s rd rm t r Bu durum yap n n mekansal olarak b y k l de korunmas na sebep olmu tur Restit syon al malar ve yap daki i ler nda mekan organi asyonu d enlenerek g n yap da yer ald d n len yeni b l c duvarlar eklenmi tir

Mal Ararlar ap str kt rel a dan genel olarak sa lam olmakla birlikte g n olmayan betonarme d emelerin tekni ine g re uygulanmad ve ta y c elli ini yitirdi i g r lmektedir at d emesinin ask ya al narak yap dan u akla t r lmas nerilirken statik raporlar nda birinci kat d emelerinin s k m n n yap ya verebilece i arar g n nde bulundurularak muhdes mo aik kaplaman n kald r larak y k n n a alt lmas na karar verilmi tir



Fi ure 23 Restorasyon u ey Cephe ve esit i imleri a Restprasyon 202

ap n n at s nda ya mur sular n n u akla t r lmas ndaki problemler yap n n g n elemanlar na arar vermektedir at ask ya al narak muhdes betonarme d emenin s k m ah ap d eme ile de i tirilmesi sonras nem sebebiyle r me ve bo ulmalar n g r ld at elemanlar n n yenilenmesi esnas nda do ru at e imleri ve kaplama mal emeleri ile bu sorun l melidir

ap n n emin kotunda g r len nem sorunlar i in beden duvarlar ndan temel kotuna kadar yap ya arar vermeden ka yap larak k t durumdaki ta lar n yenilenmesi yal t m do ru drene uygulanarak yap n n su almas engellenmesi karar al nm t r



Fi ure 2 M dahale Anali i esit i imleri a Restorasyon 202

Mal Kararları ap da g r len nem sorunlar beden duvarlar nda ah ap ve metal elemanlarda tu lanma kirlenme paslanma problemlerine sebep olmaktadır lk olarak imento esasl muhdes s valar raspa edilmeli nemin u akla t r ld beden duvarlar nda gerekli yerlerde atklara statik raporda da belirtildi i gibi hidrolik kire en eksiyonu yap larak kire esasl s va uygulamas yap lmal d r Hasar g rm ya da tamamen kaybolmu yap elemanlar uygun mal eme ve boyutta tamamlanmal d r Bo alm ve bo ulmu der lerde hidrolik kire der uygulamas yap lmas ve d etkilere ba l olarak r yen ve kaybolan ah ap elemanlar n yenilenecek durumda olanlar n gerekli bak mlar yap ld ktan sonra tekrar kullan lmas nerilmektedir ap da koro yona u rayan metal elemanlar mekanik y ntemlerle temi lenerek kullan lamayacak durumda olanlar i in yeni metal mal emeler kullan lmal d r

SO

incidere Dar leytam yap s n n g n mal emelerinin korunmas na a ami en g sterilerek a da ihtiya lara cevap verecek bir e itim yap s ng r lm t r Tarihi yap anlamsal mekansal yap sal ve estetik elli kleri ile incidere k y i in nemli oldu u kadar tarihi ve lkemi i in de nemli bir d nemi i aret etmektedir

ap n n yap sal ve mekansal b t nl bo ulmadan teknik ve teknolo ik sistemlerle g ncellenerek toplum ya am na kat lmas ve bu s re y netilirken tasar m ve donan mlar n n g ncel konfor ihtiya lar n kar lamas geli en d n en bir s rece dahil edilmesi koruman n s eklili i i in va ge ilme dir

eşer

It should be written as short as possible and expressing the contribution made without giving the number

ti Kurul O ayı

N A

A ra e erle irmesi

Externally peer reviewed

azar Kat ıları

Conceptualization H S Investigation H S Material and Methodology H S S Supervision H S E T E
Visualization S riting Original Draft H S D A riting review Editing D A S Other All authors have
read and agreed to the published version of manuscript

ı ar atışması

The authors have no conflicts of interest to declare

Fi a sal este

The authors declared that this study has received no financial support

KA AK A

Peker A i isel foto raf ar ivi

BOA Bab ali Evrak Odas Evrak BEO 37 2 7 003 H 22 0 32 M 30 0 0

Gerber M A 7 Passed Experiences Present Conditions Hope for the Future Ramsey Burns Printing Pasadena
Cal

bek 20 ayseri de Tarihi Okul ap lar La in ay nlar ayseri

Url <https://team.aow-discuforum.info/t/72> ayseri Talas incidere Ermeni Rum Protestan cemaatleri kilise
yetimhane ve tehcir htm Son Eri im Tarihi Aral k 2022

i imler Restit syon Restorasyon i imleri ve M dahale Anali i i imleri a Restorasyon 202

Assessment of Hull Corrosion in General Cargo Ships

Spirović^{1*}, Kvaček²

Abstract Corrosion can cause local damage to the structure and can also initiate huge damage that can cause partial or complete loss of the ship, loss of human life or environmental pollution. That is why numerous inspections are carried out by the Port State, Flag State and Classification Societies to identify potential hazards in a preventive manner. This is supported by mandatory maintenance activities carried out by the Ship Management Company following the International Safety Management Code. Damage to the structure depends on many factors specific to the type of ship, environmental factors, transported cargo and manipulative equipment, as well as other important influential factors. To reveal the degree of damage to the cargo holds of dry cargo ships, in this article, we investigate the impact of corrosion on the cargo holds expressed through the amount of replaced steel. Namely, each cargo hold of these ships included the longitudinal and transverse bulkheads and the tank top plating. By measuring the thickness of steel plates, systematizing measurement data and identifying corroded surfaces that need to be replaced, in this research, we analyze the cumulative amount of replaced steel. A group of 10 ships carrying different general cargoes was considered and were measured in the period from 0 to 27 years of vessel age. The considered data show that the Normal function satisfactorily describes the considered data after 10 years of exploitation. By applying regression analysis, data were obtained that describe with a high degree of precision the increase in the amount of replaced steel over time.

Keywords corrosion, general cargo ships, cargo holds, normal distribution

¹ University of Montenegro, Maritime Faculty, Cetinje, Montenegro

² University of Donja Gorica, Faculty of Applied Sciences, Mathematical Department, Podgorica, Montenegro

Corresponding author: spirovi@ucg.ac.me

1 Introduction

Numerous studies in the marine industry confirm that tankers, bulk carriers, general and dry cargo ships have the highest probability of casualties. Collision, loss of control, hull failure, contact, grounding, fire or explosion are some of the most frequently registered causes that led to numerous accidents. Accidents can lead to the loss of human life, material damage or environmental pollution.

The probability of critical casualties increases with the vessel's age and approximately 10% of losses due to structural failure are attributed to ships over the age of 10 years. Holmes and Pippenger [1]. Inadequate maintenance may have significant safety and business implications. Bright and Bell [2] reported that 23% of the failures refer to mechanical and structural components.

To keep vessels safe and secure for navigation and operations the International Maritime Organization introduced the International Safety Management Code. This Code pays special attention to the maintenance of ships. Maintenance costs increase proportionally with the age of vessels. Considering total annual technical costs, it can be assumed that approximately 20% of the ship's total operating costs, i.e. crew, technical, management and others, while maintenance reaches up to 10% of those charges, are estimated (Poggi et al. 2022).

To prevent the harmful consequences that can occur as a result of ship accidents, ship owners, ship management companies, Flag states and Classification Societies have taken numerous measures and activities regarding the reduction of accidents. Inspections are carried out on all types of ships, regardless of their age. However, there are numerous guidelines, mostly by Port State Control, that focus on certain types of ships. Flag States, previous vessels condition, age of ships and other issues connecting to the previous status of ships.

While the surface protection is effective, no corrosion on metal surfaces needs to be replaced. Usually, steel replacements during the first 10 years of exploitation are related to wastage caused by cracks or structural damage. When the surface coating breaks, the corrosion process starts and develops over the time of operation. Metal surfaces appear that need to be replaced when extensive corrosion can occur. This usually happens after 10 to 20 years of exploitation. Research on the effect of corrosion on maritime steel structures can be carried out in real seawater environment conditions (Pastor i et al. 2023) or in simulated conditions (Gudi et al. 2022). Certainly, the most significant are those studies that take into account extensive databases on the wear and tear of structural elements in different ships (Lang et al. 2022).

Corrosion can be found in different forms as general, pitting, microbacterial, local growing or other. Most investigated corrosion forms are general and pitting corrosion (Paik et al. 2003, Paik 2004, Momcilovic et al. 2023). Wastage of metals due to corrosion may be reported as weight loss expressed in grams or kilograms. In some previous research, wastage of corrosion was well considered in mm or percentage of deminution of as build thickness (Paik et al. 2003, Paik 2004, Soares and Garbatov 2004, Yamamoto and Ikegami 2004, Ivo evi et al. 2020, Ivo evi et al. 2022, Ivo evi et al. 2022).

Corrosion prevention and control are crucial to maintaining the structural integrity and safety of vessels. Regular preventive maintenance, protective coatings and corrosion resistant materials are commonly used to address and mitigate corrosion issues. Corrosion can affect various parts of a cargo vessel, but some of the most commonly corroded areas include ballast tanks, hatch covers, cargo holds, bulkheads, tank top plating, deck structure and pipes and piping systems.

Corrosion in the cargo holds of any cargo vessel can have significant negative effects on the vessel's structural integrity and cargo safety. Numerous research identifies some of the key influences of corrosion: increasing the risk of structural failure, cargo contamination, reduce vessel lifespan and increase maintenance cost. Due to specific types of cargo or cargo operation in Cargo Holds, deterioration in the cargo hold can result from factors like corrosion, wear and tear, moisture, improper maintenance or exposure to harsh conditions. Regular visual inspections, proper ventilation, regular maintenance, appropriate cargo handling, etc. can ensure the safety and integrity of the transported cargo and the vessel itself.

Damage caused by corrosion requires additional inspections and ultrasonic thickness measurements regarding the assessment of further exploitation of structural areas. Damaged surfaces need to be replaced, which greatly affects maintenance costs. Often these costs can reach values that influence the ships to be scrapped earlier. That is why it is very important to properly maintain the vessels using appropriate maintenance methods, which can include preventive and corrective activities that will ensure the desired exploitation of the vessel.

As it is prescribed in Classification Rules, corrosion intensity is measured in mm or percentage of wear concerning the as-built thickness value of specific structural members: plate, bracket, stiffener. The rules of the Classification Societies define the degree of acceptability and in this way the surfaces for replacement are identified by measurements. Corroded areas are usually treated as amounts of replaced steel expressed in kg of steel or tons of replaced steel.

The decrease in metal weight and the increase in corrosion rate increase with time and according to previous research, there are different linear and nonlinear models of corrosion. A linear model is developed by Southwell et al. [7], Soares and Garbatov [8], while non-linear models are presented by Yamamoto and Ikegami [9], Paik et al. [10], Paik [11], Paik [12], Paik [13], Melchers [14], Melcher [15], and papers by other researchers.

All models developed so far are based on exposure time, while some more advanced models take into account other parameters such as salinity, pH, seawater temperature and flow rate, the content of oxygen dissolved, sulfur pollution, and fouling [Melchers].

The most common structural damage due to corrosion occurs in ballast tanks and cargo holds. In this paper, based on measurement data on structural damage of cargo holds in general cargo ships, we consider how the amount of steel changes during exploitation.

The paper is structured through 4 chapters. The second chapter presents a related methodology, discusses the relevant database of General Cargo ships and presents the used methods. The third chapter presents research results, while the fourth chapter presents conclusion remarks.

2 Methodology

To assess the condition of the structure, the classification rules require a visual inspection of the structure and then a thickness measurement. With vessels age, the scope and intensity of measurements increase according to the rules of Classification Societies. Measurements of structural elements include three states of measurement, namely acceptable measurements, substantial corrosion, and excessive corrosion. Steel plate areas or lengths of structural elements or plate pieces with excessive values must be replaced before further exploitation of the vessel. In this sense, metal surface area, lengths or pieces of corroded metal structure are identified, which are expressed in kg, or more often in tons of replaced steel. In this way, the quantities of steel that need to be replaced in certain areas are identified, as well as the time necessary for the realization of these works. Due to specific commercial requirements, it is very important to take into account the scope of the replacement, location, contact surfaces, repair location, etc. to optimize and reduce the total maintenance costs as much as possible.

Based on huge measurements carried out on ten different general cargo ships, including complete reports on thickness measurements, an insight into excessive corrosion was made. In

this way the areas that needed to be replaced were identified and thus the amount of steel to be replaced expressed in tons. Following the above, the data on the total amount of steel during the period of exploitation are presented below. Conducted research includes information during special surveys that provide information on replaced steel quantities after 20, 22 and 27 years.

Based on the data evaluated in this research, several statistical methods were implemented in order to develop non-linear corrosion models.

2.1 Database

The database considered in this research includes ten ageing general cargo ships. According to the available data, the vessel transported steel coils, iron profiles, stone, and other types of general cargo. The trade route was missing and didn't consider as well as environmental condition parameters. The age of the ships was between 20 and 27 years, and they were measured in the period from 2000 to 2020. Measurements were made during the regular Special Survey, considering specific requirements by the Classification Society. Some vessels were observed once, twice, or three times, as shown in Table 1.

Table 1. Estimated quantity of replaced steel in Cargo Holds in tons

Ships time (years)	es 1 t s	es 2 t s	es 3 t s	es t s	es t s	es t s	es t s	es t s	es t s	es 1 t s
					0					0
20			4	20	00	3	2	20		
2	3					4	3	2	0	40
27						0	3		02	

Descriptive statistics of input empirical data are shown in Table 2, based on data grouped by year. We observe a very large variability when comparing the data for years, which is to be expected considering the relatively small database and the limited amount of available information. In addition, for data related to 20-year-old ships, it is noticeable that the mean is almost identical to the standard deviation, which significantly complicates the modelling of these data.

Table 2. Descriptive statistics of input data

variable	ea	St ev	i imum	1	e ia	3	a imum
years	20.00	4	0.00	0.00	20.00	30.00	3.00
20 years			0	0	4.0	3	240.0
2 years	0	3.4	0	3	32	2	0.0
27 years	2.0	32.4	0.00	0.0	4.00	3.2	00.00

Figure 1 shows a Box plot of the input data. The diagram shows outliers for 2 years; these are the blue dots. The existence of these outliers points to the fact that we have some very large extremes in the considered empirical data. However, we did not exclude them from consideration for the data to remain credible because we believe that there was no error in the measurements, but rather extreme conditions, influence of corrosion, exploitation conditions, and other influential factors occurred, which was necessary to replace those large amounts of steel.

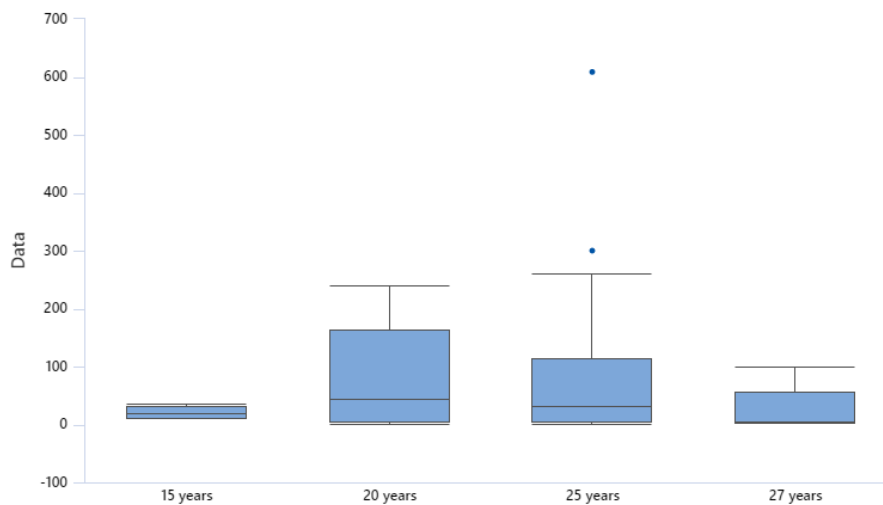


Figure 1 Estimated quantity of replaced steel in Cargo Holds in tons

Table 3 shows the confidence intervals for the mean and standard deviation. Furthermore, with certainty, we can claim that the mean value for 15 years will be between 3 tons and 200 tons, while the standard deviation of the empirical data will be in the interval 24 and 7. We observe a very wide confidence interval for the mean at 20 years and a very large variability of the data, considering that the confidence interval for standard deviation is wide and has large values of the lower and upper limits of the interval.

Table 3 Descriptive statistics of input data

Group	Mean	CI	StDev	CI
15 years	20	3 2 00	443	24 7
20 years	077	3 34 24 0	4	372 22 0
25 years	0	4 4 4	3 4	20 7 2 2
27 years	2	0 403	3 0	23 2 020

2.2 Methods

In this research, several standard scientific research methods were applied. The thickness measurement procedure was carried out using digital ultrasound devices that measure the thickness of the metal over the protective coating. These measurements obtained the initial values of the reduction in the steel thickness of structural elements of the cargo holds due to corrosion. Then, special software programs were used for data processing following the rules of the classification societies. Based on clearly defined acceptance criteria established by classification societies, the surfaces of the steel structure for replacement were identified. Considering the significant number of influencing parameters regarding the replacement of corroded surfaces, classification societies' minimum cutting surfaces, the influence of contacted areas, structural designs, etc., it is very difficult to determine precise and accurate amounts of steel replaced solely due to corrosion. This is precisely why the amount of replaced steel was estimated, which included exclusively the surface damage due to corrosion and not due to mechanical and other damages, as well as different structural requirements. Statistical data analyses were conducted on the input data obtained in this way about the estimated amount of steel to be replaced in cargo holds of general cargo ships.

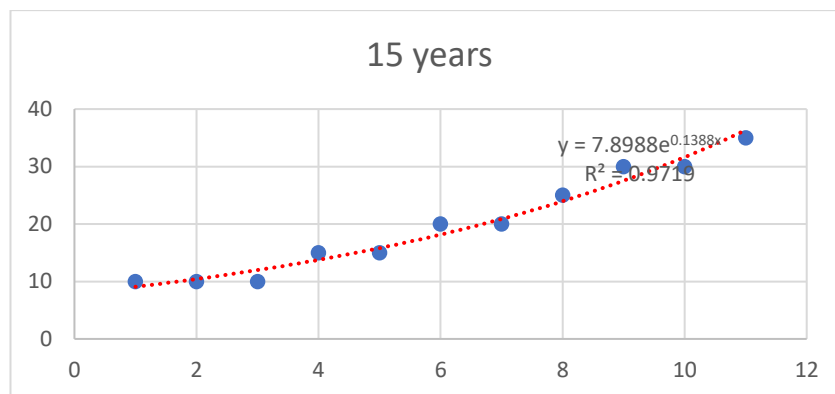
Our approach to data analysis encompassed a suite of classical statistical techniques. By utilizing descriptive analysis, box plots, and trend line visualizations, we were able to comprehensively analyze the dataset, unveil underlying patterns, and provide a robust foundation for further analysis.

In our analytical process, we executed an Anderson-Darling normality check, a method widely employed to assess the normal distribution of data. This involved calculating Anderson-Darling squared values and corresponding p-values for each dataset under scrutiny. Additionally, generated normal probability plots revealed that data are not following Normal distribution except in the case of 3 years.

Given the intricate and complex nature of the data patterns, our initial approach involved harnessing regression analysis. To capture the nuanced relationships within the data, we opted for both exponential and polynomial models. These modelling techniques are particularly adept at accommodating non-linear trends and variations that extend beyond the scope of linear models.

3 Results

Based on the Anderson-Darling test, corresponding p-values, and observing probability plots of resulting data, it was possible to conclude that empirical databases have complex structures. Having that in mind, modelling with nonlinear functions was carried out on the empirical dataset, considering that the data do not follow the Normal distribution except for 3 years. That conclusion led us to the decision to model these data with other curve shapes. We investigated the regression analysis shown in Figures 2a, b, c, and d. In each graph, we see the function that best describes the data and the R^2 value that shows how well the function follows the data. Values that are close to 1 show a higher degree of accuracy and reliability of the expressed function. As all the displayed values are always very close to 1, it means that our approximations are good on each graph. On the x-axis is the number of measurements, and on the y-axis is the amount of replaced steel. The red line is our prediction when the formula shown on the graph is taken into account.



a

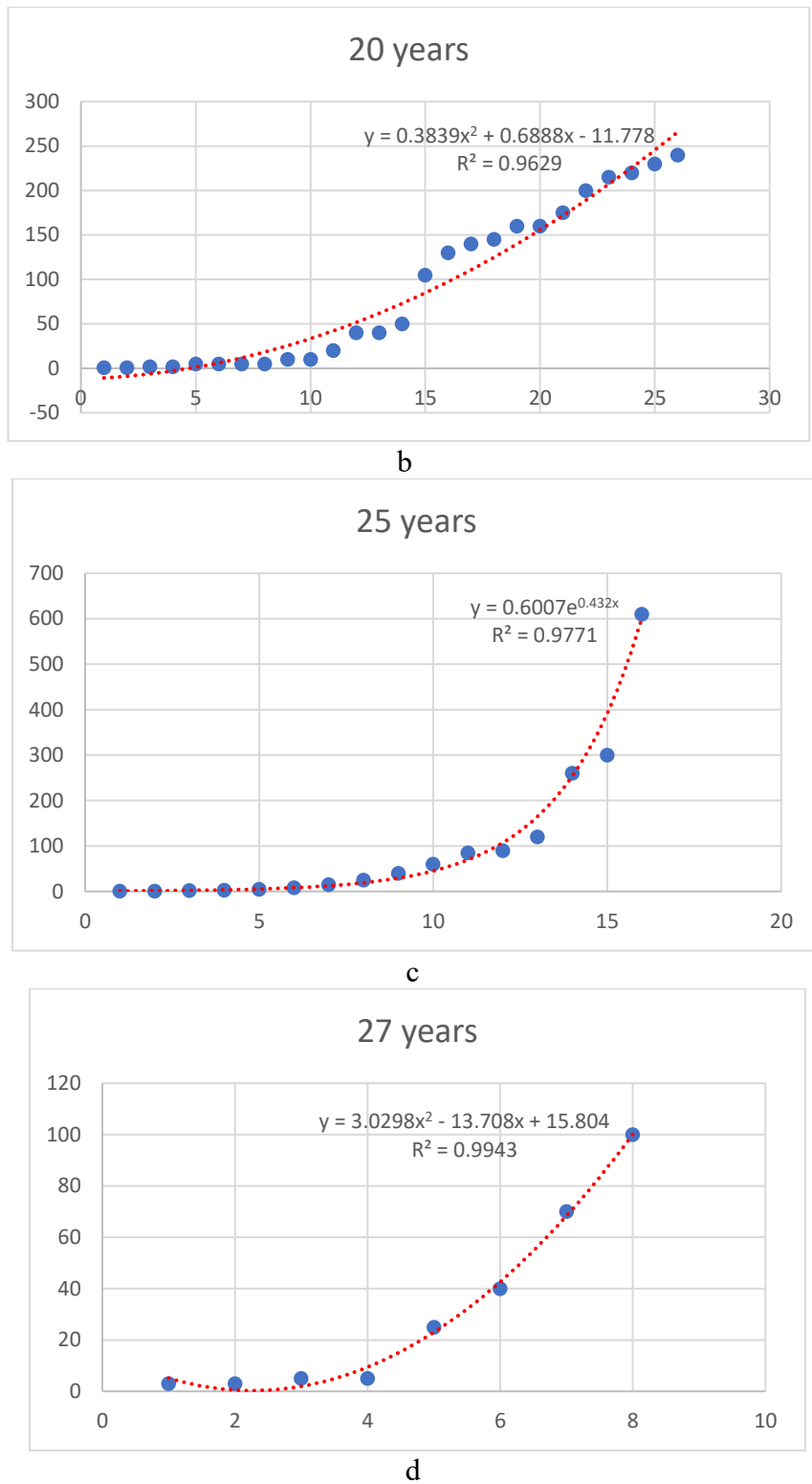


Figure 2 Modelling with non linear functions for a 20 b 2 c and 27 d years

conclusions

In this paper the authors have dealt with the development of regression models that will adequately describe the quantity of steel to be replaced in the cargo holds of ten dry cargo ships. Empirical data on the amount of replaced steel after 10 years follows a normal distribution which is not the case for the other considered time periods.

Using the regression analyses, all four presented functions follow the proposed non-linear functions with a high degree of accuracy greater than 95%, which gives us the right that they will also follow standard statistical distributions well. In the continuation of these studies, we could make an assessment of how the data behaves in accordance with the well-known probabilistic distributions. Also, it is possible to consider the total amount of replaced steel by individual structural areas of the cargo holds.

Acknowledgements

This research work has been supported by the approved Thickness Measurement Company INVAR Ivo evi Company. Some more information about the Company can be found at URL <http://www.invar.me/index.html>. Namely, the data collected and systematized during the last twenty-five years by the Company operators and experts have been included in the presented probabilistic analysis of the corrosion effects on the analyzed group of aged bulk carriers. Last decades the INVAR Ivo evi Company completed ultrasonic thickness measurement reports for vessels under the recognized classification societies such as LR, BV, DNV, GL, RINA, ABS, and ClassN. Currently, more than four hundred vessels are being inspected by the Company.

References

- Holmes, M., Pippenger, D. T., Human elements in bulk carrier inspections and repair. *Ship Structure Symposium '96*, Nov. 20, Arlington, VA.
- Bright, C., Bell, S. P., Improving human factors in marine maintenance. *Ship Structure Symposium '96*, Nov. 20, Arlington, VA.
- Poggi, L., Gaggero, T., Gaiotti, M., Ravina, E., Rizzo, C. M., 2022. Robotic inspection of ships: inherent challenges and assessment of their effectiveness. *Ships and Offshore Structures*, 17(4), 742-757. DOI: 10.1080/17445020.2020.1813737
- Momilović, N., Ilić, N., Jalađić, M., Ivo evi, Petrović, A., 2023. Pitting and uniform corrosion effects on ultimate strength of a bulk carrier. *Procedia Structural Integrity*, 4, 1-2.
- Paik, J. K., Kim, S. H., Lee, S. H., Probabilistic corrosion rate estimation model for longitudinal strength members of bulk carriers. *Ocean Engineering*, 29(1), 37-50.
- Paik, J. K., 2003. A time-dependent corrosion wastage model for bulk carrier structures. *Int. Marit. Eng. Res. Naval Arch.*, 4(2), 1-7.
- Paik, J. K., 2004. Corrosion analysis of seawater ballast tank structures. *International Journal of Maritime Engineering*, 4(A), 1-2.

Ivo evi Me trovi R ova N 20 Probabilistic estimates of corrosion rate of fuel tank structures of aging bulk carriers International Journal of Naval Architect and Ocean Engineering 77

Ivo evi ova N Mom ilovi N Vukeli G 202 Analysis of corrosion depth percentage on the inner bottom plates of aging bulk carriers with an aim to optimize corrosion margin Shipbuilding Theory and Practice of Naval Architecture Vol 72 No 3 <http://dx.doi.org/10.2271/brod7230>

Ivo evi ova N Mom ilovi N Vukeli G 2022 Evaluation of the Corrosion Depth of Double Bottom Longitudinal Girder on Aging Bulk Carriers Journal of Marine Science and Engineering 10 42 <https://doi.org/10.33044/mse.101042>

Pastorcic D Vukelic G Ivošević S 2023 Welded steel in marine environment: Experimental and numerical study of mechanical properties degradation Materials Today Communications Volume 34 1020 ISSN 23242 <https://doi.org/10.1016/j.mtcomm.2022.1020>

Melchers R E Corrosion uncertainty modelling for steel structures Journal of Constructional Steel Research 2 3

Melchers R E 2003 Probabilistic model for marine corrosion of steel for structural reliability assessment Journal of Structural Engineering 2 4443

Gudic S Nagode A Šimic Vrsalovic L Šoć S 2022 Corrosion Behavior of Different Types of Stainless Steel in PBS Solution Sustainability 4 3 <https://doi.org/10.33044/su.443>

Southwell C R Bultman D H C 1977 Estimating of service life of steel in seawater In Schumacher M editor Seawater corrosion handbook 374 3 7

Amamoto N Ikegami A study on the degradation of coating and corrosion of ship's hull based on the probabilistic approach

Soares C G Garbatov Reliability of maintained corrosion protected plates subjected to non-linear corrosion and compressive loads Marine Structure 2 42 44

Yang Sobey A Yang 202 Corrosion prediction for bulk carrier via data fusion of survey and experimental measurements Materials Design Volume 20 100 ISSN 02427

Comparison of Mechanical Properties of Cellulose Reinforced Hybrid Composites

Servet Uslum^{*1}, Uğur Emirel¹

Abstract Since hybrid composites are a more stable material type their use is starting to become widespread today compared to traditional composites. Although hybrid composites are used in the aerospace and defense industries different mechanical properties can be obtained with different arrays of fibers in layered composites. Due to this situation researches on the subject are increasing. Carbon fiber and glass fibers are the most preferred fiber types in fiber reinforced composites. If these two fibers are hybridized they enter their negative sides against each other. In addition to the different arrays of fibers there are also methods such as surface treatments and matrix reinforcement to increase the strength and reduce the delamination between layers in laminated composites. Matrix reinforcement is made using different methods such as nanoparticles, nanofiber mats and films. In addition to these methods environmentally friendly materials have become one of the preferred elements especially to increase matrix reinforcement. Cellulose fibers are one of the environmentally friendly materials due to their low density, low cost and recyclability. Cellulose fibers are a great natural resource as they are derived from plants such as kenaf, hemp, flax and bamboo. By using cellulose paper obtained from cellulose fibers between layers in layered composites these cellulose fibers take the loads on the matrix. The aim of this study is to investigate the effect of cellulose paper between layers. In this direction hybrid composites with glass/carbon fiber layer and carbon/glass fiber layer were produced and cellulose paper was added between these layers and their mechanical properties were examined.

Keywords Carbon fiber, cellulose paper, glass fiber, hybrid composite, tensile test

¹Address: Başkent University, Ahramanka Vocational School, Ankara, Türkiye

* Corresponding Author: ustulum@baskent.edu.tr

1

Kompozit malzemelerin kullanım alanlarında kullanılmaları olarak karışım yapılmaktadır. Buna bağlı olarak kompozit malzemelerin kendi içinde itlenmeye başlamaları Hibrit kompozit takviye elemanlarının birden fazla olması durumunda kompozit malzemelerin kullanım alanlarında Demir [20] Bu tür kompozitler daha stabil mekanik özellikler sunarken aynı zamanda tokluğun artmasına olanak sağlamaktadır. Hibrit kompozit tasarımı fiberlerin hibritlenmesi bir yöntem olup her bir fiberin sahip olduğu avantajları ortadan kaldırmaya yaramaktadır. Swolfs vd [20] Fiber hibritlenmesinde genellikle düşük maliyetli ve yüksek maliyetli fiberler bir arada kullanılır. Bu şekilde düşük maliyetli fiber hasarları nedeniyle yüksek maliyetli fiber bir üretilmesi için amade erine ulaşılabilmektedir. Demir [20]

Hibrit elli ilk olarak Hayashi [72] tarafından karbon cam fiber tabakalı kompozitlerde kopma yükü sadece karbon fiberden oluşan kompozitlere göre daha yüksektiği görülmüştür. Sentetik fiberlerin hibritlenmesi sertlik dayanım, nem dayanım ve korozyon direnci özellikleri katmanlı olarak [20] Sentetik fiberler düşük maliyetli düşük yoğunluklu yüksek sertlik ve dayanım sunarlar. Bundan dolayı tabakalı metal alaşımlar yerine sentetik fiberlerin kullanımı ile 30'a kadar ağırlık ve 20'ye kadar maliyetten tasarruf edilebilir. Erkendirici [2023] Aracora [2022] Matrisin aynı olup da fiber kombinasyonlarının farklı olarak kullanıldığı hibrit kompozitlerden en çok bilineni cam karbon fiber takviyeli kompozitlerdir. Ta [20] Cam karbon fiber takviyeli kompozitlerin en çok tercih edilmesinde yüksek modül ve yüksek maliyetli cam karbon fiber yapları karbon fiber yüksek maliyetli ve yüksek maliyetli cam karbon fiber yapları ile karşılaştırıldığında yüksek maliyetli cam karbon fiber yapları E cam düşük maliyetli ve yüksek maliyetli cam karbon fiber yapları ile karşılaştırıldığında yüksek maliyetli cam karbon fiber yapları sonucunda mekanik özellikleri bakımından yüksek maliyetli cam karbon fiber yapları ise minimum düşürülmüştür. Cam karbon fiber tabakalı kompozitlerde fiber tabakalarının yerlerinin de etkisi sonucunda mekanik özellikleri önemli ölçüde değişmektedir. Örneğin cam fiberler düşük maliyetli cam karbon fiberler gibi tabakalarda olacak şekilde bir tabakalanma sınırları ile cam fiberli tabakalarda karbon fiberli tabakalarda olacak şekilde bir tabakalanma sınırlarıyla ilgili olarak daha yüksek dayanım ve kopma yükü sağlanabileceği belirlenmiştir. Pandya vd [20] Ayrıca Hang vd [20] tarafından yapılan çalışmada kompozitlerin 0 si karbon fiber ve 0 si cam fiber oranında olacak şekilde üretilmesi yapıldığında dayanımının tabakalı yapıların sınırlarıyla ilgili olarak sadece ilme

dayan m n n karbon fiberlerinin en d tabakada oldu u hibrit kompo it yap lar nda en iyi sonu lar elde edildi i g r lm t r arbon fiberin hibrit kompo itlerde bu kadar ok kullan lmas nda d k yo unluk ve y ksek dayan mlar nedeniyle havac lk ve u ay sanayisi olmak ere bir ok alanda m hendislik mal emesi olarak tercih edilmektedir arbon fiberler ani ve gevrek bir bi imde hasara u ramalar sonucunda tasar mda y ksek emniyet katsay lar kullan lmas n gerektirdi inden di er elyaf t rleri ile hibritlenmektedir Literat rde karbon fiberlerin ba ta cam fiber Dong ve Davies 20 Dong vd 20 u vd 20 olmak ere evlar weben 77 hite vd 2003 im vd 20 oo 20 ba alt Dorigato ve Pegoretti 20 3 Ferrante vd 20 nylon 2 Hine vd 20 4 gibi sentetik fiberlerle kenaf Sapiai vd 20 4 kenevir Fong vd 20 2 gibi do al fiberler ve metalik fiberlerle Hannemann vd 20 20 7 hibritlendi i g r lmektedir Bu ekilde karbon fiberlerin de avanta lar ortadan kald r lmaya al lmaktad r

Hibrit kompo itlerde mekanik ellikleri daha da geli tirmek i in y ey i lemleri Nega vd 2022 fiber oryantasyonlar Seyed aghoubi vd 20 2 ve matris takviyesi hang vd 20 4 gibi e itli y ntemler de mevcuttur ompo it mal emelerin kullan m yerlerinden kaynakl olarak fiber oryantasyonunda de i imler yap lamamaktad r Bu durumda en ok tercih edilen y ntemler matris takviyesidir arei vd 20 7 Matris takviyesi olarak nanopar ac klar Nega vd 2022 nanofiber matlar Saghafi vd 20 4 ve filmler Dhaliwal ve Newa 20 tercih edilmektedir Son y llarda evre dostu mal emeler daha ok tercih edilmeye ba lanm t r Gholampour ve O bakkaloglu 2020 D k yo unluklu d k maliyetli ve geri d n t r lebilir olmas sebebiyle sel lo lifleri kompo itlerde kullan lmaya ba lan lm t r Alamri ve Low 20 2 ompo it mal emelerin mekanik ve fi iksel ellikleri erindeki etkisini incelemek i in kenaf kenevir keten bambu ve ah ap gibi e itli sel lo lifleri erinde e itli ara t rmlar yap lm t r Sel lo lif i eren tabakalar kompo itlerde matris takviyesi olarak son y llarda kullan lmaya ba lanm t r Alamri ve Low 20 2

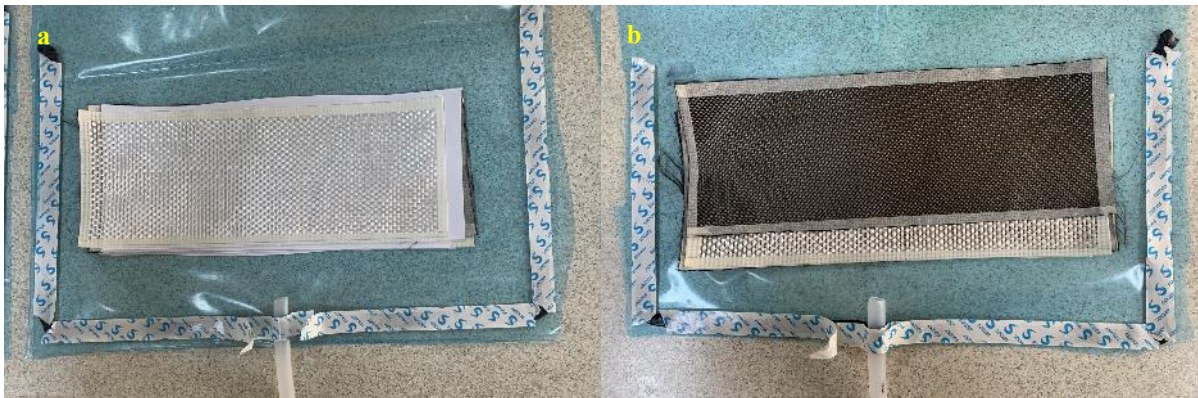
Bu al mada ka t takviyeli hibrit kompo itlerin retimi yap lm ve ka t takviyesinin dayan m erindeki etkisi ara t r lm t r a t takviyesinin tabakalar aras k r lmada etkin bir rol oynad g lenmi tir Simetrik bir kompo it yap elde edebilmek i in en d ta cam fiber i eren hibrit kompo itler ile en d ta karbon fiber i eren iki ayr hibrit kompo it retilmi tir ekme durumunda olu acak hibrit etkisi de g lemlenmi tir

2 A A O

Hibrit kompo it retimi i in gerekli olan kuma lar Dost imya firmas nda temin edilmi tir 200 g m2 lik nominal a rl a sahip d rg cam kuma lar n elyaf aplar yakla k m dir ve rg deki her elyaf demeti 3000 elyaftan olu maktad r ksek mukavemetli karbon kuma lar da 200 g m2 lik nominal a rl a sahip d rg ekinde olup elyaf aplar 7 m dir ve elyaf demeti 3000 elyaftan olu maktad r nf yon ve laminasyon elli ine sahip olan Epoksi re ine sistemi Hexion firmas taraf ndan retilmi olup d k visko iteli MGS L 0 diglisidil eter bisfenol A DGEBA epoksi ve sertle tirici olarak ayn firmaya ait MGS L2 0 amin sertle tirici tercih edilmi tir uma tabakalar aras nda kullan lacak olan sel lo ka t ise 0 g m2 olup Ve Ge firmas ndan al nm t r

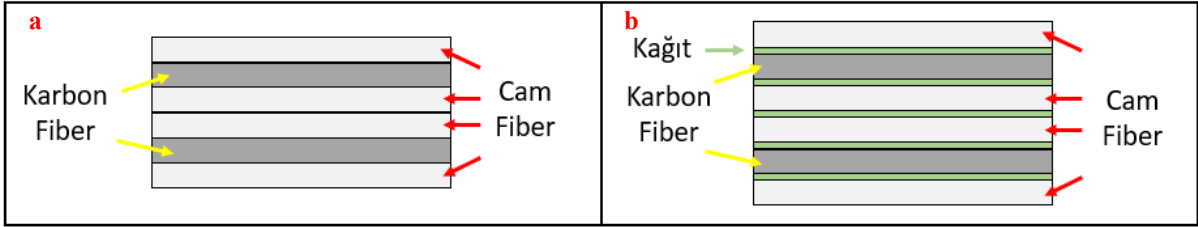
2.1 Hibrit m zitleri retimi

Hibrit kompo it mal emelerin retimi i in cam karbon kuma lar ve sel lo ka tlar belirlenen l llerde kesildi Vakum Destekli Re ine Transfer al plama VARTM retimi uygulanaca ndan dolay ayn boyutlarda ay rma kuma ve da t c file kesildi Bu retim y nteminin se ilmesindeki temel etken retim prosesinin kolay ve ok ekipman gerektirmemesidir Asim vd 20 7 Vakum naylonu ise belirtilen boyutlardan daha b y k olacak ekilde kesildi ekil

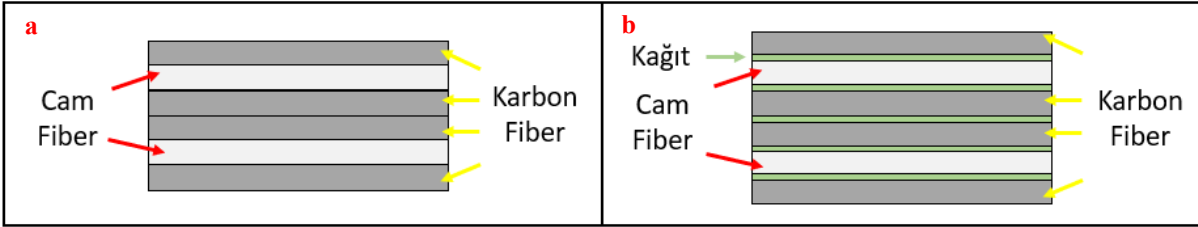


e il 1 ompo it retim ncesi ha rlık amalar a En d ta cam kuma lar n b En d ta karbon kuma lar n bulund u numuneler

Hibrit kompo iti olu turacak kuma lar kat olacak ekilde denlenmi tir uma lar n s ralamas nda iki farkl di ilim uygulanm tr Bu iki farkl di ilim i in hibrit kompo itin en d tabakas nda cam kuma lar ekil 2a ve yine en d tabakada karbon kuma lar ekil 3a olacak ekilde di ilim yap lm tr Ayr ca her iki tr di ilimde ka t takviyesi olacak ekilde her kuma tabakas aras na sel lo ka t yerle tirilmi tir ekil 2b ve 3b

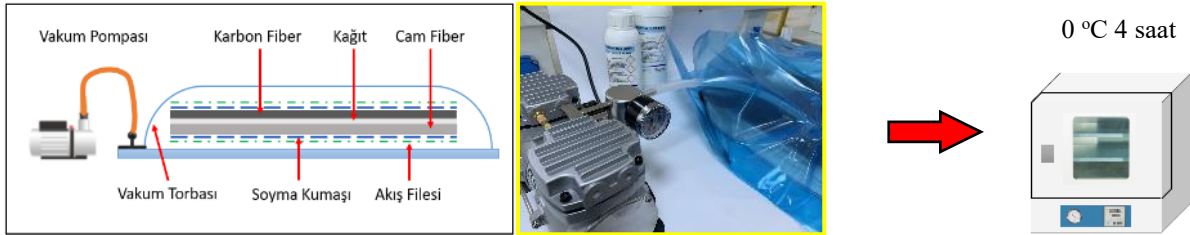


e il 2 ompo itte cam kuma lar n en d tabakada oldu u yerle im d eni a a t takviyesi b a t takviyeli



e il 3 ompo itte karbon kuma lar n en d tabakada oldu u yerle im d eni a a t takviyesi b a t takviyeli

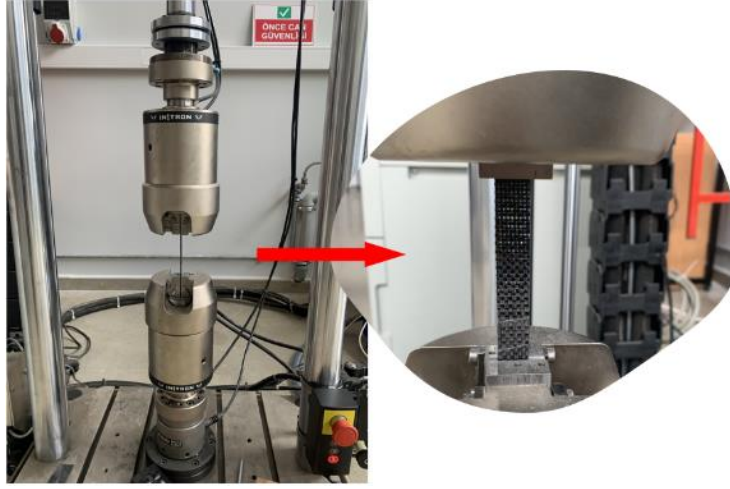
uma lar n erine s ras yla ay rma kuma ve da t c file serildi Sistemde vakum ortam sa layabilmek i in etraf na s d rma l k band ekildi ve vakum naylonu ile kapat ld Daha sonra sisteme vakum pompas ba lanarak ekil 4 te g sterildi i gibi sisteme vakum alt nda epoksi verildi ve i erideki hava ve fa la epoksi di er taraftan tahliye edildi ompo it mal eme 0 °C de 4 saat olacak ekilde k rlendi ompo it levhalar y ksek h l dairesel testere ile kesilerek ekme testi numunesi boyutlar na getirildi



e il Hibrit kompo itin retim a amalar n n ematik g sterimi

2.2 e a i test

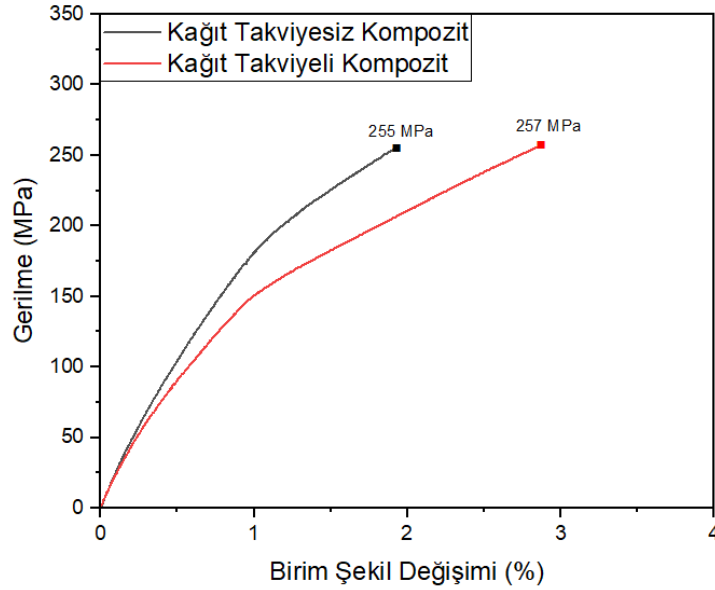
ompo it mal emelerin ekme testleri Instron 0 test ciha nda ASTM D303 standard na g re numune boyutlar 2 0 mm 2 mm 3 mm boyutlar nda olacak ekilde 2 mm dk ene ilerleme h nda ve be tekrar l oda s cakl nda yap lm tr niversal test ciha n n eneleri aras na ba lanarak ekme kuvveti uygulanan bir numuneye ait foto raf ekil te g sterilmi tir



ekme testi s ras ndaki g r nt

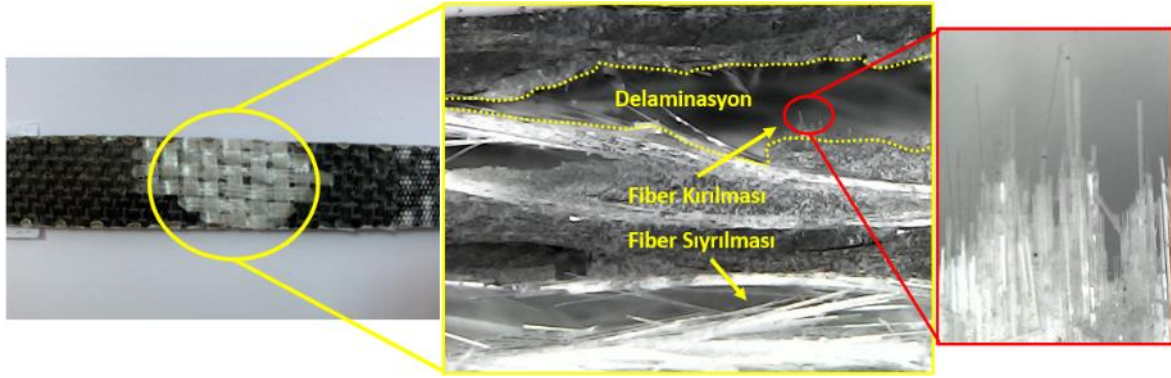
3 A

retimi yap lan kompo itler ekme testine tabi tutularak kompo itin ekme dayan m bulunmu tur Ayr ca her tabaka aras na yerle tirilen ka d n kompo itin dayan m na olan etkisine bak lm t r En d tabakada cam kuma tan olu an ka t takviyeli ve ka t takviyesi hibrit kompo ite ait gerilme birim ekil de i imi grafi i ekil da verilmi tir



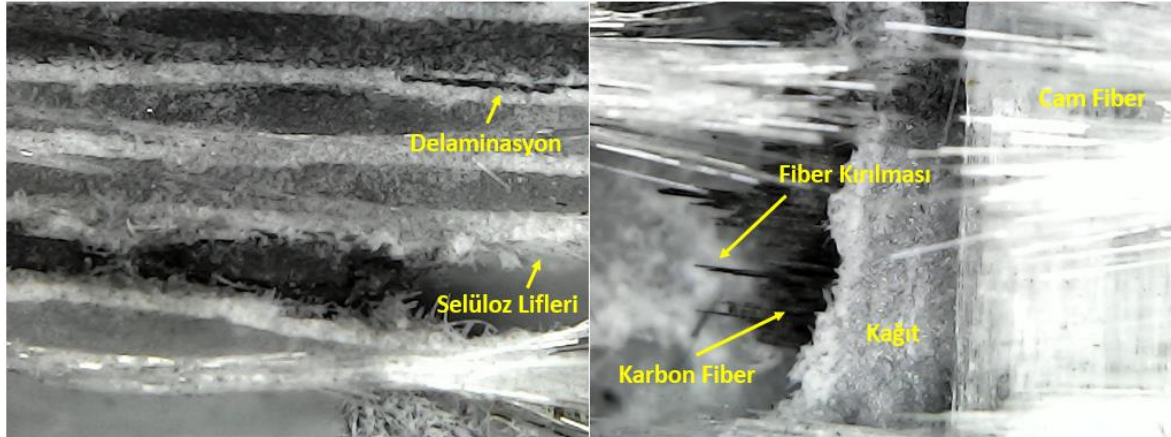
ekme testi sonu lar

Cam kuma tabakan n en d ta yer ald hibrit kompo it ka t takviyesi oldu u durumda 2 MPa l k bir ekme dayan m meydana gelirken ka t takviyeli oldu u aman 2 7 MPa l k bir sonu ortaya km t r a t takviyesi ile birlikte ekme dayan m nda nemli bir art g kme ken ekil de i iminde art a sebep olmu tur ekme testi sonucunda olu an k r lma y eyinden al nan mikroskop g r nt leri ekil 7 ve de verilmi tir a t takviyesi kompo itten al nan g r nt lerde ekil 7 cam fiberlerde fiber k r lmas ve s yr lmas n n yayg n oldu u belirlenmi tir arbon kuma tabaka ile cam kuma tabaka aras nda ise delaminasyonlar n yayg n oldu u g r lmektedir



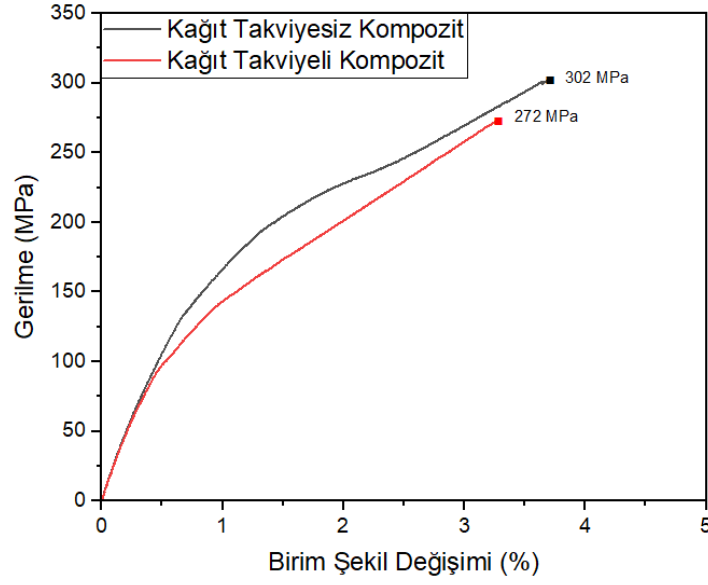
e il En d tabakada cam kuma n bulundu u ka t takviyesi hibrit kompo itin mikroskop g r nt leri

ka t takviyesi olan kompo itten al nan mikroskop g r nt lerinde ise ben er hasar t rleri mevcut olup ka t tabakas n n kuma y eylerine yap mas ndan dolay sel lo liflerin s yr lmas n g r mekteyi ine cam tabakalar aras nda delaminasyonun oldu u ve delaminasyonun oldu u b lgede ka t tabakas n n olmas ndan dolay kohe yon hasar vard r

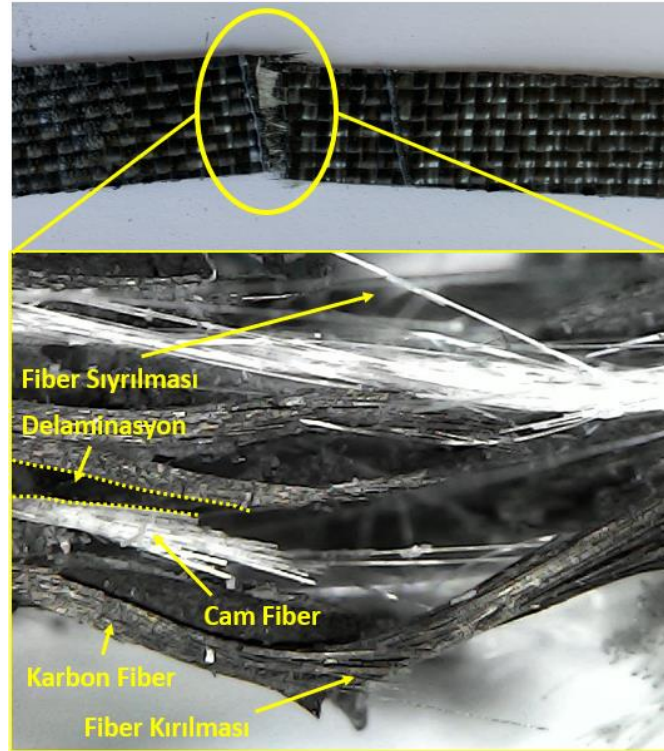


e il En d tabakada cam kuma n bulundu u ka t takviyeli hibrit kompo itin mikroskop g r nt leri

Di er di ilim t r ne sahip en d tabaka karbon kuma ka t takviyeli ve ka t takviyesi hibrit kompo itin gerilme birim ekil de i imi grafi i de ekil da verilmi tir ekme testi sonu lar incelendi inde ka t takviyesi kompo itte 302 MPa ve ka t takviyeli kompo itte ise 272 MPa l k ekme dayan m km t r arbon fiber a r l kl bir kompo itte ka t takviye edildi inde dayan mda 0 a alma meydana gelmi tir Cam fiber a r l kl kompo itle k yasland takdirde ise daha y ksek dayan m sergilemektedir Bunu da karbon fiberden kaynakl olmaktadır Ayd n vd 20 taraf ndan yap lan al mada da cam ve karbon fiberler kullanarak hibrit kompo it yap n n retimi yap ld ve bu yap n n mekanik ve dinamik elliklerini incelemi lerdir Test sonu lar na g re sadece karbon yap n n dinamik ve mekanik ellikler bak m ndan en iyi sonucu verdi i g lemlenmi lerdir

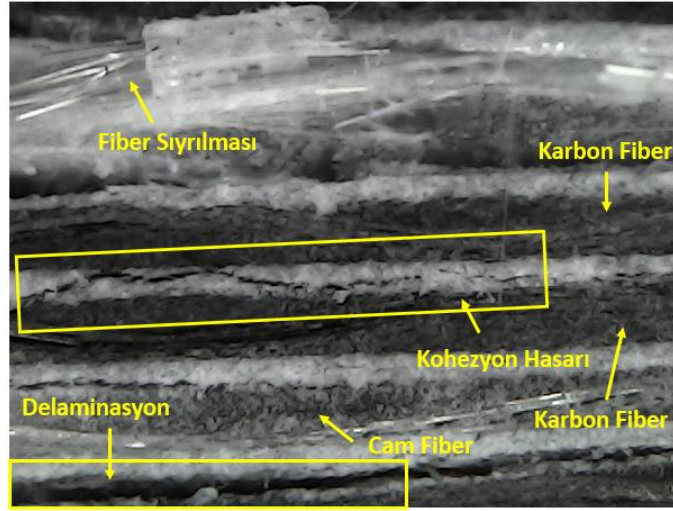


Şekil 10 En d tabakada karbon kuma n bulundu u hibrit kompo ite ait ekme testi sonu lar



Şekil 11 En d tabakada karbon kuma n bulundu u ka t takviyesi hibrit kompo itin mikroskop g r nt leri

Mikroskop g r nt leri incelendi i takdirde ka t takviyesi numunede ekil 0 ekme testinden kaynakl olarak yaygın olarak fiber kırılmalar ve sıyrılmalar mevcuttur. İnce karbon fiber tabaka ile cam fiber tabaka arasında delaminasyonların yaygın olduğu görülmektedir. Ka t takviyeli kompo itte ise sel lo ka t tabakas ndan kaynakl olarak karbon tabakalar arasında kohe yon hasarının oluştu u belirlenmiştir.



Şekil 11. En d tabakada karbon kuma n bulundu u ka t takviyeli hibrit kompo itin mikroskop g r nt leri

A A SO A

ka t takviyesinin hibrit kompo it yap lar n dayan m lerinde etkisi ara t r lm t r Bu do rultuda karbon ve cam kuma lar kullan larak kompo itler VARTM y ntemi ile retilmi tir Bu kompo itler ha rlan rken en d tabakada cam fiberler oldu u ve di er bir grup olarak da en d ta karbon fiberlerin oldu u bir di ilim tercih edilmi Tabaka say s bak m ndan 7 si karbon fiberden olu an hibrit kompo it ile 7 si cam fiberden olu an hibrit kompo itin ekme dayan m s ras yla 302 ve 2 MPa d r Ayr ca bu iki t r i in de ka t takviyesi yap lm ve her grup kendi i erisinde ekme testi sonu lar incelenmi tir Cam fiber a rkl hibrit kompo itte ka t takviyesi sonucunda birim ekil de i iminde art olurken dayan mda da ok a bir art olmu tur Fakat karbon fiber a rkl hibrit kompo itte ise ka t takviyesi ekme dayan m nda d e sebep olmaktadır ka t takviyesinde ekme dayan m n n d mesinin sebebi karbon fiberin elastik mod l n n ok y ksek olmas ndan kaynakl oldu u eklinde yorumlanabilir

KA AK A

Alamri H Low I M 20 2 Microstructural mechanical and thermal characteristics of recycled cellulose fiber halloysite epoxy hybrid nanocomposites Polymer Composites 33 4 00

Asim M awaid M Saba N Nasir M Sultan M T H 20 7 Processing of hybrid polymer composites a review Hybrid polymer composite materials 22

Ayd n M R Acar V ap c F ld Topcu M V G ndo du 20 Inter ply Hibrit ompo it ap larda Elyaf Di ili S ralamas n n Mekanik ve Dinamik elliklere Etkisi urnal of the Institute of Science and Technology 3 2 2 3 DOI 02 7 ist 4 4

Demir O 20 7 arbon Nanot p atkl Cam arbon Fiber Epoksi Hibrit Nanokompo itlerin Mekanik ellikleri ve D k h l Darbe Davran lar Sel uk niversitesi Fen Bilimleri Enstit s

Dhaliwal G S Newa G M 20 Effect of layer structure on dynamic response and failure characteristics of carbon fiber reinforced aluminum laminates CARALL urnal of Dynamic Behavior of Materials 2 3 40

Dong C Davies I 20 Flexural strength of bidirectional hybrid epoxy composites reinforced by E glass and T700S carbon fibres Composites Part B Engineering 72 7

Dong C alantari M Davies I 20 Robustness for unidirectional carbon glass fibre reinforced hybrid epoxy composites under flexural loading Composite Structures 2 3 4 3 2

Dorigato A Pegoretti A 20 4 Flexural and impact behaviour of carbon basalt fibers hybrid laminates urnal of Composite Materials 4 2 30

- Erkendirci H 2023 Cam karbon kuma ve polipropilen takviyeli hibrit kompozitlerin mekanik özelliklerinin araştırılması ve analizi Marmara Üniversitesi Fen Bilimleri Enstitüsü
- Ferrante L Tirilli Sarasini F Touchard F Ecault R Urriaga M Vignati Mellier D 2020 Behaviour of woven hybrid basalt carbon epoxy composites subjected to laser shock wave testing Preliminary results Composites Part B Engineering 7 2 73
- Fong Mariatti M Takagi H 2022 Effect of Matrix and Stacking Sequence of Recycled Waste Carbon Fiber Hybrid Laminated Composites Journal of Polymer Materials 2 4
- Gholampour A Ozbakkaloglu T 2020 A review of natural fiber composites Properties modification and processing techniques characterization applications Journal of Materials Science 3 2 2
- Hannemann B Backe S Schmeer S Balle F Breuer U P 2020 Metal fiber incorporation in carbon fiber reinforced polymers CFRP for improved electrical conductivity Steigerung der elektrischen Leitfähigkeit von kohlenstofffaserverstärkten Kunststoffen CF durch Integration von Metallfasern Materialwissenschaft und Werkstofftechnik 47 10 1023
- Hannemann B Backe S Schmeer S Balle F Breuer U P Schuster 2020 Hybridisation of CFRP by the use of continuous metal fibres MCFRP for damage tolerant and electrically conductive lightweight structures Composite structures 72 374 3 2
- Hayashi T 2022 On the improvement of mechanical properties of composites by hybrid composition In Proceedings of the 14th International Reinforced Plastics Conference pp 4 2
- Hine P Bonner M Ward I M Swolfs Verpoest I Mierwa A 2020 Hybrid carbon fibre nylon 2 single polymer composites Composites Part A Applied Science and Manufacturing 2
- İbrahim B Canlı M 2022 The effect of use of different types of matrix material on mechanical characteristics in waste carbon fiber reinforced hybrid composites Niğde Ömer Halisdemir Üniversitesi Mühendislik Bilimleri Dergisi 2 43 44
- Lim S C Lim S Moon H 2020 Experimental and numerical investigations of mode I delamination behaviors of woven fabric composites with carbon fibers and their hybrid fibers International Journal of Precision Engineering and Manufacturing 2 32 32
- Umar A Peyyalal L P Umar D B 2022 Hybridization of polymer composites International Advanced Materials Science 3 73 2
- Nega B F Pierce R S Li Liu 2022 Characterization of Mechanical and Damping Properties of Carbon Waste Fibre Hybrid SMC Composites Applied Composite Materials 2 4 37
- Pandya S Veeraru C Naik N 2020 Hybrid composites made of carbon and glass woven fabrics under quasi static loading Materials Design 32 7 40 4 40
- Saghafi H Lucchelli A Palaletti R Minak G 2020 The effect of interleaved composite nanofibrous mats on delamination behavior of polymeric composite materials Composite Structures 10 4 47
- Sapiai N Umahat A Hakim R N 2020 Tensile and compressive properties of hybrid carbon fiber kenaf polymer composite Adv Environ Biol 2 2
- Seyed Aghoubi A Liu Liaw B 2022 Stacking sequence and geometrical effects on low velocity impact behaviors of GLARE 3 2 fiber metal laminates Journal of thermoplastic composite materials 2 2 223 247
- Swolfs Gorbatikh L Verpoest I 2020 Fibre hybridisation in polymer composites A review Composites Part A Applied Science and Manufacturing 7 200
- Ta H Soykok F 2020 Tabakal Hibrit Kompozit Profillerin Doğal Frekanslarının Sonlu Elemanlar Metodu ile Belirlenmesi Doku EYL 1 Üniversitesi Mühendislik Fakültesi Fen ve Mühendislik Dergisi 20 10 104 10

White D M Taylor E A Clegg R A 2003 Numerical simulation and experimental characterisation of direct hypervelocity impact on a spacecraft hybrid carbon fibre kevlar composite structure International journal of impact engineering 29 10 777-790

Woo S C Kim T 2020 High strain rate failure in carbon kevlar hybrid woven composites via a novel SHPB-AE coupled test Composites Part B Engineering 197 3 732

Wu H Longana M L Alalvand M Isnom M R Potter D 2020 Pseudo ductility in intermingled carbon glass hybrid composites with highly aligned discontinuous fibres Composites Part A Applied Science and Manufacturing 133 3 44

Xie H Brugo T Belcari Bisadi H Minak G Lucchelli A 2017 Low velocity impact damage assessment of GLARE fiber metal laminates interleaved by Nylon nanofiber mats Composite Structures 173 23-3

Xiang H Gn S An Xiang L 2014 Impact behaviour of GLAREs with MWCNT modified epoxy resins Experimental Mechanics 54 3 3

Xiang Chaisombat He S Xiang C H 2012 Hybrid composite laminates reinforced with glass carbon woven fabrics for lightweight load bearing structures Materials Design 10 20 37-50

Yeben C 1977 Tensile strength of hybrid composites Journal of materials science 12 32 337

Nonlinear Seismic Analysis of RC Structures under Realistic Earthquake

İsmail İsmail*¹, Muhammet Karat²

Abstract Two destructive earthquakes in the Kahramanmaraş province of Turkey hit with an epicenter of Pazarcık and Elbistan on February 6, 2023. The magnitudes and depths of the earthquakes were recorded as 7.7 km for Mw 7.7 and 7 km for Mw 7.8 respectively. The earthquakes affected a wide region covering Kahramanmaraş, Gaziantep, and Adana provinces and more than 10 thousand citizens lost their lives. Absolute maximum acceleration value of the earthquake acceleration records were determined that bigger than predicted design earthquake acceleration values in some regions of the Turkey Earthquake Hazard Map (TEHM). For this reason, damages above the calculated damage were observed in the structures. In this study, a 24-story reinforced concrete building with frame and shear walls is selected. Nonlinear time history analyses of the building are obtained under two earthquake acceleration records. Damage cases are compared for two analyses results. The first earthquake records used in the analyses are data from station 44 recorded in Pazarcık, Kahramanmaraş during the Pazarcık earthquake. The second earthquake records are artificially generated by using the design acceleration spectrum graph in the Turkish Building Earthquake Code (TBEC).

Keywords Reinforced concrete building, Pazarcık Earthquake, Artificially generated earthquake records and nonlinear time history analyses

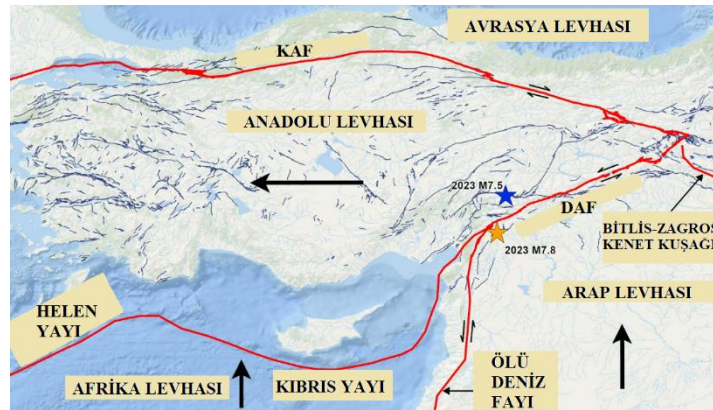
¹İsmail İsmail, Bilecik Seyyid Edebali University Faculty of Engineering, Bilecik, Turkey

²Muhammet Karat, Fırat University Faculty of Engineering, Elazığ, Turkey

*İsmail İsmail, ismail@bilecik.edu.tr

1

Deprem Türkiye'nin bulunduğu konumundan dolayı günümüz kadar ya da en fazla can ve mal kaybına neden olan afet türü Türkiye'de Alp-Himalaya depremi kuşağında ve büyük depremler üreten Anadolu Fayı (AF), Doğu Anadolu Fayı (DAF) ve Ege Dalma Batma Fayı (EBF) üzerinde yer almaktadır. 2023 yılı Ocak ayında meydana gelen Afrika-Arabistan levhalarının kuzey-kuzeydoğu hareket etmeleri ile Avrasya levhası arasında bulunan Anadolu levhasının sıkışması ile ilgilidir. Arabistan levhası kuzeydoğu itilirken Avrasya levhasının altına doğru dalma hareketine girmektedir. Ege Dalma Batma Fayı gibi Arabistan levhası ile Avrasya levhası arasında kalan Doğu Anadolu levhası sıkışmakta ve batıya doğru Ege Dalma Batma Fayı'na hareket etmektedir. Böylece AF ile DAF'ın kuzey Anadolu levhasındaki sıkışma günümüz kadar olan depremlerin ana nedenini oluşturmaktadır (Atabay, 2000).



Şekil 1 Levha hareketleri ve Anadolu levhasının batıya hareketi (USGS, 2023)

2023 yılında günümüz kadar büyük Mw 7.7 ve 7.8 büyüklüğünde olan bir ok depremin yaşandığı Anadolu A.ans 2023 Ocak ayında 06 Ocak 2023 tarihinde Pazarcık Kahramanmaraş merkezli Mw 7.7 büyüklüğünde 7 km derinliğinde ilk deprem aynı gün Elbistan Kahramanmaraş merkezli Mw 7.8 büyüklüğünde yerin 7 km derinliğinde ikinci deprem

meydana gelmi ve b y k bir y k m ya anm t r sa bir aman i inde ger ekle en iki ok iddetli deprem ili i eren ok geni bir b lgeyi etkileyerek ok say da can ve mal kayb na yol a m t r AFAD 2023 Ana depremlerden sonra meydana gelen iddetli art depremler de hasarlı binalar n hasar d eyini art rm t r 27 ubat 2023 te kaydedilen ba istasyonlar n ivme kay tlar na ait tepki spektrumlar n n geometrik ortalamas ile s n m oran ve C emin s n f i in DD Deprem er Hareketi D eyi yatay elastik tasar m ivme spektrumu kar la t r lm t r Belirli periyotlarda 0.2 s 0.5 s ve 2.0 s tepki spektrumlar n n geometrik ortalamas n n yatay elastik tasar m ivme spektrumunun erinde kald tespit edilmi tir Bu durum en ok Hatay da g r lm t r T 2023 DD2 Deprem er Hareketi D eyi 2 tasar m depreminin erinde spektral ivme de erlerinin kaydedilmesinin yan s ra T rkiye Bina Deprem netmeli i TBD 20 nde DD depremi i in olmas beklenen spektral ivme de erlerinin de a ld periyot aral klar olu mu tur Av ar vd 2023 Depremin etkisi sonucunda bir ok farkl hasar n olu tu u belirtilmi tir Akg l ve Etli 2023 Binalar n g mesine sebep olan etkenlerden biri de re onans ile birlikte binalar n do al titre im periyotlar n n depremin hakim periyodu ile ak mas sonucu binalar n davran lar ndaki beklenmedik art lard r ksek periyotlardaki b y tmeler y ksek binalar ve d k periyotlardaki b y tmeler ise y ksek olmayan binalar etkilemektedir Perk ve er 20 Ayr ca yap sal d ensi liklerden kaynaklı hasarlar da meydana gelmi olup ta y c sistemi ri itlik bak m ndan d enli olmad i in burulma davran sonucunda g melerin ya and durumlar da g r lm t r TMMOB MO 2023 Bu bak m dan binalar n ta y c sisteminde perde kullan m nem ar etmektedir Bina y ksekli ine ba l olarak y ksek binalar n ta y c sistemleri er eveli perdeli ve perdeli er eveli olarak farkl ekillerde tasarlanabilmektedir eybek 2022

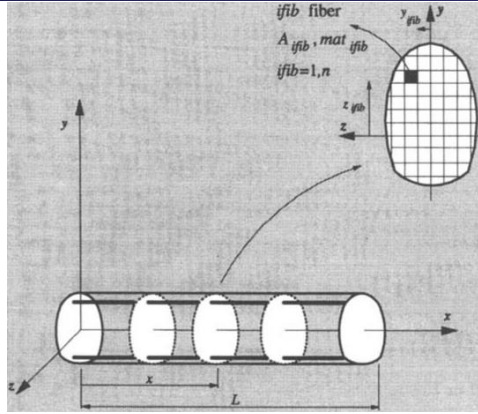
Bu al mada 24 katlı betonarme perdeli er eveli binan n TBD 20 ye g re do rusal olmayan sismik anali i yap lm t r Bina plan n n her iki do rultusunda ahramanmara ilinin 4 4 kodlu istasyonunda kaydedilen ubat 2023 ahramanmara Pa arc k ger ek deprem ivme kayd ve emin s n f D i in ayn istasyon konumu dikkate al narak TBD 20 de belirtilen yatay tasar m ivme spektrumuyla uyumlu retelen yapay deprem ivme kayd kullan lm t r Do rusal olmayan davran kuvvete dayal fiber eleman y ntemi ile hesaba kat lm t r Anal i sonucunda yap sal elemanlarda meydana gelen hasarlar incelenmi tir

2 A A O

Deprem etkisinde bina tasar m i in TBD 20 de Dayan ma uvvete G re Tasar m DGT ve ekil De i tirmeye G re De erlendirme ve Tasar m DGDT olmak ere iki yakla m mevcuttur Do rusal davran esas alan DGT de do rusal hesap y ntemleri olan e de er deprem y k y ntemi ve modal hesap y ntemleri mod birle tirme y ntemi ve mod toplama y ntemi kullan lmaktadır Deprem y klemesinin itme y ntemleri ve aman tan m alan nda do rusal olmayan hesap y ntemlerinden biri kullan larak yap ld DGDT ise deprem sebebiyle ta y c elemanlarda meydana gelen hasar hesaba kat lmaktadır Binalar n ta y c sistemleri etkiyen y kler i in do rusal davran dikkate al narak tasarlan rlar ancak deprem etkisi alt nda do rusal davran a g re yap lan hesaplar ger ek i sonu lar vermeyebilir Do rusal olmayan hesap y ntemleri do rusal hesap y ntemlerine g re mal emelerin davran n ve geometri de i imini daha kesin hesaplad i in daha ger ek i sonu lar vermektedir Aksoylu 2020

2.1 Fiber elema y ntemi

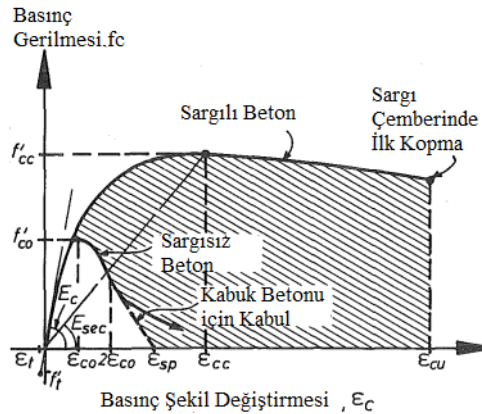
Binalarda do rusal olmayan davran i in y l ve yay l plastik davran modeli kullan lmaktadır ayl plastik davran modeli olan fiber eleman y nteminde kuvvet esneklik ve yer de i tirme deplasman esaslı olmak ere iki yakla m mevcuttur Bu y ntemde ekil 2 de g r ld gibi integrasyon noktalar ndaki kesitler kendi i inde fiber kesit h cresi lif elemanlara b l nmektedir Betonarme kesitin i inde beton ve elik fiber elemanlar n do rusal olmayan davran lar birlikte dikkate al nmaktadır Taucer vd Bu al mada kuvvete dayal fiber eleman y ntemi kullan lm olup eleman n integrasyon noktalar ndaki kesitlerinde ortaya kan i kuvvetler dikkate al narak her bir eleman n do rusal olmayan mleri elde edilmektedir Ayn amanda her bir kesitte yer alan beton fiberleri i in Mander Priestly ve Park modeli ve donat fiberleri i in ise Menegotto Pinto modeli kullan lm t r Mander vd Menegotto ve Pinto 73



Şekil 2 Eleman ve fiber h cre elemanlara b l nen kesit Taucer vd

2.1.1. a er, riestly ve ar bet m eli

Popovics 73 taraf ndan betonun tek eksenli ekme ve bas n davran n modelleyen bir e ri nerilmi tir lerleyen d nemlerde Mander vd bu modeli sarg l ve sarg s betonlar i in ekil 3 teki gerilme ekil modelini geli tirmi lerdir



Şekil 3 Sarg l ve sarg s betonun tek eksenli y kleme i in gerilme ekil de i tirme modeli Mander vd

2.1.2. e e tt i t m eli

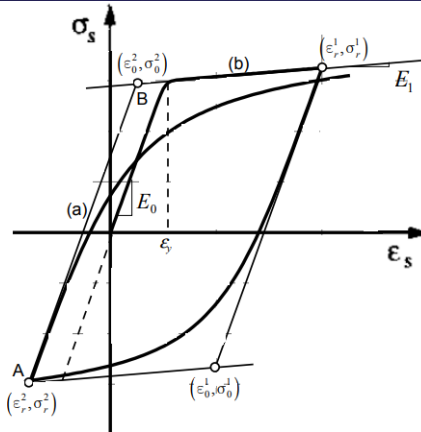
Donat eli inin do rusal olmayan gerilme ekil de i tirme davran nda Bauschinger etkisini dikkate alan model nerilmi tir Menegotto ve Pinto 73 Bu model daha sonra i otropik ekil de i tirme pekle mesini i erecek ekilde de i tirilmi tir Filippou vd 3 ekil 4 te verilen Menegotto Pinto modeline ait e itlik Denkleminde verilmi tir

$$\sigma^* = b \cdot \varepsilon^* + \frac{(1-b) \cdot \varepsilon^*}{(1 + \varepsilon^{*R})^{1/R}}$$

Bu denklemlerle E_0 e imli asimptottan a i gisi E e imli asimptota b i gisi kavisli ge i tan mlanmaktadır Denklem 2 de ε_0 ve ε_0 iki asimptotunun birle ti i B noktas ndaki σ_r ve σ_r y kn son ke bo alt ld ve tekrar y klendi i A noktas ndaki gerilme ve ekil de i tirmedir b E ve E_0 e imleri aras ndaki oran ekil de i tirme sertle me oran ve R ise ge i e risinin eklini etkileyen Bauschinger etkisini ifade etmektedir

$$\varepsilon^* = \frac{\varepsilon - \varepsilon_r}{\varepsilon_0 - \varepsilon_r}$$

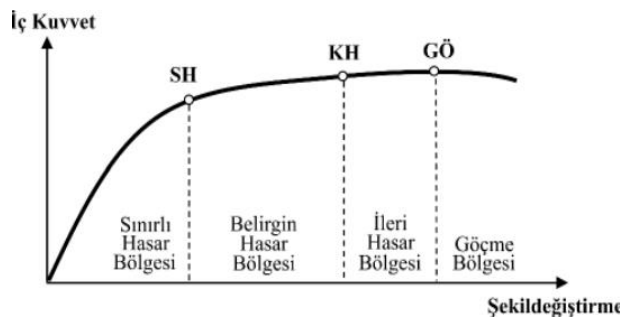
$$\sigma^* = \frac{\sigma - \sigma_r}{\sigma_0 - \sigma_r}$$



Şekil 1 Menegotto-Pinto elastik modeli (Menegotto ve Pinto, 1973)

2.2 Betonarme Elemanların Hasar Sınırları ve Hasar Bölgeleri

TBD 200'de sınırlı eleman kesitlerinde elastik-plastik davranışın sınırlı miktarda kesit dayanımını temsil eden olarak kullanılabilmesi için elde edilmiş ve ileri dönemde kullanılmak üzere sınırlı Hasar (SH), kontrol Hasar (H) ve Göçme (G) hasar durumu ve sınırlı deşimlerin tanımlanması için kritik kesitlerinin hasarının bulunduğu ve elemanların hasar durumu belirlenmektedir. Şekil 2'de SH'ye ulaşmayan elemanlar SH bölgesinde SH ile H arasında kalan elemanlar BH bölgesinde H ile G arasında kalan elemanlar H bölgesinde G'ye geçen elemanlar ise göçme bölgesinde GB yer almaktadırlar.



Şekil 2 Kesit hasar bölgeleri (TBD 200)

Şekil 2'de plastik davranış modeline göre belirlenen hasar sınırları betonarme dikdörtgen kesitli elemanların G'ye sınırlı deşimlerin Denklem 3 ve Denklem 4 kullanılarak hesaplanmaktadır.

$$\Sigma_C^{(GÖ)} = 0.0035 + 0.04 \sqrt{w_{we}} \leq 0.018 \quad (3)$$

$$w_{we} = \alpha_{se} \rho_{sh, \min} \frac{f_{ywe}}{f_{ce}} \quad (4)$$

Bu denklemlerde w_{we} , α_{se} ve $\rho_{sh, \min}$ sınırlı deşim oranı, etkin sargı donatısına ait mekanik donatı oranı, sargı donatısı etkinliği katsayısı ve dikdörtgen kesitlerde iki yatay doğrultuda hacimsel enine donatı oranının kısımlarıdır. f_{ywe} ve f_{ce} ise enine donatının ortalama akma dayanımı ve betonun ortalama basınç dayanımı olarak tanımlanmaktadır. H ve SH sınırlı deşimleri ise Denklem 3 ve Denklem 4 ile hesaplanmaktadır.

$$\epsilon_C^{(KH)} = 0.75 \epsilon_C^{(GÖ)}$$

$$\epsilon_C^{(SH)} = 0.0025$$

3.1.1 A

Bu bölümde madda 24 katlı ve katlı betonarme perdeli çerçevesiz binaların TBD 200'e göre doğrusal olmayan sismik analizi yapılmıştır. Deprem yükü olarak ahramanmara ilinin 4/4 kodlu istasyonunda kaydedilen 2003 ahramanmara Paçkırgerçek deprem ivme kaydı ve emin sınıflarının aynı istasyon konumu dikkate alınarak TBD 200'deki yatay ivme spektrumu ile uyumlu retilen yapay deprem ivme kaydı kullanılmıştır. Her iki deprem ivme kaydı binanın iki yatay doğrultusuna aynı anda uygulanmıştır. Sayısal modellerde kat deşimleri rihtiyafraam olarak kabul edilerek 1 ve hareketli yükler kirişlere yayılarak uygulanmıştır. Temel ortam ise rihtiyafraam olarak kabul edilmiştir. 3 m yükseklikli 3 m genişlikli tir binalarda çerçevesiz sistemle birlikte kullanılan perdeler binaların dış kenar ortalarında yer almaktadır. Binaların plan ve sonlu eleman modeli Şekil 3'de görülmektedir. 24

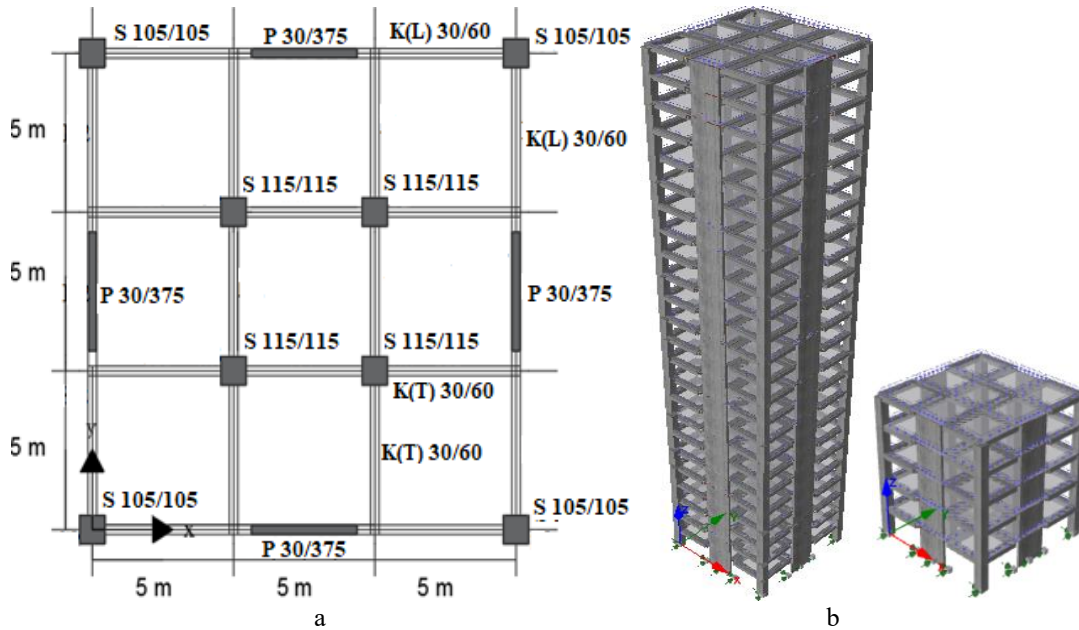
katlı binanın sonlu eleman modelinde 00 adet düğüm noktası, 12 adet perde, 2 adet kolon ve 40 adet kiriş elemanı katlı binada ise 20 adet düğüm noktası, 20 adet perde, 40 adet kolon ve 00 adet kiriş elemanı kullanılmaktadır. Uygulamaya dayalı fiber eleman yönteminde taşıyıcı elemanlar 0 adet fiber elemana kesit lif hacsi ayrılmış olup taşıyıcı elemanların donatılar ekil 7 de verilmiştir. Her bir integrasyon noktasında bir kesit dikkate alınarak elemanların doğrusal olmayan davranışları modellenmiştir. Esitlerdeki sargı b lgelerinin sargı lama etki katsayıları Tablo 2 de verilmiştir. Betonun tek eksenli basınç dayanım ve donatının akma dayanım sırasıyla 27 MPa ve 420 MPa olarak seçilmiştir. Betonun tek eksenli çekme dayanım f_{ct} ile elastisite modülü E_c ACI 308.2 e göre Denklem 7 ve Denklem 8 ile 27.2 MPa ve 23000 MPa olarak hesaplanmıştır.

$$f_{ct} = 0.5563\sqrt{f_{cc}} \text{ (MPa)}$$

7

$$E_c = 4700\sqrt{f_{cc}} \text{ (MPa)}$$

Donatının elastisite modülü ise 200000 MPa olarak dikkate alınmıştır.



Şekil 24 ve katlı binanın a) planları b) sırasıyla sonlu eleman modeli (İma, 2022)

Binaların modal analizleri 2. modülün yapılmış olup ilk modların elde edilen etkin modal kütle oranları ve periyotları Tablo 2 de verilmiştir. İlk modun periyotları kullanılarak binalardaki viskoz sınımlar hesaplanmıştır. Sınımlar olarak hesaba dahil edilmiştir. Non-merik analizleri için SeismoStruct 2022 programı kullanılmış olup binaların doğrusal olmayan davranışları için kuvvete dayalı fiber eleman yöntemi kullanılmıştır. Sismik analizleri için HHT integrasyon metodu kullanılmış olup integrasyon adımımız 0.05 s'dir. Sınımlarda gerek deprem ivme kaydı olarak Ahramanmara Paarcık depreminin 0.5 s'lik ve dağsterilen Doğu Batı DB ve üyü Gney Gbile enleri seçilmiştir. Aynı zamanda kaydın alındığı koordinatlar dikkate alınarak DD2 ve D emin sınıflarının TBD 20 deki yatay elastik tasarım ivme spektrumuyla uyumlu yapay ivme kaydı oluşturulmuştur. Ekil 10 Bu spektrum e risine ait S_{DS} ve S_D değerleri sırasıyla 2 ve 0.3 olarak belirlenmiştir. Sınımların bu ivme kayıtları 24 katlı ve katlı betonarme binalara enine ve boyuna doğrultularda etki ettirilmiştir.

Tablo 1 Sargı lama etki katsayıları aratın ve İma, 2022

Eleman	Sargı lama Etki katsayısı
P 30 37	23
S 0 0	4 4
S	3 3
30 0	02

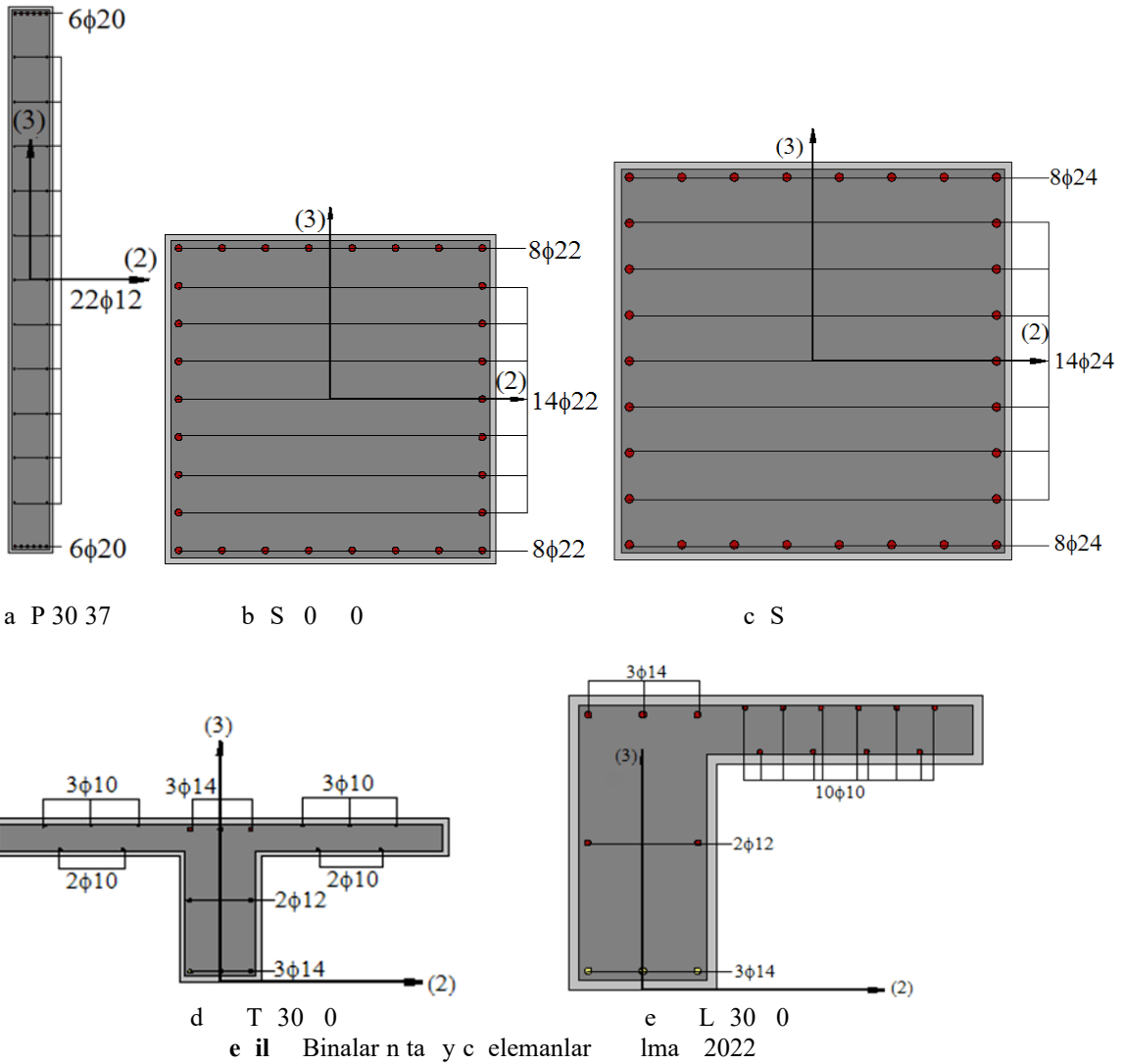
Tablo 2 Binaların modal analizleri

Bina	Etkin Modal kütle Oran U_x	Periyot T (s)

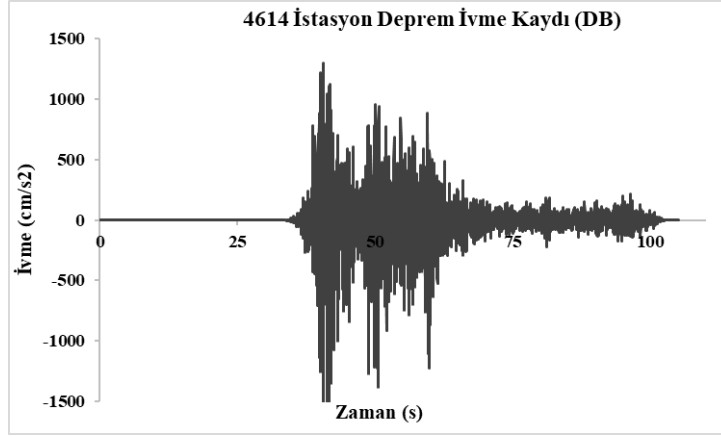
24 katlı	37 2	4
katlı	37	0 2

Tablo 3 Betonarme kesitteki hasar s n r de erleri araton ve lma 2022

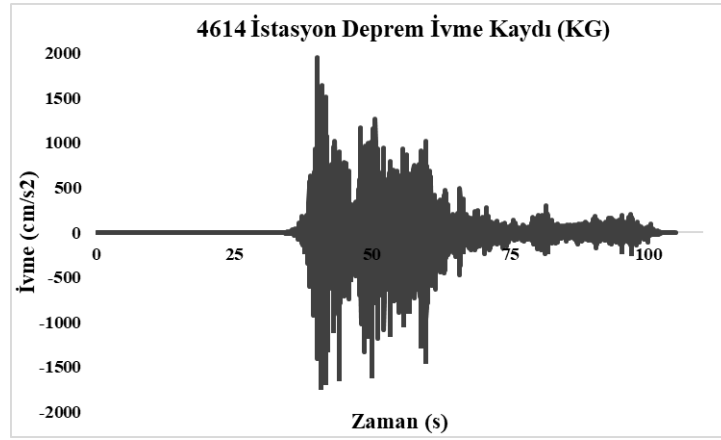
Eleman	SH	H	G
P 30 37	0 002	0 00	0 00
S 0 0	0 002	0 0 20	0 0 0
S	0 002	0 0	0 0 4
30 0	0 002	0 00 0	0 0 07



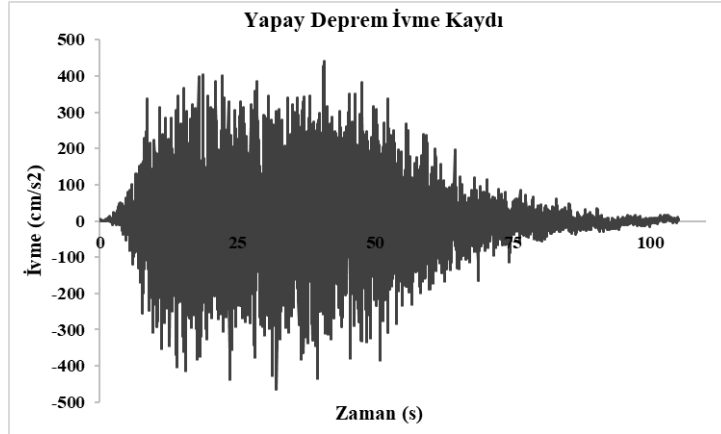
Betonarme elemanlardaki hasar s n r de erleri Tablo 3 te g r lmekte olup n merik anali lerde elde edilen hasarlar s konusu Tablo ya g re belirlenmektedir Bu ama la BH H ve GB s ras yla sar mavi ve siyah renkler ile ifade edilmi tir N merik anali lerden elde edilen hasarlar ekil ve 2 de g r lmektedir 24 katlı binaya 4 4 kodlu istasyonda kaydedilen ger ek deprem ivme kayd uyguland ır durumda emin katta adet perde ve binada toplam 00 adet kiri elemanda BH tespit edilmi tir apay ivme kayd uyguland ır nda emin katta 4 adet perde ve toplamda 2 adet kiri elemanda BH ortaya km tr Her iki m i in kolon elemanlarda herhangi bir hasar g r lmemi tir Ayn amanda katlı binaya Ger ek ve yapay deprem ivme kayd uygulanmas ır durumunda da kolonlarda hasar olu mam tr Ger ek deprem ivme kayd i in emin katta 4 adet perde elemanda ve birinci katta adet perde elemanda BH g r lm tr Binada 37 adet kiri eleman n BH 7 adet kiri eleman n H ald ır ve 7 adet kiri in ise GB de oldu u g lenmi tir apay deprem ivme kayd uygulanmas ır halinde ise kiri eleman hasar g r lmeyip sadece 2 adet perde elemanda BH meydana gelmi tir



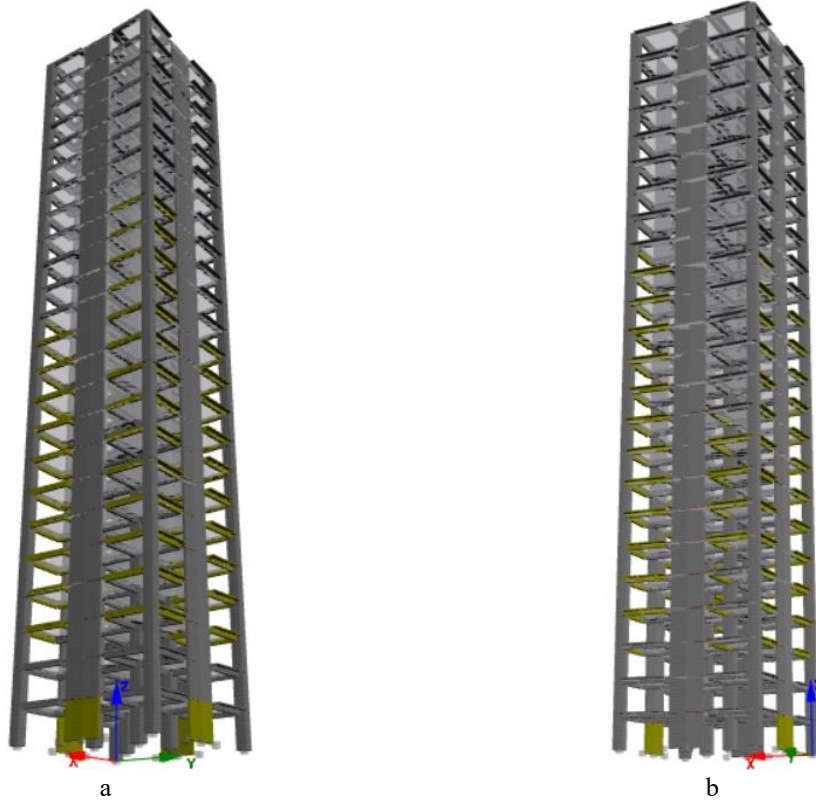
e il Ger ek deprem ivme kayd DB



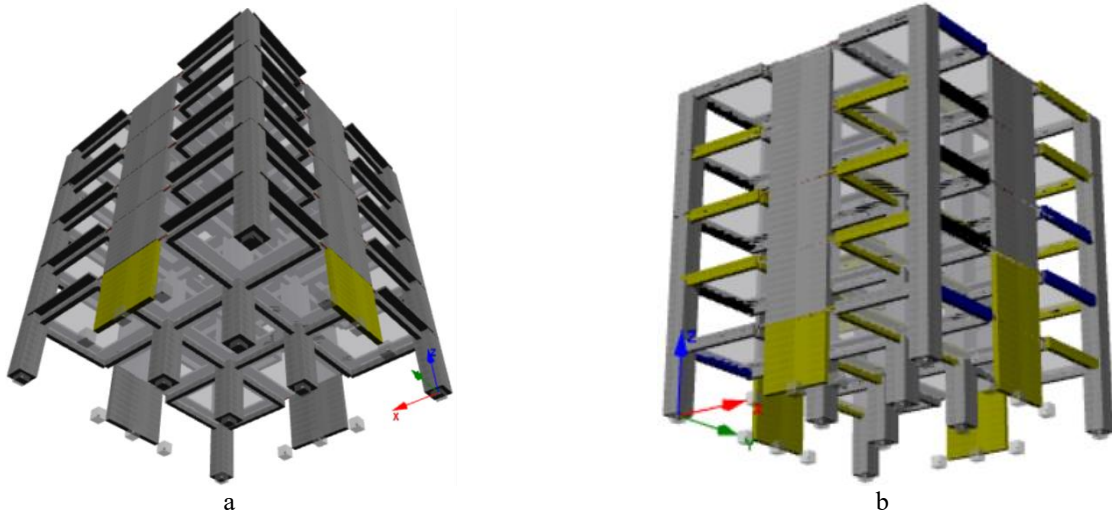
e il Ger ek deprem ivme kayd G



e il 1 apay deprem ivme kayd



Şekil 11 24 katlı binada a) yapay b) gerçek deprem ivme kaydı uygulandıktan oluşan hasarlar



Şekil 12 12 katlı binada a) yapay b) gerçek deprem ivme kaydı uygulandıktan oluşan hasarlar

A A S O A

Bu çalışmanın amacı Ocak 2023'te Türkiye'nin Kahramanmaraş'ta meydana gelen Pazarcık depreminin gerçek deprem ivme kaydı ve Türkiye Bina Deprem Yönetmeliği 2018'de belirtilen tasarım ivme spektrumu ile uyumlu yapay deprem ivme kaydı kullanılarak 24 ve 12 katlı betonarme binaların doğrusal olmayan davranışlarına olan etkilerini incelemektir. Gerçek deprem ivme kaydı 4-4 istasyonunda kaydedilen ivme verileri olup yapay deprem ivme kaydı ise Dördüncü sınıfında Deprem Hareketi Deyi 2. sınıfında belirtilen doğrusal olmayan davranış kuvvete dayalı fiber eleman yöntemi ile hesaplanmıştır. Sismik analizleri için HHT entegrasyon metodu kullanılmış olup entegrasyon zaman adım 0,005 saniye'dir.

Yapay deprem ivme kaydı altında 24 katlı betonarme binanın doğrusal olmayan analizi sonucunda BH b lgesine göre en perde ve kiriş eleman oranları sırasıyla 4,2 ve 2,0 olarak elde edilmiştir. Gerçek deprem ivme kaydı uygulandıktan sonra ise perde ve kiriş elemanların sırasıyla 10 ve 20'inin BH b lgesine göre tiğirlemiştir. Her iki ivme kaydının kullanıldığı durumda kolon elemanlarda hasarlar görülmüştür. Böylece gerçek deprem ivme kaydı

kullan lmas durumunda yapay deprem ivme kayd kullan lmas durumuna g re daha a say da perde ve kiri eleman hasarlar n n g r ld belirlenmi tir Ayr ca ayn plana sahip katl betonarme bina i in yap lan mler sonucunda ger ek deprem kayd uyguland nda perde ve kiri elemanlar n s ras yla 2 0 i ve 370 si BH b lgesine ge mi tir lave olarak kiri lerin 70 si H b lgesine ve 70 si GB ye ge mi tir apay deprem ivme kayd kullan lmas durumunda ise kiri lerde hasar meydana gelme ken perdelerde 00 BH b lgesine ge en elemanlar g r lm t r katl bina i in her iki y kleme durumunda kolonlarda herhangi bir hasar olu mam t r B ylece ger ek deprem ivme kayd kullan lmas durumu yapay deprem ivme kayd kullan lmas durumuna g re daha fa la say da perde ve kiri eleman n hasar g rmesine neden olmu tur Her iki binan n hasar durumlar kar la t r ld nda deprem y klemesinden fakl etkilendikleri g r lm t r Bu durumda katl binan n periyodunun 2 katl binan n periyoduna g re daha k sa olmas ndan dolay katl binada ivme etkisinin daha fa la g r ld sonucuna ula lm t r

ı ar atışması

a arlar n beyan edecekleri herhangi bir kar at mas bulunmamaktadır

Fi a sal este

a arlar bu al man n herhangi bir finansal destek almad n beyan etmi lerdir

KA AK A

ACI 3 Building code re uirements for structural concrete ACI 3 and commentary ACI3 R American Concrete Institute Committee 3 Farmington Hills MI USA

AFAD 2023 0 ubat 2023 Pa arc k Elbistan ahramanmara Mw 7 7 Mw 7 Depremleri Raporu Ankara AFAD Deprem dairesi ba kanl

AFAD TADAS 2023 <https://tadas.afad.gov.tr/map-eri-im-23-Temmu-2023>

Akg l M Etli S 2023 0 ubat 2023 ahramanmara Pa arc k Elbistan depremleri sonras betonarme binalarda g lenen hasar durumlar International conference on scientific and innovative studies 30 3 <https://doi.org/10.2743/isis>

Aksoylu T 2020 40 atl Asimetrik Betonarme Bir Binan n Deprem Performans n n aman Tan m Alan nda Do rusal Olmayan Hesap ntemi ile Belirlenmesi ksek Lisans Te i stanbul Teknik niversitesi Fen Bilimleri Enstit s

Anadolu A ans 2023 T rkiye ve evresi 23 lda ve eri B y kl ndeki 23 Depremle Sars ld <https://www.aa.com.tr/tr/asrin-felaketi-turkiye-ve-cevresi-23-yilda-ve-u-eri-buyuklugundeki-23-depremler-sarsildi-2-3-24> eri im 20 Temmu 2023

Atabey E 2000 Deprem <https://www.mta.gov.tr/v3/0/sayfalar/bilgi/merke-i-deprem/pdf/deprem.pdf> eri im 20 Temmu 2023

Av ar Bo er A Tunaboyu O S lev E Demirta 2023 Mw 7 7 7 ubat 2023 ahramanmara Depremlerinde 2000 Sonras ap lm Betonarme Binalar ile B lgedeki arayolu pr lerinin Sismik Performans Hatay Saha G lemleri Teknik Raporu Hatay EST

Filippou F C Popov E P Bertero V V 3 Modeling of R C oints under cyclic excitations urnal of Structural Engineering 0 2 2 4

T 2023 ubat 2023 04 7 Mw 7 ahramanmara Pa arc k T rko lu Hatay r khan ve 3 24 Mw 7 7 ahramanmara Elbistan Nurhak ardak Depremleri Nihai Rapor

araton M lma 2022 Betonarme binalar n fiber eleman y ntemiyle burulma davran n n incelenmesi Doku Eyl l niversitesi Fen ve M hendislik Dergisi 24 72 773 7 <https://doi.org/10.2202/deufmd.202224720>

Mander B Priestly M N ve Park R Theoretical Stress Strain Model for Confined Concrete urnal of the Structural Engineering ASCE 4

Menegotto M Pinto P E 73 Method of analysis for cyclically loaded R C plane frames including changes in geometry and non elastic behaviour of elements under combined normal force and bending In IABSE Symposium on Resistance and Ultimate Deformability of Structures Acted on by Well Defined Repeated Loads pp 22 Lisbon

Perk er 20 vme l er stasyonlar Alt ndaki emin elliklerinin Deprem ayd ullan larak ncelenmesi Hatay rne i T rkiye Turkish ournal of Earth uake Research 2 7 7
https://doi.org/10.4444/tdad.2332

Popovics S 73 A numerical approach to the complete stress strain curves for concrete Cement and Conor Res 3 3

Seismosoft 2022 SeismoArtif 2022 er eveli yap lar n statik ve dinamik do rusal olmayan anali i i in bir bilgisayar program

Seismosoft 2022 SeismoStruct 2022 er eveli yap lar n statik ve dinamik do rusal olmayan anali i i in bir bilgisayar program

Taucer F F Spacone E Filippou F C A fiber beam column element for seismic response analysis of reinforced concrete structures Report No UCB EERC 7 Berkeley USA Earth uake Engineering Research Center College of Engineering

TBD 20 T rkiye Bina Deprem netmeli i Afet ve Acil Durum netimi Ba kanl Ankara

TMMOB MO 2023 ubat 2023 ahramanmara Pa arc k ve Elbistan depremleri n de erlendirme raporu Eri im adresi https://www.imo.org.tr/Eklenti/7/imo-deprem-raporu-2pdf.pdf/0

USGS 2023 https://www.usgs.gov/media/images/tectonic-map-turkey-region-eri-im-20-Temmu-2023

Ima 2022 Fiber Eleman ntemi ullan larak Betonarme ap lar n Do rusal Olmayan Sismik Analisi ile Burulma Davran n ncelenmesi ksek Lisans Te i F rat niversitesi Fen Bilimleri Enstit s

n B 202 Identification of failure mechanisms in existing unreinforced masonry buildings in rural areas after April 4 20 earth uake in Turkey ournal of building engineering 43 https://doi.org/10.1080/10974462.2022.202

eybek F 2022 Deprem Etkisi Alt ndaki ksek Binalar n 20 T rk Deprem netmeli ine G re ncelenmesi ksek Lisans Te i tahya Dumlup nar niversitesi Fen Bilimleri Enstit s

Seismic Performance Evaluation of Different Structural Systems

Fatih Uzel^{*1}, Mustafa Uzel²

Abstract Seismic performance of building structures are associated with the structural systems. The structural systems are the load carrying elements transferring the vertical and lateral loads to the foundation systems in the buildings as well as delivering seismic energy dissipation. In this study, the three main structural systems and their main characteristics under earthquake events are briefly reviewed and explicitly demonstrated through response spectrum analyses. Mainly, the frame system, shear wall system and dual system consisting of frames and shear walls are explained. In addition, storey building models with different structural systems are modelled and analysed through response spectrum analyses. The results of the analyses support the typical behaviours of the frame, shear wall and dual systems. That is, the building model having frame system experiences greater lateral displacement at the lower floor levels. On the contrary, the building model owning shear wall system displaces less at the lower levels and it displaces increasingly more towards the top storey level. When the dual system is adapted, shear walls and frames limit the lateral movement at the lower and higher storey levels, respectively. Therefore, designing building structures with the involvement of both shear walls and frames shows better capacity of controlling the lateral displacement. Therefore, the dual system is always recommended in the building design, in particular, when designing mid-rise and high-rise building structures.

Keywords Earthquake load, design response spectra, lateral displacement, structural systems

¹ **Address** Iğdır University, Faculty of Engineering, Iğdır, Türkiye

² **Address** Necmettin Erbakan University, Faculty of Engineering, Eskişehir, Türkiye

* **Corresponding Author** fatih.uzel@igdir.edu.tr

1. INTRODUCTION

The rise of the immigrations from suburban areas to major cities leads to the increase of building densities that causes the limits in construction sites. In order to use these limited areas in big cities, high-rise buildings are becoming increasingly popular. With the increase in the height of the structural buildings, the rigidity of the structures and the lateral forces due to earthquake and wind loads play very crucial roles in their designs. This becomes particularly important in regions which are positioned close to the tectonic plates between which major earthquake events take place. Turkey, United States, Italy, Iran and Japan are some of the well-known places of remarkable earthquake event occurrences.

Turkey, in particular, sits on top of Anatolian and Eurasian plates neighbouring with the Arabian plates at the south-east sides. Because of the Arabian plate motion towards northwards, the Anatolian plate is forced to the westwards (Bulut et al., 2022; İvasoğlu et al., 2022). These movements have been created several earthquake events along the North Anatolian and East Anatolian Fault zones stretching within Turkey through the east-west and east-southwest directions with 1000 km and 1000 km in length, respectively (Figure 1). Some of the most memorable earthquake events occurred in these fault zones are the 1939 Van earthquake with 7.4 magnitude, the 1944 İzmit earthquake with 7.4 magnitude, the 1992 Erzincan earthquake with 7.4 magnitude and the 2003 Erzincan earthquake with 7.4 magnitude. Due to these earthquakes, considerable number of masonry and reinforced concrete buildings are severely damaged or totally collapsed as they were built not in accord with the code in place or the code design rules were not comprehended enough. This clearly indicates that when a building can stand safely under static loads, it will not mean that its dynamic performance can be sufficient enough in terms of life safety and collapse matters. Hence, with these experiences of earthquakes and their effects, consideration of seismic performance design of buildings becomes extremely vital (Gürel and Gürel, 2022).

In order to deliver the load-carrying and resistance to the gravitational and lateral forces, as well as dissipating the seismic forces, different structural systems have been implemented. For low-rise and mid-rise buildings, a frame structural system consisting of columns and beams can sufficiently carry gravitational loads when designed in compliance with the seismic design codes, e.g. Turkish Building Earthquake Code (TBEC 2018), ASCE 7 and Eurocode (EC 2004). However, when lateral forces of wind and earthquake are involved, the columns may endure the second-order moments as a consequence of lateral displacements. This will become even apparent with the rise of the building height. Therefore, the shear walls

having higher flexural rigidity than the columns are suggested in order to limit the lateral displacements causing the second order moments

Frame shear wall and Dual frame shear wall structural systems have been implementing for many years. In addition their design is being guided comprehensively in the seismic design codes. In this short work general structural characteristics of these three systems are explained. Moreover three buildings modelled in ETABS with frame shear wall and dual systems are analysed using response spectrum analysis method. Subsequently the results are discussed comparatively. Lastly the outcomes from this study are presented.

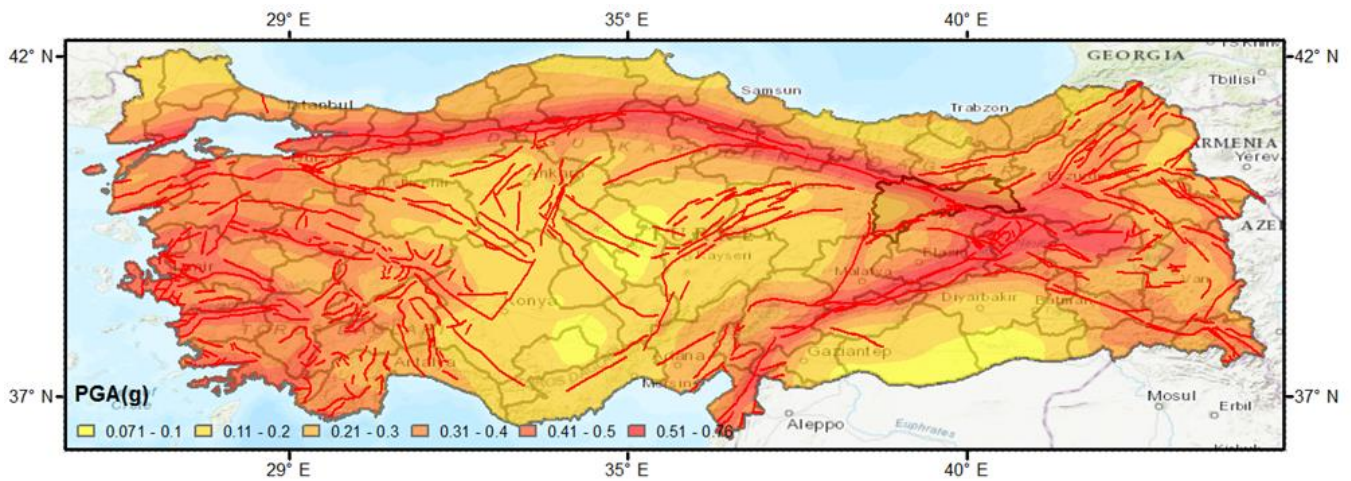


Figure 1 Seismic intensity level over the country of Turkey along with the fault lines

2 F A S S

Frame system is formed with the joints of columns, beams and plates. In general, columns and beams are the main structural elements of the system, but parts of the plates can also perform with the beam elements. It is mostly designed to withstand the vertical loads. The frame system can be used in buildings with height not greater than 20 m when it is designed in compliance with the seismic design codes and implemented rigorously (Asap et al., 2010). In Turkey, this system is in popular use in low-rise buildings as it is more economic than the shear wall system.

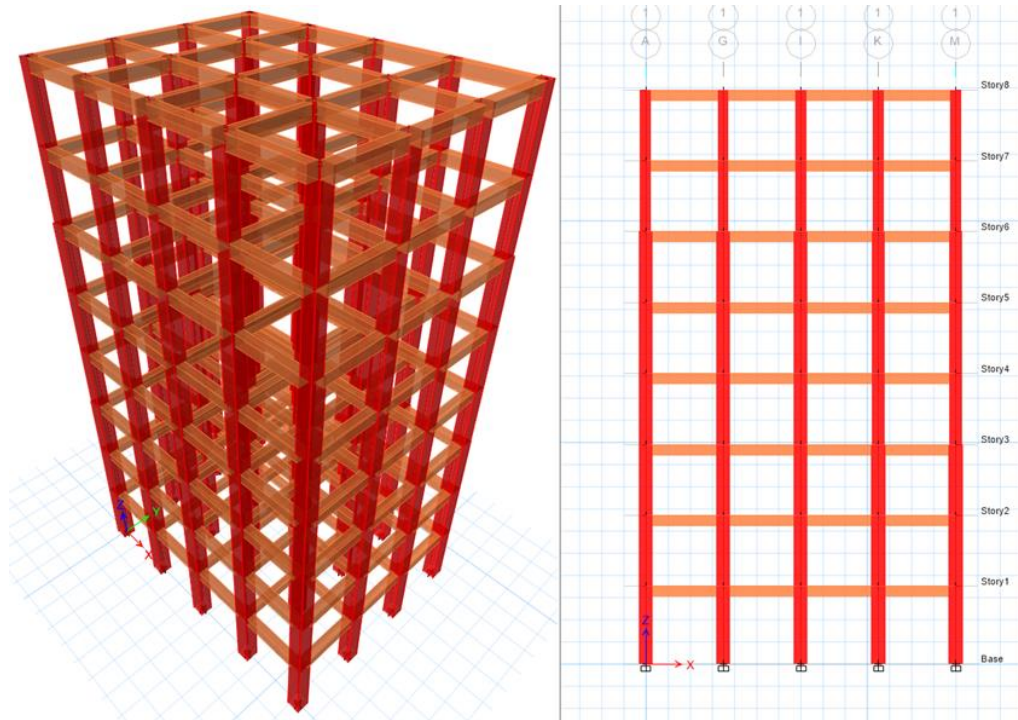


Figure 2 A sample building model consisting of a frame system used in this study

Beams should be joint to columns at least in two directions to create a frame system. Moreover, this allows to obtain enough rigidity such that second order moment and buckling effects are limited. In the frame systems, columns and beams are designed as load carrying elements transferring the vertical and lateral loads to the foundations and they are joint as rigid creating space system. When earth quake forces implemented in the one horizontal direction, the buckling effect in the other horizontal direction is thought to be minimal and negligible but may move laterally.

The columns sections can be altered with the increase of the building height but the eccentricity should be kept in minimum or should be avoided if possible in order to prevent additional moments. The general three dimensional and side view of a frame system structural model used in this study can be seen in Figure 2. Physical dimensions and reinforcement rebars of the building model is given in Table 1.

Table 1 Physical properties of the frame system structural model used in this study

System	Floor level	Column				
		size	rei	la t i s		
Frame system		0 0	22 20	Corner columns		
		0 0	20 20	The remaining columns		
	7	0 0	20 20	corner columns		
		40 40	20	remaining columns		
		eam				
		Floor level	size	rei	t rei	la t i s
			30 0	4 20	4 20	All column to column connections
	7		30 40	4 20	4 20	All column to column connections

3 SH A A S S

The vertical load carrying elements having the height at least six times of its width in plan are called shear wall TBEC 2008. One structural system can purely be formed by the shear walls or designed with the frames. The shear walls can be able to carry and transfer the loads coming from plates and beams to the foundations they can also resist the lateral loads of wind and earth quakes. Additionally due to their higher level of rigidity they limit the lateral displacements.

In general the shear wall systems are more capable of limiting the lateral displacements and keeping the damage level at low level than the frame systems. Under earth quake excitations in order to retain the buildings in function after the event and avoid the damage to the non structural elements which is essential in life line buildings like hospital nuclear power plant school etc seismic code complaint shear walls should be involved Gul 2008. Although the shear wall system cannot exhibit as such high level of ductility as the frame system the system can still be able to show satisfactory ductility when it is designed with detailed modern seismic code designs Taranath 2008.

In Figure 3 the shear wall system storey building model used in this study is demonstrated while the two U shape shear walls are modelled around the centre of the model L shape shear walls are positioned at the four corners. Two additional shear walls in the x direction and one additional shear wall in the y direction with 2 m length are designed. The thickness of all the aforementioned shear walls is assigned as 20 cm.

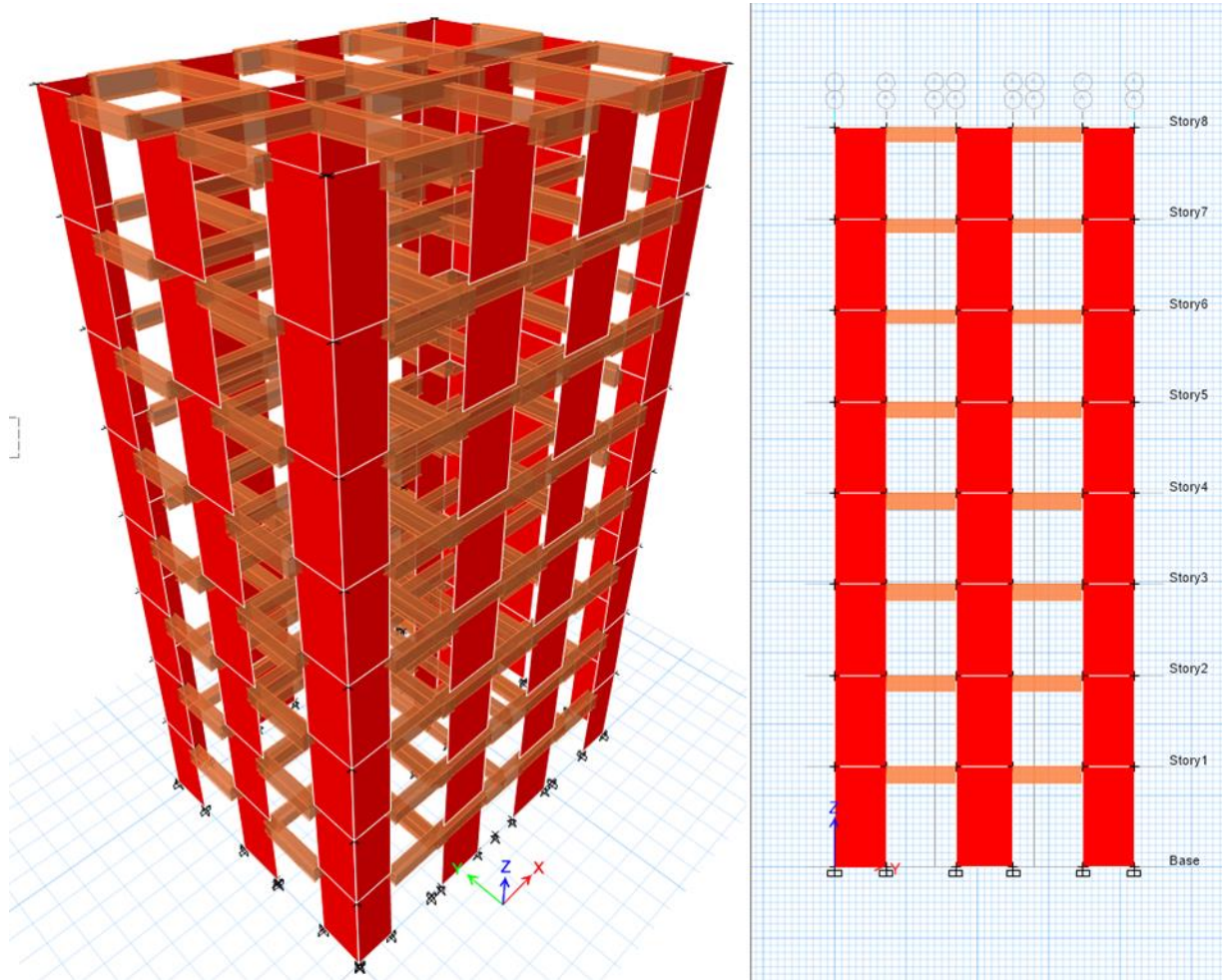


Figure 3 A sample building model consisting of a shear wall system used in this study

A S S F A S H A A

Dual systems are designed with the involvements of shear wall and frames. In multi-storey buildings, in order to decrease the relative floor deformations and limit the second order moments, it is critical that the shear walls take major parts of the lateral forces. TBEC 2000. In Turkey, frame structural systems are most widely preferred. However, contribution of the shear walls to the overall rigidity and resistance, as well as to the relative movement, necessitate the use of such structural elements, in particular in sites having high level of seismicity (Aya and Bayraktar, 2010).

As the behaviours of frame and shear wall are different under lateral forces, the shear walls act like bending resisting beam, the frames behave as though shear beams. When both systems are adapted in one single building design, there is an interaction taking place between bending and shear resistance behaviours. The shear walls experience the maximum displacement at the top floor of the building, while this occurs at the lower floors. Hence, in dual systems, the shear walls take the most of the lateral forces at the lower floors, while the frames limit the displacements at the higher floors (Akan et al., 2000). For low rise buildings, the frame systems are more economic and more ductile than the shear wall systems (Doğan et al., 2010). However, it should always be kept in mind that shear wall systems have greater level of seismic energy dissipation than the frame systems.

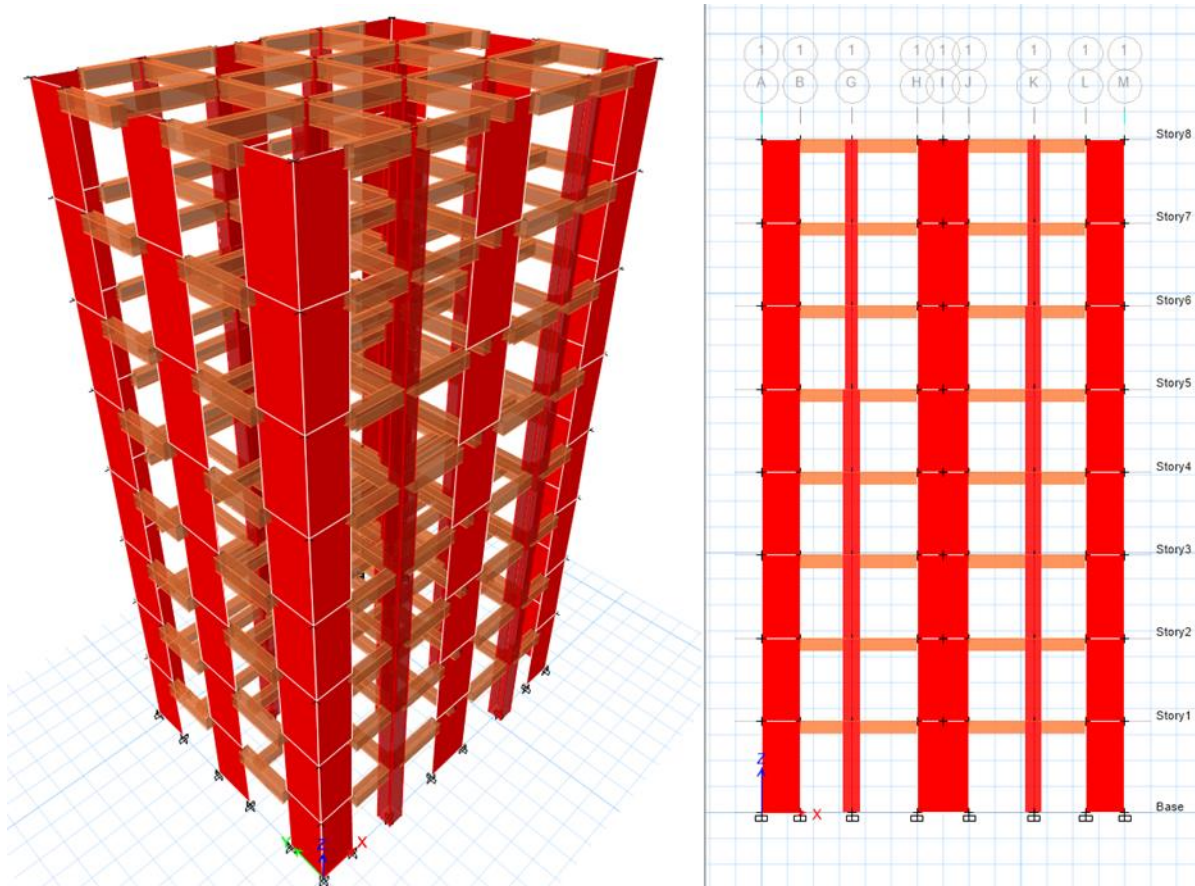


Figure 1. A sample building model consisting of a dual system (frame + shear wall) used in this study

Table 2. Physical properties of the dual system structural model used in this study

System	Floor level	Column		
		size	rei	Location
Dual system		400x400	220x200	Columns connected to shear walls
		400x400	200x200	The remaining columns

		0 0	20 20	Outer columns	
		40 40	20	Inner columns	
		eam			
	Fl r level	size	rei	t rei	la ati s
		40 0	4 20	4 20	Column to shear wall and shear wall to shear wall connections
		30 0	4 20	4 20	Column to column connections

S O OF H O A A S S

Three dimensional and side views of the frame shear wall and dual system structural models are presented in previous sections Figures 2 3 and 4 Moreover the physical properties of the models are given in Tables 2 and 3 For all the three building models 2 kN m² live loads and 7.7 kN m² dead loads are assigned Compressive strength of concrete and yield strength of rebar is equivalent to 30 MPa and 420 MPa respectively The models are residential buildings therefore the importance factor is taken as 1 All the structural elements i.e. columns beams shear walls slabs are designed in accord with TBEC guidance The shear walls and slabs thicknesses through all floors of the three building models are equal to 20 cm and 10 cm respectively The building models are modelled and analysed in ETABS platform Computers and Structures 2019 First three modes periods of the frame shear wall and dual system building models are 0.7 s 0.3 s 0.3 s and 0.3 s 0.3 s 0.3 s respectively

For the design response spectrum analyses a site in Erincan province is chosen The latitude and longitude of the location is 37°20' and 34°00' respectively The site has a reference peak ground acceleration PGA_{rock} of 0.4 g AFAD with 47 years of return period The site is designated with site class of D according to the TBEC soil classification scheme The design response spectrum curve for this specific site is given in Figure

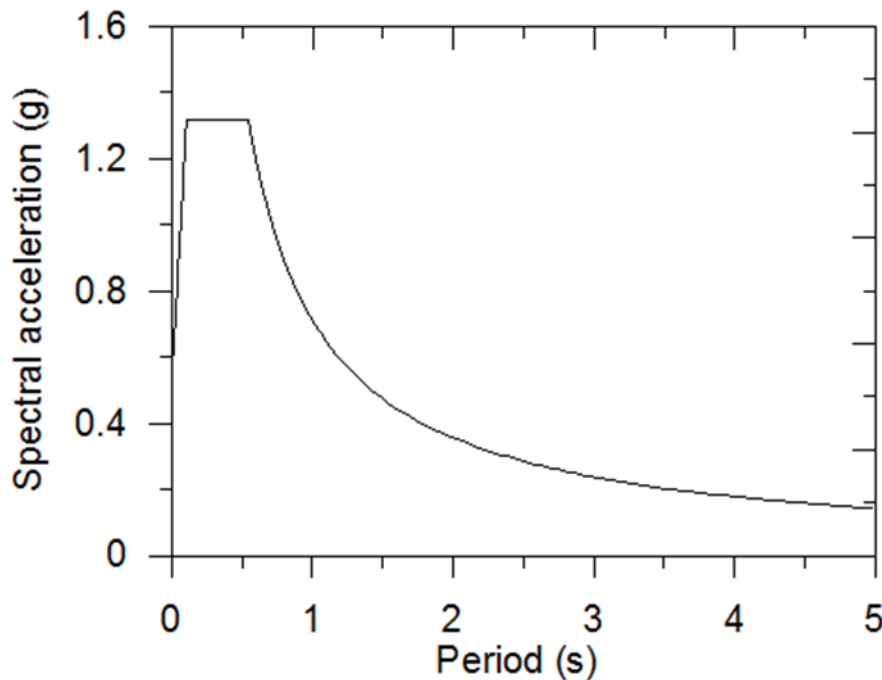


Figure The design response spectrum curve for the specific site in Erincan province

S S

The results from response spectrum analyses of the frame shear wall and dual systems building models are interpreted firstly in terms of displacement and normalized displacement by the building height. Later, the lateral forces are compared for these three different structural models.

The displacements over the building height represented in Figure 6a demonstrates that the frame system building model is experienced the greatest level of displacements at all storey levels. The model displaces about 27 mm at the first floor while this value equals to 230 mm at the top storey. However, the displacement increment is decreasing by the increase of storey level. In other words, there is a decreasing exponential displacement trend with the building height is observed. In contrast, the shear wall system structural model exhibits the least displacement values and follows almost linear increase with the increase of building height. The shear wall system building model displays lateral movement of 3 mm and 2 mm at the first and top of the storey levels accordingly. The building model with the dual system shows displacements that fits between the performances of the frame and shear wall system building models. This can also be observed from Figure 6b including the normalized displacement values over the building height.

These results directly reflect the differences in the performances of structural building models formed by discrete structural systems. Because the frame system building model tends to deform more at the lower storey levels while the shear wall system building model has relatively lower displacement at the lower storey levels but becoming greater with the height. Therefore, when the building model is designed by the dual system, part of the structural elements, the shear walls, limits the displacements at the lower storey levels. In addition, the other part of the structural elements, frames, controls the lateral movement of the building model at the higher storey levels, as can be depicted in Figures 6a, b.

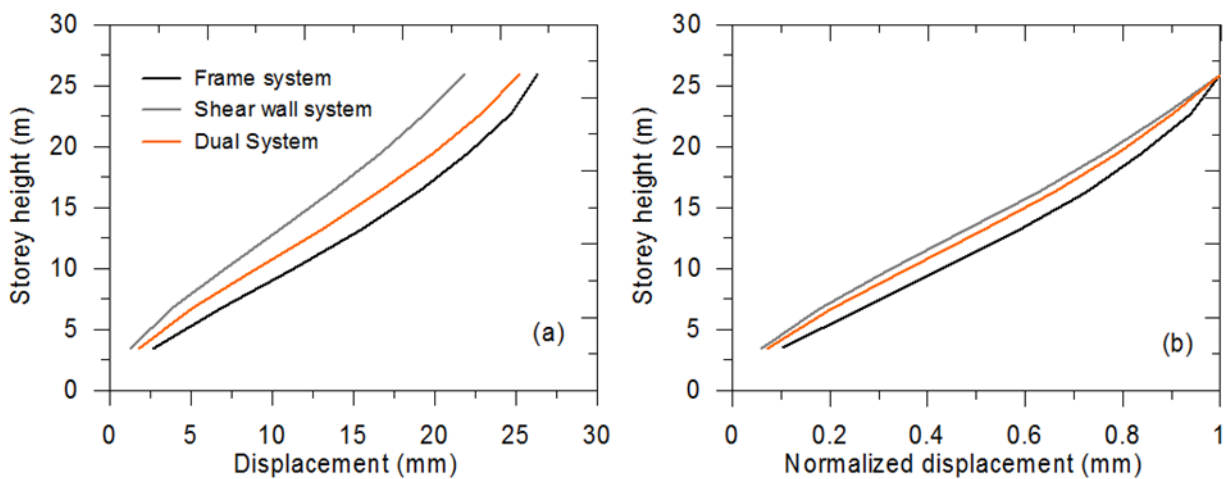


Figure 6 The results from response spectrum analyses of the building models in terms of a) storey displacements and b) normalized storey displacements

Shear forces from the response spectrum analyses are represented in Figure 7 for the building models with different structural models. From top storey to the third storey level, all three structural models illustrate almost same shear forces. Moreover, the overall shear forces acted on these building models, i.e. at the ground level, are similar too. For instance, the shear force for the frame system building model is 22 kN when it is 20 kN and 24 kN for the shear wall and dual system building models, respectively.

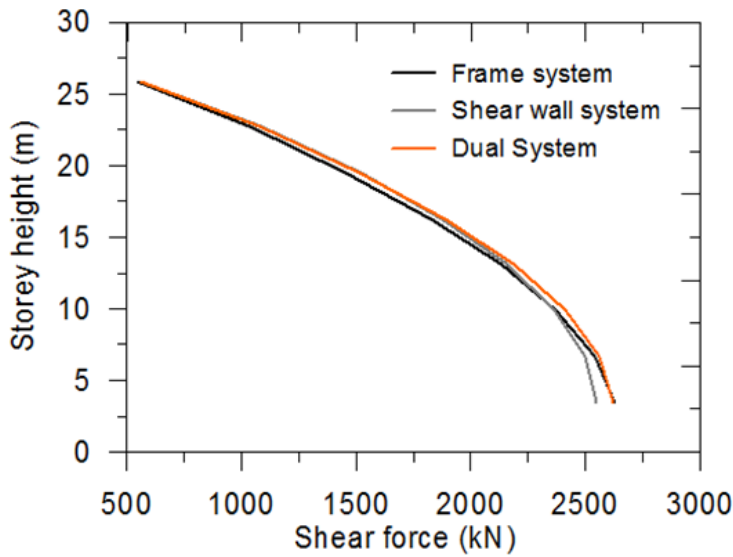


Figure Shear forces from response spectrum analyses acted on building models

O S O S

This study focuses on the main seismic performance behaviour of three different structural systems. These are the frame shear wall and dual frame shear wall systems. For this, it includes explaining the main features of these three structural systems. It also covers the modelling and analyses of three-storey building models with varied structural models. A site from the Erincan province is chosen. The PGA level of 0.4 g with 47 years of return period is considered. The major highlights of the work are:

The frame system building model tends to deform laterally more than the other two system building models at the lower storey levels.

However, the lateral movement of the shear wall system building model increases with the increase of the building height.

The dual system building model involves the characteristics of both frame and shear wall systems, hence able to control the lateral movement of the building model over the building height.

ethics committee Approval

N/A

Author Contributions

Conceptualization: F.G.; Investigation: F.G.; Material and Methodology: F.G.; Data Supervision: D.; Visualization: F.G.; Writing Original Draft: F.G.; Writing review & Editing: D.; Other: All authors have read and agreed to the published version of manuscript.

Conflict of Interest

The authors have no conflicts of interest to declare.

Funding

The authors declared that this study has received no financial support.

F S

Aka eskinel F l F elik O C 200 Betonarme stanbul Birsen ay nevi

American Society of Civil Engineers 20 7 une Minimum design loads and associated criteria for buildings and other structures American Society of Civil Engineers

Bulut F Bohnhoff M Eken T anssen C l T and Dresen G 20 2 The East Anatolian Fault one Seismotectonic setting and spatiotemporal characteristics of seismicity based on precise earth uake locations urnal of Geophysical Research Solid Earth 7 B7 <http://doi.org/10.1029/2017JB015000>

CEN 200 Eurocode Design of structures for earth uake resistance Part General rules seismic actions and rules for buildings CEN Brussels

Do ang n A 20 Betonarme ap lar n Hesap ve Tasar m stanbul Birsen ay nevi

aya G BA AE 20 Perde Ve er eveli Betonarme ap larda Perde onumunun Planda D enlenmesi Ve ap sal Davran a Etkisi M hendislik Bilimleri ve Tasar m Dergisi 7 7 7 <https://doi.org/10.2312/esd.42.07.2022.01>

G l B S 200 Perde er eve Sistemlerin Dinamik Analizi Doctoral dissertation Fen Bilimleri Enstit s Istanbul Teknik Universitesi

Gu el Gu el F 2022 Influence Of Input Motion Scaling Methods On Decoupled SSI Dynam c Analysis Eski ehir Osmanga i niversitesi M hendislik ve Mimarlk Fak ltesi Dergisi 30 30 40 <https://doi.org/10.37708/ogummf.0044.7>

Disaster and Emergency Management Presidency AFAD 20 3 present AFAD Deprem katalogu Ministry of Interior Ankara <https://deprem.afad.gov.tr/ddakatalogu> accesses 23 May 2023

asap H Necati M E R T Sevim E eber B 20 Perdeleri er eveli Ta y c Sistemli Binalarda Ta y c Sistem Se iminin ap Davran erindeki Etkisinin ncelenmesi Academic Platform urnal of Engineering and Science 3 4 <http://doi.org/10.1007/s12040-020-0442-7>

SO AE GEN 200 Perdelerdeki Bo luklar n atay telenmeye Etkisi Deprem Sempo yumu ocaeli Mart

Taranath B S 200 Reinforced concrete design of tall buildings CRC press

Turkish Building Earth uake Code 20 T rkiye Bina Deprem onetmeli i Deprem Etkisi Alt nda Binalar n Tasar m icin Esaslar Ankara

ava o lu H Tar E T ys O ak r Ergintav S 20 Determining and modeling tectonic movements along the central part of the North Anatolian Fault Turkey using geodetic measurements urnal of Geodynamics 33 343 <http://doi.org/10.1007/s00020-007-0003-0>

Computers structures 20 ETABS Extended three dimensional analysis of building systems Version 0 Berkeley

Studies in multi-media on the creative movement in space architectural spatial forms

Ferenc Sebesty^{*1}

Abstract The intense connection of experience with creative application has been an effective way to improve architectural attitude and abstract vision. In the teaching methodology of the author of this paper motion is the main means of learning and experiencing space one moment and an inspiration for space creation in the next. The use of movement based spatial experiments in architectural education is intended to develop the individual experience based sense of interior space which in turn forms the base for abstraction in the design process. The examination, recording and geometric analysis of different types complexity and dynamics of motion may effectively lead to the inception of new types of free and abstract forms. A spatial form can be a result not only of following functional needs, structural and technological logic or traditional geometry but also of other influences and creative realizations for instance through the abstract conversion of the motion's own internal mechanisms. Once one realizes that the original inspirational material's own compositional properties, its proportions, rhythm, dynamics, internal energy can be deciphered through perception and analysis and translated into our architectural toolkit, the goal, the conception of movement inspired free architectural forms at the end of the analytical and creative process has already been achieved.

Keywords space and motion, spatial perception, modelling, spatial experimenting, architecture education

¹Address: Budapest University of Technology and Economics, Faculty of Architecture, Hungary

* E-mail: sebesteny.ferenc@epk.bme.hu

1. INTRODUCTION

The first description of space through movement and the observation of the world in motion is often linked to the Futurist trends of the 20th century. Umberto Boccioni in his 1912 book *Futurist Painting, Sculpture, Plastic Dynamism* argued that Futurists launched an attack on the notion of stillness and static formality in favour of movement and dynamism, and they introduced a new interpretation of space, juxtaposing interior and exterior. Rudolf von Laban, the renowned dance theorist who, among others, studied and described the spatial relations of movement and developed the concept of Motion Space, stated: "Movement is, so to speak, living architecture, living in the sense of changing emplacements as well as changing cohesion. This architecture is created by human movements and is made up of pathways tracing shapes in space, and these we may call trace forms." The examination of space in the context of movement, alongside the extensive progress in natural sciences, primarily nuclear physics, philosophy and technology, launched a new approach from the beginning of the 20th century, as a result of which our understanding of architectural space also fundamentally transformed.

2. ARCHITECTURE AND MOVEMENT

In 2000, the author of this paper introduced the theoretical and experimental study of the relations between Space and Motion in the frame of an eponymous course at the Department of Graphics, Form and Design at the Faculty of Architecture of the Budapest University of Technology and Economics. The course, which has been offered for over two decades, focuses on a new topic every semester, thus securing its relevancy, strengthening the experimental approach and the diverse use of tools and technologies. Traditional graphics is used as well as photography, video and digital tools, traditional models and virtual spaces generated with state-of-the-art software. Stepping beyond the conventional academic framework, students of the course frequently work together with creative workshops of visual and fine arts, theaters and progressive contemporary artists.

3. SUMMARY

The methodology developed and introduced in university architecture education, the theoretical and practical examination of the interrelations between space and movement, as well as the application of the findings through

creative exercises has been found to improve the skills of architecture students in space and structural formation and to make certain spatial theoretical considerations more understandable and interactive. It also helps creative decision making considerations become more conscious in the complex process of architectural design.

S S O A O S O S

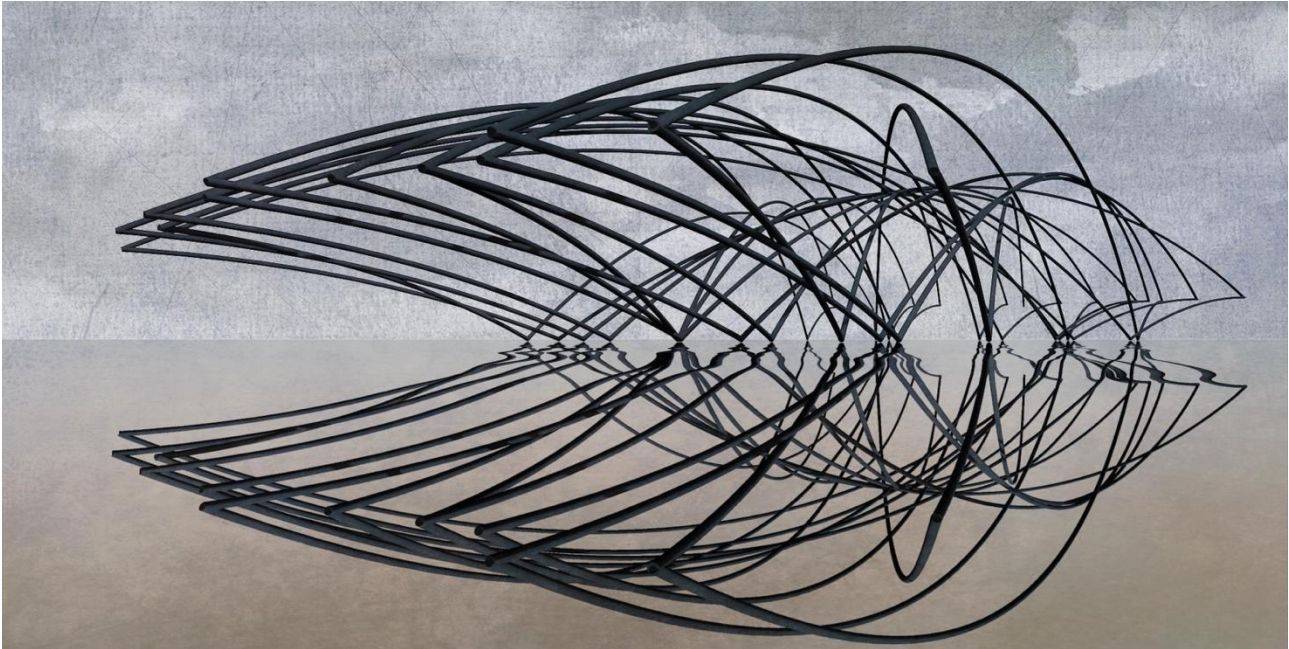


Figure 1. oltán Csakurda and Lidia ékesi Dynamic and kinetic space Space and Motion university course

Movement can be captured in space as long as its existence can be perceived with our senses Moholy Nagy L 47

The first type of experiments presented in this paper are attempts to capture and represent the temporal process of movement. The aim was to find graphic techniques that provide the opportunity to capture the dynamics abstracted from the forms and to display them spatially according to some known or arbitrary system of rules. Depending on the level of abstraction, students used a variety of approaches, from simplified human figures depicted in motion to abstract disembodied momentum arcs. Therefore, among the presented works, one finds dynamic gesture drawings that trace and capture the curve and speed of rotations and limb movements, but also linear sheet music like representations of movement beats which focus on the rhythm, emphasis, and temporality of the motion.

It is interesting to observe the parallel between the centuries-old methods of dance recording, the modern kinetographic notation systems of the 20th century, and the students' own experiments. F. Geddy 3 This similarity in form and thought is quite natural. The forms of visual representation of the essential parameters of movement inherently identify with visual elements learned from perceived stimuli. These motion images, energies, invisible force lines, occupied the attention of artists associated with the Futurist trend in the beginning of the 20th century, as well. In their 22 manifesto on 'The Dynamic Constructive System of Forces' Lasl Moholy Nagy and Alfre éme y contemplated

Carrying further the unit of construction, a dynamic constructive system of force is attained whereby man, heretofore merely receptive in his observation of works of art, experiences a heightening of his own faculties, and becomes himself an active partner to the forces unfolding themselves. The first projects looking toward the dynamic constructive system of forces can be only experimental demonstration devices for the testing of connections between man, material, forces, and space. Next comes the utilization of the experimental results for the creation of freely moving, free from mechanical and technical movement, works of art. Moholy Nagy L 47 There were various other experiments in the era in attempt to visualize motion.

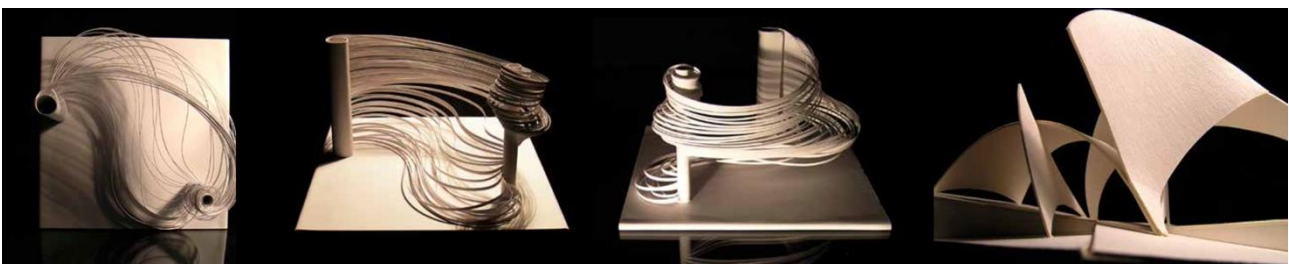


Figure 2. oltán Mac elka Capoeira Space and Motion university course

Archipenko made mobile sculpture paintings sculpture paintings Brancusi placed his sculptures on rotating stands to bring the parameter of time into the creation the sculptures of Oost Schmidt represent the space time perspective of distortion but also Giacometti and Alexander Calder harnessed in their kinetic sculptures the potential in reflecting the experience of motion Thomas Eakins who in 1874 created the famous stroboscopic action photo Man Pole Vaulting and later Harold Edgerton Herbert Matter and Moholy Nagy all implemented photographic methods which provided the opportunity to display the time factor and therefore movement in various but essentially analogous ways

These interpretations of vision in motion denote not only an artistic achievement but also an important practical step in visual perception as well as in the skill of rendering Photomontage superimpositions diagrams explosion phantom x ray cut away techniques stroboscopic motion projections and other combinations may enlarge the scope of this new method of visualization tremendously These speed photographs are of more recent date but they are astonishingly similar to futuristic paintings In fact they are their exact repetitions e.g. Nude Descending the Stairway 2 by Marcel Duchamp They all show the same juxtaposition of frozen movement



Figure 3 Lilla Sics Kinetic space Space and Motion university course

Long exposure photos are able to present a movement in its entirety but due to the continuous exposure to light as opposed to stroboscopic shots the moving parts of the body or object become blurred Most of all these images resemble billowing smoke and their character primarily enables a sculptural capture of the curvature and space of the movement In the motion capture experiments in addition to these traditional photographic techniques students can take the advantage of the possibilities offered by video and computer technology Images taken with high speed or very small endoscopic cameras can reveal never before seen details and angles of certain movements In another group of experiments students considered movement as a source of inspiration recorded its form dynamics and interpreted and visualized in an abstract way in drawing model film etc the space the movement described cut out in time This type of exercise has two important purposes Through free associations and creative thinking the abstract reinterpretation of the connections uncovers the forms and techniques with which these internal compositional principles and energies can be reinterpreted in architecture In this recreation students seek to invent and develop their own tools and set of rules which in turn will become one of the criteria and conditions for the authenticity of the creative process Capturing motion is an exceptionally difficult task There are various artworks known to have captured in a single moment the characteristic visual image internal dynamics rhythm and tension of a movement Here time the duration of a given sequence of movements takes place in the mind of the creative artist who compresses and condenses it until finally stretched into a single moment it can be presented Time is therefore merely virtually present or more precisely it is in a bound state only to be released and run in the mind of the observer However when the continuous flow of a dance movement needs to be recorded without the use of a camera the presence and passage of real time creates extreme difficulties The problem primarily is not that during the time it takes to draw to outline the main gestures the view changes but that it is the change time itself we want to capture The usual view according to which one could capture the final result of the events created and interpreted internally however is very different

from this An essentially difference in which one realises that in order to depict the movement in its temporal process and not as an image recollected from the past one has to create the way and form of expression for himself



Figure Anna Rátkai and Lidia Pékesi Mobilion Space and Motion university course

The spatial structure Mobilion designed specifically to move in space is also meant to deepen the understanding of the relationship between motion and space as it is supposed to exert its spatial and aesthetic effect during a pre-programmed movement. The design process thus begins with the vision of the future spatial movement which is then verified and adjusted during various intermediate experiments and it concludes with the construction of the structure. The task is complex since the object and the envisioned movement mutually affect each other the structure's centre of gravity stability and aerodynamic properties all influence its subsequent behaviour. In addition to the obvious forms of actions like swinging rotation uniform rectilinear motion or free fall more complicated forms of movements or even complex motion sequences are also welcome. The task includes the creative invention and aesthetic shaping of these structures and their movement. The kinetic objects are then set in motion and their movement is recorded with photo and video cameras using special techniques. The final documentation of the project is a series of photos compiled in a poster.

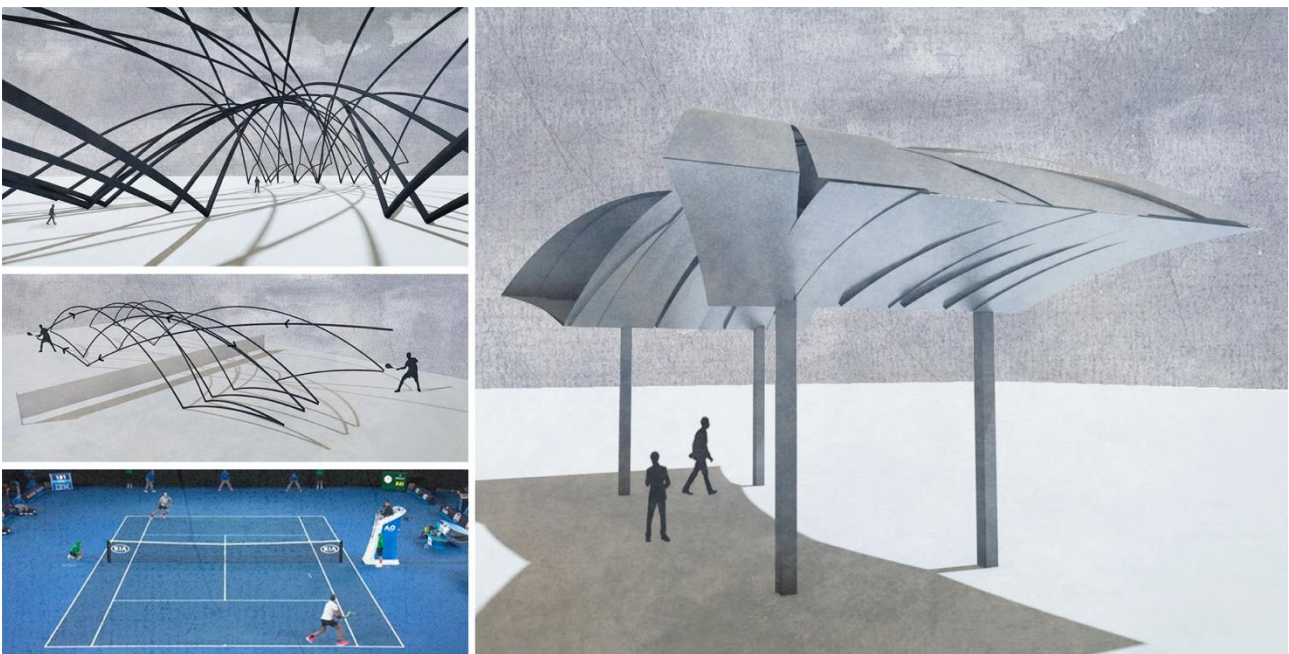


Figure István Csakurda and Lidia Pékesi Dynamic and kinetic space Space and Motion university course

A special aspect of the relationship between space and time can be grasped in relation to movement generated space. The tension between the contemporaneity of movement its confinement to the moment and the striving for eternity in architecture can be resolved in the common creative environment in the forming space which due to the way it was created carries both essences at the same time. Space constructed in this way looks for its balance on the sharp border between the here and now and timelessness and is able to articulate its independently valid philosophy.

Acknowledgements

Special thanks to the students at the Budapest University of Technology and Economics that took part in this research namely:oltán Csakurda Lidia ékesi oltán Mac elka Anna Rátkai Lilla S cs

ethics committee Approval

N A

Peer review

Externally peer reviewed

Conflict of interest

The authors have no conflicts of interest to declare

Financial

The authors declared that this study has received no financial support

References

Boccioni U 2 Pittura scultura futuriste Milano Edizioni Futuriste di Poesia

Moholy Nagy L 47 Vision in Motion Chicago Paul Theobald Company

F gedi 3 Tacle egy rends erek 3 Tacle ves et 47 4

valuati ritical Success Fact rs r i ital ucati ith Hesita t Fuzzy i uistic

A r ach

si u ul*¹, l i y z a ¹, erve ler¹

Abstract Digital education is an approach to learning that aims to optimi e the use of digital technology open source material individuali ed data and connection It strives to raise creative and inventive persons by ensuring that individuals have better living circumstances and possibilities within the context of life s sustainability This educational approach helps the student to develop himself according to the changes in society encourages students to develop their ability to apply new technologies At this point determining the factors for the success of digital education has critical importance in increasing the uality of education In this context the study aims to propose the Critical Success Factors CSFs for digital education and evaluate these factors with Hesitant Fu y Linguistic HFL method Given the complexity and uncertainty of this multi criteria decision making MCDM situation the HFL approach is used This approach is used to provide experts more flexibility by employing comparative linguistic terms and to create an evaluation environment that is more similar to human thinking In this study the CSFs are identified with the literature review and experts opinions Then the HFL Analytic Hierarchy Process AHP method is applied for the evaluation of CSFs of digital education This method is practical adaptive to varied fu y environments versatile dependable and resilient Finally an application demonstrating the potential of the proposed approach is offered

Key r s AHP critical success factors digital education hesitant fu y linguistic term sets MCDM

¹A r ess Galatasaray University Faculty of Engineering and Technology Industrial Engineering Department Istanbul T rkiye

* rres i auth r emukul gsu edu tr

1 O O

Digital education is an approach to learning that aims to optimi e the use of individuali ed data digital technology connection and open source material It strives to raise creative and inventive persons by ensuring that individuals have better living circumstances and possibilities within the context of life s sustainability This educational approach helps the student to develop himself according to the changes in society encourages students to develop their ability to apply new technologies Ibane et al 2023

Fisk 20 7 mentioned the existence of nine trends in the digital education concept These trends are as follows

- Learning may occur at any time and in any location
- Students are more exposed to pro ect based learning
- Learning is personali ed for individual learners
- Students become more involved in collaborative practices as their field experience increases such as consulting pro ects and pro ects that adopt a collaborative approach
- Students are exposed to applications that will reveal their abilities in interpreting the numbers they obtained by analy ing the data Some basic skills that seem so important today mathematical literacy memori ng formulas or dates etc are becoming irrelevant
- Students have the opportunity to determine how they want to learn
- Students are evaluated individually and traditional assessment platforms become inaduate
- Students ideas and changing needs should be taken into account in designing and updating the curriculum There is a need for more customi able and adaptable curricula
- ith the teachers taking a guiding role for the students in this process the students are freer in individual learning

In light of these trends the efficiency of digital education systems and the uality of their output are among the most important issues to be examined Digital education which has become important with the pandemic period and is

accessible fast flexible egalitarian low initial operating cost and customi able should be considered as an alternative supplement or supporter of face to face education

At this point determining the factors for the success of digital education has critical importance in increasing the quality of education In this context this study aims to propose the Critical Success Factors CSFs for digital education and evaluate these factors with Hesitant Fuzzy Linguistic HFL Multi Criteria Decision Making MCDM approach

The structure of the evaluation of CSFs for digital education is multifaceted multi actor multi disciplinary dynamic comprehensive and complicated As a result this evaluation problem is treated as an MCDM problem in this study Hwang and Moon Considering the complex and uncertain nature of this MCDM problem the HFL approach Rodrigue et al 20 2 is employed This approach is used to provide experts more flexibility by employing comparative linguistic terms and to create an evaluation environment that is more similar to human thinking The CSFs in this study are determined using a literature review and expert views Then the HFL Analytic Hierarchy Process AHP method Hu and Wu 20 4 is applied for the evaluation of CSFs of digital education This method is practical applicable to many fuzzy situations versatile dependable and resilient

This proposed approach is applied for the digital education system in Turkey to show the effectiveness of the proposed approach The contributions of this paper are proposing a new and conceptual evaluation model including CSFs for digital education presenting an analytic method such as the HFL AHP method in this area and providing an application for the evaluation of CSFs for digital education

The following is how this paper is organized The conceptual foundation of the subject is discussed briefly in the next section The study's technical basis is then supplied The proposed CSFs for digital education are shown in the fourth section and the application is shown in the fifth section Finally the final part brings the paper to a conclusion

2 ORGANIZATION

CSFs are those elements that are crucial to the performance of any organization as defined by the Massachusetts Institute of Technology study team Rockart 7 The term CSFs was coined in response to a question regarding why some organizations appear to be more successful than others

CSFs are initially utilized in project management research In general it is frequently employed in a variety of situations such as organizational management operational management and supply chain management among others CSFs should be few and controllable Freund When the research is examined it is seen that e learning is examined separately from the perspectives of technology pedagogical organization student and instructor depending on the fields of expertise of researchers In this context it is possible to say that there are not many studies that see e learning projects and their stakeholders as a whole and evaluate the factors that are effective in the success of the project and that are related to each other

There are research in the literature on success factors for digital education A comprehensive literature review is carried out in this field Table 1 lists the studies discovered as a consequence of the literature review

Table 1 Studies on CSFs for digital education

Year	Author	Aim of the Study	Country
2023	Ibanez et al	to identify key success factors for effective online teaching	Paraguay
2023	Nig et al	to determine CSFs for digital education	
2022	Anand et al	to uncover the CSFs of knowledge transfer from universities to industry	India
2022	Moya-Camacho	to develop a taxonomy for categorizing the elements influencing mobile learning acceptance	Catalonia
2022	Milic-Simeunovic	to identify the e learning CSFs with the students' perceptions	Bosnia and Herzegovina
2020	Blieck et al	to validate the quality of online learning	
2020	De Paepe et al	to present Dutch L2 learning in adult education	Germany
2020	Barclay et al	to investigate CSFs in online learning environments	Caribbean
2017	Fabito	to find out the CSFs of e learning in universities	Philippines
2020	Alrasheedi et al	to identify the factors affecting mobile learning	

20	Alrasheedi et al	to analyze studies on CSFs for success of mobile learning	
2013	Cortés Barber	to discover success criteria in online learning based on student perspective	Mexico
20	Sharma et al	to outline the CSFs for e learning at HP University	India
200	Papanikolaou Mavromoustakos	to determine CSFs for mobile learning applications	
200	Volery	to determine CSFs for online education	Australia

It is possible to say that the studies in Table belong to the last 20 years. Most of the studies are in the field of higher education. Studies have been applied in many different places such as Paraguay, Germany, Bosnia and Herzegovina, India, Catalonia, Mexico, Australia, etc.

In this study, the CSFs of the digital education system in higher education will be determined and these factors will be evaluated. This evaluation will be supported by an analytical method and this gap in the literature will be filled.

3 H A A K O

3.1 Hesitant fuzzy linguistic approach

Uncertain situations frequently present significant decision-making issues in the real world. Linguistic knowledge may be useful in managing ambiguity in this setting. Torra introduced hesitant fuzzy sets in 2010. Rodrigue et al. (2012) presented the Hesitant Fuzzy Linguistic Term Set (HFLTS). HFLTS is favored to address experts' hesitancy while expressing their ideas on the MCDM challenge. In HFLTS, experts may express themselves using language such as "at least between and at most," giving them versatility. As a result of using comparison linguistic terms in the HFLTS, a more human-like evaluation environment is created (Rodrigue et al., 2012).

The superior H_{s+} and inferior H_{s-} bounds are explained as (Torra, 2010; Rodrigue et al., 2012):

$$H_{s+} = \max(s_i) = s_j, \quad s_i \in H_s \text{ et } s_i \leq s_j \forall i$$

$$H_{s-} = \min(s_i) = s_j, \quad s_i \in H_s \text{ et } s_i \leq s_j \forall i \tag{2}$$

Liu and Rodrigue (2014) provide the envelope for HFLTS $env(H_s)$, which is a linguistic interval with superior and inferior bounds:

$$env(H_s) = [H_s^-, H_s^+], \quad H_s^- \leq H_s^+ \tag{3}$$

3.2 Hesitant fuzzy linguistic AHP method

The AHP model developed by Saaty (1980) is the most often utilized in the MCDM field. It is a strong and simple MCDM tool that prioritizes a variety of criteria when there is ambiguity in the decision-making process. HFL AHP is frequently used. Multiple alternative values reflect a tentative judgment (Hu and Wu, 2014). The AHP approach is widely used in MCDM literature due to its simple structure and ability to solve complex choice problems. The HFL AHP approach was used to calculate the criterion weights in this article. The HFL AHP stages are outlined next (Beykkan et al., 2010).

Step 1. The criteria are assessed using pairwise comparison matrices. The language expressions are then transformed to HFLTS. Table 2 depicts the linguistic scale employed in HFL AHP.

Step 2. The fuzzy envelope, which produces a trapezoidal fuzzy number, is created using the OWA operator (Liu and Rodrigue, 2014):

$A = \{a_1, a_2, \dots, a_n\}$ denotes a collection of components that will be aggregated. It is worth mentioning that it differs from the collection of alternatives. The OWA operator F is characterized as follows (Liu and Rodrigue, 2014):

$$F(a_1, a_2, \dots, a_n) = wb^T = \sum_{i=1}^n w_i b_i, \tag{4}$$

where $w = [w_1, w_2, \dots, w_n]^T$ signifies the weights vector with $w_i \in [0, 1]$ and $\sum_{i=1}^n w_i = 1$ and b signifies the related ordered values vector and $b_i \in B$ is the i th greatest value in A .

able 2 Linguistic expressions for HFL AHP Onar et al 20

Linguistic expression	Fuzzy numbers
Absolutely Low Importance (ALI)	(0.11,0.11,0.14)
Very Low Importance (VLI)	(0.11,0.14,0.2)
Essentially Low Importance (ESLI)	(0.14,0.2,0.33)
Weakly Low Importance (WLI)	(0.2,0.33,1)
Equally Low Importance (ELI)	(0.33,1,1)
Exactly Equal (EE)	(1,1,1)
Equally High Importance (EHI)	(1,1,3)
Weakly High Importance (WHI)	(1,3,5)
Essentially High Importance (ESHI)	(3,5,7)
Very High Importance (VHI)	(5,7,9)
Absolutely High Importance (AHI)	(7,9,9)

Step 3. In the pairwise comparison matrix \tilde{C} reciprocal values are calculated as

$$\tilde{c}_{ij} = \left(\frac{1}{c_{ju}}, \frac{1}{c_{jm2}}, \frac{1}{c_{jm1}}, \frac{1}{c_{ji}} \right)$$

Step 4. Each pairwise comparison matrix's consistency is checked. These matrices are defuzzified to ensure consistency. Camci et al 20. Considering TFN $A = (l, m_1, m_2, u)$ it is converted to a crisp number with

$$\mu_d = \frac{l+m_1+m_2+u}{6}$$

These equations are used to calculate the consistency ratio (CR)

$$CI = \frac{\lambda_{max} - n}{n - 1}$$

7

$$CR = \frac{CI}{RI}$$

where CI refers to the consistency index, λ_{max} is the largest eigenvector of the matrix, n is the number of criteria, and RI is the random index. Experts have to reconsider the pairwise comparison matrices if they are not consistent.

Step 5. The fuzzy geometric mean \tilde{r}_i of \tilde{C} is calculated as

$$\tilde{r}_i = (\tilde{c}_{i1} \otimes \tilde{c}_{i2} \dots \otimes \tilde{c}_{in})^{1/n}$$

Step 6. The fuzzy weight \tilde{w}_i^{CR} of every main criterion is computed as

$$\tilde{w}_i^{CR} = \tilde{r}_i \otimes \tilde{r} \otimes \tilde{r}_2 \otimes \tilde{r}_n$$

0

Step 7. Fuzzy global weights of the sub-criteria's are calculated as

$$\tilde{w}_i^G = \tilde{w}_i^{CR} \otimes \tilde{w}^{CR}$$

where \tilde{w}_{ij}^G signify sub-criteria global weight

Step 8. Trapezoidal fuzzy numbers \tilde{w}_i^G are defuzzified and normalized as

$$w_i^G = \frac{2 \cdot 2}{\dots}$$

2

$$w_i^N = \frac{w_i^G}{\sum_i \sum w_i^G}$$

3

Steps are performed for both the main and sub-criteria, and steps 7 are used to calculate the weights of the sub-criteria.

O OS A S SSFA O S FO A A O

As a result of the literature review and expert opinions the CSFs for digital education Volery 200 Sharma et al 20 Alrasheedi et al 20 Fabito 20 7 Barclay et al 20 Blicek et al 20 Moya and Camacho 202 ano ia et al 202 nig et al 2023 are structured as in Table 3

able 3 CSFs for digital education

ritical Succes Fact rs	
Technological Factors F	screen design and aesthetics F
	Internet uality F 2
	ease of access F 3
	system interactivity and system response F 4
	privacy and reliability of system F
Human Factors instructors F2	previous computer experience F2
	continuous digital awareness F22
	pedagogical digital competence F23
	timely response F24
	encourage students interaction F2
Human Factors students F3	technical competency F3
	perception of content and system F32
	students mindset about online learning F33
	self efficiency F34
	student involvement and participation F3
Organi ational Factors institution F4	technical support F4
	technical e uipment availability F42
	program flexibility F43
	course instruction authori ation F44
	digital strategy roadmap F4
Resources Factors courses F	course uality and sufficiency F
	course flexibility F 2
	curriculum management and assessment F 3
	integration of e learning into curriculum F 4
	offering more ICT related courses F

A A O

Determining the CSFs is an important step to take to increase the uality of digital education and provide an efficient education environment for students In this study the CSFs given in Table 3 were determined as a result of expert opinions and a literature review There are five main factors and twenty five sub factors An application for the evaluation of CSFs for digital education is reali ed to show the potential of the proposed approach Three experts evaluate this proposed model All experts have appropriate knowledge and expertise in the field of digital education The experts weights are regarded as e ual

To begin experts evaluate the main CSFs using the linguistic scale shown in Table 2 Table 4 shows the evaluation of the main criteria The language expressions in Table 4 are transformed into fu y numbers using 4 The weights of each main CSF are then calculated using 0 Table shows the relative weights of the main CSFs

able Pairwise comparison matrix of the main CSFs

	F1	F2	F3	F	F
F1	EE	Between EHI and HI	Between EHI and HI	Between ESHI and AHI	Between HI and ESHI
F2		EE	Between ELI and EHI	Between HI and ESHI	Between EHI and HI
F3			EE	Between EHI and HI	Between HI and ESHI
F				EE	Between ESLI and ELI
F					EE

Table 4. Relative weights of the main CSFs

	F1	F2	F3	F	F	Relative weights
F1		3	3	3 7 7 22	3 7	0 0 0 232 0 2 47
F2	0 2 0 33		0 33 3	3 7	3	0 0 0 0 27 0 3 0 0
F3	0 2 0 33	0 33 3		3	3 7	0 0 0 0 27 0 3 0 0
F	0 0 4 0 0 33	0 4 0 2 0 33	0 2 0 33		0 4 0 32 0 34	0 0 0 0 40 0 0 0 272
F	0 4 0 2 0 33	0 2 0 33	0 4 0 2 0 33	3 3 7		0 02 0 0 7 0 72 0 00

Each sub CSFs assessment matrices are generated using the linguistic scale supplied in Table 2 to determine the weights of sub CSFs. The first CSF F1 assessment matrix is shown in Table 4. Table 4 shows how the various sub CSF assessment matrices are organized.

Table 5. Pairwise comparison matrix of the first CSF F1

	F11	F12	F13	F1	F1
F11	EE	Between ESLI and ELI	Between VLI and ESLI	Between ESLI and ELI	Between ALI and VLI
F12		EE	Between ELI and EHI	Between ELI and EHI	Between ESLI and ELI
F13			EE	Between EHI and HI	Between ESLI and ELI
F1				EE	Between VLI and ESLI
F1					EE

The language expressions in Table 5 are translated into fuzzy numbers using [4]. The weights of each sub CSF are determined using [10]. The values are then normalized with [3] after being defuzzified using [2]. Table 7 contains the final findings. The CR is computed for the evaluation matrices with [11]. The results showed that experts' evaluations are consistent.

Table 6. Weights of CSFs

Sub criteria	Initial weights				Defuzzified weights	Normalized weights
F11	0 002	0 00	0 03	0 2 3	0 0 7	0 0
F12	0 004	0 032	0	0	0 2	0 0
F13	0 00	0 03	0 3	4	0 2	0 074
F1	0 003	0 022	0 0	0 43	0 4	0 042
F1	0 0	0 0	0 3	2 2	0 4	0
F21	0 002	0 023	0 0	0 4	0 0	0 0 4
F22	0 003	0 034	0 40		0 2 2	0 072
F23	0 003	0 02	0 47	220	0 2 2	0 07
F2	0 00	0 007	0 03	0 32	0 0	0 020
F2	0 00	0 007	0 03	0 40	0 0 2	0 023
F31	0 00	0 037	0 233	324	0 3	0 0
F32	0 00	0 00	0 043	0 44	0 0	0 02
F33	0 00	0 00	0 02	0 227	0 04	0 0 4
F3	0 004	0 02	0	0	0 22	0 0 4
F3	0 00	0 0	0 0 3	0 22	0 0	0 03
F 1	0 000	0 003	0 0	0 22	0 02	0 007
F 2	0 000	0 003	0 0	0 0	0 023	0 007
F 3	0 002	0 00	0 04	0 3 0	0 07	0 022
F	0 00	0 00	0 030	0 2	0 0 7	0 0
F	0 00	0 007	0 030	0 23	0 0 2	0 0
F 1	0 003	0 0	0 077	0 4	0 40	0 040
F 2	0 002	0 0	0 0	0 3	0 7	0 033
F 3	0 002	0 0 3	0 0	0 444	0 0	0 02
F	0 00	0 003	0 0	0 24	0 02	0 007
F	0 00	0 003	0 0	0 24	0 02	0 007

The most appropriate CSF is found as privacy and reliability of system F1, the second important one is technical competency F3, and the third ranked CSF is pedagogical digital competence F23.

O S O S

The aim of this study was evaluating CSFs for digital education with a HFL MCDM approach. HFL AHP method is used for the determination of the weights of CSFs. The contributions of this paper were proposing a new and conceptual evaluation model including CSFs for digital education, presenting an analytic method such as the HFL AHP method in this area, and providing an application for the evaluation of CSFs for digital education.

At the end of the application, the most important CSF is found as privacy and reliability of system. First, instructors and students need a special place where they can study online. For this reason, the first feature that the digital education approach should have in order for education to be sustainable is that the system is confidential and reliable.

For future research, the evaluation problem can be solved by the HFL Analytic Network Process (ANP) method considering the connections between the CSFs. Other extensions of fuzzy sets, for example, elicited information, pythagorean fuzzy sets, spherical fuzzy sets, may be added into the framework.

Ac k n o w l e d g e m e n t s

This work has been supported by the Scientific Research Projects Commission of Galatasaray University under grant number FOA 2020 and FOA 2023.

ethics committee Approval

NA

Peer review

Externally peer reviewed

Author contributions

Conceptualization: E M, G B, M G; Investigation: E M, G B, M G; Material and Methodology: E M, G B, M G; Supervision: G B; Visualization: E M, G B, M G; Writing Original Draft: E M; Writing review & Editing: E M, G B, M G; Other: All authors have read and agreed to the published version of manuscript.

Conflict of interest

The authors have no conflicts of interest to declare.

Financial

The authors declared that this study has received no financial support.

References

- Alrasheedi M, Capret L F, Ra a A. 2020. A systematic review of the critical factors for success of mobile learning in higher education: university students' perspective. *Journal of Educational Computing Research* 22(2): 7.
- Alrasheedi M, Capret L F, Ra a A. 2020. Management's perspective on critical success factors affecting mobile learning in higher education institutions: An empirical study. *Journal of Educational Computing Research* 42(2): 3274.
- Barclay C, Donalds C, Osei Bryson M. 2020. Investigating critical success factors in online learning environments in higher education systems in the Caribbean. *Information Technology for Development* 24(3): 2.
- Blieck Ooghe I, hu C, Depryck Struyven Pynoo B, Van Laer H. 2020. Consensus among stakeholders about success factors and indicators for quality of online and blended learning in adult education: a Delphi study. *Studies in Continuing Education* 4(3): 0.
- B y k kan G, arabulut Mukul E. 2020. A novel renewable energy selection model for United Nations sustainable development goals. *Energy* 2(0): 302.
- Cort s A, Barber E. 2023. STUDENTS PERCEPTIONS TO ARDS ONLINE LEARNING SUCCESS FACTORS. In *EDULEARN 3 Proceedings* pp. 4(0): IATED.

- De Paepe L, hu C, Depryck 20. Development and implementation of online Dutch L2 courses in adult education: educators and providers' perceptions of constraints and critical success factors. *Innovation in language learning and teaching* 3(3) 277-282
- Fabito B S. 2017 September. Exploring critical success factors of mobile learning as perceived by students of the college of computer studies National University. In 2017 International Conference on Soft Computing, Intelligent System and Information Technology (ICSIT), pp. 220-222. IEEE.
- Fisk P. 2017. Education 4.0: the future of learning will be dramatically different in school and throughout life.
- Freund P. Critical success factors. *Planning Review*
- Hwang C L. Moon. Methods for multiple attribute decision making: Multiple attribute decision making methods and applications: a state of the art survey.
- Ibanez A, Roggt A V D, Neubert M. 2023. Impact and success factors of online education methods at university level in times of COVID-19: a case study of Paraguay. *International Journal of Technology Enhanced Learning* 7(3) 73-85
- Jainoia M, Shukla B, Ali A, Joshi M. 2022. Critical success factors for leveraging technology transfer from higher education institutions to industry: Indian context. *International Journal of Innovation and Technology Management* 24(2) 100-115
- Knig C M, Arrenbauer C, Breitner M H. 2023. Critical success factors and challenges for individual digital study assistants in higher education: A mixed methods analysis. *Education and Information Technologies* 24(4) 447-462
- Liu H, Rodrigue R M. 2014. A fuzzy envelope for hesitant fuzzy linguistic term set and its application to multicriteria decision making. *Information Sciences* 272 220-235
- Milic S, Simeunovic V. 2022. Exploring e-learning critical success factors in digitally underdeveloped countries during the first wave of the COVID-19 pandemic. *Interactive Learning Environments* 30(3) 305-320
- Moya S, Camacho M. 2022. Identifying the key success factors for the adoption of mobile learning. *Education and Information Technologies* 21(2) 185-200
- Onar S, Buyukkan G, Tayibi B, Ahraman C. 2022. A new hesitant fuzzy Fuzzy Decision approach: an application to computer workstation selection. *Applied Soft Computing* 114 107645
- Papanikolaou, Mavromoustakos S. 2008 February. Critical Success Factors for the Development of Mobile Learning Applications. In *EuroIMSA*, pp. 24-30
- Rockart F. 1971. Chief executives define their own data needs. *Harvard business review* 49(2) 31-37
- Rodrigue R M, Martine L, Herrera F. 2010. Hesitant fuzzy linguistic term sets for decision making. *IEEE Transactions on fuzzy systems* 18(2) 107-118
- Saaty T L. 1980. How to make a decision: the analytic hierarchy process. *European journal of operational research* 4(3) 127-135
- Sharma, Pandit P, Pandit P. 2020. Critical success factors in crafting strategic architecture for e-learning at HP University. *International Journal of Educational Management* 34(1) 1-15
- Torra V. 2010. Hesitant fuzzy sets. *International journal of intelligent systems* 25(2) 201-213
- Volery T. 2008. Online education: An exploratory study into success factors. *Journal of educational computing research* 24(1) 77-92
- Wu B, Wu. 2014. Analytic hierarchy process hesitant group decision making. *European Journal of Operational Research* 233(3) 744-750

Effect of Strontium on Eutectic Silicon in Al-Si Alloys

Ilana Latica ^{*1}, Sara Kvačević ²

Abstract Eutectic Al-Si alloys widely applied in automotive engines because of their good mechanical properties. In order to improve mechanical properties, strontium is added to Al-Si alloy to transform the eutectic silicon. The modification treatment of Al-Si alloys by adding of Sr has been known for about a century, but the mechanisms behind the strong element assisted eutectic refinement is still not fully understood. The appropriate concentration of Sr is sufficient for well modified of the eutectic silicon.

Keywords Al-Si alloys, microstructure, properties

¹ **Address** University of Montenegro, Faculty of Metallurgy and Technology, Cetinski put bb 000 Podgorica, Montenegro

² **Address** Central School of Chemical Technology Spasice Raspopovi 000 Podgorica, Montenegro

* **Corresponding author** bilana.ucg@me

1. INTRODUCTION

Al-Si alloys are the most widely used aluminum casting alloys owing to their superior castability, light weight, low thermal expansion coefficient, excellent thermal conductivity, high wear resistance and good corrosion resistance [Liu et al., 20]. In hypoeutectic Al-Si alloy, the Si content varies from 0 to 2 wt%. There are very few data on the size of unmodified Al-Si eutectic grains. The irregular shape of the eutectic liquid interface makes accurate measurement of the Al-Si eutectic grain size difficult. Modification of Al-Si castings is standard practice. The growth characteristics of eutectic Si in unmodified and Sr-modified Al-0.7wt% Si alloys were investigated. The eutectic Si of the alloy is present as a thick needle. It is of great importance to improve the mechanical properties of Al-Si alloys by modification. Modification has been widely used because they are simple to operate and inexpensive to perform.

2. MATERIALS AND METHODS

Two alloys of composition Al-0.7wt% Si (unmodified) and Al-0.7wt% Si-0.02wt% Sr (Sr-modified) were made. The alloys were melted in an induction furnace at 720°C. The method of Sr addition is through master alloy Al-0wt% Sr. The modifying effect exerted by Sr is most pronounced if all Sr is brought into liquid solution. After the alloying step, degassing was performed for 30 minutes. The melt was poured on a temperature at 720°C into the molds. Metallographic samples were sectioned horizontally and were mounted and polished. An optical microscope was used to analyze the microstructures.

Chemical composition of the Al-Si alloys used in this study is shown in Table 1. These compositions were chosen because of their eutectic volume fractions. In the Al-0.7wt% Si (unmodified) and Al-0.7wt% Si-0.02wt% Sr, the formation of the Al-Si eutectic is the major solidification reaction because it has a large eutectic volume fraction.

Table 1 Chemical composition of the investigated alloys (in wt%)

TPE OF SAMPLE	Fe	Si	Ti	Cu	Mn	V	Cr	Mn	Mg	Sr
Al-0.7wt% Si	0.2	0.74	0.00	0.004	0.043	0.004	0.002	0.002	0.000	0.0
Al-0.7wt% Si-0.02wt% Sr	0.24	0	0.00	0.00	0.03	0.00	0.00	0.002	0.000	0.07

Properties of the Al-0.7wt% Si (unmodified) and Al-0.7wt% Si-0.02wt% Sr alloys have been investigated. Hardness has been measured by use of the Brinell method.

3 S S

Figure shows the as cast microstructure of an Al 0.7wt % Si unmodified near eutectic alloy. Figures 2 and 3 show images taken with the Sr modified sample Al 0.7wt % Si. At low magnification we can see the dendritic nature of the fine solidification structure. At high magnification this is not observed; instead we see the fine eutectic and randomly oriented α Al grains. Further in the image sequence Si needles are seen to form. Small additions of Sr modify the silicon phase. The result is an increase in mechanical properties.

100 μ m



Figure 1 Microstructure of Al 0.7wt % Si unmodified alloy

20 μ m



Figure 2 Microstructure of Al 0.7wt % Si 0.02wt % Sr alloy

100 μ m



Figure 3 Microstructure of Al 0.7wt % Si 0.02wt % Sr alloy

we have also examined the properties of these materials hardness measurement The hardness of the modified alloy is higher than the hardness of the alloy without any modification treatment Table 2

Table 2 Hardness of the investigated alloys

TYPICAL SAMPLE	HB _{average}
Al 0.7wt % Si	3
Al 0.7wt % Si 0.02wt % Sr	0

S S O A O S O S

Al Si alloys have considerable commercial importance as casting alloys Al Si based alloys are the most widely used Al based foundry alloys due to their excellent combination of mechanical properties and castability Chen and Wu 20 Near eutectic alloys generally containing eutectic modifiers are also widely used The Al Si binary phase diagram is the basis for understanding the microstructure of these alloys Our experiments were designed to investigate the effects of strontium on the eutectic silicon for Al Si alloys Solidification is a process of nucleation and growth In Al 0.7wt % Si unmodified and Al 0.7wt % Si 0.02wt % Sr alloys the first phase to be nucleated is α Al According to the Al Si phase diagram α phase has a low silicon content max The Si content determines the conditions for growth The formation of the Al Si eutectic is the major solidification reaction in the Al 0.7wt % Si alloy constituting approximately two thirds of the volume Strontium is added to Al Si alloy to transform the eutectic silicon from faceted acicular flakes to a fine fibrous structure Hegde and Prabhu 200

For hypoeutectic Al Si based alloys the modification of eutectic Si have a significant impact on the mechanical properties The results of this investigation show that the strontium modified alloy Al 0wt % Si 0.02wt % Sr had porosity level lower than Al 0.7wt % Si unmodified

F S

Liu Hang Beausir B Liu F Esling C Wu F 20 Twin controlled growth of eutectic Si in unmodified and Sr modified Al 2.7 % Si alloys investigated by SEM EBSD Acta Materialia 7 33 347

Chen Ru 20 Modeling of aluminum silicon irregular eutectic growth by cellular automaton model Research and Development 3 4 22

Hegde S Prabhu N 200 Modification of eutectic silicon in Al Si alloys Mater Sci 43 300 3027

Structure and Simulation of a Single Phase Seven Level Inverter**Abdullatif Milić^{*1}, Alijeirić Iliz²**

Abstract In this article a one phase seven level inverter structure will be examined and this inverter will be simulated in computer environment by using Matlab Simulink program. Sinus triangle pulse width modulation will be used for the control circuit of the inverter and in order to generate the trigger signal in this control structure three peak value reference values namely DC component will be added and rectified and will be realized after comparing the sinus signals with the same frequency with a carrier triangle signal. By keeping the amplitude of the said carrier triangle signal constant and its frequency being much higher than the reference rectified sine signals the output voltage of the inverter is provided to resemble a pure sine wave and the output current is provided to appear as almost pure sine with the load containing the coil. Of course because the inverter structure has seven levels sine triangle pulse width modulation is made here. In higher order inverter topologies the output voltage and current can be approximated to a pure sine form without harmonic even without applying sine triangle pulse width modulation. However in such a case the cost will increase because too many semiconductors and voltage sources will be used. However in the inverter topology realized in this study seven levels were obtained by using only six mosfets. In addition the voltage source is used as three equal level voltage sources by using 3 series connected capacitors to the voltage source. These 3 different comparison signals which are used for the inverter output voltage to be seven level will enable the switches to turn on and off respectively in the inverter structure and with the pulse width modulation the total harmonic distortion will be reduced by approaching the pure sinus form of the output voltage form. This inverter structure and everything described has been tested only in the computer environment by means of the Matlab Simulink program and the realized circuit structure can be run correctly.

Keywords Seven Level Inverter, Pulse Width Modulation, Total Harmonic Distortion

¹**Address** Coaeli University Graduate School of Natural and Applied Sciences Department of Electrical Engineering Coaeli Torkiye

²**Address** Coaeli University Faculty of Engineering Department of Electrical Engineering Coaeli Torkiye

* **Corresponding author** latifemlik@gmail.com

1. INTRODUCTION

Today multilevel inverters are used in almost every industrial application and have many different types. They are preferred because their output voltages are very close to sine. Their total harmonic distortion is also low. The higher the number of levels the higher the level of decay. However the higher the level the higher the voltage source and the number of semiconductors used. This will make the inverter structure very complex and increase the cost. For this reason inverter design should be done in accordance with the needs. When looking at the types of multilevel inverters they are diode clamped inverters, capacitor clamped inverters, H bridge inverters. In this article a bidirectional six switch H bridge inverter structure is constructed in a modified structure using a new sine triangle pulse width modulation.

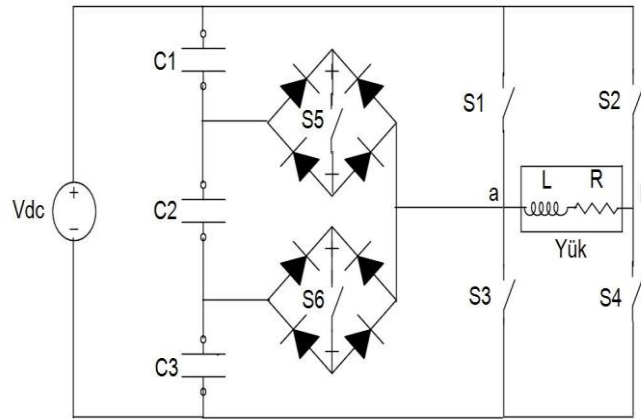


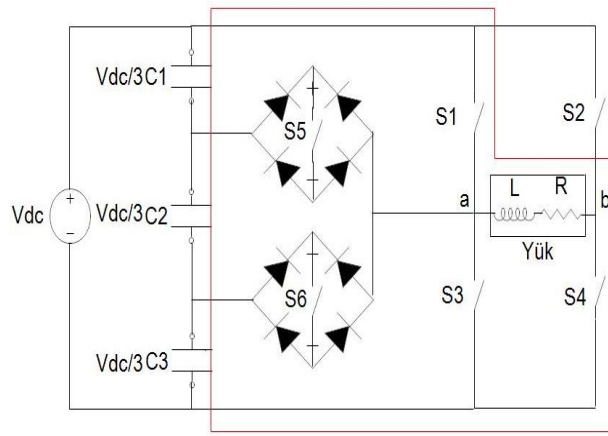
Figure 1 Phase Seven Level Inverter Circuit

2 O OS

O O O

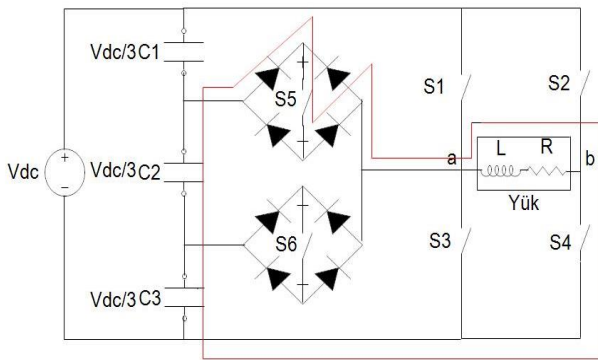
As can be seen in Figure 1 a different h bridge inverter structure is applied in this study. It consists of a combination of bidirectional switches and the traditionally used h bridge inverter. Capacitors C1, C2 and C3 are used dividing the input voltage into three equal sources. In this wide bridge inverter structure a multilevel inverter is obtained by using more power switches and power diodes. By properly switching the power switches respectively V_{dc} , $2V_{dc}/3$, $V_{dc}/3$, $0V$, $V_{dc}/3$, $2V_{dc}/3$ and V_{dc} voltages will be given to the output of the circuit. So my output voltage will become seven level. Thus we can divide the proposed inverter operating principle into 7 parts. Figure 2 represents these 7 different operating states between a and b and these situations are explained below.

- i. The maximum output voltage V_{dc} is given on the load when the S1 and S4 switches are active and all other switches are disabled and thus the voltage appearing on the load becomes the V_{dc} voltage as can be seen in Figure 2 a.
- ii. With the bidirectional switch S5 and S4 switches active and all other switches disabled a voltage of $2V_{dc}/3$ is applied to the load and thus the voltage appearing on the load is $2V_{dc}/3$. It has 3 voltages.
- iii. When the bidirectional switch S5 and S4 switches are active and all other switches are deactivated $V_{dc}/3$ voltage is applied to the load and thus the voltage appearing on the load is $V_{dc}/3$ by following the current path shown in Figure 2 c. It has 3 voltages.
- iv. In this structure which is used to get zero output voltage there are two ways to make the voltage on the load zero. The first case is when switches S3 and S4 are only active. All other switches should be disabled. The second situation is when only the S1 and S2 switches are active. All other switches should be disabled in this case. Any of these two principles will make the output voltage zero. However it would be useful to use them in order for the switches to age equally or to complete their life in the same way. Thus the voltage appearing on the load becomes $0V$ by following the current path seen in Figure 2 d.
- v. With the bidirectional switch S5 and S2 switches activated and all other switches deactivated $V_{dc}/3$ voltage is applied to the load so that the voltage appearing on the load follows the current path shown in Figure 2 e. $V_{dc}/3$ voltage becomes.
- vi. When the S5 switch and S2 switches are active and all other switches are disabled a voltage of $2V_{dc}/3$ is applied to the load and thus the voltage appearing on the load follows the current path shown in Figure 2 f. There will be a voltage of $2V_{dc}/3$.
- vii. The maximum negative output voltage $-V_{dc}$ is given on the load with the S2 and S3 switches activated and all other switches disabled and thus the voltage appearing on the load becomes $-V_{dc}$ as it can be seen in Figure 2 g.

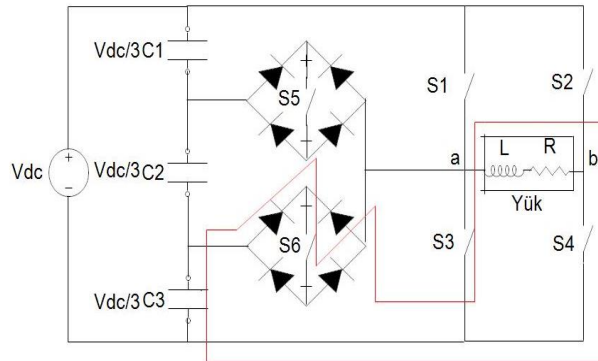


(a)

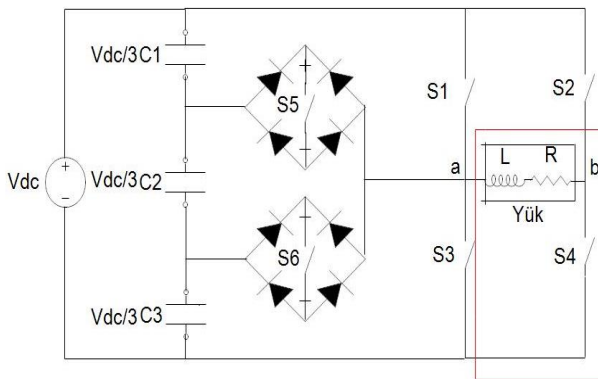
Figure 2 Required switching combinations to generate output voltage a $V_{ab} = V_{dc}$



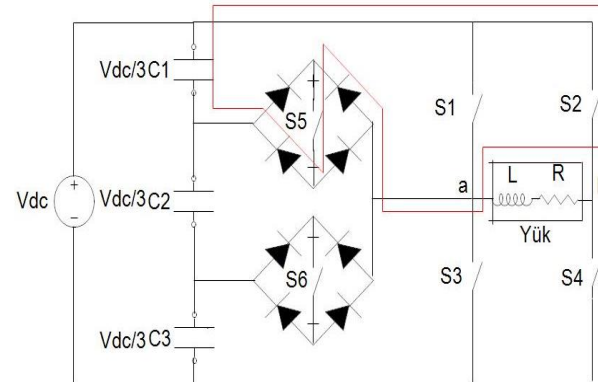
(b)



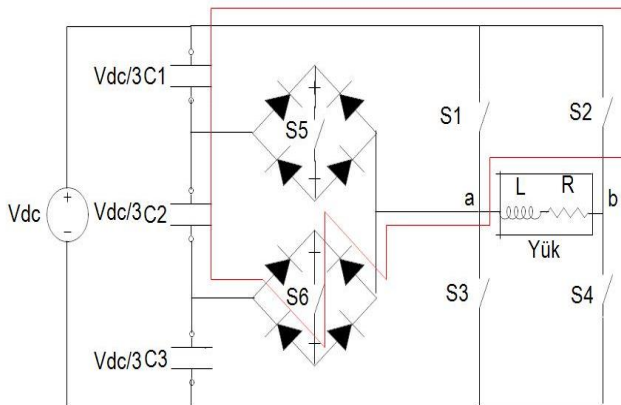
(c)



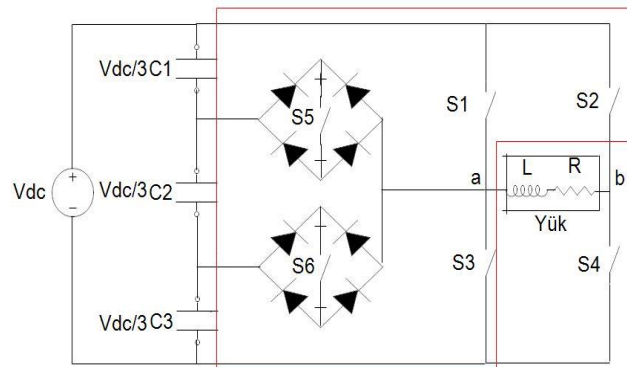
(d)



(e)



(f)



(g)

Figure 2 Continued Required switching combinations to generate output voltage b $V_{ab} = 2V_{dc}/3$ c $V_{ab} = V_{dc}/3$ d $V_{ab} = 0V$ e $V_{ab} = V_{dc}/3$ f $V_{ab} = 2V_{dc}/3$ g $V_{ab} = V_{dc}$

Table 1 Output voltage table according to whether the switches are active or not 0 is presented below

Voutput	S	S2	S3	S4	S	S
Vdc		0	0		0	0
2Vdc/3	0	0	0			0
Vdc/3	0	0	0		0	
0V	0	0			0	0
Vdc/3	0		0	0		0
2Vdc/3	0		0	0	0	
Vdc	0			0	0	0

3 S S A A H O A O

In this article a new structure was developed for sine triangle pulse width modulation. Three reference signals were generated. These reference signals named V_{ref} , V_{ref2} and V_{ref3} were compared with a carrier triangle signal to enable or disable the power switches. The frequencies of the signals created as a reference are equal and in phase with each other. Differently from the V_{ref} signal, the V_{ref2} and V_{ref3} signals have DC components, and thus the peak value of the V_{ref2} signal is reduced by one unit compared to V_{ref} . Likewise, the V_{ref3} signal was obtained by decreasing the peak value by 2 units compared to V_{ref} . It is used to create 0V level when carrier triangle signal for positive alternans is greater than V_{ref} signal. Therefore, S3 and S4 switches are activated in this interval. In cases where the carrier triangle signal is smaller than the V_{ref} signal and larger than the V_{ref2} signal, the $V_{dc}/3$ level is generated. Therefore, switches S1 and S4 are activated in this interval. A voltage of $2V_{dc}/3$ is generated when the carrier triangle signal is smaller than the V_{ref2} signal and at the same time greater than the V_{ref3} signal. Therefore, switches S1 and S4 are activated in this interval. In cases where the carrier triangle signal is smaller than the V_{ref3} signal, the V_{dc} voltage is generated. Therefore, switches S1 and S4 are activated in this interval. It is used to create 0V level when carrier triangle signal for negative alternans is greater than V_{ref} signal. Therefore, S2 and S3 switches are activated in this interval. In cases where the carrier triangle signal is smaller than the V_{ref} signal and larger than the V_{ref2} signal, the $V_{dc}/3$ level is created. Therefore, at this interval, switches S2 and S3 are activated. A voltage of $2V_{dc}/3$ is generated when the carrier triangle signal is smaller than the V_{ref2} signal and at the same time greater than the V_{ref3} signal. Therefore, switches S2 and S3 are activated in this interval. In cases where the carrier triangle signal is smaller than the V_{ref3} signal, V_{dc} voltage is generated. Therefore, S2 and S3 switches are activated in this interval. Thus, the output voltage becomes seven level. This switching structure is shown in Figure 3. As you can see, switches S1, S3, S4, and S2 operate at the speed of the carrier triangle signal. But the frequency of switches S2 and S4 is equal to the fundamental frequency.

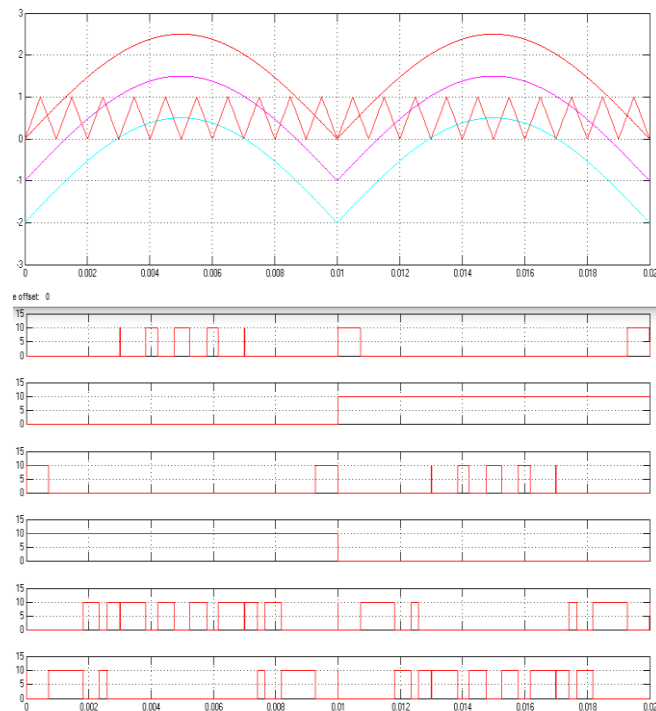


Figure 3 Switching structure for one phase seven level inverter

S A O S S

The inverter circuit realized in this article is simulated in computer environment by using Matlab Simulink program

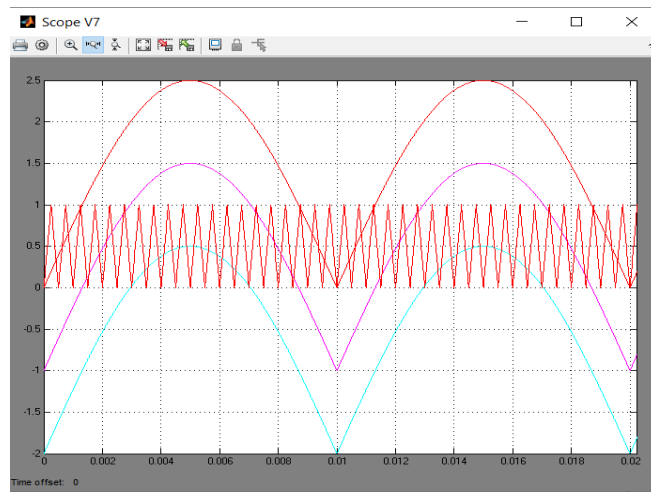


Figure Reference signals used to generate PWM switching signals

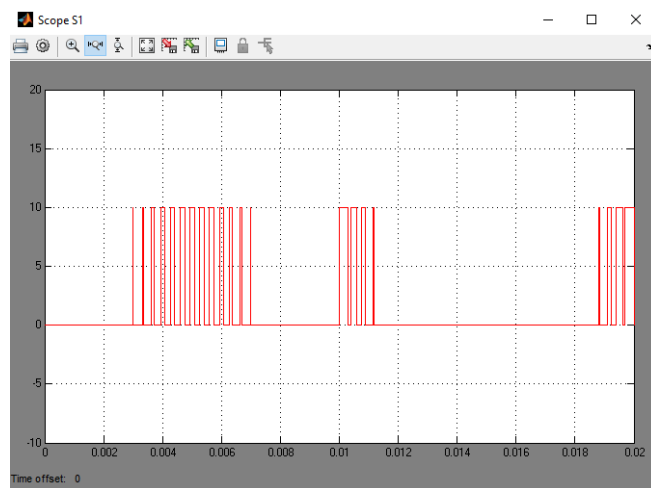


Figure PWM signal for switch S

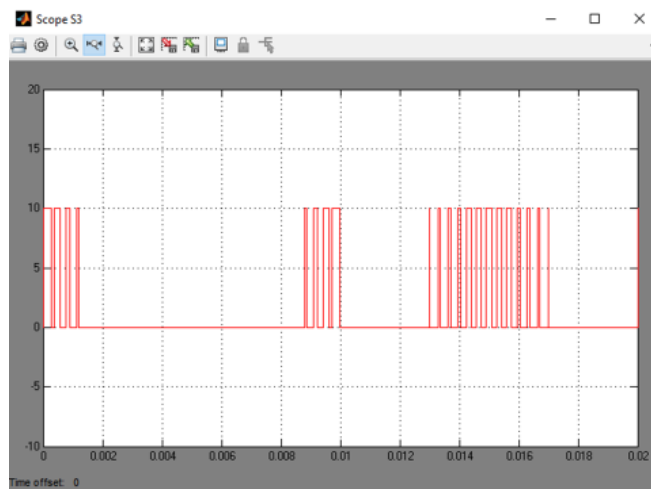


Figure PWM signal for switch S3

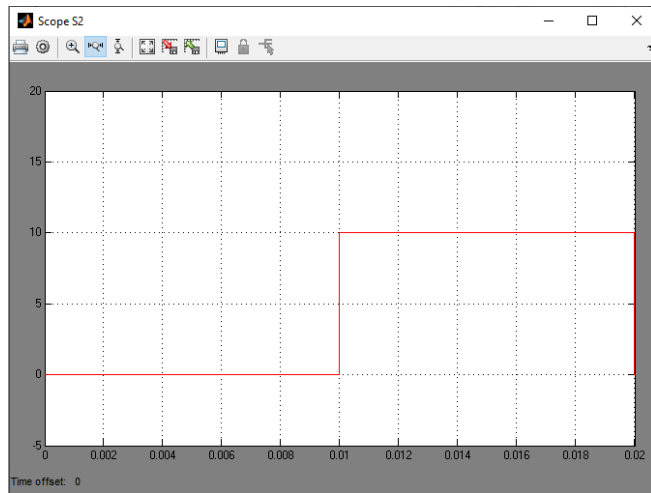


Figure P M signal for switch S2

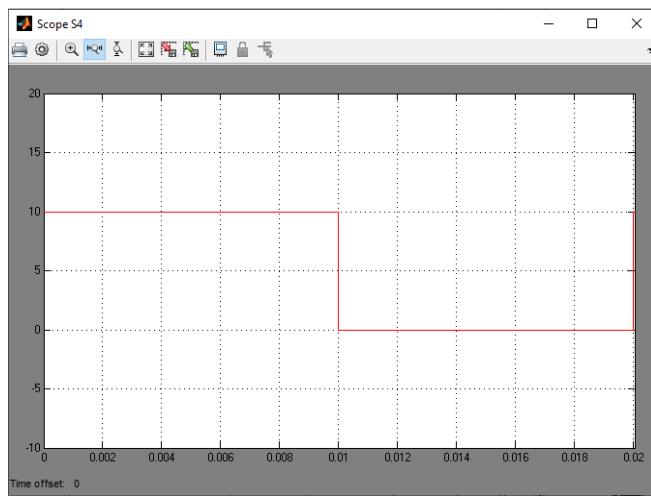


Figure P M signal for switch S4

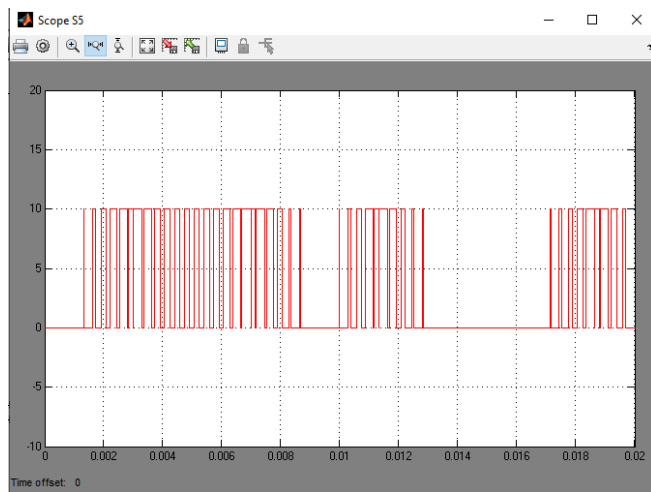


Figure P M signal for switch S

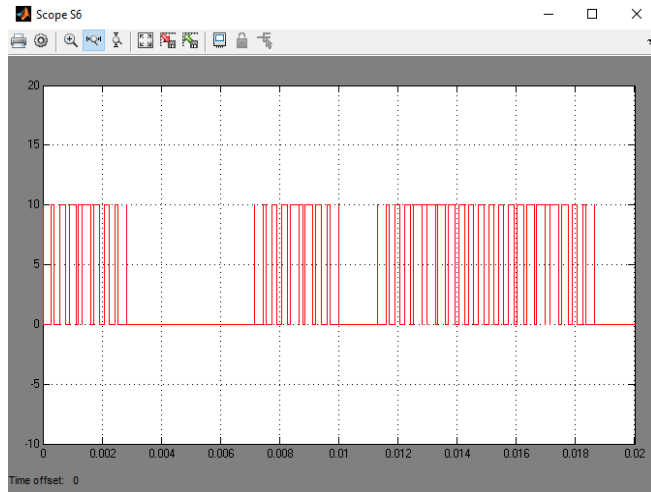


Figure 10 PWM signal for switch S

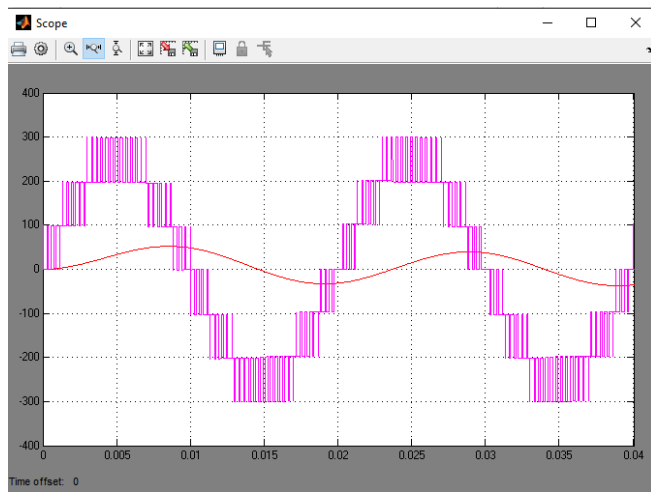


Figure 11 PWM inverter output voltage and current

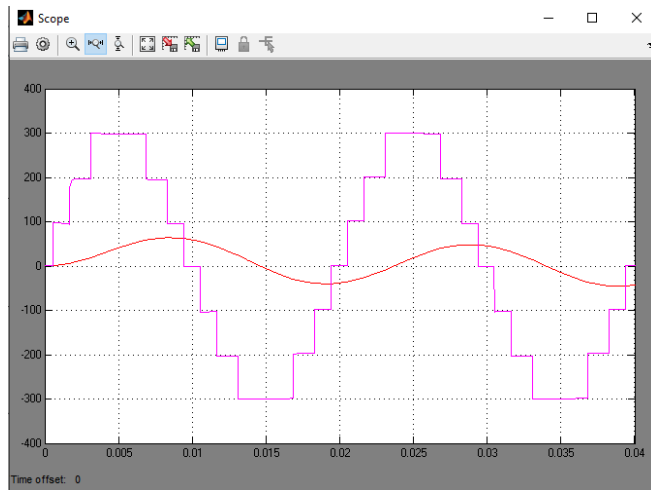


Figure 12 Inverter output voltage and current at full load without PWM

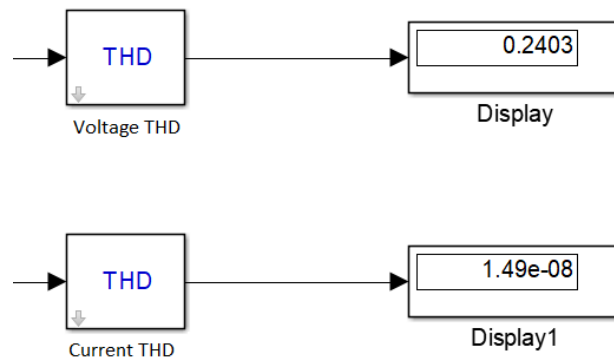


Figure 13 Total harmonic distortion values for output voltage and current

O S O S

Multilevel inverters are similar to pure sine in output voltage and thus have low total harmonic distortion. In this article, a new different pulse width modulation algorithm is implemented and three reference signals and a carrier triangle signal are compared, enabling switches to switch on and off, thus obtaining a seven-level inverter. This inverter model has been realized in a computer environment by means of the Matlab Simulink program and it has run successfully.

F S

1. Işık, İ., Balçık, E., Bayındır, R. Review of multilevel voltage source inverter topologies and control schemes. *Energy Conversion and Management*, 2014, 82, 20-30.

2. Sabarad, S., Gulikarni, G.H. Comparative analysis of SVPWM and SPWM techniques for multilevel inverter. *International Conference on Power and Advanced Control Engineering*, Bangalore, India, 2014, August 20-24.

3. Babaei, E., Hosseini, S.H. New cascaded multilevel inverter topology with minimum number of switches. *Energy Conversion and Management*, 2010, 51, 277-290.

4. Şen, S., Demir, E. Modeling, simulation and control of three-phase three-level multilevel inverter for grid-connected PV system. *SOLAR TR2 Solar Electricity Conference and Exhibition*, Antalya, Turkey, 7-11 November 2012.

5. Ray, R., Shadh, M.A. and Reza, S. Cascaded H-bridge multilevel inverter using SVPWM modulation. *International Conference on Advances in Science, Engineering and Robotics Technology (ICASERT 2010)*.

6. Islam, N., Sarker, S., Meraul Islam, N.M. and Reza, S. Implementation of finite control set model predictive control on 7-level flying capacitor multilevel inverter using space vector. *International Conference on Advances in Science, Engineering and Robotics Technology (ICASERT 2010)*.

7. T. Lipo and D. Holmes. *Pulse Width Modulation for Power Converters: Principles and Practice*. Hoboken, NJ: Wiley, 2003.

8. Ushare, B.E., A.A. Ghatol and M.S. Aphale. Survey of Interharmonics in Indian Power System Network. *Power Engineering Conference 2007 (IPEC 2007 International)*, 2007.

9. Sirisukprasert, S. Optimized Harmonic Stepped Sine Waveform For Multilevel Inverter. Master Thesis, Blacksburg, Virginia, 2007.

10. Amur, S., Arifolu, B., Behera, E., and Behera, E. Design and Application of a Novel Structure and Topology for Single Phase Five-Level Inverter. *IEEE Transactions on Electronics*, 2007.

Assessment of the Seismic Hazard for Adiyaman with Deterministic Analysis under Probable Earthquake Scenario on the Akada Segment of the Malatya Fault**Seyhan Ozyurt¹, Semir², Fatih Emir³, Mehmet Fatih Yılmaz, Ouzhan Emir**

Abstract On February 2023 at 04:17 and 03:24 hours local time in Turkey two earthquakes with an instrumental magnitude M_w of 7.7 and 7.6 with epicenters in Pazarcik, Adiyaman and Elbistan, Adiyaman occurred hours apart. It was felt in Southeastern Anatolia, Eastern Anatolia, Mediterranean and Central Anatolia regions. It caused great destruction, damage, and many casualties in Adiyaman and neighboring provinces. This study aims to determine the probable seismic hazard around Adiyaman due to a scenario earthquake in the Akada segment of the Malatya fault. According to Wells and Coppersmith (1994) an earthquake with a magnitude of M_w 7.3 is expected in the Akada segment which causes damage in Malatya and the surrounding provinces. The probable earthquake is analyzed with scenario-based seismic hazard analysis by using the earthquake information such as magnitude, longitude, latitude, dip, and rake angle and Chiou and Youngs (2000) attenuation relationship by taking into account the ground conditions in the region. The impact of the earthquake on Adiyaman province was analyzed deterministically using Openquake, an open-source seismic hazard and risk analysis software. Probable earthquake intensity (PGA, MMI) distribution around Adiyaman for the expected ground motion level is obtained and evaluated. The computational results from this study can help provide a reference for seismic hazard assessment around any region under any probable earthquake scenario.

Keywords: Earthquakes, Southeastern Anatolia, Akada Segment, Malatya fault, Seismic Hazard Assessment

¹ **Address:** Civil Engineering Department, Boğaziçi University, İstanbul, Türkiye

² **Address:** Mining and Mineral Extraction Department, Adiyaman University, Adiyaman, Türkiye

³ **Address:** Adiyaman Municipality Directorate of Planning and Urbanization, Adiyaman, Türkiye

Address: Adiyaman Municipality Directorate of Reconstruction and Urbanization, Adiyaman, Türkiye

Address: Civil Engineering Department, Gebze Technical University, İzmit, Türkiye

* **Corresponding author:** seyhan.okuyan@boun.edu.tr

1. INTRODUCTION

Turkey is a country located in a region with high earthquake risk and at the intersection of active fault lines. Earthquake is one of the natural disasters that cause the most loss of life and property in Turkey.

The Eastern Anatolia Region has been adversely affected many times by earthquakes on the Eastern Anatolia Fault Line, which was formed as a result of the collision of the Anatolian Plate and the Arabian Plate. Earthquakes in the Eastern Anatolia Region have caused great damage and death. The 1939 Erzincan Earthquake, the 1976 Eldivan Earthquake, the Van Earthquake, and the February 2023 earthquakes are some of the major earthquakes that occurred in the Eastern Anatolia Region. These earthquakes caused thousands of deaths and injuries. Earthquakes in the Eastern Anatolia Region are some of the biggest natural disasters in Turkey. The earthquake risk of the region is high, and efforts are being made to reduce this risk.

Adiyaman province is located in a seismically active region. The DAF zone is a 4-2 km wide deformation belt starting from Arslanözü in Eastern Anatolia and extending towards Antakya along a length of approximately 100 km within the provincial borders. There are Pazarcik, Erkenek, Pertge segments of the Eastern Anatolia Fault segment, Gerger and Narince segments of the Southeastern Anatolia Thrust, Besni Fault, Boğava Fault, and certain segments of the Sığirci Faults. Many earthquakes with magnitudes ranging from 7 to 7.5 have occurred in these segments along the DAF and caused severe damage. Earthquake hazard analyses are of great importance in terms of determining the earthquake risk and predicting the possible effects of earthquakes that may occur in the future. In this context, an earthquake hazard analysis was performed for Adiyaman province according to the scenario of an earthquake of M_w 7.3 on the Akada segment of the Malatya Fault, which is located around the borders of Adiyaman province and will remain within the impact area in case of an earthquake. Figure 1 with this study, it is thought that earthquake hazard analysis will provide basic data for disaster management and emergency preparedness in the Disaster Management and Emergency Preparedness phase for Adiyaman province.

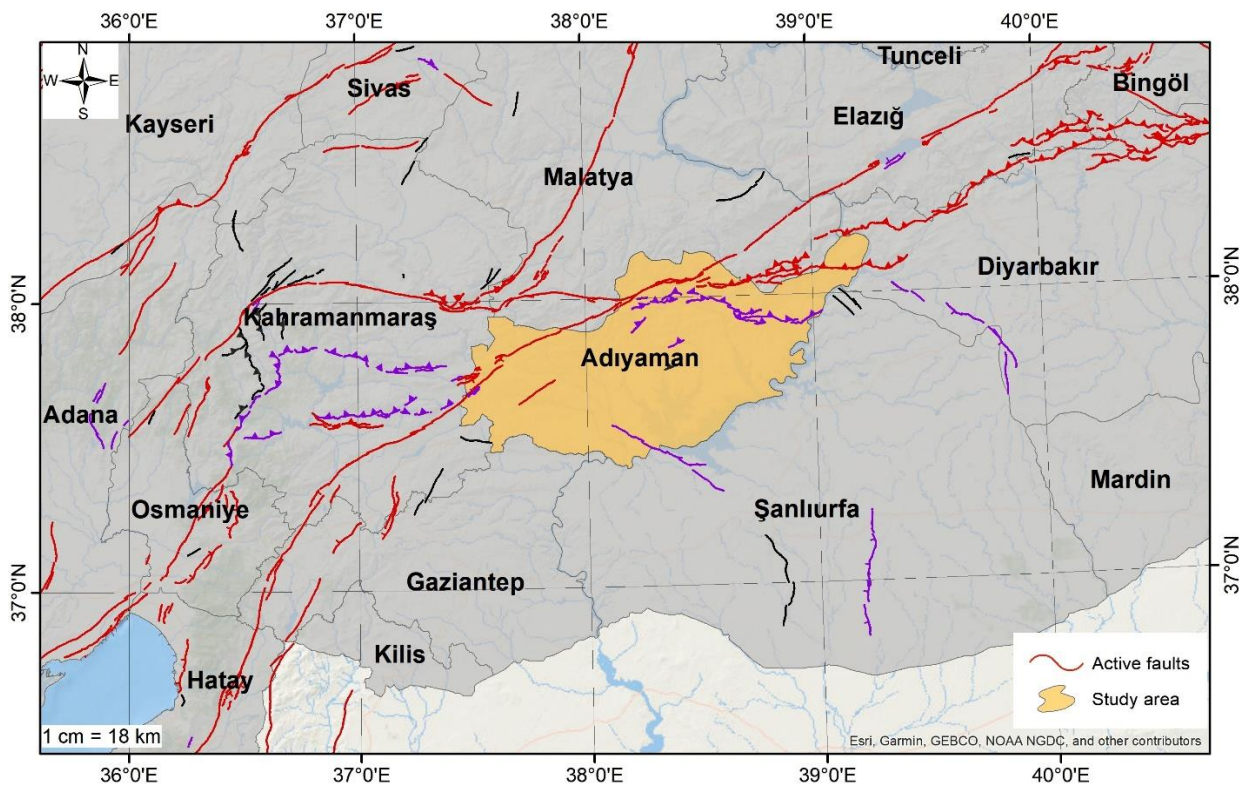


Figure Study area

2 Seismicity Adiyaman province

Adiyaman province is located in the Southeastern Anatolia Region of Turkey and is one of the provinces with high earthquake risk. There are many faults around Adiyaman, especially the Eastern Anatolia Fault, one which has the potential to produce earthquakes of 7 or more. In particular, Adiyaman province, located in the Southeastern Anatolia region, has a high risk of seismicity with approximately 420 km of active fault lines passing through the province, especially the DAF and part of the GAB.

According to historical earthquake records, the 20 earthquakes with the most destructive effects are: 22 Antakya Earthquake, Gynk arlova 72 Lake Amik Earthquake 74 and 7 Tortum Har Lake Earthquake 3 Malatya Earthquake 4 7 Erincan Erurum 04 Diyarbakır Ela and 242 Osmaniye earthquakes. According to the earthquake records of the instrumental period (00 present), 7 earthquakes with magnitude 4 and above occurred. Figure 2b shows the largest earthquake with a magnitude of 7.0 occurred on August 23, 2023, in Varto district of Muş, which is located on the DAF. 234 people lost their lives in this earthquake. The last major earthquake on the DAF occurred on January 24, 2020, with a magnitude of 6.8 centered in Elazığ. This earthquake was felt in many provinces in Turkey, such as Batman, Bingöl, Diyarbakır, Gaziantep, Hatay, Mardin, Osmaniye, Elazığ, Malatya, Kahramanmaraş, and Adiyaman. According to the instrumental earthquake records, there are many earthquakes that have had a destructive effect in Adiyaman since 2000. On March 2, 2018, an earthquake with a magnitude of 6.8 occurred in Adiyaman. This earthquake caused serious damage to buildings and infrastructure in the city. On January 24, 2020, an earthquake with a magnitude of 6.8 occurred in Samsat district of Adiyaman. In this earthquake, 2 people lost their lives and hundreds were injured. Throughout the history, the epicenter of which was Adiyaman, there were the 4 Mw 7.0 Sincik Adiyaman earthquake and 1 Samsat Adiyaman Mw 6.8 earthquake on March 02, 2017. Finally, the February 2023 earthquakes, which caused major destruction in provinces of Turkey, caused the collapse or heavy damage to approximately 100 buildings in Adiyaman province. On February 2023, at 04:17 and 03:24 hours local time in Turkey, earthquakes with epicenters in Paçarcık, Kahramanmaraş, and Elbistan, Kahramanmaraş, with an instrumental magnitude Mw of 7.7 and 7.0 occurred. The earthquakes were felt mainly in the provinces of Hatay, Kahramanmaraş, Adiyaman, Malatya, Adana, Şanlıurfa, and in the Southeastern Anatolia, Eastern Anatolia, Mediterranean, and Central Anatolia regions. The earthquake at 04:17 occurred on the Paçarcık and Amanos segments of the Eastern Anatolia Fault zone. The earthquake at 03:24 occurred on the Ardak fault starting in the southern part of Elbistan. Approximately 1000 earthquakes occurred in the region until 24:00 on July 2023. According to the Shear Wave Velocity V_s 30 map of Adiyaman province, it is seen in Figure 2c that especially the Central and Besni districts have weak ground properties.

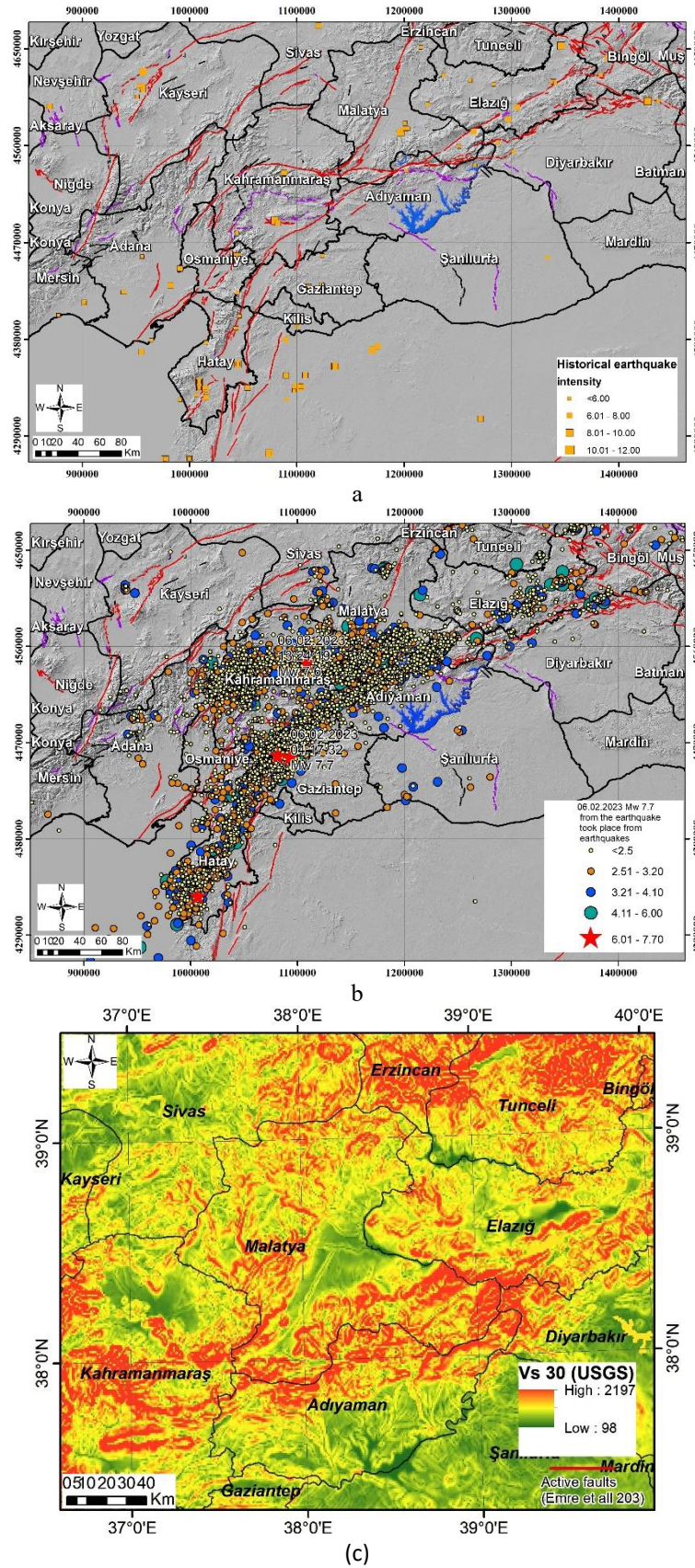


Figure 2 The earthquakes in and around the province of Adiyaman historical a and instrumental earthquake records b Vs 30 map c

An earth uake with a magnitude of Mw 6.8 occurred in the Sivrice district of Adıyaman province at 20:00 on January 24, 2020, at a depth of 10 km and lasted for 20.4 seconds around Adıyaman. As seen in the MMI intensity distribution, this earth uake had a magnitude of 7 in Adıyaman. Figure 3a. According to the USGS PGA-MMI relationship, the PGA level of this earth uake in Adıyaman ranges between 0.03g. On 02/02/2023, two earth uakes of magnitude Mw 7.7 and Mw 7.0 occurred at 04:17 and 13:24, respectively, with epicenters in Kahramanmaraş and Elbistan, Kahramanmaraş. The magnitude 7.7 earth uake occurred at a depth of 10 km, while the magnitude 7.0 earth uake occurred at a depth of 7 km. These earth uakes also had a devastating impact on the neighboring provinces. The MMI intensity distribution map of the earth uake for Adıyaman province is shown in Fig. 3. Especially in the city center of Adıyaman, the intensity was observed to be between VII on the MMI scale. As a result of the scenario analysis of the second earth uake Mw 7.7, Elbistan earth uake, it was observed that the MMI intensity distribution in Adıyaman region was between VII-10. Figure 3b.

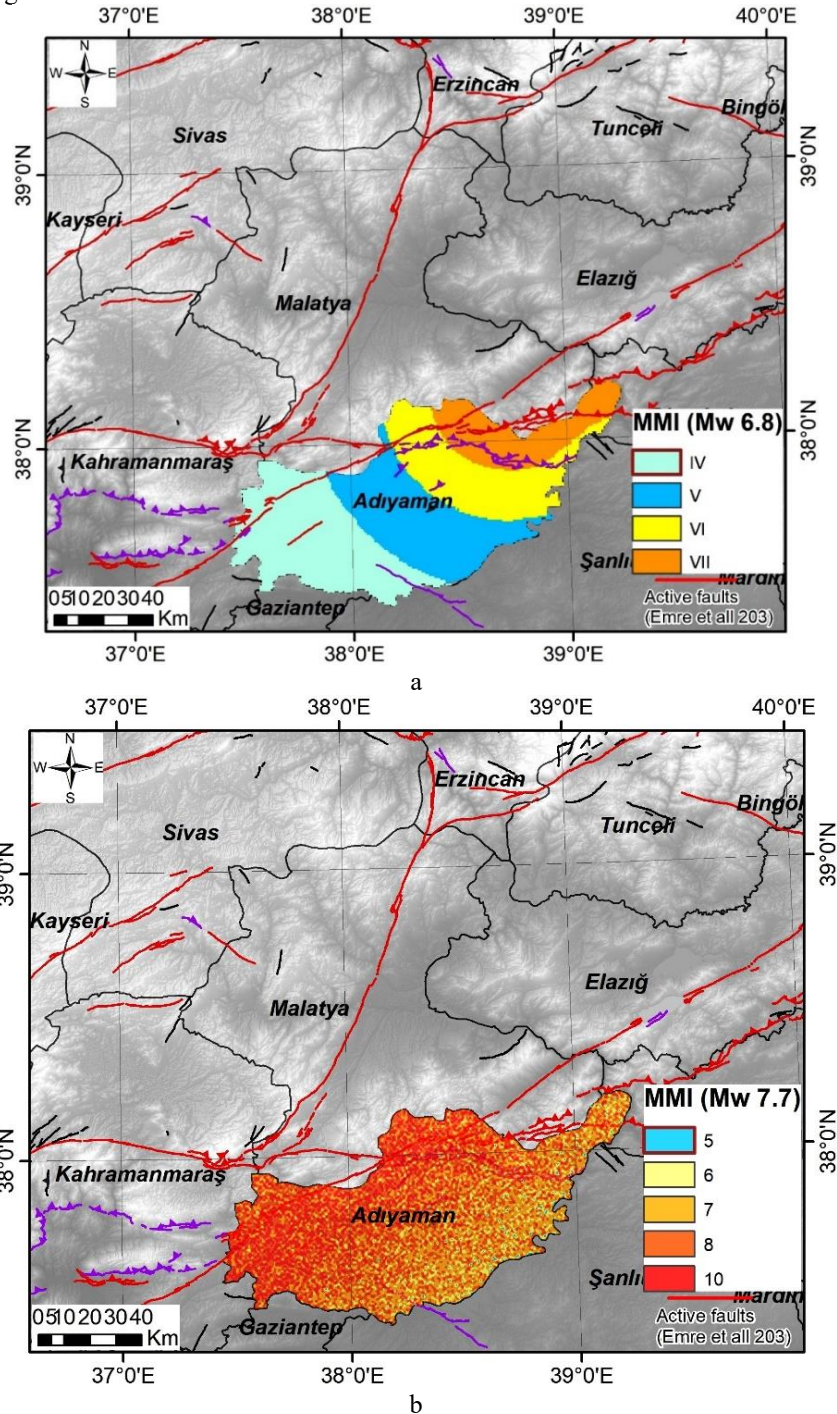


Figure 3. Adıyaman earth uake Adıyaman province MMI intensity map (a) Kahramanmaraş Kahramanmaraş Mw 7.7 earth uake scenario analysis Adıyaman province MMI distribution map (b)

3 Malatya Fault Characteristics

Malatya Fault consists of 3 segments: kemaliye segment, Akçadağ segment and Arguvan segment. Emre et al. (2013) This fault line, also referred to as the Malatya-Ovacik fault line in the literature, constitutes one of the important tectonic structures corresponding to the internal deformation of the Anatolian block during the neotectonic period. Sancar et al. (2017) The fault that forms the eastern boundary of the Malatya plain is a left-trending fault line in the northeast direction. The total length of the fault line is 173 km, of which Akçadağ segment is 74.33 km, Arguvan segment is 40 km, and kemaliye segment is 58.67 km. Figure 1 shows the location of the Malatya fault zone. Each segment has the potential to produce earthquakes of 7 and above.

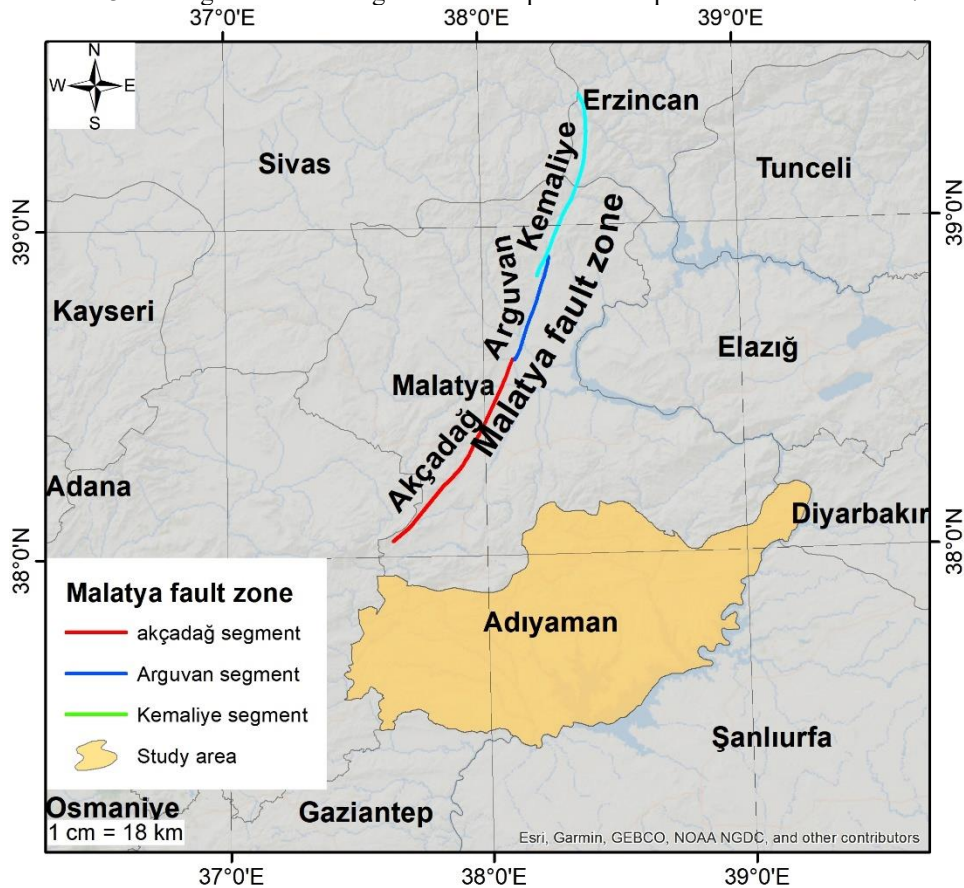


Figure 1. Malatya fault zone and segments. Emre et al. (2013)

2 Seismic Hazard Analysis

Within the scope of pre-disaster risk management, disaster scenarios created to determine the existing seismic hazard and to estimate the possible impacts damages can provide information on the rates and effects of physical, social, and economic losses that may occur after the disaster. Determination of earthquake risk requires first determining the possible earthquake hazard in the region. Griebel et al. (2000) and Erdik et al. (2004) define earthquake hazard as the probability of occurrence of the largest ground motion caused by an earthquake of a magnitude that may cause damage and loss of life at a certain place and time. There are uncertainties in the location, magnitude, and timing of expected earthquakes. Earthquake hazard analyses are pioneering in the design of structures and planning of new settlement areas. Earthquake hazard is realized by probabilistic and deterministic methods. Probabilistic seismic hazard analysis considers the probability that ground motion that may cause damage may occur at a specific location and at a specific time, taking into account uncertainties about the magnitude, location, and time of occurrence of the earthquake. In deterministic seismic hazard analyses, the level of ground motion generated by the largest earthquake that may occur in the region is determined by scenario earthquakes. In order to create earthquake scenarios using the deterministic method, the existing live fault lines and the maximum earthquake magnitudes that these fault lines can produce are determined. Probabilistic earthquake scenarios enable the determination of the probable earthquake hazard in the target region. In scenario-based earthquake hazard analysis, possible seismic sources that will affect the region are identified, the closest distance between the source and the study area is calculated, and the possible seismic hazard in the region is calculated by using ground motion prediction equations suitable for the seismic activity of the region. Figure 2 shows the effect of earthquake

magnitude earth uake source and ground information on the risk is analy ed The results obtained from the scenario analysis will enable us to see the disaster response and recovery capacity of the region

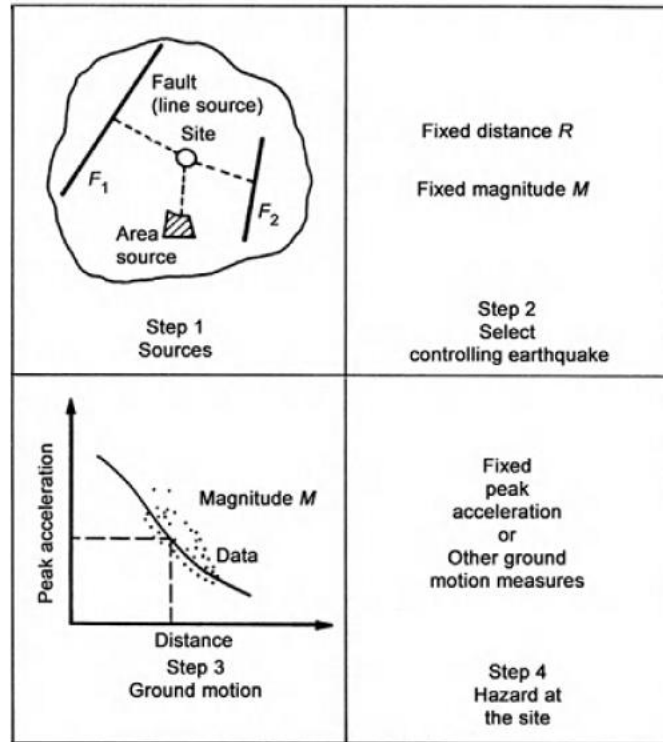


Figure Scenario seismic hazard analysis steps Marmureanu et al 3

within the scope of the study an earthquake scenario was created to predict the damage that may occur as a result of a possible earthquake in the Akada segment located in Malatya province with scenario based modeling using the OPEN UA E simulation program Pagani et al 20 4 The results of the analysis are important in terms of estimating the losses that may occur after a possible earthquake

Malatya province is located in the 1st degree earthquake zone according to the earthquake zones map of Turkey The DAF Eastern Anatolian Fault which has caused past and future earthquakes in and around Malatya extends along the Har Sincik Elifhan G lba and S rg Faults Since the earthquake magnitude one of the uncertainties of the earthquake is assumed to be the worst case scenario the magnitude of the earthquake is assumed to be Mw 7.3 in this study The impact of this earthquake on Ad yaman province was determined by earthquake hazard analysis The Open uake Engine open source software written in the Python programming language software provides calculation and assessment of seismic hazard risk and decision making tools via the data methods and standards that are being developed by GEM Global Earth quake Model and its collaborators Pagani et al 20 4

The scenario analysis of a possible Mw 7.3 earthquake on the Akada segment of the Malatya Fault was defined in the Open uake platform The fault and the possible earthquake epicenter are shown in Figure 7 In the scenario earthquake hazard analysis Chiou and Youngs 20 4 ground motion prediction equation which is generally used for Turkey was used The PGA distribution in Ad yaman province as a result of the earthquake scenario is shown in Figure 7 Figure shows the MMI distribution The expected PGA level in the north of Ad yaman reaches 0.4g As seen in the MMI distribution the MMI reaches 7 in the north of Ad yaman According to the USGS MMI PGA table Chock et al 200 the PGA value corresponding to MMI 7 corresponds to approximately 0.3 g

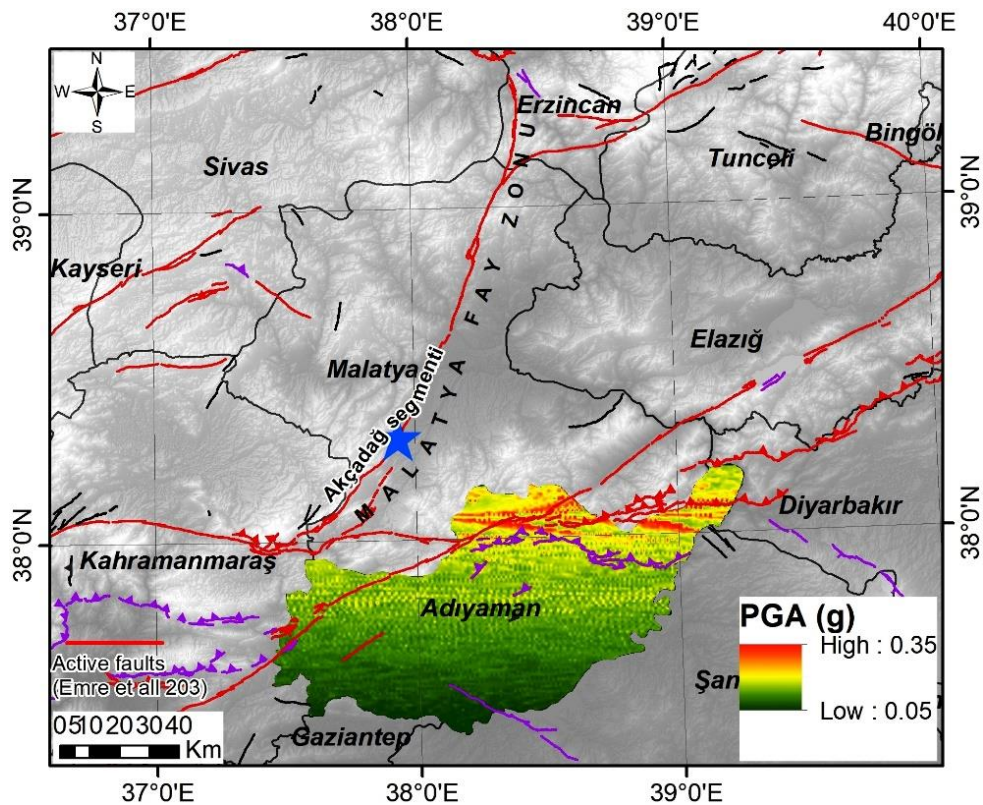


Figure 7 Scenario seismic hazard analysis PGA distribution map

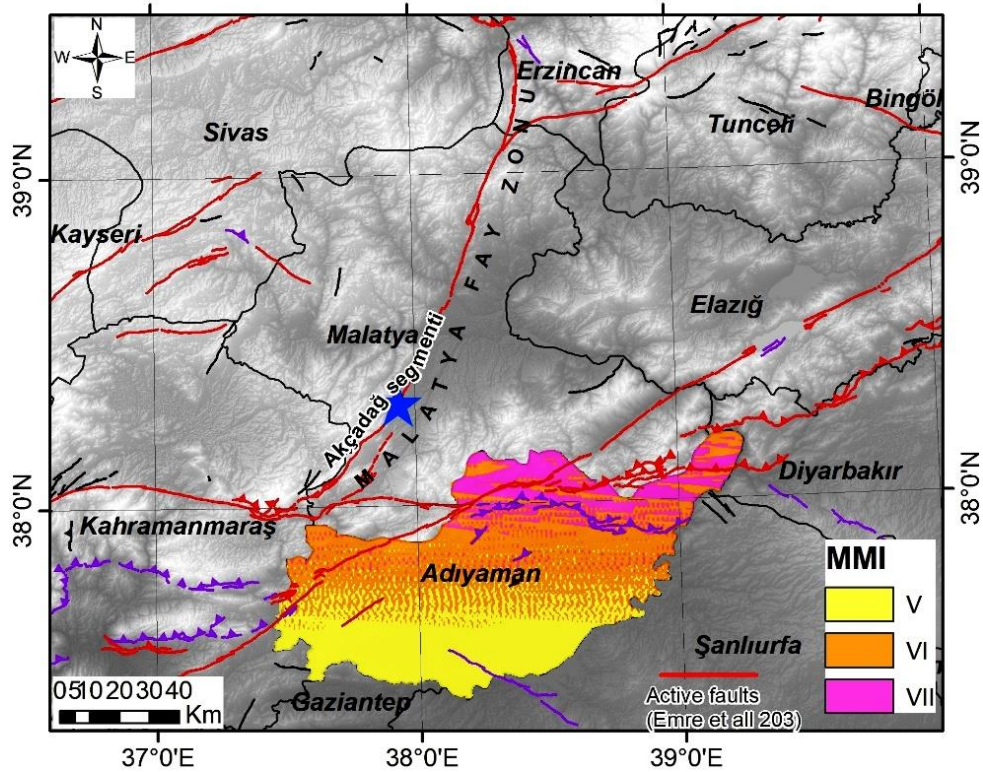


Figure Scenario seismic hazard analysis MMI distribution map

3 clusi

Adiyaman and its surroundings are one of the regions with high earthquake hazard. Therefore, it is important to be aware of the earthquake risk and to take measures to prevent the destructive effects of earthquakes. At the same time, informing

and educating the public about earth quake awareness and disaster management can help minimize post earth quake damages. Especially in construction processes earth quake hazard should be taken into consideration and buildings should be built in accordance with earth quake regulations. Thus the possible effects of earth quakes can be minimized and a safe living space can be created. In the event of a 7.3 magnitude earth quake on the Akada segment, one of the sub segments of the Malatya fault, which is one of the important seismic gaps in the region, it is seen that the earth quake hazard continues throughout the province according to the maximum ground acceleration and intensity distribution analyses for Adyaman. As a result, it is thought that the results obtained from this study will form an important basis for risk assessments to be made in the region.

Author Contributions

The authors carried out joint studies at every stage of the manuscript. All authors have read and agreed to the published version of manuscript.

References

- Chiou B S, Youngs R R. 2004. Update of the Chiou and Youngs NGA model for the average horizontal component of peak ground motion and response spectra. *Earthquake Spectra* 30(3): 7-33.
- Chock G, Robertson I, Nicholson P, Brandes H, Medley E, Okubo P, Holmes. 2000. Compilation of observations of the October 2000 Kiholo Bay Mw 7 and Mahukona Mw 6 earth quakes. *Hawaii Earthquake Engineering Research Institute* 3: 3.
- Emre Duman, Talp S, Elmac H, Olgun and Eroglu. 2003. Active fault map of Turkey.
- Erdik M, Demircioglu M, Sesetyan, Durukal E, Siyahi B. 2004. Earth quake hazard in Marmara region Turkey. *Soil Dynamics and Earthquake Engineering* 24: 0-3.
- Gurba C, Aktar M, Eyidogan H, Cisternas A, Haessler H, Barka A, Ergin M, Turkelli N, Polat O, Ucer B, Uleli S, Baris S, Ayapak B, Bekler T, Tor E, Bicmen F, Toruk A. The seismotectonics of the Marmara region, Turkey: results from a microseismic experiment. *Tectonophysics* 2000 3: 7.
- Marmureanu G, Cioflan C O, Marmureanu A, Ionescu C, Manea E F. 2003. Bridging the Gap Between Nonlinear Seismology as Reality and Earthquake Engineering. *Perspectives on European Earthquake Engineering and Seismology* 2: 40.
- Pagani M, Monelli D, Weatherill G, Danciu L, Crowley H, Silva V, Vigano D. 2004. Openquake engine: An open hazard and risk software for the global earthquake model. *Seismological Research Letters* 3: 2702.
- Sanar T, Abc C, Arabacak V, Aici M, Akyu H S. 2000. Geometry and Paleoseismology of the Malatya Fault, Malatya-Ovacik Fault Zone, Eastern Turkey: Implications for intraplate deformation of the Anatolian Scholle. *Journal of Seismology* 23(3): 340-0007 s 0 00 0.

Level meta analysis as solar air base system fresh water generation as comprehensive thermodynamic assessment

Fatih Ilmaz^{*1}

Abstract One of the important ways to struggle with global warming and environmental challenges is the effective use of renewable energy resources. In this context, solar energy is almost the basis of renewable energy sources. It is also noted that humanity is required clean and drinkable water as well as a clean energy source. That is the clean water scarcity is been in many counties around the world. Therefore, this study examines the design and analysis of a solar and wind powered model for clean electricity and water generation. This work comprises of a solar photovoltaic thermal (PV/T) subsystem, wind turbines, an Organic Rankine cycle with the R32 refrigerant, and a reverse osmosis (RO) desalination unit. The thermodynamic performance investigation is conducted by applying the energy and exergy efficiency methods. Also, to define the system performance change versus some different factors, a parametric study is done. Based on analysis results, total energy generation and fresh water capacity are computed as 34.7 kW and 2.0 kg/s. The energetic and exergetic efficiency of the developed study is determined as 37.0% and 3.7%.

Keywords Energy, exergy, solar, PV/T, thermal, wind

¹**Address** Department of Mechatronics Engineering, Faculty of Technology, Isparta University of Applied Sciences, Isparta, Türkiye

^{*}**Corresponding author** fatiyilma7@gmail.com

1. Introduction

Energy demand is increasing day by day due to many factors such as population growth, industrial development, and industrialization. It is a fact that fossil fuels are still preferred to meet this increasing demand. In this case, as a result of the use of carbon-based fuels, global warming and acid rain, etc., which are expressed as environmental problems arise (Venkatesh et al., 2022). For the future of the globe, these environmental problems must be elaborated and destroyed, and at this point, renewable energy sources are coming to the fore because renewable energies have many advantages; for example, there is no emission and independence from other countries. Among these resources is an plentiful primary energy source that can be used in cost-effective and reliable ways for thermodynamic cycles in solar energy plants, as well as for electrical power generation for heating or cooling purposes (Herrando et al., 2023). Moreover, solar and wind energy can be an appreciated source of sustainable energy with insignificant environmental challenges (Hossain et al., 2022).

Another important aspect is that concerns about worldwide water accessibility and effects have been stated in recent years using the worrying terms "global water crisis" and "water scarcity" (Dhakal et al., 2022). Parallel to global warming, people's access to clean water is getting harder day by day, and water shortages are emerging. For this reason, especially for today and for the future, using renewable energy technologies and meeting needs such as clean water is one of the most fundamental issues that need to be solved. For this motive, numerous academic trainings and projects have been carried out in these fields in the literature in recent years, and active studies are continuing. In 2023, for zero-emission hydrogen generation, Aik and Erle (2023) proposed a solar and wind energy system for electrolysis. They used a proton exchange membrane to generate clean hydrogen. They determined that PEM can generate an average 1.5 cc/min of hydrogen with an efficiency of 7%. Bamisile et al. (2023) illustrate an analysis of the solar-wind-geothermal-assisted multigeneration system for cleaner products. Their proposed system's energetic and exergetic efficiencies are 4% and 3%, respectively. Sherwani (2022) examines the assessment of the solar energy-based ORC refrigeration cycle. For more details, some recent studies are presented here: Hassan et al. (2022), Mousavi et al. (2022), Abu Rayash and Dincer (2023), Ata et al. (2023), and U et al. (2023).

This study deals with the clean and sustainable power and freshwater generation employed by solar and wind energy sources. Also, the thermodynamic performance analysis is conducted with energy and exergetic efficiency methods. Moreover, the system is investigating the efficiency aspects and also the irreversibility rate.

2 S S F O A A A S S

The suggested plant is presented in Figure which is the layout of the developed cycle for power and freshwater generation. The system consists of a series of PV/T collectors for generating both power and heat, a series of wind turbines that generate power, an ORC plant for power, and finally RO technology for freshwater generation.

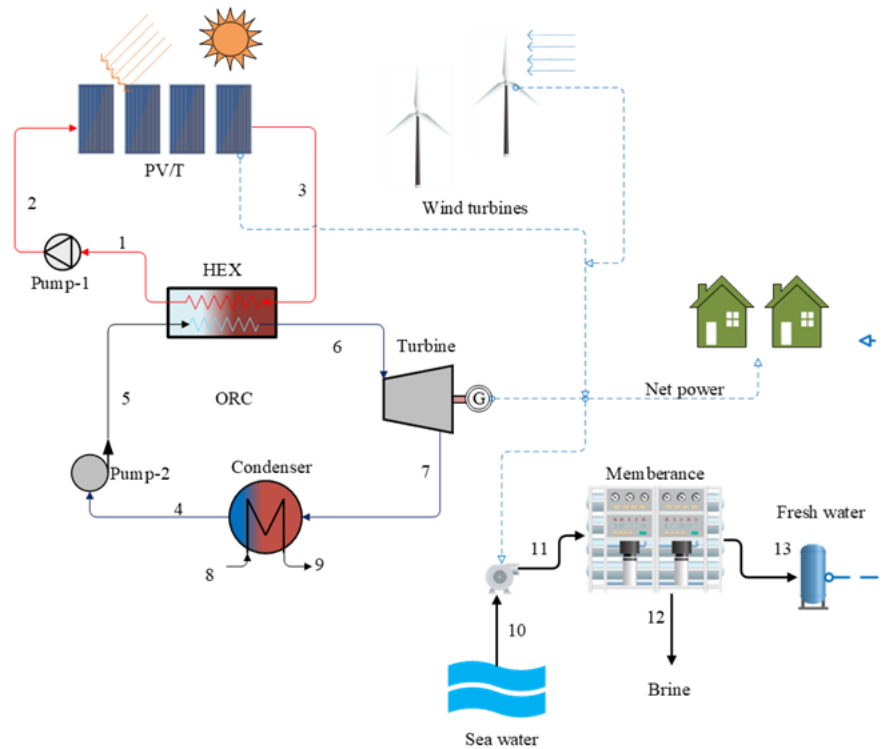


Figure A schematic flow chart of the proposed system

The power is generated by PV/T and ORC units and the freshwater is also produced by the RO unit. The required electrical power of the RO unit is met with the ORC system. Here, a hybrid model for solar and wind has been designed and analyzed. Before performing the thermodynamic analysis, some assumptions made for the system can be listed below:

- The system works in steady state conditions
- Turbines and pumps have isentropic efficiency
- Solar flux is constant 1000 W/m^2
- The working fluid of the ORC is selected R32
- Sea water inlet temperature is assumed $30 \text{ }^\circ\text{C}$
- Dead state temperature and pressure are taken into $25 \text{ }^\circ\text{C}$ and 101.325 kPa

This study has been extensively investigated from a thermodynamic perspective and a series of examines have been carried out. Moreover, the system design and assumed constraints are presented in Table

Table System design and inputs boundaries

Parameters	Unit	Value
PV/T subsystem		
Solar radiation	m ²	00
PV reference temperature	°C	2
Optic efficiency of PVT		0
PV reference temperature coefficient		0.004
Number of PV		20
Wind speed	m/s	3
Working fluid		Therminol 72
ORC		
Working fluid		R32
Pump inlet pressure	kPa	7
Pump pressure ratio		3
Pump inlet temperature	°C	Saturated liquid at P4 pressure
Pinch point temperature	°C	
Turbine isentropic efficiency		
Reverse osmosis		
T _{sea}	°C	30
P _{sea}	kPa	0.32
Sea water inlet mass rate	kg/s	2
Sea water salinity rate	ppm	42000
Brine salinity rate	ppm	70000

For thermodynamic calculations the equilibrium equations mass energy entropy and exergy as below are handled separately and applied to each component Cengel and Boles 2002 Bejan et al 2009 Dincer 2020

$$\sum \dot{m}_{in} = \sum \dot{m}_{out}$$

$$\sum \dot{m}_{in} h_{in} + \sum \dot{Q}_{in} + \sum \dot{W}_{in} = \sum \dot{m}_{out} h_{out} + \sum \dot{Q}_{out} + \sum \dot{W}_{out} \tag{2}$$

$$\sum \dot{m}_{in} s_{in} + \sum \left(\frac{\dot{Q}}{T} \right) + \dot{S}_{gen} = \sum \dot{m}_{out} s_{out} \tag{3}$$

$$\sum \dot{m}_{in} ex_{in} + \dot{E}x_{in}^{\dot{Q}} + \dot{E}x_{in}^{\dot{W}} = \sum \dot{m}_{out} ex_{out} + \dot{E}x_{out}^{\dot{Q}} + \dot{E}x_{out}^{\dot{W}} + \dot{E}x_D \tag{4}$$

In these equations the sub terms of in and out describe the inlet and outlet flow of the state Also ṁ is mass flow rate Q̇ is heat transfer rate and Ẇ is work rate After that ex is define the specific exergy flow The generated power from the solar and wind turbine can be formulated as

$$\dot{W}_{PVT} = G \times A_{PVT} \times \eta_{PVT} \times n_{PVT}$$

where G is the solar flux rate A_{PVT} is the area of PVT unit η_{PVT} is the efficiency of the PTV and n_{PVT} is the number PVT units

$$\dot{W}_{wt} = 1/2 \times \rho_{air} \times C_p \times n_{wt} \times A \times V^3$$

here C_p is the Betz limit n_{wt} is the number of wind turbines A is the swept area and V is the wind speed To sum up the energetic and exergetic efficiency of the total plant can be modeled as

$$\eta_{total} = \frac{\dot{W}_{net} + \dot{m}_{fw} h_{fw}}{\dot{Q}_{solar} + \dot{W}_{wt,ava}} \tag{7}$$

$$\psi_{total} = \frac{\dot{W}_{net} + \dot{m}_{fw} ex_{fw}}{\dot{E}x_{Q,solar} - \dot{W}_{wt,ava}}$$

3 S S A S S S O

With the above declared in Table assumptions and system parameters the thermodynamic analysis is conducted and the main findings are offered in Table 2. The power production rate of the PV T and wind turbine are 037 k and 3 k respectively. Also the freshwater production rate is determined as 2.0 kg/s. As finally the total energetic and exergetic efficiency of the developed schema is 37.0% and 3.7% respectively.

Table 2 Analysis results of the developed plant

Parameters	Unit	Value
PVT power rate	k	037
PVT thermal energy rate	k	3
Wind turbine power rate	k	3
Net power rate	k	34.7
Freshwater generation rate	kg/s	2.0
Efficiencies		
η_{ORC}		23.44
Ψ_{ORC}		37
$\eta_{overall}$		37.0
$\Psi_{overall}$		3.7

After the main results parametric analysis was performed to examine the effects of system parameters. Figure 2 and Figure 3 examine the variation of net power generation and thermal losses in a PV T system versus solar radiation value. According to Figure 2 a rise of 200 W/m² in solar radiation increases the net electricity production from 338 kW to 344 kW. However, it is seen in Figure 3 that the losses in the PV T system increase in response to this increase.

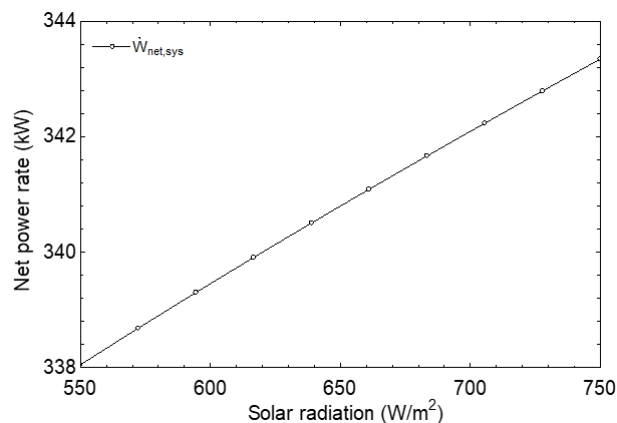


Figure 2 The effect of solar flux on net power production rate

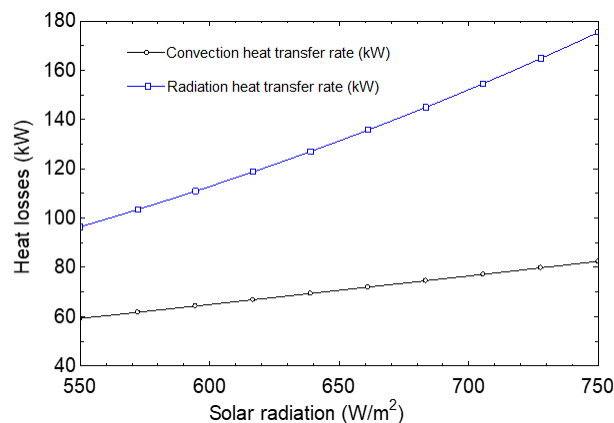


Figure 3 Impact of solar flux on the heat losses

The increase in work and thermal energy from the PV T module relative to the increase in solar radiation is presented in Figure 4. The increase in radiation increases the useful products obtained from the PV T module. Then the negative effect of the increase in solar irradiance on the performance of the whole system is seen in Figure 5. Both the energy and exergy performance of the whole system increases negatively as a result of the losses in the PV T. The reason for this efficiency drop can be expressed as the thermal losses pictured above (Figure 3).

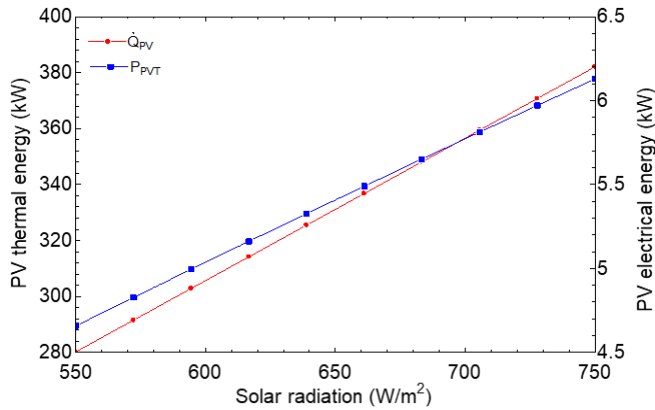


Figure Effect of the solar radiation on the PV T thermal and power rate

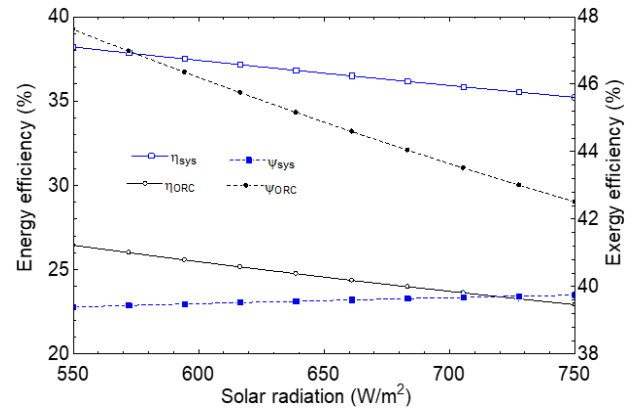


Figure Influence of solar flux on the developed system s performance

Another important parameter is wind speed variation Figure shows the goes up in the net power and wind turbine capacity produced by the increase in wind speed from 2 m s to 2 m s Parallel to this increase Figure 7 shows a linear increase in the designed system performance with increasing wind speed Up to a certain speed limit the increase in wind speed rises the net work obtained from the model and also the system s performance

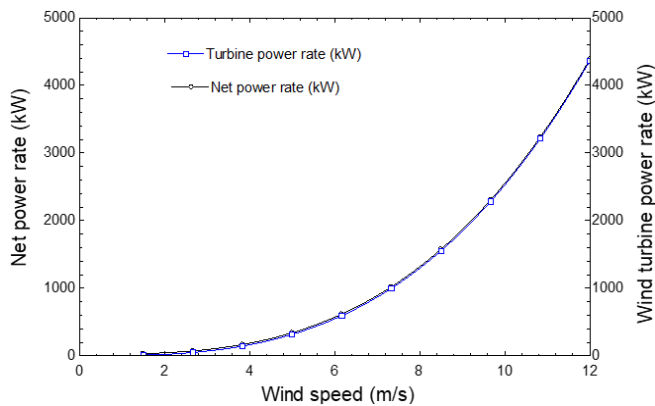


Figure Variations of net power and wind turbine power rate vs wind speed

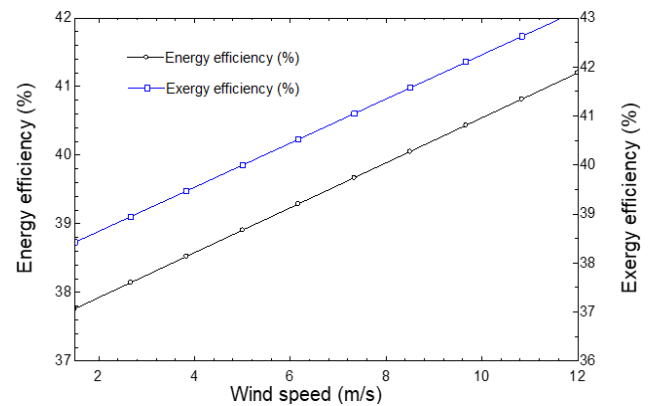


Figure Variations of the system s performance vs wind speed

Figure examines the impact of the H pinch point temperature on the developed system s efficiency hen the H pinch point temperature increases from 2 °C to 22 °C the developed system s performance that is energy and exergy efficiencies are decreases It is noted that the high difference the temperature of pinch point is means of increasing the irreversibility rate of H and then decreasing the plant s performance

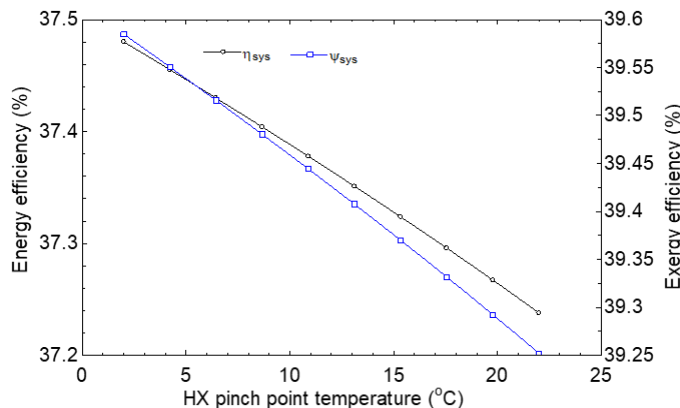


Figure Variations of the developed system s performance with H pinch point temperature

O S O

In this developed study a solar and wind energy supported a hybrid model is designed and proposed for production of clean power and potable water. This system entails of a solar PV/T unit, an ORC, wind turbines and RO unit. Comprehensive thermodynamic performance analysis is also conducted to determine the system's performance in light of the energy and exergy efficiency methods. Moreover, the exergy destroyed analysis performed to define the system irreversibility. According to analyses results, the main conclusions can be drawn as below:

- The generated power and fresh water rate are determined as 34.7 kW and 2.0 kg/s respectively.
- The power and thermal energy generation capacities of the PV/T system are 0.37 kW and 3 kW respectively.
- Energy and exergy efficiencies are computed as 23.44% and 37% for the ORC subsystem.
- Energy and exergy efficiency of the total system are to be 37.0% and 3.7% respectively.

F

Abu Rayash A, Dincer I. 2023. Development and assessment of an integrated wind-solar based energy system for sustainable communities. *Energy Conversion and Management* 277: 1-10.

Ata S, Se Tutumlu H, Al Ho A. 2023. High power cycle is the best fit for parabolic trough solar collectors: A comparative and comprehensive case study for six sub-configurations of the three main cycles. *Energy Conversion and Management* 291: 1-13.

Bamisile O, Cai D, Adedeji M, Dagbasi M, Li H, Huang H. 2023. Thermo-environmental exergoeconomic analysis and multi-objective optimization of a novel geothermal solar-wind micro-multi-energy system for cleaner energy production. *Process Safety and Environmental Protection* 170: 1-7.

Bejan A, George T, Moran M. Thermal design and optimization. Wiley.

Cengel A, Boles MA. Thermodynamics: an engineering approach. 4th ed. Mc New York: McGraw-Hill; 2002.

Dhakal N, Salinas Rodriguez S, G Hamdani, Abushaban A, Sawalha H, Schippers C, Kennedy M. D. 2022.

Is desalination a solution to freshwater scarcity in developing countries. *Membranes* 12(4): 3.

Dincer I. Thermodynamics: A Smart Approach. USA: John Wiley & Sons Ltd; 2020.

Hassan A, A Elwardany A, E Ookawara S, Sekiguchi H, Hassan H. 2022. Energy-exergy-economic and environmental 4E assessment of hybrid solar system powering adsorption parallel-series ORC multigeneration system. *Process Safety and Environmental Protection* 164: 1-7.

Herrando M, Yang H, Huang G, Otanicar T, Mousa O, B Agathokleous R, A Markides C, N. 2023. A review of solar hybrid photovoltaic thermal (PV/T) collectors and systems. *Progress in Energy and Combustion Science* 97: 10072.

Hossain F, Arim M, R Bhuiyan A, A. 2022. A review on recent advancements of the usage of nano fluid in hybrid photovoltaic thermal (PV/T) solar systems. *Renewable Energy* 188: 1-4.

Mousavi S, A Mehrpooya M, Delpisheh M. 2022. Development and life cycle assessment of a novel solar-based cogeneration configuration comprised of diffusion-absorption refrigeration and organic Rankine cycle in remote areas. *Process Safety and Environmental Protection* 159: 10003.

Sherwani A, F. 2022. Analysis of solar energy driven organic Rankine cycle vapor compression refrigeration system. *Thermal Science and Engineering Progress* 35: 100477.

Venkatesh T, Manikandan S, Selvam C, Harish S. 2022. Performance enhancement of hybrid solar PV/T system with graphene-based nanofluids. *International Communications in Heat and Mass Transfer* 130: 1074.



Wu, Li, Riang, Sang, Li. 2023. Quantitative sustainability assessment and sensitivity analysis for a solar driven combined heating and power system integrated with organic Rankine cycle and ground source heat pump. *Applied Thermal Engineering* 220: 722.

Maik, S. 2023. Solar and wind energy in Poland as power sources for electrolysis process. A review of studies and experimental methodology. *International Journal of Hydrogen Energy* 48(3): 2-3.

Classification of Mechanical Faults in Electric Motors based on Power Spectral Density Vibrational Analysis

Umut Akar^{1*}

Abstract Unplanned shutdowns caused by mechanical and electrical failures of electric motors are among the most significant and preventable losses in manufacturing facilities. In the past few decades, the subject of preventive and predictive maintenance has attracted the intense interest of many researchers. Several studies have demonstrated that vibration, sound, temperature, and some electrical quantities of electric motors contain information about the current and potential faults. Extracting the best distinguishing feature by various methods is one of the significant issues in the field. This study focuses on the vibration signals corresponding to healthy operation and five distinct fault conditions in electric motors, like imbalance, misalignments, and bearing malfunctions. The effectiveness of measurements taken from 3-axis accelerometers placed in two different positions has been examined to classify these six cases. The power spectral densities of the vibration signals have been extracted to input for commonly employed machine learning algorithms. The performances of the machine learning methods have been presented comparatively. According to the results, one vibration signal recorded from the radial axis is adequate to distinguish the suspected mechanical faults with accuracies over

Keywords Electric motor classification, machine learning, power spectral density, predictive maintenance, vibration

Address Selcuk University, Faculty of Technology, 41080, Sivasli, Turkey
Corresponding Author akar@selcuk.edu.tr

1. INTRODUCTION

Electric motors are among the most crucial components of today's industry. Owing to converting electrical energy into mechanical energy, places electric motors at the heart of mobility in industry and at the core of mass production. An average of 70% of the energy consumption of electrical motors in production plants indicates their pivotal role. Saidur (2010). Given their critical position, preventing failures in electric motors is one of the primary challenges in the industry. Companies must define their most suitable maintenance strategy for this purpose. In the literature, maintenance activities are categorized into three main titles: corrective, preventive, and predictive maintenance.

Corrective maintenance refers to repairing or replacing faulty equipment after a failure has occurred. This approach can be preferred when the repair or replacement is quickly completable, the failure does not significantly impact overall system operations, and the time required to address the malfunction isn't overly lengthy.

In contrast, preventive maintenance represents actions taken to prevent or delay a failure. It's crucial that breakdowns do not coincide with critical periods, especially when production is intensive. Based on the statistically determined usable life of the equipment, maintenance or replacement should be conducted before any failure occurs. However, the excess personnel in facilities, spare parts inventory, and early replacement or maintenance makes the approach inefficient.

Lastly, predictive maintenance enables personalized maintenance for equipment by continuously or periodically monitoring them using various sensors. It provides detection before a failure occurs or reaches a critical level and offers insights into the progression of the malfunction. When compared to preventive maintenance, many studies have highlighted the superiority of predictive maintenance because it does not require keeping excess personnel and spare parts on standby and prevents overly premature action taking. Popescu et al. (2022), Ran et al. (2020), Vafaei et al. (2020). Selcuk (2017) has illustrated the preeminence of predictive maintenance over preventive maintenance using a critical example. Selcuk (2017) She attracts attention to the failure time of previously tested identical bearings spanning a wide range from 100 to 300 hours. As can be inferred from the example, a maintenance activity planned based on an average lifespan calculated statistically will not prevent failures for all bearings. When considering the shortest endurance time, maintenance would have to be performed much earlier than the lifespan for some.

For predictive maintenance activities of electric motors, two distinct approaches emerge: current-based and vibration-based. While current-based methods stand out for not requiring direct mounting on the electric motor and being

facilitated by inexpensive current sensors vibration based ones offer early diagnosis opportunities especially for vibrations caused by mechanical failures The techniques used in both methods are very analogous and with the base of time frequency transformation

The frequency content of the recorded signals is extracted using spectral methods such as Fast Fourier Transform FFT Borghesani et al 2013 Short Time Fourier Transform STFT Wu 2014 wavelet based methods Al Badour et al 2015 autoregressive moving average ARMA Chukwueke et al 2016 and Power Spectral Density PSD Li et al 2022

The extracted frequency information is provided to classifiers directly or through additional feature extraction approaches As the first step of predictive maintenance failure classification is realized at the stage of the classifier output Later on predicting the progression of the malfunction and preparing a maintenance plan based on the progression and system priorities culminate the whole process

In this study the focus has been on the classification of failures which is the initial phase of predictive maintenance Section 2 explains the data and method used for the mentioned purpose The results are discussed comparatively in Section 3 Finally Section 4 concludes the study

2 DATA ANALYSIS

Fault types in electrical machines are fundamentally divided into mechanical and electrical Principal electrical faults include short circuits open circuits and ground faults in windings Additionally rotor bars can experience wear cracks and breaks On the other hand wear and deformations in bearings misalignments and eccentricity are common mechanical faults

An electrical machine fault dataset Riberio 2019 containing data for one healthy and five different mechanical fault classes is subjected in this paper The dataset includes vibration signals obtained by two three axis accelerometers for the faults of horizontal misalignment vertical misalignment bearing malfunctions for two locations imbalance errors and a normally operating case Marins et al 2020 Healthy working data class involves vibration signals for 4 speeds between 737 rpm and 3000 rpm The vibration data for 44 revolutions create 333 imbalance data classes for imbalance states originating with seven independent weights ranging from 0.3 g to 3 g The number of data for horizontal and vertical misalignments created by sliding the motor shaft is respectively 7 and 30 Data for bearing faults are recorded in two different classes based on the position where the faulty bearing is placed Vibration signals for bearing faults are recorded with consciously created imbalances to make them practically detectable There are 100 data for the underhang position where the bearing is between the motor and the rotor and 100 data for the overhang position where the rotor is in the middle A visual of the experimental setup is shown in Figure 1

The six vibration signals recorded axially radially and tangentially for two positions were evaluated separately Each vibration signal sampled at a 1000 Hz sampling rate and recorded as 1 second was divided into 1000 second sections Each of these one second vibration signals has been considered a separate signal thus increasing the dataset size fivefold The number of data for each class in the reorganized dataset is given in Table 1

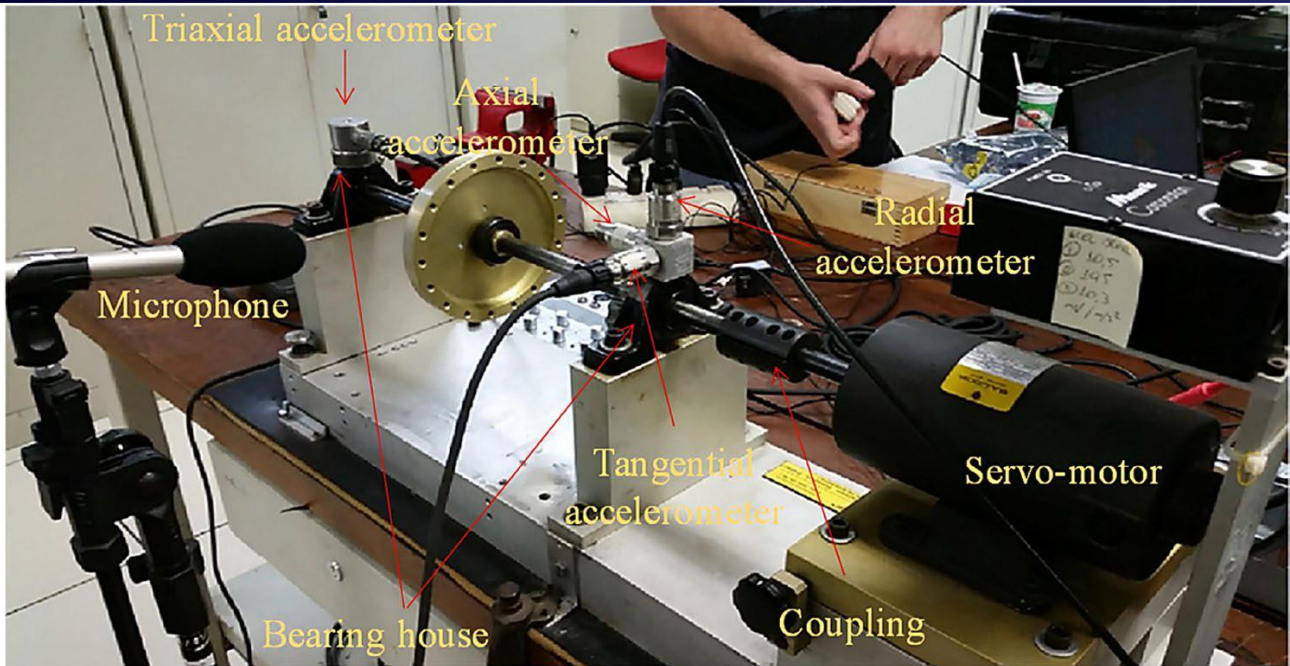


Figure Spectra uest Experimental Testbench System Marins et al 20

Table Amount of data per each class

lass	umber	ata
Hori ontal misalignment	7x	
Imbalance	333x	
Normal	4 x	24
Overhang	3x	2
Underhang	x	27 0
Vertical misalignment	30 x	0
tal	7	

2.1 Power Spectral Density (PSD)

The power spectral density (PSD) is a mathematical measure that depicts how the power of a signal is distributed across the frequency spectrum. It is widely used in analyzing the vibration characteristics of systems (in et al 2023, noise analysis Nielsen et al 2023, optical applications Dwik et al 2023) and many other applications (Massara et al 2023, Mitishita et al 2023).

Estimation methods for power spectral density are divided into two categories such as parametric and non-parametric approaches. Parametric approaches like AR, MA, and ARMA assume that it is possible to model the system with a certain number of parameters. Estimating PSD becomes more challenging as the data size increases, and the accuracy of the estimation is proportional to the accuracy of the parametric model formed. On the other hand, non-parametric approaches like the periodogram provide a more general estimate with their flexible structures. As there's no need for any parametric model, non-parametric techniques are often preferred for systems that are difficult to model. Because it is difficult to model the electric motors linearly, the PSD was estimated using the Welch method, one of the non-parametric approaches. The Welch approach can essentially be summarized in 3 stages: Firstly, the signal is divided into K segments of length M with a certain overlap ratio, and these segments are multiplied by a window function $w(n)$. Given a window impulse response of R , the weighted segments $x_m(n)$ are calculated as shown in Equation

$$x_m(n) \cong w(n)x(n + mR), n = 0,1,2, \dots, M - 1, m = 0,1,2, \dots, K - 1$$

Subsequently, the periodogram is calculated using the square of the absolute value of the N length Fourier transform of these segments. The periodograms for each segment are computed as shown in Equation 2.

LD has no correct classification for class 3 the normally operating state possibly because of the lower amount of class data NN is the best one considering the accuracy but it requires a very long training time compared to others

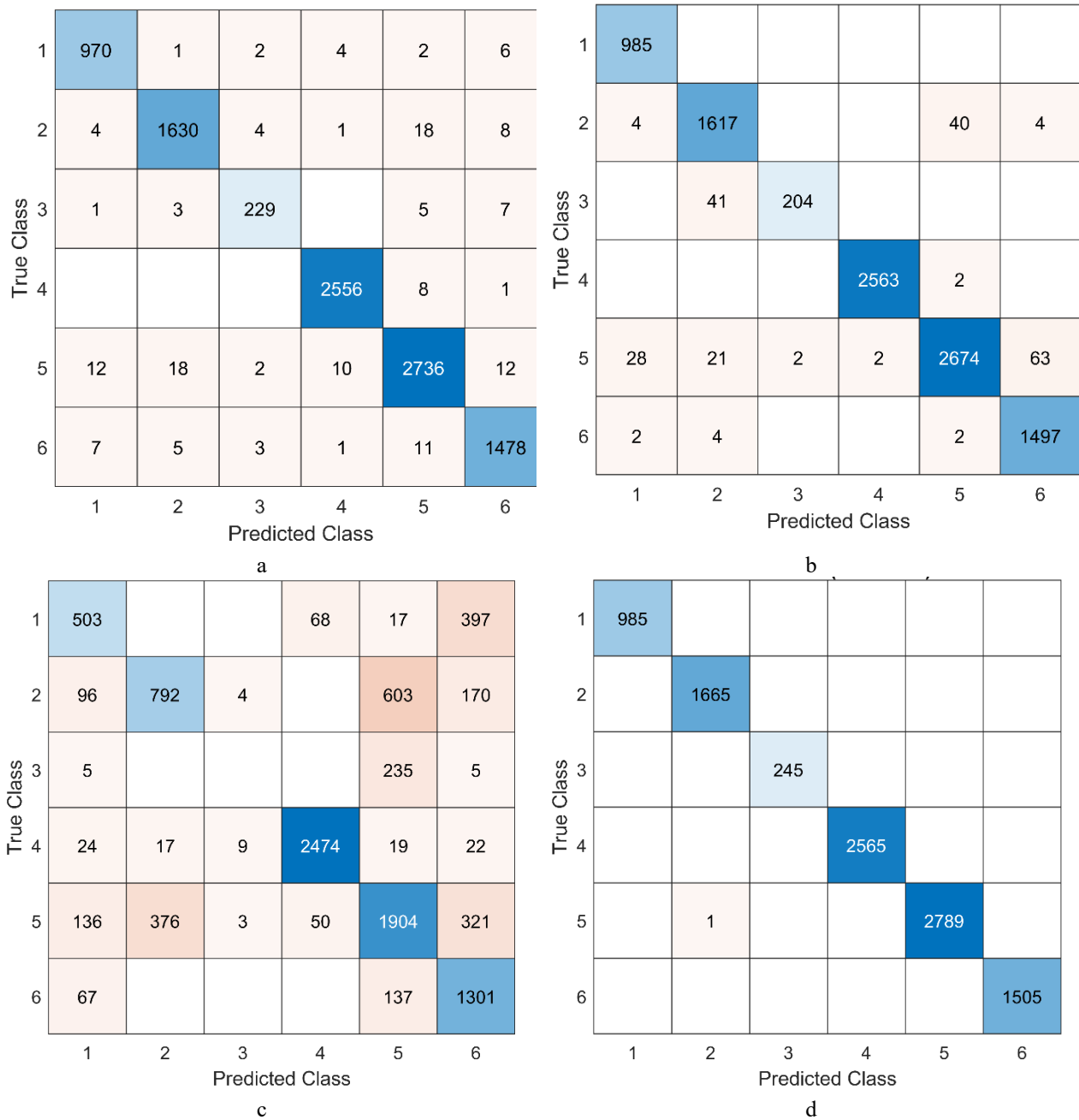


Figure 2 The confusion matrices obtained by using a DT b SVM c LD and d NN with the radial measurements

O S O S

Fault classification in electric motors one of the most critical equipment of today's industry is the subject of this study. Healthy operation and a total of five malfunctions like imbalance misalignments and bearing failures have been studied. It has been investigated which of the six vibration data obtained from the accelerometers in two different positions from the axial radial and tangential directions is more successful in classifying the faults. The PSD of the vibration signals has been extracted by the Welch method. It has been seen that the data recorded only on the radial axis from the underhang position is sufficient alone to classify the faults. The performances of the popular machine learning methods have been compared in terms of accuracy and learning time with the input of PSD on radial axis data. It is concluded that the DT method is the most successful when the learning time and accuracy are considered. In applications where longer learning time is not a problem the performance of the NN method which correctly classifies almost all failures is quite remarkable.

ethics committee Approval Kurul O ayı
N A

peer review Ara e erle irmesi
Externally peer reviewed

lict terest
The author has no conflicts of interest to declare

Fu i
The author declared that this study has received no financial support

F S

- Al Badour F Sunar M Cheded L 20 Vibration analysis of rotating machinery using time frequency analysis and wavelet techniques *Mechanical Systems and Signal Processing* 25 20 3 2 0
- Borghesani P Pennacchi P Randall R Sawalhi N Ricci R 20 3 Application of cepstrum prewhitening for the diagnosis of bearing faults under variable speed conditions *Mechanical Systems and Signal Processing* 36 2 370 3 4
- Chukwuekwe D O Glesnes T Sch lberg P 20 Condition Monitoring for Predictive Maintenance Towards Systems Prognosis within the Industrial Internet of Things
- Dwik S Sasikala G Natara an S 2023 Design and Simulation of a Reconfigurable Multifunctional Optical Sensor *Optical Memory and Neural Networks* 32 2 47 7
- in ang He an u L ei C in G 2023 Improving vibration performance of electric vehicles based on in wheel motor active suspension system via robust finite frequency control *IEEE Transactions on Intelligent Transportation Systems* 24 2 3 43
- Marins M A Ribeiro F M Netto S L Da Silva E A 20 Improved similarity based modeling for the classification of rotating machine failures *Journal of the Franklin Institute* 355 4 3 30
- Massara E Villaescusa Navarro F Hahn C Abidi M M Eickenberg M Ho S Lemos P Di gah A M R galdo Saint Blancard B 2023 Cosmological information in the marked power spectrum of the galaxy field *The Astrophysical Journal* 951 70
- Mitshita R S Elfring G Frigaard I A 2023 Statistics and spectral analysis of turbulent duct flows with flexible and rigid polymer solutions *Journal of Non-Newtonian Fluid Mechanics* 311 04 2
- Nielsen Christensen M G Boldt B 2023 An Analysis of Traditional Noise Power Spectral Density Estimators based on the Gaussian Stochastic Volatility Model *IEEE/ACM Transactions on Audio, Speech, and Language Processing*
- Popescu T D Aiordachioaie D Culea Florescu A 2022 Basic tools for vibration analysis with applications to predictive maintenance of rotating machines an overview *The International Journal of Advanced Manufacturing Technology* 7
- Ran hou Lin P en Deng R 20 A survey of predictive maintenance Systems purposes and approaches ar iv 20 *arXiv preprint arXiv:1912.07383*
- Riberio F M L 20 *MAFAULDA - Machinery Fault Database.*
<http://www02.smt.ufr.br/offshore/mfs/page0.html>
- Saidur R 20 0 A review on electrical motors energy use and energy savings *Renewable and sustainable energy reviews* 14 3 77
- Selcuk S 20 7 Predictive maintenance its implementation and latest trends *Proceedings of the Institution of Mechanical Engineers, Part B: Journal of Engineering Manufacture* 231 70 7
- Vafaei N Ribeiro R A Camarinha Matos L M 20 Fu y early warning systems for condition based maintenance *Computers & Industrial Engineering* 128 73 74
- i C ang H hou Hu hou P Lin 2022 An Adaptive Harmonic Product Spectrum for Rotating Machinery Fault Diagnosis *IEEE Transactions on Instrumentation and Measurement* 72 2



u G 20 A concentrated time frequency analysis tool for bearing fault diagnosis *IEEE Transactions on Instrumentation and Measurement* 69 2 37 3

Development of Sustainable and Innovative Approach to Develop Food Packaging Materials Using Green Synthesized Carbon Dots Derived from Pumpkin Waste

Cemhan Dogan^{1*}, Yobu Edu Tr

Abstract Food packaging plays a critical role in preserving the quality and safety of food products. However, the widespread use of synthetic packaging materials has raised concerns about their environmental impact. In this study, we propose a sustainable and innovative approach to develop food packaging materials using green synthesized carbon dots derived from pumpkin waste. The synthesis of carbon dots was carried out using a hydrothermal reactor, which provided an eco-friendly and cost-effective method. Pumpkin waste, a readily available agricultural byproduct, was utilized as the carbon source for the synthesis. To integrate the carbon dots into food packaging materials, sodium alginate, a natural biopolymer derived from seaweed, was used as the film-forming matrix. The incorporation of carbon dots into the sodium alginate film resulted in the development of multifunctional packaging materials with enhanced properties. The synthesized carbon dot-integrated sodium alginate films were evaluated for their antioxidant and antimicrobial activities. The films demonstrated significant antioxidant potential, as determined by their ability to scavenge free radicals using DPPH (2,2-diphenylpicrylhydrazyl) assays. The presence of carbon dots in the films contributed to their antioxidant activity, which can help mitigate oxidative degradation of packaged food products. Furthermore, the carbon dot-integrated films exhibited remarkable antimicrobial properties against two common foodborne pathogens, *E. coli* and *S. aureus*. The films effectively inhibited the growth of these bacteria, indicating their potential for extending the shelf life of perishable food items and reducing the risk of foodborne illnesses. The utilization of pumpkin waste for green synthesis and the integration of carbon dots into sodium alginate films present a sustainable and eco-friendly approach to food packaging. The multifunctional properties of the resulting films, including antioxidant and antimicrobial activities, offer promising avenues for enhancing the quality and safety of packaged food products. This study highlights the potential of green synthesized carbon dots derived from pumpkin waste as a valuable resource for the development of sustainable food packaging materials, contributing to the reduction of environmental impact in the food industry.

Keywords: green synthesis, carbon dots, pumpkin waste, food packaging, antioxidant activity, antimicrobial activity

¹Address: Boga University, Boga liyan Vocational School, Department of Food Technology, Boga liyan, Montenegro

*Corresponding author: cemhan.dogan@yobu.edu.tr

1. INTRODUCTION

The surge in demand for processed and packaged foods is experiencing an unprecedented rise due to the swiftly evolving global human lifestyle. In response, the food industry is tirelessly working to satisfy the growing consumer appetite for food that is both secure and conveniently accessible. The current market is inundated with an array of processed food options, spanning from minimally processed items to fully heated products. While significant strides have been made in the preservation and packaging of pre-cooked and heated foods, the preservation methods for minimally processed foods, such as fresh fruits and thinly sliced raw meat, still face significant challenges. Notably, among these items, minimally processed meat products stand out as a staple, prone to rapid deterioration throughout storage and distribution, necessitating specialized preservation techniques and packaging solutions (Asgher et al., 2020).

Carbon dots (CDs), a novel addition to the realm of carbon nanomaterials, exhibit exceptional chemical and photochemical stability. Distinctively resembling semiconductor quantum dots (QDs), CDs have garnered attention as a promising contender within the domain of carbon nanomaterials. The allure of CDs emanates from their robust attributes, including remarkable fluorescence, strong photoluminescence (PL), hydrophilicity, favorable biocompatibility, and minimal toxicity. These qualities substantiate their potency, particularly in the sphere of biological applications, positioning them as a viable substitute for conventional QDs, often with comparable or superior

performance Li vd 202 Recent years have witnessed CDs unleash their substantial potential across an array of domains These encompass photocatalysis solar energy harnessing light emitting diodes antibacterial and antioxidant activities chemical sensing as well as bioimaging Remarkably CDs have ventured into the realm of sustainable food packaging polymers where they serve as environmentally sound secure and non toxic fillers hen integrated into packaging materials CDs confer noteworthy antioxidant and antimicrobial attributes thereby augmenting the longevity of packaged foods Moreover research has documented the synthesis of CDs from sustainable sources expressly for application in food packaging E ati vd 2022 Furthermore CDs eclipse alternative functional additives in the realm of food packaging Notably derived from agricultural byproducts they offer economic advantages over chemically synthesi ed nanomaterials like metal oxides which fre uently find employment in food packaging contexts Adding to their appeal CDs owing to their natural origins boast high levels of biocompatibility and a lack of toxicity attributes that often pose significant concerns with artificially manufactured nanomaterials Moradi vd 2023

Pumpkin waste an abundant byproduct of food processing and consumption has garnered increasing attention as a valuable and sustainable resource in various applications The efficient utili ation of pumpkin waste presents a multifaceted solution addressing both environmental concerns and the uest for novel bioresources Typically arising from pumpkin carving culinary preparation and industrial processing this waste stream encompasses peels seeds and fibrous matter In recent years researchers have explored innovative avenues to harness the untapped potential of pumpkin waste transforming it into a resource rich matrix for applications such as biofuel production value added food products natural pigments and bioactive compounds By converting this underutili ed waste into functional materials an opportunity arises not only to mitigate environmental burdens but also to tap into a source of bioactive compounds that could contribute to various industries aligning with the principles of a circular economy Norfe ah vd 20 The utili ation of pumpkin waste as a precursor for the synthesis of CDs holds substantial promise in the realm of nanotechnology and materials science Pumpkin waste an abundant agricultural byproduct offers a sustainable and environmentally friendly source for the production of CDs These CDs characteri ed by their intriguing optical and chemical properties have emerged as a novel class of nanomaterials with a wide range of applications The inherent carbon rich composition of pumpkin waste can provides a foundation for the creation of CDs through cost effective and eco friendly synthesis routes These CDs can exhibit exceptional fluorescence biocompatibility and low toxicity making them suitable candidates for food packaging By tapping into pumpkin waste as a resource for CD synthesis researchers not only address waste management challenges but also contribute to the development of innovative sustainable materials with diverse technological implications

The primary aim of this study was to explore the potential of integrating carbon dots CDs into food packaging materials by employing sodium alginate a natural biopolymer derived from seaweed as the film forming matrix The ob ective was to create multifunctional packaging materials with improved properties by incorporating CDs into the sodium alginate films The synthesi ed CD integrated sodium alginate films were sub ected to evaluation for their antioxidant and antimicrobial activities The investigation sought to assess the films ability to scavenge free radicals using DPPH 2 2 diphenyl picrylhydra yl and ABTS 2 2 a ino bis 3 ethylben othia oline sulfonic acid assays indicative of their antioxidant potential Additionally the study aimed to determine the antimicrobial efficacy of the CD integrated films against E coli and S aureus common foodborne pathogens Through this approach the study aimed to contribute to the creation of sustainable and environmentally friendly food packaging solutions offering enhanced preservation and safety of packaged food products while minimi ng the environmental impact of the food industry

2 A A A HO

2 1 aterial

Pumpkins were sourced from local farmers in Bo a l yan o gat Turkey The strains of Escherichia coli ATCC 3 2 and Staphylococcus aureus ATCC 2 2 3 were ac uired from the culture collection at Boga liyan Vocational High School Turkey Pathogenic microorganisms were consistently stored at 4 C and sub ected to periodic subculturing The chemicals and microbial media utili ed for the analyses were procured from Merck Sigma Aldrich Darmstadt Germany unless otherwise specified

2 1 s sy thesis

Pumpkin waste based CDs was synthesi ed method following the hydrothermal procedure outlined by E ati vd 2022 For this purpose 20 g of pumpkin waste was mixed with 0 mL of distilled water and the mixture was placed in a Teflon lined stainless steel reactor 2 0 mL The reactor was kept in an oven at 200 C for hours After removal from the oven the reactor was allowed to cool down to 2 C followed by centrifugation at 0 000 rpm for 20 minutes The collected supernatant was filtered through a micro membrane filter with a pore si e of 0 22 m hatman

International Ltd Maidstone England The filtrate was subsequently lyophilized to obtain a powdered form The obtained CDs were stored at 4 °C until their use in film production

2.2 Film production

Film solutions were prepared by mechanically stirring sodium alginate (0.1 g/L) film solution and glycerol (0.1 g/L) in a water bath (~30 °C) at a speed of 100 rpm for 2 hours to dissolve them in 30 mL of water Different concentrations of CDs (SA CDs (0.1 g/L), SA CDs (0.2 g/L) and SA CDs (0.4 g/L) film solution) were added to the solution along with CaCl₂ (0.1 g/L) to reinforce the films After an additional 10 minutes of mixing at 30 °C the total solution volume was adjusted to 400 mL using distilled water To remove air bubbles the solutions were centrifuged at 100 G for 3 minutes and then poured onto plexiglass plates (200 mm x 200 mm) The films were separated from the mold after approximately 24 hours of drying at 30 ± 2 °C in an oven and used for analyses

2.3 Antioxidant activity

The assessment of antioxidant activity (AA) was conducted employing the 2,2-diphenyl-1-picrylhydrazyl (DPPH) method, a widely recognized approach for gauging antioxidant potential In this experimental phase, a precise combination of 0.1 mL of the extracted substance and 3 mL of a methanolic DPPH solution (at a concentration of 2 mg/L) was meticulously prepared The resulting mixture was allowed to incubate undisturbed in a darkened environment at room temperature for a duration of 30 minutes Following the incubation period, the absorbance of the concoction was meticulously gauged at a wavelength of 517 nm The quantification of antioxidant activity was subsequently conducted using the computational formula outlined below (Bajraktari et al., 2020)

$$AADPPH = \frac{\text{Absorbance control} - \text{Absorbance sample}}{\text{Absorbance control}} \times 100$$

2.4 Antimicrobial activity

The antimicrobial activities of the samples were assessed against the foodborne pathogens Gram-negative bacteria *E. coli* and Gram-positive bacteria *S. aureus* Initially, pathogen stock cultures were regenerated For this purpose, cultures were inoculated into 10 mL of Mueller Hinton Broth (MHB) and incubated at 37 °C overnight After incubation, the cultures were diluted using optical density (OD₆₀₀) measurements until reaching a concentration of 10⁶ CFU/mL The antimicrobial activity was determined using the disk diffusion method as follows

A volume of 0.1 mL of the diluted bacterial cell suspension was inoculated into Mueller Hinton Agar (MHA) and the agar surface was inoculated in a spreading method by rotating the sterile loop in a clockwise direction for three complete turns with small intervals The inoculated medium was left for 15 minutes to allow liquid absorption and subsequently sterilized via UV exposure films with a diameter of 6 mm were placed onto the agar surface The Petri dishes were then incubated at 37 °C for 24 hours Following incubation, the zones formed around the disks were measured using a caliper This approach allowed the assessment of the inhibitory effects of the samples against the bacterial growth by measuring the diameter of the inhibition zones (Doan et al., 2022)

2.5 Statistical analysis

The statistical evaluation was performed using the IBM SPSS 22.0 software package (SPSS Inc., Chicago, IL, USA) The results were subjected to analysis through one-way analysis of variance (ANOVA) and subsequently presented as mean ± standard deviation Moreover, significant disparities (P < 0.05) among the means were identified using Tukey's multiple comparison test

3. Results and Discussion

3.1 Antioxidant activity

The DPPH assay, a widely recognized method for assessing radical scavenging ability, was employed to measure the films' efficacy in neutralizing free radicals, thus illuminating their potential as robust antioxidants (Gómez Estaca et al., 2014) In contrast to the control film, which exhibited a modest antioxidant activity of 42%, the introduction of CDs into the film formulation heralded a significant upsurge in antioxidant potential Notably, the SA CDs film displayed a substantial enhancement in antioxidant activity, registering a commendable 24% This preliminary outcome underscores the favorable impact of even lower concentrations of CDs in augmenting the antioxidant capacity of the films However, the most striking strides in antioxidant potential emerged with escalating CD concentrations The SA CDs film stood out with an impressive antioxidant activity of 24.7%, while the pinnacle was reached with the SA

CDs film showcasing a remarkable 3 antioxidant activity Table The dose dependent amplification of antioxidant activity potentially arises from the inherent characteristics of CDs such as their diverse surface chemistry and capacity to trap free radicals which were further accentuated at higher concentrations

These findings align harmoniously with prior research E ati vd 2022 Li vd 202 Moradi vd 2023 establishing carbon dots as potent candidates for exhibiting substantial antioxidant properties The augmented antioxidant activity observed in our study is likely attributed to a synergistic interplay between CDs and the sodium alginate matrix hile CDs contribute to radical scavenging the sodium alginate not only provides a stable structure but also potentially amplifies the overall antioxidant effect of the resulting film The ascending tra ectory of antioxidant activity with increasing CD concentrations not only underscores the potential of pumpkin waste derived CDs but also accentuates their viability as efficient antioxidants for application in food packaging This becomes especially pertinent in the context of extending the shelf life of packaged foods and bolstering food uality by mitigating oxidative deterioration In summation the successful integration of pumpkin waste derived carbon dots into sodium alginate films engendered a marked augmentation in antioxidant activity The discernible correlation between CD concentrations and heightened antioxidant potential substantiates the promise of CDs as effective antioxidants within food packaging materials This study not only showcases the merit of harnessing CDs from pumpkin waste but also offers a sustainable and effective avenue for enhancing the antioxidant prowess of food packaging films This promising endeavor opens doors to environmentally conscious packaging solutions thus contributing to both food preservation and environmental sustainability Lindh vd 20

able 1 Antioxidant and antimicrobial activity of films

	Antioxidant Activitiy	Antimicrobial activity	
	DPPH	<i>E.coli</i> mm	<i>S. aureus</i> mm
Control	4 2 0 °	n d	n d
SA CDs	2 4 03 ^b	3 4 0 °	4 3 0 7 ^c
SA 0CDs	2 47 24 ^a	4 0 ^b	7 42 0 2 ^b
SA CDs	3 32 ^a	3 0 2 ^a	0 33 ^a

3 2 vitr a timier bial activity

The antimicrobial activity of the films as assessed through the disk diffusion test against *E. coli* and *S. aureus* offered insights into the potential of pumpkin waste derived CDs integrated sodium alginate films as effective antimicrobial agents For *E. coli* the control film exhibited a non detectable one of inhibition indicating minimal inhibition of bacterial growth In contrast films containing CDs displayed increasingly prominent ones of inhibition as CD concentrations rose The SA CDs film demonstrated a one of inhibition measuring 3 4 mm followed by a noticeable augmentation in the SA 0CDs film with a 4 mm one of inhibition The most substantial inhibition was witnessed with the SA CDs film which showcased an impressive 3 mm one of inhibition against *E. coli* Similarly in the case of *S. aureus* the control film displayed no detectable one of inhibition indicative of limited antimicrobial effect The introduction of CDs into the film matrix led to enhanced antimicrobial activity The SA CDs film exhibited a 4 3 mm one of inhibition which further expanded in the SA 0CDs film with a notable 7 42 mm one of inhibition The pinnacle of antimicrobial inhibition was achieved with the SA CDs film recording a substantial mm one of inhibition against *S. aureus* These results underscore the potential of CDs in significantly augmenting the antimicrobial activity of sodium alginate films The escalating trend of increasing CD concentrations correlating with larger ones of inhibition suggests a clear dose dependent effect The antimicrobial efficacy observed can be attributed to the CDs inherent properties which may disrupt the bacterial cell membrane thus inhibiting growth

The results revealed a notable discrepancy in the antimicrobial activity exhibited by the films against *S. aureus* compared to *E. coli* The films demonstrated a consistently larger one of inhibition against *S. aureus* as compared to *E. coli* This distinct variation in antimicrobial efficacy between the two bacterial species could be attributed to several underlying factors One contributing factor is the intrinsic structural and physiological differences between *S. aureus* and *E. coli* *S. aureus* a Gram positive bacterium possesses a relatively thick peptidoglycan layer in its cell wall rendering it more susceptible to disruption by antimicrobial agents Eaton vd 200 In contrast *E. coli* a Gram negative bacterium features an outer membrane that serves as an additional barrier often providing greater resistance to antimicrobial substances Tenover 200 Moreover the diverse mechanisms of action of antimicrobial agents can result in varying degrees of efficacy against different bacterial species Tenover 200 The CDs integrated into the films may exhibit interactions with specific components of *S. aureus* that render it more susceptible to inhibition Ghirardello vd 202 Conversely the intricate cell wall structure of *E. coli* might present some resistance against the CDs antimicrobial effects Another influencing factor could be the distinct metabolic and growth characteristics of *S. aureus* and *E. coli* The differential response might stem from variations in growth rates cellular metabolism and

susceptibility to external stressors. These factors collectively contribute to the differing antimicrobial outcomes observed. Furthermore, bacterial species may exhibit varying levels of sensitivity to specific antimicrobial agents due to inherent genetic differences and adaptations. *S. aureus* and *E. coli* might possess dissimilar genetic makeup, resulting in diverse susceptibility profiles to the CDs' antimicrobial actions. The nuanced response highlights the need for comprehensive investigations into the antimicrobial efficacy of innovative materials, enabling a more targeted and effective approach to food safety and preservation through advanced packaging solutions.

These findings align with previous studies that have reported the antimicrobial potential of carbon dots derived from various sources. Ahdari, Moradi (2022), E. Ati vd (2022), Moradi vd (2023). The enhanced antimicrobial activity observed in this study is a testament to the synergistic effect between CDs and the sodium alginate matrix, where CDs contribute to antimicrobial activity while sodium alginate provides a stable film structure. In conclusion, the integration of pumpkin waste-derived carbon dots into sodium alginate films led to a considerable enhancement in antimicrobial activity. The increasing zone of inhibition with higher CD concentrations highlights the potential of CDs as effective antimicrobial agents within food packaging materials. This study accentuates the value of utilizing CDs from pumpkin waste to bolster the antimicrobial capacity of food packaging films, offering a sustainable approach to enhancing food safety and quality through innovative packaging solutions.

CONCLUSIONS

The present study illuminates the promising potential of pumpkin waste-derived carbon dot (CD)-integrated sodium alginate films as multifunctional materials with enhanced antioxidant and antimicrobial properties. The incorporation of CDs into the film matrix yielded remarkable improvements in both antioxidant activity and antimicrobial efficacy. This innovative approach showcases the sustainable utilization of agricultural waste for the development of functional packaging solutions, aligning with the principles of a circular economy. The significant enhancement in antioxidant activity observed with increasing CD concentrations underscores the viability of CDs as efficient scavengers of free radicals. This holds profound implications for prolonging the shelf life of packaged foods by mitigating oxidative degradation. Additionally, the escalating antimicrobial efficacy against *Staphylococcus aureus* and *Escherichia coli* underscores the potential of CDs to reinforce the antimicrobial capacity of sodium alginate films. The dose-dependent responses highlight the versatility of CDs in curbing bacterial growth, offering a valuable tool for enhancing food safety and quality. The differential responses of *S. aureus* and *E. coli* to the films' antimicrobial activity elucidate the intricate interplay between bacterial species, structural characteristics, and susceptibility to antimicrobial agents. This insight underscores the need for tailored approaches to antimicrobial applications, reflecting the complex nature of microbial interactions. The successful integration of pumpkin waste-derived CDs into sodium alginate films signifies a remarkable stride towards sustainable and functional food packaging. By repurposing agricultural waste into valuable resources, this study exemplifies the potential of green technologies to address environmental challenges while simultaneously contributing to advanced packaging solutions that extend beyond conventional preservation. In conclusion, the synergistic combination of pumpkin waste-derived CDs and sodium alginate films presents an innovative pathway towards enhancing food safety, extending shelf life, and promoting sustainable practices within the food packaging industry. This research paves the way for further exploration of novel materials derived from agricultural waste, driving the evolution of packaging technologies that align with both consumer demands and environmental stewardship.

ETHICS COMMITTEE APPROVAL

N/A

PEER REVIEW

Externally peer reviewed

AUTHOR CONTRIBUTIONS

Conceptualization: CD, ND; Investigation: CD, ND; Material and Methodology: CD, ND; Supervision: CD, ND; Visualization: CD, ND; Writing Original Draft: CD, ND; Writing review & Editing: CD, ND; Other: All authors have read and agreed to the published version of manuscript.

CONFLICTS OF INTEREST

The authors have no conflicts of interest to declare.

FINANCIAL SUPPORT

The authors declared that this study has received no financial support.

F S

- Asgher M, Amar S, A Bilal M, I bal H, M N 2020 Bio based active food packaging materials Sustainable alternative to conventional petrochemical based packaging materials *Food Research International* 137 0 2 <https://doi.org/10.1016/j.foodres.2020.107202>
- A hdari S, Moradi M 2022 Application of antimicrobial coating based on carboxymethyl cellulose and natamycin in active packaging of cheese *International Journal of Biological Macromolecules* 209 2042 204 <https://doi.org/10.1016/j.ijbiomac.2022.107044>
- Ba yi it B, Ala alvar H, Do an N, Do an C, Berkta S, am M 2020 Mild mustard *Sinapis arvensis* parts: Compositional analysis, antioxidant capacity and determination of individual phenolic fractions by LC-ESI-MS/MS *Journal of Food Measurement and Characterization* 14 3 7 <https://doi.org/10.1007/s11402-020-0042-2>
- Do an N, Do an C, Eticha A, Gungor M, Akgul 2022 Centrifugally spun micro nanofibers based on lemon peel oil gelatin as novel edible active food packaging: Fabrication, characterization and application to prevent foodborne pathogens *E. coli* and *S. aureus* in cheese *Food Control* 139 0 0 <https://doi.org/10.1016/j.foodcont.2022.107040>
- Eaton P, Fernandes C, Pereira E, Pintado M, E avier Malcata F 200 Atomic force microscopy study of the antibacterial effects of chitosans on *Escherichia coli* and *Staphylococcus aureus* *Ultramicroscopy* 108 0 2 34 <https://doi.org/10.1016/j.ultramic.2000.04.002>
- E ati P, Rhim, Molaei R, Priyadarshi R, Roy S, Min S, im, H, Lee S, G, Han S 2022 Preparation and characterization of B S and N doped glucose carbon dots: Antibacterial, antifungal and antioxidant activity *Sustainable Materials and Technologies* 32 e003 7 <https://doi.org/10.1016/j.susmat.2022.e0037>
- Ghirardello M, Ramos Soriano, Galan M, C 202 Carbon Dots as an Emergent Class of Antimicrobial Agents *Nanomaterials* 11 Article <https://doi.org/10.3390/nano11071077>
- G me Estaca, L pe de Dicastillo C, Hern nde Mu o P, Catal R, Gavara R 20 4 Advances in antioxidant active food packaging *Trends in Food Science & Technology* 35 42 <https://doi.org/10.1016/j.tifs.2023.03.000>
- Li S, Li L, Tu H, hang H, Silvester D, S Banks C, E ou G, Hou H, i 202 The development of carbon dots: From the perspective of materials chemistry *Materials Today* 51 207 <https://doi.org/10.1016/j.mat.2022.07.022>
- Lindh H, Olsson A, illiams H 20 Consumer Perceptions of Food Packaging: Contributing to or Counteracting Environmentally Sustainable Development *Packaging Technology and Science* 29 3 23 <https://doi.org/10.1002/pts.2434>
- Moradi M, Molaei R, ousheh S, A T, Guimar es, McClements D 2023 Carbon dots synthesized from microorganisms and food by products: Active and smart food packaging applications *Critical Reviews in Food Science and Nutrition* 63 4 43 <https://doi.org/10.1080/10407813.2022.207233>
- Norfe ah M, N Hardacre A, Brennan C, S 20 Comparison of waste pumpkin material and its potential use in extruded snack foods *Food Science and Technology International* 17 4 3 7 373 <https://doi.org/10.1111/1365-3113.12444>
- Tenover F, C 200 Mechanisms of Antimicrobial Resistance in Bacteria *The American Journal of Medicine* 119 Supplement 3 S 0 <https://doi.org/10.1016/j.amjmed.2000.03.003>
- aharia D, C Muntean A, A Popa M, G Steriade A, T Balint O, Micut R, Ifene C, Tofolean I, Popa V, T Baicus C, Bogdan M, A Popa M, I 20 3 Comparative analysis of *Staphylococcus aureus* and *Escherichia coli* microcalorimetric growth *BMC Microbiology* 13 7 <https://doi.org/10.1186/1471-2164-13-7>

Investigation of Performance Analysis of a Stirling Engine with Bell Crank Drive Mechanism

Özge Özlü

Abstract Today efforts to develop power generation systems that can use renewable energy sources continue to solve the environmental problems created by fossil based fuels. The working principles of Stirling engines date back to ancient years. These engines have been known for over two centuries and are continuing to develop studies. Stirling engines can generate mechanical or electrical power using any heat source that can provide sufficiently high temperatures. The thermal efficiency, harmful exhaust emission values, noise and vibration levels of these engines are quite good compared to internal combustion engines. In this study, thermodynamic and kinematic analysis of a beta type Stirling engine with bell crank drive mechanism were conducted. The volume and pressure changes depending on the crank angle of the engine with the bell crank drive mechanism were calculated using the isothermal analysis method. In this study, the fundamental parameters related to engine performance such as working fluid mass, charge pressure, heater and coolant temperature, the effects on the amount of net power are examined in detail. The simulation and optimization analysis of the bell crank drive mechanism for the beta type Stirling engine were made using the MSC Adams program. Part drawings and assemblies of the models used in the MSC Adams program were created in the SolidWorks program.

Keywords Stirling engines, Bell crank, Thermodynamic analysis, kinematic analysis, Isothermal analysis

Address Özlü University, Department of Automotive Technology, Şah İhan Özlü T. K. İyeye

Corresponding Author ozge.ozlu@ozlu.edu.tr

1. INTRODUCTION

Stirling engines are an external combustion power generation system that can use all kinds of heat energy [1]. Today these engines are used commercially for electric power generation in spacecraft of NASA and combi systems at houses. In addition, there are different application areas where it is used for electrical energy generation from solar energy and as a water pump [2]. Different drive mechanisms are used to convert heat energy into mechanical energy in Stirling engines [3]. Different drive mechanisms such as bell crank, slider crank, wobble yoke, rhombic drive, swash plate, scotch yoke, and ross yoke are used in kinematic Stirling engines [4]. The drive mechanisms differ according to engine type and power. Different drive mechanisms can be developed by engine designers to ensure higher engine power and efficiency are obtained from this type of engine [5].

The bell crank drive mechanism is known to be the first drive mechanism used in Stirling engines [6]. The bell crank drive mechanism is a simple part used to change the direction of movement. The inlet and outlet direction of the movement can be approximately 90° different. The bell crank mechanism can be used for different purposes besides converting linear motion to circular motion in many mechanical systems [7]. It has been reported in the literature that the bell crank mechanism provides better performance results for single cylinder small engines [8]. This mechanism is not preferred very often in large size engines due to negative conditions such as the weight of the mechanism and balance [9]. In this drive mechanism, it is seen as a disadvantage that the lateral friction forces occurring between the displacer/piston rod and the power piston are higher than in other mechanisms [10]. In Figure 1, the 3D design pictures of the Stirling engine with bell crank drive mechanism developed for this study, created in the SolidWorks program are shown.

In this study, it is aimed to investigate of design and thermodynamic analyses of a Stirling engine with bell crank drive mechanism. It is planned to manufacture the Stirling engine by evaluating the results obtained according to the design and analysis results. Power and torque values of the Stirling engine with bell crank drive mechanism will be experimentally determined by using a dynamometer in the next stages of manufacturing. Due to the wide usage area of

Stirling engines it is foreseen that bringing a local original design to the industry will contribute significantly to our country's economy

2 A A A HO

More efficient design and testing of mechanical systems is a challenging process for engineers. In particular, the inability to fully examine the interaction of finite elements and rigid body dynamics analyses with each other during designs may cause the systems to have very different behavior after production. Therefore, the complexity of the events that occur in the real life operating conditions of Stirling engines directs researchers to theoretical analysis.

Kinematics examines only the movements of objects without considering their masses and the forces acting on them. The kinematic analysis method is used to determine the properties of parameters such as position, displacement, velocity, and acceleration of machine parts. MSC Adams Automatic Dynamic Analysis of Mechanical System software is one of the most widely used dynamic and kinematic analysis software in the world. MSC Adams program is advanced software used to analyze the parameters such as force, velocity, position, acceleration, and moment of a system designed in a computer environment in real life operating conditions. With these features, the MSC Adams program has better features than other CAD programs. MSC Adams program, the design quality of the systems increases, while the design and prototype costs are significantly reduced. In this study, kinematic analyses of a Stirling engine with bell crank drive mechanism were made using the MSC Adams program. Part drawings and assemblies of the models used in the MSC Adams program were created in the SolidWorks program, a CAD program.

Many methods, Isothermal, Schmidt, and nodal analysis, etc., are used in the literature in thermodynamic analysis, which is the basis for the design of Stirling engines. In this study, the isothermal analysis method is preferred. With the Isothermal analysis method developed by Gustav Schmidt, the performance parameters of the existing system, such as pressure, volume, and power, can be determined theoretically before the production of engine prototypes.

All heat losses in the Stirling engine are neglected in this analysis. Therefore, in the analysis, the temperatures of the gas masses in the expansion volume, compression volume, and regenerator are taken as equal to the wall temperatures of these parts. The equations used to determine the net work and pressure changes obtained from Stirling engines are given in below. Pressure and volume changes are taken into account in net work of engine calculations.

$$M = [m_c + m_k + m_r + m_h + m_e] \tag{2}$$

$$m = [pV \quad RT] \tag{2.2}$$

$$M = [p \quad V_c \quad T_k + V_k \quad T_k + V_r \quad T_r + V_h \quad T_h + V_e \quad T_h \quad R] \tag{2.3}$$

$$T_r = [T_h - T_k \quad \ln T_h \quad T_k] \tag{2.4}$$

$$p = \left[MR \left(\frac{V_c}{T_k} + \frac{V_k}{T_k} + \frac{V_r \ln T_h \quad T_k}{T_h - T_k} + \frac{V_h}{T_h} + \frac{V_e}{T_h} \right)^{-1} \right] \tag{2}$$

$$W = \left[\sum_{i=1}^{i=k} P_i \quad V_i - V_{i-1} \right] \tag{2}$$

$$W = [W_c + W_e] \tag{2.7}$$

$$\eta = [W \quad Q_e] \tag{2}$$

The linear reciprocating motion of the pistons between the bottom dead center and the top dead center in the cylinder is converted into circular motion via the drive mechanism. The faster this movement of the pistons in the cylinder, the higher the engine speed. In fact, although the velocity of a point on the crankshaft and flywheel is constant at constant engine speed, the velocity and direction of the piston are constantly changing. Piston velocities are a frequently used quantity as a comparison value between engines [20, 21]. The velocity changes of the power piston and displacer piston obtained with the MSC Adams program depending on the 100 and 200 rpm engine speeds of the Stirling engine with bell crank drive mechanism are given in Figure 7 and Figure 8. When the graphics are examined, it is seen that when the pistons go up to the top dead center at 100 rpm, they reach a speed of nearly 1 m/s, and the power piston and the displacer pistons move at different speeds when descending towards the bottom dead center. It is seen that the displacer piston reaches a velocity of approximately 2.3 m/s as it descends toward the lower dead point. At 200 rpm engine speed, the pistons reach a speed of approximately 2 m/s as they move towards the top dead center, and the power piston reaches a speed of 2 m/s and the displacer piston reaches a speed of 3 m/s when descending towards the bottom dead center. As seen in Figure 7 and Figure 8, the engine is in 1 second, it performs 10 cycles for 100 rpm engine speed and 20 cycles for 200 rpm engine speed.

In this section, the work topic should be stated in the previous work on the subject, the purpose of working with the relevant references supported. The entire article will be written in Times New Roman in 10 pt with a single line spacing. In this section, the work topic should be stated in the previous work on the subject, the purpose of working with the relevant references supported. The entire article will be written in Times New Roman in 10 pt with a single line spacing.

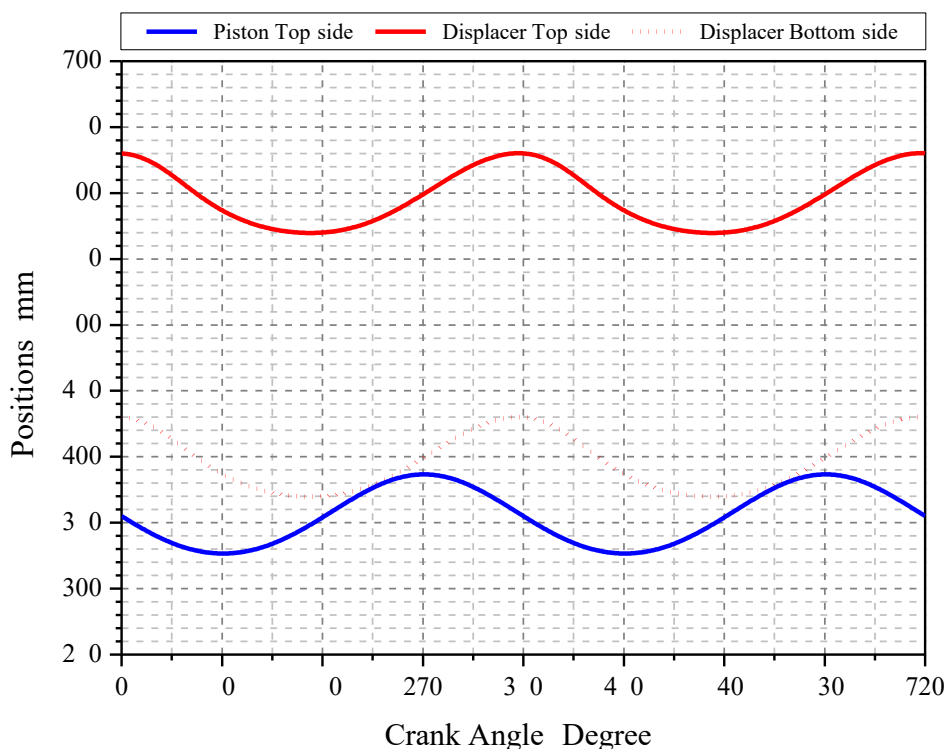


Figure 2 The variations of piston and displacer positions according to crank angle

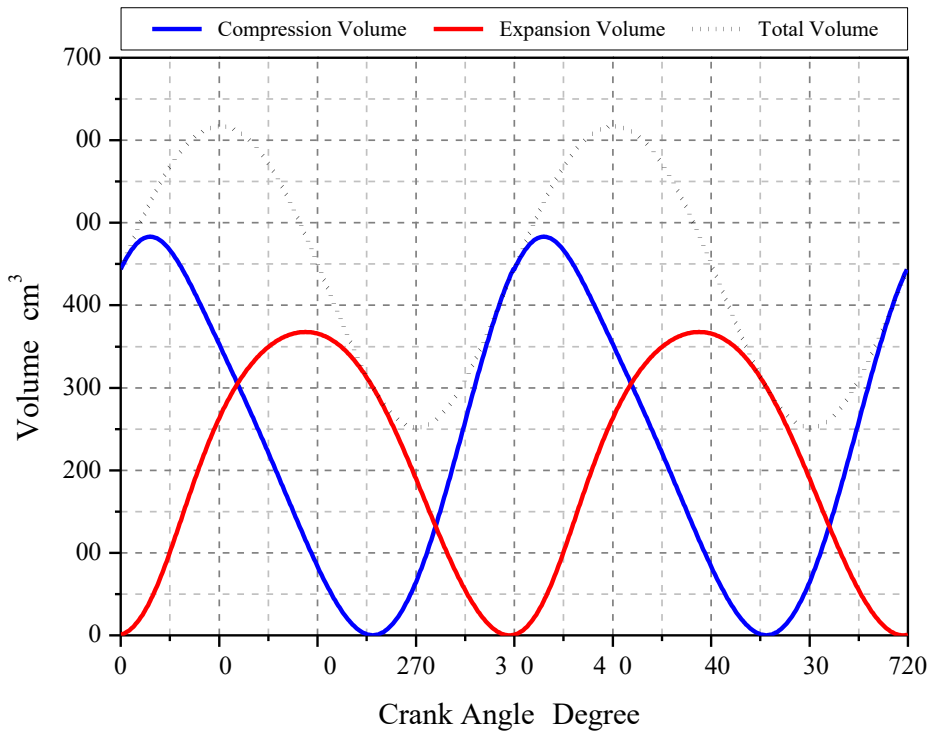


Figure 3 The variations of volume according to crank angle

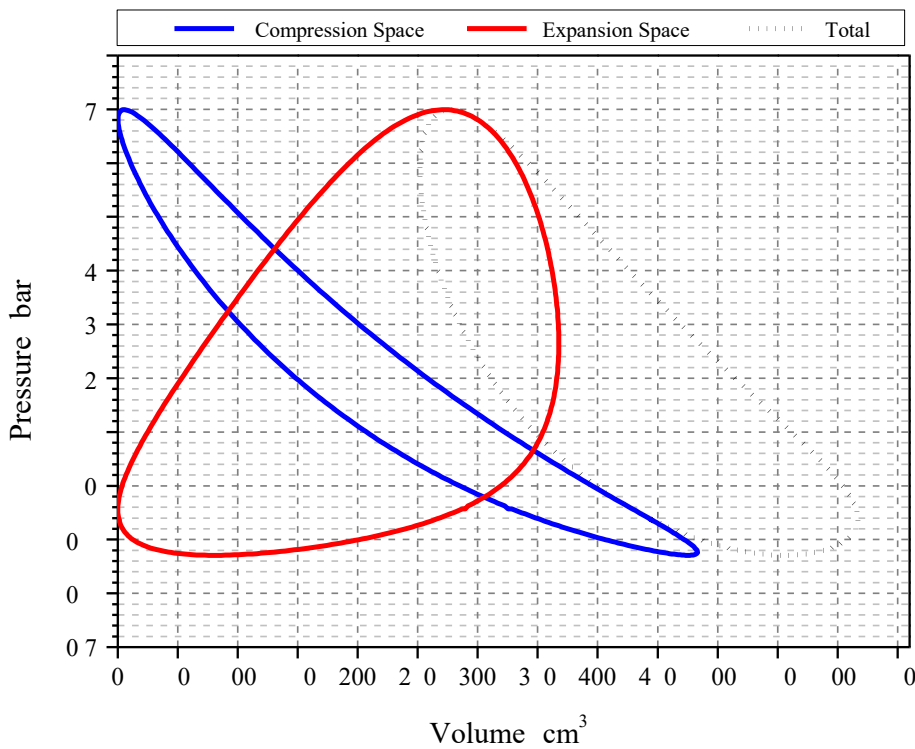


Figure Comparison of expansion and compression chambers P V diagrams

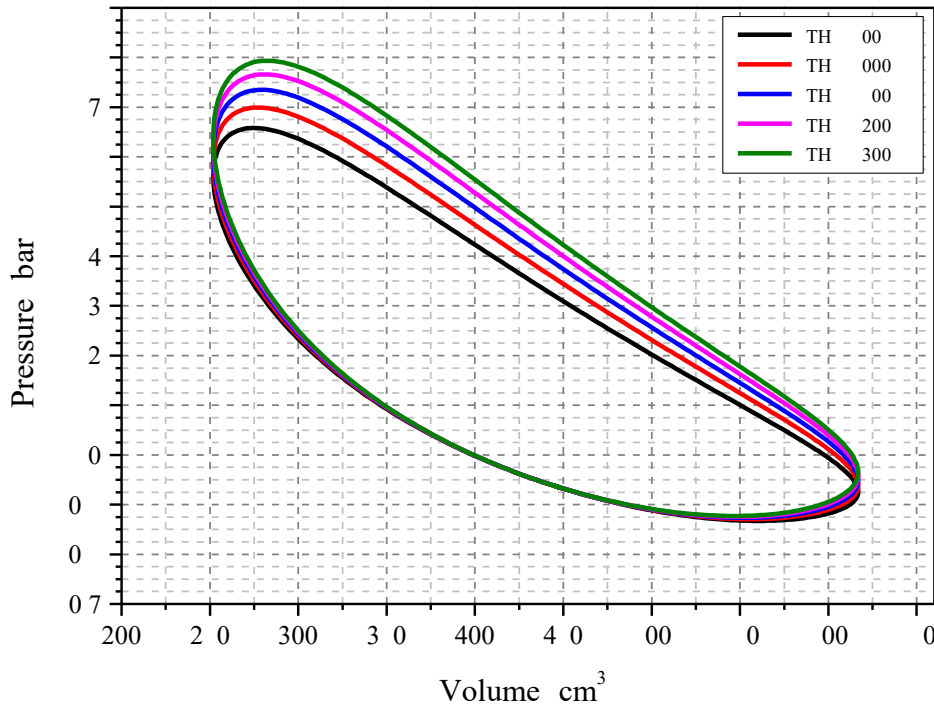


Figure Comparison of P V diagrams for different heater temperatures

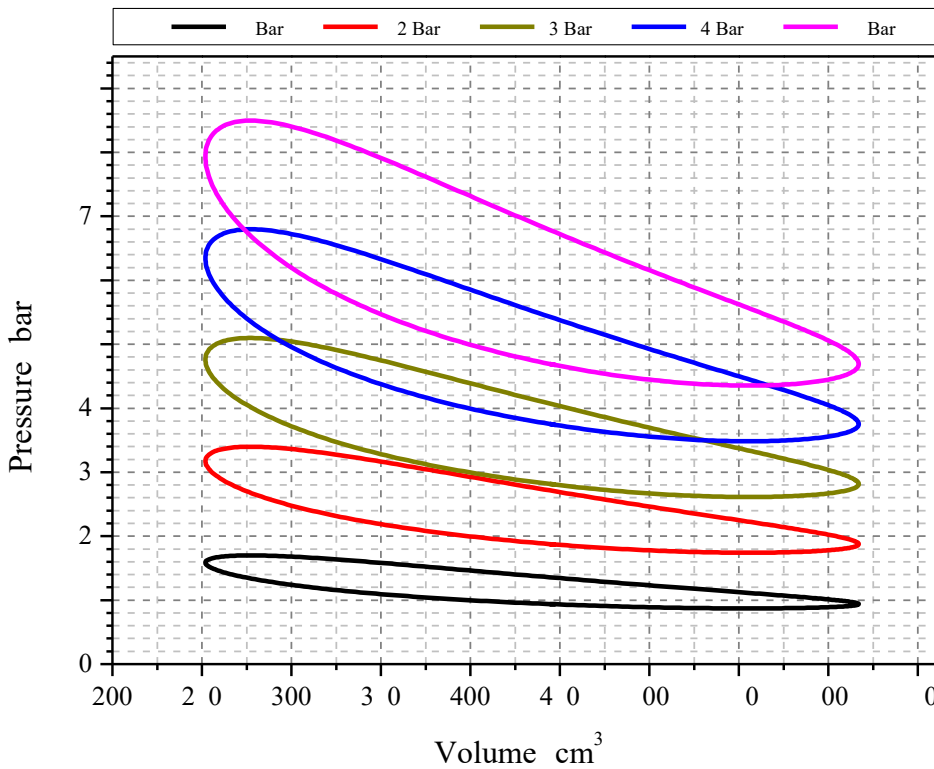


Figure Comparison of P V diagrams for different charge pressures

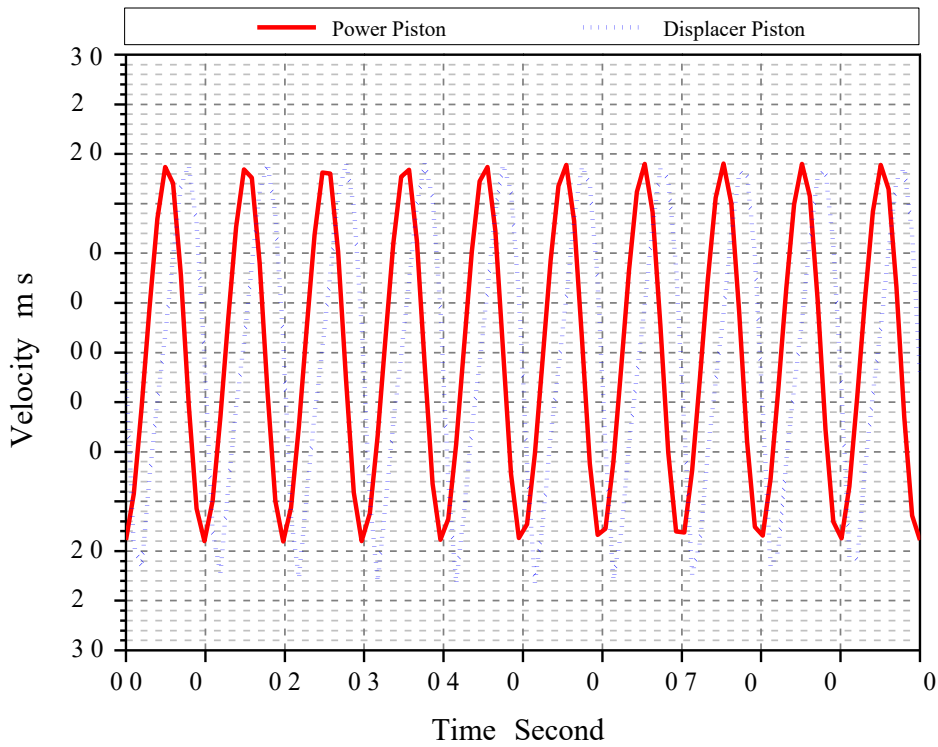


Figure The variations of piston velocities according to time 1000 rpm

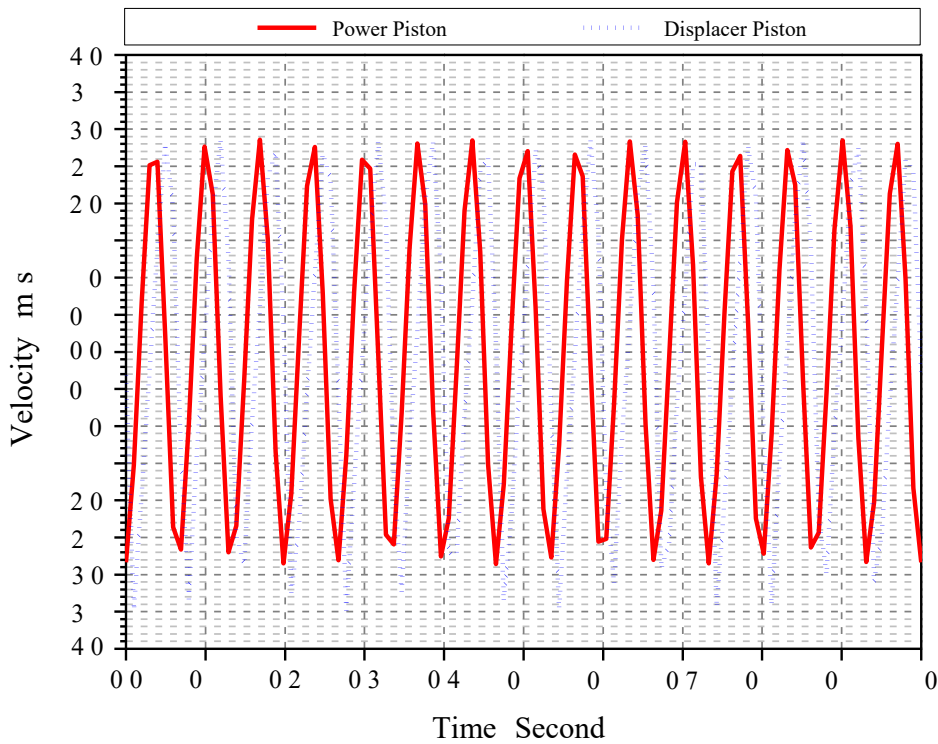


Figure The variation of piston velocities according to time 3000 rpm

O S O S

In this study thermodynamic and kinematic analysis of a beta type Stirling engine with bell crank drive mechanism were examined. The fundamental parameters related to engine performance such as working fluid mass, charge pressure, heater and coolant temperature, the effects on the amount of net power are investigated. The pressure and volume changes of a beta type Stirling engine with bell crank drive mechanism were determined using the MSC Adams program. In addition, velocity changes of the power and the displacer pistons were calculated at the 100 and 200 rpm engine speeds. It has been observed that the highest piston velocity values occurred at 200 rpm engine speed. It was determined that the velocities of the power and displacer pistons are nearly equal when they are moving toward the top dead center. The both pistons velocities of moving towards the bottom dead center are different from each other.

Acknowledgements

This study was supported within the scope of project number 2023-01 by the Scientific Research Projects Coordination Unit of Sremska University. I would like to thank the Scientific Research Projects Coordination Unit of Sremska University for their support.

Ethics Committee Approval

N/A

Conflict of Interest

The author declares that they have no known competing financial interests or personal relationships that could have appeared to influence the work reported in this paper.

References

1. Erol D, Daman H. Do an B A review development of rhombic drive mechanism used in the Stirling engines. *Renewable and Sustainable Energy Reviews*, 2017; 77: 1044-1077.
2. Mei er R. The Philips Stirling thermal engine: analysis of the rhombic drive mechanism and efficiency measurements. Thesis. Technical University Delft, 2010.
3. Erol D and Alkan S. The examination of performance characteristics of a beta type Stirling engine with a rhombic mechanism: the influence of various working fluids and displacer piston materials. *International Journal of Energy Research*, 2024; 372-3747.
4. Hargreaves C M. The Philips Stirling engine. Elsevier, New York.
5. Finkelstein T and Organ A. Air engines: the history, science and reality of the perfect engine. New York: The American Society of Mechanical Engineers, 2004.
6. Stirling R. Improvements for diminishing the consumption of fuel and in particular, an engine capable of being applied to the moving of machinery on a principle entirely new. British Patent No. 40.
7. Walker G. Stirling engines. United States by Oxford University Press, 2010.
8. Delyova I, Hroncova D, Frankovsky P, Durisova E and Rakay F. Kinematic analysis of crank-rocker mechanism using MSC Adams. View. *Applied Mechanics and Materials*, 2014; 60-7.
9. Doane. Machine analysis with computer applications for mechanical engineers. John Wiley and Sons, 2010.
10. Arabulut H, Aksoy F and Turk E. Thermodynamic analysis of a beta type Stirling engine with a displacer driving mechanism by means of a lever. *Renewable Energy*, 2020; 34: 202-210.

- Arabulut H, Nar C, Turk E and Cesu H S Torque and power characteristics of a helium charged Stirling engine with a lever controlled displacer driving mechanism *Renewable Energy*, 2003, 3, 43
- 2 Erol D andalkan S Comparative study on the performance of different drive mechanisms used in a beta type Stirling engine through thermodynamic analysis *International Journal of Automotive Engineering and Technologies*, 2022, 44, 0
- 3 Eenen F L V 47 The Construction of the Philips air engine *Philips Technical Review*, 47, 2, 34
- 4 Martin G H *Kinematics and dynamics of machines*aveland Press Inc United State of America 2002
- aldron in el G L and Agrawal S *Kinematics, dynamics, and design of machinery*ohn iley Sons 20
- Orlandea N V Multibody systems history of Adams *Journal of Computational and Nonlinear Dynamics*, 2020, 0, 030
- 7 Shabana A A An important chapter in the history of multibody system dynamics *Journal of Computational and Nonlinear Dynamics*, 2020, 0, 0303
- Schmidt G Theorie der Lehmann schen Calorischen Maschine Theory of Lehmann s caloric machine eitschrift des Vereins deutscher Ingenieure 7
- Urieli I and Berchowit D M Stirling cycle engine analysis Adam Hilger Ltd Bristol 4
- 20 Taylor C F The internal combustion engine in theory and practice Massachusetts Institute of Technology London England
- 2 Ferrari G Onorati A and D Errico G Internal combustion engines Societa Editrice Esculapio 2024

ri ritizati ybersecurity Strate ies A Hesita t Fuzzy i uistic A r ach

erve ler*¹, I i y z a ², si u ul³

Abstract Cybersecurity threats have become a significant challenge for any important digital infrastructure and numerous cyber attacks have also become a major concern for society. Cybersecurity is an approach of guarding against digital attacks on systems, networks, and programs. Institutions aim to create effective cybersecurity procedures, create in-house awareness, train their employees on this issue, and strengthen their cybersecurity infrastructure. A strategic approach is required for institutions to effectively implement cybersecurity measures. This study aims to address security challenges and present a cybersecurity strategy prioritization model that would guide institutions in their cybersecurity operations. Hesitant Fuzzy Linguistic Term Sets (HFLTS) technique is used to represent Decision Makers (DMs) opinions by addressing the problem of expressing concepts through crisp numbers and ambiguity. The HFL AHP (Analytic Hierarchy Process) approach is used to compute the weights of the assessment criteria, while the HFL VI OR (Vise riteri umsaOptimaci a I ompromisnoResenje) method is used to prioritize the alternatives. The HFL AHP method was chosen because it is flexible, intuitive, practical, and considers consistency. The HFL VI OR method was chosen because it is a method that provides a consensus-based solution. To demonstrate the effectiveness of the proposed research methodology, a case study is provided. Finally, the results are presented along with suggestions for further research.

Key words: AHP, Cybersecurity, Hesitant Fuzzy Linguistic Term Sets, MCDM, VI OR

^{1,2,3}A **ress** Galatasaray University, Faculty of Engineering and Technology, Istanbul, Turkey

* **rres** i **auth** r mguler gsu.edu.tr

1 O O

Recently, cyber attacks and security breaches of technological systems have been increasing rapidly. In most of the studies, it has been emphasized that the new generation technologies are an attack element and that the systems used have become targets. Cyber attacks are actions that aim to steal, change, or even destroy sensitive information by taking advantage of security vulnerabilities and generally aiming to gain financial gain. The target of these attacks may be the critical infrastructures of countries, energy, communication, health, finance, dams, pipelines, etc. Therefore, cyber attacks cause material and moral damage to many organizations around the world. For this reason, it is inevitable for institutions to attach importance to cybersecurity.

Cybersecurity is the set of measures taken against cyber attacks. Organizations need to prioritize their strategies to effectively establish cybersecurity procedures, create internal awareness, train their employees, strengthen their cybersecurity infrastructure, and ultimately increase their cyber resilience (Erdoğan et al., 2020). The aim of the cybersecurity strategy is to increase the security of the systems and infrastructures that individuals and institutions use in their business and services. As a matter of fact, in this study, it is aimed to address the security issues of institutions and to propose a cybersecurity strategy prioritization model that will guide institutions in their cybersecurity practices.

The cybersecurity strategy prioritization problem should be considered from various dimensions. Therefore, due to the nature of the problem, there are many factors and uncertainties to consider. In this study, Hesitant Fuzzy Linguistic (HFL) Multi-Criteria Decision Making (MCDM) approach is applied. To overcome hesitation in decision makers (DMs) decisions, Hesitant Fuzzy Linguistic Term Sets (HFLTS) technique proposed by Rodriguez et al. (2010) is used. In the first part of the study, the weights of the factors in the cybersecurity model are found by the HFL AHP (Analytical Hierarchy Process) method. HFL AHP method is chosen because it is flexible, intuitive, practical, and considers consistency. In the second part of the study, cybersecurity strategy alternatives are ranked with the HFL VI OR (Vise riteri umsaOptimaci a I ompromisnoResenje) method. HFL VI OR method is chosen because it is a method that provides a consensus-based solution. In addition, VI OR provides maximum group benefit for the majority of experts and minimum personal regret for dissenters. The evaluation model presented in the study is determined by reviewing the literature, examining industry reports, and taking the opinions of experts. Then, a case study of the proposed approach is carried out, and the results of the study are given.

In recent years the studies about cybersecurity strategies has grown intensely while some of the previous studies have examined the subject with various MCDM methods Ganin et al 2020 Umar et al 2020 Torbacki 2022 Torbacki 2022 proposed a cybersecurity structure with Decision Making Trial and Evaluation Laboratory DEMATEL Analytic Network Process ANP and Preference Ranking Organization Method for Enrichment Evaluation II PROMETHEE II methods for sustainable manufacturing Ganin et al 2020 presented a model for cybersecurity risk assessment with Multi Criteria Decision Analysis MCDA technique Umar et al 2020 utilized fuzzy AHP Technique for Order Preference by Similarity to an Ideal Solution TOPSIS approaches for evaluating cybersecurity systems of health information systems As a result the primary contribution of this paper is the first use of the HFL AHP and HFL VI OR methods in prioritizing cybersecurity strategies

The remainder of this paper is organized as follows The research methodology is described in the second section A presentation of the case study is included in the third section The final section includes a summary of the findings and potential research areas for future research

2 SAH HO O O

The proposed HFL AHP HFL VI OR methodology includes 3 steps as seen in Figure

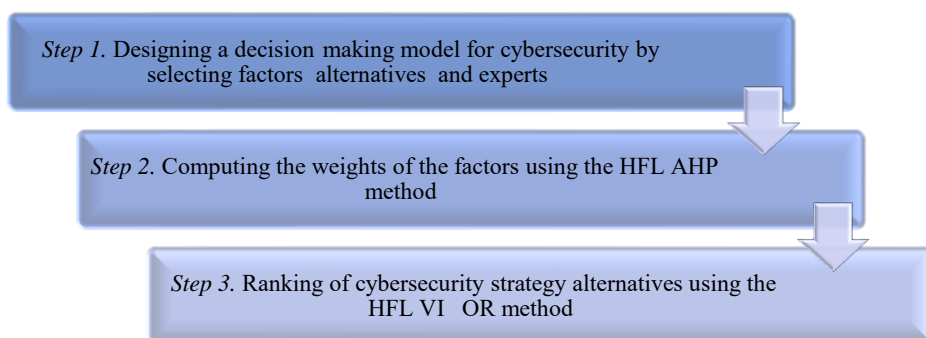


Figure 1 The main steps of the proposed research methodology

The HFLTS technique which was proposed by Rodriguez et al 2013 was created using a collection of HFLTS Please see Rodriguez et al 2013 for further details on the HFLTS technique The next section explains the steps of the HFL AHP and HFL VI OR approaches

2.1 HFAHP method

Step 1. The experts evaluated the criteria by using the linguistic term set provided in Table

Table 1 The linguistic term set used in HFL AHP method Gulak Ahraman 200

Linguistic terms	Fuzzy Numbers
Useful	
Equally important	2 3 2
Slightly more important	3 2 2
Strongly more important	3 2 2 2
Very strongly more important	2 2 3
Absolutely more important	2 3 7 2

Step 2. The linguistic terms are translated into HFLTS and pairwise comparison matrices are constructed

Step 3. A matrix for pairwise comparison (C-tilde) is found The reciprocal values are obtained Buyukcan Guler 2020

$$\tilde{c}_i = \frac{1}{c_{i1}}, \frac{1}{c_{i2}}, \dots, \frac{1}{c_{im}}, \frac{1}{c_{i1}}$$

Step 4 The fuzzy geometric mean r-tilde_i of matrix C-tilde is calculated as follows



$$\tilde{r}_i = \tilde{c}_i \otimes \tilde{c}_{i2} \otimes \dots \otimes \tilde{c}_{in} \quad n \tag{2}$$

Step 5. The fuzzy weight \tilde{w}_i^{CR} of every main criteria is calculated

$$\tilde{w}_i^{CR} = \tilde{r}_i \otimes \tilde{r} \otimes \tilde{r}_2 \otimes \dots \otimes \tilde{r}_n \tag{3}$$

Step 6. The fuzzy global weights of sub criteria are computed

$$\tilde{w}_i^G = \tilde{w}_i^{CR} \otimes \tilde{w}^{CR} \tag{4}$$

where \tilde{w}_{ij}^G is the global weight of sub criteria

Step 7. The trapezoidal fuzzy numbers \tilde{w}_i^G using are defuzzified and they are normalized

$$w_i^G = \frac{2 \cdot 2}{\dots}$$

$$w_i^N = \frac{w_i^G}{\sum_i \sum w_i^G}$$

2.2 HF-KO method

Step 1. The experts evaluated the criteria by using the linguistic term set provided in Table 2

Table 2 The linguistic term set used in HFL VI-OR method Chou et al. 200

Linguistic terms	Fuzzy Numbers
Very bad	0 0 3
Bad	0 3 3
Medium	2
Good	7 7 0
Very good	7 0 0 0

Step 2. The linguistic terms are translated into HFLTS

Step 3. The elements of the \tilde{R}_{ij} are computed as Býkkan Gler 202

$$\tilde{r}_{ij} = \left(\frac{x_{ij}}{x_{ij4}^+}, \frac{x_{ij2}}{x_{ij4}^+}, \frac{x_{ij3}}{x_{ij4}^+}, \frac{x_{ij4}}{x_{ij4}^+} \right) \quad C_j \in B \tag{7}$$

$$\tilde{r}_{ij} = \left(\frac{x_{ij}}{x_{ij}^-}, \frac{x_{ij2}}{x_{ij}^-}, \frac{x_{ij3}}{x_{ij}^-}, \frac{x_{ij4}}{x_{ij}^-} \right) \quad C_j \in C$$

where $x_{ij4} = \max_i \{ \tilde{X}_{ij} \}, C_j \in B$ and $x_{ij} = \min_i \{ \tilde{X}_{ij} \}, C_j \in C$

Step 4. The normalized matrix R_{ij} with crisp numbers is computed as

$$\text{Defuz} (X_{ij}) = \frac{\int \frac{\mu(x) \cdot x dx}{\mu(x) \cdot dx} = \frac{\int_{x_{ij1}}^{x_{ij2}} \left(\frac{x-x_{ij1}}{x_{ij2}-x_{ij1}} \right) \cdot x dx + \int_{x_{ij2}}^{x_{ij3}} x dx + \int_{x_{ij3}}^{x_{ij4}} \left(\frac{x_{ij4}-x}{x_{ij4}-x_{ij3}} \right) \cdot x dx}{\int_{x_{ij1}}^{x_{ij2}} \left(\frac{x-x_{ij1}}{x_{ij2}-x_{ij1}} \right) dx + \int_{x_{ij2}}^{x_{ij3}} dx + \int_{x_{ij3}}^{x_{ij4}} \left(\frac{x_{ij4}-x}{x_{ij4}-x_{ij3}} \right) dx} = \frac{-x_{ij1}x_{ij2}^2 + x_{ij3}x_{ij4}^2 + \frac{2}{3}(x_{ij4}-x_{ij3})^2 (x_{ij2}-x_{ij1})^2}{-x_{ij1}^2x_{ij2} + x_{ij3}^2 + x_{ij4}^2}$$

Step 5. The weighted normalized matrix elements are calculated as

$$v_{ij} = r_{ij} \cdot w_j \tag{8}$$

Step 6. The ideal f_j^* and f_j^- values ($j = 2, \dots, n$) are determined. If the j^{th} function is related with benefit factors then

$$f_j^* \max f_{ij} \quad f_j \min f_{ij}$$

If the j^{th} function is related with cost factors then

$$f_j^* \min f_{ij} \quad f_j \max f_{ij} \tag{2}$$

Step 7. The S_i, R_i and Q_i values $i= 2, \dots, I$, are computed as

$$S_i = \sum_j^n w_j \frac{f_j^* \cdot f_{ij}}{f_j \cdot f_j^*} \tag{3}$$

$$R_i = \max \left[w_j \frac{f_j^* \cdot f_{ij}}{f_j \cdot f_j^*} \right] \tag{4}$$

$$Q_i = \theta \frac{S_i - S^*}{S - S^*} \quad \theta \frac{R_i - R^*}{R - R^*}$$

$$S^* = \min S_i \quad S = \max S_i$$

$$R^* = \min R_i \quad R = \max R_i \tag{7}$$

3 AS S

Cyber attacks are actions that aim to steal change or even destroy sensitive information by taking advantage of security vulnerabilities and generally aiming to gain financial gain. The target of these attacks may be the critical infrastructures of countries energy communication health finance etc. Cyber attacks cause material and moral damage to many organizations around the world. It is inevitable for institutions to attach importance to cyber security. As stated in the National Cyber Security Strategy and Action Plan 2020-2023 report Turkey needs to establish a good cyber security strategy to increase the cyber resilience of institutions. T.C. Ulaştırma ve Altyapı Bakanlığı (2023)

This study proposes a model for prioritizing cybersecurity strategies that was developed after evaluating academic articles industry reports and expert opinions. Deloitte (2022), arabacak et al. (2020), P. C. (2020), Tu et al. (2020), eoh et al. (2022), ammani et al. (2020). Figure 2 provides an illustration of this model. The cybersecurity alternatives are determined based on reports. These alternatives are T.C. Ulaştırma ve Altyapı Bakanlığı (2023)

- 1 Protecting Critical Infrastructures and Increasing Strength A1
- 2 Developing National Capacity A2
- 3 Organic Cyber Security Network A3
- 4 Security of Next Generation Technologies A4
- 5 Fighting Cybercrime A5
- 6 Development and Support of Domestic and National Technologies A6
- 7 Integration of Cyber Security into National Security A7
- 8 Developing International Cooperation A8

HFL AHP method is used in the first phase to compute the factors weights. Table 3 displays the evaluations made by the DMs. The HFL AHP method's stages are applied with Eqs. (1)-(6). Table 4 illustrates the final factor weights.

Table 3 The evaluation about factors

	F1	F2	F3	F4	F5
F1	ust e ual	At least weakly more important	At most weakly more important		
F2		ust e ual			
F3		At least weakly more important	ust e ual		
F4	At most e ually important	At least strongly more important	At least weakly more important	ust e ual	At most e ually important
F5	At most e ually important	At least strongly more important	At least weakly more important		ust e ual

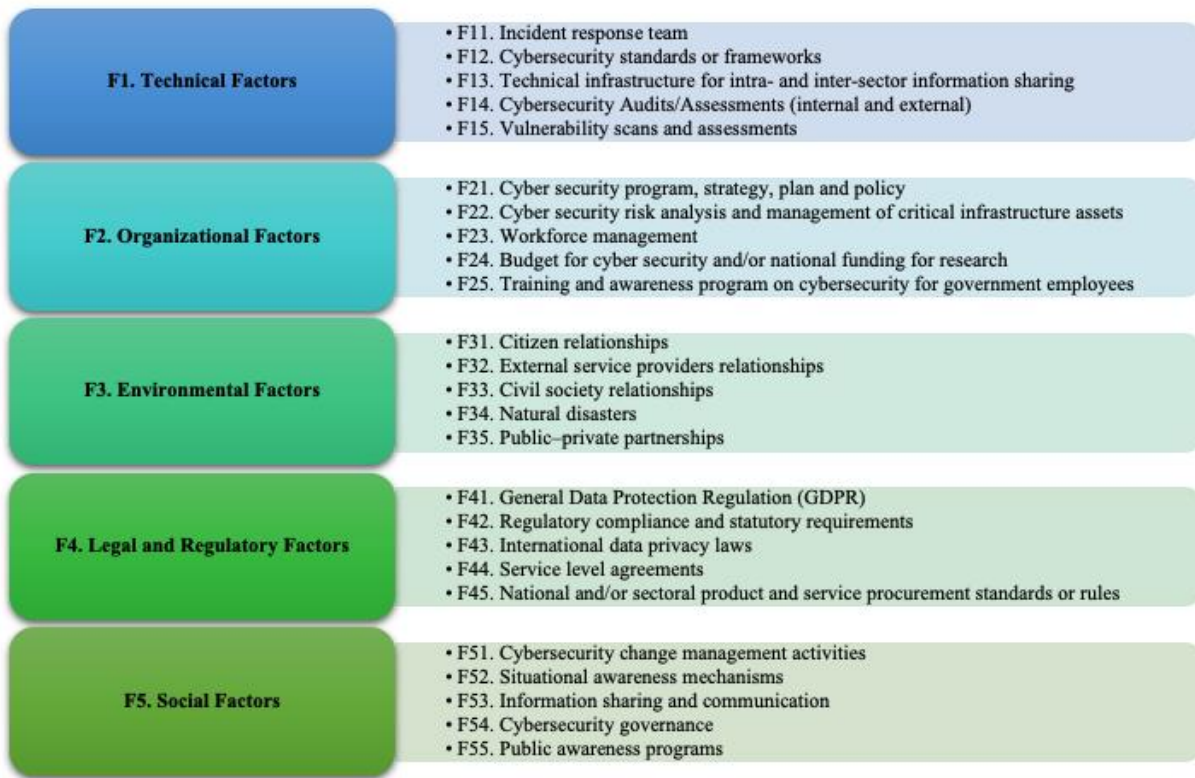


Figure 2 The factors in the proposed model Deloitte 2022 arabacak et al 20 P C 20 Tu et al 20 eoh et al 2022 ammani et al 20

Table The weights of the factors

Main Factors	Weights	Sub Factors	Local Weights	Weights	Ranking
F1	0.0	F11	0.20	0.04	2
		F12	0.040	0.00	24
		F13	0.20	0.023	
		F14	0.377	0.074	3
		F15	0.37	0.073	2
F2	0.0	F21	0.20	0.040	3
		F22	0.037	0.007	2
		F23	0.27	0.042	
		F24	0.302	0.0	
		F25	0.23	0.047	0
F3	0.23	F31	0.7	0.03	
		F32	0.044	0.00	23
		F33	0	0.037	4
		F34	0.27	0.0	
		F35	0.24	0.07	7
F4	0.307	F41	0.4	0.0	
		F42	0.2	0.02	
		F43	0.0	0.03	22
		F44	0.4	0.02	
		F45	0.0	0.02	20
F5	0.33	F51	0.7	0.03	
		F52	0.072	0.04	2
		F53	0.4	0.02	7
		F54	0.24	0.00	
		F55	0.33	0.0	4

The most important criterion is found as F4 General Data Protection Regulation GDPR the second important one is F3 Vulnerability scans and assessments and the third ranked criterion is F4 Cybersecurity Audits Assessments

In the second step the alternatives are assessed by using HFL VI OR method First experts evaluated the alternatives regarding factors by using the linguistic scale given in Table 2 Table 3 shows the evaluations made by the DMs Then by using Eqs 7-9 the steps of the HFL VI OR technique are applied Table 4 displays the ranking lists

Table 3 The assessment about alternatives

	F1	F2	F3	F4	F5
A1	At least very good	At least very good	At least very good	Between good and medium	Vg
A2	At most bad	Between bad and very bad	Between bad and very bad	At most bad	Between bad and very bad
A3	Between good and medium	Between medium and good	At most medium	At most bad	Between medium and good
A4	Between good and medium	At least very good	At least very good	Between good and medium	At least very good
A5	At least very good	At most medium	At most medium	Between good and medium	At least very good
A6	At least very good	At least very good	At least vg	Between good and medium	At least very good
A7	Between medium and good	At most medium	At most medium	Between bad and very bad	Between bad and very bad
A8	At most bad	Between good and medium	Between bad and very bad	At most bad	Between bad and very bad

Table 4 The result of HFL VI OR method

	$Q_i v 0$	Ranking	S_i	Ranking	R_i	Ranking
A1	0.4		3.23		3.02	
A2	0.4		3.00		3.02	
A3	0.20	3	3.2	3	3.00	3
A4	0.00		3.7		3.02	
A5	0.37	2	3.7	2	3.00	3
A6	0.72	4	3.072	4	3.02	
A7	0.000		3.27		3.00	3
A8	0.7	7	3.3	7	3.02	

C1. Acceptable advantage:

The condition $Q(a'') - Q(a') \geq DQ (**)$ is not satisfied $0.37 \geq 0.43$ here $DQ = 0.43$

C2. Acceptable stability in decision making:

Alternative a should also be the best ranked according to S and or R values A7 is the best alternative according to both Q and S values this condition is met

If condition C1 is unsatisfactory alternatives $a', a'', \dots, a(M)$ and $a(M)$ are determined by the relation for maximum M Therefore A7, A5 and A3 alternatives are included in the compromise solution

S SSO A O SOS

Rapid digitalization in advanced economies during COVID-19 has led to new cyber vulnerabilities McLennan Group 2022 In particular elements such as communication banking services public activities defense systems military systems and network systems have become the main target (Urtul, Eyveli 2022) As a result of rising threats and actual attacks critical infrastructure cyber resilience has become a key necessity of national security (Arabacak et al. 2020)

The aim of this study was addressing the security issues of institutions and to propose a cybersecurity strategy prioritization model that will guide institutions in their cybersecurity practices HFL AHP HFL VI OR methodology is used for the first time in this field At the end of the application the most important factor is found as F4 General Data Protection Regulation GDPR and the first ranked alternative is determined as A7 which is Integration of Cyber Security into National Security Cybersecurity is an integral part of national security In our high level national

security policies it is aimed to protect our country from hybrid threats including cyber elements and to increase deterrence T C Ula t rma ve Altyap Bakanl 2023

For future studies the interaction between the factors can be taken into account and the HFL ANP method can be applied Group decision making approach can be used Furthermore it is possible to improve work with advanced decision making techni ues

Ac le eme ts

This work has been supported by the Scientific Research Pro ects Commission of Galatasaray University under grant number FOA 202 0 and FOA 2023

thics mmittee A r val

N A

eer revie

Externally peer reviewed

Auth r tributi s

Conceptuali ation M G G B E M Investigation M G G B E M Material and Methodology G B M G E M Supervision G B Visuali ation M G G B E M riting Original Draft M G riting review Editing M G G B E M Other All authors have read and agreed to the published version of manuscript

lict terest

The authors have no conflicts of interest to declare

Fu i

This work has been supported by the Scientific Research Pro ects Commission of Galatasaray University

F S

- By k kan G G ler M 2020 Analysis of companies digital maturity by hesitant fu y linguistic MCDM methods Journal of Intelligent and Fu y Systems 3 32 https doi org 0 3233 IFS 7 473
- By k kan G G ler M 202 A combined hesitant fu y MCDM approach for supply chain analytics tool evaluation Applied Soft Computing 2 07 2
- Chou S Chang H Shen C 200 A fu y simple additive weighting system under group decision making for facility location selection with ob ective sub ective attributes European Journal of Operational Research 32 4 https doi org 0 0 e or 2007 0 00
- Deloitte 2022 Cybersecurity Strategy In Reimagining OT cybersecurity strategy
- Erdo an M ara an A aya Budak A olak M 2020 A fu y based MCDM methodology for risk evaluation of cyber security technologies Advances in Intelligent Systems and Computing 02 042 04 https doi org 0 007 7 3 030 237 23
- Ganin A A uach P Panwar M Collier A eisler M Marchese D Linkov I 2020 Multicriteria Decision Framework for Cybersecurity Risk Assessment and Management Risk Analysis 40 3 https doi org 0 RISA 2
- arabacak B ildirim S O Baykal N 20 A vulnerability driven cyber security maturity model for measuring national critical infrastructure protection preparedness International Journal of Critical Infrastructure Protection 47 https doi org 0 0 i cip 20 0 00
- ulak O ahraman C 200 Fu y multi attribute selection among transportation companies using axiomatic design and analytic hierarchy process Information Sciences 70 2 4 2 0
- umar R Pandey A Ba A Alhakami H Alhakami Agrawal A han R A 2020 Fu y based symmetrical multi criteria decision making procedure for evaluating the impact of harmful factors of healthcare information security Symmetry 2 4 https doi org 0 33 0 S M 2040 4
- urtul A eyvel M F nd Siber G venlik Raporu
- McLennan M Group S 2022 The Global Risks Report 2022 https www weforum org reports global risks report 2022
- P C 20 Cyber Risk Having better conversations on cyber PwC www pwc com sg risk assurance
- Rodr gue R M Martine L Herrera F 20 Hesitant fu y linguistic term sets for decision making IEEE Transactions on Fu y Systems 20 0
- Rodr gue R M Mart ne L Herrera F 20 3 A group decision making model dealing with comparative linguistic expressions based on hesitant fu y linguistic term sets Information Sciences 24 2 42



- T C Ula t rma ve Altyap Bakanl ın d Ulusal Siber G venlik Strate isi ve Eylem Plan 2020 2023
Torbacki 202 A hybrid mcdm model combining danp and promethee ii methods for the assessment of
cybersecurity in industry 4 0 Sustainability Swit erland 3 https doi org 0 33 0 su 3 33
- Tu C uan Archer N Connelly C E 20 Strategic value alignment for information security
management a critical success factor analysis Information and Computer Security 2 2 0 70
https doi org 0 0 ICS 0 20 7 0042
- eo h ang S Popovi A Chowdhury N H 2022 A systematic synthesis of critical success factors for
cybersecurity Computers and Security https doi org 0 0 cose 2022 02724
- ammani M Ra ali R Singh D 20 Factors contributing to the success of information security management
implementation International urnal of Advanced Computer Science and Applications 0 3 4 3
https doi org 0 4 I ACSA 20 0 0 3

Analysis and Comparison of Three Level Inverters

Eray Sabuncu¹, Ali Emir iliz¹

Abstract With the widespread use of renewable energy systems the design and features of the power equipment used in these systems are gaining importance day by day. In systems involving solar and wind energy we come across inverters that work synchronously with the grid for energy transfer to the electricity grid. In inverter topologies it is expected that the values that are critical for the network and important in terms of converter quality parameters such as harmonic distortion values, power factor and efficiency parameters are kept high or the quality standards are complied with. Therefore many different techniques and topologies are applied to correct for efficiency and other operating values. The reason for the use of topologies at high power values is that there are rooms of the level numbers and different switching techniques in the inverters. In particular the size of the level dimensions and the output harmonic values and the limitation of the filter limits used accordingly together with lower switching and reduction losses multilevel inverters provide many advantages both in terms of cost and performance. In this study diode clamped and active clamped T type structures in the three level topology which is frequently used as a multi level inverter are considered and their efficiency and performance values are compared.

Keywords Multi level Inverter, Three Level T Type Inverter, Three Level Diode Clamped Inverter, Vector Control, Total Harmonic Distortion

¹Address: Sogutlu University, Department of Electrical Engineering, Sogutlu, Turkey

* Corresponding author: berkaysabuncu0@gmail.com

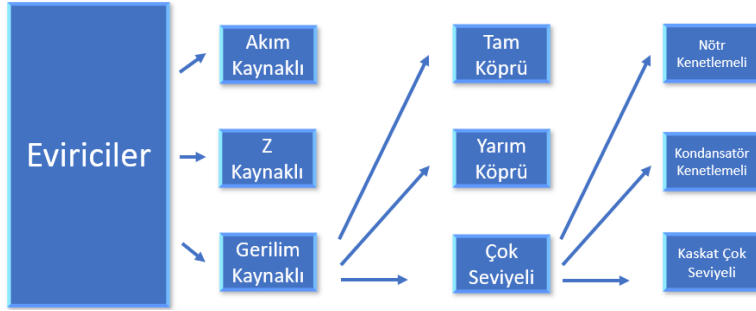
1

Genelde yeni enerji kaynakları üzerinde ara tirmalar yapmakta olup elimizde var olan enerji kaynakları ekonomik şekilde kalitesini artırarak kullanıya ulaştırılmaya çalışılmaktadır. Enerji ihtiyacının arttığı genelde yenilenebilir enerji sistemleri üzerine oldukça yoğun yatırımlar yapılmaktadır. Bu alanda rüzgar ve güneş enerjisi sistemlerine yapılan yatırımlar ve projeler ciddi önem taşımaktadır.

Yenilenebilir enerji sistemleri incelendiğinde sistemlerin normal şartlarda sürekli güç transferi yapması için yeterli güçleri nedeniyle enerji depolama sistemleri ve bunların ebekeye entegrasyonunu sağlayacak güç elektroniği ekipmanlarının tasarlanması gerekli görülmüştür. Depolama haricinde yenilenebilir enerji kaynağından elde edilen güç elektrik ebekeye aktarılabilmesi için de enerjinin uygun forma getirilmesi gerekmektedir. Bu amaçla ebekeye uygun formda alın ve standartlarda gerekli parametrelere uyan eviricilerin tasarlanması önemlidir.

1.1 Eviricilerin Sınıflandırılması

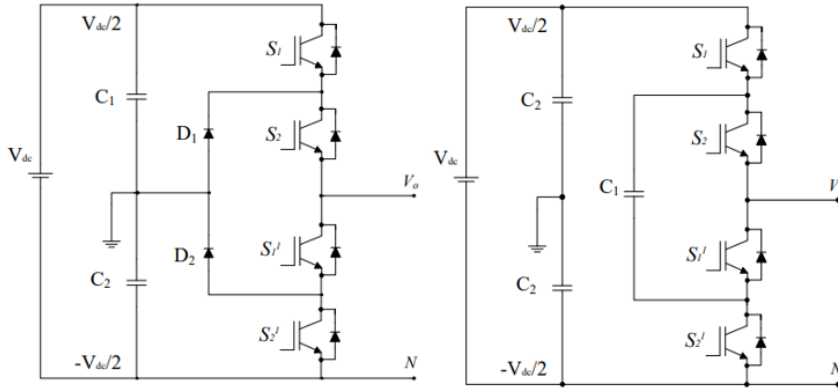
Eviriciler yapılarına göre incelendiğinde akım kaynağı, empedans kaynağı ve gerilim kaynağı olarak ayrılırlar. Akım kaynağı eviriciler genel olarak girişi DC akım kaynağına dayalı olarak çalıştırılmaktadır. Empedans kaynağı eviriciler girişi bir empedans grubunun bağlanması ile girişleri kontrol edilmektedir. Uygulamalar genel olarak incelendiğinde gerilim kaynağı eviricilerin yaygın olarak kullanılmaktadır. Gerilim kaynağı eviriciler DC girişlerinde kondansatör grubunun eklenmesiyle gerekli olan DC gerilimi kararlaştırılır.



Şekil 11.11 Gerilim Kaynaklı Evirici Topolojileri

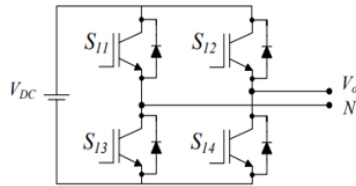
Çok Seviyeli Eviriciler

Çok seviyeli eviricilerin nötr noktası kenetlemeli, kondansatör kenetlemeli ve kaskat bağlı olmak üzere farklı tip topolojilerle geliştirilebilir. Çok seviyeli eviriciler özellikle yüksek verim ve yüksek güç transferi gerektiren uygulamalarda tercih edilmektedir. Diğer bilinen iki seviyeli topolojilere kıyasla gerilim seviyelerini daha yüksek seviyelerde tutarak çıkış geriliminin kalitesini arttırmakta ve kullanacak filtre elemanlarının da boyutlandırılmasında yarar sağlamaktadırlar.



a)

b)



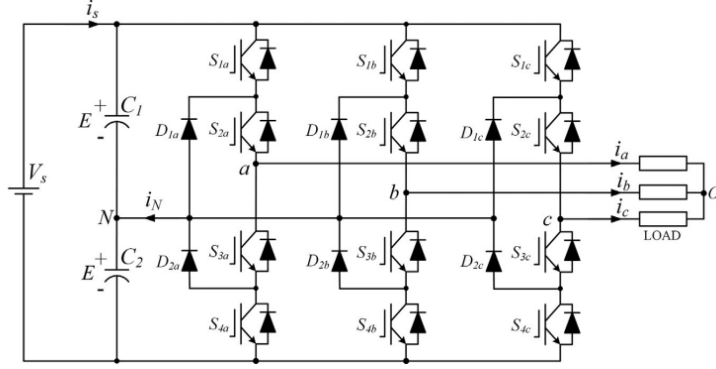
c)

Şekil 11.12 a) Diyot kenetlemeli Çok Seviyeli Evirici b) Kondansatör kenetlemeli Çok Seviyeli Evirici c) Kaskatlı Çok Seviyeli Evirici

Şekil 11.2'deki nötr noktası kenetlemeli eviriciler incelendiğinde giriş gerilimleri kondansatör gruplarıyla ikiye bölünmüş durumda. Anahtarların devreye girmesiyle $V_{dc}/2$, $V_{dc}/2$ ve 0 olmak üzere farklı gerilim düzeyleri oluşur.

1.2 Seviyeli Fazlı Tr Ke etlemeli Viriciler

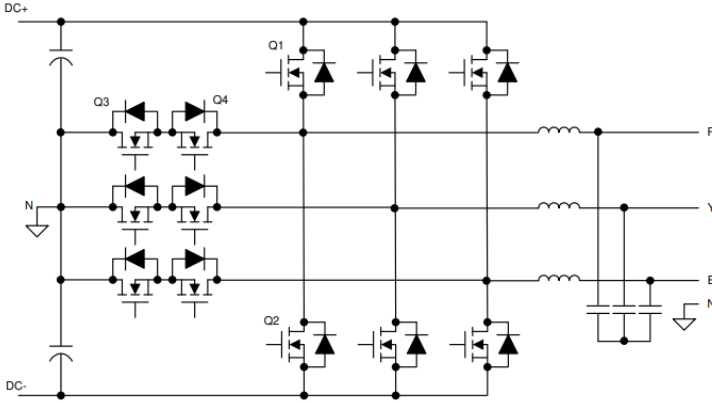
Resim 2 de seviyeli fazlı diyot kenetlemeli evirici topolojisi gösterilmiştir. Devrede her bir faz için bir faz diyot ve bir frekans diyot kullanılmaktadır. Evirici bloku üzerine uygulanacak DC gerilim kondansatörler ile bir frekans ortas noktası olarak alınmaktadır.



Resim 2.1 Seviyeli Fazlı Diyot Kenetlemeli Evirici

Topoloji incelendiğinde yüksek gerilim uygulamalarında kondansatör gerilimlerini pasif olarak dengelemek için kullanılan kenetleme diyotları hem maliyet açısından hem de kontrol tekniğinin getirdiği avantajlardan dolayı diyot kenetlemeli çok seviyeli eviricilerin kullanım alanlarının belli oranda sınırlanmaktadır. Bu nedenle diyot kenetlemeli çok seviyeli evirici topolojileri beş seviye ve üzeri uygulamalarda tercih edilmemektedir. Anahtarlama metodu temel frekansta kare dalga olarak uygulanabileceği gibi vektör kontrol gibi gelişmiş modülasyonların tercih edilmesi de bu topolojiye uygulanabilir.

T tipi kenetlemeli evirici topolojisi incelendiğinde diyot kenetlemeli yapıdan farklı olarak fazların nötr bağlantı noktalarıyla ters bağlantı anahtarları ile bağlantıdır. Bu nedenle kondansatörlerdeki gerilim dengesi için aktif kenetleme yardımıyla ciddi anlamda sağlanabilir.



Resim 2.2 Seviyeli Fazlı T Tipi Kenetlemeli Evirici

Topoloji incelendiğinde yüksek gerilim uygulamalarında kondansatör gerilimlerini aktif olarak dengelemek için kullanılan 3 ve 4 anahtarlar hem maliyet açısından hem de kontrol tekniğinin getirdiği avantajlardan dolayı T tipi kenetlemeli seviyeli evirici yüksek güç ve yüksek verim gerektiren uygulamalarda oldukça yaygın olarak tercih edilmektedir. Anahtarlama metodu temel frekansta kare dalga olarak uygulanabileceği gibi vektör kontrol gibi gelişmiş modülasyonların tercih edilmesi de bu topolojiye uygulanabilir.

Vektör kontrol uygulamasında kontrol sinyallerinin referans vektörüne göre gerekli birtakım işlemler sırasıyla

Referans Gerilim Vektörünün Genliğinin ve Amplitüdünün Hesaplanması

Vektör Diyagramında Sektör Belirleme

Sektöründe Bileşen Belirleme

Referans Sinyallerinin Belirlenmesi

Darbe Sinyallerinin Belirlenmesi

olup gerekli sinyaller oluşturulur Referans vektörünün genliği ve amplitüdü

$$V_a = V_m \cdot \sin \omega t \quad (1.3.1)$$

$$V_b = V_m \cdot \sin\left(\omega t - \frac{2\pi}{3}\right) \quad (1.3.2)$$

$$V_c = V_m \cdot \sin\left(\omega t + \frac{2\pi}{3}\right) \quad (1.3.3)$$

$$\begin{bmatrix} V_d \\ V_q \end{bmatrix} = \frac{2}{3} \times \begin{bmatrix} 1 & -1/2 & -1/2 \\ 0 & \sqrt{3}/2 & -\sqrt{3}/2 \end{bmatrix} \times \begin{bmatrix} V_a \\ V_b \\ V_c \end{bmatrix} \quad (1.3.4)$$

$$V_{ref} = V_d + i \cdot V_q = \frac{2}{3} * (V_a + a \cdot V_b + a^2 \cdot V_c) \quad (1.3.5)$$

$$|V_{ref}| = \sqrt{V_d^2 + V_q^2} \quad (1.3.6)$$

$$\theta = \tan^{-1}\left(\frac{V_q}{V_d}\right) \quad (1.3.7)$$

olacak şekilde hesaplanır Belirlenen açı değeri ile referans vektörünün konumu

Her açı $0 \leq \theta < 60^\circ$ ise referans vektör A sektöründedir

Her açı $60 \leq \theta < 120^\circ$ ise referans vektör B sektöründedir

Her açı $120 \leq \theta < 180^\circ$ ise referans vektör C sektöründedir

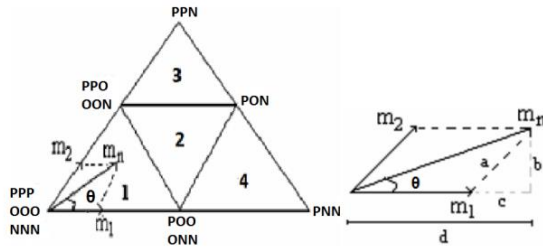
Her açı $180 \leq \theta < 240^\circ$ ise referans vektör D sektöründedir

Her açı $240 \leq \theta < 300^\circ$ ise referans vektör E sektöründedir

Her açı $300 \leq \theta < 360^\circ$ ise referans vektör F sektöründedir

durumlar kontrol edilerek belirlenir

Referans vektörünün belirlenmiş sektörün hangi bileşeninde olduğunu belirlemek için



e il 1 3 3 A Sekt r nde Belirtilmi Referans Vekt r ve Sekt r erindeki B lgeler

$$a = m_2 = \frac{b}{\sin\left(\frac{\pi}{3}\right)} = \frac{2 \cdot b}{\sqrt{3}} = \frac{2}{\sqrt{3}} \cdot m_n \cdot \sin\theta \quad (1.3.8)$$

$$m_1 = m_n \cos\theta - \left(\frac{2}{\sqrt{3}} \cdot m_n \cdot \sin\theta\right) \cdot \cos\left(\frac{\pi}{3}\right) \quad (1.3.9)$$

$$m_1 = m_n \cdot \left(\cos\theta - \frac{\sin\theta}{\sqrt{3}}\right) \quad (1.3.10)$$

E er m_2 ve $m_1 + m_2 < 0,5$ ise referans vekt r b lgededir

E er $m_1 > 0,5$ ise referans vekt r 4 b lgededir

E er $m_2 > 0,5$ ise referans vekt r 3 b lgededir

E er m_1 ve $m_2 > 0,5$ ve $m_1 + m_2 > 0,5$ ise referans vekt r 2 b lgededir

Sekt r ve b lge belirlemelerinin yap lmas n n ard ndan konumu belirlenmi referans vekt r n n konum s releri T_a T_b ve T_c s releri

$$V_{ref} \cdot T_s = V_1 \cdot T_a + V_8 \cdot T_b + V_2 \cdot T_c \quad (1.3.10)$$

$$T_s = T_a + T_b + T_c \quad (1.3.11)$$

$$T_a = T_s - 2K \sin(\theta) \quad (1.3.12)$$

$$T_b = 2K \sin\left(\frac{\pi}{3} + \theta\right) - T_s \quad (1.3.13)$$

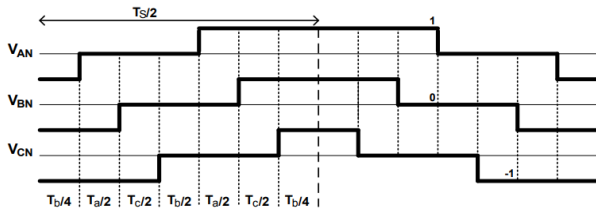
$$T_c = T_s - 2K \sin\left(\frac{\pi}{3} - \theta\right) \quad (1.3.14)$$

$$K = \left(\frac{4\sqrt{3}}{3}\right) (m_a \cdot T_s) \quad (1.3.15)$$

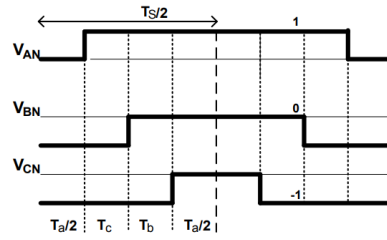
$$m_a = \left(\sqrt{3} \frac{V_{ref}}{V_{dc}}\right) \quad 0 \leq m_a \leq 1 \quad m_a: \text{modülasyon indeksi} \quad (1.3.16)$$

olarak belirlenir

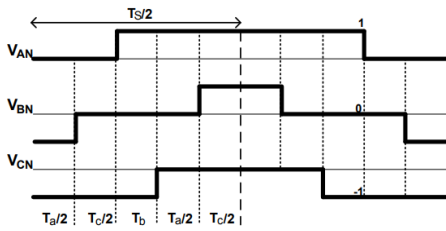
Sonu olarak uygulanan bu matematiksel algoritma sonucu A sekt r erindeki b lgelerde olu turulan anahtarlama i aretleri ekil 3 4 teki gibidir



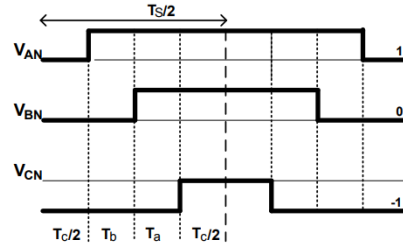
a Sekt r A B lge 1



b Sekt r A B lge 4



b Sekt r A B lge 2

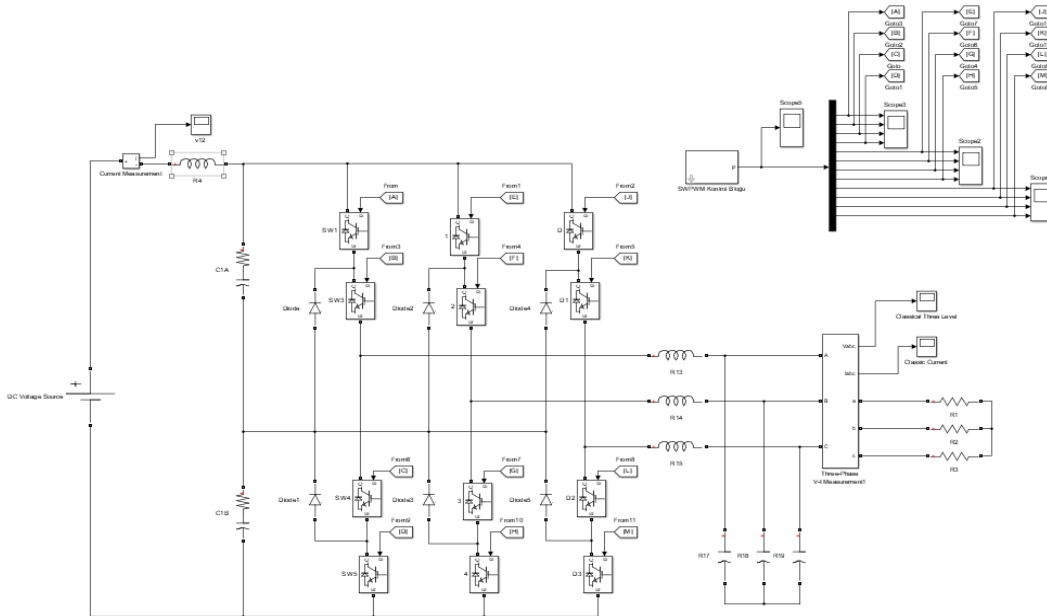


d Sekt r A B lge 3

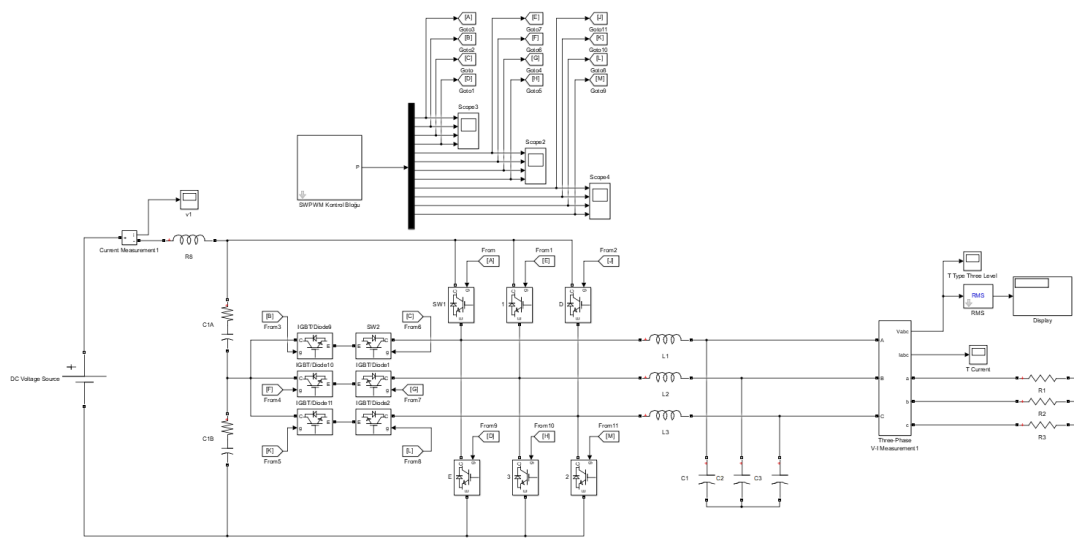
e il 13 Sekt r A Referans Vekt r n n B lgelere G re Anahtarlama Durumu

2 A A O

Bu al mada seviyeli eviricilerin en s k kullan lan iki topo lo si olan diyot kenetlemeli ve T tipi kenetlemeli evirici topo lo leri vekt r kontrol metoduyla ele al nm tr Ele al nan sistemler Matlab Simulink ortam nda sim le edilerek sonu lar ayr ayr incelenmi tir Giri b l m nde ele al nan seviyeli eviriciler i in vekt r kontrol metodu bu sim lasyonda uygulanm tr Ele al nan iki evirici modelinin Simulink erindeki modellenmesi ekil 2 ve ekil 2.2 de g sterilmi tir

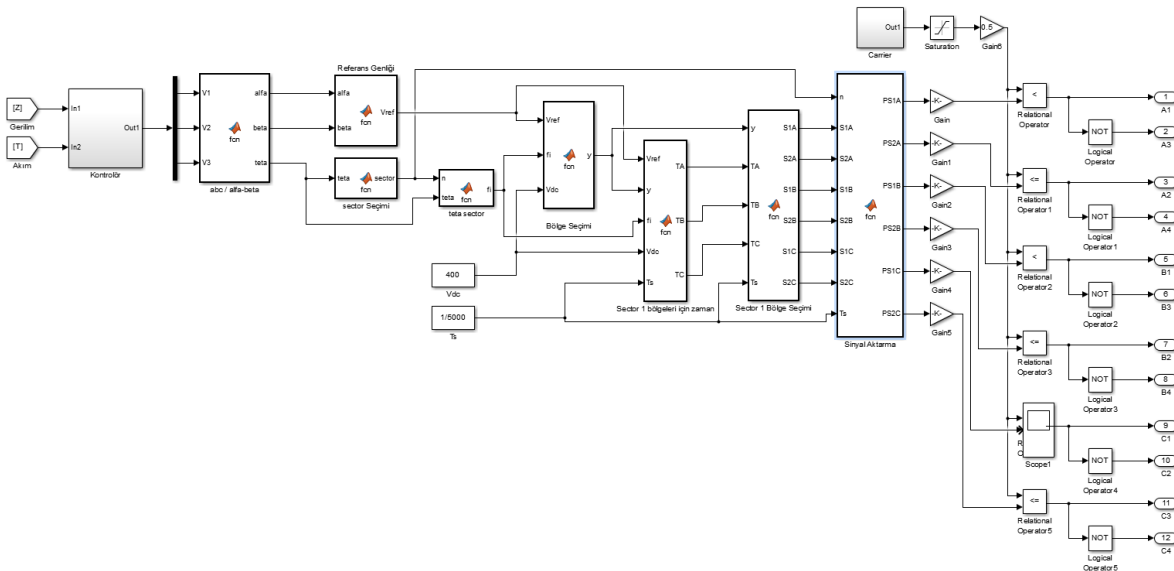


e il 2.1 Diyot kenetlemeli Evirici Simulink Modellemesi



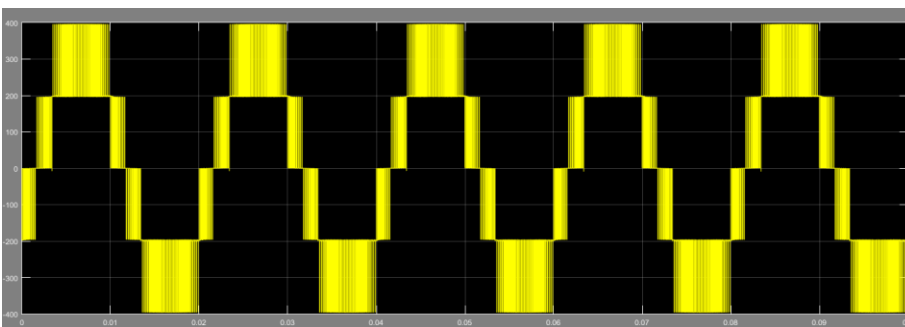
Şekil 2.2 T Tipi Evirici Simulink Modellemesi

Sistemlerde kullanılan anahtarlama elemanları ortak olup vektör kontrol tabanlıdır. Giriş bölümünde belirtilen adlarla uygulanması Şekil 2.3'de belirtilen kontrol bloğu oluşturulmuştur.



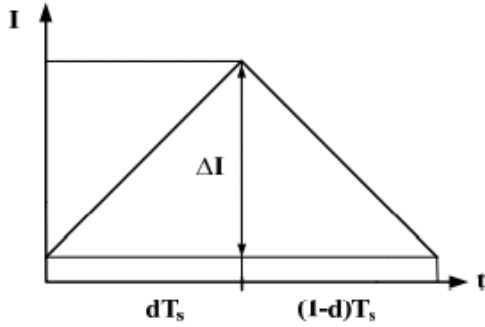
Şekil 2.3 Seviyeli Evirici için Vektör Kontrol Bloğu ve Sinyaller

Eviricilerin çıkış filtreleri uygulanmayıp kontrol bloğunun alınmasıyla çıkışta elde edilen faz-faz gerilim dalgaları Şekil 2.4'teki gibidir.



Şekil 2. Evirici Kontrol Bloğunun Oluşturulmuş Faz-Faz Gerilimi

bu formunda uygulanması için evirici simülasyonunda LC filtre boyutlandırılması için LC filtre boyutlandırılabilirken evirici çıkış akım dalgaları referans alınarak boyutlandırılabilir. L değerinin saptanması için endüksiyon denklemini kullanarak akım dalgalarına bağlı olarak elde edilmiştir.



Şekil 2 Evirici Çıkış Akım Dalgaları

$$V_L = L_f \left(\frac{\Delta I}{\Delta T} \right) \quad (2.1)$$

Anahtarlama durumuna bağlı olarak endüksiyon geriliminde denklemler 2.2 ve denklemler 2.3 ifadelerinde belirtilen gerilim değerleri olacaktır.

$$L_f \left(\frac{\Delta I}{dT_s} \right) = \frac{V_{DA}}{2} \quad (2.2)$$

$$L_f \left(\frac{\Delta I}{(1-d)T_s} \right) = 0 \quad (2.3)$$

Bu iki denklemin ortak çözümlerine bağlı olarak akım dalgalanmasına bağlı endüksiyon ifadesi denklemler 2.4 teki gibidir. Burada f_s anahtarlama frekansı, V_{DA} DC bara gerilimi ve d anahtarlama doluluk oranıdır.

$$\Delta I = \left(\frac{V_{DA}}{2L_f f_s} \right) d(1-d) \quad (2.4)$$

Denklemler 2.4 ve Şekil 2 dikkate alınarak endüksiyonun sıfır olması durumunda akım dalgalarının ifadesinin maksimum değere ulaşacağı noktada maksimum akım dalgaları ifadesi denklemler 2.5 teki gibidir. Denklemler 2.2 te V_{DA} DC bara gerilimi, f_s anahtarlama frekansı ve L_f ise hesaplanacak endüksiyon değeri olacaktır.

$$\Delta I = \left(\frac{V_{DA}}{8L_f f_s} \right) \quad (2.5)$$

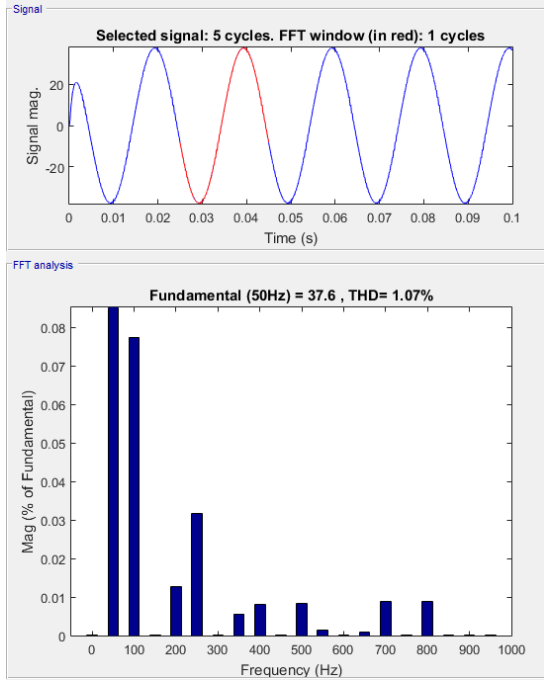
Belirlenecek akım dalgalarına bağlı olarak endüksiyon değeri hesaplanabilir. C değerinin belirlenmesinde LC filtre bloğunun anahtarlama frekansında filtreleme yapmasını sağlamak için belirlenen L değeri kullanarak denklemler 2.6'ya göre C değeri hesaplanabilir.

$$f_r = \left(\frac{1}{2\pi\sqrt{LC}} \right) \quad (2.6)$$

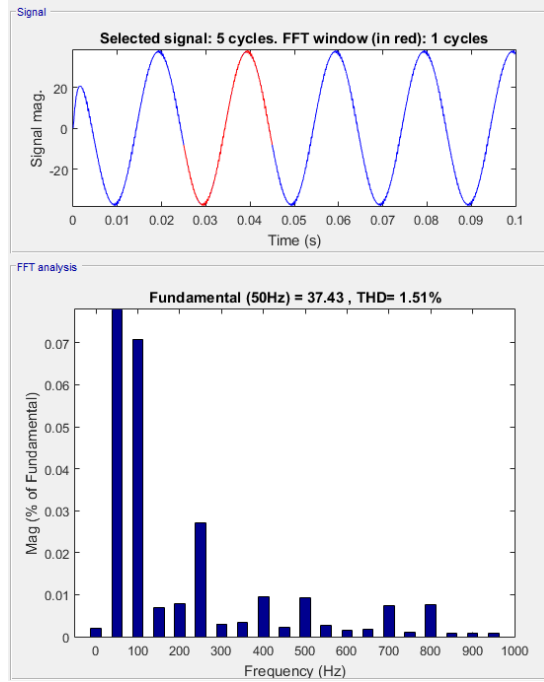
3 A

3.1 Fazlı Seviyeli İki ve İki Keçitli Keçitli Evirici Simülasyonları

Ekil 2 ve ekil 2.2 de gösterilmekte olan evirici simülasyonlarında her iki topolojide de 2 kHz frekansına göre seçilmiş ve 3mH ve 2uF değerlerinde L ve C filtre elemanları kullanılarak 0V DC giriş gerilimi uygulanmakta olup evirici çıkışında 3 0V AC fazla gerilimi elde edilmektedir. Kullanılan bu değerler ile simülasyon yapıldığında ekil 3 de gösterilmekte olan çıkış harmonik bozunum değerleri görülmektedir.



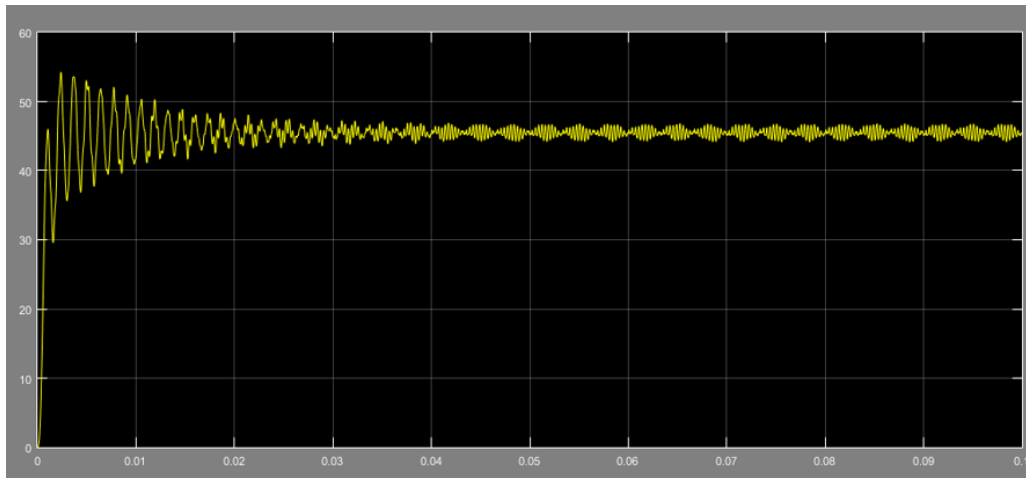
a Diyot keçitli Evirici



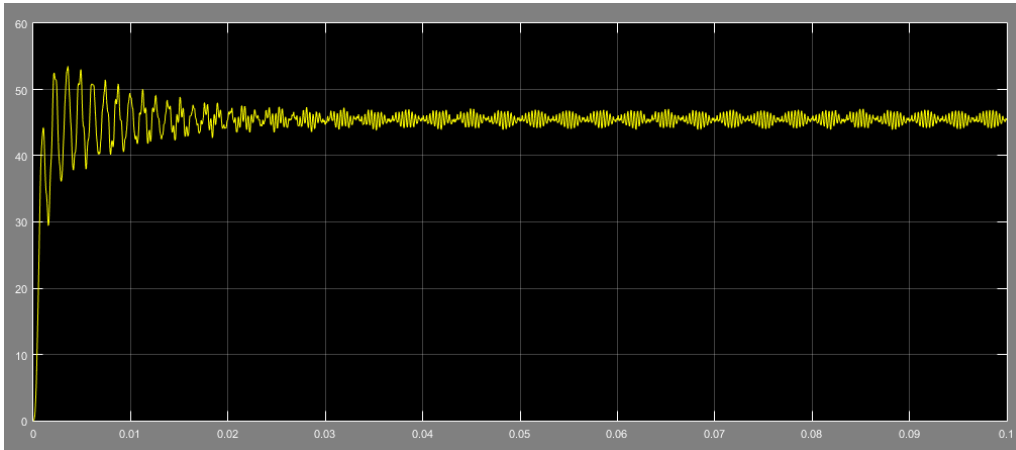
b T Tipi keçitli Evirici

ekil 3.1 Evirici Çıkış Gerilimi Harmonik Bozunum Değerleri

Simülasyon sonuçları 0V DC giriş gerilimi için çıkış harmonik bozunumundan incelendiğinde ekil 3.2 ve ekil 3.3 deki sonuçlar elde edilmektedir.



ekil 3.2 Diyot keçitli Eviricide Giriş Akım Formu ve Çıkış Akım Değeri 4 A



Şekil 3.3 T Tipi Üç Fazlı Eviricide Giriş Akımı Formu ve Amplitud Değeri 44 A

A A SO A

Bu çalışmada evirici uygulamalarında sık kullanılan üç seviyeli topolojilerden T tipi kenetlemeli evirici ve diyot kenetlemeli evirici yapıları ele alınmıştır. Üç seviyeye uyarlanmış vektör kontrol algoritması ve matematiksel modellemesi incelenmiştir.

Vektör kontrolün üç seviyeli topolojilerde kullanılmasıyla modülasyon aralıkları skaler kontrol yöntemlerine göre daha fazla genişlik kazanmış ve özellikle motor kontrol uygulamalarında moment kontrolü daha etkili bir şekilde yapılabilmektedir. Bununla birlikte kontrol tek bir referans vektöründen yapıldığından kontrol değişkenleri alt lüpe sistemin donanım gerektirmesi daha ilgisiz hale getirilebilir.

Vektör kontrol uygulamasının üç seviyeli T tipi evirici ve diyot kenetlemeli evirici yapıları uygulanmasıyla elde edilen verim ve harmonik bozunum değerleri simülasyon ortamında analiz edilmiştir. Sonuçlara bakıldığında çıkış harmonik bozunumu bakımından diyot kenetlemeli evirici 2 kV'lık uygulamada yaklaşık 0.1 degerinde T tipi kenetlemeli eviriciye göre avantajlıdır. Fakat topolojilerin verimleri karşılaştırıldığında T tipi vericinin aktif kenetleme avantajı nedeniyle DC girişten diyot kenetlemeli yapıya göre daha yüksek etkinliği görülmüştür.

Evirici uygulamalarının topoloji seçimlerinde verim ve harmonik bozunum değerlerinin sistem açısından nemi iyice araştırıldıktan sonra uygun topolojilerin kullanılması gerekmektedir.

KA AK A

Bilhan A. B. İnce ve Sektör Tespitinde Kullanılan Üç Fazlı Vektör Darbe Geniçlik Modülasyon Kontrolü. Yüksek Lisans Tezi, İstanbul Kültür Enstitüsü, İstanbul, 2022.

Canver M. Design And Implementation Of A Three Phase Grid Connected Sic Solar Inverter. Yüksek Lisans Tezi, Middle East Technical University, Ankara, 2020.

Das S. Narayanan G. Novel switching sequences for a space vector modulated three level inverter. Industrial Electronics IEEE Transactions on, 2002, 3(4): 477-484.

İçkol E. İncebalcı R. Bayındır. Review of multilevel voltage source inverter topologies and control schemes. Energy Conversion and Management, 2020, 204: 115422.

İncebalcı E. Üç Fazlı Yüksek Verimli Üç Seviyeli T Tipi Evirici İçin Bir SDGM Tekniğinin Geliştirilmesi. İstanbul Kültür Enstitüsü, İstanbul, 2020.

İncebalcı E. Üç Seviyeli Eviriciler İçin Yeni Bir SDGM Tekniğinin Geliştirilmesi. İstanbul Kültür Enstitüsü, İstanbul, 2020.

İncebalcı E. Üç Seviyeli Enerji Sistemleri İçin Üç Seviyeli Bir Eviricinin Geliştirilmesi. İstanbul Kültür Enstitüsü, İstanbul, 2020.

The Effect of Titanium and Boron on the Structure and Properties of the Al-Si Alloys

Milica Laticinić¹, Sara Kvačević²

Abstract Al-0.3 wt% Si and Al-2.3 wt% Si alloys were modified with Al-Ti-B master alloy. The effect of the added Al-Ti-B on the microstructure and mechanical properties of the Al-Si alloys were investigated using an optical microscope and a hardness measurement. The results show that the size of the primary Si decreased with the titanium addition. It is of great importance to improve the mechanical properties of the Al-Si alloys by refining the primary Si. The mechanical properties of the alloy were improved after modification.

Keywords Al-Si alloys, microstructure, properties

¹Address: University of Montenegro, Faculty of Metallurgy and Technology, Cetinski put bb 000 Podgorica, Montenegro

²Address: Central School of Chemical Technology, Spasoje Raspopovića 000 Podgorica, Montenegro

*Corresponding author: biljana.ucg@ucg.me

1. INTRODUCTION

Grain refinement is achieved in aluminium alloys by inoculating the molten metal with small amounts of titanium and boron. The refined grain size depends on the Ti content, Ti/B ratio and the matrix alloy composition. Although the exact grain refining mechanism is still being debated, the high melting point intermetallic phases TiAl₃ and TiB₂ present in these master alloys are thought to have an important role to play.

Grain refinement in Al-Si casting alloys improves the mass feeding characteristics during solidification, resulting in reduced shrinkage, porosity and the promotion of smaller and improved porosity dispersion. Also, a fine grain size creates a more uniform distribution of secondary intermetallic phases in addition to pores which form from the evolution of dissolved gas in the melt. Agarwal [20]

2. MATERIALS AND METHODS

Experimental work can be divided in two phases. The first phase comprises melting and casting of six alloys of composition Al-0.3 wt% Si and Al-2.3 wt% Si. The solidification structure was modified by the addition of the Al-Ti-B master alloy to give alloys containing 0.0, 0.1, 0.2 titanium. The alloys were melted in an induction furnace at 900°C. After the alloying step, degassing was performed for 30 minutes. The second phase includes characterization of cast samples with optical microscope.

Chemical composition of the Al-Si alloys used in this study is shown in Table 1. Properties of the materials have been investigated, e.g., hardness has been measured by use of the Brinell method.

Table 1 Chemical composition of the investigated alloys in wt%

TYPICAL SAMPLE	Fe	Si	Ti	Cu	Mn	V	Cr	Mn	Mg	Sr
Al-0.3 wt% Si	0.0 Ti	0.20	0.3	0.00	0.003	0.04	0.002	0.000	0.002	0.000
	0.1 Ti	0	0.34	0.2	0.003	0.047	0.002	0.000	0.002	0.000
	0.2 Ti	0	0.3	0.24	0.003	0.04	0.002	0.000	0.002	0.000
Al-2.3 wt% Si	0.0 Ti	0.2	2.3	0.007	0.004	0.03	0.004	0.000	0.002	0.000
	0.1 Ti	0	2.2	0.04	0.004	0.03	0.004	0.000	0.002	0.000
	0.2 Ti	0	2.2	0.240	0.004	0.040	0.004	0.002	0.002	0.000

3 S S

Figure shows the as cast microstructure of an Al 2.3wt % Si unmodified alloy. Figures 2, 3 and 4 show images taken with the Ti modified samples of Al 2.3wt % Si.

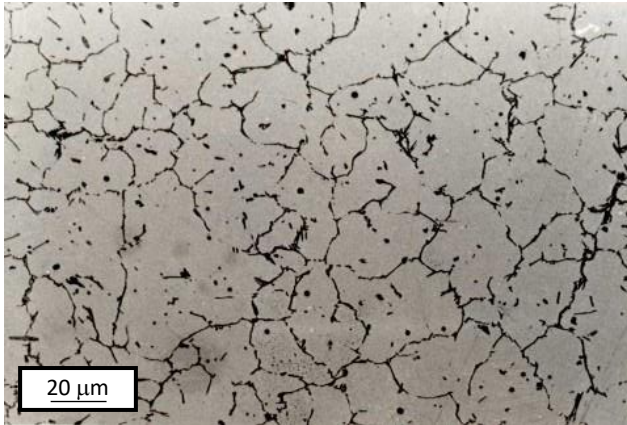


Figure 1 Microstructure of Al 2.3wt % Si unmodified alloy

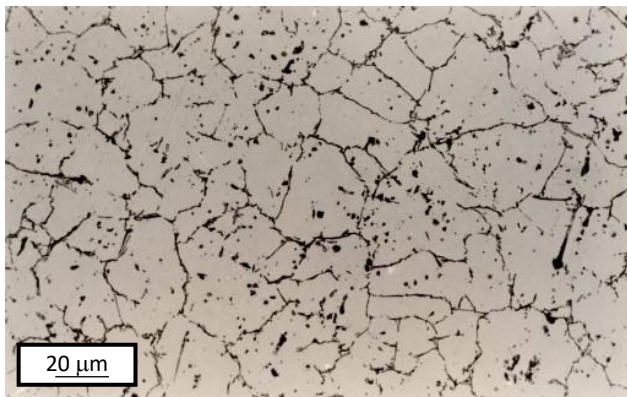


Figure 2 Microstructure of Al 2.3wt % Si 0.0 wt % Ti alloy

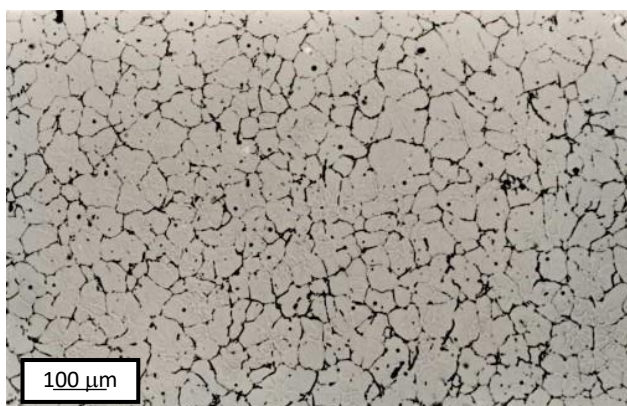


Figure 3 Microstructure of Al 2.3wt % Si 0 wt % Ti alloy

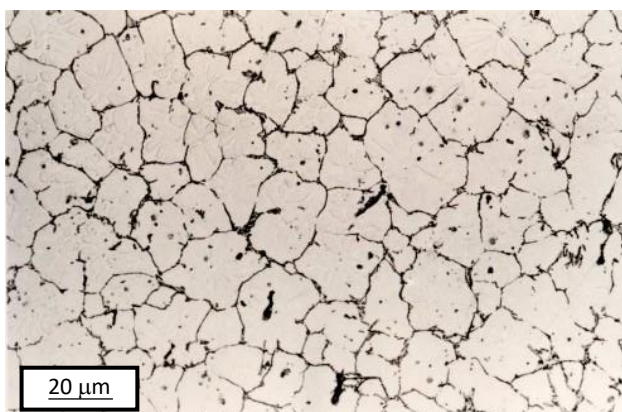


Figure Microstructure of Al 2.3wt Si 0.2wt Ti alloy

We have also examined the properties of these materials hardness measurement. The hardness of the modified alloy is higher than the hardness of the alloy without any modification treatment. Table 2

Table 2 Hardness of the investigated alloys

TYPE OF SAMPLE		HB _{average}
Al 0.3 wt Si	0.0 Ti	3
	0 Ti	3
	0.2 Ti	32
Al 2.3wt Si	0.0 Ti	34
	0 Ti	37
	0.2 Ti	3

S S O A O S O S

Grain refinement of castings is way to control the microstructure. Grain refinement of aluminum alloys has been used commercially and it has been a main feature in the control of quality products manufactured from aluminum alloys. Grain refinement of Al Si casting alloys is commonly assessed by the presence of Ti and B in the melt. The binary Al Si phase diagram is based on the study by Murray and McAlister [4]. The eutectic reaction occurs at 2 wt Si and 77°C. Additions of certain elements to aluminum alloys melts can provide nuclei for grain growth. Titanium has a nucleating effect and is the most commonly used grain refiner. The addition of boron together with titanium produces finer grains. Experimentation on Al Si alloys has show the importance of boron in Al Ti B master alloy. Ratio Ti B is important. Various theories have emerged from this practice and the exact mechanism of grain size reduction is still in dispute. The mechanical properties of the Al Si alloys were improved after modification. Chen and Wu [20]. It is also important to appreciate that the effects of grain refinement in aluminum castings can be further enhanced when varying other production parameters such as pouring temperature, cooling rate, silicon morphology and heat treatments.

F S

Agarwal S [20]. Grain refinement in Al Si alloys. International Journal of Recent Advances in Engineering and Technology. 33 (3)

Murray L, McAlister A [4]. The Al Si Aluminum Silicon system. Bull Alloy Phase Diagrams. 74 (4)

Chen R, Wu [20]. Modeling of aluminum silicon irregular eutectic growth by cellular automaton model. Research and Development. 34 (22)

Optimization of the leaching process of magnesium and iron from chromium ore processing tailings by different acid solutions

Huseyin Azizci*¹

Abstract The present study aimed to determine the optimum operational conditions for leaching of magnesium (Mg) and iron (Fe) from chromium ore processing tailings which was rich in terms of Mg, Fe and Si content by different acid solutions. For this purpose, different leaching reactants including nitric (HNO₃), sulphuric (H₂SO₄) and ortho phosphoric (H₃PO₄) acid solutions were used to investigate the effect of varying acid concentrations (0.4-0.8 molar M), reaction times (20-120 min), material dosages (3-15 g/L) and temperatures (20-50 °C) on the leaching efficiency. To determine the leaching performance of the acid solutions under the investigated operational conditions, residual concentrations of Mg and Fe as well as nickel (Ni), aluminum (Al), chromium (Cr) and silicon (Si) were measured in the obtained leachates by inductively coupled plasma optical emission spectrometry (ICP-OES). Experimental results showed that the optimum concentration of HNO₃, H₂SO₄ and H₃PO₄ was found to be 0.4, 0.4 and 0.4 M respectively. An acid concentration higher than the given optimum values did not cause any remarkable increase in the leaching efficiency of Mg and Fe. Similarly, an increase in the material dosage up to 15 g/L did not cause any decrease in the leaching efficiency of Mg and Fe. However, the leaching efficiency of Mg and Fe as well as Al, Ni and Cr significantly increased with the increasing reaction time and temperature. The optimum values for the reaction time and temperature were found to be 60 min and 50 °C for each of the acid solutions used. Under the optimized conditions, the leaching efficiencies using HNO₃ and H₃PO₄ were maximized at values of 22% and 30% for Mg and 4% and 14% for Fe respectively, while over 90% of the initial Mg and Fe content of the material (0.30 and 0.20 mg/L) respectively could be leached with H₂SO₄. At the same time, the highest leaching efficiency for Al, Ni, Cr and Si was determined to be 100% with H₂SO₄, 100% with H₂SO₄, 70% with H₃PO₄ and 44.2% with HNO₃ respectively.

Keywords Tailings leaching, magnesium, iron, acid solution

¹Address: Isparta University of Applied Sciences, Vocational School of Aksu Mehmet Seyya Demiraslan, Department of Environmental Protection Technologies, 32000 Isparta, Turkey

*Corresponding author: huseyinyazici@isparta.edu.tr

1. INTRODUCTION

Expansion of industrial applications with the improved technologies and rapid increase in the generation of waste materials together with the ever-growing global population has created a motivation for research and development activities on waste recycling issues. Erst et al. (2023). Among the wastes, metal finishing industry waste, medical waste, spent petroleum catalysts, fly ash, battery wastes, and electronic scraps have been shown some of the largest industrially generated wastes (rishnan et al. 2022). Beside these wastes, mining wastes pose a huge threat to the environment (lvare et al. 2022) since a huge amount of waste material is created due to the long-term mining and metallurgical activities (an et al. 2022). It is estimated that the worldwide production of solid waste from the primary production of mineral and metallic raw materials is over 100 billion tons per year (de Palacios and Rodrigue, 2022).

Mining wastes refer to a broad group of waste materials that are originated from extracting the ground and processing the mineral sources to varying stages during the ore processing and enrichment phases (BRGM, 2000). These materials have low or no economic value since they are considered as unusable mineralized materials and hence are stored or discarded rather than processed (Hitch et al., 2010). Usually, mining wastes are in the form of fine suspended materials (0.075 mm) including dissolved metals and reagents, chemicals, and inorganic and organic additives (Araujo et al., 2022). Typically, these wastes are classified as waste rocks, processing waste, and tailings (Bellenfant et al., 2013; Carmo et al., 2020) which can be present in the form of solid, liquid, and gaseous depending on the physical form of residues (Araujo et al., 2022).

Disposal options of mining wastes include underground backfilling, submarine tailing disposal, regeneration of ground vegetation, producing glass or fertilizer, and utilization as construction materials for roads, dams, and wall bricks (Lu and Cai, 2012). Because transportation of the waste to another site is not economically viable, mining wastes are

commonly deposited in large man made embankments referred to as tailings dams near mining production site Araujo et al 2022 However if these wastes are not managed properly significant pollutions can occur both through air pathways dust and gas emissions and water leaching acid mine drainage L bre and Corder 20 Furthermore failure to manage can result in high cost re uiring catastrophic consequences Up to now several environmental problems as well as multiple human risks have been originated due to the failures in tailings dam storage Ivare et al 2022 Recent events such as the Los Frailes tailings dam failure in Spain and the Brumadinho tailings dam failure in Bra il 20 have resulted in heightening attention of the industry and society to the catastrophic impacts of mining wastes Tayebi horami et al 20 Although tailings pose several environment risks as stated above some extractive mining wastes still contain valuable and or critical metals Ivare et al 2022 However the composition of mining waste remains largely unknown since mining companies generally do not monitor the waste they generate This prevents opportunities for extracting further material from it or even reducing its generation which add value for a better disposal option of the waste However an alternative waste management oriented towards resource recovery could potentially mitigate environmental impacts L bre and Corder 20 At this point an evaluation of waste materials for the recovery of their metal values together with stabili ation of toxic elements present in them by proper waste management strategies for environmental safety has been considered as the driving force for research and development activities Er st et al 2023 Nevertheless the drive for most mining operations is to reduce the costs associated with the development of processes and procedures that have to be put in place to make sure that the tailings discharged meet the re uired environmental standards Ndlovu et al 20 7

Reprocessing of tailings ensures benefits on the transforming a linear economy into a circular economy and therefore reducing the dependence on reserve extraction an et al 2022 Therefore related to the circular economy strategy some of these wastes have been considered as secondary source of raw materials in recent years Ivare et al 2022 Various metal recovery processes involve physical chemical and thermal characteristics of waste streams and target metals for separation and extraction rishnan et al 202 It is well known that hydrometallurgy is one of the most efficient technologies to recover valuable metals from low grade ores and wastes Ivare et al 2022 Atmospheric acid leaching refers to hydrometallurgical processes that utilize non pressurized stirred reactor applications with temperatures 00 C URL 20 Typical steps involved in this process are leaching concentration purification and recovery rishnan et al 202 Using this process several research efforts have been put into recovering heavy metals and rare earth elements from different wastes such as printed circuit boards Oliveira et al 200 ha et al 20 0 electrical and electronic e uipment Marra et al 20 and fly ashes from municipal solid waste incineration eibel et al 202

As one of the mined metals chromium and its compounds find their widespread applications in the field of metallurgy foundry and tanning and they use in dyes and pigments wood preservatives catalysis and interconnectors for solid oxide fuel cells Lunk 20 The global mine production of the transition metal chromium has been accounted for a gross weight of 4 0 tons in 2022 URL 2 2023 and its leading producers have been reported as South Africa India a akhstan and Turkey Coet ee et al 2020 During enrichment of chromium related ores a considerable amount of fine si ed processing tailings is produced Tailings generated from the processing plant is generally dumped and therefore causes space and environmental concerns umar et al 202 Because tailings are not recycled or re used and due to their potential to release Cr they belong to the third ha ardous group of waste generated by chromite mining Bola os Ben te et al 20

Motivated by these concepts the main objective of the present study was to determine the optimum operational conditions for leaching of Mg and Fe from chromium ore processing tailings by different leaching solutions For this purpose different leaching reactants including HNO_3 H_2SO_4 and H_3PO_4 were used to investigate the effect of acid concentration reaction time material dosage and temperature on the leaching efficiency

2 A A A HO

2 1 aterials

All chemicals used in the experiments were of analytical grade and were used without further purification All solutions were prepared with distilled water HNO_3 H_2SO_4 and H_3PO_4 solutions were obtained from Merck Germany The input material chromium ore processing tailings used in experiments was collected from a tailing dam at a chrome mine in Deni li T rkiye The main composition of the input material was represented in Table Before use in experiments the material was powdered using a grinder at 2 000 rpm for min and then dried in an oven at 0 C for 24 h The obtained material was stored in a desiccator until further use

Table 1 Chemical composition of the chromium ore processing tailings

Compound	wt	Compound	wt
MgO	43	Al ₂ O ₃	0.4
SiO ₂	3.3	Cr ₂ O ₃	0
Fe ₂ O ₃	7.43	NiO	0.3
CaO	0.33	Loss of Ignition	

2.2 Leaching procedure

Leaching experiments were performed by adding a known weight of the powdered material into 100 mL of acid solutions HNO₃, H₂SO₄ and H₃PO₄ that were prepared for a desired molar concentration. The prepared suspension was placed on an analogue hotplate stirrer with temperature controller (Mestir MSH 20D, Daihan Scientific Co., Korea) and was mixed in three-neck round bottom flask under reflux condition at a constant agitation speed of 400 rpm. To determine the optimum operational conditions of the leaching process, a four-stage experimental run was conducted for each of the acid solutions according to the following experimental design (Table 2).

Table 2 Experimental design for the leaching process

Stage	Acid concentration (Molarity)	Reaction time (min)	Material dosage (g/L)	Temperature (°C)
1	0, 0.2, 0.3, 0.4	30	2	20
2	Optimum molar concentration determined in Stage 1	30, 40, 0, 20	2, 3	20, 0, 0
3		Optimum reaction time determined in Stage 2	Optimum dosage determined in Stage 3	
4				

2.3 Sample analysis measurements

At the end of the leaching reaction, the mixture was cooled down to room temperature if required. Then 2 mL of sample was taken and filtered through filter papers (Millipore AP40). The concentrations of Mg, Fe, Al, Ni, Cr, and Si in the filtrate samples were measured by ICP-OES (Perkin Elmer Optima 2000 DV). According to the obtained data, leaching efficiency for each of the analyte was calculated by the following equation:

$$\text{Leaching efficiency (\%)} = \frac{m_i - m_f}{m_i} * 100 \tag{E}$$

where m_i is the initial amount of the analyte corresponding to the amount of the powdered material added into 100 mL of acid solution (mg/L) and m_f is the measured concentration of the analyte in the filtrate sample (mg/L). The initial amount of the analytes was calculated based on the related wt% given in Table 1.

3. Results and Discussion

3.1 Effect of acid concentration

The effect of acid concentration on the leaching efficiency was investigated by testing different concentration values ranging between 0 and 4.0 M under the conditions of 20 °C, 30 min, 2 g material/L, and 400 rpm for each of the acid solutions. The experimental results showed that there was no remarkable change in the leaching efficiency of both Mg and Fe with the increasing acid concentration of HNO₃ and H₃PO₄ (Fig. 1a and b). The leaching efficiencies with HNO₃ were found to be in the range of 23% and 2% for Mg and 44% and 44% for Fe under the examined acid concentration conditions while the use of H₃PO₄ resulted in obtaining almost close leaching efficiencies ranging between 2% and 24% for Mg and 42% and 40% for Fe. In the case of the leaching with H₂SO₄, relatively higher efficiencies for both Mg and Fe were obtained than those obtained with HNO₃ and H₃PO₄, especially for the acid concentration 0.3 M. An increase in the acid concentration of H₂SO₄ from 0.1 to 0.3 M increased the leaching efficiency from 24% to 30% for Mg and 43% to 44% for Fe while there was no significant increase in the leaching efficiency of both Mg and Fe under the increasing concentration conditions up to 4.0 M.

The leaching efficiency of Al, Ni, and Cr was also investigated as a function of the acid concentration. The experimental results showed that the increasing acid concentration up to 4.0 M did not stimulate the leaching of Al and Ni for each type of acids while the leaching efficiency of Cr increased gradually with the increasing acid concentration for all of the acids used (Table 3). The highest leaching efficiency for Al, Ni, and Cr was found to be 3% with 4.0 M H₂SO₄, 2% with 3.0 M H₂SO₄, and 2% with 4.0 M H₃PO₄, respectively. Even though over half of the total Ni content was leached from the material compared to Al and Cr, it should be noted that the initial wt% of Al, Ni, and Cr

in the material composition was 0. These results implied that Al, Ni, and Cr could be determined only with negligible amounts in the supernatant after the leaching reaction compared to Mg and Fe.

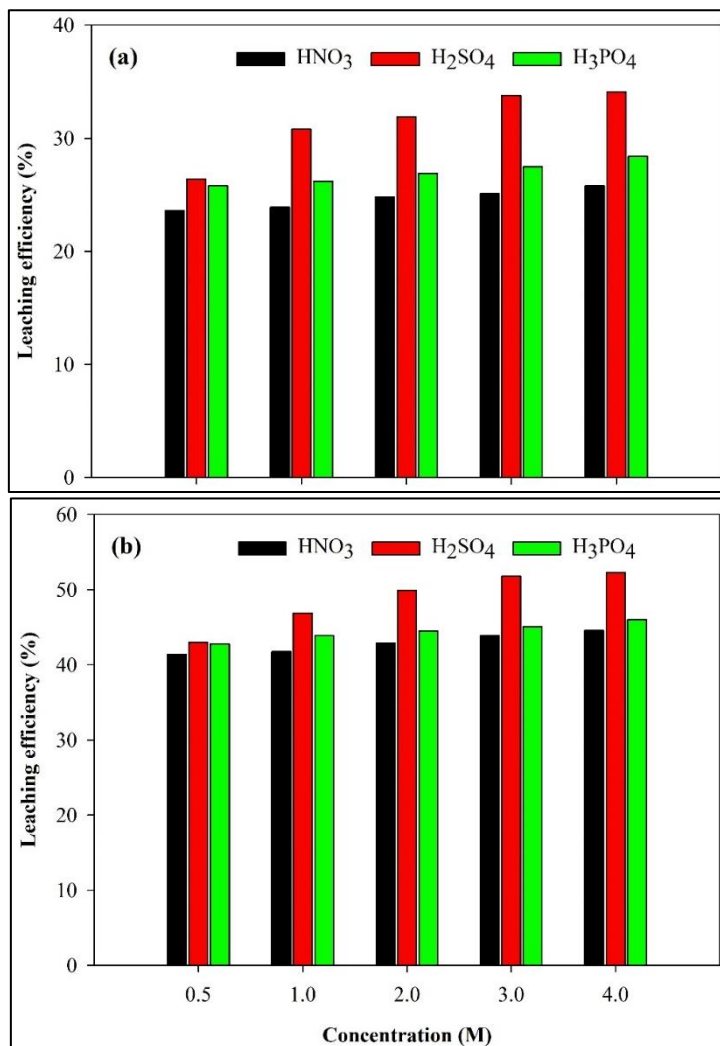


Figure 1 The effect of acid concentration on the leaching efficiency of Mg (a) and Fe (b). Mixing speed: 400 rpm; reaction time: 30 min; material dosage: 2 g/L; temperature: 20 °C.

Table 3 The effect of acid concentration on the leaching efficiency of Al, Ni, and Cr.

Type of acid	Concentration	Leaching efficiency		
		Al	Ni	Cr
HNO ₃	0	2	2	0.4
	0	2.0	0	0.7
	2.0	2		7.2
	3.0	2.7	4	4
	4.0	3	4	2
H ₂ SO ₄	0	2.2		0.24
	0	2.7		0.32
	2.0	3	2	0.3
	3.0	3		0.42
	4.0	3	0	0.43
H ₃ PO ₄	0		3.7	0.2
	0	4		0
	2.0	7	2.3	0.20
	3.0	7	3	0.23
	4.0	2.0	4	0.2

3.1 Effect of reaction time

The effect of reaction time on the leaching efficiency was investigated by testing varying reaction times in the range of 15 and 120 min under the same experimental conditions applied for the acid concentration. The experimental results showed that the leaching efficiency for both Mg and Fe increased gradually with the increasing reaction time for all acid reagents (Fig. 2a and b respectively). The leaching efficiencies with HNO₃ were found to be in the range of 17.4 and 32.0% for Mg and 33.0 and 40.2% for Fe while the leaching efficiencies with H₃PO₄ were found to be in the range of 20.0 and 34.2% for Mg and 37.0 and 40.2% for Fe. In the case of the leaching with H₂SO₄, relatively higher efficiencies were obtained for both Mg and Fe than those obtained with HNO₃ and H₃PO₄. The leaching efficiencies with H₂SO₄ varied between 28.0 and 48.3% for Mg and 44.0 and 60.4% for Fe with the increasing reaction time. These results revealed that the highest leaching efficiency for both Mg and Fe followed the order H₂SO₄ > H₃PO₄ > HNO₃.

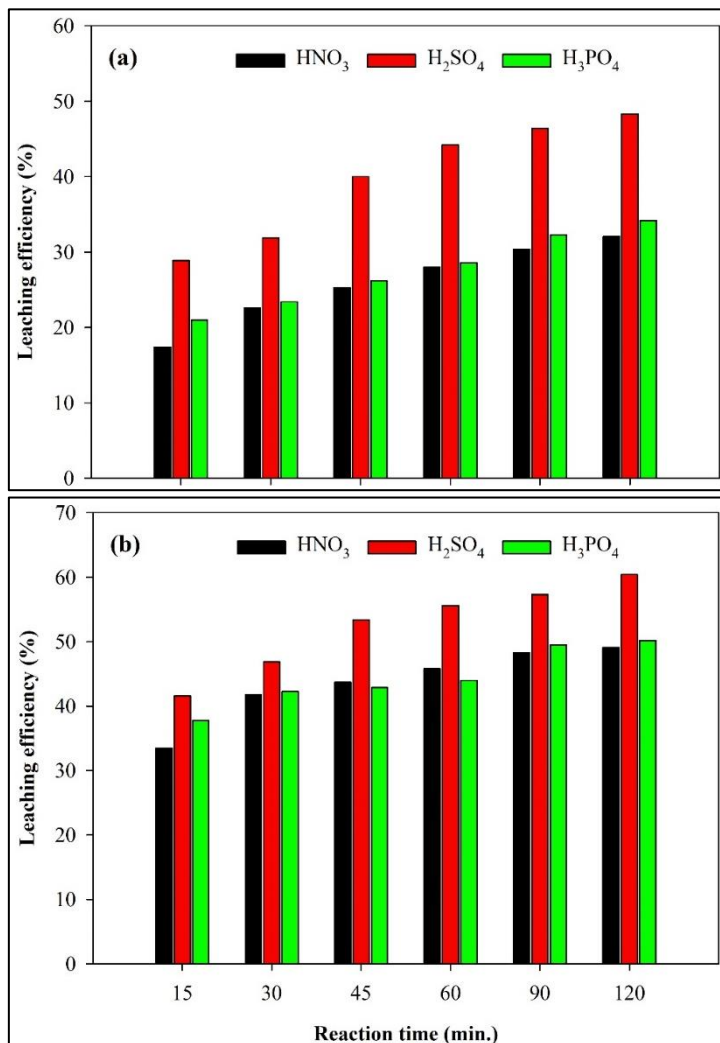


Figure 2 The effect of reaction time on the leaching efficiency of Mg (a) and Fe (b). Mixing speed: 400 rpm; material dosage: 2 g/L; temperature: 20 °C; acid concentration: 0.1 M HNO₃, 0.1 M H₂SO₄, 0.1 M H₃PO₄.

To quantify the magnitude of change in the efficiency values (η_{ef}) as a function of the varying reaction time, a set calculation was done based on the obtained experimental data (Table 4). According to the calculated data, the highest η_{ef} value was obtained to be 23.0 and 40.2% respectively when the reaction time increased from 15 to 30 min for both Mg and Fe in the case of leaching with HNO₃. On the other hand, in the case of leaching with H₂SO₄, the highest η_{ef} value was obtained to be 20.3 and 22.2% respectively when the reaction time increased from 30 to 45 min for both Mg and Fe. However, the highest η_{ef} value was obtained to be 34.2 and 40.2% respectively when the reaction time increased from 90 to 120 min for both Mg and Fe in the case of leaching with H₃PO₄. These results indicated that a relatively longer reaction time was required to achieve a satisfactory leaching efficiency for both Mg and Fe when using H₂SO₄ or H₃PO₄ as leaching reactant compared to HNO₃. This finding was confirmed by the calculated data for the rate of the reaction completion. According to the data, 40.7 and 50.0% of the total leaching reaction was completed for Mg and Fe respectively in the first 30 min with 0.1 M HNO₃ while only 22.0 and 22.0% of the total leaching reaction for

Mg and 3.7 and 3.2 of the total leaching reaction for Fe were completed in the case of the leaching with 0 M H₂SO₄ and 0 M H₃PO₄ respectively under the same conditions. Although the leaching with HNO₃ exhibited a relatively faster reaction for Mg and Fe compared to H₂SO₄ and H₃PO₄ over 0 of the total leaching reactions for both Mg and Fe were completed generally in 0 min for all of the leaching reactants used. Therefore the optimum reaction time was decided to be 0 min for each of the reactants to achieve a satisfactory leaching efficiency.

Table 4. Leaching efficiency values and rate of the reaction completion values for the leaching of Mg and Fe

Reaction time min	Mg					
	HNO ₃		H ₂ SO ₄		H ₃ PO ₄	
	ef	Cumulative ef a	ef	Cumulative ef a	ef	Cumulative ef a
30	23.0	23.0 (40.7)	4	4	0.3	0.3 (22)
4	0.7	33.7	20.3	2.7 (2)	0.7	2.0 (4)
0		43.3 (7)		3.2 (2.0)	4	2.4 (3.2)
0	7	2.0	4.7	43.3 (4)		40.7
20	3	00	3	47.00		4.00
Total ef to 20 min			47		4	
Reaction time min	Fe					
	HNO ₃		H ₂ SO ₄		H ₃ PO ₄	
	ef	Cumulative ef a	ef	Cumulative ef a	ef	Cumulative ef a
30			3	3.3 (7)	0	0.3 (2)
4	4.3	24.2 (7)	2.2	23.0	4	2.0 (4.4)
0	4	2.0	4.0	27.7 (2)	2	4.3 (7)
0	2	34.0	3.0	30		2.4
20		3.00		3.00	4	27.0 (00)
Total ef to 20 min	3		3		27.0	

a The given values in parenthesis represent the value of rate of the reaction completion which was calculated by dividing the cumulative ef value to the total ef value.

According to the total ef value which means the total magnitude of the change in the leaching efficiencies at the end of 20 min of reaction time the highest total ef value followed the order HNO₃, H₂SO₄ and H₃PO₄ for the leaching of Mg whereas it followed the order HNO₃, H₂SO₄ and H₃PO₄ for the leaching of Fe (Table 4). This result showed that the leaching with 0 M HNO₃ yielded a relatively higher leaching efficiency for Mg at the end of the 20 min of reaction time as compared those obtained by 0 M H₂SO₄ or 0 M H₃PO₄. Combining the results obtained for the leaching efficiencies, the rate of the reaction completion and the total ef it could be concluded that leaching with a mixture of 0 M HNO₃ and 0 M H₂SO₄ which will be prepared in a proper volume combination might have a positive impact for achieving the same or higher leaching efficiencies for Mg and or Fe within a shorter reaction time.

The results of the effect of reaction time on the leaching efficiency of Al, Ni and Cr was shown in Table 5. According to the results the leaching efficiencies of Al, Ni and Cr gradually increased with the increasing reaction time for each of the acid reactants. These results showed that the increasing reaction time had an effect similar to that of the effect of the increasing acid concentration on the leaching efficiency of Al, Ni and Cr. The highest leaching efficiency for Al, Ni and Cr was found to be 2 with H₂SO₄, 2 with H₂SO₄ and 0 with H₃PO₄ respectively.

Table 3. Effect of reaction time on the leaching efficiency of Al, Ni and Cr

Type of acid	Reaction time min	Leaching efficiency		
		Al	Ni	Cr
HNO ₃	0	0.2	42	0.07
	30		3.7	0.2
	4		4.3	0.20
	0	2.0	2	0.2
	0	2		0.30
	20	2	7.4	0.32
H ₂ SO ₄	0	2	4	0.3
	30	2.7		0.32
	4	4.4	0.7	0.2
	0	4	0	0.4
	0	4		0
	20		2	0.7
H ₃ PO ₄	0	2	4.7	0.42
	30	2	2	0.7
	4	2.0	0	0.3
	0	2	3.2	0
	0	3.2	7	0.7
	20	3.4	3	0

3.3 Effect of material dosage

The effect of material dosage on the leaching efficiency was investigated by testing different material dosages ranging between 1 and 3 g/L. Principally, it was expected that the leaching efficiency should have decreased with the increasing material dosage for a given volume of the acid reactant due to the decreasing volume of acid reactant per the increasing amount of the material. However, interestingly, the experimental results showed that increasing the material dosage did not cause any remarkable change in the leaching efficiency of both Mg and Fe for all of the acid reactants (Fig. 3). The leaching efficiencies with HNO₃ were found to be in the range of 2.7 and 30.4% for Mg and 42.0 and 4.3% for Fe, while the use of H₃PO₄ resulted in relatively higher leaching efficiencies ranging between 3.7 and 34% for Mg and 4.4 and 4% for Fe. In the case of the leaching with H₂SO₄, the efficiencies varied between 44.4 and 4.4% for Mg and 3 and 7.4% for Fe.

The results of the effect of the material dosage on the leaching efficiency of Al, Ni, and Cr were represented in Table 3. According to the results, the leaching efficiencies of Al, Ni, and Cr exhibited a fluctuating trend with the increasing material dosage for each of the acid reactants. In addition, it was observed that the increasing material dosage did not have any remarkable impact on the leaching efficiency of Al, Ni, and Cr. The highest leaching efficiency for Al, Ni, and Cr was found to be 4.7% with H₂SO₄, 42% with HNO₃, and 0% with H₃PO₄, respectively.

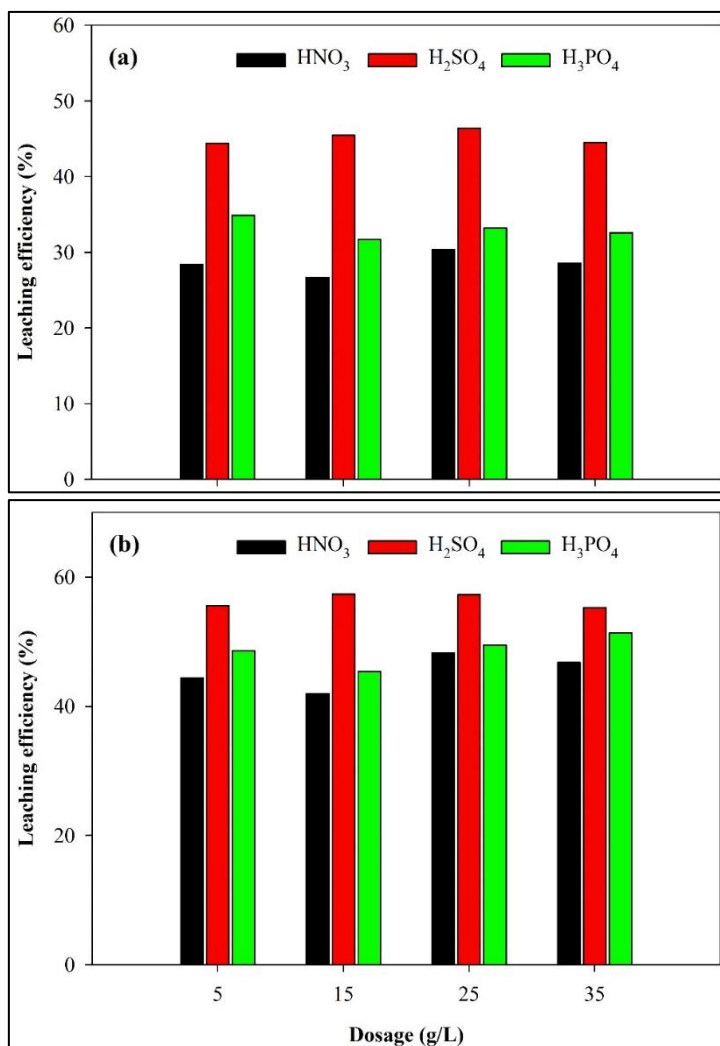


Figure 3 Effect of the material dosage on the leaching efficiency of Mg (a) and Fe (b). Mixing speed: 400 rpm, reaction time: 30 min, temperature: 20 °C, acid concentration: 0.1 M HNO₃, 0.1 M H₂SO₄, 0.1 M H₃PO₄.

Table 3 Effect of the material dosage on the leaching efficiency of Al, Ni, and Cr

Type of acid	Dosage (g/L)	Leaching efficiency		
		Al	Ni	Cr
HNO ₃			2	
		0.2	4	
	2	2		0.30
H ₂ SO ₄	3		4	0.7
		3		0.3
	2	4		0
H ₃ PO ₄	3	4.7		0
			2	0
	2	0	4	0
	2	3.2		0.7
	3	2.3	4	0

* Not calculated since the measured concentration value was lower than detection limit of 0.0 mg/L

3.3 Effect of temperature

The effect of temperature on the leaching efficiency was investigated under the conditions of 20, 30, and 40 °C. The experimental results showed that the leaching efficiencies of both Mg and Fe significantly increased with the increasing temperature for each of the acid reactants, especially for H₂SO₄. (Fig. 4) The leaching efficiency with HNO₃ were found

to be 24.2 and 22.2 for Mg and 4.4 and 4.4 for Fe under the temperature condition of 20 °C and 0 °C respectively while the leaching with H₃PO₄ resulted in quite close leaching efficiencies ranging between 33.4 and 30.0 for Mg and 0 and 4 for Fe. In the case of the leaching with H₂SO₄ the leaching efficiencies were found to be 43.7 and 37 for Mg and 37 and for Fe at 20 °C and 0 °C respectively. This result showed that over 0 of the total Mg and Fe content of the material could be leached with H₂SO₄ at 0 °C. Furthermore, under this temperature condition, almost and 2 fold higher leaching efficiencies were obtained for Fe and Mg respectively for each of the acid reactants. Based on the overall results of the study, one can be concluded that temperature had an impact on the leaching efficiency of both Mg and Fe much more than the other examined operational conditions.

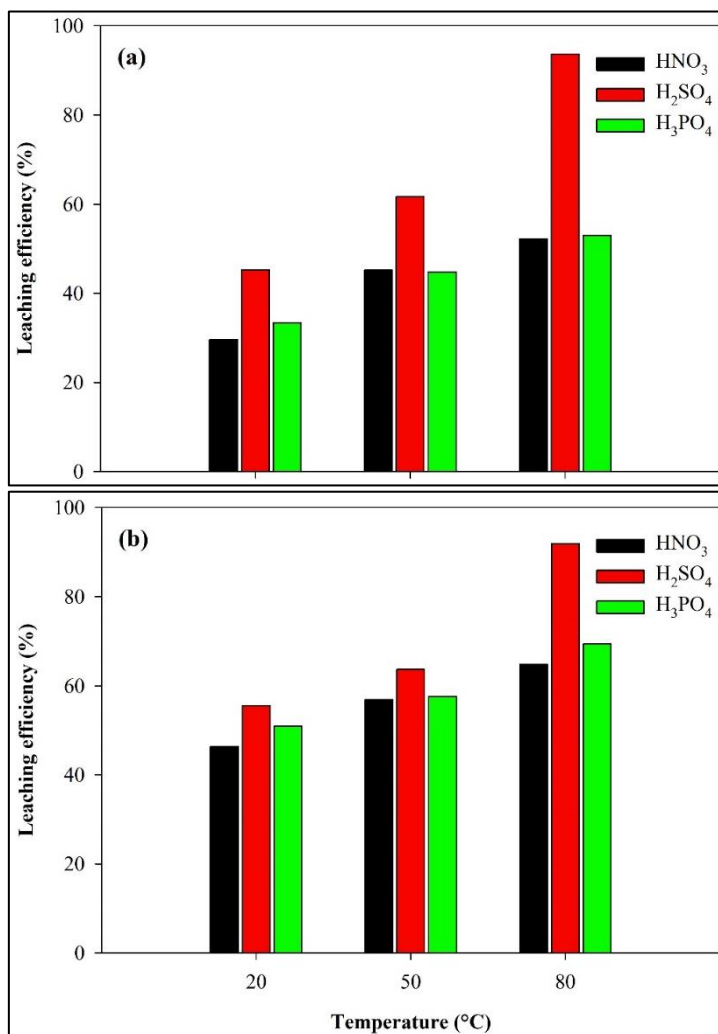


Figure 1 Effect of temperature on the leaching efficiency of Mg (a) and Fe (b). Mixing speed: 400 rpm; reaction time: 60 min; material dosage: 3 g/L; acid concentration: 0.1 M HNO₃, 0.1 M H₂SO₄, 0.1 M H₃PO₄.

To determine how the examined operational conditions affected the leachability of Si from the material, the residual Si concentration was also measured, as well as Al, Ni, and Cr, in this experimental stage. The obtained results showed that the increasing temperature gradually increased the leaching efficiency of Al, Ni, Cr, and Si (Table 1). The highest leaching efficiency for Al, Ni, Cr, and Si was found to be 70.5% with H₂SO₄, 70.0% with H₂SO₄, 71.7% with H₃PO₄, and 44.2% with HNO₃, respectively. According to the results, although the leaching efficiency of Ni reached a maximum value of 70.0% with H₂SO₄ at 80 °C, only 70.0% of the total Al content could be leached under the same condition. In addition to this, the leaching of Cr was maximized at an efficiency of 71.7% in the case of the leaching with H₃PO₄ at 80 °C. On the other hand, the obtained results for the leaching efficiency of Si showed that only a small fraction (44.2%) of the total Si content could be leached from the material, meaning that the examined experimental conditions or acid reactants did not have any significant impact on the recovery of Si from the material.

20 reported that the leaching efficiency of Mg and Fe increased with the increasing temperature between 2 and 0 C and the increasing reaction time between and 0 min However the increasing trend for the leaching efficiencies decreased after 20 min of reaction time These findings were in accordance with the findings of the present study

Table Comparison of the leaching efficiencies obtained under optimi ed conditions for several literature studies

Reference	Optimum conditions	Leaching efficiency				
		Amount of the recovered analyte measured in the leachate mg L				
		Mg	Fe	Al	Ni	Cr
Habbache et al 20 7	<ul style="list-style-type: none"> • Acid concentration 2 0 M HCl • Solid to li uid ratio 2 • Reaction time 30 min • Temperature 0 C 	NA *	NA	NA	00	NA
Top 20 4	<ul style="list-style-type: none"> • Acid concentration 7 0 M HCl • Solid to li uid ratio • Reaction time 30 min • Temperature 0 C 	2 3372 mg L	73 mg L	NA	7 0 mg L	7 2 0 mg L
Matus et al 2020	<ul style="list-style-type: none"> • Acid concentration 0 M HCl • Solid to li uid ratio 0 • Reaction time 0 min • Temperature 0 C 	40 4 NA	40 4 NA	NA	30 3 NA	NA
Moyo et al 2022	<ul style="list-style-type: none"> • Acid concentration 0 M HCl • Solid to li uid ratio 0 • Reaction time 0 min • Temperature 70 C 	2 3 40 mg L	NA	NA	NA	NA
This study	<ul style="list-style-type: none"> • Acid concentration 0 M H₂SO₄ • Solid to li uid ratio 3 • Reaction time 0 min • Temperature 0 C 	3 7 4 mg L	72 mg L	4 mg L	0 0 mg L	32 3 mg L

* Not available

The overall results of the present study showed that a considerable amount of Mg and Fe could be recovered from the material using HNO₃, H₂SO₄ and H₃PO₄. This means the obtained leachates contained Mg and Fe up to a certain level after leaching of the material implying that the leachates could be used as Mg and or Fe source for several applications. For example the Mg rich leachate obtained with H₃PO₄ presents itself as a great opportunity for struvite precipitation process where the external addition of both Mg and PO₄ sources is re uired to obtain a desired molar ratio for the formation of struvite crystals. Using magnesit MgCO₃ as a low cost Mg source G nay et al 200 showed that struvite precipitation with MgCO₃ significantly lowered the amount of ammonium phosphate suspended solid and turbidity from high ammonium contained landfill leachate. On the other hand the leachates that are rich in terms of both Mg and Fe can also be used to synthesi e MgFe layered double hydroxides which are commonly synthesi ed by co precipitation of Mg and Fe salts in an alkaline medium ameliya et al 2023. These potential uses of such leachates may trigger new research studies for cost effective alternative metal resources.

Ac le eme ts

The author appreciates Dr Barbaros Salih umbul s generous help and efforts in the preparation of the material and experimental set up. The author would also like to express his gratitude to Prof Dr amil Ekinci for supplying the tailings.

thics mmittee A r val

NA

eer revie

Externally peer reviewed

Auth r tributi s

H seyin a c Conceptuali ation Investigation Material and Methodology Supervision Visuali ation riting Original Draft riting review Editing Other The author has read and agreed to the published version of manuscript

lict terest

The authors have no conflicts of interest to declare

F u i

The financial support for ICP OES measurements from Mehmet Ararat G m l is thankfully acknowledged by the author

F S

Ivare M L Gasc G Rodrigue Pacheco R Pa Ferreiro M nde A 2022 Recovery of metals from mine wastes The effect of biochar Fe composites in the immobili ation of arsenic urnal of Sustainable Metallurgy 4 42 <https://doi.org/10.1007/s4030220044>

Arau o F S M Taborda Llano I Nunes E B Santos R M 2022 Recycling and reuse of mine tailings A review of advancements and their implications Geosciences 2 3 <https://doi.org/10.330/geosciences2003>

Bellenfant G Gue ennec A G Bodenan F D Hugues P Cassard D 20 3 Reprocessing of mining waste combining environmental management and metal recovery In Tibbett M Fourie A B Digby C Eds Mine Closure 20 3 Proceedings of the Eighth International Seminar on Mine Closure Australian Centre for Geomechanics Cornwall U pp 7 2 <https://doi.org/10.347ACGrep324Bellenfant>

Bola os Ben te V van Hullebusch E D Lens P N L uantin C van de Vossenber Subramanian S Sivry 20 Bio leaching behavior of chromite tailings Minerals 2 <https://doi.org/10.330/min002>

BRGM 200 Management of mining uarrying and ore processing waste in the European Union https://ec.europa.eu/environment/pdf/waste_studies/mining_0204finalreportbrgm.pdf accessed August 2023

Carmo F F Lanchotti A O amino L H 2020 Mining waste challenges Environmental risks of gigatons of mud dust and sediment in megadiverse regions in Bra il Sustainability 2 4 <https://doi.org/10.330/su2204>

Coet ee Bansal N Chirwa E M N 2020 Chromium in environment its toxic effect from chromite mining and ferrochrome industries and its possible bioremediation Exposure and Health 2 2 <https://doi.org/10.1007/s24030024>

Er st C Akcil A Gahan C S Tuncuk A Deveci H 20 3 Biohydrometallurgy of secondary metal resources a potential alternative approach for metal recovery urnal of Chemical Technology and Biotechnology 2 2 32 <https://doi.org/10.1002/ctb44>

G nay A arada D Tosun turk M 200 Use of magnesit as a magnesium source for ammonium removal from leachate urnal of Hazardous Materials 23 <https://doi.org/10.1016/j.hamat.2007.207>

Habbache N D erad S Tifouti L 20 7 Optimi ation of the operation conditions for NiO dissolution with different leachants Process Engineering urnal 7

Hitch M Ballantyne S M Hindle S R 20 0 Revaluing mine waste rock for carbon capture and storage International urnal of Mining Reclamation and Environment 24 4 7 <https://doi.org/10.1007/978-0-30024302>

ha M Shivendra umar V Pandey B D umar R Lee 20 0 Leaching studies for the recovery of metals from the waste printed circuit boards PCBs in Vidal E E Ed Proceedings of EPD Congress ohn iley Sons ashington USA 4 2

ameliya Verma A Dutta P Arora C Vyas S Varma R S 2023 Layered double hydroxide materials A review on their preparation characteri ation and applications Inorganics 2 <https://doi.org/10.330/inorganics0302>

rishnan S ulkapli N S amyab H Taib S M Din M F B M Ma id A Chaiprapat S en o I Ichikawa Nasrullah M Chelliapan S Othman N 202 Current technologies for recovery of metals from industrial wastes An overview Environmental Technology Innovation 22 0 2 <https://doi.org/10.1002/eti.20202>

umar P Patra S Tripathy S Sahu N 202 Efficient utili ation of nickel rich Chromite Ore Processing Tailings by carbothermic smelting urnal of Cleaner Production 3 2 04 <https://doi.org/10.1016/j.clepro.2022.04>

- L bre E Corder G 20 Integrating industrial ecology thinking into the management of mining waste Resources 477 <https://doi.org/10.330/resources40407>
- Lu Cai M 2022 Disposal methods on solid wastes from mines in transition from open pit to underground mining Procedia Environmental Sciences 772 <https://doi.org/10.1016/j.proenv.2022.000>
- Lunk H 20 Discovery properties and applications of chromium and its compounds ChemTexts <https://doi.org/10.1007/s40200-020-0007>
- Marra A Cesaro A Belgiorno V 20 Recovery opportunities of valuable and critical elements from EEE treatment residues by hydrometallurgical processes Environmental Science and Pollution Research 27 <https://doi.org/10.1007/s11356-020-040>
- Matus C Stopic S Et old S remer D otruba H Dertmann C Telle R Friedrich B nops P 2020 Mechanism of nickel magnesium and iron recovery from olivine bearing ore during leaching with hydrochloric acid including a carbonation pre treatment Metals 10 <https://doi.org/10.330/met.000>
- Moyo LB Simate GS Mamvura TA 2022 Magnesium recovery from ferrochrome slag kinetics and possible use in a circular economy Heliyon 8 <https://doi.org/10.1016/j.heliyon.2022.e27>
- Ndlovu S Simate GS Matinde E 2020 Mining and beneficiation waste production and utilization in Ndlovu S Simate GS Matinde E Eds Waste Production and Utilization in the Metal Extraction Industry CRC Press London U pp 2
- Oliveira PC Cabral M Taborda C Margarido F Nogueira CA 200 Leaching studies for metals recovery from printed circuit boards scrap in Proceedings 2nd International Conference Electronics Battery Recycling 0 Toronto Canada
- de Palacios LT Rodrigue AE 2022 In mining not everything is a circular economy Case studies from recent mining projects in Iberia Resources Policy 77 <https://doi.org/10.1016/j.resourpol.2022.027>
- an R Ristic I Ceplak B 2022 Mining and metallurgical waste as potential secondary sources of metals A case study for the West Balkan Region Minerals 12 <https://doi.org/10.330/min.20.047>
- Tayebi horami M Edraki M Corder G Golev A 20 Re thinking mining waste through an integrative approach led by circular economy aspirations Minerals 12 <https://doi.org/10.330/min.20.02>
- Top S 2024 Preparation of carnallite from Adana Alada chromite ore beneficiation plant tailings M Sc Thesis in Turkish ukurova University Institute of Natural and Applied Sciences Department of Mining Engineering Adana Turkey pp 7
- Top S ld r m M 20 Magnesium sulphate MgSO₄ synthesis from chromite concentration plant tailings Madencilik 47 <https://doi.org/10.1501/ma47>
- URL <https://ec.europa.eu/research/participants/documents/downloadPublic?documentIds=09090e37ba-c37b-appId=PPGM-S> accessed 2 July 2023
- URL 2 2023 <https://www.statista.com/statistics/320/mine-production-of-chromium-worldwide> accessed 27 July 2023
- eibel G appatini A olffers M Ringmann S 2022 Optimization of metal recovery from MS I fly ash by acid leaching Findings from laboratory and industrial scale experiments Processes 10 <https://doi.org/10.330/pr.02032>
- o ertuo lu E 2023 Multi metal recovery from flotation tailings with citric acid on the NaCl media Journal of Scientific Reports A 373 <https://doi.org/10.1038/s41598-023-2434>

Simulati on ve Geri Dönüş Analizi için Fatih Dönüş Array**Yusuf Güzel¹**

Abstract Predictions of seismic input motion characteristics at a site is seen as a tool of earthquake hazard mapping and earthquake hazard mitigation. The predictions can be conducted via modelling and simulating the soil layers under equivalent linear or nonlinear analyses in frequency or time domains. In order the predictions to be reliable for the use in building designs, it is necessary to verify the performances of the approaches through the actual input motions recordings at downhole arrays at different depths. When the elastic and nonlinear soil properties are two main driving inputs of the approaches, the modelling depth can be critical in the predictions, too. In this study, it is aimed to test the performance of the equivalent linear approach when the recorded input motions are simulated at different depths in Fatih Downhole Array Istanbul. For this, the recorded input motions at the bottom, i.e. 3 m from the surface, at 0 m and at 23 m are applied to the models having identical heights. The results demonstrate that the prediction at the surface changes quite dramatically with the changes of soil model height. When the predictions in the East-West direction can be seen as indication of actual spectral accelerations, this is not relatively valid in the North-South direction. The study concludes that the spectral acceleration predictions express great dependency to the soil model length.

Keywords Fatih Downhole Array, site response analysis, equivalent linear approach, Aegean earthquake, spectral acceleration

¹**Address** Necmettin Erbakan University, Faculty of Engineering, Eskişehir, Turkey

* **Corresponding Author** yusufkurdereli@hotmail.com

1.0.0

A well known natural hazard that causes primarily human losses and huge economic losses is called an earthquake. The risks to urbanized areas associated with such a natural disaster are presented using the maximum ground acceleration (PGA) that reaches to the site of interest (ramer, 2000). Magnitude of an earthquake event can articulate little about its damages to the surrounding urban areas as earthquake energy is dissipated at rock and soil layers. Therefore, the seismic level of an area or intensity of the earthquake event is represented by the PGA level (Ambraseys et al., 2000; Idriss, 2004).

When the PGA level for a site of interest depends on its distance to the fault lines, the local site condition is also very critical (Yusuf Güzel, 2020). Because the local site can alter the main characteristics of the input motions. Such as frequency content, peak ground values (e.g. peak ground acceleration (PGA), peak ground velocity (PGV) and peak ground displacement (PGD)), predominant period and important duration of the input motions can be changed. Hence, the site response analysis can be very useful in order to predict such changes in the input motion characteristics (Sextos et al., 2000).

Site response analysis is carried out through with linear or equivalent non-linear methods in the frequency or time domain (Elia, 2000; Güzel et al., 2020). Actual earthquake data recorded from the bottom soil layers is required to test whether the developed method can provide reliable predictions. In this regard, instrumented geotechnical arrays have been deployed in several seismic tectonic regions. For example, Lotung, Treasure Island, Parkfield, Turkey Flat, and La Cienega Geotechnical Arrays are some of the most popular geotechnical arrays installed. The seismic data collected in these arrays have been used in several studies to test equivalent linear and non-linear ground response approaches (Amorosi et al., 2007; Güzel et al., 2020; Hallal and Cox, 2002; Salvati and Pestana, 2000).

This study focuses on the input motion recordings at the Fatih Downhole Array (FTH) and their simulations from different depths. It mainly purposes to reveal the impact of the depth of soil model simulation to the spectral response predictions at the surface. In the following section, site properties of the array are explained. The locations of the considered earthquake event and the downhole array and properties of the actual input motion recordings are presented in the following section. Subsequently, spectral response predictions are illustrated along with the actual ones.

2 FA H O HO A A

Fatih Geotechnical Array (FTH) is positioned on top of stiff soil underlain by rock. It is closer to the historical mosque known as Fatih Mosque. It has been installed by Kandilli Observatory and Earthquake Research Institute of Bogaziçi University (OERI) and by German Research Center for Geosciences (GFZ) in 2001 (Turgutlu, 2010).

Geological formation from the Paleozoic age forms the engineering bedrock at the site named as Trakya Formation. This formation is overlain by the Bakirkoy and Gungoren Formations from the Miocene age. The Trakya formation is observed to be reached up until the 0 to 10 m depths. Geotechnical surveys conducted at the site demonstrate that the unweathered greywacke is encountered between 33 m and 80 m depths and overlain by weathered greywacke up to the depth of about 40 m. The top 40 m of the soil deposit consists of alternating clay, silty sand and clay soil layers.

The shear wave velocity profile of the array site is depicted from the PS logging tests as represented in Figure 1. The shear wave velocity distribution clearly explains the different soil layering as it changes through the depths. Dikmen et al. (2010). In other words, the V_s alters quite smoothly from soil layers between 300 m/s and 400 m/s up to the depth of 40 m; it increases sharply in the weathered greywacke to almost 800 m/s and in particular in the unweathered greywacke to 1200 m/s. The average V_s profile at the top 30 m equals to 333 m/s and hence classified as soil class C according to Eurocode (EC8). The water table is about 4 m depth down from the surface.

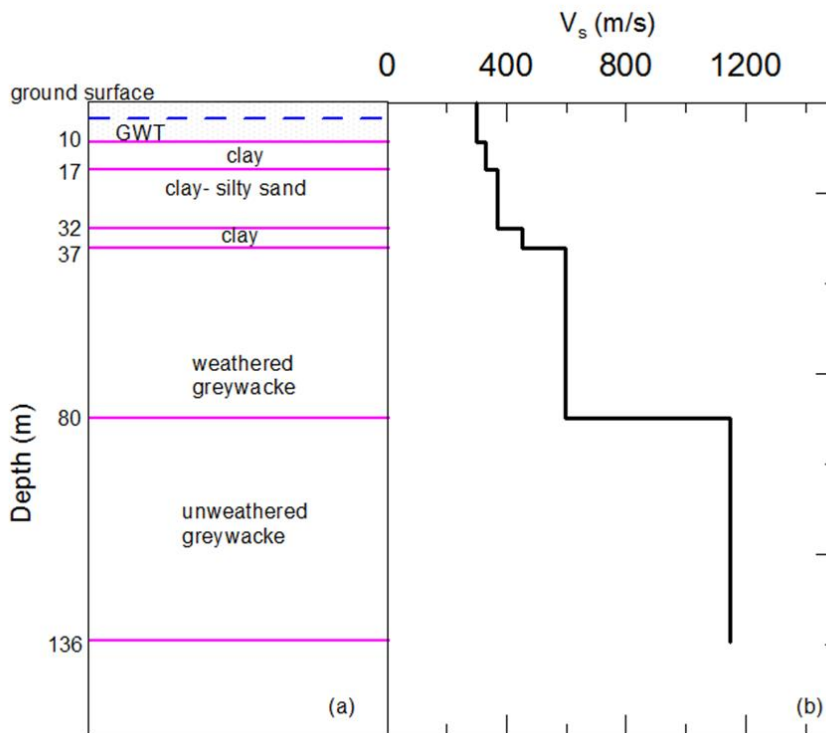


Figure 1 a) geological features of the site and b) measured V_s values up to the depth of 136 m

3 O O O S

On April 24, 2014, an earthquake event was occurred in Aegean sea with moment magnitude of 6.7. Input motions of the earthquake event called as Aegean earthquake were recorded at the FTH downhole array when the earthquake epicentre located in 40.200 latitude and 27.30730 longitude, the FTH array located in 40.072 latitude and 27.4 longitude. The locations are demonstrated in Figure 2. The direct distance between the earthquake epicentre and the array is about 320 km.

The acceleration time histories in the East-West (E-W) and North-South (NS) directions of the input motions in the East-West (E-W) and North-South (NS) directions recorded at 3 m, 10 m, 23 m and at the ground surface are shown in Figure 3. The associated PGA values are also given in Table 1. The PGAs at the bottom of the array are 0.42 m/s² and 0.07 m/s² in the E-W and NS directions, respectively. The PGA reaches to 0.03 m/s² in the E-W direction when it reaches to 10 m, showing deamplification. In the NS direction, however, it amplifies to the PGA level of 0.07 m/s². After 10 m, the

PGA values in the both horizontal directions amplify at the recorded depths. More precisely they are equal to 0.0 m/s^2 and 0.0 m/s^2 at 23 m and 0.3 m/s^2 and 0.0 m/s^2 at the ground surface in the E and NS directions respectively.

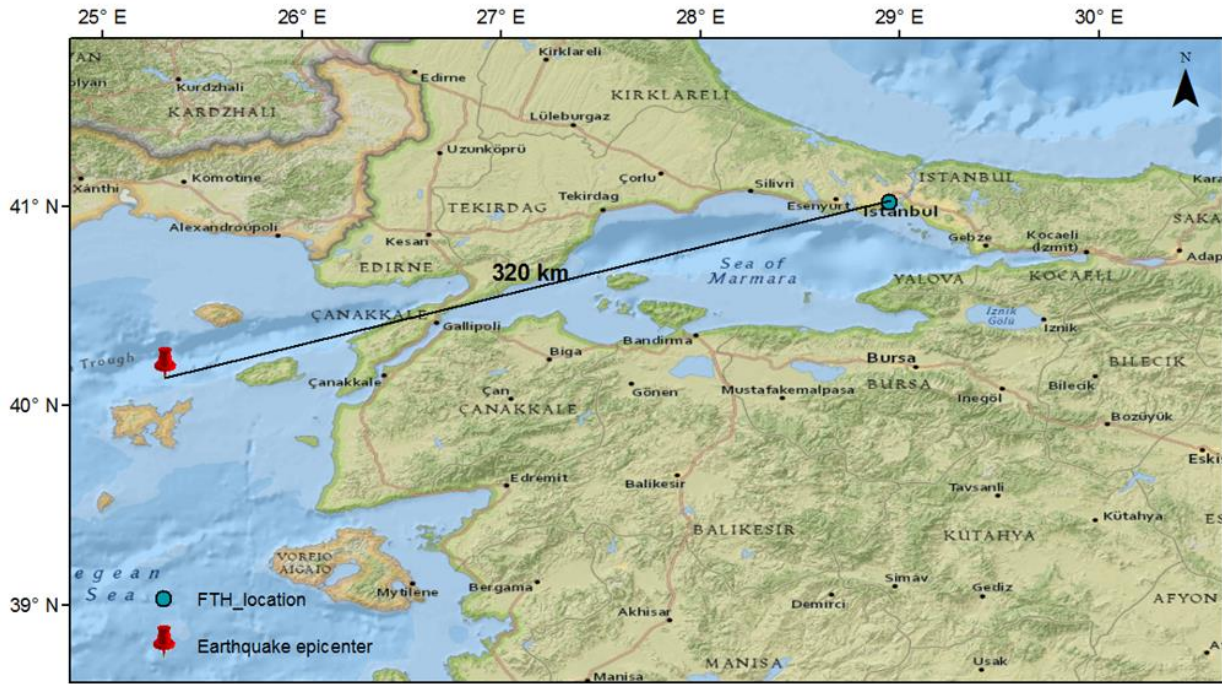


Figure 2 Locations of the Aegean earthquake event and FTH downhole array and distance between them

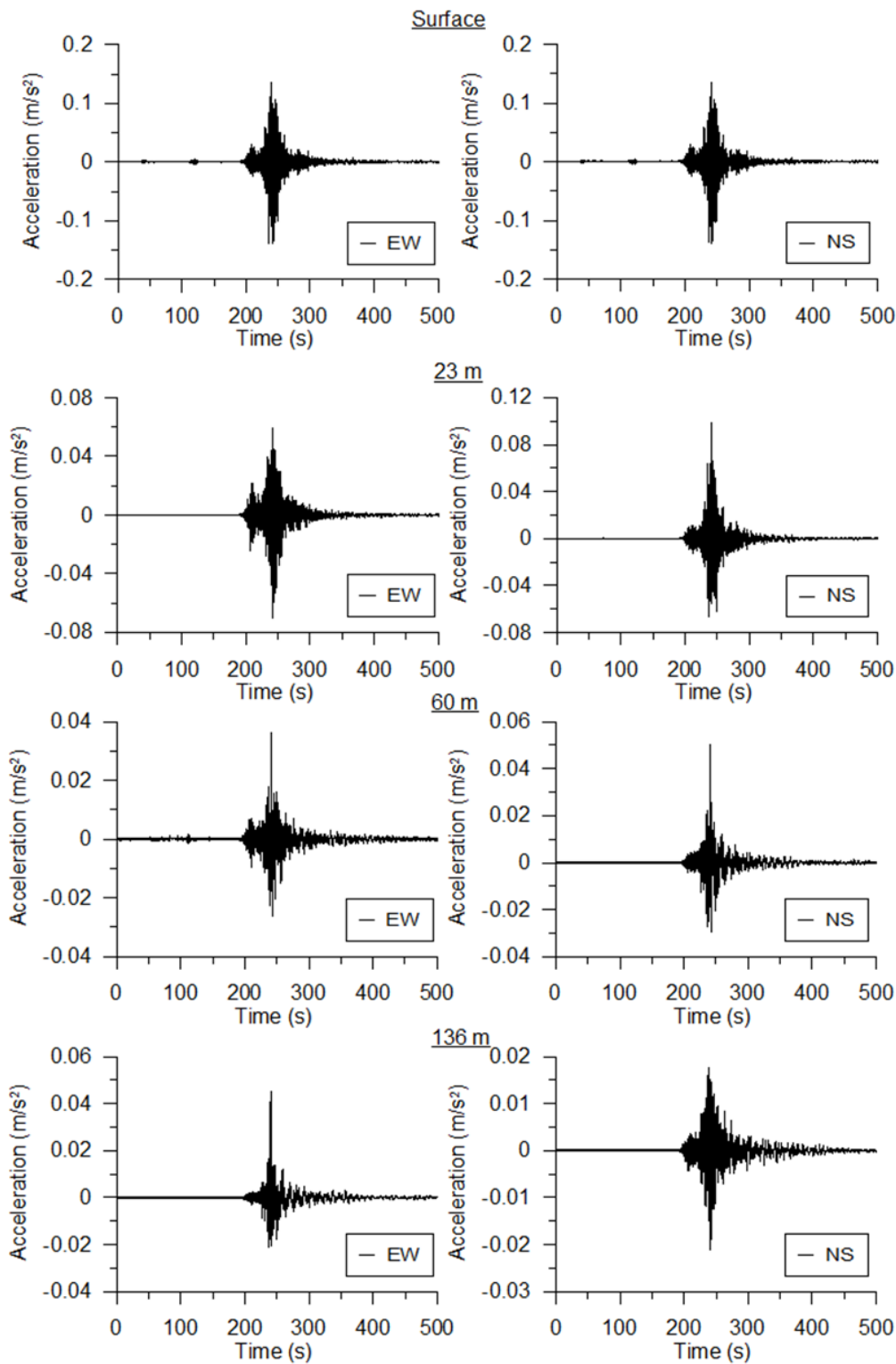


Figure 3 Acceleration time histories of the input motions from the Aegean earthquake event recorded at the ground surface in the EW and NS directions

able 1 PGA values of the recorded input motions at different depths

Depth m \ Directions	PGA m s ²	
	E	N S
Ground surface	0.3	0.0
23	0.4	0.0
0	0.034	0.0
3	0.04	0.07

3 S S A S S O S

The PGA and spectral acceleration predictions from the equivalent linear site response analyses Deepsoil of the FTH downhole array are illustrated in this section. When the PGA values are regarded as valuable to show the earthquake intensity, the spectral acceleration curves are very crucial for building behaviours too (Malhotra, 2000).

In Table 2, the predicted PGA values when the FTH downhole array is simulated by the input motions at the 3 m depth are compared with the recorded ones in both horizontal directions. It is clear that the predicted PGA value at 0 m shows amplification from 0.04 m s² to 0.0 m s² while the recorded values deamplify with the value of 0.034 m s² in the E direction. At 23 m and at the ground surface, both predicted and recorded PGA values intend to amplify to 0.02 m s² and 0.3 m s² and to 0.4 m s² and 0.3 m s² respectively. However, both the predicted and recorded PGA values are always in line of amplification at all measured depths. As the predicted and recorded PGA values are always equal to each other, being 0.047 m s² and 0.0 m s² respectively, they differ from each other towards the ground surface. More precisely, the predicted PGA value increases sharply to the value of 0.22 m s² and the recorded ones reach just to the value of 0.0 m s².

able 2 Predicted PGA values at 0 m, 23 m and at the ground surface when the 3 m of the FTH downhole array is simulated

Depth m \ Directions	PGA m s ²			
	Recorded E	Predicted E	Recorded N S	Predicted N S
Ground surface	0.3	0.3	0.0	0.22
23	0.4	0.02	0.0	0.073
0	0.034	0.0	0.0	0.047

The PGA values at 23 m and at the ground surface from the simulation of 0 m of the FTH downhole array are given in Table 3. The predicted PGA values reduce significantly and are well lower than the recorded ones in the E direction, being 0.04 m s² at 23 m and 0.0 m s² at the ground surface. In contrast, the reductions in the NS direction are relatively minimal as the predicted PGA values are 0.07 m s² at 23 m and 0 m s² at the ground surface.

able 3 Predicted PGA values at 23 m and at the ground surface when the 0 m of the FTH downhole array is simulated

Depth m \ Directions	PGA m s ²			
	Recorded E	Predicted E	Recorded N S	Predicted N S
Ground surface	0.3	0.0	0.0	0
23	0.4	0.04	0.0	0.07

In terms of spectral acceleration values, the predictions show a relatively good match with the recorded ones in the E direction at 23 m and at the ground surface, but the period at which the spectral peaks occurred are not captured well (Figure 4). For instance, the recorded spectral peak is about 0.7 m s² at 0 s, the predicted one equals to 0.77 m s² at 0.72 s at the ground surface. The corresponding values at 23 m are 0 m s² at 0.44 s (recorded one) and 0.3 m s² at 0.72 s (predicted one).

one However the equivalent site response analysis cannot able to predict the recorded spectral values well at all considered depths in particular at the ground surface and at the 0 m depth

When the 0 m of the FTH downhole array is simulated the spectral predictions become better only at 23 m in the NS direction as seen in Figure Also the period of spectral peak seems to be well captured at the ground surface in the E direction

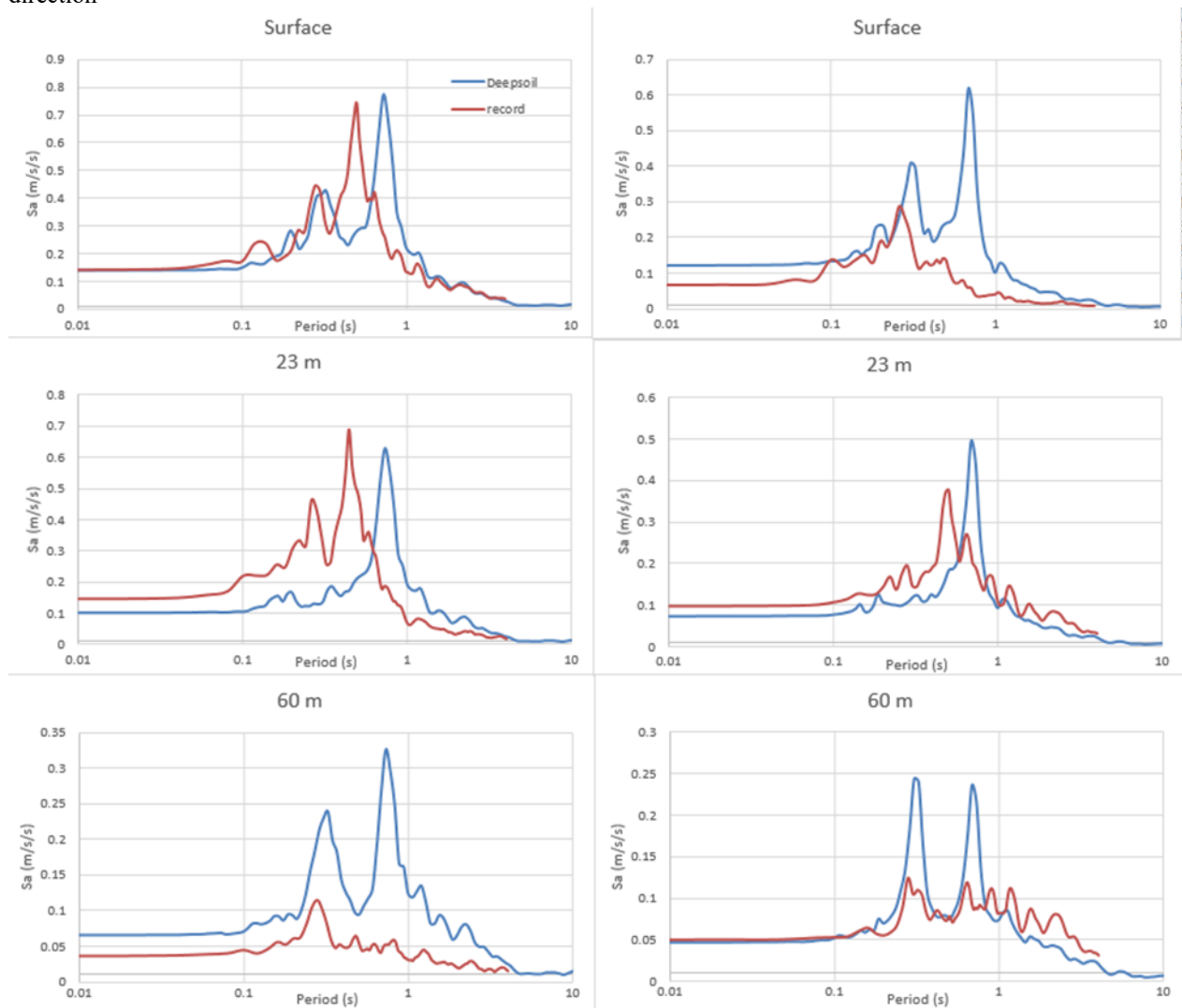


Figure Spectral acceleration curves of the recorded and predicted input motions at 0 m 23 m and at the ground surface when the recorded input motions at 3 m are simulated

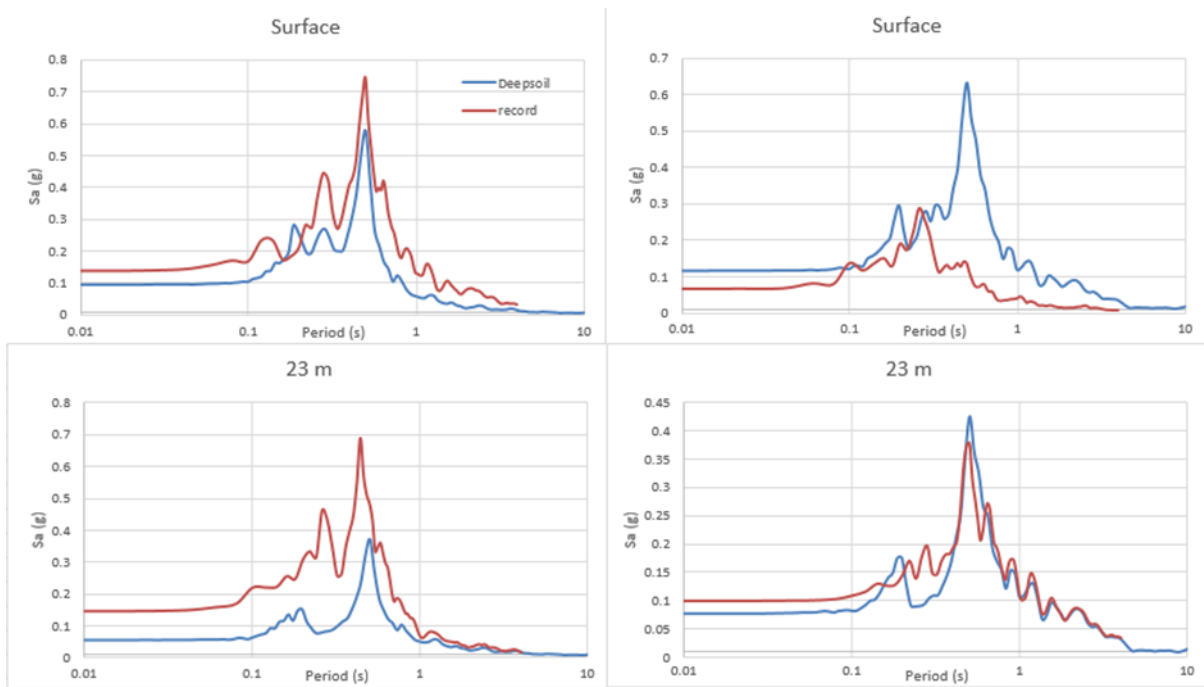


Figure Spectral acceleration curves of the recorded and predicted input motions at 23 m and at the ground surface when the recorded input motions at 0 m are simulated

O S O S

In this study the dependency of the PGA and spectral acceleration values on the soil model length is studied at the Fatih Downhole array. The recorded input motions from the Aegean earthquake event occurred on April 24, 2020 are used for simulation and comparison purposes. The equivalent linear site response analyses are conducted.

The results indicate that the PGA predictions in the E direction demonstrate good indication of the recorded values in the case of applying input motions at 3 m, especially at the ground surface. The predictions in the NS direction are also improved when the 0 m of the array is simulated. These assessments are valid for the spectral acceleration predictions too. Therefore, the site response predictions express great dependency to the depth at which the input motions applied.

Ac le eme ts

The author acknowledges the help of Prof. Erdal Kafak at Bogaziçi University in attaining the recorded data.

thics mmittee A r val

N/A

eer revie

Externally peer reviewed

Auth r tributi s

Conceptualization: G; Investigation: G; Material and Methodology: G; Supervision: G; Visualization: G; Writing Original Draft: G; Writing review & Editing: G; Other: All authors have read and agreed to the published version of manuscript.

lict terest

The authors have no conflicts of interest to declare.

Fu i

The authors declared that this study has received no financial support.

F S

- Ambraseys N N Douglas Sarma S Smit P 200 Equations for the estimation of strong ground motions from shallow crustal earthquakes using data from Europe and the Middle East: horizontal peak ground acceleration and spectral acceleration *Journal of Bulletin of Earthquake Engineering* 3 3
- Amorosi A Boldini D di Lernia A 2017 Dynamic soil structure interaction: A three dimensional numerical approach and its application to the Lotung case study *Computers and Geotechnics* 10 34-44 doi: 10.1016/j.compgeo.2017.01.000
- Dikmen S U Edinçliler A Pinar A 2019 Northern Aegean Earthquake Mw 6.7 Observations at three seismic downhole arrays in Istanbul *Soil Dynamics and Earthquake Engineering* 127 32-33 doi: 10.1016/j.soildyn.2019.07.000
- Elia G 2019 Site response for seismic hazard assessment *Journal of Encyclopedia of earthquake engineering*
- EC 2004 Design of structures for earthquake resistance Part 1: General rules, seismic actions and rules for building *2004*
- Gu el 2019 Influence of input motion selection and soil variability on nonlinear ground response analyses Newcastle University
- ESRI 2019 ArcGIS Redlands CA Environmental Systems Research Institute
- Gu el Rouainia M Elia G 2020 Effect of soil variability on nonlinear site response predictions: Application to the Lotung site *Computers and Geotechnics* 122 doi: 10.1016/j.compgeo.2020.103444
- Hallal M M Cox B R 2021 An H V geostatistical approach for building pseudo 3D Vs models to account for spatial variability in ground response analyses Part I: Model development *Earthquake Spectra* 37(3) 203-204 doi: 10.1177/073217232093020
- Hashash M Musgrove M Harmon 2019 Nonlinear and equivalent linear seismic site response of one dimensional soil columns User Manual v7.0 Deepsoil Software University of Illinois at Urbana Champaign
- Idriss I 2014 An NGA best2 empirical model for estimating the horizontal spectral values generated by shallow crustal earthquakes *Journal of Earthquake Spectra* 30(3) 777-782 doi: 10.1177/073217231426432
- ramer S L 2019 Geotechnical earthquake engineering Pearson Education India
- urtulu A 2019 Istanbul geotechnical downhole arrays *Bulletin of Earthquake Engineering* 17(4) 443-444 doi: 10.1007/s10080-019-00200-0
- Malhotra P 2000 Smooth spectra of horizontal and vertical ground motions *Bulletin of the Seismological Society of America* 70(2) 399-401 doi: 10.1785/BSSA-70-2-399
- Salvati L A Pestana M 2000 Small strain behavior of granular soils II: Seismic response analyses and model evaluation *Journal of Geotechnical and Geoenvironmental Engineering* 126(3) 202-209 doi: 10.1061/(ASCE)1090-0248(2000)126:3(202)
- Sextos A De Risi R Pagliaroli A Foti S Passeri F Ausilio E Immaro P 2019 Local site effects and incremental damage of buildings during the 2016 Central Italy Earthquake sequence *Earthquake Spectra* 34(4) 343-354 doi: 10.1177/073217231987544M

Performance Comparison of Feature Extraction Methods in Alzheimer's Disease MRI Images

Yıldırım Hilmi Acar^{*1}, Fatih Aşit¹, Kamil Ayutal²

Abstract Neuroimaging is a discipline that aims to unravel the complex anatomy and functioning of the brain. Magnetic Resonance Imaging (MRI) is one of the most commonly used neuroimaging techniques. With the help of high performance computing tools, neurological abnormalities can be detected and analyzed based on the images obtained through MRI. Research on the diagnosis of diseases using MRI data is still ongoing, with some of the systems working directly with the original data while others require preprocessed data. This study focuses on the diagnosis of an Alzheimer's disease stage using MRI data from patients in the non-demented and very mild demented classes. The diagnosis is performed either by directly using the MRI images or by extracting meaningful features from the data. The discrete wavelet transform, statistical method (mean, standard deviation, and entropy), and deep learning (ResNet) model are employed as feature extractors, both individually and in combination. The performance of these methods is analyzed by a decision tree, support vector machine, k-nearest neighbor, traditional machine learning, and ResNet deep learning methods. The results are compared with classification criteria calculated using confusion matrices. The results have shown that the highest classification accuracy is achieved by deep features extracted by the ResNet model on the original MRI dataset and classified by support vector machine algorithm.

Keywords: Magnetic resonance imaging, feature extraction, deep learning, machine learning

¹Address: Selçuk University, Faculty of Technology, 43100, Turkey

²Address: Selçuk University, Adnan Faik İl Vocational School, 43100, Turkey

* Corresponding Author: yulehayilma@selcuk.edu.tr

1. INTRODUCTION

Neuroimaging provides detailed information about the structure and functioning of the brain, allowing complex system analysis. Beaulac et al. (2023) Magnetic Resonance Imaging (MRI) technology is a frequently used method for the detection of neurodegeneration in soft tissue. Along with these analyzing relationships between high-dimensional data and image sets are problems waiting to be solved. Machine Learning (ML) solutions provide models that systematically analyze these complex structures and data. Traditional ML algorithms require a feature extraction step; on the other hand, deep learning can work on raw data without a feature extraction step. The feature extraction process is to reveal meaningful information and connections about the disease by examining the data in depth. Chakraborty et al. (2023)

Various approaches have been proposed for feature extraction methods from MRI images. Aplan et al. investigate Parkinson's disease MRI images using a pyramid histogram of oriented gradients (HOG) feature extraction method. This approach handles the images segment by segment. Each segment is created as a grid by implementing HOG. After the segments are aggregated to form a feature vector. Aplan et al. (2022) Sharma et al. conduct brain tumor detection using HOG features. The analyses are performed to find the appropriate block size for HOG transformation, and the resulting feature vector is used as a ResNet input. Sharma et al. (2023) Üwül proposes a statistical feature extraction method for different types of medical images. According to this method, data distributions of medical images are examined and skews are analyzed. Thus, hidden features are revealed. Üwül (2022) Tasci et al. in their approach uses many pre-trained deep learning models as feature extraction method on diffusion MRIs of patients with ischemic acute infarction. The models are tested according to the classification performance metrics in the ML algorithm, and the pre-trained models that give the features that best describe the data are selected as feature extractors. The obtained deep features from the selected models are combined and sent to the feature selection model for feature reduction. Tasci, Tasci (2022)

In this study two stages of Alzheimer's disease (non-demented and very mild demented) are classified on brain MRI images. Discrete wavelet transform (DWT), statistical methods, and deep learning methods are used as feature extraction methods from MRI images, both separately and in combination, and the performances of the methods are compared. As the statistical method, the standard deviation, mean, and entropy values of each MRI image are used as features. Another method is the DWT, which is an image compression method and is also used for feature extraction. Haar wavelet mother function, widely preferred in biomedical images, is used in the study. Lastly, ResNet, a deep learning model, is used as both a classifier and a feature extractor. Performance comparisons are made through classifiers to measure the success of the methods. As classifiers, tree types of decision tree algorithms (fine, medium, and coarse), six types of support vector machine (SVM) (linear, quadratic, cubic, fine Gaussian, medium Gaussian, and coarse Gaussian), six types of k-nearest neighbor (k-NN) (fine, medium, coarse, cosine, cubic, and weighted), NN, and ResNet, a deep learning model, are preferred. Based on the confusion matrices, the performance metrics are calculated, and the success of feature extraction methods are compared.

The organization of the paper is as follows: The dataset and feature extraction methods are explained in the material and method in the second part. The performance metrics, classification algorithms, and results are in the third section. The comparison of the feature extraction methods according to the metrics and conclusions is given in the fourth section as the discussion and conclusions part.

2 MATERIALS AND METHODS

In this section, the dataset and feature extraction methods are introduced. Figure 1 represents the process of the study.

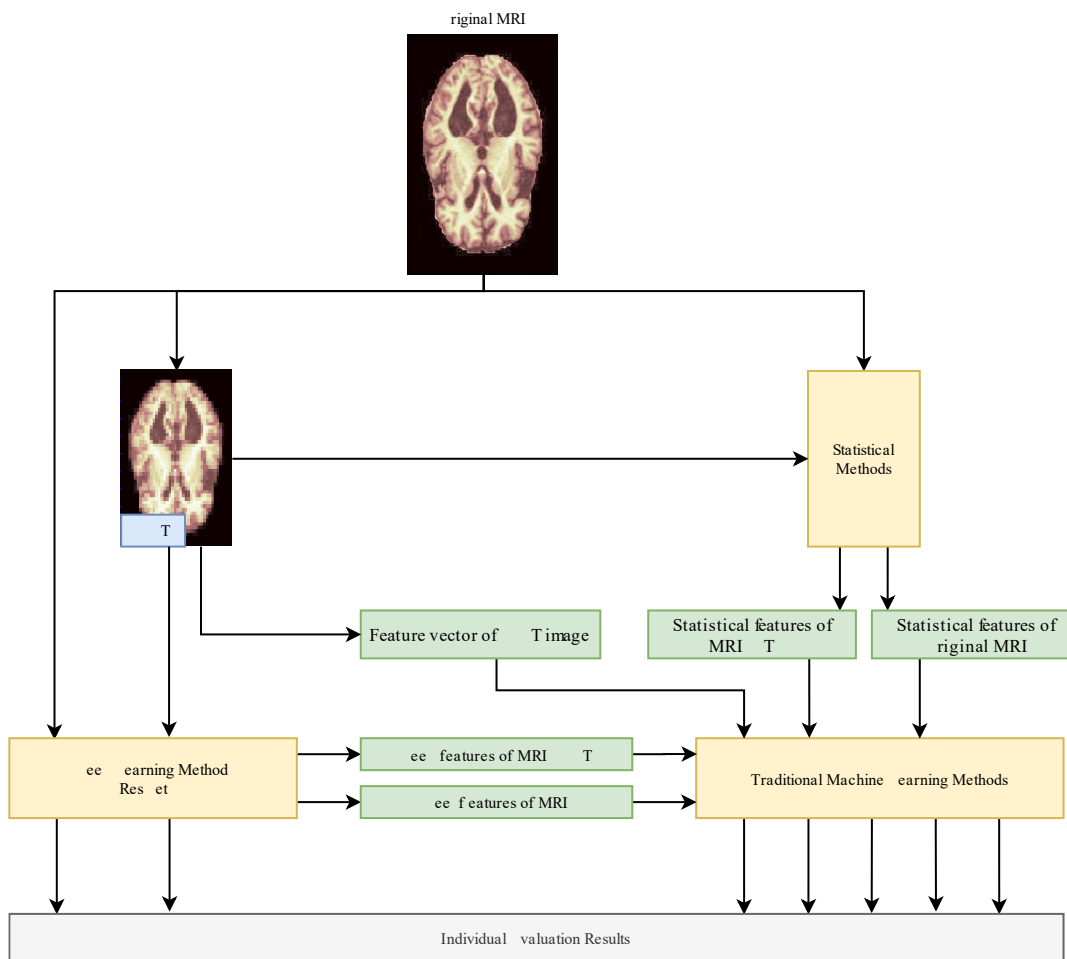


Figure 1 The process of the study

2.1 Dataset

The MRI dataset used in the study is related to Alzheimer's disease. It is available on the open source Kaggle website <https://www.kaggle.com/tourist/alheimers-dataset-4-class-of-images> accessed on 02/08/2023. Since there is an imbalance problem between the classes in the dataset, two classes of similar size are studied. These classes are non-demented and very mild demented. Some images of the dataset are shown in Figure 2.

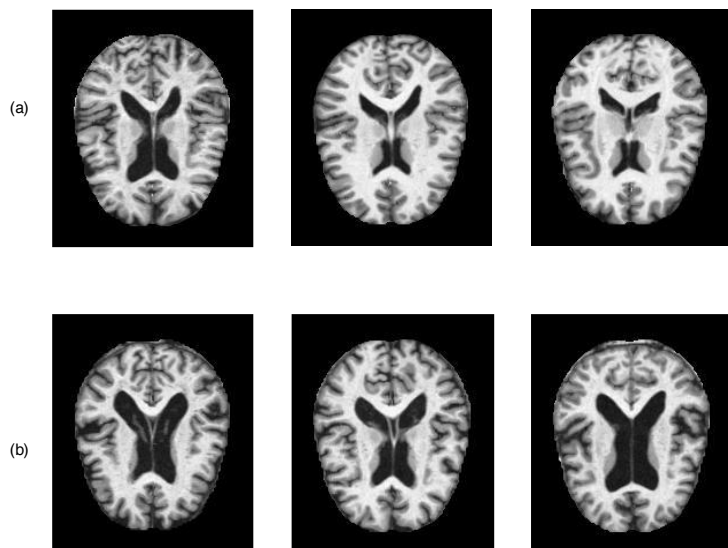


Figure 2 a) the row with non-demented MRI images b) the row with very mild demented MRI images

The dataset contains 3200 images from the non-demented class and 2240 images from the very mild demented class respectively, with a total of 5440 images in the train and test sets. After the feature extraction step, score normalization is applied to all images. In addition, RGB formats of images are used as deep learning input types.

2.2 Feature Extraction Methods

In this study, feature extraction methods are performed on the raw and the compressed data by applying DCT. One of the aims of this study is to investigate whether there is an advantage in using the DCT of large-sized MRI images as a preprocess and using compressed data as input. On the other hand, the data obtained with the DCT is used directly as a feature vector in the study. Thus, the statistical method DCT and deep features are considered both separately and as a combination. Afterward, the dataset is classified. The classifiers and input data types used in the study are listed in Table 1.

Table 1 Input data and feature extraction methods

Classifiers	Inputs
Deep Learning ResNet	MRI
	MRI-DCT
Traditional ML Decision Tree SVM NN	MRI-DCT
	MRI-Statistical
	MRI-DCT-Statistical
	Deep features of MRI
	Deep features of MRI-DCT

The first feature extraction method used is the statistical method. In the study, three features of the data as mean, standard deviation, and Shannon wavelet entropy are used when extracting the features from the image matrices; two different results are obtained by taking both the original and mean value of the statistical results. The applied process is shown in Figure 3.

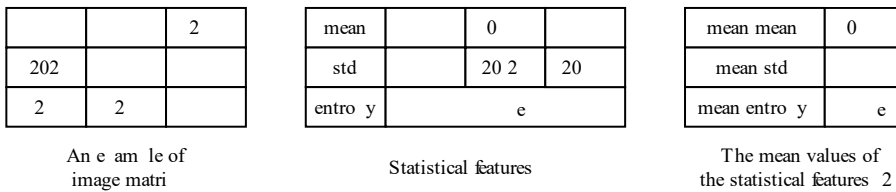


Figure 3 The implementation of the mean operation

The other method used as a feature extraction method is the wavelet transform. Discrete wavelet transform (DWT) is utilized in this study. This method is a signal analysis method that performs multiple resolution analysis of signals. Mallat's method is used. Relationships across rows and columns of 2D MRI images are explored. This DWT is used as a feature extraction method. In the study, the Haar wavelet mother function is applied from the second level as the wavelet family. Figure 4 shows the obtained MRI image when DWT with the Haar wavelet mother function is applied.

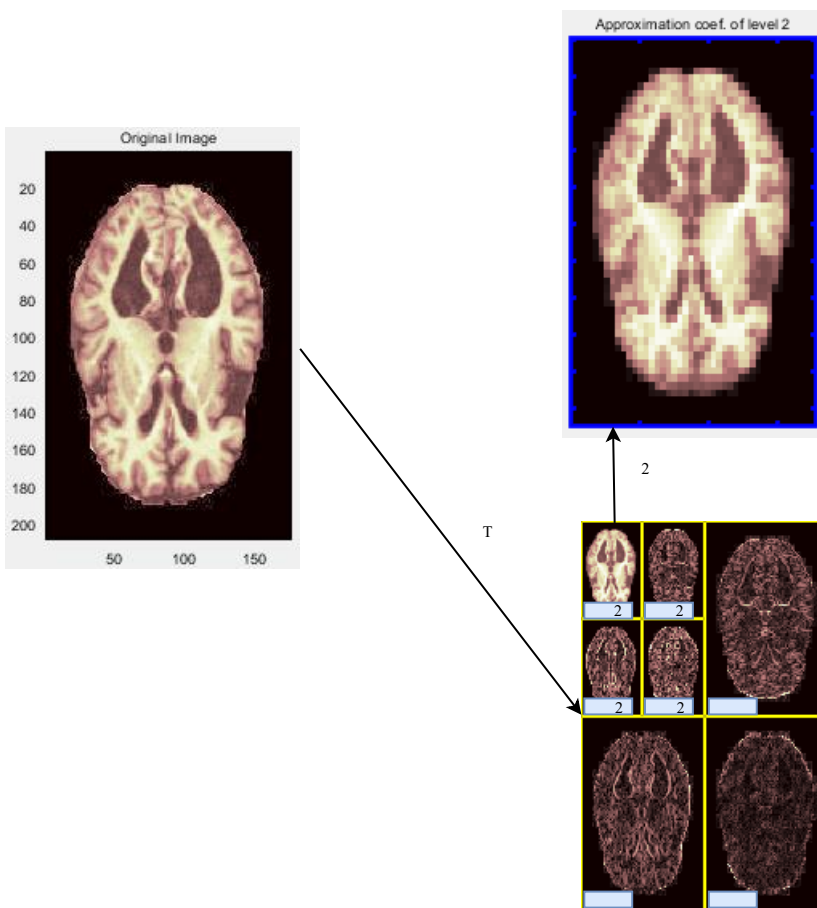


Figure 4 The application of the DWT

The LL2 image in Figure 4 is the detailed image and contains the most meaningful information (Ima Acar Bafti Ekmecki 2022). The LL2 image expressed as MRI DWT and statistical features are extracted from this image. Here it is aimed to investigate the success of applying DWT to high-dimensional MRI data and creating a smaller image set. The procedures in Figure 3 are also applied for MRI DWT and are also named LL2 and LL2. The LL2 image is also converted into vector form as directly a feature vector.

Finally, since deep learning is both an effortless and popular method of recent times, the pre-trained ResNet deep learning architecture is utilized in the study. ResNet is a convolutional neural network model consisting of layers. He, Hang, Ren, Sun, 2018. Input data has been converted to RGB images. The original MRI data and the MRI DWT are the individual input data of ResNet. Hereby, it is aimed to compare the success of the MRI DWT image set and the original image set in the deep learning method. Besides, after applying ResNet to both sets, the features obtained

by the model in the last stage are also stored as deep features and given to traditional ML algorithms for classification. The feature extraction performance of the ResNet model is examined.

3 S S

The output of the study is the combination of the input data and the feature extraction method that reaches the highest accuracy value. In this section, feature extraction methods are compared based on performance metrics. Extracting the most essential features from the data dramatically affects the results obtained by the classifiers. For this reason, many methods are handled in different ways and the results are examined.

Alzheimer's disease brain MRI datasets are used in the study. The information about the dataset is given in Table 2.

Table 2 The number of images in the dataset

Dataset	rai		est	
	class 1 normal	class 2 dementia	class 1 normal	class 2 dementia
Alzheimer's disease MRI images	20	72	40	44

Feature extraction methods produce the feature numbers in Table 3.

Table 3 The number of features of the feature extraction methods

Method	Number of features
Statistical features	2
Statistical features 2	3
Statistical features of MRI D T	73
Statistical features of MRI D T 2	3
Vectorial form of MRI D T	22
Deep features of the original MRI	2
Deep features of MRI D T	2

Data is classified using traditional ML algorithms using the number of features given in Table 3. The classifiers used in the study are three types of decision tree algorithms: fine, medium, and coarse tree; six types of SVM: linear, quadratic, cubic, fine gaussian, medium gaussian, and coarse gaussian SVM; six types of NN: fine, medium, coarse, cosine, cubic, and weighted NN; and ResNet model.

The success of the methods is compared by calculating the classification performance metrics over the confusion matrices obtained from each classifier. The confusion matrices and metrics are shown in Figure.

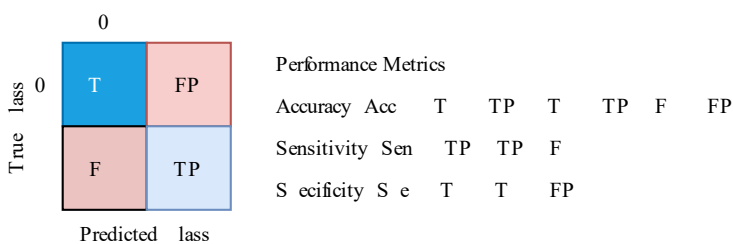


Figure The confusion matrix and performance metrics

In Figure, TN is referred to as True Negative, FP is False Positive, FN is False Negative, and TP is True Positive. The formulas of the metrics are included in the figure.

The performance results are obtained from all traditional ML algorithms. In addition, the original and MRI D T images are classified with the ResNet model. The best results among all classifiers are listed in Table 4.

Table 4. The classification results

Methods	Classifier	Performance Metrics		
		Accuracy (Acc)	Sensitivity (Sen)	Specificity (Spe)
Statistical features	NN medium	0.2	0.33	0.44
Statistical features 2	Decision Tree coarse	0.73	0.347	0.77
Statistical features of MRI D T	NN weighted		0.200	0.00
Statistical features of MRI D T 2	SVM fine gaussian	0.7	0.42	0.7
Vectorial form of MRI D T	Decision Tree fine	0.3	0.402	0.707
Deep features of the original MRI	SVM medium gaussian			0.77
Deep features of MRI D T	SVM fine gaussian	0.7	0.33	0.2
Original MRI dataset	ResNet	0.742	0.4	0.2
MRI D T dataset	ResNet		0.24	0.32

According to Table 4 it is presented that the results are below the 0.5 Acc value for statistical features on both the original MRI and MRI D T datasets. Additionally, the Sen values, which are the classification rate of the very mild demented class, are very low. On the other hand, the Spe values, which are the classification rate of the non-demented class, are at a sufficient level. A very low Sen value and a very high Spe value indicate that the classifiers failed in the training process and mostly classified the data into non-demented classes. The classification success is to reach balanced and sufficient Sen and Spe values as well as Acc values.

MRI D T images are converted to vectorial form and used as a feature vector. This method produces 0.3 Acc, 0.402 Sen, and 0.707 Spe values in the decision tree classifier. It reveals a more meaningful feature vector with a high Acc value and more balanced Sen and Spe values compared to the statistical features.

The ResNet model makes classification with two types of input data. The first is the original raw MRI dataset, and the other is the MRI D T dataset. According to the results obtained with the original dataset, relatively good results are obtained with 0.742 Acc, 0.4 Sen, and 0.2 Spe values. However, the data belonging to the non-demented class are still classified more accurately; on the other hand, the data of the very mild demented class are not classified accurately enough. There appears to be a tendency towards the non-demented class. Besides, the MRI D T dataset demonstrates the result with 0.24 Acc, 0.2 Sen, and 0.32 Spe values, which is lower than the original MRI dataset. The results show both a low Acc and an immoderate Sen and Spe values, and not being able to adequately distinguish both class groups. Here, it can be concluded that the D T process causes a loss of information about the dataset for deep learning.

Looking at the methods and classifiers table, it is seen that the best combination is achieved with the SVM classifier using ResNet deep features. The ResNet model is trained using the original train MRI dataset; then the activations obtained by the architecture are stored. In addition, the activations of the test MRI dataset are extracted over the trained network. By using the activations as features, the SVM is utilized as the classifier. This method produces the highest Acc value with 0.7 and also obtains stable and balanced results with 0.747 Sen and 0.77 Spe values. The results show that it can distinguish the patient and healthy class. This combination has been the method showing the highest success compared to other methods, especially in the highest true positive rate classification of the patient class. On the other hand, deep features of the MRI D T dataset produce a 0.7 Acc value but a low Sen value of 0.33 and a nonproportional high Spe value of 0.2.

The confusion matrices obtained by the methods are given in Figure 1. In the figure, the value 0 represents the healthy class (non-demented) and the value 1 represents the patient class (very mild demented).

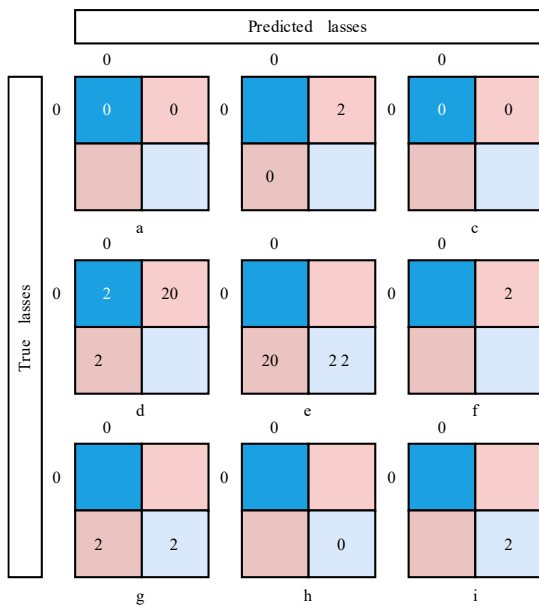


Figure The confusion matrices a statistical features b statistical features 2 c statistical features of MRI D T d statistical features of MRI D T 2 e vectorial form of MRI D T f deep features of original MRI g deep features of MRI D T h original MRI dataset i MRI D T dataset

S S S O A O S O S

MRI data contains very complex and meaningful information about the brain. The analysis of MRI images is an important role in the diagnosis of the disease. Various analysis and disease detection studies have continued to be carried out with machine learning solutions. In this study, a classification study is carried out using the Alzheimer's disease brain MRI dataset. The results are analyzed and interpreted by applying various feature extraction methods. In the study, seven different feature groups are analyzed separately, including statistical features obtained from the original MRI dataset in the study with two different processes: statistical features obtained from the MRI D T dataset with two different processes: directly MRI D T vectorial form and ResNet deep features of original MRI and MRI D T dataset. The feature groups are classified with sixteen classifiers, including three types of decision trees, six types of SVM, six types of NN, and the ResNet deep learning model.

According to the results, it shows that the statistical features are insufficient in the feature extraction process. In terms of the vectorial form of MRI D T, the method is open to improvement, but this combination creates a disadvantage for deep learning. The results of classification performance, both in itself and over deep features, are unsuccessful since the significant features are lost. On the other hand, the best feature extraction method according to the performance results of all methods is the deep features obtained by the ResNet model, and the classification of these features with the SVM algorithm. This result demonstrates the success of the deep learning model in making sense of in-depth features in the data. Besides, it shows that the SVM algorithm continues to produce high classification results, especially on biomedical data.

Acknowledgements

I thank Selçuk University and Scientific Research Projects Commission.

Ethics Committee Approval

Not applicable.

Peer review

Externally peer reviewed.

Author Contributions

Conceptualization: A, F, B; Investigation: A, F, B; A, G; Material and Methodology: A, F, B; Supervision: F, B; Visualization: A, F, B; A, G; Writing Original Draft: A; Writing review & Editing: A, F, B; A, G; Other: All authors have read and agreed to the published version of manuscript.

Conflict of Interest

The authors have no conflicts of interest to declare

Funding

This study is supported by Sel uk University Scientific Research Projects Commission with project number 2370 3

References

- Beaulac C, Gu S, Gibson E, Miranda M, F. Cao, Rocha L, Nathoo F. S. 2023. Neuroimaging feature extraction using a neural network classifier for imaging genetics. *BMC bioinformatics* 24: 27. <https://doi.org/10.1186/s12859-023-0344-x>
- Chakraborty D, Huang Y, H. Fiecas M, B. Shen, Pan. 2023. Deep Learning Based Feature Extraction with MRI Data in Neuroimaging Genetics for Alzheimer's Disease. *Genes* 14: 3. Retrieved from <https://doi.org/10.3390/genes1403027>
- He H, Hang Y, Ren S, Sun. 2020. 27-30 June 2020. Deep Residual Learning for Image Recognition. Paper presented at the 2020 IEEE Conference on Computer Vision and Pattern Recognition (CVPR).
- Apalan E, Altunisik E, Ekmekyapar F, Datta Barua P, Dogan S, Baygin M, Raendra Acharya U. 2022. Novel nested patch based feature extraction model for automated Parkinson's Disease symptom classification using MRI images. *Computer Methods and Programs in Biomedicine* 224: 107030. <https://doi.org/10.1016/j.cmpb.2022.107030>
- Uwil F. H. 2022. A new feature extraction approach of medical image based on data distribution skew. *Neuroscience Informatics* 2(3): 000-7. <https://doi.org/10.1016/j.neuri.2022.100007>
- Mallat S. G. A theory for multiresolution signal decomposition: the wavelet representation. *IEEE Transactions on Pattern Analysis and Machine Intelligence* 7(7): 74-93. <https://doi.org/10.1109/34.243123>
- Men G, Chen S. 2020. A new denoising method for fMRI based on weighted three dimensional wavelet transform. *Neural Computing and Applications* 2(2): 23-27. <https://doi.org/10.1007/s00202-020-07217-7>
- Sharma A, Nandal A, Dhaka A, Polat A, Alwadi R, Alenezi F, Alhudhaif A. 2023. HOG transformation based feature extraction framework in modified Resnet 10 model for brain tumor detection. *Biomedical Signal Processing and Control* 4: 04737. <https://doi.org/10.1016/j.bspc.2023.104737>
- Tasci B, Tasci I. 2022. Deep feature extraction based brain image classification model using preprocessed images. *PDRNet. Biomedical Signal Processing and Control* 7: 03-4. <https://doi.org/10.1016/j.bspc.2022.103040>
- Ima Acar, Bahtiyar F, Kmekci A. 2022. Future activity prediction of multiple sclerosis with 3D MRI using 3D discrete wavelet transform. *Biomedical Signal Processing and Control* 7: 03-40. <https://doi.org/10.1016/j.bspc.2022.103040>

Design and Implementation of a Battery Management System for a Solar Charger

Ömer Akın¹, Mehmet Ali Şen¹, Hammettullah Amiri², Hayati Mamur^{1*}

Abstract Batteries are used to store energy in areas where there is no grid and they need various DC DC converters to use this stored energy. In this study, the current and voltage monitoring system required to operate the maximum power point tracking (MPPT) algorithms from the battery with microcontrollers (MCU) was designed and implemented. Current, voltage, battery output power, and duty cycle data of metal oxide semiconductor field effect transistor (MOSFET) were visualized and instantly monitored on the computer screen using STM32F407VGT microcontroller (MCU). A voltage divider circuit is used to determine the battery output power used for MPPT. These current and voltage values are digitized for MPPT algorithms. Voltages up to 10 V DC are detected using a voltage divider for the voltage of the load. Ten-bit analog-to-digital converter (ADC) is made by transmitting the voltage information of the voltage divider to the analog inputs of the MCU. Thus, all data were collected on the STM32F407 MCU and both the current, voltage, and power data of the battery output were visualized and digitized by recording. As a result, these data have been brought to a state where they can be easily used in the inputs of MPPT algorithms.

Keywords MPPT converter, current sensor, voltage sensor, microcontroller

¹Address: Manisa Celal Bayar University, Faculty of Engineering, Manisa, Turkey

²Address: Islamic University, Department of Electrical and Electronic Engineering, Dhaka, Bangladesh

*Corresponding author: hayati.mamur@cbu.edu.tr

1. Introduction

Battery management is critical for the efficient operation of electronic devices. Engineers and researchers are working on the best use of power. Various battery management systems (BMS) are being developed to ensure that electronic devices have a longer life and work for longer periods. The more efficient the BMS is designed, the more efficient the operation of electronic devices.

BMS generally works on 24 V DC voltage. Power electronic circuits such as buck converter, boost converter, or buck-boost converter are used to regulate this voltage. Voltage to be used with these circuits. It is converted into voltage at which electronic devices can operate. These systems can provide uninterrupted electrical energy to the user, especially in cases where there is no grid or the grid becomes fault. In addition, they are useful in storing energy and managing the distribution of this energy by using BMSs in thermoelectric generators (TEG) or photovoltaic panel (PV) hybrid systems.

BMS uses DC DC converters with MPP tracker (MPPT) algorithms for both voltage regulation and MPP. To use these MPPT algorithms, the current and voltage at the output of the DC DC converter must be known. For this, current and voltage sensors are used. With these sensors, this information is obtained, and the power value is calculated. As a result, MPP monitoring is performed by changing the duty cycle of the metal oxide semiconductor field effect transistor (MOSFET) in the DC DC converter. Mamur and Şen (2020)

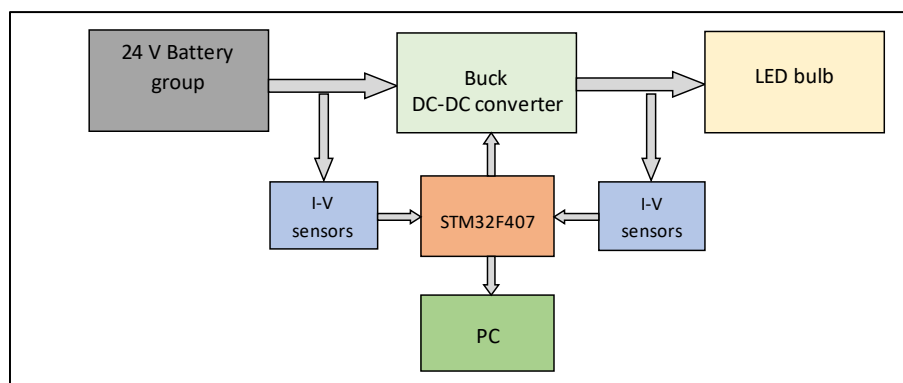
In the literature, it is seen that the measurement of battery current and voltage value is done by using various electronic equipment. Dalala *et al.* (2020) carried out their studies for MPPT by making current and voltage detections with voltage divider resistors without using any physical connection in their systems. They used the current-voltage general characteristic of TEG as the basis of their system. Twaha *et al.* (2021) investigated the performance of DC DC converter with incremental conductivity (IC) MPPT algorithm. They used both current and voltage sensors in their systems. Chandrarathna and Lee (2022) made a double-stage amplifying converter in the MPPT system they developed. They made their measurements using a current mirror for current and voltage divider resistors for voltage. Gabbar *et al.* (2022) designed a BMS that monitors

battery status using a wi fi signal Rodr gue *et al.* Rodr gue *et al.* 2022 conducted a study following the open circuit MPPT algorithm for wireless sensor networks They have only detected the open circuit voltage which is a re uirement of their algorithm with the voltage divider They delivered the current and voltage measurements to the microcontroller MCU system with the help of sensors

In this study a current mirror has been developed to measure the output voltage and current value of a DC DC converter In order for the user to monitor these values a computer program called Tera Term is used to make the variables in the system appear instantly In addition the output current and voltage values of the step down DC DC converter used and the value of the duty cycle in which the MOSFET is triggered are visuali ed on this software and instant information about the performance of the system is obtained In this part of the study after a general introduction materials and methods are given in the second part Outputs and comments are given in the third section and the results are presented in the fourth section

2 A A A HO

STM32F407 MCU is one of the main materials used in this study The block diagram of the system is given in Figure



Fi ure 1 The block diagram of the system

Tera Term software was used to visuali e the data in this system It was designed and manufactured by performing calculations of a step down DC DC converter for making MPPT A voltage divider circuit capable of measuring up to 0 V is used to detect the current and voltage values at the output of this buck DC DC converter These data are sent to the STM32F407 MCU via USART communication The measurement of the voltage value at the output of the buck DC DC converter is detected by the voltage divider and transmitted to the analog input of the STM32F407 and converted to a 0 bit digital value The voltage value passing over k in a voltage divider connected in 00 k and k series connected to the voltage measurement buck converter was determined and delivered to the MCU

A 24 buck DC DC converter designed during the working process is connected to the output of the battery and an LED bulb is connected to the output of this converter To prevent this designed converter from being affected by sudden voltage fluctuations two 47 F 0 V capacitors are connected to its input The coil value was chosen as 0 H N schotky diode is used to prevent reverse electromotive force in the coil The n channel IRF 44N MOSFET in the system was triggered at 30 kHz Since the voltage from this circuit will fluctuate a capacitor of 47 F 0 V is used to regulate it The P M pin of the STM32F407 MCU is used to trigger this circuit element This MCU can only output 3.3 V However for the circuit to be triggered the MOSFET must be triggered at a voltage higher than V For this reason MOSFET driver integrated circuit IC named IR2 0 is used for triggering For this IC to work a 0 resistor and a flyback diode have been added to the MOSFET output side hen 2 V and V input voltages are applied to this circuit the output voltage is at least 3 V and at most 23 V while the input current reaches a minimum of 0.0 A and a maximum of 2.0 A

The visuali ation and instantaneous monitoring of the variables in this designed system is done through Tera Term software For the MCU to work with Tera Term software it provides serial communication with the USART feature which is standard in STM32F4 Since this method works with the USART communication protocol there are only transmitter T and receiver R communication ends In the UART protocol the serial T end of the computer is connected to the R end of the MCU and the R end is connected to the T end of the MCU since the data in the MCU can receive this data from the receiver end while the data in the MCU is going through the transmitter channel USART block diagram between STM32F407 MCU and computer is given in Figure 2

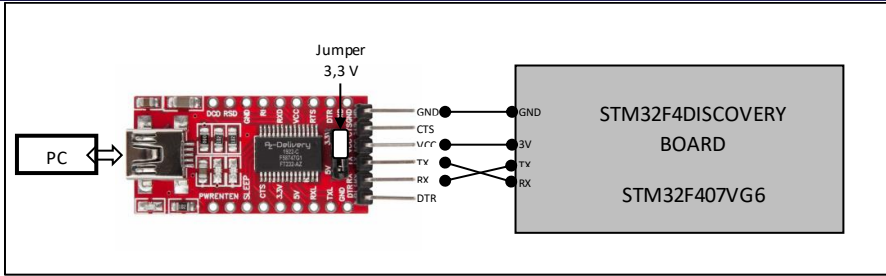


Figure 2 PC FT232RL USB TTL converter and MCU connection

The design of the interface used in the visualization of the system was made over Tera Term software. In this program, by making serial port communication with the USART protocol over the MCU. Thanks to this software, it can transfer the data from the MCU to the user in a simplified way. The current, voltage, power, and duty cycle values of the buck DC/DC converter, which should be at the interface of the designed system, are included in this design. In addition, a chart layout has been used so that these values can appear more regularly. To receive data from this designed interface, it is connected to the USB input of the computer using a FT232RL USB TTL converter and reflected on the screen with a bandwidth of 200.

The software of the STM32F407 MCU was written in the compiler called STM32 Cube Integrated Development Environment (STM32 Cube IDE) to be able to switch the DC/DC converter and display the output current, voltage, power, and duty cycle values of this converter on Tera Term software and to run MPPT algorithms. In this program, it can read up to 0 V voltage by using the analog signal output between 0 V and 3.3 V from the voltage divider circuit connected to the output of the battery. Variables are assigned to hold these input analog values and convert the raw value to voltage. Project configuration of STM32F407 MCU via Cube IDE is shown in Figure 3.

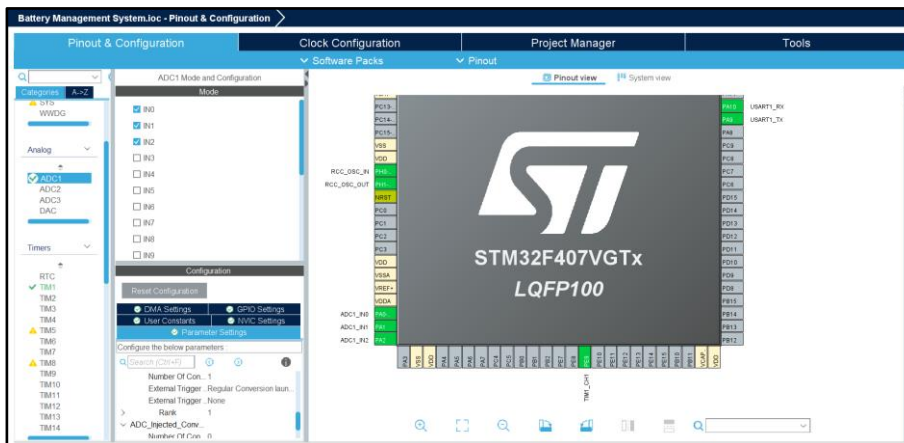


Figure 3 STM32CubeIDE interface in STM32CubeIDE

Separate variables were used for PWM and duty cycle, and MCU configurations were made. It is setup to a 30 kHz PWM signal using the first channel timer for the STM32F407 MCU via the STM32CubeIDE compiler. To provide this signal, the clock speed is set to 100 MHz. To read the analog values coming from the voltage divider, the analog values are converted to digital values by assigning the pin on the first ADC channel of the ADC, and the voltage reading is made. USART channel is used to make serial communication between MCU and computer, and USB TTL converter is used to provide the necessary connection. If necessary, MPPT algorithms can be added to this program.

3. Results

The image of the computer screen showing the variables of the implemented system is given in Figure 4. Input current, voltage, and power data of the output of the step-down DC/DC converter are reflected via this software.

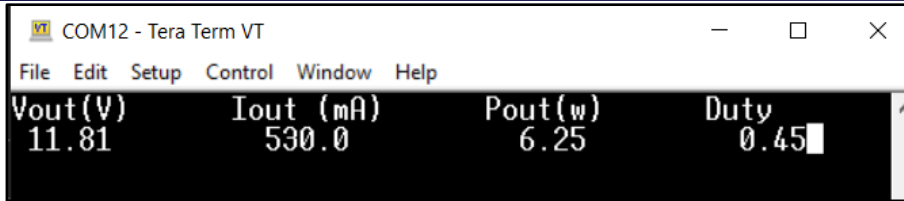


Figure Tera Term interface

It has been possible to instantly monitor the output data of the buck DC DC converter on the computer screen. In addition, since this data is digitized, it can be stored in any desired cloud network for later analysis. In addition, since this system will be used in battery MPPT algorithms, it is possible to instantly look at the duty cycle value of the MOSFET. Thus, when the load changes, the change in the output power of the buck DC DC converter can be monitored. However, the efficiency of this buck DC DC converter can be calculated with the visualization of the variables in this developed battery management system, a convenience has been created for MPPT software developers.

S S O A O S O S

In this study, for the control of LED lighting in places where there is no grid, the appropriate voltage regulation of the 24 V battery for the LEDs and the power measurement monitoring system were designed and implemented. The output power variables of the buck converter connected to the battery output are visualized on the computer screen. It is possible to monitor the duty cycle, which is an important criterion in MPPT monitoring and constantly changes depending on the load changes, with this developed system, LED lighting can be controlled by regulating the battery voltage in places where there is no grid.

Ac le eme ts

This paper was supported by the Manisa Celal Bayar University Scientific Research Projects Coordination Unit, Project Number 2023 04.

thics mmittee A r val

N A

eer revie

Externally peer reviewed

Auth r tributi s

Conceptualization: M R A B and H M; Investigation: O E G; Material and Methodology: O E G and M A U; Supervision: M R A B and H M; Visualization: O E G and M A U; Writing Original Draft: O E G and H M; Writing review: Editing: O E G, M R A B and H M; Other: All authors have read and agreed to the published version of manuscript.

lict terest

The authors have no conflicts of interest to declare.

Fu i

This paper was supported by the Manisa Celal Bayar University Scientific Research Projects Coordination Unit, Project Number 2023 04.

F S

Chandrarathna S C, Lee 20 A dual stage boost converter using two dimensional adaptive input sampling MPPT for thermoelectric energy harvesting. *IEEE Transactions on Circuits and Systems I: Regular Papers*, 2024, 4(4): 400.

Dalala M, Saadeh O, Bdour M, ahid U 20 A new maximum power point tracking MPPT algorithm for thermoelectric generators with reduced voltage sensors count control. *Energies*, 2023, 16(7): 2.

Gabbar H A, Othman A M, Abdussami M R 2022 Review of battery management systems: BMS development and industrial standards. *Technologies*, 2022, 12(2): 2.

- Mamur H oban 2020 Termoelektrik enerat rler i in al altan y kselten eviricili maksimum g noktas takibi ben etimi Pamukkale niversitesi M hendislik Bilimleri Dergisi 2 2
- Rodr gue Garc a Mer R Lamar D G Sebasti n 2022 A novel version of the ripple modulation techni ue for enabling the use of single phase buck converters in VLC applications IEEE ournal of Emerging and Selected Topics in Power Electronics
- Twaha S hu an Li B Huang 20 7 Performance analysis of thermoelectric generator using dc dc converter with incremental conductance based maximum power point tracking Energy for Sustainable Development 37

Stacked Autoencoder Feature Selection for Zero Day Threat Detection

Mahmut Tokmak¹, İbrahim Nkongolo²

Abstract Zero day attacks exploit previously unknown vulnerabilities in software, hardware, or networks. Since these vulnerabilities are not yet patched or protected against, they present a significant risk. Detecting zero day attacks is crucial due to their exploitation of unknown vulnerabilities, posing significant risks to cybersecurity. Timely detection allows for swift response and deployment of countermeasures, minimizing the window of opportunity for attackers. It protects sensitive data, mitigates financial losses, safeguards reputation, and strengthens cybersecurity practices. Detecting zero day attacks provides insights into attack vectors, improves security measures, and enhances incident response capabilities. It helps prevent future attacks by understanding adversary techniques and updating defense mechanisms. Overall, zero day attack detection plays a critical role in mitigating risks, protecting assets, and staying ahead in the evolving threat landscape. This study explores the application of stacked autoencoder (SAE), a type of artificial neural network, for feature selection and zero day threat classification using a Long Short Term Memory (LSTM) scheme. The process involves preprocessing the UGRansome dataset and training an unsupervised SAE for feature extraction. Fine tuning with supervised learning is then performed to enhance the discriminative capabilities of this model. The learned weights and activations of the autoencoder are analyzed to identify the most important features for discriminating between zero day threats and normal system behavior. These selected features form a reduced feature set that enables accurate classification. The results indicate that the SAE LSTM performs well across all three attack categories by showcasing high precision, recall, and F1 score values, emphasizing the model's strong predictive capabilities in identifying various types of zero day attacks. Additionally, the balanced average scores of the SAE LSTM suggest that the model generalizes effectively and consistently across different attack categories. The SAE LSTM model excels in detecting signature attacks, while synthetic signature and anomaly attacks pose challenges due to abnormality or absence of patterns. The methodology we put forth utilizes the SAE LSTM technique, resulting in a remarkable accuracy of 95%, outperforming prior intrusion detection studies. Hence, this research aims to contribute to advanced cyberintelligence to proactively mitigate zero day threats. Future cyberintelligence can progress by refining the proposed feature selection model, addressing computational efficiency of the UGRansome dataset, and integrating hybrid methodologies for improved intrusion detection capabilities.

Keywords Stacked Autoencoder, Feature Selection, Zero Day Threats, Machine Learning, Deep Learning, UGRansome, Cyberintelligence

¹**Address** Burdur Mehmet Akif Ersoy University, Bucak, İliha Tolunay School of Applied Technology and Management, Burdur, Turkey

²**Address** University of Pretoria, Faculty of Engineering, Built Environment and Information Technology, Department of Informatics, Pretoria, South Africa

* **Corresponding Author**: mahmuttokmak@mehtakif.edu.tr

1. Introduction

In the ever-evolving landscape of cybersecurity, the emergence of advanced and elusive threats poses unprecedented challenges to organizations, governments, and individuals alike. Among these threats, zero day attacks have garnered substantial attention due to their potential to exploit undiscovered vulnerabilities and wreak havoc on digital infrastructure. A zero day attack refers to a cyber assault that targets a previously unknown vulnerability in software, hardware, or network systems. These vulnerabilities, referred to as zero day vulnerabilities, are named as such because developers have zero days to address and patch them before malicious actors exploit them. Zero day attacks are particularly effective because they can strike unexpectedly and catch defenders off guard. This surprise factor lets them evade regular security measures. Unlike known vulnerabilities, zero day vulnerabilities have no documented fixes or protections, giving attackers a notable upper hand. Consequently, zero day attacks present a daunting challenge for defenders, as they often evade signature-based detection systems and intrusion prevention tools. Nkongolo, Tokmak (2023), Thomas et al. (2022), Tokmak (2022). In the era of big data, extracting meaningful and representative features from high-dimensional datasets has become a cornerstone of modern data analysis and machine learning. Among the myriad of techniques, stacked autoencoders (SAEs) have emerged as a powerful tool for automated feature learning

enabling the discovery of intricate data structures and patterns. Rooted in the field of deep learning, DL SAEs offer a compelling solution to the challenge of high dimensional data representation, presenting a pathway towards enhanced predictive modeling, efficient dimensionality reduction, and insightful data interpretation. Boussaad, Boucetta, 2021; Kim et al., 2020. Feature selection with SAEs has been explored in several papers. Feature extraction using SAEs has been explored in various domains.

Yang et al. proposed the broad autoencoder features (BAF) which consist of four parallel interconnected SAEs with different activation functions. Tian, Yang et al., 2021. Yang et al. used a stacked autoencoder with L2 norm regularization for dimensionality reduction and feature extraction from electricity load data. Yang et al., 2020. Yang et al. introduced a stacked supervised autoencoder (SSAE) to acquire fault relevant attributes from raw input data and improve fault classification accuracy. Yang et al., 2020. Chatterjee et al. integration of SAE characteristics with wavelet based and morphological fractal texture attributes for the classification of skin disorders achieved high accuracy. Chatterjee et al., 2021. Kim et al. suggested an enhancement in tool condition diagnosis through the utilization of SAE based CNC machine tool prognosis incorporating feature extraction from discrete wavelet transform. Kim et al., 2020. Zero day threat detection involves identifying and mitigating attacks that exploit unknown vulnerabilities, such as a cybercriminal targeting a newly discovered weakness in a popular software program before the software developer has a chance to release a patch. Nkongolo et al. introduced the UGRansome dataset, which facilitates the identification of anomalies and zero day attacks that cannot be recognized by known threat signatures. Nkongolo et al., 2021. Umar and Sinha proposed a resilient and smart cyber attack detection model that uses the notion of prominent entities and network structure techniques to detect zero day attacks. Umar, Sinha, 2021. Sarhan et al. proposed a zero shot learning approach for assessing the effectiveness of machine learning models in detecting zero day attacks. Sarhan et al., 2023.

Millar et al. suggested a deep neural network for Android malware detection without prior knowledge of malicious characteristics, achieving high detection rates for zero day scenarios. Millar et al., 2021. Blaise et al. proposed the utilization of the Split and Merge technique to promptly identify emerging botnets and recently exploited vulnerabilities, reducing false positives. Blaise et al., 2020. Long Short Term Memory (LSTM) networks have displayed significant potential in unknown vulnerabilities and malware detection. Researchers have dedicated significant efforts to studying LSTM hyperparameters for the development of Intrusion Detection Systems (IDS). They have explored diverse LSTM setups and configurations. What they have discovered is that the significance of these hyperparameters in the context of IDS varies from their importance in language model applications. The interplay of hyperparameters significantly influences the assessment of their respective significance. Considering this interaction, the precise order of importance for LSTMs in IDSs includes batch size as the most critical, followed by dropout ratio and padding. Additionally, sensitivity based LSTM models have been proposed for designing System call Behavioral Language (SBL) for malware detection. These models achieve impressive Area Under the Curve (AUC) values and specificity on unknown attack datasets.

Another approach involves using LSTM with word embedding and attention mechanisms to effectively represent and classify malware files, achieving high accuracy and F1 scores. Sewak et al., 2021. Jie et al., 2020. Jie et al., 2020. Hang, 2020. A method for zero day detection using LSTM is proposed in the paper by Fang et al. The model is designed to detect malicious JavaScript code injected into web pages. It extracts features from the semantic level of bytecode and optimizes the method of word vector. The LSTM based detection model outperformed existing models based on Random Forest and Support Vector Machine (SVM) algorithms. Fang et al., 2021. Another paper by Roberts and Nair introduces a neural architecture for anomaly detection in discrete sequence datasets. Their model combines a modified LSTM autoencoder with an array of One Class SVMs to find anomalies within sequences. The proposed method shows improved stability and outperforms standard LSTM and sliding window anomaly detection systems. Roberts, Nair, 2021.

This study aims to leverage the synergistic capabilities of SAE and LSTM networks to improve the identification and categorization of zero day threats using the UGRansome dataset. The primary objective is to integrate feature selection techniques into the SAE architecture to streamline the extraction of pertinent and differentiating features from raw data. By carefully choosing the input data, the subsequent LSTM network can adeptly capture temporal relationships within the feature domain. Ultimately, this research strives to advance proactive and resilient cybersecurity strategies by introducing an innovative approach: a feature selection driven SAE based LSTM model. The subsequent sections of this work delve into the methodology, experimental setup, results, and discussions, all of which culminate in a comprehensive analysis of the proposed SAE based LSTM model for zero day threats detection using the UGRansome dataset.

2 A A A HO

2.1 Crime Dataset

In 2022 Nkongolo et al. [20] introduced the UGRansome dataset, a novel and comprehensive anomaly detection dataset designed to detect unknown network attacks, including zero-day threats. Unlike existing datasets in the IDS field, UGRansome includes previously unexplored unknown and ransomware attacks. The dataset comprises various attack categories, namely Signature (S), Anomaly (A), and Synthetic Signature (SS). Each category includes labeled instances of zero-day threats such as Locky, CryptoLocker, advanced persistent threats (APT), SamSam, AnnaCry, Ransomware, Globe Tower, and more. Table 1 provides an overview of the UGRansome features, while Table 2 displays the distribution of the UGRansome subsets. To gain a comprehensive understanding of the dataset statistics, we direct readers to Figure 3, which presents its key characteristics.

Table 1 The data structure of the UGRansome dataset

Feature	Category	Type	Feature	Category	Type
f1	SS	Categorical	f2	Cluster	Numeric
f3	S	Categorical	f4	A	Categorical
f5	Spam	Categorical	f6	BTC	Numeric
f7	Blacklist	Categorical	f8	Bytes	Numeric
f9	Nerisbonet	Categorical	f10	USD	Numeric
f11	UDP scan	Categorical	f12	igSA	Categorical
f13	SSH	Categorical	f14	Port	Numeric
f15	DoS	Categorical	f16	CryptoLocker	Categorical
f17	Port scanning	Categorical	f18	annaCry	Categorical

Table 2 The UGRansome subsets

Subset	A	S	SS
UGRansome Train	40,323	2,22	
UGRansomeVal		43	73
UGRansome Test	4,70	3,40	4
Total	3	3	34
Average avg	4	2	

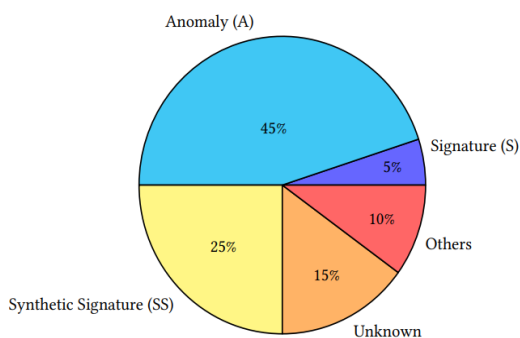


Figure 3 Distribution of zero-day threats categories of the UGRansome dataset

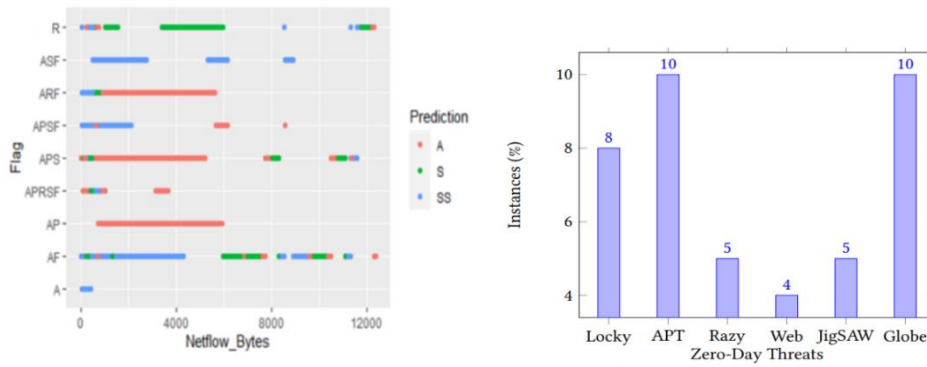


Figure 2 The network flags and distribution of zero day threats of the UGRansome dataset

Dataset Statistics

Number of Variables	14
Number of Rows	207533
Missing Cells	0
Missing Cells (%)	0.0%
Duplicate Rows	58491
Duplicate Rows (%)	28.2%
Total Size in Memory	106.9 MB
Average Row Size in Memory	540.2 B
Variable Types	Numerical: 4 Categorical: 9 GeoGraphy: 1

Figure 3 The characteristic of the UGRansome dataset

2.2 Stacked Autoencoder

SAEs are a type of neural network NN architecture that is used for feature extraction and dimension reduction in various tasks including biometrics recognition image recognition natural language processing and automatic speech recognition Tokmakov et al. 2022. It is called stacked because it consists of multiple layers of autoencoders where each layer is trained to reconstruct the output of the previous layer. The training of SAEs involves two steps: unsupervised pre-training and supervised fine-tuning. In the unsupervised pre-training step, each layer of the network is trained individually using autoencoders which learn internal data representations. These representations are then used to initialize the network weights and improve generalization.

In the supervised fine-tuning step, the pre-trained layers are stacked together and trained in a supervised manner using labeled data. This approach has been shown to achieve high accuracy rates in biometrics recognition tasks Boussaad and Boucetta 2022. In the context of automatic speech recognition, SAEs have been used to design networks for recognizing speech sounds articulated by children, achieving high accuracy rates (Liu et al. 2020). SAEs can also be enhanced by incorporating data weighting techniques which improve the robustness and discriminative power of the network (Sun et al. 2022). Additionally, SAEs have been used for automatic voice quality evaluation in call centers, achieving better correlation coefficients compared to traditional methods (Liang et al. 2022). In the field of intrusion detection, stacked sparse autoencoders have been proposed for dimensionality reduction and classification, achieving better results compared to existing methods (Mananatha Gogoi 2022). It has also been used effectively in malware detection (Rathore et al. 2020; Samaneh et al. 2022; Hu et al. 2022). Figure 4 illustrates a SAE architecture.

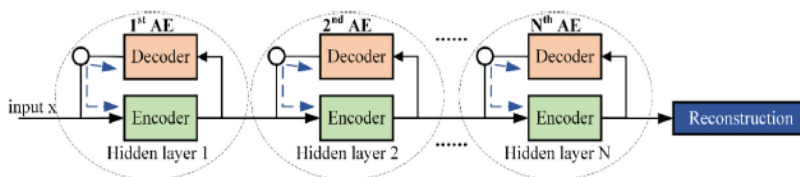


Figure 4 Structure of SAE model (Luo et al. 2022)

2.3 Short-term memory

Recurrent Neural Network (RNN) is a variation of the feedforward neural network (NN). The architecture of the feedforward NN encompasses several layers, each comprised of neurons with connections between layers proceeding

unidirectionally resulting in a sequential arrangement of layers. RNN introduces a recurrent structure within the NN by establishing connections from each node (neuron) to itself. This self-connection mechanism allows the RNN to retain previous inputs, potentially impacting the network's output. (Fan et al., 2017; Naik, Mohan, 2019; Wang et al., 2020). In RNN, the inference process is similar to the feedforward NN, completed by forward propagation. Training in RNN is done through the mechanism of backpropagation through time, updating the weights using the gradient.

In RNN, the gradient for each output depends not only on the current layer but also on the previous layer. If backpropagation is continuously updated at intervals, the gradient can approach zero, leading to the vanishing gradient problem, followed by the problem of weakening gradients. Similarly, when gradients become too large, the result can grow significantly, leading to the exploding gradient problem. (Metin, Arasulu, 2019). The LSTM DL algorithm was developed by Hochreiter and Schmidhuber in 1997 as a variant of the RNN model, aiming to mitigate the drawbacks associated with traditional RNN architecture. (Hochreiter, Schmidhuber, 1997). Distinct from classical RNN, LSTM introduces the concept of memory cells for its nodes, enabling the linkage of prior data information to the present nodes. Each LSTM node encompasses three gating mechanisms: an input gate, a forget gate, and an output gate. (Figure 1)

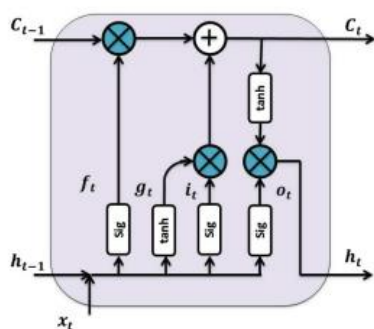


Figure 1 LSTM architecture (Smagulova, Ames, 2020)

2 Performance Evaluation

After the data preprocessing steps, the dataset obtained, consisting of a total of 20,000 examples, was split into 80% training and 20% testing.

```
The UGRansome columns names
df.columns = ['Time', 'Protocol', 'Flag', 'Family', 'Clusters', 'SeddAddress', 'ExpAddress',
              'BTC', 'USD', 'Netflow Bytes', 'IPaddress', 'Threats', 'Port', 'Prediction']
```

```
Drop the columns to exclude from the analysis
columns to drop = ['column to drop', 'column to drop', 'column to drop', 'column to drop', 'column to drop']
ugransome_df.drop(columns=columns_to_drop, inplace=True)
```

```
Split the DataFrame into features and labels
ugransome_df.drop(columns='target column', inplace=True)
features = ugransome_df
y = ugransome_df['target column']
```

```
Split the data into training and testing sets while preserving specific columns
train, test = train_test_split(features, y, train_size=0.8, test_size=0.2, random_state=42,
                               preserve_df=True)
```

The evaluation of the training and testing performance of the established models was conducted by calculating accuracy, precision, recall, and F-scores. The accuracy metric, denoting the proportion of accurately classified instances used to assess the training and testing effectiveness of the formulated model, is mathematically expressed in Equation 1. The precision metric, quantifying the accuracy of positive predictions among the actual positives, is formally defined in Equation 2. The recall metric, indicating the proportion of true positive values correctly identified, is represented as Sensitivity/Recall in Equation 3. The F-Score, a composite metric of recall and precision, is mathematically defined as score = 2 * (precision * recall) / (precision + recall).

$$Accuracy = \frac{TP + TN}{TP + FN + TN + FP}$$

$$Precision = \frac{TP}{TP + FP} \quad 2$$

$$Sensitivity = \frac{TP}{TP + FN} \quad 3$$

In this study the training and testing of the proposed data preprocessing feature extraction and classification models were conducted with the Python programming language version 3.0.2. The methodology employed for this work is explained in this section. The framework of the study is illustrated in Figure 1 and Algorithm 1.

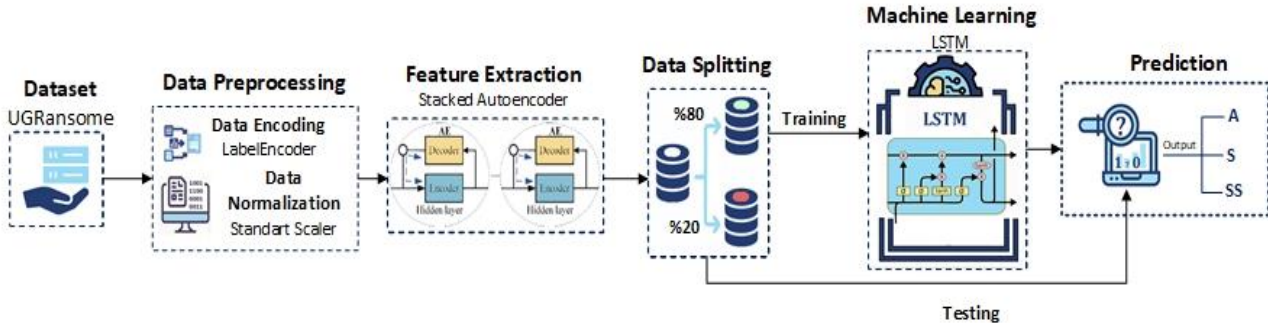


Figure 1 Proposed study model

Algorithm 1 Feature Selection SAE-based LSTM model

```

Require:
1: UGRansome dataset
Ensure:
2: Prediction results
3: function COMBINEDAPPROACH
4:   LoadDataset
5:   PreprocessRowsdata
6:   ApplyNormalizationdata
7:   ApplyFeatureExtractiondata
8:   (X_train, y_train), (X_test, y_test) = SplitDatasetdata
9:   TrainLSTMX_train, y_train
10:
11:   model = TrainLSTMX_train, y_train
12:   PerformPredictionmodel, X_test
13:
14:   predictions = PerformPredictionmodel, X_test
15:   AnalyzeResultsy_test, predictions
16:   FeatureSelection
17:   selected.features = FeatureSelectionX, a, b, c
18:
19:   return final_results
20: function FEATURESELECTION(X, a, b, c)
21:   Normalize input features X
22:   Calculate membership degrees μ(x; a, b, c) for each feature x ∈ X
23:   Initialize feature importance scores I = {0, 0, ..., 0}
24:   for i = 1 to n do
25:     for j = 1 to n do
26:       I[i] ← I[i] + μ(x_j; a, b, c)
27:   Sort features based on importance scores in descending order
28:   X_selected ← top-ranked features from X based on I
29:   return X_selected
    
```

Algorithm 1 The proposed SAE LSTM feature selection algorithm where a denotes anomaly class, b signature class and c synthetic signature class.

The training and testing processes of the suggested data encoding, normalization, SAE, and LSTM model were conducted using the Google Colaboratory cloud system. This system provides ready access to numerous Python libraries and offers its services for free (Colab 2023) within the Colab platform. Nvidia CUDA technology was employed to leverage GPU acceleration for faster algorithm execution. Tasks such as file uploading, data preprocessing, setting up the data frame, and more were carried out using Python libraries including numpy, pandas, statistics, sklearn, matplotlib, pyplot, and seaborn. As for the suggested SAE and LSTM architecture, the Python TensorFlow library was utilized. The suggested SAE layers and parameters are given in Table 3. In the established SAE architecture, three encoders with 7, 0, and 3 layers and three decoders with 0, 7, and 3 layers were employed. The activation function was set to relu, the optimizer parameter to Adam, the loss parameter to mse, and the epoch parameter to 10. The suggested LSTM layers and params are given in Table 4. The constructed LSTM network consists of 3 layers, each containing 100 neurons. The loss parameter was set to sparse categorical crossentropy, the optimizer parameter to Adam, and the epoch parameter to 400.

Table 3 SAE layers and params

Layer type	Output Shape	Param
input InputLayer	None 3	0
dense Dense	None 7	0 0
dense Dense	None 0	3 00
dense 2 Dense	None 3	3
dense 3 Dense	None 0	700
dense 4 Dense	None 7	3 2
dense Dense	None 3	
Total params		02

Table 4 LSTM layers and params

Layer type	Output Shape	Param
lstm 3 LSTM	None	22 304
dense 2 Dense	None 3	07
Total params		22

3 S S

After completing the data preprocessing and feature extraction steps the trained LSTM model was tested resulting in the following performance metrics accuracy precision recall and F score were measured as 0.40 0.40 0.40 and 0.40 respectively. These metrics are summarized in Table and Figure 7.

Table Performance metrics

	Precision	Recall	F score	Support
A	0.77	0.3	0.73	320
S	0.4	0.7024	0.4	23
SS	0.7	0.437	0.0	4
Accuracy			0.4	4.07
Average	0.004	0.4	0.424	4.07

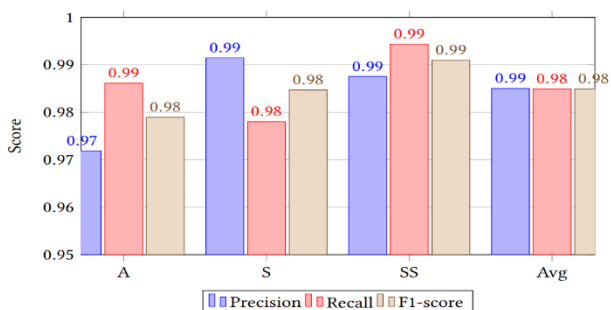


Figure 7 Visualization of the performance metrics

In summary Table and Figure 7 indicate that the SAE based LSTM model performs well across all three attack categories Anomaly A Signature S and Synthetic Signature SS. It showcases high precision recall and F score values emphasizing the model's strong predictive capabilities in identifying various types of attacks. Additionally, the balanced average scores suggest that the model generalizes effectively and consistently across different attack categories. The confusion matrix is a tool used in machine learning and classification tasks to visualize the performance of a model by presenting the number of true positive (TP), true negative (TN), false positive (FP), and false negative (FN) predictions. It is particularly useful when evaluating the accuracy of a classification algorithm. The confusion matrix showing the test results of the proposed work is shown in Figure

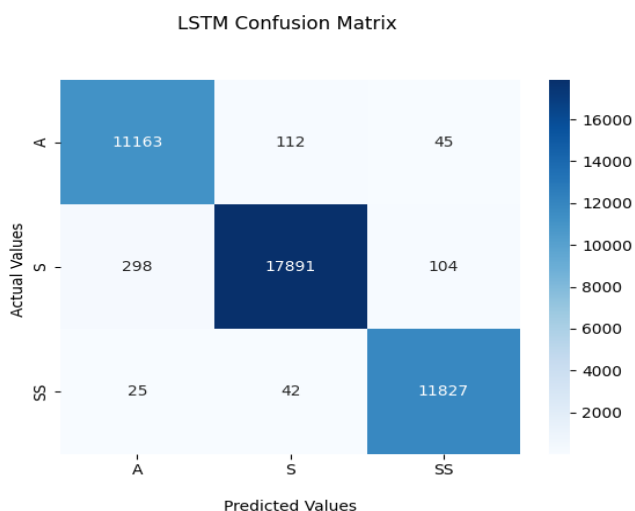


Figure Confusion matrix

The SAE based LSTM models superior precision recall and F score in detecting signature attacks compared to synthetic signature and anomaly attacks signifies its effectiveness in identifying known threat patterns Figure 7 Signature attacks are recogni ble due to established patterns and the models adeptness in pinpointing instances aligned with these patterns is pivotal for real time threat detection Synthetic signature attacks involve modified or novel attack signatures and the models slightly lower performance could suggest difficulty in identifying unconventional or altered signatures underscoring the challenge of evolving threat detection Figure 7 Anomaly attacks representing ero day or novel threats pose a greater detection challenge as their lack of discernible patterns complicates identification Figure 7 Future work in the IDS landscape can potentially use the UGRansome dataset and improve the proposed model parameters to enhance anomaly detection adapt the model for modified signatures implement continuous learning for emerging threats explore ensemble approaches and develop interpretable techni ues In essence the proposed models strong detection of signature attacks and potential improvements for synthetic signatures and anomalies highlight avenues for advancing IDSs

S SS O

Table presents a comparative assessment of different intrusion detection studies each employing distinct datasets and models Our proposed methodology centered around the UGRansome dataset leverages the SAE LSTM techni ue to achieve an impressive accuracy surpassing the performance of previous investigations Additionally this approach offers distinct advantages particularly within critical infrastructure contexts Notably several discussed studies within the IDS literature share the common limitation of feature selection Contrasting this im et al 2020 reali ed a 7 accuracy utili ng a signal autoencoder model on signal data promising for signal processing albeit lacking a tool diagnosis model hang 2020 harnessed LSTM on malware data achieving accuracy while addressing invasive software though grappling with dependency issues Sun et al 202 embraced SAE across diverse datasets achieving a commendable 0 accuracy with data weighting advantages although computational time remains a concern Blaise et al 2020 adopted the Split Merge techni ue on MA I and UCSD datasets yielding accuracy with exceptional attack detection albeit with false positives

Lastly Tokmak 2022 applied deep learning to the UGRansome dataset securing 7 accuracy with a pronounced focus on ero day threat detection also involving feature selection Pertaining to ero day attack detection our approach not only underscores its significance but also highlights its robust accuracy and emphasis making strides in addressing evolving threats Considering the importance of ero day attack detection our approach not only underscores its significance but also demonstrates robust accuracy and a proactive stance in tackling evolving threats To further advance cyberintelligence future efforts could concentrate on refining feature selection techni ues addressing computational efficiency challenges and exploring ways to integrate various methodologies to enhance overall intrusion detection capabilities

Table A comparative analysis with existing IDS studies

Auth r	ear	ataset	el	Accuracy	A va ta e	imitati
Nkongolo M Tokmak M	2023	UGRansome	Fu ification		Critical Infrastructure	Feature Selection

im et al	2020	Signal data	SAE	7	Signal Processing	Tool diagnosis model
hang	2020	Malware	LSTM		Invasive Software	Dependency
Sun T et al	202	MNIST CIFAR 10 and UCI	SAE	0	Data eighting	Computational time
Blaise et al	2020	MA I and UCSD	Split Merge		Attack Detection	False Positive
Tokmak M	2022	UGRansome	Deep Learning	7	ero Day Threat Detection	Feature Selection

O S O S

The detection and mitigation of zero day threats have emerged as critical imperatives in the landscape of cybersecurity. Zero day threats, by their very nature, exploit vulnerabilities that are yet unknown to software vendors and security teams, posing substantial risks to organizations and individuals. As attackers constantly evolve their techniques, the need for robust and adaptive zero day threat detection mechanisms becomes increasingly pressing. This research endeavors to harness the potential of deep learning techniques to effectively counter the ever-evolving landscape of zero day threats. By capitalizing on deep learning's ability to process unstructured data to provide classification and prediction analysis, we present a robust framework for zero day threat recognition. This framework integrates the LSTM approach with SAE feature extraction. The encouraging results obtained from our detection system underscore its significant effectiveness, thus offering valuable guidance and inspiration for forthcoming research pursuits in the field. In conclusion, the fight against zero day threats demands a multi-faceted approach that integrates cutting-edge technology, collaborative efforts, and robust risk management practices. While machine learning and deep learning are potent tools, they must be complemented by human expertise to effectively counteract the sophistication of modern cyber threats. As the cybersecurity landscape continues to evolve, the ability to detect and mitigate zero day threats will be a defining factor in ensuring the security and stability of digital ecosystems.

ethics committee Approval

N/A

peer review

Externally peer reviewed

Author Contributions

M T and M N contributed to the design and implementation of the research, to the analysis of the results and to the writing of the manuscript.

Conflict of Interest

The authors have no conflicts of interest to declare.

Financial

The authors declared that this study has received no financial support.

References

Blaise A, Bouet M, Conan V, Secci S. 2020. Detection of zero day attacks: An unsupervised port based approach. *Computer Networks* 180: 073.

Boussaad L, Boucetta A. 2021. Stacked Auto Encoders Based Biometrics Recognition. *2021 International Conference on Recent Advances in Mathematics and Informatics (ICRAMI)*.

Chatterjee S, Dey D, Munshi S. 2020. Morphological texture and auto encoder based feature extraction techniques for skin disease classification. *2019 IEEE 16th India Council International Conference (INDICON)* 4.

Fang, Huang C, Liu L, Yue M. 2022. Research on Malicious JavaScript Detection Technology Based on LSTM. *IEEE Access* 6(2): https://doi.org/10.1109/ACCESS.2022.740

Google Colaboratory. 2023. Colaboratory. <https://colab.research.google.com>

- Lim Lee H eon Lim M Lee H U Lim S 2020 Stacked auto encoder based CNC tool diagnosis using discrete wavelet transform feature extraction *Processes* 8 4 4
- Long Lin R ou H 2020 Feature extraction of load curve based on autoencoder network *2020 IEEE 20th International Conference on Communication Technology (ICCT)* 4 2 4
- umar V Sinha D 202 A robust intelligent zero day cyber attack detection technique *Complex & Intelligent Systems* 7 22 2234 <https://doi.org/10.1007/s40747-021-003>
- Luo S Huang ang Luo R hou 2022 Transfer learning based on improved stacked autoencoder for bearing fault diagnosis *Knowledge-Based Systems* 256 0 4
- Manunatha B A Gogoi P 2022 An Improved Stacked Sparse Auto Encoder Method for Network Intrusion Detection *Emerging Research in Computing, Information, Communication and Applications: ERCICA 2020, Volume 1* 03
- Millar S McLaughlin N del Rincon M Miller P 202 Multi view deep learning for zero day Android malware detection *Journal of Information Security and Applications* 58 027
- Nkongolo M Tokmak M 2023 Zero Day Threats Detection for Critical Infrastructures In A Gerber M Coetsee Eds *South African Institute of Computer Scientists and Information Technologists* pp 32 47 Springer Nature Switzerland <https://doi.org/10.1007/978-3-03-12-3>
- Nkongolo M Van Deventer P asongo S M 202 Ugansome A novel dataset for anomaly detection and zero day threats *Information* 12 0 40
- Nkongolo M van Deventer P asongo S M 2022 The Application of Cyclostationary Malware Detection Using Boruta and PCA In *Computer Networks and Inventive Communication Technologies* pp 47 2 Springer
- Rathore H Agarwal S Sahay S Sewak M 20 Malware detection using machine learning and deep learning *Big Data Analytics: 6th International Conference, BDA 2018, Warangal, India, December 18–21, 2018, Proceedings* 6 402 4
- Roberts C Nair M 20 Arbitrary discrete sequence anomaly detection with zero boundary LSTM *ArXiv Preprint ArXiv:1803.02395*
- Samaneh M Dima A Ghorbani A A 2022 Effective and Efficient Hybrid Android Malware Classification Using Pseudo Label Stacked Auto Encoder *Journal of Network and Systems Management* 30
- Sarhan M Layeghy S Gallagher M Portmann M 2023 From zero shot machine learning to zero day attack detection *International Journal of Information Security* 22 4 47 <https://doi.org/10.1007/s12072-023-00710-7>
- Sewak M Sahay S Rathore H 2022 LSTM Hyper Parameter Selection for Malware Detection Interaction Effects and Hierarchical Selection Approach *2021 International Joint Conference on Neural Networks (IJCNN)* <https://doi.org/10.1109/IJCNN43720.2021.9733323>
- Smagulova Ames A P 20 A survey on LSTM memristive neural network architectures and applications *The European Physical Journal Special Topics* 228 0 23 3 2324
- Sun T Ding S u 2022 An iterative stacked weighted auto encoder *Soft Computing* 25 4 33 4 43 <https://doi.org/10.1007/s00100-020-0407-7>
- Thomas V E Ugwu C Onyegbu L 2022 Comparative Analysis of Dimensionality Reduction Techniques on Datasets for Zero Day Attack Vulnerability *Journal of Software Engineering and Simulation* 7 4
- Tokmak M 2022 Deep forest approach for zero day attacks detection In S Tasdemir A O Okan Eds *Innovations and Technologies in Engineering* pp 44 Eitim aynevi
- Tokmak M ksille E U 2022 Comparative Analysis of Dimension Reduction and Classification Using Cardiocography Data In M araboyac A Demir al Eds *Versatile Multidisciplinary Engineering Research* pp 4 4 SRA Academic Publishing

- ang L ang hao G Su hao ang L 202 Automatic voice quality evaluation method of IVR service in call center based on Stacked Auto Encoder *IOP Conference Series: Earth and Environmental Science* 827 0 202
- ang T Ng Li wong S 202 Broad Autoencoder Features Learning for Classification Problem *International Journal of Cognitive Informatics and Natural Intelligence (IJCINI)* 15 4
- ang ang H uan Shardt A ang C Gui 2020 Deep learning for fault relevant feature extraction and fault classification with stacked supervised auto encoder *Journal of Process Control* 92 7
- ei P hao 20 A novel speech emotion recognition algorithm based on wavelet kernel sparse classifier in stacked deep auto encoder model *Personal and Ubiquitous Computing* 23 3 2 2
<https://doi.org/10.1007/s0077-0-0-24>
- ie ang in 2020 Malware Family Classification using LSTM with Attention *2020 13th International Congress on Image and Signal Processing, BioMedical Engineering and Informatics (CISP-BMEI)* 70 <https://doi.org/10.1007/978-3-03-202-234-7>
- ie u S ou S i 2020 A System call Behavior Language System for Malware Detection Using A Sensitivity based LSTM Model *Proceedings of the 2020 3rd International Conference on Computer Science and Software Engineering* 2 <https://doi.org/10.1007/978-3-03-202-234-7>
- hang 2020 DeepMal A CNN LSTM Model for Malware Detection Based on Dynamic Semantic Behaviours *2020 International Conference on Computer Information and Big Data Applications (CIBDA)* 3 3 3
<https://doi.org/10.1007/978-3-03-202-000-7>
- hu H ang L M hong S Li Sheng V S 202 A hybrid deep network framework for android malware detection *IEEE Transactions on Knowledge and Data Engineering* 34 2 70

İller e ulu a azar eri Sayıları ı eteklili leri i Araştırılması

ur a e ay*¹, r em lha ¹

Özet retici ve t keticinin ticaret amac ile do rudan bulu tu u pa aryerleri tarih boyunca ticaretin geli ti i ve kent merke lerinin hareketlendi i alanlar olmu tur Her t rl alt sekt rlere ait r nlerin sat ld pa aryerleri ellikle T rkiye de k lt rel a dan k kl bir ge mi e sahiptir Pa ar yerleri ekonomik sosyal ve k lt rel yapıdaki de i klikler ula m tercihlerinin farklı la mas AVM ve s permarket kullan m n n aman i erisinde yayg nla mas il elerde yer alan pa aryerleri ile ilgili bilgilerin tam olarak belirlenememesi gibi etkenler sebebiyle g n ge tik e a almaktadır Pa ar yerlerinin mek n say ve b y kl klerinin do ru bir ekilde belirlenememesi bu alanlar n yetersi kalmas na sebep olmaktadır Pa ar yerlerinin yer se imi planlama standartlar ve planlama ilkeleri do rultusunda yapılmaktadır Devamla il elerde ka tane pa ar yeri kurulaca ve bu alanlar n b y kl klerinin ne olaca konusunda analitik y ntemler ve niceliksel modeller konusunda literat rde bo luklar bulunmaktadır N fusla do ru orant l olarak kent merke ine yak n il elerde pa ar yerleri say ve b y kl kleri artmakta ve e perlerdeki il elere do ru a almaktadır Pa ar yerlerinin say lar ve alansal b y kl kleri aras nda ili ki bulunmaktadır Pa ar yerleri alansal olarak b y kse il edeki pa ar yeri say s a olmakta e er ki say s oksa alansal b y kl kleri k k olmaktadır Bu al mada mir ve Deni li illerindeki pa ar yeri say lar ve alansal b y kl kleri aras ndaki ili ki oklu do rusal regresyon modeli yard m yla bulunmu tur Bu do rultuda mir ve Deni li iline ait il elerdeki pa ar yeri say lar ve alansal b y kl kleri l mlenmi tir l elerdeki n fus verileri de kullan larak ki i ba na d en pa ar yeri alan ve pa ar yeri ba na d en ki i say lar hesaplanm tr Daha sonra an lan de erler a s ndan il e ba nda ortalama alt nda ve st nde kalan yerle meler tespit edilerek bu b lgelerde pa aryerlerinin geli tirilmesi nerilmi tir al ma kapsam nda elde edilen model ile pa aryerleri say lar b y kl klerinin ve n fus b y kl klerinin gelecekte farklı la mas sonucunda ya da ba ka ehirlerde nerilen modellerden yararlan larak hangi il elerde say ve alan b y kl gerekti inin tespit edilebilece i de erlendirilmektedir

A ahtar Kelimeler Pa ar yeri oklu do rusal regresyon anali i mir Deni li

¹**A res** Pamukkale niversitesi Mimarlık ve Tasarım Fak ltesi Deni li T rkiye

***S rumlu aazar** demiraydurdane gmail.com

1

Pa ar yerleri tarihi d nemlerden bu yana retici ve t keticilerin bulu ma alanlar olmu tur Belediye taraf ndan haftan belirli g nleri veya her g n sat yapılmaz i in nceden belirlenmi meyve seb e g nl k ihtiya mal emeleri giyim ve ev e yas gibi bir ok ihtiya n sat ld yerler pa ar yeri olarak tan mlanmaktadır Ero lu 7 Pa ar yerleri k rsal b lgelerde genellikle haftada bir ke g nl k ger ekle irken mevsimlik olarak kurulan pa ar yerleri daha u un s reli panay r ekinde ger ekle mektedir entsel yerle melerde ise ihtiya lar n bir k sm bakkal manav market veya al veri merke lerinden kar lan rken farklı amanlarda kurulan haftal k semt pa arlar ndan da kar lanmaktadır Tun el 2003 nsanlar n hem sosyal ili kiler kurmas n sa layan hem de ihtiya lar n kar lanmas na olanak tan yan pa arlar ilk a kentlerindeki agoralardan bu yana varl klar n s rd rmektedir rsal yerle melerde pa ar k lt r r n da t m ve toplama sisteminin nemli bir eleman d r Tun el 200 Pa arlarla ilgili bilim insanlar mensubu olduklar ara t rma alanlar kapsam nda al malar y r tm ve literat rde e itli tan mlamalar yapılm tr avramsal a dan pa arlar n tan mlamas n

Tax 3 Pa ar alanlar insanlar aras e amanl faaliyetler i ermektedir Pa ar yerlerinin g r ve konforlu bir alan olmas ekonomistlerin m kemmel pa ar n ifade etmektedir ekinde yapm tr EF Ba man pa ar sat c lar n r nleri sat n almak veya satmak i in ortak bir alanda bir araya gelmesini ifade etmektedir Coulson ve Cor 2 ise pa ar yerlerini hayvansal ve bitkisel r nlere ula man n kolay oldu u al m sat m i lemelerinin ger ekle ti i alan olarak ifade etmi tir Hodder ve Bromley e g re pa arlar ortak konumda belirlenen s relerde al c ve sat c lar n bir araya geldi i kamusal organi asyon olarak tan mlanm tr Hodder ve Ukwu ya g re pa ar yerleri s n rlar ve aman kabaca belirlenmi retici al c ve sat c lar n ticaret yapma amac yla bir araya geldikleri kurumsal bir faaliyeti ifade etmektedir Pa arlarla ilgili tan mlamalar n bir k sm nda ekonomik ve sosyal boyuta dikkat ekilmi tir Ullman a g re

pa arlar insan faaliyetlerinin merke inde yer ald i in bir b lgenin ya am nda olduk a nemli bir olgudur Smailes 4 ilerleme kaydeden lkelerin kasabalar nda kurulan pa arlar n y re halk n n sosyal ya am nda ma a a ve al veri merke lerinden daha nemli oldu u sonucu erinde durmu tur Hodder pa ar yerlerinin sosyal ve ekonomik ya am n en nemli unsurlar ndan biri oldu unu vurgulam t r Afolabi 72 pa ar kurulan alanlar ticaret merke lerinden ok nemli kav ak noktalar nda sosyal dini tesis ve siyasi ili kilerin kuruldu u alanlar olarak ifade etmi tir ebber ve Symanski 73 pa arlar n yaln ca al veri ama l yap lmad n bununla birlikte sosyal ihtiya lar n kar lanmas nda nemli oldu unun alt n i mi tir Bromley Symanski ve Good 7 periyodik pa arlar n kurulma amanlar n n yaln ca ay mevsim gibi unsurlarla ilgili oldu u de il ayn amanda festival dini t ren gibi toplumsal olaylarla da ili kili oldu u vurgulam t r Tun el 20 T rkiye de haftal k pa arlar erine hem teorik hem de uygulamal olarak bir ok al ma yap lm t r Baykara 4 y l nda Bir Osmanl a pa ar n n k n ele almaktad r y l nda Do u aradeni yaylalar nda pa ar yerlerinin tarihsel s recini inceleyen Bak rc ellikle ula m n geli mesiyle yaylalar n ekonomik neminin a ald n de erlendirmi tir Pa arlarla ilgili bir di er al ma g l ve Mitchell taraf ndan 2000 y l nda yap lm t r stanbul daki periyodik pa arlar konu alan al ma pa arlar n al c sat c ve mal ili kilerini incelemi tir en ve lhan ise 2003 y l nda mir B y k ehir genelinde ge imini pa ar l k yaparak sa layan kesimin kentle me s recindeki konumlar n ele alm lard r El ehrinde yer alan pa arlar de erlendiren Tun el 2003 y l nda haftal k pa arlar n tarih esini tercih nedenlerini ve da l etki alanlar n topolojik olarak de erlendirmi tir Pa arlarla ilgili bir di er al ma Bursa da kurulan pa arlar konu alan al kan taraf ndan 200 y l nda yap lm t r al kan a g re cadde sokaklarda kurulan pa arlar sosyo ekonomik faydalar n yan s ra ehir ya am a s ndan genellikle b y k sorunlara sebep olmaktadır D kmeci vd 200 y l nda stanbul da yapt klar al mada geli mi lkelerle k yasland nda stanbul da geleneksel ve modern ticaret sisteminin birlikteli ine vurgu yapm lard r 200 y l nda can Anadolu Sel uklu D nemi Pa ar ve Panay r erle melerinin Mek nsal kurulu unu ekonomik demografik b y kl klerini ve evrim s recini ele alm t r lma 200 y l nda Samsun ehrinde kurulan pa arlar n genel ellikleri ve sorunlar erinde durmu tur al kan 2007 y l nda Bursa ve anakkale ehrindeki pa arlar ele alm t r 200 y l nda Tun el T rkiye de k rsal kesim kasaba ve ehirlerde kurulan pa arlar n farkl la mas n ele alm t r

Pa ar yerlerinin kurulu uyla ilgili birbirinden farkl iki g r bulunmaktadır lk g r e g re pa ar yerlerinin kurulma sebepleri ehirlerdir nsanlar rettikleri r nlerini t keticiye ula t rmak i in ortak bir alana ihtiya duymu lar ve rettikleri r nleri satmak i in ehirlere getirmi lerdir Bu ekilde pa ar alanlar olu mu tur Ak i 20 kinci g r e g re de pa ar alanlar ehrin kurulu sebebi olmu tur Tarihi d nemlerden bu yana insanlar sahip oldu u becerileri sebebiyle rettikleri gere leri veya r nleri birbirleriyle takas etmi lerdir Takas i lemi i in herhangi bir alana gerek duyulmam t r Ge mi d nemlerde pa arlar yollar n kesi im noktas nda cami gibi dini alanlarda ve yak nlar nda ve limanlar gibi ortak kullan m bulunan alanlarda kuruldu u i in milletlerin bulu ma alan olmu tur Roma da pa ar yerleri e lence vesilesi olarak g r l rken unan ekonomisinde ve y y llarda ar ve pa arlar n yer ald bilinmektedir Bu d nemde pa arlar b lgesel ihtiya kar larken geni i erikli ekonomik de i meyi kapsayan panay rlar da geli meye ba lam t r Ero lu 7 Orta a a gelindi inde Antik unan ve Roma da yer alan agora ve forumlar n ben eri panay r ve fuarlar ortaya km t r Osmanl d neminde halk bir noktada birle tirmek ve al veri i o alana ta mak i in ARASTA ad verilen d kkanlar yap lm t r Ce ar lkemi de kentlerde sanayi devrimiyle birlikte ehirler yatay olarak geni lemeye ba lam ve pa ar yerleri yetersi kalm bu sebeple kentlerin farkl b lgelerinde insanlar n ihtiya lar na cevap verebilecek pa ar alanlar olu maya ba lam t r Pa ar kurulan yerin co rafi konumu iklim ellikleri hedef kitlenin varl ula m ve ula t rma ko ullar ve idari yap gibi e itli unsurlar nem ta maktadır Pa ar olu turan kriterlerin ba nda finans gelmektedir Finans gerekli paran n sa lanmas ve y netimini i ermektedir Berkmen Bir di er kriter fiyat olu umudur Pa arlamak bu konuda t m etkenleri dikkate almal d r Pa ar olu turan bir di er kriter depolamad r Depolama ile r nlerin uygun ko ullarda bekletilmesi ve sonras nda sat a sunulmas sa lanmaktadır Pa ar olu turan kriterlerden bir di eri risk ta mad r Risk arar etme olas l anlam na gelmektedir arar olas l k ger ekle ti inde ortaya kmaktadır Risk ortaya kt nda mal n sahibi arar kar lamaktadır Berkmen Pa ar yerleri kurulma sorumlulu u 0 say l Belediyeler yasan n Maddesinin 42 F kras ile belediyelere verilmi tir Fen leri M d rl taraf ndan ncelikle pa ar kurulacak alan n ara i m lkiyet durumu incelenmektedir M d rl k pa ar yerlerinin se iminde kriter yo unluk evresel ili kiler ve evre pa arlara olan u akl dikkate almaktadır Bunlarla birlikte pa ar konusunda pa ar yerleri esnaf derne i g r al nmaktadır Aksoy 200 ktisat leri M d rl pa ar yerlerinin y netiminden sorumludur Pa ar yerlerinin denetiminden ise ktisat leri M d rl Veteriner M d rl Sa l k M d rl Hesap leri M d rl ab ta leri M d rl ve Pa ar yerleri Esnaf Derne i sorumludur Aksoy 200 Pa ar yerlerinin imar planlar nda belirlenmesinde 20 2 tarih ve 2 3 say l resm ga etede G mr k ve Ticaret Bakanl nca yay nlanarak y r l e giren Pa ar erleri Hakk nda netmelik ten faydalan lmaktadır netmelikte yer alan h k mler belediyeler taraf ndan dikkate al nmaktadır Pa ar yerlerinin aman i erisinde g sterdi i de i iklikler belirlenmi ehir i indeki konumlar na say ve b y kl klerine ili kin mir ve Deni li illerinde kurulan pa arlar n ba ellikleri ortaya konmu tur Pa ar yerlerinin say ve b y kl klerinin belirlenmesi i in model nerisi geli tirilmi tir mir ve Deni li illerinde kurulan pa arlar n mek n erindeki da l mlar say ve b y kl kleri tespit edilmi tir mir ve Deni li illeri

pa ar yerleri say ve b y kl klerinin belirlenmesinde regresyon anali inden yararlan lm t r Bunun sonucunda mir ve Deni li illerinin pa ar alanlar kar la t r lm t r

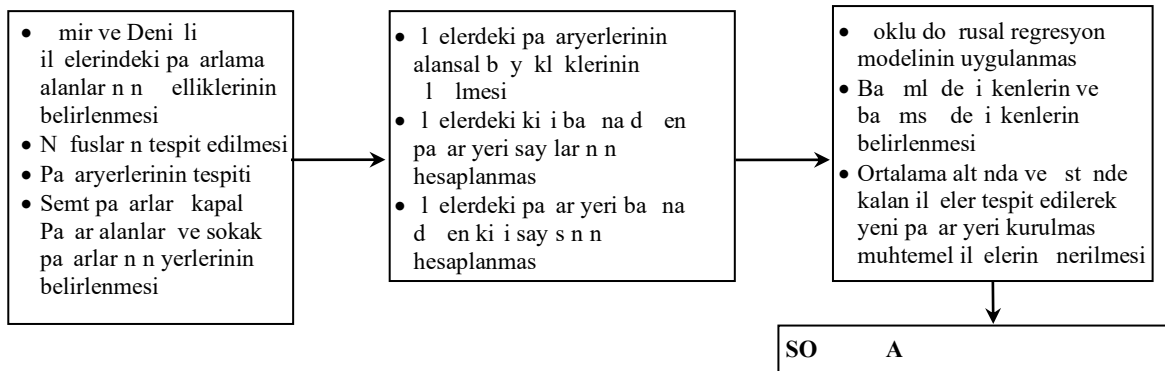
2 A A O

Pa ar yeri say ve alansal b y kl kleri ihtiya lar n n belirlenmesi i in al mada a amal bir y ntem geli tirilerek mir ve Deni li il eleri kapsam nda uygulanm t r Geli tirilen y ntemde kullan lan veriler sanal veri depolar yerinde ara t rma g lem konu ile ilgili yay nlanm rapor ve al malar derlenerek idari kurumlardan ilgili konu kapsam nda sorular sorularak elde edilmi tir Harita l mleme metodu ile pa ar alanlar n n b y kl kleri l lm t r ekil de an lan y ntemin ak emas verilmi tir

ETAP 1 al ma alan n belirlenmesi ve Pa ar yerlerinin tespiti

ETAP 2: Pa aryerlerine y nelik l m ve hesaplamalar n yap lmas

ETAP 3: Say ve alan b y kl aras ndaki ili kinin bulunmas



e il 1 Ak emas

Etap de al ma alan ve ellikleri belirlenmi tir al ma alan olarak se ilen mir ve Deni li illeri kapsam nda demografik veriler ve pa aryerlerinin konumlar belirlenerek haritalara i lenmi ve tablo haline getirilmi tir Pa aryerlerinin ellikleri ve gruplama i lemeleri yap larak l me ha r hale getirilmi tir Etap 2 de mir ve Deni li ili il elerindeki pa aryerleri tespit edilerek say lar tablolara i lenmi tir Her bir pa ar yerinin alansal olarak b y kl haritalar erinden yakla k olarak l mlenerek tablo haline getirilmi tir Daha sonra il elerdeki ki i ba na d en pa ar yeri say lar ve pa ar yeri ba na d en ki i say lar hesaplanarak ortalamalar bulunmu tur Etap 3 te ba ml ve ba ms de i kenler tan mlanarak oklu do rusal regresyon anali i yap lm t r ap lan anali sonucunda modelin anlaml l k d eyleri ve ba ms de i kenleri anlaml l k d eyleri sorgulanarak yorumlanm t r Daha sonra ortalama alt nda ve st nde kalan il eler tespit edilerek ula m ve eri ilebilirlik ili kileri de dikkate al narak yeni pa ar yeri kurulmas ya da alansal olarak b y t lmesi muhtemel il eler nerilmi tir Bununla birlikte mir ve Deni li Pa aryerleri modeli sonu lar kapsam nda ben er ve farkl lklar ortaya koymak il elerde ki i ba na d en pa ar alan ve pa ar ba na d en ki i say lar n n kar la t rmas n yaparak bu kapsamda kan sonu lar ortaya koymak ve de erlendirmeye sunmak amac yla kar la t rma y ntemi de kullan lm t r al ma kapsam nda uygulanan oklu do rusal regresyon anali i detayl olarak anlat lm t r

2.1 lu rusal e resy A alizi

Regresyon bir de i ken ile farkl bir veya birden fa la de i kenler aras nda ili ki kurma eklidir Ba ms de i kenlerin farkl de erlerine kar l k ba ml de i kenin alaca de erin tahmin edilmesi Regresyon denklemi kapsam nda yap lmaktad r Regresyon anali inin farkl alt ba lklar bulunmaktad r al ma kapsam nda kullan lan metod da regresyon anali inin bir e idi olan oklu do rusal regresyon anali idir Regresyon anali inde birden fa la ba ms de i ken bulunuyorsa bu modellere oklu Do rusal Regresyon Analisi denmektedir oklu do rusal regresyon denkleminde yer alan ba ms de i kenlerin gelecekte alacaklar de erler farkl pro eksiyo y ntemleri ile hesaplanarak denklemde bu de erlerin yerine konulmas ile gelecek i in sonu lar ortaya konmaktad r oklu Do rusal Regresyon e itli i l n arslan 20 2

a_0 b x $b_{2 \times 2}$ $b_{3 \times 3}$ b_{ixi}

Bu form lde

Ba ml de i ken

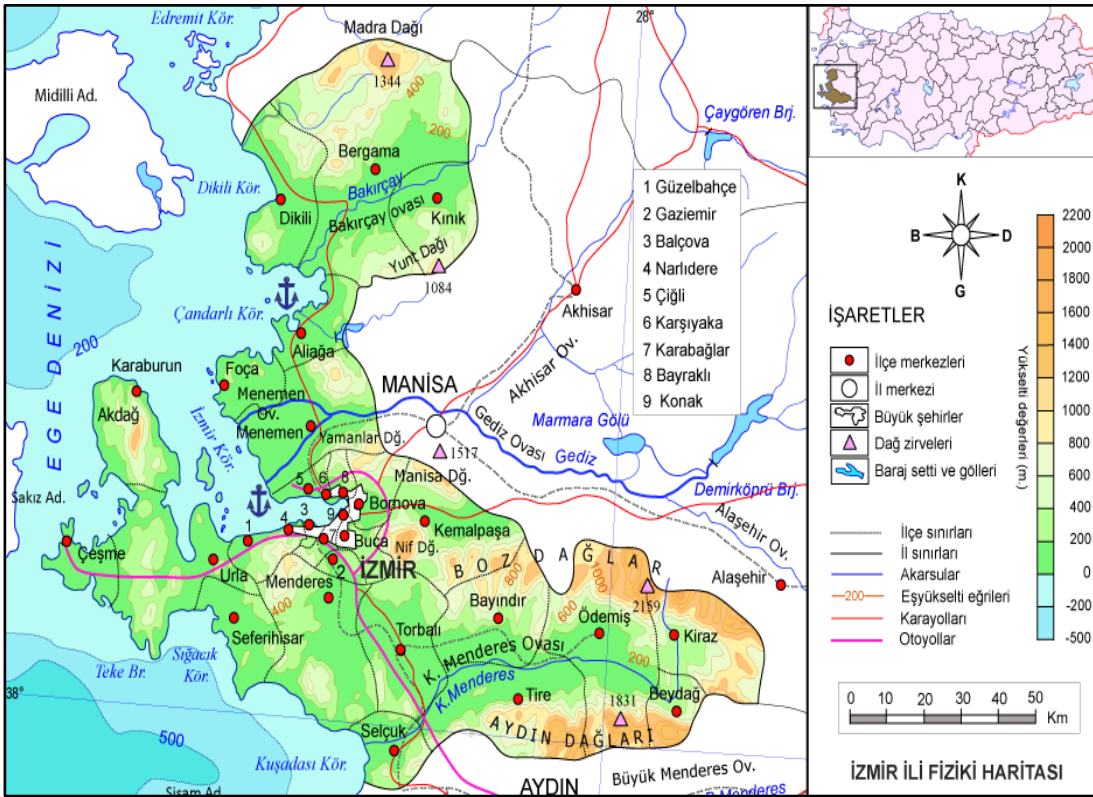
a_0 b b_2 b_3 b_i katsay lar

x x_2 x_i ba ms de i kenler n fus ara sahiplili i vb

Regresyon anali inde ba ms de i kenlerin detayl olarak birbirleriyle ve ba ml de i kenle incelendi i hesaplamalar n sonu lar korelasyon katsay s R ile kontrol edilmelidir ksek korelasyon de eri veren ba ms de i ken form lde kalmal d r

2.2. Alışma Alanı

Te al mas kapsam nda al ma alan olarak mir ve Deni li illeri se ilmi tir mir ve Deni li illeri detayl olarak anali edilmi tir mir ili T rkiye nin bat k sm nda Ege B lgesi nde yer almaktad r 2 ile 2 20 do u boylamlar ve 37 4 ile 3 ku ey enlemleri aras nda bulunan il 2 0 2 km² y l m ne sahiptir mir ku eyde Mandra da lar g neyde u adas k rfe i bat da e me ar madas n n Tekne Burnu do uda ise Ayd n ve Manisa il s n rlar ile evrilidir Bat da ise mir k rfe ine ba lanmaktad r ekil 2 de ilin co rafı konumu g sterilmi tir



ekil 2 Ege b lgesi fi iki haritası

mir ilinin Adrese Dayal N fus ay t Sistemi sonu lar na g re 2022 y l n fusu 4 4 2 0 ki i olarak tespit edilmi tir Bu n fusun 4 l k orana sahip 2 2 7 s erkek 0 34 l k orana sahip 2 24 340 kad nlardan olu maktad r lde kilometrekareye 372 ki i d mektedir lin n fus yo unlu u 372 ki i km² dir mir ilinin 30 il esi bulunmaktad r Bu il eler Alia a Bal ova Bay ndr Bayrakl Bergama Beyda Bornova Buca e me i li Dikili Fo a Ga iemir G elbah e araba lar araburun ar yaka emalpa a nk ira onak Menderes Menemen Narl dere demi Seferihisar Sel uk Tire Torbal ve Urla d r al ma kapsam nda anali edilen bir di er il ise Deni li dir Anadolu ar madas n n g neybat s nda Ege b lgesinin de g neydo usunda yer alan Deni li Ege ve Akdeni b lgerleri aras nda yer al p Ege b lgesine ba l bir ildir 1 2 30 2 30 do u meridyenleri ile 37 2 3 2

ku ey paralelleri aras nda yer almaktadır T C Denizli Valili i 2022 Denizli nin batısında Aydın ve Manisa g neyinde Mu la ku eyinde U ak illeri bulunmaktadır ekil 3



ekil 3 Denizli ili konumu

Denizli ilinin Adrese Dayal N fus ayıt Sistemi sonu lar na g re 2022 y l n fusu 0 332 ki i olarak tespit edilmi tir Bu n fusun 4 73 lk orana sahip 2 3 u erkek 0 27 lik orana sahip 30 73 kad nlardan olmaktadır lde kilometrekareye ki i d mektedir lin n fusu yo unlu u ki i km² dur Denizli de merke e ba l il e bulunmaktadır Bu il eler Ac payam Babada Baklan Bekilli Beya a Bo kurt Buldan al ameli ardak ivril G ney Hona ale Merke efendi Pamukkale Sarayk y Serinhisar ve Tavas tr

3 A

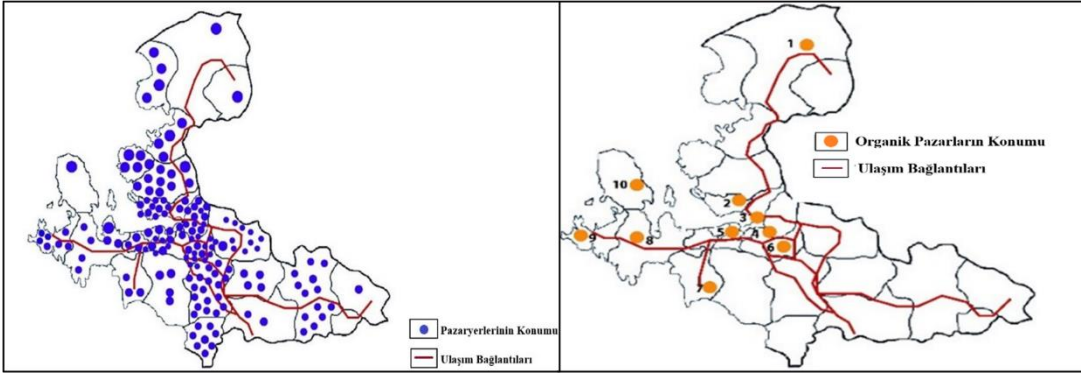
3 1 zmir azar erleri erleri i la ması ve Öl mle mesi

mir il e Belediyeleri s n rlar na g re mevcut Pa ar erleri ve konumlar na ili kin olarak bir da l m bilgisi al maya veri olarak aktar lmam tr Bu nedenle mevcut durum haritalardan ve resmi kurum internet siteleri taranarak bir veri ortam yaratlmaya al lm tr S konusu veriler erinden eri ilebilen bilgilere dayal olarak de erlendirmeler yap lm tr Ticari ara y k dinami mi lo istik faaliyetlerin k melenmesi ve sosyo ekonomik ellikler dikkate al narak mir al ma kapsam nda ana ekirdek b lgeye ayrı lm tr mir ili il elerinde yer alan pa ar yerleri bilgileri Tablo de verilmi tir Tablo da 2 ve 3 ekirdeklerde yer alan standart geleneksel halk pa ar alanlar organik ve do al r n pa ar alanlar bilgileri g r lmektedir Veriler B y k ehir Belediyesi yay nlar ve harita tabanlı l mlemeler sonucu elde edilmi tir ekirdeklerde yer alan il eler ise toplam olarak verilmi tir

Tabl 1 Mir ili pa ar alanlar bilgileri

İller	Yüzölçümü	Ortalama Alanlar (m ²)	Ortalama Alan Sayısı	Ortalama Alan (m ²)	Kişi başına Ortalama Alan	Kişi başına Ortalama Alan Sayısı
Alia a	3 2	20 232	4	0	0 2	23
Bay nd r	40 4	3	4	0	0 0	0
Bergama	03	27 2		2 4	0 27	03
Beyda	2 07	00		0	0 00	0 00
e me	43 4		7	0	0 0	2
Dikili	44 72	3	4	0	0 2	04
Fo a	33 3	4 3		0	0 4	3
araburun	0 03	4		04	0 04	0 0
emalpa a	0 2	3 02	0	0	0 2	0 3
n k	2 03	00		0	0 00	0 00
ira	43	3 0		0	0 0	43
Menderes	3 7	0 2 7	4	0	0	23 4
Menemen	74 4	3 27	0	0	0 23	7 4
demi	32	7 2	3	0	0 0	0
Seferihisar	43 4	0	3	2 4	0 3	4 2
Sel uk	3 3 0	47		0	0	4
Tire	4 4 7	440	2	0	0 0	42 23
Torbal	7 772	4 2 7		0	0 02	4
Urla	3 0	74	4	07	0	
ekirdek	2 47 000	20 32		04	0 04	3
2 ve 3 ekirdek Ortalaması					0	

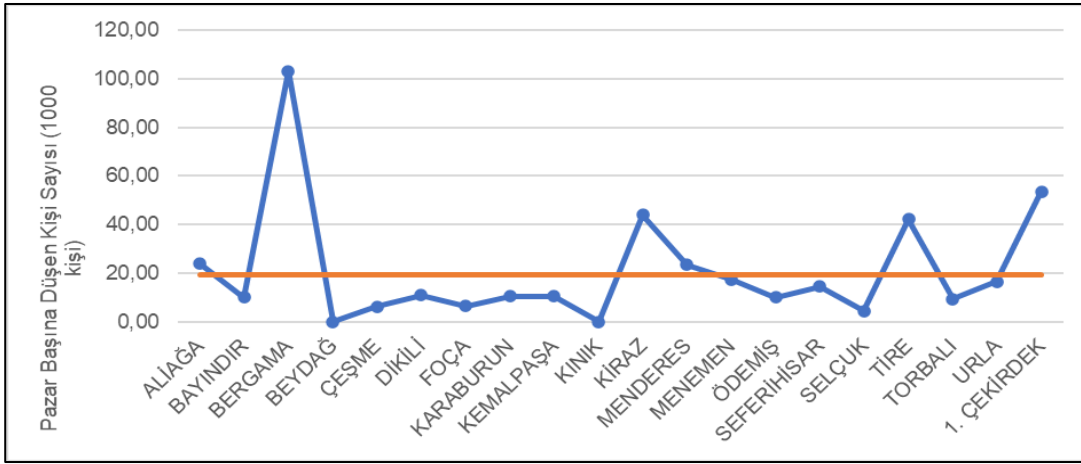
Mir ili genelinde ortalama bin kişi için bir pa ar kurulmaktadır. Bu de er kentsel alan olarak tan mlanan ekirdekte yakla k 4 000 olarak hesaplanm t r l genelinde Beyda ve n k il elerinde b y k ehir belediyesi envanterinde yer alan pa ar yeri bulunmamakta olup b lgede faaliyet g steren pa ar yerleri tespit edilmi tir. Son y llarda yayg nla an organik pa arlar ise il genelinde denetimli olarak Bal ova ve Bostanl olmak ere iki il ede kurulmaktadır. Di erleri ise pa arlar i erisinde kurulan do al r n sat noktalar d r. Pa ar alanlar n n konumlar ve il s n rlar i indeki da l m bi imi verilmi tir. ekil 4 ekil



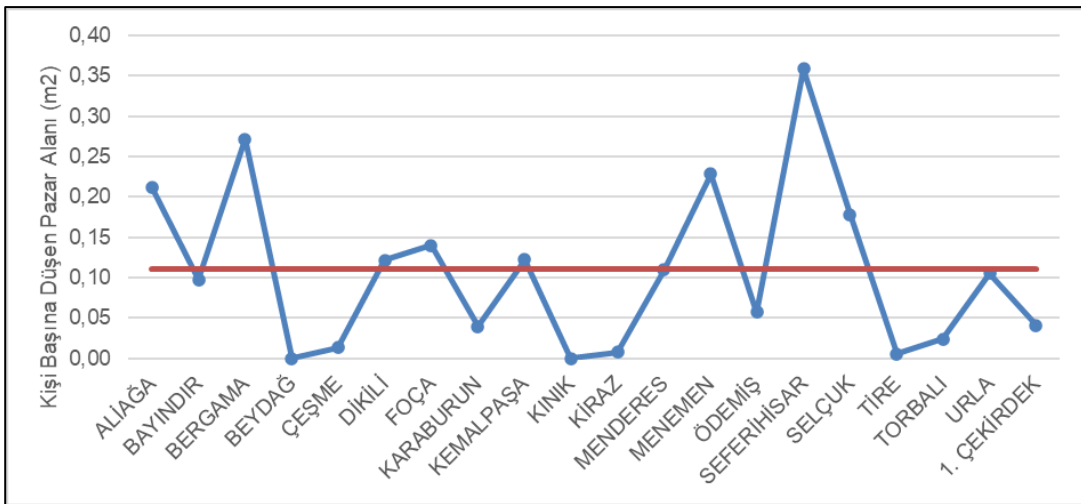
e il Pa ar yerlerinin konumlar

e il Organik pa arlar n konumlar

mir ili pa ar yerleri bilgileri toplad ktan sonra elde edilen veriler yard m ile ki i ba na d en pa ar alan b y kl ve pa ar ba na d en ki i say lar hesaplanm ve oklu do rusal regresyon anali i yap lm tr i i ba na d en pa ar alan b y kl incelendi inde 2 ve 3 ekirdekte yer alan pa arlar ba al nd nda ki i ba na ortalama 0 m² pa ar alan d erken kentsel alanda bu rakam 0 04 m² ye d mektedir ekil 7



e il Pa arlara g re ki i say lar n n da l m i i Say s Pa ar



e il Pa ar alan i i da l m

rsal il elerde bulunan pa ar alanlar say lar n n n fus ve alansal b y kl klerle olan ili kişi oklu do rusal regresyon anali i ile ara tr lm tr Bu ama la retici ve semt pa arlar bilgilerinin de yararlı olaca d n lebilir Tablo 2

abl 2 retici ve semt halk pa arlar et tablosu

l eler	azar eri Sayısı	us	azar Ala ları m ²	Kişi aşı a azar Ala ı	azar aşı a şe Kişi Sayısı
Alia a		3 2	20 232	0 2	23 4
Bay nd r		40 4	3	0 0	0 4
Bergama	2	03	30 33	0 30	3
Beyda	1	2 07	00	0 04	2 07
e me		43 4	4	0 02	43
Dikili		44 72	3	0 2	043
Fo a		33 3	4 3	0 4	2
araburun	2	0 03		0 0	302
emalpa a	1	0 2	3 02	0 2	0 30
n k	1	2 03	00	2	2 3
ira	1	43	3 0	1	3
Menderes		3 7	02 7	11	23
Menemen	1	74 4	3 27	0 23	7 4
demi	13	32	7 2	0 0	0 3
Seferihisar		43 4	00	0 37	0 7
Sel uk		3 3 0	47	0	4 4
Tire	2	4 4 7	440	1	2 22
Torbali	1	7 772	4 2 7	0 02	40
Urla		3 0	7 0	0	3 272
Ortalama	,12	1 1			

ukar daki tabloda retici ve semt pa ar alanlar birle tirilerek ki i ba na pa ar alanlar ve pa ar yerleri ba na d en ki i say lar bulunarak ortalamalar verilmi tir ani bir anlamda an lan regresyon modelinin istatistik sonu lar verilmi tir Tablo 3

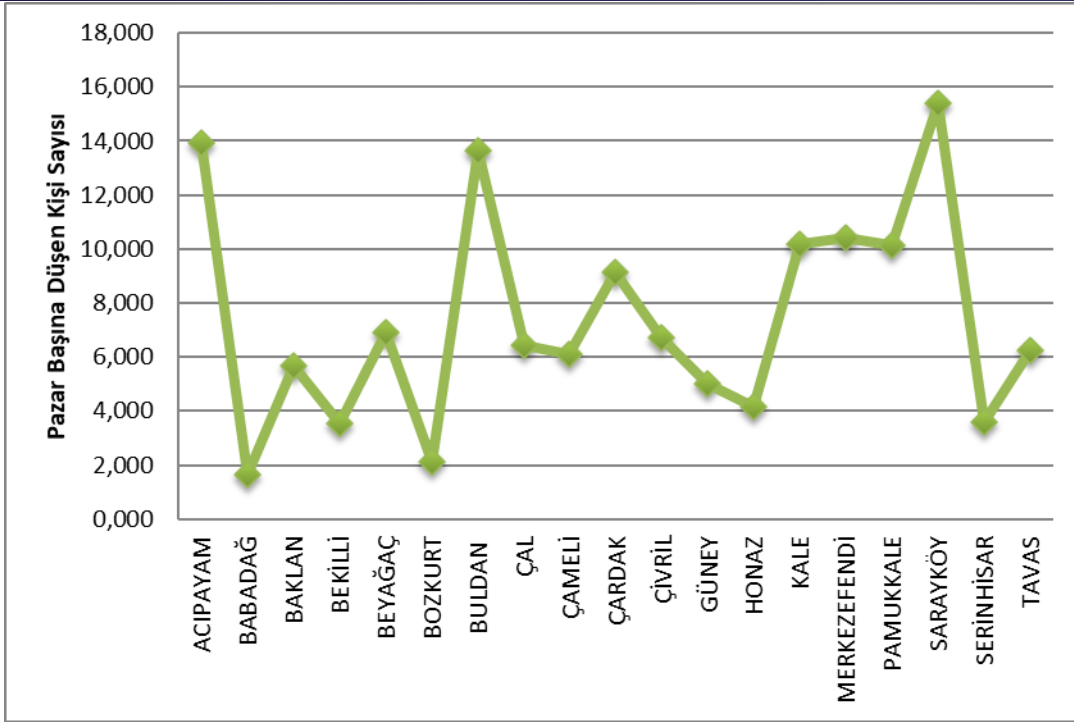
abl 3 Pa ar yerleri modeli regresyon istatistikleri tablosu

a ımlı e iş e azar eri Sayısı			
Kare	2		
Ba ms De i kenler	atsay	Standart Hata	t stat
N fus	E 0	2 47 E 0	1
Pa ar Alan	0 000	7 43 E 0	2 32 1

Model sonucuna g re il elerdeki Pa ar Alan say lar n fus ve pa ar alan ile ili kildir i i ba na d en pa ar alan ortalamas alt nda ve pa ar ba na d en ki i erinde kalan il eler belirlenmi tir Model sonu lar na g re ikinci ekirdekte Menderes ve nc ekirdekte n k ira ve Tire il elerindeki pa ar alanlar n n say lar n n ve eri ilebilirliklerinin olanaklar n n ara tr larak arttr lmas nerilmektedir

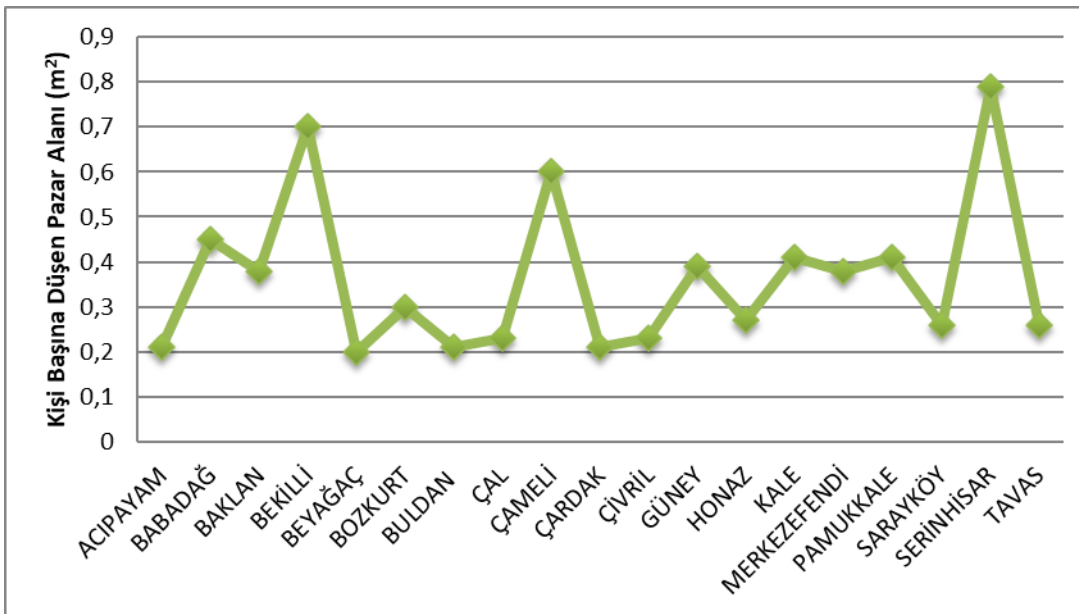
3 2 e izli azar erleri erileri i la ması ve Öl mle mesi

Deni li genelinde ortalama 7 4 4 ki i i in bir pa ar kurulmaktad r i i ba na d en pa ar alan b y kl ortalama 0 3 m² pa ar alan d mektedir Deni li ilinde toplam 24 adet pa ar yeri bulunmaktad r Toplam pa ar yerleri alan yakla k olarak 234 43 m² olarak hesaplanm tr ekil den de g r ld ere pa ar ba na d en ki i say s en fa la Sarayk y il esinde 3 4 ki i en a Babada il esinde 3 ki i d mektedir



e il Pa ar ba na d en ki i say s

ekil dan da anla laca ere ki i ba na d en pa ar alan miktar n n 0 7 m² ile en fa la Serinhisar il esinde iken 0 20 m² ile en a Beya a il esinde oldu u tespit edilmi tir



e il i i ba na d en pa ar alan m²

Modelde ba ml de i ken olarak pa ar yeri say lar (Y_1) ba ms de i kenler n fus (X_1) pa ar alan (X_2) ki i ba na d en pa ar alan (X_3) pa ar ba na d en ki i say s (X_4) olarak belirlenmi tir Model s namas ndan nce merke i il e olarak tan mlanan Merke efendi ve Pamukkale l eleri kategoriden kart lm tr ap lan oklu do rsal regresyon modelinin sonu lar verilmi tir Tablo 4

abl oklu do rusal regresyon modeli istatistik sonu lar

R^2	1		
Ba ms De i kenler	atsay	Standart Hata	T e eri
N fus(X_1)	0 0002	0 000	13
Pa ar alan (X_2)	0 0003	0 0002	1 313
i i ba na d en pa ar alan (X_3)	7 7	2 324	3
Pa ar ba na d en ki i say s (X_4)	0 0003	0 000	3 221

i i ba na d en pa ar alan ortalamas n n alt nda kalan ve ayn amanda pa ar ba na d en ki i say s ortalamas n n st nde kalan il elerde pa ar olanaklar n n ara t r larak geli tirilmesi de erlendirilmektedir An lan de erlerin tespit edilmesi i in ortalamalar al narak iki ko ulu da ayn anda sa layan il eler Tablo te i aretlenmi tir

abl Ortalama e ikleri ayn anda ge en il eler

l eler	Kişi aşı a azar Ala ı	azar aşı a şe Kişi Sayısı
Ac payam	21	13 12
Babada	0 4 0	3
Baklan	0 3	4
Bekilli	0 702	3 33
Beya a	0 203	03
Bo kurt	0 30	2 3
Buldan	213	13 21
al	0 23	420
ameli	0 03	0
ardak	212	1
ivril	0 232	7 4
G ney	0 3	4
Hona	0 27	4 4
ale	0 4 7	0 7
Sarayk y	2	1 3
Serinhisar	0 7 7	3 0
Tavas	0 2	2 4
O A A A	3 3	

Tablo teki ortalama de erler incelendi inde ayn anda iki ortalama e ik de eri s n rlar n ge en il eler Ac payam Buldan ardak ve Sarayk y olarak belirlenmi tir Dolay s ile bu il elerde bulunan pa aryeri say lar n n veya alanlar n n geli tirilmesinin ara t r lmas ve artt r lmas n n ncelikli olarak ara t r lmas nerilmektedir

3 3 zmir ve e izli azar erleri eli Karşılaştırması

mir li genelinde ortalama bin ki i i in bir pa ar kurulmaktadır Bu de er kentsel alan olarak tan mlanan ekirdekte yakla k 4 000 olarak hesaplanm t r Deni li linde merke e ba l toplam adet il e bulunmaktadır Her il ede a k veya kapalı pa aryeri bulunmaktadır l genelinde ortalama 7 4 4 ki i i in bir pa ar kurulmaktadır mir de ki i ba na d en pa ar alan b y kl incelendi inde 2 ve 3 ekirdekte yer alan pa arlar ba al nd nda ki i ba na ortalama 0 m² pa ar alan d erken kentsel alanda bu rakam 0 04 m² ye d mektedir Deni li ilinde ise ki i ba na d en pa ar alan b y kl ortalama 0 3 m² pa ar alan d mektedir mir ili model sonu lar na g re Pa ar ba na d en ki i say s n n en fa la Bergama da ki i ba na d en pa ar alan b y kl n n ise en fa la Bergama ve Seferihisar da oldu u g lemlenmi tir Bununla birlikte model sonu lar na g re ikinci ekirdekte Menderes ve nc ekirdekte nk ira ve Tire il elerindeki semt ve retici pa ar alanlar n n say lar n n ve eri ilebilirliklerinin olanaklar n n ara t r larak artt r lmas nerilmektedir Deni li ilinde ise pa ar ba na d en ki i say s n n en fa la Sarayk y il esinde en a Babada il esinde oldu u tespit edilmi tir i i ba na d en pa ar alan miktar n n ise en fa la Serinhisar il esinde en a Beya a il esinde oldu u tespit edilmi tir Elde edilen veriler do rultusunda Deni li ili il eleri i in regresyon anali i yap lm ayn anda iki ortalama e ik de eri s n rlar n ge en il eler Ac payam Buldan ardak ve Sarayk y olarak belirlenmi tir Dolay s ile bu il elerde bulunan pa aryeri say lar n n veya alanlar n n geli tirilmesinin ara t r lmas ve artt r lmas n n ncelikli olarak ara t r lmas nerilmektedir

3 azar erleri Sayıları ı em ra i ve S sy mi A ılar a A alizi

mir ve Deni li ili il eleri i in ki i ba na d en pa ar alan b y kl ve pa ar ba na d en ki i say lar hesaplanarak yap lan oklu regresyon anali i sosyo ekonomik ve demografik de i kenler kapsam nda yeniden de erlendirilmi tir Pa ar yeri say lar n n belirlenen ba ms de i kenlerden hangileri ile ili kili oldu u belirlenmi tir Tablo da mir ili pa ar yeri say lar pa ar alanlar ortalama hanehalk b y kl tar m alan ve n fus yo unlu u bilgileri g r lmektedir

abl mir ili pa ar alan sosyo ekonomik ve demografik veriler

l eler	azar eri Sayısı	us	azar Ala ları m ²	Kişi aşı a azar Ala ı	azar aşı a şe Kişi Sayısı	Ortalama Ha ehal ı y l	arım Ala ı e ar	us u lu u
Alia a		3 2	20 232	0 2	23 4	3 0	2 74	2 2
Bay nd r		40 4	3	0	0 4	2 0	304 7	74
Bergama	2	03	30 33	0 3	3	2 7	3 4 2	7
Beyda	1	2 07	00	0 04	2 07	2	4 2	73
e me		43 4	4	0 02	43	2		3
Dikili		44 72	3	0 2	0 43	2 33		3
Fo a		33 3	4 3	0 4	2	2 42	44 02	32
araburun	2	0 03		0 0	302	2 23	37	2
emalpa a	1	0 2	3 02	0 2	0 3	3 20	2 43	
n k	1	2 03	00	, 2	2 , 3	3 23	4 0	2
ira	1	43	3 0	, 1	3,	2	7 0	77
Menderes		3 7	02 7	,11	23,	2	227 270	2
Menemen	1	74 4	3 27	0 23	7 4	3 7	204 43	30
demi	13	32	7 2	0 0	0 3	2 7	330 7	30
Seferihisar		43 4		0 37	0 7	2	77	
Sel uk		3 3	47	0	4 4	2 0	47 74	
Tire	2	4 4 7	440	, 1	2,22	2 70	2 0	
Torbal	1	7 772	4 2 7	0 02	40	3 27	2 2 2	3 0
Urla		3	7 0	0	3 272	2	70 3 2	

Pa ar yeri say s ile belirlenen ba ms de i kenler aras ndaki ili kinin regresyon modelinin istatistik sonu lar verilmi tir Tablo 7

abl mir ili regresyon istatistikleri tablosu

a ımlı e iş e azar eri Sayısı			
2	, 2 1		
Ba ms De i kenler	atsay	Standart Hata	t stat
Ortalama Hanehalk B y kl	0 20 0 4	0 7 7 2	0 7247 7
Tar m Alan	7 E 0	7 43332E 0	30 344 3
N fus o unlu u	0 04204 044	0 0 0 0 7	3,

Modelde ba ml de i ken olarak pa ar yeri say lar (Y_1) ba ms de i kenler ortalama hanehalk b y kl (X_1) tar m alan (X_2) n fus yo unlu u (X_3) olarak belirlenmi tir Model sonucuna g re il elerdeki Pa ar Alan say lar n fus yo unlu u ile ili kildir mir ili regresyon de erlendirmesi sonras nda Deni li ili i in de pa ar yeri say lar n n sosyo ekonomik ve demografik de i kenler ile aras ndaki ili ki anali edilmi tir Tablo

abl Deni li ili pa ar alan sosyo ekonomik ve demografik veriler

İ l e r	azar eri Sayısı	us	azar Ala ları m ²	Kişi aşı a azar Ala ı	azar aşısı a şe Kişi Sayısı	Ortalama Ha ehal ı y ı l	arım Ala ı e ar	us u lu u
Ac payam	4	4	2 0	0 2	3 2	2 72	44 07	34
Babada	4	22	3 000	0 4	3	2 7	2 7	4
Baklan		4	2 200	0 3	4	2 7	2 3	
Bekilli	2	7 0	4 0	0 7	3 33	2 24	7 347	22
Beya a		03	400	0 2	03	2 73	3 00	
Bo kurt		2 7	3	0 3	2 3	2 3	3 04	3
Buldan	2	27 24	00	0 2	3 2	2	4 7	4
al	3	2	4 4 0	0 23	420	2 3	3 4 27	22
ameli	3	2	000	0	0	2	22 322	2
ardak		44	3	0 2	44	2 7		3
ivril		0 42	4 000	0 23	7 4	2	0 7 0	4
G ney	2	7	3 00	0 3	4	2 4		
Hona		33 4	000	0 27	4 4	3	30 4 0	
ale	2	20 3 3	00	0 4	0 7	2	3 3	3
Merke efendi	2	302 2 3	77	0 3	0 42	3 0	3	04
Pamukkale	34	344 0	43	0 4	0 20	2	2 33	42
Sarayk y	2	30 7	300	0 2	3 4	2 2	2 0 2	
Serinhisar	4	4 430	0	0 7	3 0	2	3 7	3
Tavas	7	43 4	2	0 2	2 4	2 7	47	2

Pa ar yeri say s ile belirlenen ba ms de i kenler aras ndaki ili kinin regresyon modelinin istatistik sonu lar verilmi tir Tablo

abl Deni li ili regresyon istatistikleri tablosu

a ımlı e iş e azar eri Sayısı			
2	, 11 21 1		
Ba ms De i kenler	atsay	Standart Hata	t stat
Ortalama Hanchalk B y kl	0 442 2	0 7 230 407	0 7 3 7047
Tar m Alan	4E 07	4E 0	0 2 3
N fus o unlu u	0 0 2 4	0 0 42 74	, 2 3

Model sonucuna g re n fus yo unlu u artt k a pa ar yeri say s n n artt n fus yo unlu u a ald k a pa ar yeri say s n n a ald tespit edilmi tir

A A SO A

mir ve Deni li illeri sanayi ve ticaretin en yo un oldu u kentlerdir mir ili ticari ara y k dinami mi lo istik faaliyetlerin k melenmesi ve sosyo ekonomik ellikler dikkate al narak ana e kirdek b lgeye ayrı lm t r mir ilinde ortalama 000 ki i i in bir pa ar kurulurken Deni li ilinde haftan n yedi g n ortalama 7 4 ki i i in bir pa ar kurulmaktadır mir ilinde 2 ve 3 e kirdekte ki i ba na ortalama 0 m² pa ar alan d erken kentsel alanda ki i ba na ortalama 0 04 m² pa ar alan d mektedir Deni li ilinde ki i ba na ortalama 0 3 m² pa ar alan d mektedir mir ilinde pa ar ba na d en ki i say s en fa la Bergama il esinde Deni li ilinde pa ar ba na d en ki i say s en fa la Sarayk y il esinde en a Babada il esindedir mir ilinde ki i ba na d en pa ar alan en fa la Bergama ve Seferihisar il elerinde Deni li ilinde ise en fa la Serinhisar en a Beya a il elerindedir mir ilinde 2 e kirdekte Menderes 3 e kirdekte n k ira ve Tire il elerinde semt ve retici pa arlar n n say s n n artt r lmas nerilmektedir Deni li ilinde ise Ac payam Buldan ardak ve Sarayk y il elerinde pa ar yeri say lar n n ve alanlar n n artt r lmas nerilmektedir l elerde ka tane pa ar yeri olmas gerekti i il elere ait bir ok konu ile ilgilidir Bu kapsamda mir ve Deni li ili il eleri i in ki i ba na d en pa ar alan b y kl ve pa ar ba na d en ki i say lar hesaplanarak yap lan oklu regresyon anali i sosyo ekonomik ve demografik de i kenler kapsam nda yeniden de erlendirilmi tir Modelde her iki il ve il eleri i in de ba ml de i ken olarak pa ar yeri say lar (Y_i) ba ms de i kenler ortalama hanchalk

bykl (X_1) tar m alan (X_2) n fus yo unlu u (X_3) olarak belirlenmi tir Model sonucuna g re her iki ilin il elerindeki Pa ar Alan say lar n fus yo unlu u ile ili kildir

KA AK A

Ak i 20 Alternatif Al veri Mekan Olan Geleneksel Semt Pa arlar n n ap s leyi i ve Sorunlar n n ncelenmesi Ad yaman rne i Akademik Sosyal Ara t rmalar Dergisi 22 247

Aksoy 200 Pa ar erlerinin ehir Planlamas Standart ve lkeleri n nden ncelenmesi stanbul li Bak rk y l esi rne i ukurova niversitesi Sosyal Bilimler Enstit s Dergisi

Berkmen H stanbul da Semt Pa arlar erine Bir Ara t rma Be ikta ad k y Fatih Pa arlar ksek Lisans Te i T Fen Bilimleri Enstit s

Ce ar M Tipik ap lar yla Osmanl ehircili inde ar ve lasik D nem mar Sistemi. stanbul Milli E itim ay n Evi

Ero lu G 7 urtulu Semt Pa ar Ara t rmas Bitirme Te i T Mimarlk Fak ltesi

l n arslan T 20 2 entsel Ula m Ula m Sistemi Toplu Ta m Planlama Politikalar Ninova ay nc l k T C Deni li Valili i 2022 Co rafi onum Eri im Adresi <http://www.deni.li.gov.tr/cografi/konu>

Tun el H 2003 Anadolu ehirlisinde Semt Pa arlar Ela rne i urnal of Social Science 4

Tun el H 200 T rkiye nin rsal Pa ar B lgeleri Ankara Ankara niversitesi IV Ulusal Co rafya Avrupa Birli i S recindeki T rkiye de B lgesel Farkl l klar Sempo yumu 2 2 May s 200 Ankara

Tun el H 20 T rkiye deki Periyodik Pa arlar n S n fland r lmas T CAUM 30 l Uluslararası Co rafya Sempo yumu Bilecik eyh Edebali niversitesi Fen Edebiyat Fak ltesi Co rafya B l m

Development of Gas-Cooled Modular Reactor Based Helium Gas Turbine with Bottoming Transcritical CO₂ Rankine Cycle and Hydrogen Production

Gamze Soy Turk¹, Onder Kizilkan*¹, Shoaib Khanmohammadi²

Abstract: The development of a gas-cooled modular reactor (GCMR) based on a helium gas turbine with a bottoming transcritical CO₂ Rankine cycle and hydrogen production represents a significant advancement in the field of nuclear energy. The system designed in this study combines multiple technologies to increase energy conversion efficiency and produce clean hydrogen, a versatile energy carrier. The use of helium as a coolant in the GCMR offers several advantages, including its excellent heat transfer properties, chemical inertness, and ability to operate at high temperatures. These characteristics enable efficient heat extraction from the reactor core, minimize the likelihood of corrosion, and increase thermal efficiencies and power output. The integration of a bottoming transcritical CO₂ Rankine cycle with the helium gas turbine is a key feature of this design. By utilizing waste heat from the gas turbine, the system generates additional power through the CO₂ Rankine cycle, thereby maximizing energy conversion efficiency and resource utilization. Furthermore, the system incorporates a hydrogen production module, allowing to produce clean hydrogen as a byproduct of the nuclear energy production process. Hydrogen is a versatile energy carrier that can be used for various applications, contributing to the sustainability of the system and offering opportunities for transportation, industry, and energy storage. According to the results of the analysis, the highest exergy destruction is in the reactor core with 91282 kW. HE PEM has the lowest exergy destruction among system components, with 3.56 kW. In addition, this study includes parametric studies to investigate the effect of helium exit temperature and pressure ratio on system performance.

Keywords: Gas-Cooled Modular Reactor Based Helium Gas, transcritical CO₂ Rankine Cycle, hydrogen Production, energy, exergy

¹**Address:** Isparta University of Applied Sciences, Technology Faculty, Department of Mechanical Engineering, Isparta/Türkiye

²**Address:** ²Department of Mechanical Engineering, Kermanshah University of Technology, Kermanshah, Iran

***Corresponding author:** onderkizilkan@isparta.edu.tr

1. INTRODUCTION

The development of advanced nuclear power technologies holds great potential for addressing global energy challenges while minimizing environmental impact. One promising avenue of research is the integration of Gas-Cooled Modular Reactors (GCMRs) with innovative power conversion systems, such as helium gas turbines and transcritical carbon dioxide (CO₂) Rankine cycles, along with concurrent hydrogen production. This integrated approach aims to enhance overall system efficiency, increase power generation capabilities, and enable the production of clean hydrogen as a versatile energy carrier (Wang et al., 2022). GCMRs utilize helium as the coolant, providing advantages over traditional water-cooled reactors, including higher thermal efficiency, improved safety features, and reduced water consumption. The utilization of helium allows for efficient heat extraction from the nuclear reactor core, enabling the transfer of heat to the power conversion systems (Wang and Dai, 2016). The integration of a helium gas turbine with a bottoming transcritical CO₂ Rankine cycle within the GCMR system is a significant development in advanced nuclear power technology. The helium gas turbine serves as the primary power conversion system, harnessing the energy from the hot helium to drive turbine blades and generate electricity. The utilization of helium, with its exceptional heat transfer properties, enables higher operating temperatures, thereby enhancing the overall thermodynamic efficiency of the system. To further optimize energy extraction, a bottoming transcritical CO₂ Rankine cycle is integrated into the system. This secondary power conversion cycle captures waste heat from the helium gas turbine and utilizes CO₂ as the working fluid. The transcritical CO₂ Rankine cycle operates at high pressures and temperatures, facilitating efficient power generation by effectively utilizing the available heat energy. In addition to improved energy efficiency, this integrated system enables concurrent hydrogen production. Excess heat from the GCMR can be utilized in a thermochemical water-splitting process to produce hydrogen. Hydrogen is a clean energy carrier with various applications, including fuel cells, transportation, and industrial processes. The development of a Gas-Cooled Modular Reactor Based Helium Gas Turbine with a bottoming

transcritical CO₂ Rankine cycle and hydrogen production represents a significant advancement in nuclear power technology. This integrated system offers the potential for higher thermal efficiencies, reduced greenhouse gas emissions, and the production of a clean, versatile fuel source (Labar et al., 2004). Dardoura et al. (2007) presented the successive stages that led to the development of physical and mathematical models enabling the calculation of desalination costs of the gas turbine-modular helium-cooled reactor and the pebble bed modular reactor providing free thermal energy. El-Genk and Tournier (2008) investigated the attributes and limitations of noble gases and binary mixtures as potential working fluids for gas-cooled nuclear power plants with closed Brayton cycles. They compared the heat transfer coefficient and pressure losses of helium and other noble gases and binary mixtures at typical operating conditions in commercial power plants (7.0 MPa and 400–1200 K) for the same molecular flow rate and geometry. Tournier and El-Genk (2008) conducted a review of the properties of the noble gases helium, neon, argon, krypton, and xenon and their binary mixtures at pressures from 0.1 to 20 MPa and temperatures up to 1400 K. An extensive database of experimental measurements is compiled and used to develop semi-empirical properties correlations. Zhao and Peterson (2008) predicted the performance of the helium Brayton cycles with multiple reheat and intercooling states for SFRs with reactor outlet temperatures in the range of 510–650 °C. The resulting thermal efficiencies range from 39% to 47%, which is comparable with that of supercritical recompression CO₂ cycles. The study indicates that the multiple reheat helium cycle is the preferred choice over the sCO₂ cycle for sodium-cooled fast reactors. In this study, it is aimed to investigate the performance of the gas-cooled modular reactor-based system that integrates a helium gas turbine with a bottoming transcritical CO₂ Rankine cycle while concurrently facilitating hydrogen production. At the same time, parametric studies were carried out to investigate the effects of helium temperature and pressure ratio at the reactor outlet on the cycle performance.

2. SYSTEM DESCRIPTION

Figure 1 shows the schematic representation of the integrated system consisting of a gas-cooled modular reactor, a helium gas turbine, a transcritical CO₂ Rankine cycle, and a hydrogen generation system. The GCMR serves as the core component of the system. It utilizes helium as the coolant, providing advantages such as higher thermal efficiency, improved safety features, and reduced water consumption. The GCMR produces high-temperature helium gas because of nuclear fission, which is used as a heat source for subsequent power conversion processes. The helium gas turbine is the primary power conversion system in the integrated setup. It utilizes the high-temperature helium gas from the GCMR to drive the turbine blades and generate electricity. The gas turbine operates based on the principles of thermodynamics, extracting energy from the hot helium, and converting it into mechanical energy, which is then transformed into electrical energy through a generator.

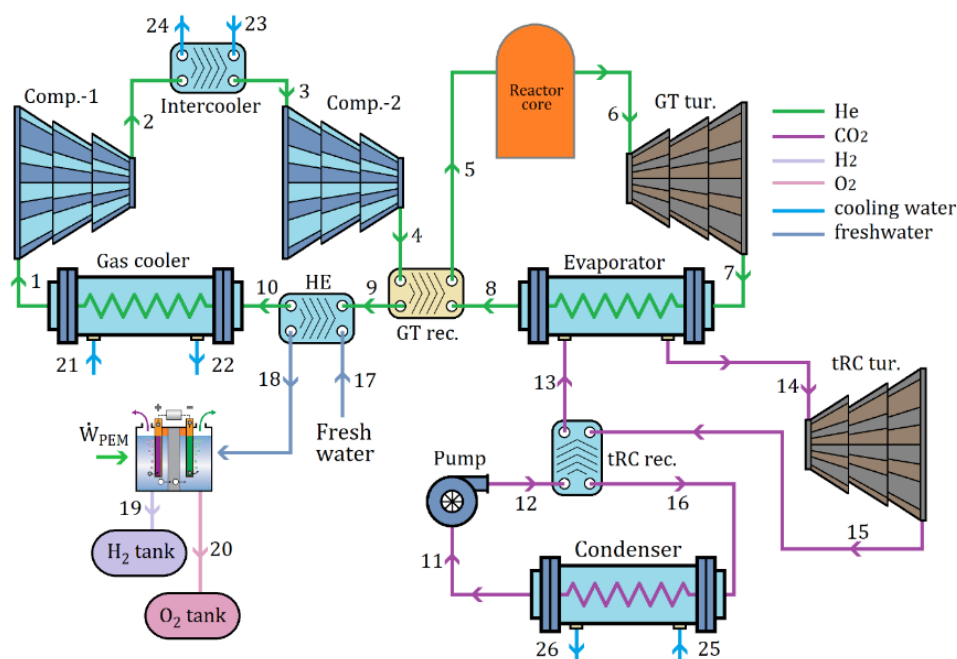


Figure 1. Schematic diagram of a gas-cooled modular reactor combined with the TRC cycle and hydrogen production.

To further optimize the system's energy extraction, a bottoming transcritical CO₂ Rankine cycle is incorporated. This secondary power conversion cycle captures waste heat from the helium gas turbine. The transcritical CO₂ Rankine cycle

operates at high pressures and temperatures, making efficient use of the waste heat by utilizing CO₂ as the working fluid. The CO₂ expands through a turbine, driving a generator to produce additional electricity. Concurrent with power generation, the system facilitates hydrogen production. Excess heat from the GCMR, which is not utilized by the gas turbine or the bottoming transcritical CO₂ Rankine cycle, is diverted to a thermochemical water-splitting process. This process utilizes the excess heat to separate water molecules into hydrogen and oxygen, generating clean hydrogen as a valuable byproduct. The hydrogen can be captured, stored, and utilized for various applications, such as fuel cells, transportation, and industrial processes. Overall, the integrated system operates in a closed-loop manner, with heat being extracted from the GCMR using helium as the coolant. The high-temperature helium is used to drive the gas turbine, generating electricity. Waste heat from the gas turbine is further harnessed through the bottoming transcritical CO₂ Rankine cycle, maximizing the energy extraction from the system. Concurrently, excess heat is utilized in a thermochemical process for hydrogen production, enhancing the overall efficiency and sustainability of the system.

3. METHODOLOGY

In this subchapter, a detailed definition of the thermodynamic methodology utilized in this paper is introduced. Energy and exergy analyses are performed using the Engineering Equation Software (EES) (Klein, 2022) program for the performance evaluation of the system. In this paper, the thermodynamic analysis is made under the following assumptions:

- The steady-state and steady-flow conditions are chosen for all system elements.
- The energetic change for kinetic and potential energies is neglected.
- The heat losses from pumps and turbine are neglected.
- The pressure drops through the pipelines and heat exchangers are neglected.
- The reference state properties are 20°C and 101.325 kPa.

The mass balance equation for steady-state and steady-flow processes can be written as (Cengel and Boles, 2006):

$$\sum \dot{m}_{in} = \sum \dot{m}_{out} \quad (1)$$

Here, \dot{m} is the mass flow rate, and the subscript in denotes inlet and out denotes outlet. The energy balance is expressed as:

$$\dot{Q} + \sum \dot{m}_{in}h_{in} = \dot{W} + \sum \dot{m}_{out}h_{out} \quad (2)$$

where \dot{Q} is the heat transfer rate, \dot{W} is the work, and h is the specific enthalpy. For the exergy analysis, the balance equation is defined as (Dincer and Rosen, 2007):

$$\dot{E}x_Q - \dot{E}x_W = \sum \dot{E}x_{in} - \sum \dot{E}x_{out} + T_0\dot{S}_{gen} \quad (3)$$

where the first and the second terms are exergy of heat and work, respectively, $\dot{E}x$ is the rate of flow exergy, T_0 is the reference state temperature, and the last term is entropy generation. In the above equation, each term is defined as follows:

$$\dot{E}x_{dest} = T_0\dot{S}_{gen} \quad (4)$$

$$\dot{E}x_Q = \dot{Q} \left(\frac{T - T_0}{T} \right) \quad (5)$$

$$\dot{E}x_W = \dot{W} \quad (6)$$

$$\dot{E}x_W = \dot{m} ex \quad (7)$$

In Equation (7), ex is the specific flow exergy and can be calculated using the equation below:

$$ex = (h - h_0) - T_0(s - s_0) \quad (8)$$

3. RESULTS

In this study, it is purposed to examine the performance of the gas-cooled modular reactor-based system that integrates a helium gas turbine with a bottoming transcritical CO₂ Rankine cycle while concurrently facilitating hydrogen production. At the same time, parametric studies were carried out to examine the effects of helium temperature and pressure ratio at the reactor outlet on the cycle performance. Using the balance equations and under the assumptions given above, the analyses are performed by EES software. The assumed operational parameters of the proposed system are tabulated in Table 1.

Table 1. The assumed operational parameters

Parameter	Value
Reference temperature	25 °C
Reference pressure	100 kPa
Thermal power from the reactor	600 MW (Gauthier et al., 2006)
Gas cycle turbine inlet temperature	750 °C (Wang et al., 2002)
Gas cycle turbine inlet pressure	8000 kPa (Wang et al., 2002)
Gas cycle compressor inlet temperature	30 °C (Genk and Tournier, 2008)
Gas cycle compressor inlet pressure	2500 kPa
Gas cycle recuperator efficiency	0.9
tRC pump inlet temperature	23.5 °C
tRC pressure ratio	1.45
tRC turbine isentropic efficiency	0.90
tRC pump isentropic efficiency	0.85
tRC recuperator efficiency	0.85
PEM temperature	80 °C

Figure 2 shows the exergy destruction rate of the components that make up the system. The green color on the right side of the graph shows the exergy destruction rate in the reactor core, and the blue color on the left shows the exergy destruction rate on the other components of the system. As seen in the figure, the highest exergy destruction is in the reactor core with 91282 kW. The reactor core is followed by the evaporator, gas cooler, gas turbine intercooler, and gas turbine, respectively. The lowest exergy destruction among the system components is in the HE PEM, with 3.56 kW.

Parametric studies have been carried out to examine the effects of helium temperature at the reactor exit on the system performance. Figure 3 shows the effect of helium temperature at the reactor outlet on total power generation and energy efficiency. As seen in the figure, when the helium temperature at the reactor outlet is increased from 700 °C to 900 °C, the total power generation and overall energy efficiency increase.

The effect of helium temperature at the reactor outlet on total exergy destruction and overall energy efficiency is shown in Figure 4. It is quite clear that as the helium temperature at the reactor exit increases, the exergy destruction rate decreases; on the contrary, the exergy efficiency increases.

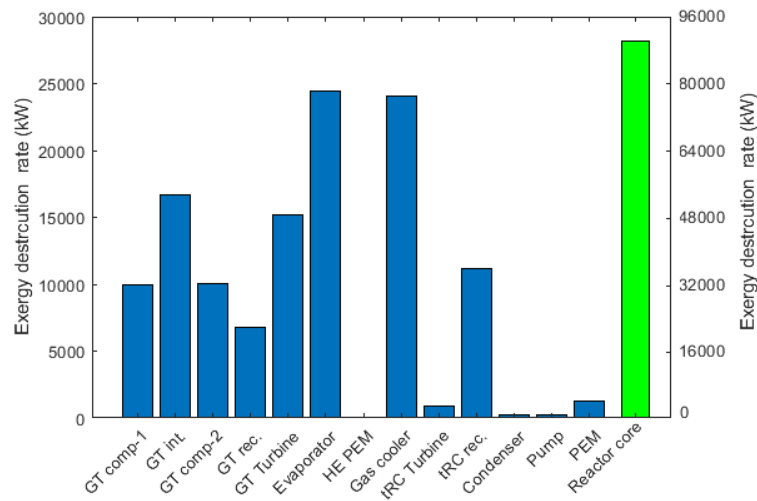


Figure 2. Total exergy destruction rates of system components

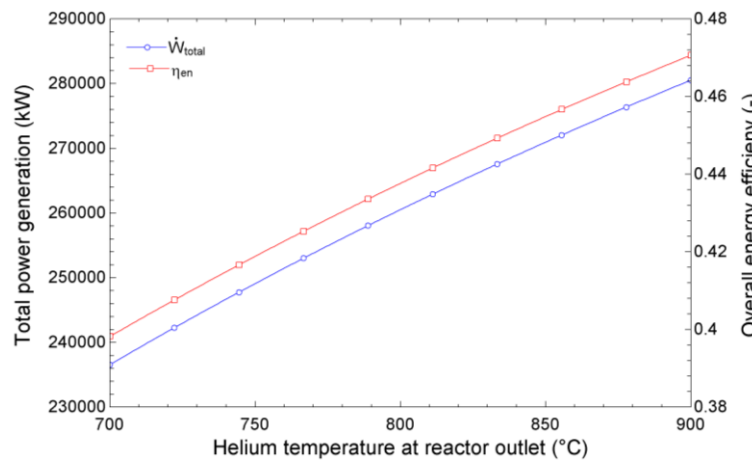


Figure 3. Effect of helium temperature at the reactor outlet on total power generation and overall energy efficiency

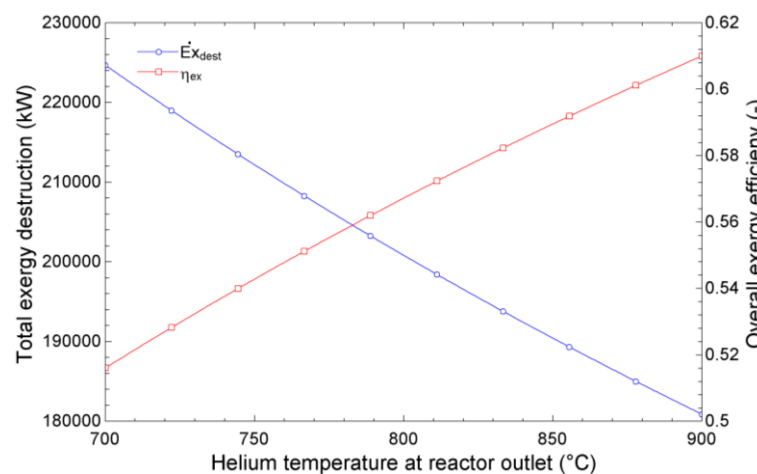


Figure 4. Effect of helium temperature at the reactor outlet on total exergy destruction and overall exergy efficiency

The effect of helium temperature at the reactor outlet on hydrogen production and tRC net power generation is shown in Figure 5. As seen in the figure, as the helium temperature at the reactor outlet increases, hydrogen production and the net power output of the tRC decrease. As expected, hydrogen production decreases as the power generation of the transcritical Rankine cycle decreases.

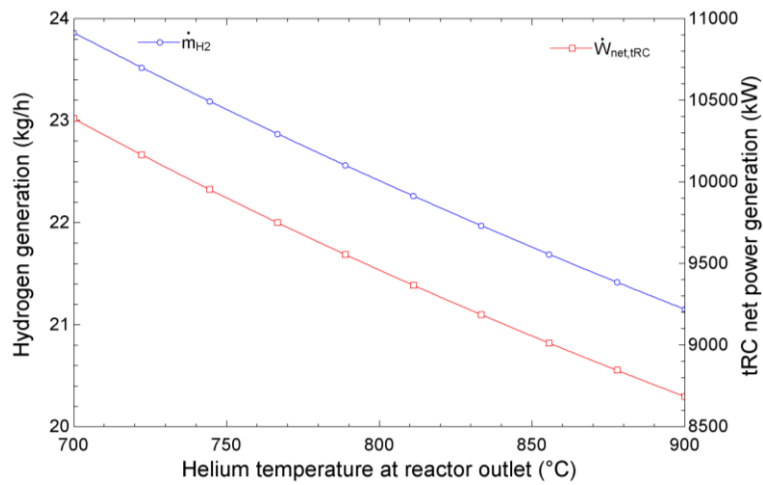


Figure 5. Effect of helium temperature at the reactor outlet on hydrogen generation and tRC net power generation

The effect of the pressure ratio on overall power generation and overall energy efficiency is shown in Figure 6. Total power generation and efficiency increase with turbine inlet temperature and show a maximum value relative to the pressure ratio at any temperature. This maximum value shifts to higher pressure ratios when higher turbine inlet temperatures are used. Increasing temperature increases the average temperature of heat reception of the cycle, which increases the corresponding Carnot and, as a result, our cycle efficiency. Increasing temperature also increases the enthalpy difference across the turbine, allowing more power to be produced and consequently achieving higher efficiencies for all the cycles. Moreover, increasing temperature results in a higher turbine inlet temperature and pressure in the tRC, leading to produce more power in the tRC turbine.

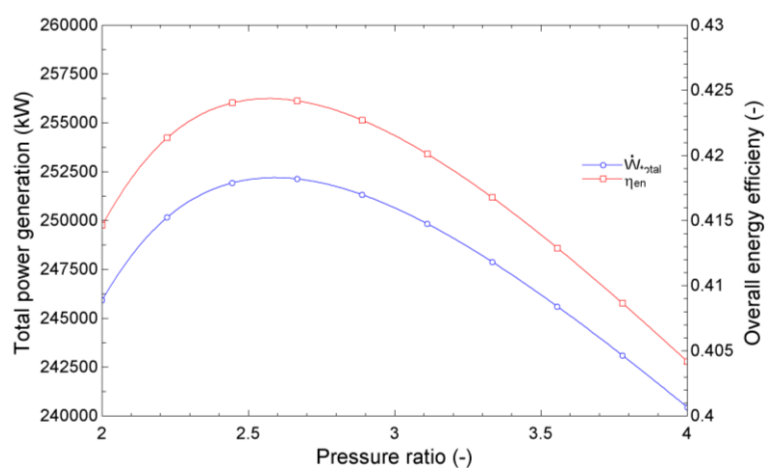


Figure 6. Effect of pressure ratio on total power generation and overall energy efficiency

Figure 7 shows the effect of the pressure ratio on total exergy destruction and overall exergy efficiency. It is seen that the energy efficiency seen in Figure 6 and the increasing-decreasing trend of the exergy efficiency seen here are the same. Also, the effect of the pressure ratio on hydrogen production and tRC net power generation is shown in Figure 8. The hydrogen production and tRC net power generation decrease with the pressure ratio.

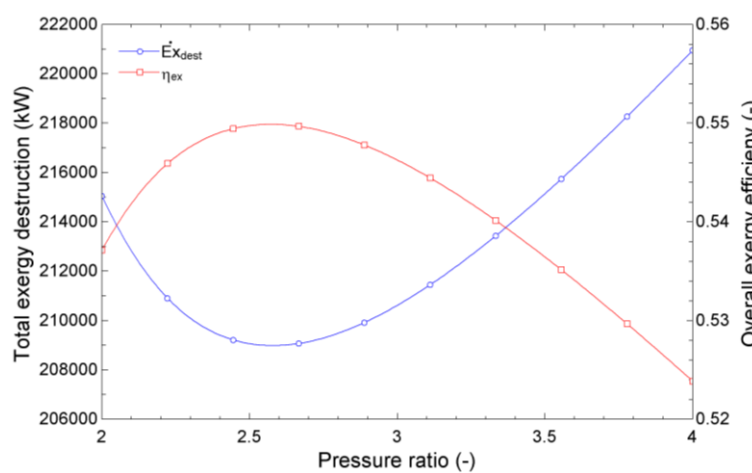


Figure 7. Effect of helium temperature at the reactor outlet on hydrogen generation and tRC net power generation

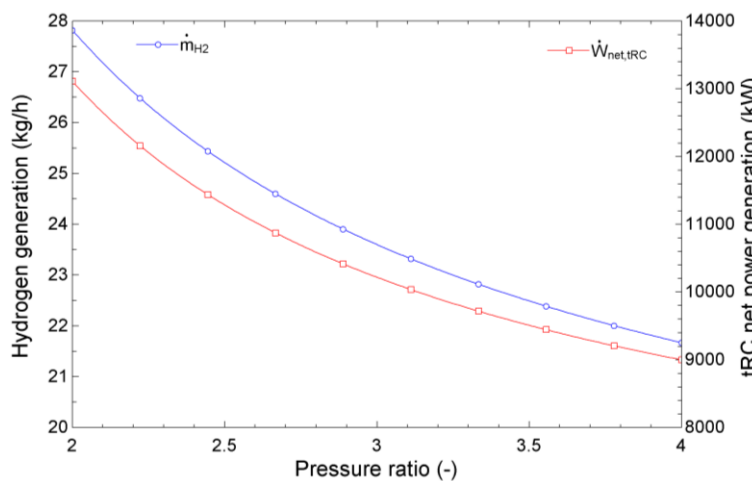


Figure 8. Effect of helium temperature at the reactor outlet on hydrogen generation and tRC net power generation

4. CONCLUSIONS

In this study, the performance of a gas-cooled modular reactor-based system that facilitates hydrogen production while integrating a helium gas turbine with the bottoming out transcritical CO₂ Rankine cycle is investigated. At the same time, parametric studies were carried out to investigate the effects of helium temperature and pressure ratio at the reactor outlet on the cycle performance. According to the results of the analysis, a net power of 241679 kW was obtained from the gas turbine and 9902 kW from the tRC cycle. In addition, the amount of hydrogen produced was 23.11 kg/h, and the amount of O₂ was calculated as 183.4 kg/h. The total exergy destruction rate in the system is 212199 kW, the overall energy efficiency of the system is 41.8%, and the overall exergy efficiency is 54%. At the same time, in this study, parametric studies were carried out to investigate the effects of helium temperature and pressure ratio at the reactor outlet on the cycle performance.

In conclusion, the development of a GCMR based on a helium gas turbine with a bottoming transcritical CO₂ Rankine cycle and hydrogen production holds significant promise for advancing the field of nuclear energy. This innovative approach combines multiple technologies to enhance the overall efficiency of the system while enabling the production of hydrogen, a clean and - versatile energy carrier. The use of helium as a coolant in the GCMR offers several advantages. Helium has excellent heat transfer properties, allowing for efficient heat extraction from the reactor core. It is also chemically inert, reducing the likelihood of corrosion or chemical reactions within the system. Furthermore, helium operates at high temperatures, enabling higher thermal efficiencies and increased power output. The integration of a bottoming transcritical CO₂ Rankine cycle in conjunction with the helium gas turbine is a key feature of this design. By utilizing the waste heat from the gas turbine, the system can generate additional power through the CO₂ Rankine cycle, thereby maximizing the overall energy conversion efficiency. This approach enhances the sustainability of the system by optimizing resource utilization and minimizing waste. Another significant benefit of this integrated system is the

production of hydrogen. Hydrogen is a clean and versatile energy carrier that can be used for various applications, including transportation, industry, and energy storage. By incorporating a hydrogen production module within the GCMR system, it becomes possible to generate hydrogen as a byproduct of the nuclear energy production process, further enhancing the system's economic viability and environmental sustainability. The development of a gas-cooled modular reactor based on a helium gas turbine with a bottoming transcritical CO₂ Rankine cycle and hydrogen production represents a crucial step towards the realization of advanced nuclear energy systems. This integrated approach offers a range of advantages, including high thermal efficiency, reliable and safe operation, reduced environmental impact, and the production of clean hydrogen. However, further research, development, and demonstration efforts are required to optimize and validate the technical and economic feasibility of this concept at a larger scale. With continued advancements in nuclear technology and a focus on sustainable energy solutions, the gas-cooled modular reactor with a bottoming transcritical CO₂ Rankine cycle and hydrogen production holds immense potential for transforming the energy landscape and driving us toward a greener and more sustainable future.

REFERENCES

- Cengel, Y.A., Boles, M.A. (2006). *Thermodynamics: an engineering approach*. McGraw-Hill, New York.
- Dincer, I., Rosen, M.A. (2007). *Exergy: Energy, Environment and Sustainable Development*. Elsevier Science.
- Dardoura, S., Nisan, S., Charbit, F. (2007). Utilization of Waste Heat from GT-MHR and PBMR Reactors for Nuclear Desalination. *Desalination*. 205, 254–268.
- El-Genk, M.S., Tournier, J.M. (2008). On the Use of Noble Gases and Binary Mixtures as Reactor Coolants and CBC Working Fluids. *Energy Conversion and Management*. 49, 1882–1891.
- Gauthier, J.C., Brinkmann G., Copsey B., Lecomte, M. (2006). ANTARES: The HTR/VHTR project at Framatome ANP. *Nuclear Engineering and Design*. 236, 526–533
- Klein, S.A. (2022) *Engineering Equation Solver (EES) V11, F-Chart Software*, Madison, USA. <http://www.fchart.com>
- Labar, M., Shenoy, A.S., Simon, W.A., Campbell, E.M. (2004). The Gas-Turbine Modular Helium Reactor. *Nuclear Energy*. 43(3), 165-175.
- Tournier, J.M., El-Genk, M.S. (2008). Properties of Noble Gases and Binary Mixtures for Closed Brayton Cycle Applications. *Energy Conversion and Management*. 49, 469–492.
- Zhao, H., Peterson, P.F. (2008). Multiple Reheat Helium Brayton Cycles for Sodium Cooled Fast Reactors. *Nuclear Engineering and Design*. 238, 1535–1546.
- Wang, Q., Liu, C., Luo, R., Li, D., Juan, R.M. (2022). Thermodynamic Analysis and Optimization of the Combined Supercritical Carbon Dioxide Brayton Cycle and Organic Rankine Cycle-Based Nuclear Hydrogen Production System. *International Journal of Energy Research*. 46, 832-859.
- Wang C, Ballinger RG, Stahle PW, Demetri E, Koronowski M, (2002). Design of a power conversion system for an indirect cycle, helium cooled pebble bed reactor system. In: *Proceedings of first international topical meeting on HTR technology (HTR2002)*, international atomic energy agency, 22–24 April 2002, Vienna, Austria, Petten, Netherlands; 2002.
- Wang, X., Dai, Y. (2016). An Exergoeconomic Assessment of Waste Heat Recovery from a Gas Turbine-Modular Helium Reactor Using Two Transcritical CO₂ Cycles. *Energy Conversion and Management*. 126, 561-572.

Dynamic Modeling of a Photovoltaic/Thermal (PV/T) Collector for Isparta

Gamze Soy Turk¹, Onder Kizilkan^{*1}

Abstract: Although the performance of photovoltaic/thermal (PV/T) panels has been studied both computationally and experimentally for some time, the thermal models created in previous research were mostly steady-state models to predict annual efficiencies. In this study, solar thermal collector and photovoltaic (PV) cells are combined to form a PV/T collector, and water-ethylene glycol is used as a coolant to lower the temperature of the PV panels. The aim of this study is to analyze a water-ethylene glycol-based PV/T collector in Isparta conditions numerically. Time-dependent dynamic analyzes were performed using the MATLAB software program. Research has also been conducted on how the generated electrical energy and fluid output and the temperature of the PV/T surface change over time.

Keywords: Photovoltaic/Thermal collector, solar energy, thermal efficiency, electrical efficiency, ethylene glycol

¹**Address:** Isparta University of Applied Sciences, Technology Faculty, Department of Mechanical Engineering, Isparta/Türkiye

***Corresponding author:** onderkizilkan@isparta.edu.tr

1. INTRODUCTION

The growing demand for renewable energy sources has led to extensive research and development in the field of photovoltaic/thermal (PV/T) collectors. These innovative devices combine the benefits of both solar photovoltaic and solar thermal technologies, enabling simultaneous electricity generation and heat production. The dynamic modeling of PV/T collectors plays a crucial role in optimizing their performance and assessing their feasibility for specific locations. The hybrid photovoltaic/thermal (PV/T) solar collector integrates a PV module with a solar thermal collector, simultaneously producing electric and thermal energy. In this way, a reduction of the PV cell temperature, which is beneficial for the electric conversion efficiency, and a simultaneous increase of coolant (air or water) temperature are achieved. Although the electrical and the thermal performance of PV/T collectors are lower than the ones of separate PV and conventional thermal collectors, the converted energy per unit surface area is usually than the one produced by one PV panel and one thermal collector next to each other and, therefore, the PV/T technology results strongly attractive for applications where the surface area availability is a constraint (Zondag and Vries, 1999). The development of both thermal and electric models and their coupling are necessary to predict the performance of PV/T solar collectors accurately. Different approaches are found in the scientific literature leading to various models, from simple to complex. Zondag et al. (2002) developed and validated a 3D dynamical model and three steady-state (3D, 2D, and 1D) models of a double-glazed PV/T collector. The electric modeling was based on the adoption of the power coefficient to correct the power production at different temperatures. Numerical data agreed with experimental ones within 5%. Chow (2003) developed a dynamic model for a single-glazed flat plate PV/T collector based on the control-volume approach. The influence of cell temperature on collector power production was accounted for using the typical power coefficient correction. The model was later updated and validated by Bhattarai et al. (2012) through a comparison with experimental data, finding that the maximum difference between the measured and predicted values was 1.17 K for water temperature at the collector outlet, 2% for collector thermal efficiency and 0.2% for collector electrical efficiency. Amrizal et al. (2013) developed a dynamic model of a flat plate PV/T collector based on the equation reported in the report coupled with the single-diode photovoltaic model. The model required four parameters to simulate the dynamic operation of the PV/T collector calibrated against experimental data. Once calibrated, the model accuracy was satisfactory. Touafek et al. (2014) developed a dynamic model of a sheet-and-tube PV/T collector, assuming an average value of the temperature for each layer and using the power coefficient relation between cell temperature and conversion efficiency to account for its influence on power production. Khelifa et al. (2014) developed and validated a dynamic model of a sheet-and-tube PV/T collector using a 2D control-volume approach. The influence of cell temperature on cell power production was accounted using the power coefficient relation. The model was validated using in-house experimental results, finding that the root mean square of percentage deviations is equal to 2.66% for water outlet temperature and 16.17% for useful thermal energy. Haurant et al. (2015) developed and validated a 3D dynamic model for a sheet-and-tube PV/T collector. The Shockley single-diode approximation to describe the PV cell was implemented. The model was validated under steady-

state and transient conditions, showing a tendency to overestimate the collector power production with a maximum difference equal to 1.7 W in steady-state conditions and larger values in transient ones. Moreover, the fluid temperature at the collector outlet was predicted within 0.2 K and 2 K during steady and transient conditions, respectively. Aste et al. (2015) developed a dynamic model of an innovative roll bond PV/T collector, assuming a uniform temperature in each layer and using the power coefficient to correct the PV cell conversion efficiency. The model was validated against in-house experimental results finding a root mean square percentage deviation of around 15% for the power production and around 4–5% for the water temperatures. Later this model was improved to simulate a commercial roll-bond PV/T collector (2016). After a calibration of the model parameter using a best-fitting procedure, an agreement between the measured and model collector daily electrical energy and the water temperatures within 2.52% and within 0.27 K was found, respectively. This paper focuses on the dynamic modeling of a PV/T collector specifically designed for the city of Isparta. Isparta, located in southwestern Turkey, experiences a Mediterranean climate characterized by abundant sunshine throughout the year. Such favorable weather conditions make Isparta an ideal location for harnessing solar energy and evaluating the efficiency of PV/T collectors. Dynamic modeling involves the simulation and analysis of various factors that influence the performance of PV/T collectors over time. These factors include solar radiation, ambient temperature, wind speed, and system design parameters. By employing mathematical models and computer simulations, researchers can accurately predict the electrical and thermal outputs of PV/T collectors under varying weather conditions. The outcomes of this dynamic modeling study provide valuable insights into the energy generation potential and efficiency of PV/T collectors in Isparta. By accurately predicting the system's performance, researchers and engineers can optimize the design and operation of PV/T collectors, leading to improved energy utilization and cost-effectiveness.

2. MATHEMATICAL MODELING

In photovoltaic thermal systems, some solar irradiation is transformed into electrical energy, while a large part of it creates a thermal load on the material. This thermal load can reduce the collector's efficiency and damage the material's structure. PV/T systems have been designed to minimize this thermal load created by solar irradiation that cannot be converted into electrical energy in the collector. These hybrid systems can simultaneously provide hot air or domestic water and electrical power. The most widely used PV/T type is the system where hot water is provided. While these systems generate electrical energy with the modules on their upper surfaces, they store the domestic water with the copper plates on the back of the collector. Thanks to the working fluid in the collector, the temperature of the cell is diminished, and the electrical energy efficiency is raised. The schematic representation of the PV/T panel is shown in Figure 1. As seen from the figure, the PV/T collector comprises a set of PV panels, a glass cover, pipes, an absorber surface, and insulation. In Figure 1, the thermal resistance network of the PV/T panel is shown.

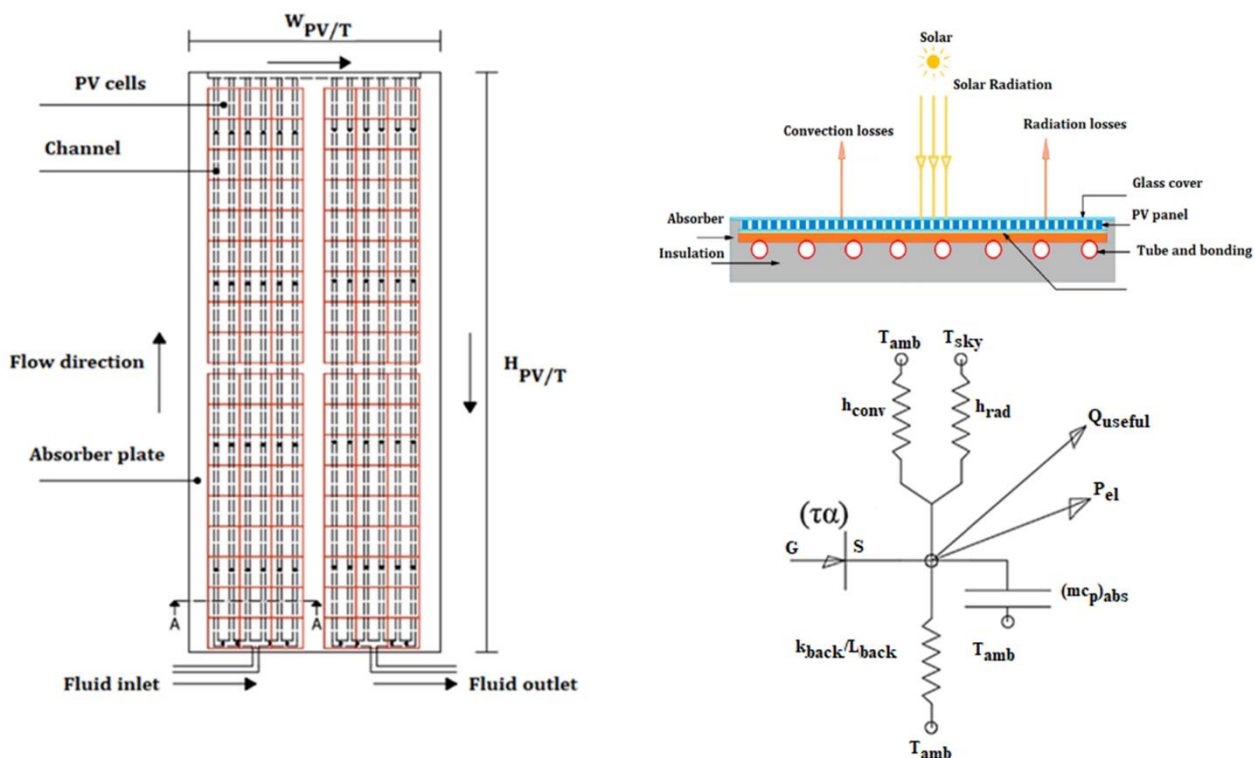


Figure 1. PV/T collector schematic and thermal resistance network

The following assumptions were considered in the PV/T mathematical modeling (Sakellariou and Axaopoulos, 2018):

- 1) PV/T panels are connected in series.
- 2) Air gaps between the glass cover and the PV cells are neglected.
- 3) PV/T is considered as a single layer, and heat transfer between layers is neglected.
- 4) PV/T mass and specific heat capacity are neglected.
- 5) Heat transfer by natural convection is neglected, and heat losses by wind are only considered for the upper surface of the collector.
- 6) The heat losses from the edge surfaces of the PV/T panel are neglected.
- 7) The thermal capacities of the PV/T components are neglected. Only the thermal capacities of the heat transfer fluid are considered.

The properties of the PV/T panel used in the mathematical modeling are given in Table 1.

Table 1. Properties of PV/T panel working with ethylene glycol –water mixture (Sakellariou and Axaopoulos, 2018):

Basic data		Value
PV/T length	L(m)	1.649
PV/T width	W (m)	0.992
PV/T total area	A _{PV/T} (m ²)	1.635
PV/T cell area	A _{cell} (m ²)	1.417
PV/T mass	m _{PV/T} (kg)	3.75
PV/T specific heat	C _{pPV/T} (J/kgK)	8081
PV/T conductivity	k _{PV/T} (W/mK)	187.1
PV/T thickness	λ _{PV/T} (m)	0.0065
Absorptivity coefficient	α	0.85
Emissivity coefficient	ε	0.88
Transmissivity coefficient	τ	0.9
Packing factor	PF	0.9
Electrical data		
Cell type		p-Si
Reference electrical efficiency	η _{ref} (%)	0.143
Temperature power coefficient	β (1/K)	0.0046
Thermal data		
Mass flow rate	m _{HTF} (kg/s)	0.02
Number of tubes	n _{tube}	10
External tube diameter	D (m)	0.008
Internal tube diameter	D _i (m)	0.006
Distance between tubes	w (m)	0.099
Insulation thickness	λ _{back} (m)	0.03
Insulation conductivity	k _{back} (W/mK)	0.04
Boundary conductivity	k _{bond} (W/mK)	250
Boundary width	b _{bond} (m)	0.01
Boundary thickness	λ _{bond} (m)	0.05
Boundary heat transfer coefficient	h _{ca} (W/m ² K)	30.3214

In this work, heat that had accumulated in various parts of the hybrid solar system was removed using ethylene glycol-water as a heat transfer fluid. 50% by weight ethylene glycol-water mixture has been shown to have a higher energy and exergy efficiency than pure ethylene glycol and a lower freezing point than pure ethylene glycol when used as the working fluid for PV/T. As a result, ethylene glycol-water mixture (50 percent by weight) was utilized as a working fluid that was appropriate for cold climates. Temperature-dependent thermophysical properties for ethylene glycol (50%) were formulated using curve-fit curves from the Engineering Equation Solver (EES) database. Required property values in the following equation:

$$y = a + bT + cT^2 + dT^3 + eT^4 + fT^5 + gT^6 \tag{1}$$

In the above equation, y is the thermophysical property (C_p, k, ρ, μ, Pr), and the coefficients a, b, c, d, e, f, and g are obtained for the temperature of T = 25°C and pressure of P = 101.325 kPa. Various thermophysical property coefficients can be defined for different temperature and pressure values. These coefficients are obtained from the real table value

with the help of curve-fitting methods. In determining the size of the linear regression error in curve fittings, the correlation coefficient 'R²' is determined. An R² value close to 1 means that the fitted curve best expresses the data. Table 2 shows the equation coefficients of the thermophysical properties of the water-ethylene glycol mixture (50% by weight).

Table 2. Coefficients of the thermophysical properties in Equation (1)

	Cp (kj/kgK)	k (W/m ² K)	ρ (m ³ /kg)	μ (kg/ms)	Pr
a	3202.88	0.37	1074.62	0	67.19
b	5.64	0.0006	-0.43	-0.0002	-2.48
c	-0.008	3.17×10 ⁻⁷	-0.002	0.000009	0.081
d	-0.0003	-50	0.000006	-42	-0.0029
e	0	0	0	7.3×10 ⁻⁹	0.00006
f	0	0	0	-80.3	-64.7
g	0	0	0	2.39×10 ⁻¹³	1.98×10 ⁻⁹

The heat transfer coefficient of the working fluid in the pipe by convection is calculated as follows:

$$h_f = \frac{Nuk}{D_i} \quad (2)$$

Here, h_f (W/m²K) is the heat transfer coefficient of the fluid, and k (W/mK) is the thermal conductivity of the fluid. To calculate the h_f value of the working fluid, the Reynolds (Re) number must first be determined.

$$Re = \frac{\rho V D_i}{\mu} \quad (3)$$

where ρ (kg/m³) is the density of the fluid, V (m/s) is the velocity of the fluid, D_i (m) is the inner diameter of the pipe, and μ (kg/ms) is the absolute viscosity. If Re < 2500, laminar flow occurs, if Re ≥ 2500, turbulent flow occurs in the pipe (Çengel and Ghajar, 2014).

L (m), the hydrodynamic inlet length, is expressed as the length from the pipe inlet where the shear stress (and, therefore, the friction factor) approaches the fully developed value by 2% pipe (Çengel and Ghajar, 2014). The hydrodynamic inlet lengths in laminar and turbulent flow are calculated as follows:

$$L_{laminar} = 0.05 Re D \quad (4)$$

$$L_{turbulent} = 10 D \quad (5)$$

$$x^* = \frac{L}{Re Pr D} \quad (6)$$

Here, Pr is the Prandtl number, and D (m) is the hydraulic diameter.

The Nusselt number for thermally developing laminar flow is determined by Equation (7) and Equation (8):

$$Nu = 1.953(x^*)^{-\frac{1}{3}} \quad x^* \leq 0.03 \quad (7)$$

$$Nu = 4.364 + \frac{0.0722}{(x^*)^{-\frac{1}{3}}} \quad x^* > 0.03 \quad (8)$$

In the case of turbulent flow, the Nusselt number can be determined by Equation (9) as pipe (Çengel and Ghajar, 2014):

$$Nu = \frac{\frac{f}{8}(Re-1000)Pr}{1+12.7\left(\frac{f}{8}\right)^{\frac{1}{2}}\left(\frac{2}{3}Pr-1\right)} \quad (9)$$

Here f is the friction factor, and it is determined by Equation (10) (Kalagirou, 2015):

$$f = \frac{1}{(0.79 \ln(Re) - 1.64)^2} \quad (10)$$

The total heat loss coefficient U_L (W/m²K) in the collectors is calculated by Equation (11). Here, U_e (W/m²K) heat losses from the side surfaces are disregarded, while the total heat loss from the collector is calculated with the sum of the heat losses from the upper and lower surfaces pipe (Kalagirou, 2015):

$$U_L = U_t + U_b \quad (11)$$

where U_t (W/m²K) denotes the heat loss coefficient from the collector top surface, and U_b (W/m²K) represents the loss coefficient from the collector back surface (Kalagirou, 2015):

$$U_t = h_{conv} + h_{rad} \quad (12)$$

Here, h_{conv} (W/m²K) denotes the heat transfer coefficient with forced convection, and h_{rad} (W/m²K) denotes the heat transfer coefficient with radiation (Kalagirou, 2015):

$$h_{conv} = 2.2V_{wind} + 8.3 \quad (13)$$

$$h_{rad} = \varepsilon\sigma(T_{PV/T}^2 + T_{sky}^2)(T_{PV/T} + T_{sky}) \quad (14)$$

$$T_{sky} = 0.0552T_{amb}^{1.5} \quad (15)$$

Here, V_{wind} (m/s) represents the average wind speed, $T_{PV/T}$ (K) means the average PV /T surface temperature, T_{sky} (K) represents the sky temperature, and T_{amb} (K) the ambient temperature (Kalagirou, 2015):

$$U_b = \frac{k_{back}}{\lambda_{back}} \quad (16)$$

Here, k_{back} (W/mK) represents the thermal conductivity of the back surface insulation material, and λ_{back} (m) refers to the thickness of the back surface insulation material.

A one-dimensional steady-state model was developed to study the thermal and electrical efficiency of PV/T systems, and Hottel-Whillier equations were employed in these calculations. The overall energy balance of the PV/T collector is calculated by Equation (17) (Sakellariou and Axaopoulos, 2018):

$$\dot{Q}_u = F_R \left(I(\alpha\tau)(A_{PV/T} - A_{cell}\eta_{el}) \right) - \left(A_{PV/T}U_L(T_{in} - T_{out}) \right) \quad (17)$$

Here, \dot{Q}_u (W) represents the useful heat supplied from the collector, I (W/m²) solar radiation, $(\alpha\tau)$ absorbance-permeability coefficient, η_{el} collector electrical efficiency, $A_{PV/T}$ (m²) collector surface area, A_{cell} (m²) PV/T cell area, T_{in} (K) fluid inlet temperature.

The collector heat gains factor (F_R) is calculated by Equation (18) as follows (Kalagirou, 2015):

$$F_R = \frac{\dot{m}_{HTF}c_p}{A_{PV/T}U_L} \left(1 - \exp\left(\frac{-A_{PV/T}U_L F'}{\dot{m}_{HTF}c_p}\right) \right) \quad (18)$$

Here, \dot{m}_{HTF} (kg/s) is the mass flow rate of the fluid, c_p (J/kgK) is the specific heat capacity of the fluid, and F' is the collector efficiency factor.

$$F' = \frac{\frac{1}{U_L}}{w \left(\frac{1}{U_L(D+(W-D)F)} + \frac{1}{h_{ca}} + \frac{1}{\pi D_i h_f} \right)} \quad (19)$$

Here, w (m) is the space between the pipes through which the PV/T fluid passes, D (m) is the outer diameter of the tube, h_{ca} (W/m²K) is the boundary heat transfer coefficient, D_i (m) is the inner diameter of the tube, h_f (W/m²K) represents the heat transfer coefficient of the fluid.

$$F = \frac{\tanh\left(\frac{m(w-D)}{2}\right)}{\frac{m(w-D)}{2}} \quad (20)$$

The value of m here is calculated by Equation (21) (Kalagirou, 2015):

$$m = \sqrt{\frac{U_L}{(k\lambda)_{PV/T}}} \quad (21)$$

P_{el} , which is the electrical power gained from PV/T, is calculated by Equation (22) (Sakellariou and Axaopoulos, 2018):

$$P_{el} = \eta_{el} I A_{cell} (\alpha\tau) \quad (22)$$

Average PV/T temperature $T_{PV/T}$ is calculated by Equation (23) (Sakellariou and Axaopoulos, 2018):

$$T_{PV/T} = T_{in} + \left(\frac{\dot{Q}_u}{A_{PV/T} F_R U_L} \right) (1 - F_R) \quad (23)$$

Also, the fluid mean outlet temperature T_{HTF} (K) can be found by Equation (24):

$$T_{HTF} = \dot{Q}_u + \frac{\dot{m}_{HTFCp}(T_{in}-T_{out})dt}{m_{HTFCp}} + T_{out} \quad (24)$$

Electrical and thermal efficiencies of PV/T could be calculated using Equation (25) and Equation (26) (Yazdanifard et al., 2016):

$$\eta_{el} = \eta_{ref} \left(1 - \beta(T_{PV/T} - T_{amb}) \right) \quad (25)$$

Here, η_{ref} denotes the electrical efficiency at the reference point, and β denotes the temperature power coefficient.

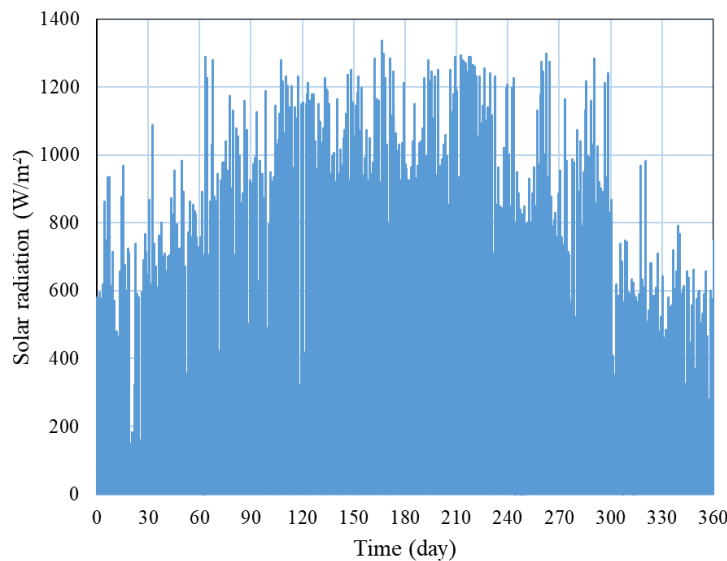
$$\eta_{th} = \frac{\dot{m}_{HTFCp}(T_{HTF}-T_{in})}{I(\alpha\tau)A_{PV/T}} \quad (26)$$

The total efficiency of the PV/T system is determined by Equation (27):

$$\eta_{PV/T} = \eta_{el} + \eta_{th} \quad (27)$$

3. RESULTS

Using the equations given in the previous section, analyzes were carried out for a water-ethylene glycol-based PV/T collector for Isparta conditions. For the time-dependent dynamic investigation, meteorological information such as annual solar radiation, wind velocity, and environment temperature of Isparta is obtained and shown in Figure 2.



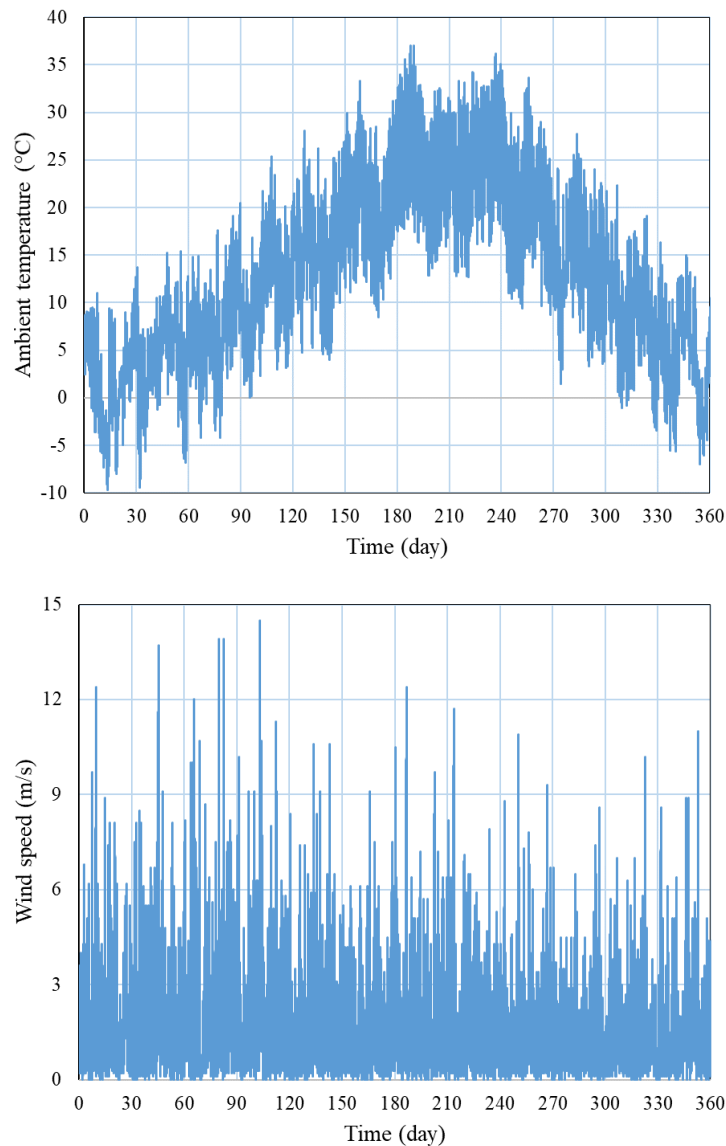


Figure 2. Meteorological data for Isparta

In the second part of the study, the validation of the modeling was carried out. In Figure 3, the graph of variation of the collector flow factor (F'') and the dimensionless number $(\dot{m}c_p) / (AU_L F)$ in the reference study by Duffie and Beckman (2013) was shown to validate the current mathematical model. As can be seen from the figure, the trend in the PV/T mathematical modeling and the trend in the reference study are compatible with each other.

Figure 4 shows the thermal efficiency based on the $(T_{in} - T_{amb}) / I_{solar}$ ratio, which is an indicator for evaluating the performance of PV/T. As can be observed in the figure, for flow rates of 0.03, 0.1, 0.2, 0.3, and 0.36 kg/s, there was a tendency for thermal efficiency to decrease as the $(T_{in} - T_{amb}) / I_{solar}$ increased due to the rise in heat losses due to the temperature difference between the working fluid and the ambient air. In addition, verification studies were carried out considering the reference study of Kim and Kim (2012), and the average efficiency at a flow rate of 0.36 kg/s reached the highest value of 40% when the difference between the inlet temperature and the ambient temperature was zero. As seen in the figure, in the current study, thermal efficiency reaches 40% from 26% by raising the mass flow rate from 0.03 kg/s to 0.36 kg/s under 800 W/m² radiation conditions.

The variation in the electrical efficiency of PV/T according to the temperature difference is shown in Figure 5. As in thermal efficiency verification studies, electrical efficiency variation was observed for flow rates of 0.03, 0.1, 0.2, 0.3, and 0.36 kg/s depending on the $(T_{in} - T_{amb}) / I_{solar}$ ratio. As can be seen in the figure, verification studies were carried out with the reference study of Kim and Kim (2012), and it was observed that the $\Delta T / I_{solar}$ ratio and the electrical efficiency tended to decrease.

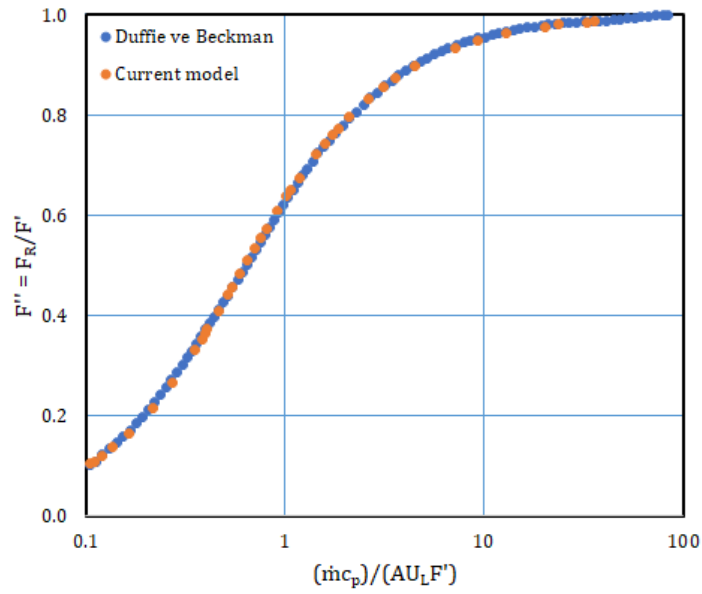


Figure 3. PV/T collector flow factor F'' as a function of $(\dot{m}_{HTF} C_p)/(A_{PV/T} U_L F')$

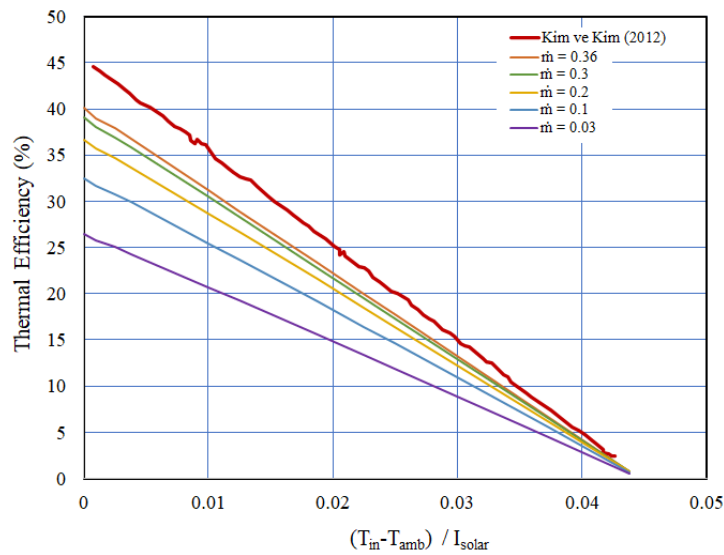


Figure 4. PV/T thermal efficiency curve according to $\Delta T/I_{solar}$

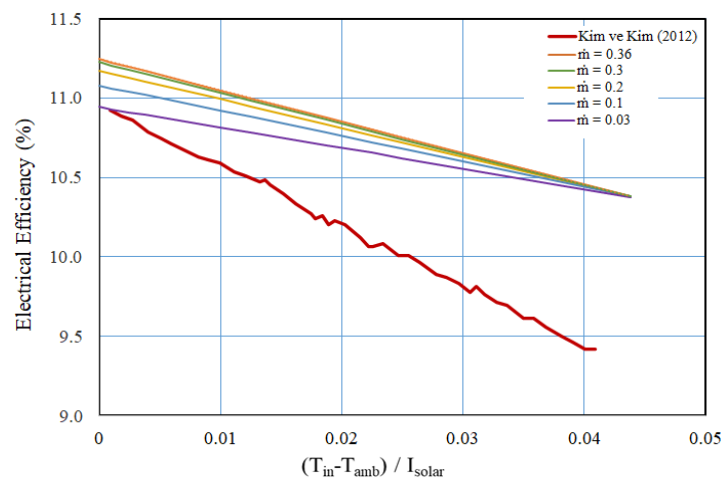


Figure 5. PV/T electrical efficiency curve according to $\Delta T/I_{solar}$

Figure 6 depicts the PV/T surface temperature's fluctuation over the first five days of January. The PV/T surface temperature rises as solar irradiation rises, as shown in the figure. The three-day analysis produced a maximum panel temperature estimate of about 37°C. Figure 7 shows the change in the heat transfer fluid's output temperature over time. The output temperature of the heat transfer fluid rises with an increase in solar radiation, as seen in the image. The maximum exit temperature of the heat transfer fluid was determined to be almost 12.5°C as a result of the five-day analysis.

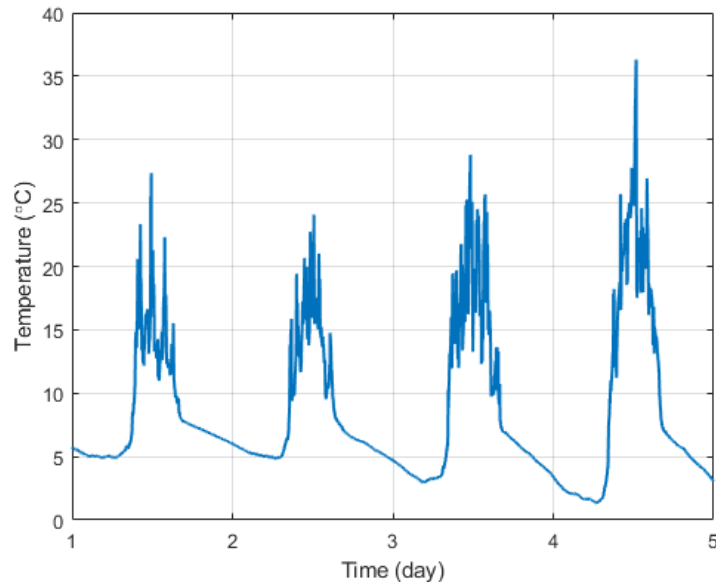


Figure 6. Variation of the PV/T surface temperature

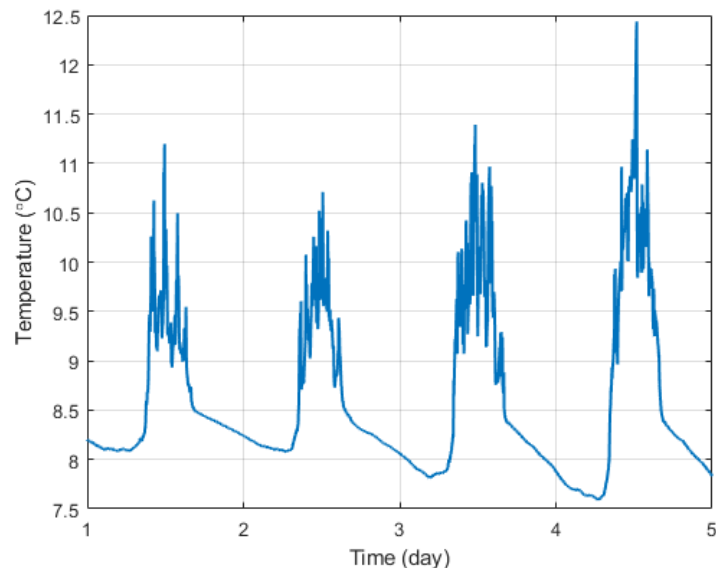


Figure 7. Variation of the outlet temperature of the HTF

Figure 8 depicts the fluctuation in the working fluid outlet temperature and PV/T surface temperature for the chosen three days. The change of the PV/T surface temperature and the working fluid outlet temperature follow the same trend, as shown in the figure. In rare circumstances, the working fluid's output temperature climbs above the PV/T surface temperature. This is since just the mass and specific heat of the working fluid are considered in the PV/T mathematical modeling, but the PV/T has no resistance and heats up and cools down quickly.

The electrical power's change over time is depicted in Figure 9. Throughout the analysis time, the solar radiation value changed simultaneously with the electrical power produced by the PV collector and the PV/T panel, and the highest electrical efficiency was attained at noon when the radiation was at its highest.

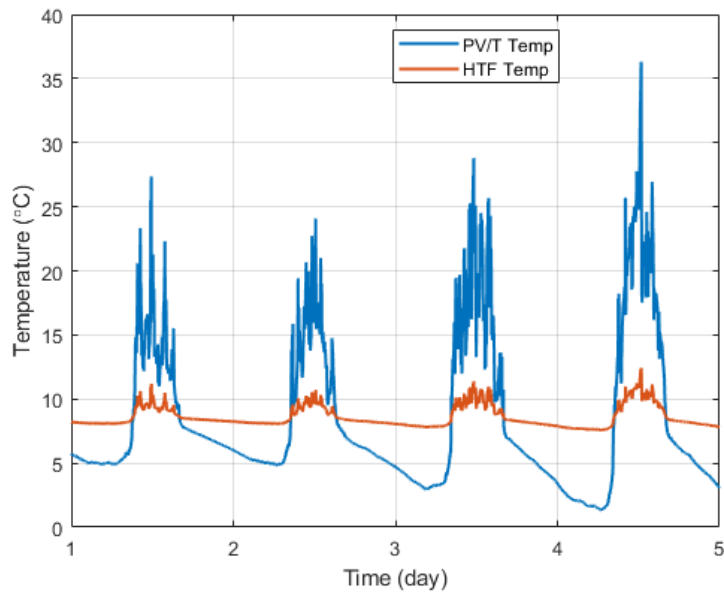


Figure 8. Variation of the outlet temperature of the heat transfer fluid and PV/T surface temperature with time

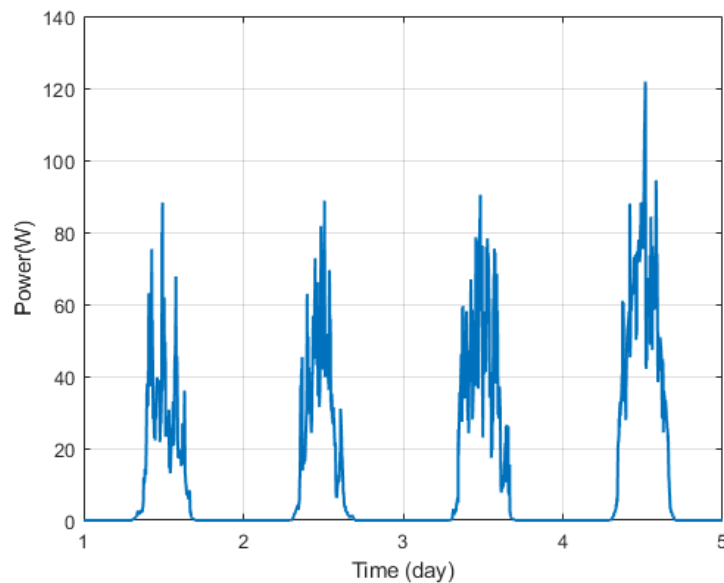


Figure 9. Variation of the electrical power

4. CONCLUSIONS

In this study, a mathematical model was conducted with the purpose of validating the water-ethylene glycol-based PV/T panel. Based on the energy balance of the PV/T panel, which is made up of several parts, including PV cells, insulation, transparent cover, pipes, plate absorber, and fluid inside the pipe, a model has been created to predict the dynamic behavior of the PV/T panel. Comparing the data found in the literature allowed us to confirm that the obtained theoretical results were in good agreement. During the analyses, the mass flow rate was taken as 0.02 kg/s, and the change of PV/T surface temperature, fluid outlet temperature, and electrical power over time was calculated for three days selected in Isparta conditions. As a result of the analysis, the maximum surface temperature of PV/T panels is 37°C. Also, the maximum power of PV/T is calculated as 122 W. In summary, the dynamic modeling of a PV/T collector for Isparta offers a detailed understanding of the system's performance and its potential contributions to sustainable energy generation. By combining photovoltaic and thermal technologies, this approach represents a significant step towards achieving cleaner and more efficient energy utilization in the region and beyond.

REFERENCES

- Amrizal, N., Chemisana, D., Rosell, J.I. (2013). Hybrid Photovoltaic-Thermal Solar Collectors Dynamic Modeling. *Applied Energy*. 101797–807.
- Aste, N., Del Pero, C., Leonforte, F., Manfren, M. (2016). Performance Monitoring and Modeling of an Uncovered Photovoltaic-Thermal PVT Water Collector. *Solar Energy*. 135, 551–568.
- Aste, N., Leonforte, F., Del Pero, C. (2015). Design, Modeling and Performance Monitoring of a Photovoltaic-Thermal PVT Water Collector. *Solar Energy*. 112, 85–99.
- Bhattarai, S., Oh, J.H., Euh, S.H., Kafle, G.K., Kim, D.H. (2012). Simulation and Model Validation of Sheet and Tube Type Photovoltaic Thermal Solar System and Conventional Solar Collecting System in Transient States. *Solar Energy Mater. Sol. Cells*. 103, 184–193.
- Chow, T.T. Performance Analysis of Photovoltaic-Thermal Collector by Explicit Dynamic Model. (2003). *Solar Energy* 75, 143–152.
- Çengel, YA., Ghajar, A. (2014). *Heat and Mass Transfer*, McGraw Hill Education.
- Duffie JA, Beckman WA. (2013). *Solar Engineering of Thermal Processes* (4th ed.). New York: Wiley.
- Haurant, P., Ménézo, C., Gaillard, L., Dupeyrat, P. (2015). Dynamic Numerical Model of a High Efficiency PV-T Collector Integrated into a Domestic Hot Water System. *Solar Energy*. 111, 68–81.
- Kalogirou, SA. (2015). *Solar Energy Engineering Processes and System*, Elsevier.
- Khelifa, A., Touafek, K., Moussa, H.B. (2014). Approach For the Modelling of Hybrid Photovoltaic-Thermal Solar Collector. *IET Renewable Power Generation*. 207–217.
- Kim, JH., Kim, JT. (2012). Comparison of Electrical and Thermal Performances of Glazed and Unglazed PVT Collectors. *International Journal of Photoenergy*.
- Sakellariou, E., Axaopoulos, P. (2018). An Experimentally Validated, Transient Model for Sheet and Tube PVT Collector. *Solar Energy*, 174, 709-718.
- Touafek, K., Khelifa, A., Adouane, M. (2014). Theoretical and Experimental Study of Sheet and Tubes Hybrid PVT Collector, *Energy Conversion and Management*. 80, 71–77.
- Yazdanifard, F., Ebrahimnia-Bajestan, E., Ameri, Mehran. (2016). Investigating the Performance of a Water-Based Photovoltaic/Thermal (PV/T) Collector in Laminar and Turbulent Flow Regime. *Renewable Energy*. 99, 295-306.
- Zondag, H., Vries, D., Van Steenhoven, A.A., Van Helden, W.G.J. (1999). Van Zolingen, R.J.C. The Thermal and Electrical Yield of a Combi-Panel, in: *Proceedings of ISES World Congress*. Jerusalem. vol. 3, pp. 96–101.
- Zondag, H.A., De Vries, D.W., Van Helden, W.G.J., Van Zolingen, R.J.C., Van Steenhoven, A.A. (2002). The Thermal and Electrical Yield of a PV-Thermal Collector. *Solar Energy*. 72, 113–128.

The Effect of Grape Seed on Phenolic Properties in Different Fermentation Applications and Production Process in Wine Produced from Öküzgözü Grape

Alev Akpınar Borazan, *¹, Berrin Bozan ²

Abstract: The effect of grape seed on phenolic compounds and antioxidant activity of the wine production process from Öküzgözü grape was investigated. Öküzgözü wine was produced by using 3 different fermentation methods; classical, enzyme addition, and thermovinification. The change in phenolic properties during the production process in each fermentation method was monitored in terms of total phenolic content, total flavanol, and total anthocyanin contents and determined in five production stages: I- maceration/marc fermentation, II- alcoholic fermentation, III- final fermentation/resettle, IV- stabilization and clarification, V- bottling and aging. In addition, to observe the effect of seed on processes and phenolic properties, marc fermentation (5 days, 25 °C) was made in two different applications both skin and skin & seed. Spectrophotometric methods were used to determination of phenolic compounds and anthocyanins. Antioxidant activity was evaluated by DPPH free radical scavenging activity. In all fermentations and stages, the total phenolic contents varied from 2.72 to 1.41 g GAE L⁻¹ by skin & seed extracts; from 1.70 to 0.8 g GAE L⁻¹ by skin extracts; the total flavan-3-ol contents varied from 6.00 to 1.11 g catechin L⁻¹ by skin & seed extracts; from 5.31 to 0.44 g catechin L⁻¹ by skin extracts; the total anthocyanin contents varied from 0.1552 to 0.0170 g Mvd-3-O-glu L⁻¹ by skin & seed extracts; from 0.1835 to 0.0201g Mvd-3-O-glu L⁻¹ by skin extracts. As a result, the highest phenolic contents were determined in all fermentation applications and stages in marc fermentation, where seeds and skins were used together, and the lowest values were determined at the end of alcohol fermentation and 3rd month maturation. On the other hand, the total anthocyanin value was not as high as expected in all fermentations in which marc fermentation was applied without using seeds. The highest total amount of phenolic compounds and antioxidant activity were observed in the wines obtained by the thermovinification process, which was pre-processed at 65 °C for 8 hours. The amounts of phenolic compounds and antioxidant activity were affected by each step of the wine process.

Keywords: Öküzgözü, Fermentation, Seed, Phenolics, Antioxidant activity.

¹Address: Bilecik Seyh Edebali University, Faculty of Chemical, Bilecik/Turkiye

²Address: Eskişehir Technical University, Faculty of Chemical, Eskişehir/Turkiye

*Corresponding author: alev.akpinar@bilecik.edu.tr

1. INTRODUCTION / GİRİŞ (Times New Roman 10pt)

Experimental studies in the literature have confirmed that foods rich in antioxidants show significant positive effects in the prevention of many diseases (Roussis et.al. 2008). Some beverages such as tea, red wine and cocoa, which are frequently consumed in many different cultures, are also rich in phenolic phytochemicals, which are known for their high antioxidant activities (Tabart, et.al. 2009; Lee, et.al. 2003). The phenolic composition of wine depends on many factors: viticulture practices, quality of grapes used in wine production, maturity level, grape variety, winemaking conditions and techniques etc. (Garciafalcon et.al., 2007; Gutiérrez-Escobar et.al., 2021; Merkytė et.al., 2020; Coletta et.al., 2013). According to those factors, red wine contains many important antioxidant phenolics at different level.

Phenolic compounds are extracted from the skin, pulp and seeds of grapes during the wine production process, and their levels may change with the factors applied during the production process (Feliciano et.al., 2009; Gutiérrez-Escobar et.al., 2021).

The aim of the present study was the assessment of the influence of the fermentation process, changing of the phenolics from maceration to bottling stages during winemaking, and differentiation of extraction with skin /seed&skin on the phenolic fraction öküzgözü wines produced in Turkey

2. MATERIAL AND METHOD / MATERYAL VE METOT

The optimum mature Öküzgözü grapes were harvested manually in the Kırklareli area. They were kept into cold storage until begins to production. The procedures in Öküzgözü red winemaking, respectively, are given figure 1.

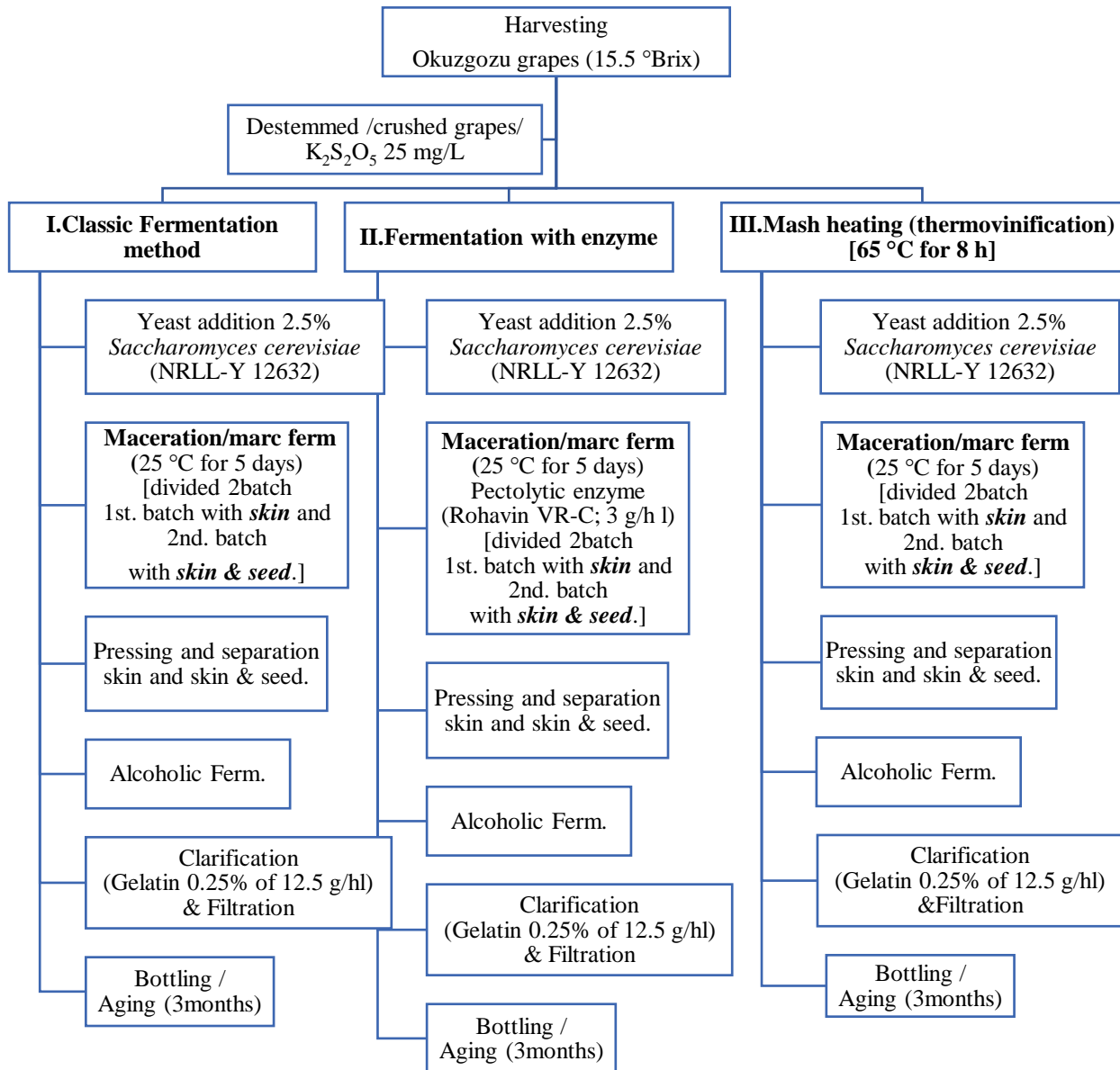


Figure 1 Scheme of generating Öküzgözü grape-to-wine with different fermentation techniques

2.1. Determination of total phenolic, total flavanol, total anthocyanin content and antiradical activity

The total phenolic (TP) content in the samples was determined by the Folin–Ciocalteu colorimetric method (Prior et al., 1998).

The total phenolic content was expressed as gallic acid (g GAE/L) equivalents. The total flavan-3-ol (TF) content was estimated by the vanillin–HCl method (Price, Van Scoyoc, & Butler, 1978). The total flavan-3-ol content was expressed as (+)-catechin (g catechin/L) equivalents. The total anthocyanins (TA) were estimated by a pH differential method (Lee, Durst, & Wrolstad, 2005), using a spectrophotometer (SP-3000, Optima). The results were calculated as mg malvinidin-3-O-glucoside equivalents per L

The antiradical activity of phenolic extracts was measured using DPPH method (Sanchez-Moreno, Larrauri, & Saura-Calixto, 1998), and expressed as EC₅₀ (µg/mL), the concentration necessary for 50% reduction of DPPH.

2.2. Statistical analysis

Phenolic analyses were performed in either two or three replicates, and the determined results are presented as mean ± standard deviation. Analysis results were subjected to ANOVA test. Multiple comparisons of means were performed with the least significant difference (LSD) test at the $\alpha = 0.05$ level.

3. RESULTS / BULGULAR

The phenolic properties during the production process with different fermentation methods were determined in five production stages. Analyzes were made on the samples taken at the stages when the relevant processes were completed. The effect of seed on processes and phenolic properties are given in Table 1-3.

Table 1. Effect of grape seed on phenolic properties during Öküzgözü wine making processes by classical fermentation

a) Process (maceration with skin&seed)	Total Phenolic (g GAE/L)	Total Flavanol (g catechin/L)	Total Anthocyanin (g Mvd-3-o-glu/L)	DPPH (EC ₅₀ , µg/mL)
Maceration/marc ferm.	2.61±0.15 ^b	2.47±0.24 ^c	0.1552±3.1E-3 ^d	57.79±2.74 ^b
Alcoholic ferm.	1.70±0.11 ^a	1.11±0.77 ^a	0.0362±7.0E-3 ^{ab}	45.69±0.98 ^a
Finish ferm./resettle	1.97±0.18 ^a	1.48±0.18 ^{ab}	0.0529±5.5E-3 ^c	58.16±5.93 ^b
Stabilize and Clarify	1.68±0.05 ^a	1.91±0.34 ^{abc}	0.0435±0.4E-3 ^{bc}	53.72±1.03 ^b
Bottling /aging (3mnths)	2.51±0.26 ^b	1.98±0.24 ^{bc}	0.0266±24.4E-3 ^a	54.48±1.58 ^b

b) Process (maceration with skin)	Total Phenolic (g GAE/L)	Total Flavanol (g catechin/L)	Total Anthocyanin (g Mvd-3-o-glu/L)	DPPH (EC ₅₀ , µg/mL)
Maceration/marc ferm.	1.70±0.09 ^b	1.20±0.09 ^{bc}	0.1835±20.6E-3 ^c	87.35±7.78 ^b
Alcoholic ferm.	1.05±0.05 ^a	1.22±0.10 ^c	0.0872±0.3-3 ^b	94.67±7.03 ^b
Finish ferm./resettle	1.12±0.14 ^a	1.04±0.29 ^{bc}	0.0367±4.4E-3 ^a	123.82±0.48 ^c
Stabilize and Clarify	1.02±0.06 ^a	0.77±0.08 ^{ab}	0.0429±4.7E-3 ^a	93.24±5.13 ^b
Bottling /aging (3mnths)	1.71±0.17 ^b	0.44±0.41 ^a	0.0386±37.E-3 ^a	76.06±6.94 ^a

* Mean values marked with the same letters in the same column ($p < 0.05$) there is no difference

Table 2. Effect of grape seed on phenolic properties during Öküzgözü wine making processes by addition of the Pectolitic Enzyme

a) Process (maceration with skin&seed)	Total Phenolic (g GAE/L)	Total Flavanol (g catechin/L)	Total Anthocyanin (g Mvd-3-o-glu/L)	DPPH (EC ₅₀ , µg/mL)
Maceration/marc ferm.	1.96±0.13 ^b	1.33±0.07 ^a	0.0902±5.8E-3 ^c	52.46±2.24 ^b
Alcoholic ferm.	1.41±0.08 ^a	1.88±0.15 ^b	0.0209±1.9E-3 ^a	45.37±0.45 ^a
Finish ferm./resettle	1.45±0.06 ^a	1.87±0.02 ^b	0.0179±0.2E-3 ^a	45.66±5.45 ^a
Stabilize and Clarify	1.41±0.20 ^a	1.74±0.22 ^b	0.0485±0.9E-3 ^b	52.13±3.12 ^b
Bottling /aging (3mnths)	1.47±0.10 ^a	1.91±0.16 ^b	0.0496±50.8E-3 ^b	54.20±2.36 ^b

b) Process (maceration with skin)	Total Phenolic (g GAE/L)	Total Flavanol (g catechin/L)	Total Anthocyanin (g Mvd-3-o-glu/L)	DPPH (EC ₅₀ , µg/mL)
Maceration/marc ferm.	1.41±0.13 ^c	1.22±0.13 ^a	0.0763±4.0E-3 ^d	92.84±7.32 ^b
Alcoholic ferm.	1.03±0.05 ^b	1.37±0.10 ^a	0.0761±1.5E-3 ^d	73.46±5.92 ^a
Finish ferm./resettle	1.00±0.12 ^b	1.82±0.29 ^b	0.0295±2.8E-3 ^b	73.79±2.67 ^a
Stabilize and Clarify	0.80±0.14 ^a	1.36±0.14 ^a	0.0409±1.1E-3 ^c	113.58±13.26 ^c
Bottling /aging (3mnths)	0.77±0.01 ^a	1.88±0.19 ^b	0.0176±16.2E-3 ^a	87.34±0.09 ^{ab}

* Mean values marked with the same letters in the same column ($p < 0.05$) there is no difference

Table 3. Effect of grape seed on phenolic properties during Öküzgözü wine making processes by thermovinification

a) Process (maceration with skin&seed)	Total Phenolic (g GAE/L)	Total Flavanol (g catechin/L)	Total Anthocyanin (g Mvd-3-o-glu/L)	DPPH (EC ₅₀ , µg/mL)
Maceration/marc ferm.	2.72±0.12 ^c	6.00±0.51 ^c	0.0626±5.3E-3 ^b	51.86±3.69 ^b
Alcoholic ferm.	1.79±0.02 ^a	5.53±0.18 ^{bc}	0.0939±0.5E-3 ^c	28.56±0.09 ^a
Finish ferm./resettle	1.81±0.12 ^a	4.54±0.30 ^a	0.0845±0.2E-3 ^c	56.44±1.34 ^c
Stabilize and Clarify	2.25±0.10 ^b	4.98±0.29 ^{ab}	0.0570±4.6E-3 ^b	40.09±2.32 ^{ab}
Bottling /aging (3mnths)	2.22±0.15 ^b	4.40±0.32 ^a	0.0433±49.6E-3 ^a	46.14±2.83 ^{ab}

b) Process (maceration with skin)	Total Phenolic (g GAE/L)	Total Flavanol (g catechin/L)	Total Anthocyanin (g Mvd-3-o-glu/L)	DPPH (EC ₅₀ , µg/mL)
Maceration/marc ferm.	1.53±0.07 ^c	3.69±0.11 ^a	0.0201±7.0E-3 ^a	81.50±6.14 ^b
Alcoholic ferm.	1.08±0.01 ^a	3.07±0.26 ^a	0.0564±0.8E-3 ^b	62.34±2.23 ^a
Finish ferm./resettle	1.17±0.04 ^a	3.13±0.32 ^a	0.0547±6.8E-3 ^b	118.50±8.65 ^c
Stabilize and Clarify	1.34±0.04 ^b	3.57±0.46 ^a	0.0474±3.6E-3 ^b	72.10±6.79 ^{ab}
Bottling /aging (3mnths)	1.15±0.10 ^a	5.31±0.38 ^b	0.0254±24.8E-3 ^a	72.16±6.58 ^{ab}

* Mean values marked with the same letters in the same column ($p < 0.05$) there is no difference

4. DISCUSSION AND CONCLUSIONS / TARTIŞMA VE SONUÇLAR

Total phenolic content has changed in different processes in wine production with different methods (classical, enzyme added and hot maceration). The differences in the values were found to be statistically significant ($p > 0.05$). The total amount of phenolic compounds showed their maximum values in applications where seeds and grape skin were used together. Total phenolic component values, respectively; It decreased gradually in hot maceration, classical fermentation, and enzyme added fermentation applications. There was a significant decrease in all methods with the clarification process. The clarifying agent used here is thought to be effective. While no significant difference could be determined in the amount of total phenolic compounds between alcoholic fermentation, resting and clarification processes, the highest value was generally reached in maceration/marc fermentation stages.

It was determined that the total flavanol value showed statistically significant differences in different fermentation applications and process stages. The total flavanol value had the highest value within the mash heating method, with and without seeds, among the fermentation and processing stages applied. In the literature, it has been stated that high-temperature applications increase the tannin and the prolongation of the contact time of the seeds with the must also increases the flavanols. Complex formation between anthocyanins and tannins and reactions between polyphenols and acetaldehyde during the aging process of the wine affected the total amount of flavanols.

Total anthocyanin was determined to be higher in each process with applied only skin maceration as expected. It was observed that the wines obtained from the fermentation processes in which only the skin was used were rich in phenolic acid and monomeric anthocyanin compounds, and the products obtained from the fermentation processes in which the grape skin and seed were used were rich in catechin derivatives (catechin, epicatechin).

In the study was determined, the antioxidant activity values are largely in correlation with the total phenolic component content. The highest antioxidant activity value in wines was obtained by the mash heating/maceration method in all processes. Wine producers minimize the phenol content due to turbidity and adverse taste, but when the health-protective effect is considered, these problems can be eliminated to provide more phenolic substances and the thermovinification method can be preferred in wine production.

In applications made with grape skin maceration, all values are lower than in fermentation applications and stages where grape skin and seed are macerated together.

Author Contributions

Conceptualization: B.B.; Investigation: A.A.B; Material and Methodology: A.A.B., B.B.; Supervision: B.B.; Writing-Original Draft: A.A.B., B.B.; Writing-review & Editing: A.A.B., B.B.: All authors have read and agreed to the published version of manuscript.

Conflict of Interest

The authors have no conflicts of interest to declare.

Funding

The authors declared that this study has received no financial support.

REFERENCES

- Coletta, A., Trani, A., Faccia, M., Punzi, R., Dipalmo, T., Crupi, P., Antonacci, D., & Gambacorta, G. (2013). Influence of viticultural practices and winemaking technologies on phenolic composition and sensory characteristics of Negroamaro red wines. *International Journal of Food Science & Technology*, 48(11), 2215-2227. doi.org/10.1111/ijfs.12207
- Feliciano, R.P., Bravo, M.N., Pires, M.M. et al. Phenolic Content and Antioxidant Activity of Moscatel Dessert Wines from the Setúbal Region in Portugal. *Food Anal. Methods* 2, 149–161 (2009). <https://doi.org/10.1007/s12161-008-9059->
- Garciafalcon, M., Perezlamela, C., Martinezcarballo, E., & Simalgandara, J. (2007). Determination of phenolic compounds in wines: Influence of bottle storage of young red wines on their evolution. *Food Chemistry*, 105(1), 248–259. doi:10.1016/j.foodchem.2006.11.006
- Gutiérrez-Escobar R, Aliaño-González MJ, Cantos-Villar E. (2021) Wine Polyphenol Content and Its Influence on Wine Quality and Properties: A Review. *Molecules*. 30;26(3):718. doi: 10.3390/molecules26030718.
- Lee, J., Durst, R. W., & Wrolstad, R. E. (2005). Determination of Total Monomeric Anthocyanin Pigment Content of Fruit Juices, Beverages, Natural Colorants, and Wines by the pH Differential Method: Collaborative Study. *Journal of AOAC International.*, 88(5), 1269–1278. <https://doi.org/10.1093/jaoac/88.5.1269>
- Lee, K. W., Kim, Y. J., Lee, H. J., & Lee, C. Y. (2003). Cocoa Has More Phenolic Phytochemicals and a Higher Antioxidant Capacity than Teas and Red Wine. *Journal of Agricultural and Food Chemistry*, 51(25), 7292–7295. doi:10.1021/jf0344385
- Merkytė V, Longo E, Windisch G, Boselli E. (2020) Phenolic Compounds as Markers of Wine Quality and Authenticity. *Foods*. 9(12):1785. doi.org/10.3390/foods9121785
- Price, M. L., Van Scoyoc, S., & Butler, L. G. (1978). A critical evaluation of the vanillin reaction as an assay for tannin in sorghum grain. *Journal of Agricultural and Food Chemistry*, 26, 1214–1218. <https://doi.org/10.1021/jf60219a031>
- Prior, R., Cao, G., Martin, A., Sofic, E., McEwen, J., O'Brien, C., Lischner, N., Ehlenfeldt, M., Kalt, W., Krewer, G., & Mainland, C. (1998). Antioxidant capacity as influenced by total phenolic and anthocyanin content, maturity, and variety of *Vaccinium* species. *Journal of agricultural and food chemistry*, 46, 2686-2693. <https://doi.org/10.1021/jf980145d>
- Roussis, I. G., Lambropoulos, I., Tzimas, P., Gkoulioti, A., Marinos, V., Tsoupeis, D., & Boutaris, I. (2008). Antioxidant activities of some Greek wines and wine phenolic extracts. *Journal of Food Composition and Analysis*, 21(8), 614–621. doi:10.1016/j.jfca.2008.02.011
- Sanchez-Moreno, C., Larrauri, J. A., & Saura-Calixto, F. A. (1998) Procedure to measure the antiradical efficiency of polyphenols. *Journal of the Science of Food and Agriculture*, 76, 270–276. Doi: 10.1002/(SICI)1097-0010(199802)76:2<270::AID-JSFA945>3.0.CO;2-9
- Tabart, J., Kevers, C., Pincemail, J., Defraigne, J.-O., & Dommes, J. (2009). Comparative antioxidant capacities of phenolic compounds measured by various tests. *Food Chemistry*, 113(4), 1226–1233. doi:10.1016/j.foodchem.2008.08.013

A Barrier-Free City Proposal for Disabled Individuals Gostivar/North Macedonia Example

Ayşe ARICI*¹

Abstract: In this study, while an ergonomic, convenient, comfortable urban planning design is designed so that the people of the city can live their lives in a healthy, equal life, safe, free, happy, and peaceful way, it will improve the welfare of the people of the city at minimum cost with the proposals of building materials suitable for the current situation in the most economical way. Is to develop a solution proposal that will increase. For this purpose, it has been investigated whether urban outdoor spaces and urban equipment are compatible with the living conditions of disabled individuals. In the study, It is important that all the spaces in the city appeal to all segments of society and should be designed in this way, and what features should be added for the region that is the study universe? The answer to the question has been sought. In this context, in the example of the city of Gostivar, North Macedonia, especially in the streets and streets in the city center, the city center, parks, playgrounds, the entrances of religious places of worship and accessibility, the floor elements in public areas (ramps, stairs, pedestrian paths, parking areas), urban equipment (living and rest areas, lighting elements, garbage cans), access opportunities to public buildings, and access opportunities at the entrances to the buildings have been taken into account. As a result of the findings, it has been revealed how easily disabled users can use the problems they experience outdoors and what their expectations are from the city. As solution proposals, suggestions were made regarding the suitability for the new conditions, how to make changes in the current situation, the existence of the transformation, and the spatial use and organizational structure for the change, planting, and ecology in order to provide solutions for the transformation and change needs.

Keywords: Disability, Urban Accessibility, Building Materials, Sustainability.

¹**Address:** VizyonUniversity, Faculty Of Architecture Engineering, Gostivar/Nort Makedonia

***Corresponding author:** aysearici.iut@gmail.com

1. INTRODUCTION

Today, the principles of equality and inclusiveness for all segments of society are becoming more important by combining them with the goals of sustainability and livability. Disability, urban accessibility, building materials, and sustainability are key concepts that come together to transform the construction industry and build a more inclusive future.

Disability refers to the difficulties an individual faces in different areas of life due to limitations in their physical, mental, or sensory abilities. Disability not only affects the daily lives of individuals but also affects all layers and infrastructures of society. One of the problems with disability is the lack of accessibility in urban areas. Many cities are littered with obstacles such as narrow roads, stairs, or buildings full of obstacles, making it difficult for people with disabilities to enjoy basic rights such as independence, employment, and social inclusion.

Disability is understood as the inequalities of opportunity and limitations that arise between individuals based on the principle of equality in society. This definition emphasizes the difficulties that prevent disabled people from taking part in society on an equal basis with other individuals and their full participation in activities in various fields. Disability is associated with deficiencies in existence and active participation in areas such as information, communication, and education. These deficiencies are considered factors that prevent people with disabilities from integrating with society and interacting fully. (Çınar et al., 2015).

Urban accessibility aims at minimizing or eliminating physical barriers so that individuals with disabilities and other disadvantaged groups can perform their daily living activities. These include planning and arranging various infrastructure and services in a city, such as roads, sidewalks, buildings, public transport systems, parks, and utilities, to suit accessibility needs. Urban accessibility encourages the full and equal participation of people with disabilities in society while enabling everyone to live in a more comfortable and usable environment. Measures such as disabled

ramps, elevators, low-floor buses, non-slip floors, and information systems for the hearing and visually impaired can be given as examples of urban accessibility. Urban accessibility aims to increase the access of people with disabilities to basic rights, independence, freedom, and quality of life. It also enables disadvantaged groups such as the elderly, pregnant women, children, and other individuals with temporary disability or injuries to access activities and services in the city easily.

The "barrier-free or accessible city" approach has been put forward as a solution proposal for the accessibility problem of people with disabilities in urban areas. Today, cities are accepted as focal points of social, cultural, economic, and political interaction of society. The fact that people with disabilities can move freely in the urban space and have access to all kinds of resources, services, and physical environment forms the basis of the idea of a barrier-free city. With this approach, it is aimed that disabled people to participate effectively in all areas of life and live independently. (Erten and Aktel, 2020).

According to the concept of universal design, the needs and expectations of individuals belonging to different groups are taken into account. Solutions are offered to facilitate the use of everyone, such as the elderly, children, pregnant women, or people with temporary disability, as well as disabled individuals. In this way, barriers to social participation are removed, and it is ensured that everyone can be found in spaces of independence, safety, and comfort (Pouya, 2021).

The squares that play a central role in urban life and the urban furniture in these squares should be designed to meet the needs of everyone. Unfortunately, applications made by ignoring the needs of elderly and disabled individuals are quite common in our country (Aykil et al., 2018).

The diversity and intensity of disability problems necessitate a large number of services to be provided to people with disabilities in terms of quantity and variety. Although disability is handled from the perspective of human rights, individuals with disabilities face problems such as not being able to access health services, education, and employment opportunities equally, not getting the disability services they need, and not being able to participate in daily life activities (Arab et al., 2021).

The ability of a person to develop within the social structure and to benefit equally from the opportunities offered by social life is closely related to the access and use of the space. However, the ability of disabled individuals to live in the same conditions as all other individuals depends on the accessibility of the built environment for them. In order to ensure the full participation of disabled people in social life, the design and arrangement of the spaces should be carried out in accordance with accessibility standards. In this way, disabled people's access to the spaces becomes easier, their use becomes unhindered, and it is ensured that they can take a full place in society (Çivici and Gönen, 2015).

In this context, this article aims to research the building entrances of public institutions in the Municipality of Gostivar in North Macedonia and the roads to be accessed to this building, suitable for the disabled, elderly, and raising children, and to offer solutions to the deficiencies in this area. This study was carried out with the aim of making better use of the accessibility difficulties for the disabled, elderly, and children in the surrounding area and disseminating applicable solutions to reveal these problems. In addition, developments in building materials and accessibility offer a promising way to address these challenges. The construction industry is developing new concepts and technologies to design and build more barrier-free and accessible structures based on sustainability and usability accessibility. The sustainability of building materials is also of great importance in terms of reducing environmental impacts, increasing energy efficiency and creating long-lasting structures. This article will highlight the relationship between urban accessibility, building materials and sustainability in the fight against disability by evaluating the accessibility status of public institutions in the Municipality of Gostivar and offering solutions. This work is an important step towards raising awareness about disability and contributing to the building of a more inclusive society in the future.

2. MATERIAL AND METHOD

The main material of the study is the streets and sidewalks that provide access to the public institutions in the city center of Gostivar Municipality in North Macedonia and to these institutions. In addition, the Vardar River, which flows through the city of Gostivar, has great importance for the city's people and is an important natural resource in the context of sustainability as a global value. For this reason, the city park and walking paths around the river were also examined, and the content of the study was further enriched. The river offers the residents of Gostivar the opportunity to spend time with nature, relax and engage in physical activities. At the same time, the contribution of the river to the city's ecosystem and environmental balance is remarkable. The city park and walking paths allow people to discover natural beauty and continue their recreational activities. However, they must be designed in an environmentally friendly way. In addition, it has been examined whether this urban park is suitable for the comfort of disabled, elderly, or sick

individuals. The fact that it has an important location that can be used for walking by patients providing transportation to the hospital, which is close to this city park, and patients in the hospital increases the importance of this park. In this way, the city of Gostivar plays a leading role in the conservation of natural resources and the sustainable use of natural beauties by offering sustainable living space to its local people and local and foreign visitors. For this purpose, in this study, the necessary measures will be researched so that the city of Gostivar can appeal to all segments of the city, and it will contribute to the acquisition of a comfortable urban identity in accordance with the standards for the disabled, the elderly and the sick. The method of the study includes the determination of the purpose and scope first, and a literature review of similar studies on the subject has been made. Current and valid resources in areas such as the arrangement of roads for the disabled, urban planning, accessibility, design standards, and the needs of people with disabilities have been researched. Useful information on academic resources, research articles, regulations, and national and international standards were reviewed.

During the data collection phase, data on the arrangement of roads for people with disabilities were collected, field studies were carried out, and interviews were conducted with disabled individuals. Measurements were made in the sample areas in the study universe and were processed into observation forms and visual materials. The measurement results were evaluated in terms of compliance with the standards determined for people with disabilities, and suggestions were developed based on the results. Within the scope of the study, the suitability of urban outdoor elements for disabled individuals was investigated in the example of the Municipality of Gostivar. While the research includes examining the standards for people with disabilities in national and international standards, areas such as floor elements, open parking areas, reinforcement elements, and public building entrances are emphasized. The study, organized in this way, aims to contribute to the city of Gostivar to gain a sustainable urban identity suitable for disabled individuals.

3. RESULTS

Gostivar Municipality Building, Municipal Support Building, Provincial Directorates Building, Court of First Instance Building, İşkur Building and Social Security and Health Institution Building, Gostivar Post Office Building, Gostivar Culture House Entrance, and Transportation When the accessibility arrangements made for Gostivar, Vardar River Walkways and City Park are examined. It was observed that some important shortcomings were identified. Accessibility improvements need to be made in these buildings. Deficiencies were identified and visual materials and measurements supported possible arrangements. In this direction, if we make an academic analysis, the following points include suggestions for accessibility regulations:

GOSTIVAR MUNICIPAL BUILDING AND MUNICIPAL SERVICE BUILDING		
		
A- Municipal Service Building Entrance	B- Municipal Service Building Entrance Stair Tread Height: 15 cm Step Width: 30 cm Stair Width: 280 cm There is no stair railing.	C- Municipal Service Building Entrance ramp width: 140cm
		
D- The width of the pavement in front of the Municipal Service Building, the Municipality Building and the Provincial Directorates: 278 cm	E- Municipal Service Building - Entrance to the area where the Municipality Building and Provincial Directorates are located	F- City Hall Main Entrance - Stair Tread Height: 15cm Step Width: 30 cm Stair Width: 480cm There is no ramp.

Figure 1. Gostivar City Hall and Municipal Support Building Entrances and Access (ARICI A,2023)

An important factor limiting the mobility of persons with disabilities is difficulties in transportation. Participants in the research emphasize that difficulties in accessing transportation vehicles and the lack of audio signaling for the visually impaired and colored/light signaling for the deaf and hard of hearing are prominent problems (Doğruel, 2022).

According to the deficiencies identified in the entrances and transportation of the Gostivar Municipality Building and the Municipality Support Building, the following arrangements can be made suitable for the disabled, the sick, and the elderly: Stairs: They should be arranged in a way that is suitable for the access of disabled people. The stair step height must be lower than the existing 15 cm. Preferably, a 10 cm high step should be added, and a platform or border should be created that will enable visually impaired individuals to perceive with their walking sticks. Also, stair railings should be added. Ramp: Municipal Service Building Entrance ramp width should be wider than the current 140 cm. Braille signs are not used. There are no non-slip floor coverings. There are no discretionary sidewalks. There are no colored road signs. There are no reactive road signs. These arrangements will facilitate the access of the disabled, the sick, and the elderly to the town hall and support the building and ensure their safety. When making arrangements, it is important to comply with local regulations and disability accessibility standards. In addition, suitable building materials should be used, and all arrangements should be designed in a way that disabled people can easily perceive and use.

The diversity and intensity of disability problems necessitate many services to be provided to the disabled in terms of quantity and variety. Although disability is handled from the perspective of human rights, individuals with disabilities face problems such as not being able to access health services, education, and employment opportunities equally, not getting the disability services they need, and not being able to participate in daily life activities (Arab et al., 2021).

GOSTIVAR PROVINCIAL DIRECTORATES BUILDING ENTRANCE AND TRANSPORTATION		
		
<p>A- Gostivar, Provincial Directorates Building Entrance Stair Tread Height: 16 cm Step Width: 30 cm Stair Width: 320 cm No handrail is on the stairs.</p>	<p>B- Gostivar, Provincial Directorates Building Entrance Stair Tread Height: 16 cm Step Width: 30 cm Stair Width: 320 cm No Ramp</p>	<p>C- There are no suitable passages for wheelchairs when crossing the street, no directions for walking for the visually impaired, and no voice warning system.</p>

Figure 2. Gostivar Municipality Provincial Directorates Building Entrance and Transportation (ARICI. A ,2023)

According to the deficiencies detected in the entrances and transportation of the Gostivar Provincial Directorates building, the following arrangements can be made: Stairs: The stair step height should be lower than the existing 16 cm so that people with disabilities can use it easily. Generally, an acceptable height of up to 10-12 cm is preferred. The stair step width is specified as 30 cm; this size can be considered appropriate. Railings should be added. Handrails allow disabled people to use stairs safely. Railings should be designed with an average height of 80-90 cm and a suitable holding surface. Braille signs are not used. There are no non-slip floor coverings. There are no discretionary pavements. There are no colored road signs. There are no responsive road signs. Ramp: Ramps should be constructed to provide convenient passages for wheelchair users. The slope and width of the ramp should be such that disabled people can easily pass. Generally, the slope rate is accepted as 6%. The ramp surface should be equipped with non-slip floor coverings. Non-slip floor coverings will ensure the safety of people with disabilities and reduce the risk of slipping. A 10 cm high platform or border should be provided for visually impaired individuals to perceive with the help of a walking stick.

GOSTIVAR, COURT BUILDING ENTRANCE


		
<p>A- Gostivar, Court Building Entrance</p>	<p>B- Ramp Width: 130 cm</p>	<p>C- Stair Step Height: 15 cm Step Width: 30 cm Stair Width: 330 cm There is no railing on the stairs.</p>

Figure 3. Gostivar Court of First Instance Entrance and Transportation ARICI.A,2023)

The following arrangements can be made for the Gostivar Court of First Instance building in order to solve the identified deficiencies and make it suitable for all types of disability: Stairs: The stair step height must be lower than the existing 15 cm. Preferably, a 10 cm high step should be added, and a platform or border should be created that will enable visually impaired individuals to perceive with their walking sticks. Railings should be added on the stairs. Handrails are important to provide grip and stability when using stairs. Ramp: The width of the ramp must be wider than the current 130 cm. A ramp should be provided where disabled people can easily pass using a wheelchair or walking aid. The ramp slope should be determined according to appropriate standards. Generally, 6% slope is preferred. The ramp surface must be non-slip and properly designed to ensure a safe passage. Braille Signs: Signs written in the Braille alphabet should be used to enable visually impaired individuals to access information. Non-slip floor coverings should be used. Discreet pavements should be used for the road safety of visually impaired individuals. Colored road signs should be used for road safety and guidance for visually impaired individuals. Signs in different colors can be used to identify a particular route or landmarks within the building. Reactive Road Signs: Responsive road signs should be used to improve road safety for people with disabilities. Building materials that can be used to achieve these regulations are: Rubber coatings or antistatic materials may be preferred for durable and non-slip floor coverings. Stainless steel or aluminum materials can be used for ramp and stair railings. Aluminum or plexi materials can be preferred for Braille signs. For discretionary pavements, polymeric or epoxy coatings can be used. Durable paint or colored stones can be preferred for colored road signs. Electronic systems and audible warning devices can be used for responsive road signs. These building materials provide advantages for facilitating the access of people with disabilities, ensuring their safety, and complying with current standards. Having durable, cleanable, and long-lasting features, they can offer an effective solution for solving the deficiencies in the building. In addition, with the use of materials, it is aimed to increase the independence and participation of disabled people, ensure social accessibility, and ensure that everyone can use the building comfortably.

GOSTIVAR İŞKUR BUILDING ENTRANCE- GARDEN- TRANSPORTATION

		
<p>A- Gostivar, İşkur Building Entrance Stair Tread Height: 16 cm Step Width: 30 cm Stair Width: 320 cm There is no handrail on the stairs.</p>	<p>B- Stair Step Height: 22 cm Step Width: 30cm Stair Width: 325 cm There is no railing on the stairs.</p>	<p>C- While crossing the street, there are no suitable passages for wheelchairs, there are no directions for walking for the visually impaired, and there is no voice warning system.</p>

Figure 4. Gostivar İşkur Building Entrance and Access (Arıcı, 2023)

The following arrangements can be made for the Gostivar İşkur building in order to solve the identified deficiencies and make it suitable for all types of disability: Stairs: The stair step height should be lower than the existing 16 cm. Preferably, a 10 cm high step should be added, and a platform or border should be created that will enable visually impaired individuals to perceive with their walking sticks. Railings should be added on the stairs. Handrails are important to provide grip and stability when using stairs. Disabled Crossings: Appropriate transitions for wheelchairs should be provided when crossing the street. For this, ramps or smooth ground transitions of appropriate width and slope should be created. Directions and audio warning systems should be added for walking for the visually impaired.

Direction signs should be equipped with signs in embossed or Braille. Non-slip floor coverings should be used. Non-slip surfaces should be preferred to prevent slipping, especially on wet floors. Non-slip floor coverings should be applied at the ramp and stair entrances. Non-slip floor coverings should be durable and easy to clean. Discreet pavements should be used for the road safety of visually impaired individuals. Colored road signs should be used for road safety and guidance for visually impaired individuals. Responsive road signs should be used to increase road safety for people with disabilities. With these arrangements, the Gostivar Işkur building can be made suitable for all types of disability, and accessibility can be provided. Appropriately sized ramps, wide passages, and Braille signs will make it easier for people with disabilities to use the building comfortably and access information. Non-slip floor coverings, discreet pavements, and colorful and responsive road signs will increase their safety and make their journey safer.




GOSTIVAR SOCIAL SECURITY AND HEALTH INSTITUTION BUILDING ENTRANCE AND TRANSPORTATION		
		
<p>A- Gostivar, Social Security and health institution Building Entrance</p>	<p>B- Stair Step Height: 17 cm Step Width: 30 cm Stair Width: 170 cm There is no railing on the stairs.</p>	<p>C- When crossing the street, there are no wheelchair-friendly passages, no walking directions for the visually impaired, and no voice warning system.</p>

Figure 5. Gostivar Social Security and Health Institution Building Entrance and Transportation (Arıcı,2023)

Gostivar Social Security and Health Institution accessibility arrangements for construction must be made. Information on correcting the detected deficiencies and the suitable dimensions: Stair tread tension must be lower than the current 17 cm. A 10 cm long step should be added to create a platform or border that will enable visually impaired people to perceive a walking stick. Railings should be added on the stairs. Handrails are important to provide grip and stability when using stairs. Disabled Crossings: Appropriate transitions for wheelchairs should be provided when crossing the street. For this, ramps or smooth ground transitions of appropriate width and slope should be created. Directions and audio warning systems should be added for walking for the visually impaired. Direction signs should be equipped with signs in embossed or Braille. Signs written in the Braille alphabet should be used to enable visually impaired individuals to access information. Braille signs must be placed. Braille signs should be made of durable materials and be long-lasting.

Non-slip floor coverings should be used. Non-slip surfaces should be preferred to prevent slipping, especially on wet floors. Non-slip floor coverings should be applied at the ramp and stair entrances. Discreet pavements should be used for the road safety of visually impaired individuals. There are no Colored Road Signs. Responsive road signs should be used to increase safety. With these arrangements, the Gostivar Social Security and Health Institution building can be made suitable for all types of disability, and accessibility can be provided. Appropriately sized stairs, ramps, transitions, and Braille signs make it easier for people with disabilities to use the building comfortably and access information. Non-slip floor coverings, discreet pavements, and colorful and responsive road signs should increase their safety and make their journey safer.




GOSTIVAR POSTHOUSE ENTRANCE- TRANSPORTATION		
		
A- Post Office Building Entrance	B- Stair Step Height: 15 cm Step Width: 32 cm Stair Width: 300 cm There is no railing on the stairs.	C- There are no directions for walking on the pavement for the visually impaired and no audio warning system. In addition, there are no discretionary pavements for the visually impaired on the pavement.

Figure 6. Gostivar Post Office Building Entrance and Access (Arıcı,2023)

Accessibility arrangements need to be made for the Gostivar Post Office building. Below is information on how the detected deficiencies can be eliminated and which dimensions are appropriate: Stairs: Stair step height must be lower than the existing 15 cm. Preferably, a 10 cm high step should be added, and a platform or border should be created that will enable visually impaired individuals to perceive with their walking sticks. Railings should be added on the stairs. Handrails are important to provide grip and stability when using stairs. Disabled Crossings: Directions and audio warning systems should be added for walking for the visually impaired. Visually impaired individuals should be able to perceive directions by using embossed or Braille signs on the pavement. Discreet pavements should be used. Discretionary pavements make a crackling sound on the wheeled surface of the cane, allowing disabled people to cross the pedestrian path and realize the dangers. Ramp: A suitable ramp should be added to the entrance. The ramp allows wheelchair users to enter the building easily. The ramp width must be at least 90 cm. The slope should not be more than 6%. Doors: Entrance doors should be suitable for the passage of disabled individuals. It is preferred that the doors are sufficiently wide and equipped with automatic opening features.



GOSTIVAR CULTURAL ENTRY- TRANSPORTATION		
		
A- Culture House Building Entrance	B- Stair Step Height: 13cm Step Width: 40 cm 1. Ladder Width:630 cm 2. Ladder Width:230 cm There is no railing on the stairs. There is no ramp.	C- When crossing the street, there are no wheelchair-friendly passages, and there are no walking directions for the visually impaired, and there is no voice warning system.

Figure 7. Gostivar Culture House Entrance and Transportation (Arıcı,2023)

Accessibility arrangements need to be made for the Gostivar Post Office cultural house building. Below is information on how the detected deficiencies can be eliminated and which dimensions are appropriate: Stairs: The stair step height must be lower than the existing 13 cm. Preferably, a 10 cm high step should be added, and a platform or border should be created that will enable visually impaired individuals to perceive with their walking sticks. Railings should be added on the stairs. Handrails are important to provide grip and stability when using stairs. Disabled Crossings: Directions and audio warning systems should be added for walking for the visually impaired. Visually impaired individuals should be able to perceive directions by using embossed or Braille signs on the pavement. Discreet pavements should be used. Discretionary pavements make a crackling sound on the wheeled surface of the cane, allowing disabled people to cross the pedestrian path and realize the dangers. Ramp: A suitable ramp should be added to the entrance. A ramp should be built. Moreover, the ramp allows wheelchair users to enter the building with ease. The ramp width must be at least 90 cm. The slope should not be more than 6%. Doors: Entrance doors should be suitable for the passage of disabled individuals. It may be preferable that the doors are sufficiently wide and equipped with an automatic opening feature.

GOSTIVAR VARDAR RIVER WALKING PATH AND CITY PARK		
		
A- Gostivar, The Pedestrian Pavement on the Bridge Over the Vardar River, is 200 cm wide.	A- Gostivar, Vardar River is divided into two parts by a bridge. On the left side of the bridge, there is no area for bicycles, and there is no special walking area for disabled people.	C- Gostivar, the walking area along the Vardar River The area reserved for walking is 240 cm wide.
		
D- In Gostivar, there is no walking area along the Vardar River and no access to a walking area for people with disabilities.	E- General view of the walking area along the Vardar River in Gostivar	F- Gostivar, walking area along the Vardar River; The width of the bicycle path indicated in red is 160cm 80cm between the bicycle path and the middle reflux
		
G- Gostivar, walking area along the Vardar River, walkway width 240 cm	L- Gostivar, Stairs used for access to the walking area along the Vardar River; step height: heights vary in steps. It has 12 cm-16 cm and 17cm heights. The step width is 30 cm, stair width is 320 cm.	F- Gostivar, the city park walking area next to the Vardar River, has a wide area. However, the walking paths in the park do not have the opportunity to walk around with a wheelchair, and there are no other measures for people with disabilities.

Figure 8. Gostivar, Vardar River Walkways and City Park (Arıç1, 2023)

One of the biggest reasons why people with disabilities cannot benefit from important social policies such as education, health, and employment is the limited and limited accessibility of living spaces. Therefore, central and local governments should organize the physical environment in accordance with universal design principles. Urban furniture should not be placed randomly, and factors such as pavement width (minimum 150 cm) and slope (maximum 2%) should be planned in accordance with the use of disabled individuals. Opinions and suggestions of disabled individuals should be included in the decisions to be taken on these issues (Bektaş et al., 2020).

We can evaluate the compliance of parks and walking paths in Gostivar with disability standards. The precautions to be taken and the materials to be used in order to provide comfortable and safe transportation for people with disabilities are as follows:

The width of the walkways should be a minimum of 200 cm. Special walking areas should be reserved for people with disabilities along the walking path. These areas should be a minimum of 240 cm wide and should be arranged in a way that allows easy passage with wheelchairs. The road surface should be non-slip and smooth. It is important to use a non-slip floor covering. For visually impaired individuals, there should be a 10 cm high platform or border on the road to enable them to perceive with the help of a walking stick. Directions such as braille signs, directional signs, and colored road signs should be used. There should be low-response sidewalks along the way. The step heights of the stairs should be close to each other. Step heights should be between 10 cm and 12 cm. Also, steps of different heights should be

avoided. A non-slip surface coating should be used. This ensures that the stairs are safe even when wet or slippery.

The walking paths in the park should be suitable for walking around with a wheelchair. Paths must be smooth, non-slip, and unobstructed. Braille signs and directions should be used for visually impaired individuals. For example, signposts at the entrance of the park may contain directional and informational signs. Benches, picnic tables, and other seating areas should be suitable for use by people with disabilities. For example, it should be of suitable height and accessibility for wheelchair users. Toilets are required in the park. It is important to have suitable toilets for people with disabilities. These toilets should be wide enough and equipped for wheelchairs to enter easily.

Construction Materials, Rubber, or similar materials specially designed for non-slip floor coverings can be used. Durable and non-slip materials should be preferred for stair steps. It may be necessary to add a non-slip coating to wooden or metal steps. Durable and tactile materials should be used for braille signs and directions. For example, embossed lettering and steel plates may be preferred.

4. DISCUSSION AND CONCLUSIONS

In order to solve the accessibility problems of stairs that are not suitable for people with disabilities, there is information with solutions and measures below:

Ramp Construction: Ramp slope: The optimal slope ratio for disabled ramps is 1:12. This means a 2.5 cm rise for every 30 cm horizontally. Ramp width: The minimum ramp width is at least 90 cm for wheelchair users. Ramp surface: A non-slip surface coating should be used on the ramp to ensure safety.

Platform Lift: Platform dimensions: Platform width should be at least 90 cm, and depth should be at least 140 cm for wheelchair users to sit comfortably. Platform height: The platform should go up and down by the height of the stairs.

Stairlift: Stairlift dimensions: A platform with a minimum width of 80 cm and a depth of 110 cm is usually required to provide adequate space for wheelchair users.

Building an Alternative Road: Road width: A road wide enough for disabled people to pass side by side should be created. The minimum width can be considered as 150 cm. Road surface: A non-slip and flat surface should be preferred to provide a safe walking surface. In case there is no ramp suitable for people with disabilities, it is necessary to produce a cost-effective solution, and the recommendations should be implemented as follows. **Alternative Crossing Point:** An alternative crossing point can be provided to the building for persons with disabilities. For example, consider adding a ramp or elevator by arranging a nearby entrance.

Temporary Ramps: Portable or foldable ramps can provide temporary access to the building for people with disabilities. These ramps can be used when needed, offering a lower-cost solution.

Project Support: You can request support for accessibility projects from public institutions or local administrations. It is possible to benefit from the funds provided to improve the access of persons with disabilities.

Solution suggestions were presented to create resting areas for the disabled and the elderly on the walking paths;

Seating Units: Seating height: The seating units should be between 45-50 cm for disabled individuals to sit comfortably. Seating area width: A minimum width of 90 cm is recommended to provide a suitable seating area for wheelchair users. Backrest angle: Backrests should be positioned at an ergonomically appropriate angle.

Shades and Umbrellas: Canopy height: The canopies' height should be at least 210 cm for disabled people to pass easily. Width and depth: Generally, shades should be at least 120 cm wide and 120 cm deep.

Dimensions and features of handicapped tables: At least 70 cm of space should be left under the table to provide unhindered access. Seat height and width must be suitable for wheelchair users. Generally, a height of 45-50 cm and a width of 90-120 cm are recommended. The surface of the desk should have a non-slip coating and should have a smooth surface for users to access it comfortably.

Dimensions and features of fountains designed for people with disabilities: Height: The height of the fountains should generally be between 75-85 cm for easy access by wheelchair users. Handles: There should be handles in fountains so that disabled people can get support. Pressurized water: Providing pressurized water in fountains can be beneficial in terms of ease of use.

The standards and dimensions of the toilets suitable for people with disabilities are as follows: Door height: The door height must be at least 90 cm for wheelchair users to enter the session. Indoor maneuvering area: Covering a maneuvering area of at least 150 cm x 150 cm for wheelchair users. Handles: In toilets, the handles should be at a suitable height and above to provide support. Stepping on the sink: There should be approximately 70 cm from the sink for wheelchair users to watch.

Features of signs and information boards: High contrast: High contrast of signs and texts makes it easier for visually impaired individuals to perceive. Braille signs: Information marked with the Braille alphabet enables visually impaired individuals to access information. Sufficient size: Enough size of the text improves readability. Correct placement: Signs must be placed correctly so users can easily notice and read them.

Disabled-friendly roads should be designed according to the following dimensions and standards: Road width: At least 150 cm width should be provided so that disabled people can pass side by side comfortably. Discretionary sidewalks: There should be discretionary ramps on sidewalks for wheelchair users.

Colored road signs: Colored markings can be used to separate different sections of roads. Responsive road signs: To attract the attention of people with disabilities, road signs can provide audio or tactile feedback.

The absence of a 10 cm high platform or border for the perception of people with disabilities may cause accessibility problems. To remedy this situation: Adding a platform or border: A 10 cm high platform or border can be added to facilitate the perception of visually impaired individuals. High-contrast markings: High-contrast markings can be used to attract the attention of visually impaired individuals. Smooth surface: Providing a smooth and non-slip floor on walkways increases safety.

The types, names, and properties of building materials that can solve the identified deficiencies should be as follows;

Non-Slip Ceramic or Tile Coatings: Non-slip ceramic or tile coatings are specially designed to prevent slipping on their surfaces. Thanks to its high coefficient of friction, it reduces slippage and provides safe walking. It provides grip even on wet or slippery surfaces. Advantages: It provides a safe and non-slip floor; it must be durable and easy to clean.

Stainless Steel or Aluminum Railings: Railings made of stainless steel or aluminum provide a secure hold on stairs and ramps. It is durable, corrosion-resistant, and long-lasting.

It is preferably ergonomically designed to facilitate the use of people with disabilities. Advantages: Provides a secure hold, is durable, and is long-lasting.

Braille Sign Materials: Braille sign materials contain braille writings especially suitable for the Braille alphabet.

Stainless steel or plastic materials can be used. It is touchable, durable, and weather resistant.

Advantages: Provides visually impaired individuals access to information, is durable and long-lasting.

Non-Slip Floor Coverings: Non-slip floor coverings are specially designed to reduce the risk of slipping. Different materials can be used, for example, non-slip rubber or non-slip epoxy coatings. It prevents slipping even on wet or slippery floors. Advantages: Provides safe walking, reduces the risk of slipperiness, is durable, and is easy to clean.

These building materials are the preferred options for facilitating the access and safety of people with disabilities. Factors such as durability, safety, cleanability, and longevity should be considered in material selection. It is also important to comply with local legislation and standards.

These building materials are the preferred options for facilitating the access and safety of people with disabilities. Factors such as durability, safety, cleanability, and longevity should be considered in material selection. It is also important to comply with local legislation and standards.

REFERENCES

Arap, S. K., Yücebaş, E., & Arap, İ. (2021). Local Governments' Goal Of Life Without Barriers: The Case Of The Izmir Metropolitan Municipality. *Anemon Muş Alparslan University Journal of Social Sciences*, 9(1), 139-156.

Aykıl, F. D., Erbaş, M., & Meltem. (2018). The Suitable Design of Urban Furniture for Elderly and Disabled: The Suitability Analysis on Elazig Town Squares. *Inonu University Journal of Art and Design*, ISSN: 1309-9876, E-ISSN: 1309-9884.

Bektaş, B., & Develi, A. (2020). Engelli Bireylerin Erişilebilirlik Sorunu: Destekler, Eksiklikler. *Uluslararası Anadolu Sosyal Bilimler Dergisi*, 4(3).

Çınar, H., Arslan, A. R., Öztürk, A. M., & Bülbül, R. (2015). Public Buildings: Life Analysis for the Disabled and Furniture Use Reinforcement. *Suleyman Demirel University Journal of Engineering Sciences and Design*, 3(3), 329-337. SI: Ergonomi2015. ISSN: 1308-6693. Special Issue of 21. National Congress of Ergonomics, Turkey.

Çivici, T., & Gönen, D. (2015). Evaluating Accessibility to Social Areas for Physical Disabled Students in Balıkesir University Çağış Campus. *Süleyman Demirel Üniversitesi Mühendislik Bilimleri ve Tasarım Dergisi*, 3(3), 639-646. ÖS: Ergonomi2015. ISSN: 1308-6693. Special Issue of 21. National Congress of Ergonomics, Turkey.

Doğruel, F. (2022). Accessibility Experiences of People with Disabilities at the Intersection of Body, Individual, and Society. *Journal of Sociological Research*, 25(2), ISSN 2148-9947.

Enginöz, E., B. (2015). *Herkes için Tasarım, Mimarlık*, 381.

Erten, Ş., & Aktel, M. (2020). Right of Accessibility of People with Disabilities: An Assessment in the Framework of Barrier-Free City Approach. *Süleyman Demirel University Visionary Journal*, 11(28), 898-912. ISSN: 1308-9552.

Mutluer, S. Y. (1997). *Tekerlekli Sandalye Kullanan Bedensel Özürlüler İçin Uygun Konut Tasarımı ve Çevre Düzenlemesi*. Yüksek Lisans Tezi. Selçuk Üniversitesi, Konya.

Pouya, S. (2021). The importance of universal equipment designs for people with disabilities and some design suggestions in the related landscape areas. *Sosyal Çalışma Dergisi*, 5(2), 209-229.

Comparison of Two Sensorless Control Methods for PMSM based on High-Frequency Signal Injection

Fehmi Sevilmiş*¹

Abstract: In recent years, there has been a growing interest in the development and implementation of sensorless control methods for permanent magnet synchronous motor (PMSM) in various fields, such as electric vehicles and industrial applications. Since there is no need for a mechanical sensor to obtain the rotor position, sensorless control methods bring many advantages such as low-cost, robustness, and reliability in PMSM control. For sensorless operation of PMSM at zero and low speeds, high-frequency (HF) signal injection methods are used to estimate the rotor position. Among these methods, HF rotating signal injection and HF pulsating signal injection techniques are broadly operated for sensorless control of PMSM. A HF rotating signal is injected into the stationary reference frame while a HF pulsating signal is injected into the estimated synchronous reference frame. This paper presents a comparison for the two HF signal injection methods. The principle of these techniques is analyzed first. Then, the two methods are compared with each other, and the obtained findings are summarized.

Keywords: high frequency rotating signal injection, high frequency pulsating signal injection, permanent magnet synchronous motor (PMSM), sensorless control.

¹**Address:** Selçuk University, Faculty of Technology, Konya/Türkiye

***Corresponding author:** fehmisevilmis@selcuk.edu.tr

1. INTRODUCTION

Recently, permanent magnet synchronous motor (PMSM) has gotten a widespread usage in many applications, especially electric vehicles, thanks to its high power density and efficiency. In order to properly control the PMSM, a field-oriented control (FOC) is usually preferred. But, the FOC needs accurate rotor position information. This information can be obtained by a mechanical sensor (e.g., encoder). The encoder gives the rotor position precisely; however, it causes some problems such as an increase in the risk of failure and cost (Li et al., 2020). To overcome these issues, many sensorless control methods for detecting rotor position information are presented in literature (Wang et al., 2020).

Sensorless control techniques can be divided into two categories based on motor speed. These are model-based sensorless control and saliency-based sensorless control (Wang et al., 2020). The first one is employed in middle and high speed ranges based on electromotive force (EMF). In EMF-based methods, extended Kalman filter (Yin et al., 2019), disturbance observer (Xu et al., 2021), and sliding mode observer (Zuo et al., 2023) are widely used. Since the magnitude of back EMF is quite small at zero and low speeds, these methods are not suitable for such speeds. Therefore, the second one is applied in zero and low speed ranges based on high frequency (HF) signal injection. Saliency-based sensorless control can be mainly subdivided into HF rotating voltage injection in the stationary reference frame and HF pulsating voltage injection in the estimated reference frame.

This study presents a comparison with two saliency-based sensorless control methods for PMSM. This paper is organized as follows. In section II, the HF rotating voltage injection and HF pulsating voltage injection techniques are analyzed, respectively. Section III summarizes the findings.

2. SALIENCY-BASED SENSORLESS CONTROL METHODS

The dynamic model of PMSM in dq -axis rotor frame can be expressed as

$$\begin{bmatrix} u_d \\ u_q \end{bmatrix} = \begin{bmatrix} R_s & \omega_e L_q \\ \omega_e L_d & R_s \end{bmatrix} \begin{bmatrix} i_d \\ i_q \end{bmatrix} + \begin{bmatrix} L_d & 0 \\ 0 & L_q \end{bmatrix} \frac{d}{dt} \begin{bmatrix} i_d \\ i_q \end{bmatrix} + \begin{bmatrix} 0 \\ \omega_e \psi_f \end{bmatrix} \quad (1)$$

where u_d and u_q are the d - and q -axis stator voltage components, i_d and i_q are the d - and q -axis stator current components, L_d and L_q are the d - and q -axis inductances, R_s is the stator resistance, ω_e is the electrical angular speed of the rotor, and

ψ_f is the permanent magnet flux linkage, respectively. This equation should be transformed into the estimated dq -reference frame or stationary $\alpha\beta$ -reference frame because it, which states the actual dq -reference frame, cannot be used directly for rotor position detection (Wang et al., 2019). When the motor operates at very low speed ranges (i.e., ω_e is approximately zero), (1) can be rewritten as

$$\begin{bmatrix} u_d \\ u_q \end{bmatrix} = \begin{bmatrix} R_s & 0 \\ 0 & R_s \end{bmatrix} \begin{bmatrix} i_d \\ i_q \end{bmatrix} + \begin{bmatrix} L_d & 0 \\ 0 & L_q \end{bmatrix} \frac{d}{dt} \begin{bmatrix} i_d \\ i_q \end{bmatrix} \quad (2)$$

If the injection signal is high enough, the voltage drop on stator resistance can be neglected. Then, at zero or low speed range, the HF model of PMSM can be approximated in the rotor frame as (Wang et al., 2020)

$$\begin{bmatrix} u_d^h \\ u_q^h \end{bmatrix} = \begin{bmatrix} L_d & 0 \\ 0 & L_q \end{bmatrix} \frac{d}{dt} \begin{bmatrix} i_d^h \\ i_q^h \end{bmatrix} \quad (3)$$

where superscript “h” denotes the HF component.

Using a proper transformation, (3) can be obtained in the $\alpha\beta$ -reference frame as

$$\begin{bmatrix} u_\alpha^h \\ u_\beta^h \end{bmatrix} = \begin{bmatrix} L_0 + L_1 \cos(2\theta_e) & L_1 \sin(2\theta_e) \\ L_1 \sin(2\theta_e) & L_0 - L_1 \cos(2\theta_e) \end{bmatrix} \frac{d}{dt} \begin{bmatrix} i_\alpha^h \\ i_\beta^h \end{bmatrix} \quad (4)$$

where L_0 and L_1 are average and differential inductances, respectively, i.e., $L_0 = (L_d + L_q)/2$, $L_1 = (L_d - L_q)/2$, and θ_e is the actual rotor position.

2.1. HF Rotating Voltage Injection

Figure 1 shows the schematic of HF rotating voltage injection based sensorless control method. As shown, rotating sinusoidal voltages are injected into $\alpha\beta$ -reference frame. These voltages are

$$\begin{bmatrix} u_\alpha^h \\ u_\beta^h \end{bmatrix} = U_h \begin{bmatrix} \cos(\omega_h t) \\ \sin(\omega_h t) \end{bmatrix} \quad (5)$$

where U_h and ω_h represent the amplitude and angular frequency of injected voltages. The inverse of (4) is taken to obtain the induced currents as follows.

$$\frac{d}{dt} \begin{bmatrix} i_{\alpha_h} \\ i_{\beta_h} \end{bmatrix} = \frac{1}{L_0^2 - L_1^2} \begin{bmatrix} L_0 - L_1 \cos(2\theta_e) & -L_1 \sin(2\theta_e) \\ -L_1 \sin(2\theta_e) & L_0 + L_1 \cos(2\theta_e) \end{bmatrix} \begin{bmatrix} u_\alpha^h \\ u_\beta^h \end{bmatrix} \quad (6)$$

If (5) is substituted into (6), we can rewrite as

$$\frac{d}{dt} \begin{bmatrix} i_{\alpha_h} \\ i_{\beta_h} \end{bmatrix} = \frac{U_h}{L_0^2 - L_1^2} \begin{bmatrix} L_0 \cos(\omega_h t) - L_1 \cos(2\theta_e - \omega_h t) \\ L_0 \sin(\omega_h t) - L_1 \sin(2\theta_e - \omega_h t) \end{bmatrix} \quad (7)$$

The induced HF currents can be calculated by taking the integral of (7) as follows. Note that these currents are obtained by passing through high-pass filters (HPFs), as shown in Figure 1.

$$\begin{bmatrix} i_{\alpha_h} \\ i_{\beta_h} \end{bmatrix} = \frac{U_h}{\omega_h (L_0^2 - L_1^2)} \begin{bmatrix} L_0 \sin(\omega_h t) + L_1 \sin(2\theta_e - \omega_h t) \\ -L_0 \cos(\omega_h t) - L_1 \cos(2\theta_e - \omega_h t) \end{bmatrix} \quad (8)$$

To estimate the rotor position from (8), a synchronous frame filter (SFF) is used. In SFF, firstly, (8) is transformed into HF rotating frame as

$$\begin{bmatrix} i_d^h \\ i_q^h \end{bmatrix} = \frac{U_h}{\omega_h (L_0^2 - L_1^2)} \begin{bmatrix} L_0 \sin(2\omega_h t) + L_1 \sin(2\theta_e) \\ -L_0 \cos(2\omega_h t) - L_1 \cos(2\theta_e) \end{bmatrix} \quad (9)$$

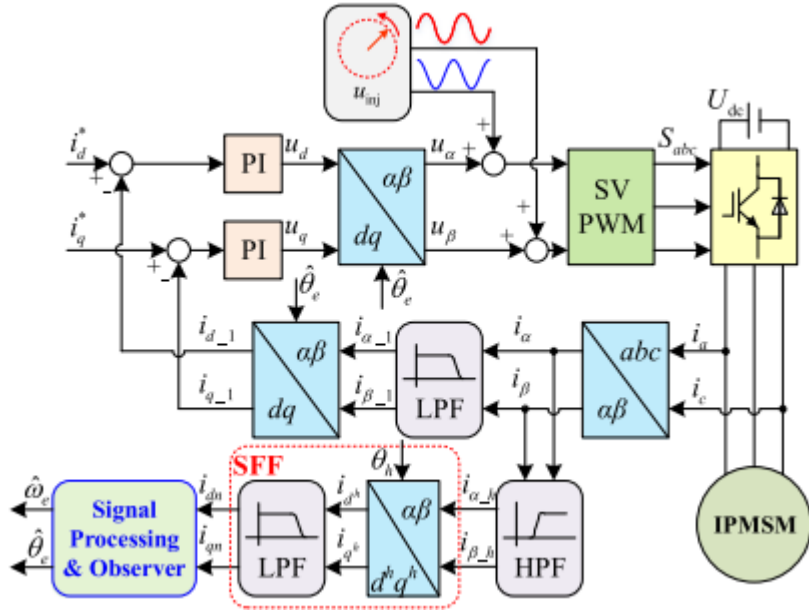


Figure 1. Schematic of HF rotating voltage injection method (Wang et al., 2020)

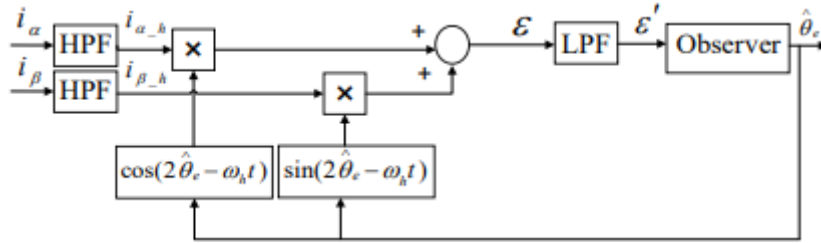


Figure 2. Schematic of heterodyning demodulation (Naderian et al., 2023)

Then, two low-pass filters (LPFs) are used to filter out the first components in (9) with a frequency of $2\omega_h$. And this formula can be rewritten as

$$\begin{bmatrix} i_{dh} \\ i_{qh} \end{bmatrix} = \frac{U_h}{\omega_h (L_0^2 - L_1^2)} \begin{bmatrix} L_1 \sin(2\theta_e) \\ -L_1 \cos(2\theta_e) \end{bmatrix} \quad (10)$$

Finally, the rotor position can be derived as

$$\theta_e = \frac{1}{2} \arctan \left(-\frac{i_{dh}}{i_{qh}} \right) \quad (11)$$

Another way to estimate rotor position is to use the structure in Figure 2, called heterodyning demodulation. In this approach, the induced HF currents in $\alpha\beta$ -reference frame given in (8) are respectively multiplied by the cosine and sine functions. Then, the error signal (ε) is passed through a LPF. After some mathematical operations, the filtered error (ε') can be approximated by

$$\varepsilon' = \frac{U_h}{(L_0^2 - L_1^2)} \frac{L_1}{\omega_h} \sin 2(\theta_e - \hat{\theta}_e) \approx \frac{2U_h L_1}{\omega_h (L_0^2 - L_1^2)} (\theta_e - \hat{\theta}_e) \quad (12)$$

where $\hat{\theta}_e$ is the estimated rotor position. ε' converges to zero through an observer. The observer structure is the same as the control loop of a phase locked loop (PLL), i.e., consisting of a PI controller and an integrator.

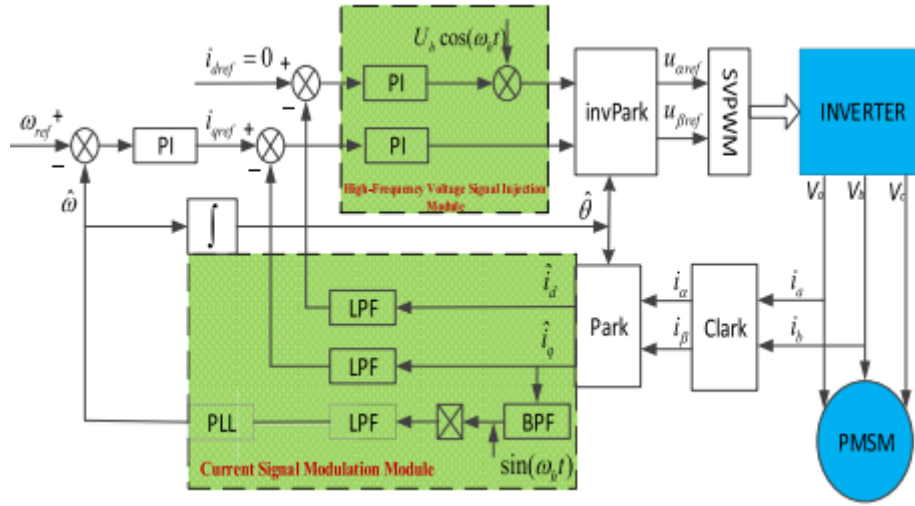


Figure 3. Schematic of HF pulsating voltage injection method (Wang et al., 2019)

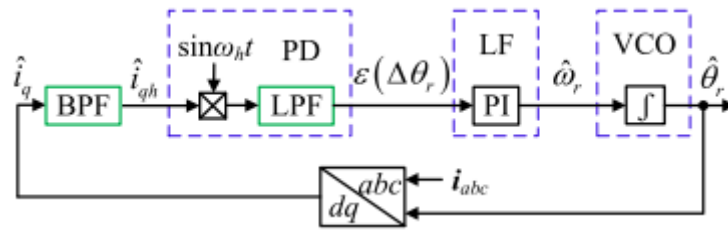


Figure 4. Schematic of signal demodulation algorithm (Li et al., 2020)

2.2. HF Pulsating Voltage Injection

Figure 3 illustrates the block diagram of HF pulsating voltage injection based sensorless control method. As observed, pulsating sinusoidal voltages are injected into the estimated dq -reference frame. They are

$$\begin{bmatrix} \hat{u}_d^h \\ \hat{u}_q^h \end{bmatrix} = U_h \begin{bmatrix} \cos(\omega_h t) \\ 0 \end{bmatrix} \quad (13)$$

Based on (3) and (13), and making some mathematical manipulations, the induced HF currents in estimated dq -axis can be obtained as

$$\begin{bmatrix} \hat{i}_{dh} \\ \hat{i}_{qh} \end{bmatrix} = \frac{U_h \sin(\omega_h t)}{\omega_h (L_0^2 - L_1^2)} \begin{bmatrix} L_0 - L_1 \cos(2\Delta\theta_r) \\ -L_1 \sin(2\Delta\theta_r) \end{bmatrix} \quad (14)$$

where $\Delta\theta_r$ is the position error and equals to $\theta_r - \hat{\theta}_r$. Here, θ_r and $\hat{\theta}_r$ are the actual and estimated rotor positions, respectively.

To detect the rotor position, the current \hat{i}_{qh} is preferred because it converges to zero if $\Delta\theta_e = 0$. Figure 4 shows the signal modulation algorithm based on type-2 PLL structure. The PLL composes of phase detector (PD), loop filter (LF), and voltage controlled oscillator (VCO). As shown, a band-pass filter (BPF) is used to derive the HF current \hat{i}_{qh} the q -axis current \hat{i}_q . Then, \hat{i}_{qh} is multiplied by $\sin(\omega_h t)$, and a LPF is used to obtain the position error at the PD output. This error can be determined as

$$\varepsilon(\Delta\theta_r) = \text{LPF} \left[\hat{i}_{qh} \sin(\omega_h t) \right] = -\frac{L_1 U_h \sin(2\Delta\theta_r)}{2\omega_h (L_0^2 - L_1^2)} \quad (15)$$

Finally, to estimate the speed $\hat{\omega}_r$ and rotor position $\hat{\theta}_r$, a PI controller and an integrator are used, respectively.

3. DISCUSSION AND CONCLUSIONS

In this paper, two saliency-based sensorless control methods for PMSM, called the HF rotating voltage injection and HF pulsating voltage injection methods, are discussed. Comparative results are summarized as follows:

- 1) Two sinusoidal voltages, i.e., $U_h \cos(\omega_h t)$ and $U_h \sin(\omega_h t)$, are injected into $\alpha\beta$ -reference frame in HF rotating voltage injection method while only one sinusoidal voltage, i.e., $U_h \cos(\omega_h t)$ or $U_h \sin(\omega_h t)$, is injected into estimated dq -reference frame in HF pulsating voltage injection method. This means that HF pulsating voltage injection technique provides convenience in terms of signal injection.
- 2) If an evaluation is made in terms of the signal demodulation algorithm used to estimate the rotor speed and position information, the HF pulsating voltage injection method is more advantageous. Because, it needs less filtering than the HF rotating voltage injection method. The reason of this, the HF rotating voltage injection method uses $\alpha\beta$ -axis currents i_α and i_β (see Figure 2) while the HF pulsating voltage injection method uses only \hat{i}_q (see Figure 4).

Consequently, HF pulsating voltage injection method based sensorless control method offers a simpler structure and ease of implementation. So, this method has received more attention, as in (Li et al., 2020; Lu et al., 2021; Zhang et al., 2018).

Acknowledgements

The authors would like to acknowledge the Scientific Research Projects Coordinating Office of Selçuk University for financial support.

Ethics Committee Approval

N/A

Peer-review

Externally peer-reviewed.

Author Contributions

Conceptualization: F.S.; Investigation: F.S.; Material and Methodology: F.S., Visualization: F.S.; Writing-Original Draft: F.S., Writing-review & Editing: F.S.; Other: All authors have read and agreed to the published version of manuscript.

Conflict of Interest

The authors have no conflicts of interest to declare.

Funding

The authors declared that this study has received a financial support from the Scientific Research Projects Coordinating Office of Selçuk University (SÜBAP Project No: 23701129).

REFERENCES

- Li, H., Zhang, X., Xu, C., Hong, J. (2020). Sensorless control of IPMSM using moving-average-filter based PLL on HF pulsating signal injection method. *IEEE Transactions on Energy Conversion*, 35(1), 43-52. <https://doi.org/10.1109/TEC.2019.2946888>
- Lu, Q., Wang, Y., Mo, L., Zhang, T. (2021). Pulsating high frequency voltage injection strategy for sensorless permanent magnet synchronous motor drives. *IEEE Transactions on Applied Superconductivity*, 31(8), 1-4. <https://doi.org/10.1109/TASC.2021.3094426>
- Naderian, M., Markadeh, G. A., Karimi-Ghartemani, M., Mojiri, M. (2023). Improved Sensorless Control Strategy for IPMSM Using an ePLL Approach with High-Frequency Injection. *IEEE Transactions on Industrial Electronics (Early Access)*. <https://doi.org/10.1109/TIE.2023.3270528>
- Wang, S., Yang, K., Chen, K. (2019). An improved position-sensorless control method at low speed for PMSM based on high-frequency signal injection into a rotating reference frame. *IEEE Access*, 7, 86510-86521. <https://doi.org/10.1109/ACCESS.2019.2925214>
- Wang, G., Valla, M., Solsona, J. (2020). Position sensorless permanent magnet synchronous machine drives—A review. *IEEE Transactions on Industrial Electronics*, 67(7), 5830-5842. <https://doi.org/10.1109/TIE.2019.2955409>
- Xu, B., Zhang, L., Ji, W. (2021). Improved non-singular fast terminal sliding mode control with disturbance observer for PMSM drives. *IEEE Transactions on Transportation Electrification*, 7(4), 2753-2762. <https://doi.org/10.1109/TTE.2021.3083925>
- Yin, Z., Gao, F., Zhang, Y., Du, C., Li, G., Sun, X. (2019). A review of nonlinear Kalman filter applying to sensorless control for AC motor drives. *CES Transactions on Electrical Machines and Systems*, 3(4), 351-362. <https://doi.org/10.30941/CESTEMS.2019.00047>
- Zhang, X., Li, H., Yang, S., Ma, M. (2018). Improved initial rotor position estimation for PMSM drives based on HF pulsating voltage signal injection. *IEEE Transactions on Industrial Electronics*, 65(6), 4702-4713. <https://doi.org/10.1109/TIE.2017.2772204>
- Zuo, Y., Lai, C., Iyer, K. L. V. (2023). A Review of Sliding Mode Observer based Sensorless Control Methods for PMSM Drive. *IEEE Transactions on Power Electronics*, 38(9), 11352-11367. <https://doi.org/10.1109/TPEL.2023.3287828>

APF Based Control Algorithm for Voltage Regulation of Self Excited Induction Generator Using DSTATCOM

Ali Sait Özer¹, Hulusi Karaca*², Fehmi Sevilmiş³

Abstract: Distribution Static Compensator (DSTATCOM) systems are widely used for voltage regulation of self-excited induction generator (SEIG). DSTATCOM provides the reactive power that SEIG and the load need. The performance of DSTATCOM depends on its control algorithm. The main goal of the control algorithm is to generate switching signals for the voltage source inverter (VSI) in the structure of DSTATCOM. These signals are estimated by reference currents. The active and reactive components required to generate the reference currents are obtained from the SEIG individual phase voltages and 90-degree lagging-phase. For this, SOGI and EPLL based current synchronous detection (CSD) methods have been suggested in the literature. The filtering capabilities of these methods are satisfactory, but they are relatively complex. In this paper, all pass filter (APF) based CSD method is proposed. This method is a simple and effective method with less mathematical calculations. The suggested algorithm has been tested under linear and nonlinear load conditions. The obtained results clearly represent the effectiveness of the suggested APF based CSD control algorithm.

Keywords: Distribution static compensator (DSTATCOM), Self-excited induction generator (SEIG), Wind energy conversion systems (WECS), Current synchronous detection (CSD) method, All pass Filter (APF)

¹**Address:** Konya Technical University, Department of Control and Automation Technology, Konya/Turkiye

²**Address:** Selçuk University, Department of Electrical and Electronics Engineering, Konya/Turkiye

³**Address:** Selçuk University, Department of Electrical and Electronics Engineering, Konya/Turkiye

***Corresponding author:** hkaraca@selcuk.edu.tr

1. INTRODUCTION

Nowadays, due to increasing energy demand and environmental concerns, the interest in renewable energy sources has increased significantly (Kewat & Singh, 2019). Self-excited induction generator (SEIG) is commonly used to generate the power in renewable energy systems. SEIG has many advantages such as simple structure, low maintenance and cost, brushless construction, and self-protection against short circuits (Tandekar, Ojha, & Jain, 2019). However, its performance deteriorates when unbalanced and nonlinear loads are connected to SEIG's terminals. That is, terminal voltages of SEIG are drop because the reactive power required for SEIG is not supplied.

To provide voltage regulation of SEIG, distribution static compensator (DSTATCOM)-based control method is very popular. DSTATCOM consists of IGBT-based voltage source inverter (VSI) and DC bus capacitor. The performance of DSTATCOM depends on the reference signals generated for the VSI. In the literature, many methods have been proposed to generate reference signals. One of the widely used methods is current synchronous detection (CSD) based theory.

The CSD method have been proposed to control DSTATCOM-based SEIG (Singh et al. 2015). This method includes a second-order generalized integrator to filter the measured SEIG voltages and estimate the amplitudes of each phase voltages. Özer et al. (2022) have suggested an enhanced phase locked loop (EPLL)-based CSD control algorithm. These methods present a high disturbance rejection capability in case of unbalanced and nonlinear loads. But they have complex structures that increases computation burden.

In this paper, a simple structured APF-based CSD method is proposed. The performance of the proposed method has investigated under linear nonlinear load conditions. The results obtained demonstrated the effectiveness of the APF-based method.

2. DSTATCOM-BASED SEIG STRUCTURE

Fig. 1 shows the configuration of the DSTATCOM-based SEIG system. The system consists of an induction generator, a star connected three-phase capacitor bank for self-excitation, consumer loads, and a DSTATCOM. The capacitor bank

is required to provide the reactive power to produce the rated voltage at no-load. The DSTATCOM includes IGBT-based VSI with DC bus capacitor. The inductor (L_f) is connected in series with the point of common coupling (PCC) to minimize the high frequency noise generated by the VSI. The DSTATCOM regulates the terminal voltage.

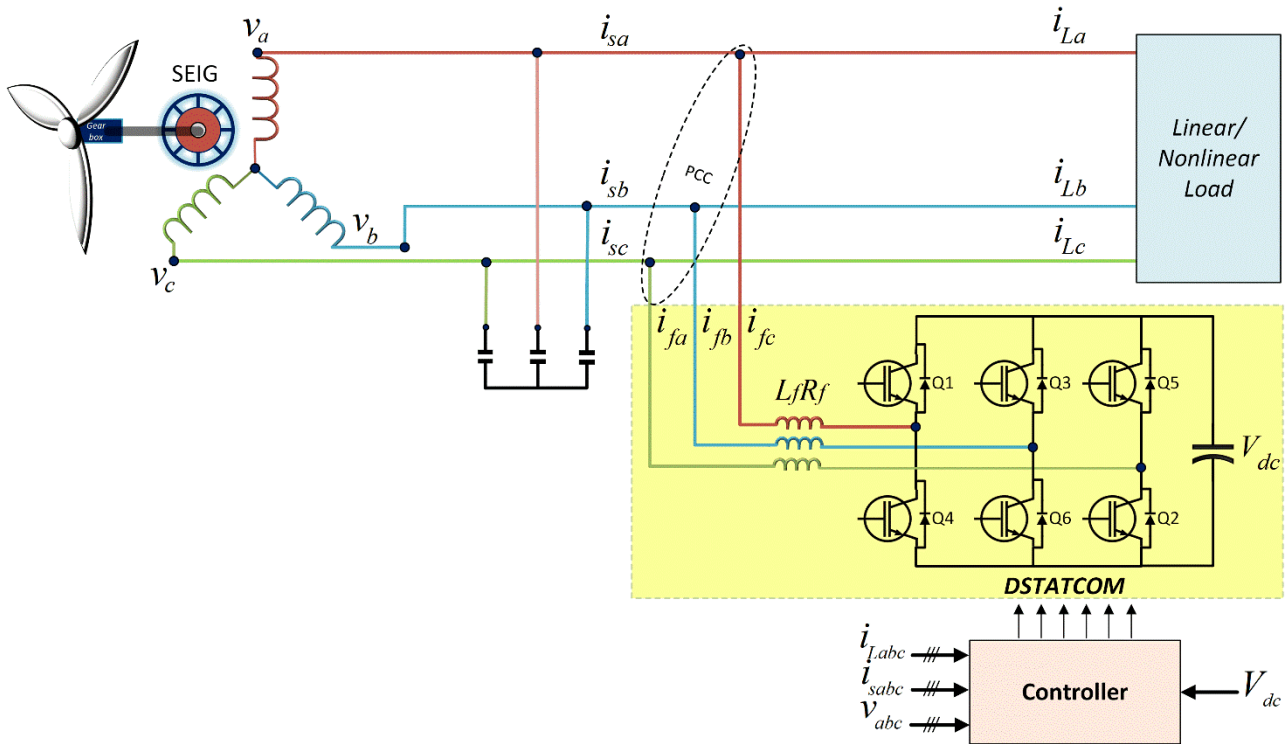


Figure 1. Schematic of DSTATCOM-based SEIG system

3. APF-BASED CSD CONTROL ALGORITHM

Fig. 2 shows the block diagram of suggested APF-based CSD method. As shown, proposed method employs an APF for each phase voltages (i.e., v_a , v_b , and v_c). The aim of using the APF is to create a 90° lagging-phase of PCC voltages. Thus, the amplitude of PCC voltages can be easily obtained to realize the CSD technique as follows.

$$V_{am} = \sqrt{v_a^2 + qv_a^2}, V_{bm} = \sqrt{v_b^2 + qv_b^2}, \text{ and } V_{cm} = \sqrt{v_c^2 + qv_c^2} \quad (1)$$

where qv_a , qv_b , and qv_c denote the 90° lagging-phase of v_a , v_b , and v_c , respectively.

APF is widely preferred for generation of virtual orthogonal signal due to its several advantages such as fast dynamic response and simple structure. Its transfer function that features a low-pass filter can be obtained as (Sevilmiş and Karaca, 2020)

$$\text{APF}(s) = \frac{-s + \omega}{s + \omega} \quad (2)$$

where ω is angular frequency.

The schematic of APF is illustrated in Fig. 3, here v and qv are input signal and its 90° lagging-phase, respectively. As shown, it requires only two subtractions, one multiplication, and one integrator. So, APF can be simply implemented in CSD method.

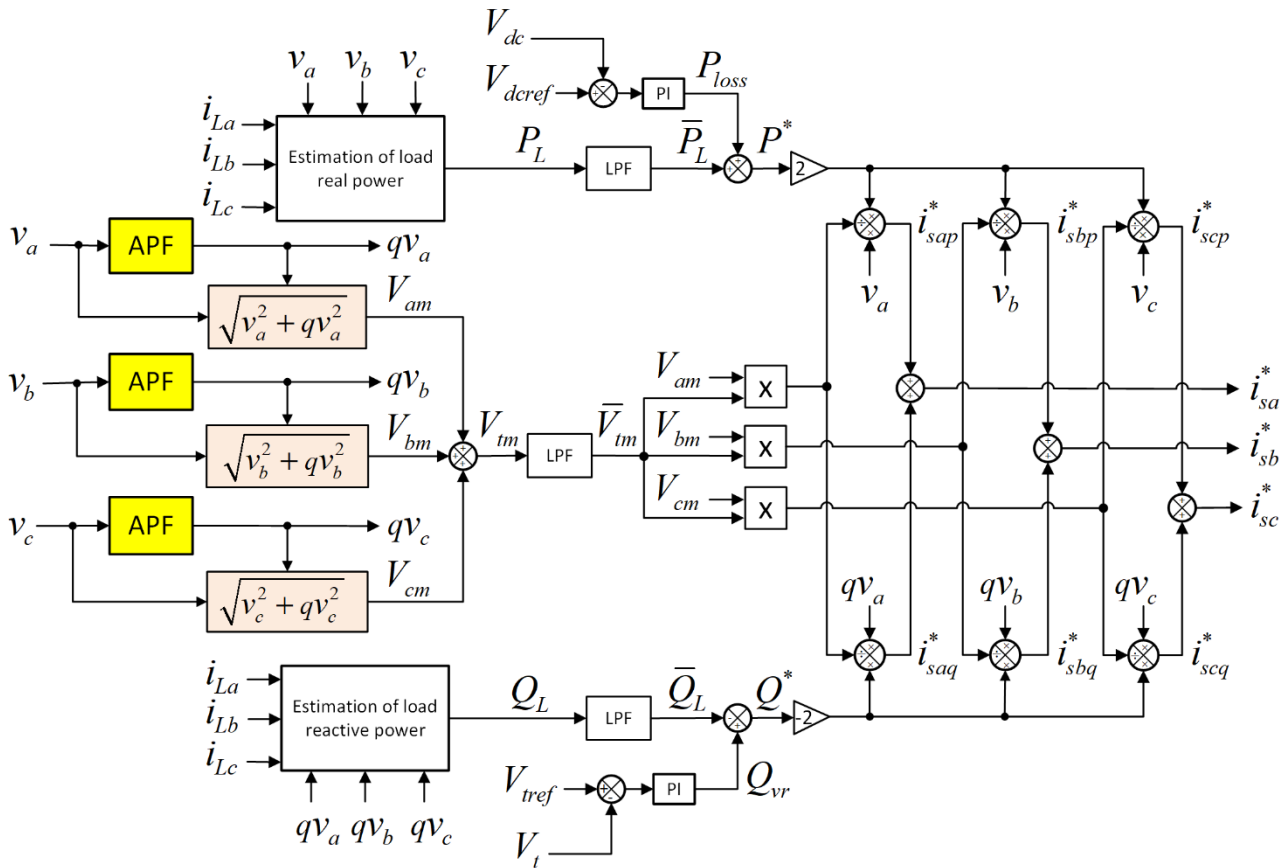


Figure 2. Schematic of proposed APF-based CSD method

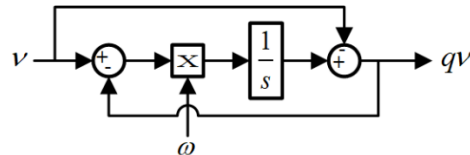


Figure 3. Block diagram of APF

In the proposed APF-based control algorithm, the active power of the load is calculated by using the load currents and phase voltages as follows.

$$P_L = v_a i_{La} + v_b i_{Lb} + v_c i_{Lc} \quad (3)$$

The active power of the load includes DC ($\overline{P_L}$) and AC components. SEIG's output power can be affected by AC component. This component is filtered using the LPF.

DC bus voltage must always be kept higher than the peak value of the PCC voltage. The DC bus voltage is compared with the reference value (V_{dcref}) and the obtained error is fed into the PI controller. The power at the PI output (P_{loss}) compensates for the power requirement of DSTATCOM. The reference active power (P^*) is calculated as

$$P^* = P_{loss} + \overline{P_L} \quad (4)$$

The active components of the reference currents are estimated by

$$i_{sap}^* = \frac{2P^*v_a}{\sqrt{v_m}V_{am}} ; i_{sbp}^* = \frac{2P^*v_b}{\sqrt{v_m}V_{bm}} ; i_{scq}^* = \frac{2P^*v_c}{\sqrt{v_m}V_{cm}} \quad (5)$$

where $\overline{V_{tm}}$ is obtained by filtering after summing the peak values of phase voltages.

The instantaneous reactive power consumed by the load is expressed as

$$Q_L = qv_a i_{La} + qv_b i_{Lb} + qv_c i_{Lc} \quad (6)$$

(6) can contain oscillations due to the nonlinear loads. In order to achieve sinusoidal and balanced reference currents, the disturbance components in the reactive power should be eliminated. Hence, the instantaneous reactive power of load (Q_L) is filtered using LPF. To keep the SEIG voltage constant at the reference value, reference reactive power (Q^*) can be calculated as follows.

$$Q^* = Q_{VR} - \overline{Q_L} \quad (7)$$

where Q_{VR} , as shown in Fig. 2, is the reactive power at the output of PI controller. The error signal in the PI input is determined by comparing V_{ref} with V_t . Here, V_t can be calculated by $\overline{V_{tm}}/3$ and V_{ref} denotes its reference value.

The reactive components of the reference currents are obtained as

$$i_{saq}^* = -\frac{2Q^*qv_a}{\overline{V_{tm}}V_{am}}; \quad i_{sbq}^* = -\frac{2Q^*qv_b}{\overline{V_{tm}}V_{bm}}; \quad i_{scq}^* = -\frac{2Q^*qv_c}{\overline{V_{tm}}V_{cm}} \quad (8)$$

As a result, using (5) and (8), reference currents can be calculated as

$$i_{sa}^* = i_{sap}^* + i_{saq}^*; \quad i_{sb}^* = i_{sbp}^* + i_{sbq}^*; \quad i_{sc}^* = i_{sbp}^* + i_{scq}^* \quad (9)$$

4. PERFORMANCE OF DSTATCOM-BASED SEIG UNDER THE LINEAR AND NONLINEAR LOAD CONDITIONS

The performance of DSTATCOM with the proposed APF-based CSD control algorithm is acquired under various linear and nonlinear load conditions. These conditions are given as follows.

Test condition-1: To examine the proposed APF-based CSD controller under linear load, resistive load is connected in 2.9-3.1 s.

Test condition-2: To examine the proposed SEIG-DSTATCOM controller under a nonlinear load, three-phase diode rectifier with resistive load is connected as a load in 3.1-3.3 s.

Test condition-3: To test the suggested method against the different loads, three-phase diode rectifier with capacitive filter and resistive load is tied to PCC point in 3.3-3.5 s.

In Fig. 4, the load currents (i_{Labc}), DSTATCOM currents (i_{fabc}), SEIG currents (i_{sabc}), and SEIG terminal voltages (v_{ab}, v_{bc}, v_{ca}) of proposed APF-based CSD algorithm are shown, respectively. Fig. 5 illustrated the amplitude of the SEIG voltages (V_t) and the DC bus voltage (V_{dc}), respectively.

In test-1, the load currents are balanced due to the linear load as shown in Fig. 4(a). Fig. 4(b) demonstrated the currents injected by DSTATCOM into the system to provide the reactive power needed by the SEIG. Thanks to the proposed APF-based CSD, SEIG currents and voltages are obtained in sinusoidal and balanced form as illustrated in Fig. 4(c) and Fig. 4(d), respectively. Also, the amplitude of SEIG voltage (V_t) and DC bus voltage (V_{dc}) are also observed to be constant and maintained at reference values as shown in Fig. 5(a) and Fig. 5(b), respectively.

In test-2, the harmonics occur in load currents because of the nonlinear load as illustrated in Fig. 3(a). Therefore, DSTATCOM suppresses load harmonics and keeps SEIG currents nearly sinusoidal by injecting compensating currents as shown in Figure 4(b). SEIG currents and voltages are obtained in balanced form as illustrated in Fig. 4(c) and Fig. 4(d), respectively. When the V_t and V_{dc} voltages are examined, there was a voltage decrease of about 1V at the first moment when the nonlinear load was activated and it settled to the reference value within 0.1 second as shown Fig. 5(a) and Fig. 5(b), respectively.

In Test-3, it is seen in Fig. 4(a) that the current increases due to the increase in the power of the load. As shown in Fig. 4(b), DSTATCOM injects more current into the system to meet the reactive power demand. Depending on the load, the SEIG currents increase but are not unbalanced thanks to the proposed APF based algorithm as shown in the Fig.4(c). When the SEIG voltage is examined, it is seen in Fig 4(d) that it is balanced and sinusoidal. As soon as the power of the nonlinear load increased, the V_t and the DC bus voltage decreased by about 1V but reached the reference value in a few cycles as illustrated Fig. 5(a) and Fig. 5(b).

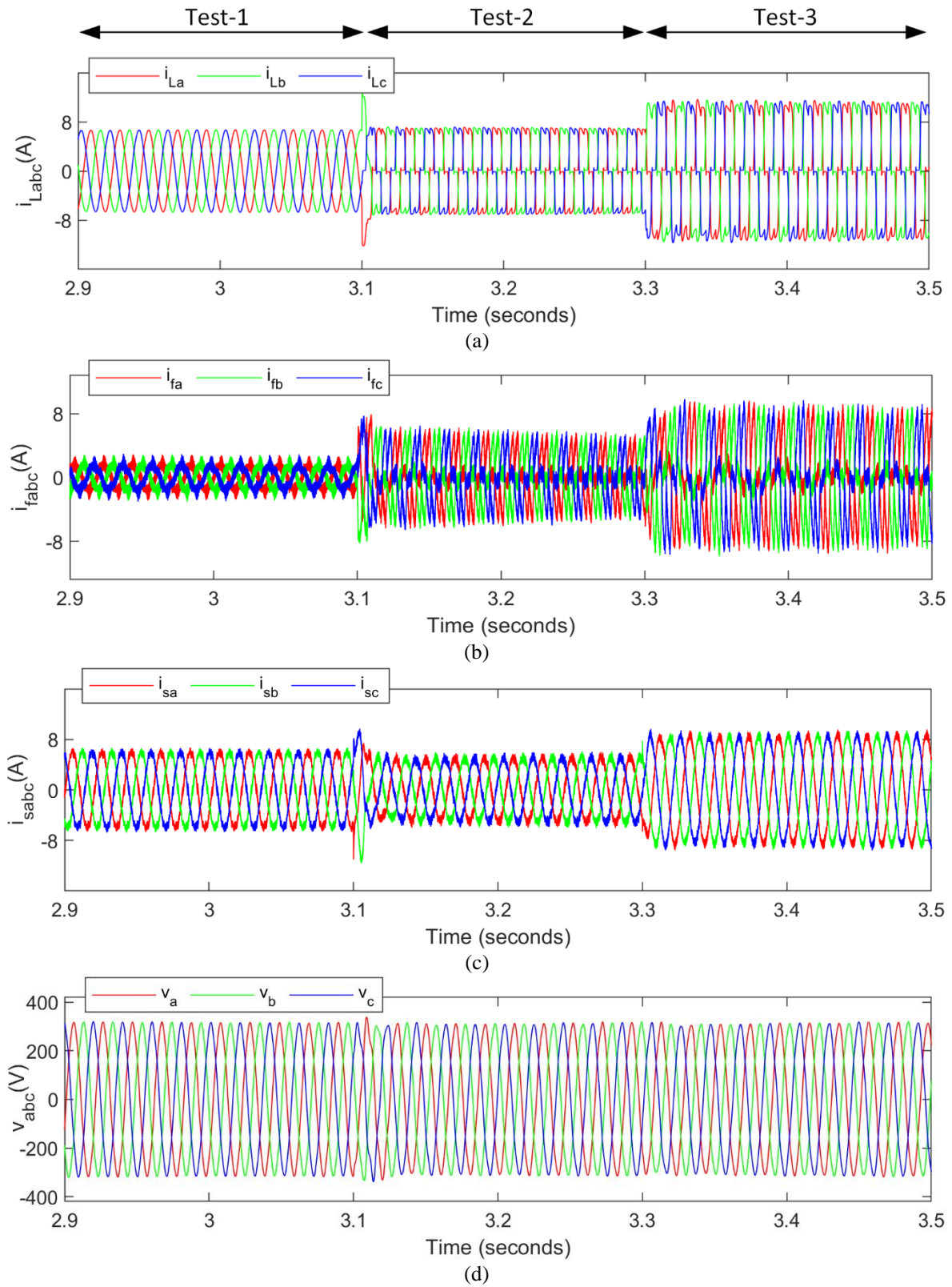


Figure 4. Performance of proposed APF based SEIG-DSTATCOM system under linear and nonlinear loads (a) Load currents, (b) DSTATCOM currents, (c) SEIG currents, (d) SEIG terminal voltages.

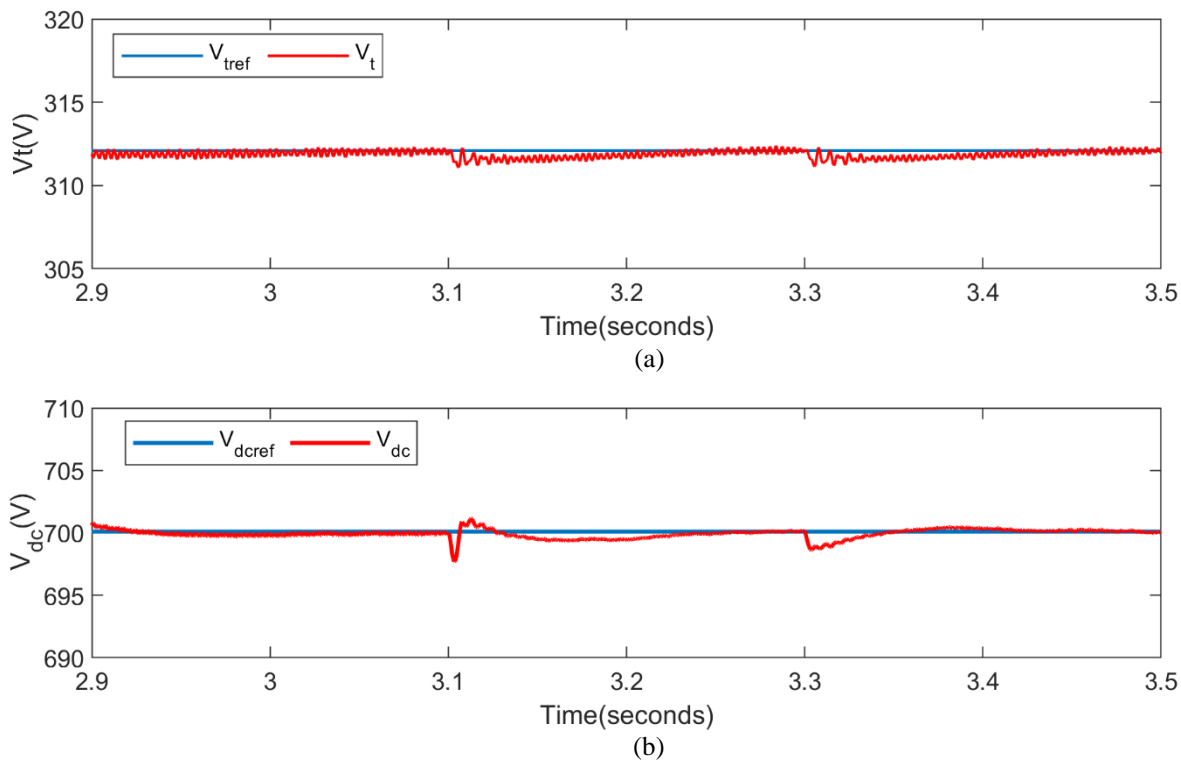


Figure 5. (a) Amplitude of SEIG voltages and (b) DC bus voltage

5. CONCLUSIONS

In this paper, an APF-based CSD control algorithm is proposed for DSTATCOM control and implemented for SEIG voltage regulation. The peak amplitudes of phase voltages are estimated separately for each phase by using the APF. In this way, there is no need to use complex structures. The obtained results clearly demonstrated the effectiveness of the APF-based CSD algorithm.

REFERENCES

- Kewat, S., & Singh, B. (2019). Modified amplitude adaptive control algorithm for power quality improvement in multiple distributed generation system. *IET Power Electronics*, 12(9), 2321-2329. <https://doi.org/10.1049/iet-pel.2018.5936>
- Özer, A. S., Sevilmiş, F., Karaca, H., & Arabacı, H. (2022). Enhanced control method for voltage regulation of DSTATCOM based SEIG. *Energy Reports*, 8, 839-847. <https://doi.org/10.1016/j.egy.2022.05.191>
- Sevilmiş, F., & Karaca, H. (2020). A fast hybrid PLL with an adaptive all-pass filter under abnormal grid conditions. *Electric Power Systems Research*, 184, 106303. <https://doi.org/10.1016/j.epsr.2020.106303>
- Singh, B., Murthy, S. S., Reddy, R. S., & Arora, P. (2015). Implementation of modified current synchronous detection method for voltage control of self-excited induction generator. *IET Power Electronics*, 8(7), 1146-1155. <https://doi.org/10.1049/iet-pel.2014.0718>
- Tandekar, J. K., Ojha, A., & Jain, S. (2019). SEIG-based renewable generation for MVDC ship power system with improved power quality. *Electric Power Components and Systems*, 47(1-2), 27-42. <https://doi.org/10.1080/15325008.2019.1570394>

A Comparative Study on Effects of The Number of Hidden Layers in Classification of Induction Motor Rotor Faults with Deep Neural Network

Hayri Arabaci*¹

Abstract: Induction motors are widely used in industry. The motors are of solid construction. However, in case of any fault, it causes the system to which it is connected to stop or operate inefficiently. For this reason, it is important to detect the faults of induction motors. In few decades, studies on fault detection have been carried out using many methods in the literature. Motor current is the most used motor parameter for fault detection. In the studies, the frequency spectrum of the motor current is generally used as a feature. Machine learning and especially artificial neural networks are used in fault classification. In recent years, deep learning approaches have started to be used in this field as well. The deep neural network (DNN) comes to the fore in deep learning approaches because it requires less processing capacity. One of the parameters affecting the accuracy of the results obtained with DNN is the number of hidden layers. For this reason, in this study, the effects of the number of hidden layers on classification accuracy in the detection of broken rotor bar faults were investigated. Three different motors for experimental work were operated at rated loads in four different conditions: healthy motor, one broken bar fault, 2 broken bar faults, and 3 broken bar faults. The motor current for each condition was sampled and saved. The frequency spectrum of the currents was obtained using the fast Fourier transform. These frequency spectrums are used as input data for the deep neural network. The network was trained and tested on nine different hidden layers. The obtained test results were compared based on both the detection errors of the healthy motors and the test errors. The test results obtained show that test errors increase in cases where the number of hidden layers is low or high, and it gives the best results when the number of hidden layers is three. The error rate of 0.92% in the optimum network structure showed that the DNN approach could be used for rotor fault detection.

Keywords: Deep neural network, fault classification, hidden layers, induction motor, rotor faults.

¹**Address:** Selcuk University, Faculty of Technology, Konya/Turkiye

***Corresponding author:** hayriarabaci@selcuk.edu.tr

1. INTRODUCTION

Induction motors are used as drive machines in many systems in the industry due to their robustness, reliability and low cost. If one of the motors fails, it will cause the system it drives to stop and thus industrial processes will be adversely affected. For this reason, detection and classification of induction motor faults have been studied for many years. The majority of faults are usually in moving parts, but rarely in solid parts such as rotor bars. Induction motor faults are examined in four different groups (Hassan, 2018):

- Stator faults
- Rotor faults
- Eccentricity faults
- Bearing faults

The symptoms of stator faults can clearly be observed and can therefore be detected using simple methods. Symptoms of other faults are not obvious. Therefore, it requires extensive analysis (Vas, 1993). Vibration analysis, sound analysis and current analysis methods are generally used in the detection of rotor faults, misalignment faults and bearing faults (Hassan, 2018). Vibration signals are obtained for the motor and the connected system by attaching vibration sensors for vibration analysis (Nath, 2020; Morales, 2018). The sensors are difficult to place and require precision. In addition, vibration sensors are expensive. For this reason, the use of vibration analysis and diagnosis method has gradually decreased. Microphones and ultrasonic sensors are used for fault detection with sound signals (Yaman, 2021). However, environments with motors in industry often have intense sound noise. Therefore, it becomes difficult to distinguish the noise in the recorded sound data from the sound data that carries the fault characteristic. For this reason, fault detection with the sound signal becomes difficult.

In current analysis-based approaches, the motor current can only be made with a current sensor connection. In addition, current sensors are inexpensive and easy to connect to the system. For this reason, current analysis has been widely used in the detection of motor faults in recent studies. In the first studies for fault detection, studies were carried out to

distinguish whether the motor is defective or not (Haji, 2001). In the following years, the focus has been on fault classification.

Among the motor faults, rotor faults were the most difficult to detect due to the minimal effects on the motor. In particular, the fact that broken rotor bar faults start as a small occurrence and grow gradually makes detection difficult. In the event of a broken bar, the motor air gap flux will change, which will be reflected in the motor current. This effect on the motor current is used as the fault characteristic. Time domain components and frequency domain components are used to extract the features of the fault. The current in the time domain is not used much in fault classification because the effects of the rotor bar fault are less pronounced in the data. The effects of rotor bar fault in the frequency domain appear in multiples of the fundamental frequency due to the slip as shown in Equation (1). For this reason, frequency domain components are more commonly used for feature extraction.

$$f_{brb}=(1\pm 2ks)f \quad (1)$$

where s is the slip, f is the current fundamental frequency. Numerous methods have been used to obtain the frequency components of the current: Discrete Wavelet Transform (Siddiqui, 2012), Prony Analysis (Chen, 2010), Fast Fourier Transform (FFT) (Ameid, 2017), Zoom-FFT (Kim, 2012), Hilbert Transform (Rangel, 2017), Extended Kaman Filter (Naha, 2016) and Multiple Signal Classification (Singh, 2018). However, studies have mostly focused on FFT. It is seen from Equation (1) that the effects of rotor bar fault will be in close values just around the fundamental current component. Therefore, it is important for the classification accuracy to include the frequency components (sidebands) close to the fundamental current component within the frequency region where feature extraction will be used.

Rotor faults generally occur during the production stages or as a result of an error made during the production process. However, not all faults are at the same level. While the fault sometimes negatively affects the conductivity of a rotor bar (high reactance bar fault), sometimes the error causes the complete loss of conductivity of the bar (a broken bar fault). Additionally, after the motor is put into use following production, the bars are subjected to magnetic and thermal stresses, which cause the bars to be strained. Fault continues to develop due to these stresses: a high reactance bar can cause a broken bar situation, or a broken bar can cause a second broken bar to occur. Considering these situations, the following fault conditions are usually included in the fault detection studies:

- Healthy motor condition
- A broken bar fault condition
- Two broken bars fault condition
- Three broken bars fault condition

The input data to be used for rotor fault detection and classification is a column matrix consisting of the frequency domain components of the current. The output is 4 conditions representing healthy and faults. For this reason, machine learning has a very suitable data structure for artificial intelligence applications. Therefore, to classify rotor faults, Adaptive Neural Fuzzy Inference System (Mohamed, 2020), Artificial Neural Network (ANN) (Zolfaghari, 2018), Principal Component Analysis (Georgoulas, 2013), Support Vector Machines (Arabaci, 2020), K Nearest Neighborhood (Yaman, 2021). Traditional machine learning algorithms such as and various combinations of the algorithms are frequently used. On the other hand, in recent years, deep learning approaches have been especially focused on fault classification (Nath, 2021). The structure of machine learning algorithms generally has one hidden layer. Especially in ANN, a single hidden layer is preferred. With the development of technology, hardware and software limitations have begun to disappear. Accordingly, the capacity of ANN has been greatly expanded by allowing to increase the number of computation layers of traditional ANN (LeCun, 2015). The enhanced version of ANN is called a deep neural network (DNN). When combined with more intelligent training schemes and fine-tuning, DNNs have found widespread applications in various fields such as natural language processing, image processing, and speech recognition.

It is evident that thanks to its structure, DNN is highly suitable for fault detection and classification purposes. Numerous studies in the literature have shown that if a DNN has a sufficient number of hidden layers, it can achieve desired results in systems with any kind of linear or nonlinear behavior (Hanin, 2019). The proposed method can use the frequency spectrum of the current signal for fault classification without the need for an additional filter and a mathematical relationship. This spectrum, which is used as input data, is very suitable for DNN use because it has a column matrix structure.

In studies on the classification of rotor faults, one motor is generally used. Classification data set was created by taking motor current for full load values over one motor. A network is created using this data. However, a question arises here: "Can the obtained classification structure be used for fault classification on another motor with a different nominal power?"

In order to answer this question, 3 different power motors were used in this study. Each motor was run at full load. For each motor, current data are taken for 3 different fault conditions and healthy motor condition. Feature extraction was done separately for each motor and input matrices were created. A single DNN network structure was created for all motors. In addition, one of the main aims of this study has been to investigate the optimal number of hidden layers that yield results with minimum error.

2. MATERIAL AND METHOD

Motor current is used as input data to classify rotor fault in induction motors with deep learning. In a healthy motor, the currents flowing through the rotor bars are balanced. If one of the bars is faulty, no current will flow through that bar. In this case, the current distribution through the rotor bars will become unbalanced. This unbalanced current distribution will adversely affect the air gap magnetic flux. These effects will be reflected in the motor current depending on the slip and the motor current fundamental frequency (as seen in Equation 1). Frequency components representing the fault can be to the right and left of the main frequency component. These are called sidebands. The sidebands are shown in Figure 1. Rotor bar fault can be detected by looking at the sideband components in the frequency spectrum of the current. The place of these components in the spectrum and the amplitude of these components will vary according to the load level of the motor and the size of the rotor bar fault. Therefore, it is difficult to determine the magnitude of the fault (class of fault), although it can be detected by looking at the sidebands that there is a rotor fault in the motor.

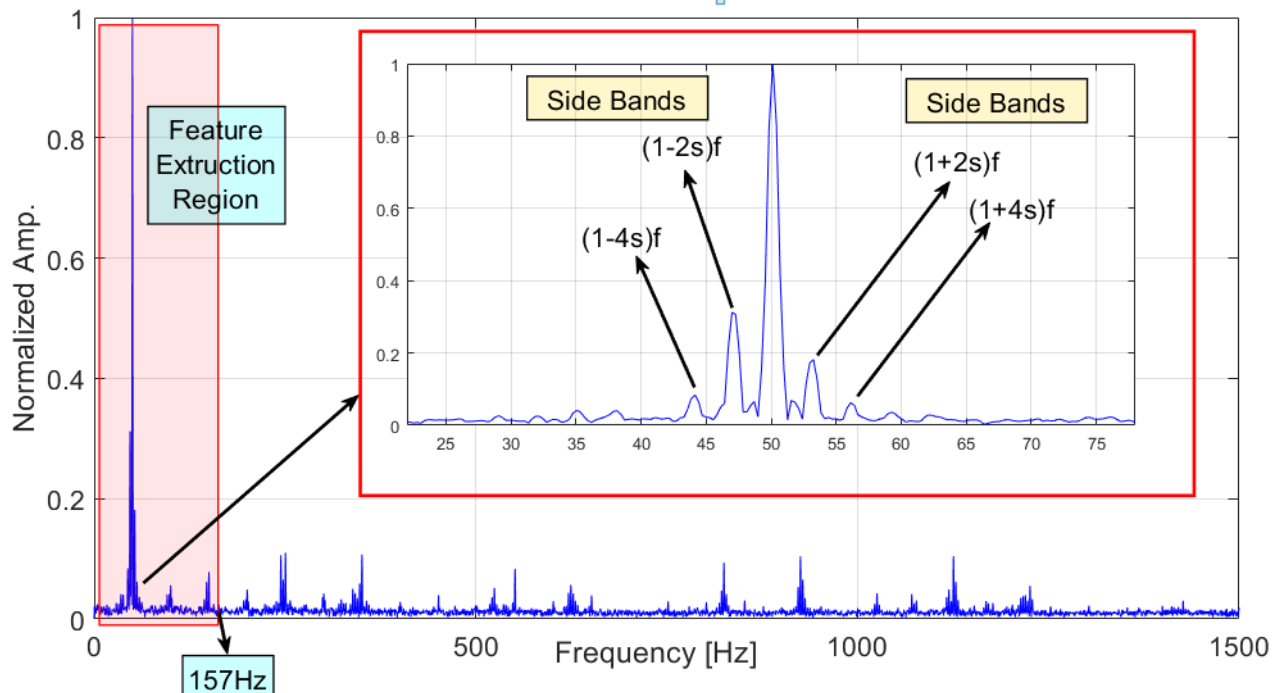


Figure 1. Motor current frequency spectrum and the frequency region used for the feature matrix.

In this study, it is aimed to determine the optimum number of hidden layers in the DNN structure that can make fault classification independent of motor rated power and motor loading status. Therefore, 3 different power induction motors were used in the experiments. Current values are sampled by loading each motor at full load level. The frequency spectrum of the current was obtained by using FFT from the current data. The fact that the power and load conditions of the motors used are different causes the effects of the fault effects on the spectrum to be different. In order to evaluate similar fault situations under the same conditions, the obtained frequency spectrum has been normalized. The fault indicators are most prominent in the frequency range of 0-157 Hz. Therefore, this range has been used as the input data.. The normalized frequency spectrum of the motor current is given in Figure 1. In the figure, the frequency range used for the feature matrix is shown in the frame.

Each motor was loaded at full load in 4 different motor states and 18 data were obtained. Thus, a total of 216 data sets were prepared. Each data is generated by sampling the current signal for approximately 3 seconds. Each sample has 20000 data points. As a result of feature extraction, the input data to be used for DNN has been reduced to 542 points. The obtained 216 data sets were split into two halves, with 108 of them used for training and the other half for testing. In this study, DNN was used as the classification method. The inputs of the DNN are a column matrix of 542 data, consisting of frequency components in the range 0-157 Hz. The output of the DNN is a matrix of 4 columns with data. The equivalents of these output matrix data are followed:

- Healthy motor: $[1000]^T$
- One broken bar fault: $[0100]^T$
- Two broken bar faults: $[0010]^T$
- Three broken bar faults: $[0001]^T$

Most approaches involving deep learning have a set of hyperparameters that profoundly influence the behavior and performance of the DNN according to the desired objectives. Therefore, these hyperparameters need to be carefully selected beforehand. Some of them are provided in Table 1.

Table 1. (Some important hyperparameters and options in the DNN structure)

Hyperparameters	Selection Options
Number of hidden neurons	Positive integer
Number of hidden layers	Positive integer
Neuron initiation	He, Lecun, Random, Xavier
Optimization algorithm	Adagrad, Adam, RProp, SGD
Non-Linearity	ELU, ReLU, Sigmoid, Tanh

As can be seen from Table 1, the number of permutations of possible options is very large. In addition, an increase in the number of hidden layers and neurons will increase the selection and use of hyperparameters, thus increasing the number of calculations. In conclusion, it is clear that a lot of work will be required to find the right combination of hyperparameters. A number of hyperparameter optimization algorithms are available that look for the best combination of hyperparameters for any focused problem (How, 2020). However, hyperparameter optimization is such a broad topic that it can be considered as a separate study. For this reason, hyper parameter analysis was not included in the study. Each hyperparameter can affect the behavior of the DNN. But the most influential hyperparameter is the number of layers. Therefore, investigating the number of hidden layers has been the main subject of this study. The other hyperparameters were selected based on empirical experience through previous work. The selected hyperparameter for the proposed DNN structure is given in Table 2.

Table 2. (The selected hyperparameters for the proposed DNN)

Hyperparameters	Selection Options
Number of hidden neurons	350
Number of hidden layers	1-9 (Variable)
Neuron initiation	Random
Optimization algorithm	RProp
Non-Linearity	Sigmoid

The training and optimization algorithm to be used is critical for training the DNN structure. In addition to these, it is very important to determine the loss functions and error measurement methods to create a stable structure. In the training process of this study, weight updates of DNN models were performed using the backpropagation algorithm. To assess the appropriateness of the determined weights, Mean Squared Error (MSE) was utilized for evaluation. In order to determine the most suitable number of hidden layers, first of all, the most suitable number of nodes was determined by making trials. In this process, robustness error and diagnostic error were used as reference criteria:

- Healthy error: It is the percentage expression of the ratio of the number of the created network classifying as defective for the healthy motor to the total number of samples.
- Diagnostic error: It is the percentage expression of the created network, the ratio of the number of misdiagnoses to the total number of samples.

By keeping the determined number of nodes constant, the number of hidden layers was increased from one to nine. Results were obtained for each value. The optimum number of hidden layers was determined by comparing the robustness error and diagnostic error values. After the training was completed, tests were conducted with other data not used in the training.

2.1. Experimental Study

In order to carry out the experimental study, the motor-generator experiment set was used. A generator is connected to the motor shaft to load the motors. Motors are loaded at full load by connecting a resistive load to the generator terminals. The block diagram of the experimental setup is given in Figure 2.

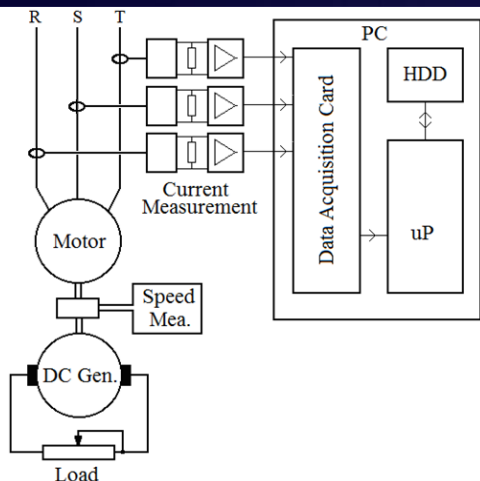


Figure 2. Experimental setup block diagram

Three different motors with 50HP, 30HP and 25HP power were used in the experiments. All motors are 3-phase, nominal operating voltage is 380V and frequency is 50Hz. For each motor, 4 different cases were examined:

- Healthy motor condition
- A broken bar fault condition
- Two broken bar fault condition
- Three broken bar fault condition

Each fault condition is created in the factory environment. First, the copper rotor bar was hammered in two separate pieces from both sides of the rotor cavity, leaving a gap in the middle to form the broken rotor bar. Thus, the electron transition in the corresponding bar is completely eliminated. For two broken and three broken bar faults, the same procedure was applied for 2 and 3 bars fault conditions. The illustration for a generated fracture fault situation and the photograph of the motors used are given in Figure 3. After the fault was created, the rotor balances were taken and mounted. Thus, a negative effect on the current due to the balance and interference with the rotor bar fault is prevented.



Figure 3. Photographs of the faulty rotor; a- Broken bar fault, b-Motors used

Motor current data is read from each of the three phases. To measure the current, the Hall-effect based current sensor "LA-205-S" manufactured by LEM company has been used. With the PCI-1716 data access card of Advantech company, the data were obtained from the sensors, transferred to the computer and saved on the HDD. The sampling frequency is 7500 Hz. The photograph of the experimental setup from which the data was taken is shown in Figure 4.



Figure 4. Photograph of the experimental setup

3. RESULTS

During the DNN training and testing processes, the ideal number of hidden layers was sought in the fixed number of nodes. For this process, first of all, experiments were made on the number of nodes in various numbers to determine the number of nodes. Test results are given in Table 3.

Table 3. (Error values obtained in fixed number of hidden layers)

Hidden Neurons	Hidden Layers	Healthy Error [%]	Diagnosis Error [%]
100	3	7,4074	13,8889
200	3	2,7778	4,6296
250	3	6,4815	7,4074
300	3	1,8519	4,6296
350	3	1,8519	3,7037
400	3	3,7037	3,7037
450	3	7,4074	12,037
500	3	2,7778	5,5556
100	3	7,4074	13,8889

Here it is seen that the best results are obtained at 350 hidden neurons. 350 neurons are used in the DNN structure to search for the ideal number of hidden layers. First, tests were made with a hidden layer DNN structure and then the number of hidden layers was increased one by one from two to nine, and results were obtained by using the DNN structures. The results obtained are given in Table 4.

Table 4. (Error values obtained in fixed number of hidden neurons)

Hidden Neurons	Hidden Layers	Healthy Error [%]	Diagnosis Error [%]
350	1	36,11	30,55
350	2	20,37	18,51
350	3	0,92	1,85
350	4	3,70	3,70
350	5	13,88	13,88
350	6	25	100
350	7	25	100
350	8	25	100
350	9	25	100

4. DISCUSSION AND CONCLUSIONS

As can be seen from Table 4, the best classification accuracy was achieved in the 3 hidden layer structure. In this case, the diagnostic error was 0.92% and the robustness error was 1.85%. If the number of hidden layers is increased, the errors increase. This shows that it is not meaningful to increase the hidden layer too much. Classification accuracy also decreases in low number of hidden layer structures.

The results obtained in this study showed us the following:

- Increasing the hidden layer in the DNN structure does not increase the classification accuracy proportionally.
- With the proposed DNN structure, rotor faults can be detected with high accuracy (99.08%). In fault classification, the error rate remains at 1.85%. These error rates show that the proposed DNN has a strong structure in rotor fault detection.
- The use of motors of different powers in the optimization process and the resulting accuracy rate show that the proposed DNN structure can also be used for testing motors of different rated powers.

Acknowledgements

The study has been supported by Scientific Research Project of Selcuk University.

Ethics Committee Approval

N/A

Peer-review

Externally peer-reviewed.

Author Contributions

Conceptualization: H.A.; Investigation: H.A.; Material and Methodology: H.A.; Supervision: H.A.; Visualization: H.A.; Writing-Original Draft: H.A.; Writing-review & Editing: H.A.; Other: All authors have read and agreed to the published version of manuscript.

Conflict of Interest

The authors have no conflicts of interest to declare.

Funding

The authors declared that this study has received no financial support.

REFERENCES

- Ameid, T., Menacer, A., Talhaoui, H., & Harzelli, I. (2017). Rotor resistance estimation using Extended Kalman filter and spectral analysis for rotor bar fault diagnosis of sensorless vector control induction motor. *Measurement*, 111, 243-259. <https://doi.org/10.1016/j.measurement.2017.07.039>
- Arabaci, H., & Mohamed, M. A. (2020). A knowledge-based diagnosis algorithm for broken rotor bar fault classification using FFT, principal component analysis and support vector machines. *International Journal of Intelligent Motorering Informatics*, 8(1), 19-37. <https://doi.org/10.1504/IJIEI.2020.105431>
- Chen, S., & Živanović, R. (2010). Estimation of frequency components in stator current for the detection of broken rotor bars in induction machines. *Measurement*, 43(7), 887-900. <https://doi.org/10.1016/j.measurement.2010.03.006>
- Georgoulas, G., Mustafa, M. O., Tsoumas, I. P., Antonino-Daviu, J. A., Climente-Alarcon, V., Stylios, C. D., & Nikolakopoulos, G. (2013). Principal Component Analysis of the start-up transient and Hidden Markov Modeling for broken rotor bar fault diagnosis in induction machines. *Expert Systems with Applications*, 40(17), 7024-7033. <https://doi.org/10.1016/j.eswa.2013.06.006>
- Haji, M., & Toliyat, H. A. (2001). Pattern recognition-a technique for induction machines rotor broken bar detection. *IEEE Transactions on Energy Conversion*, 16(4), 312-317. <https://ieeexplore.ieee.org/document/969469>

- Hanin, B. (2019). Universal function approximation by deep neural nets with bounded width and relu activations. *Mathematics*, 7(10), 992. <https://doi.org/10.3390/math7100992>
- Hassan, O. E., Amer, M., Abdelsalam, A. K., & Williams, B. W. (2018). Induction motor broken rotor bar fault detection techniques based on fault signature analysis—a review. *IET Electric Power Applications*, 12(7), 895-907. <https://doi.org/10.1049/iet-epa.2018.0054>
- How, D. N., Hannan, M. A., Lipu, M. S. H., Sahari, K. S., Ker, P. J., & Muttaqi, K. M. (2020). State-of-charge estimation of li-ion battery in electric vehicles: A deep neural network approach. *IEEE Transactions on Industry Applications*, 56(5), 5565-5574. <https://ieeexplore.ieee.org/document/9122534>
- Kim, Y. H., Youn, Y. W., Hwang, D. H., Sun, J. H., & Kang, D. S. (2012). High-resolution parameter estimation method to identify broken rotor bar faults in induction motors. *IEEE Transactions on Industrial Electronics*, 60(9), 4103-4117. <https://ieeexplore.ieee.org/document/6355663>
- LeCun, Y., Bengio, Y., & Hinton, G. (2015). Deep learning. *nature*, 521(7553), 436-444. <https://doi.org/10.1038/nature14539>
- Mohamed, M. A., Mohamed, A. A. A., Abdel-Nasser, M., Mohamed, E. E., & Hassan, M. M. (2021). Induction motor broken rotor bar faults diagnosis using ANFIS-based DWT. *International Journal of Modelling and Simulation*, 41(3), 220-233. <https://doi.org/10.1080/02286203.2019.1708173>
- Morales-Perez, C., Rangel-Magdaleno, J., Peregrina-Barreto, H., Amezcua-Sanchez, J. P., & Valtierra-Rodriguez, M. (2018). Incipient broken rotor bar detection in induction motors using vibration signals and the orthogonal matching pursuit algorithm. *IEEE Transactions on Instrumentation and Measurement*, 67(9), 2058-2068. <https://ieeexplore.ieee.org/document/8333785>
- Naha, A., Samanta, A. K., Routray, A., & Deb, A. K. (2016). A method for detecting half-broken rotor bar in lightly loaded induction motors using current. *IEEE Transactions on Instrumentation and Measurement*, 65(7), 1614-1625. <https://ieeexplore.ieee.org/document/7450652>
- Nath, A. G., Sharma, A., Udmale, S. S., & Singh, S. K. (2020). An early classification approach for improving structural rotor fault diagnosis. *IEEE Transactions on Instrumentation and Measurement*, 70, 1-13. <https://ieeexplore.ieee.org/document/9300170>
- Nath, A. G., Udmale, S. S., & Singh, S. K. (2021). Role of artificial intelligence in rotor fault diagnosis: A comprehensive review. *Artificial Intelligence Review*, 54, 2609-2668. <https://doi.org/10.1007/s10462-020-09910-w>
- Rangel-Magdaleno, J., Peregrina-Barreto, H., Ramirez-Cortes, J., & Cruz-Vega, I. (2017). Hilbert spectrum analysis of induction motors for the detection of incipient broken rotor bars. *Measurement*, 109, 247-255. <https://doi.org/10.1016/j.measurement.2017.05.070>
- Siddiqui, K. M., & Giri, V. K. (2012, March). Broken rotor bar fault detection in induction motors using wavelet transform. In *2012 International Conference on Computing, Electronics and Electrical Technologies (ICCEET)* (pp. 1-6). IEEE. <https://ieeexplore.ieee.org/document/6203753>
- Singh, G., & Naikan, V. N. A. (2018). Detection of half broken rotor bar fault in VFD driven induction motor drive using motor square current MUSIC analysis. *Mechanical Systems and Signal Processing*, 110, 333-348. <https://doi.org/10.1016/j.ymssp.2018.03.001>
- Vas, P. (1993). *Parameter estimation, condition monitoring, and diagnosis of electrical machines*, Oxford University Press, London.
- Yaman, O. (2021). An automated faults classification method based on binary pattern and neighborhood component analysis using induction motor. *Measurement*, 168, 108323. <https://doi.org/10.1016/j.measurement.2020.108323>
- Zolfaghari, S., Noor, S. B. M., Rezazadeh Mehrjou, M., Marhaban, M. H., & Mariun, N. (2017). Broken rotor bar fault detection and classification using wavelet packet signature analysis based on fourier transform and multi-layer perceptron neural network. *Applied Sciences*, 8(1), 25. <https://doi.org/10.3390/app8010025>